ANALYTIC ELEMENT MODELING OF GROUNDWATER FLOW

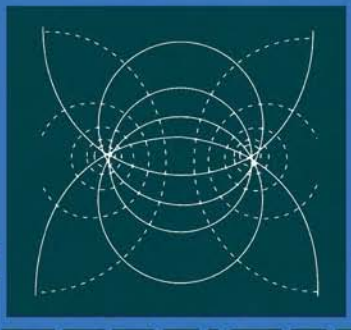

H. M. HAITJEMA

ANALYTIC ELEMENT MODELING OF GROUNDWATER FLOW

This Page Intentionally Left Blank

ANALYTIC ELEMENT MODELING OF GROUNDWATER FLOW

H. M. Haitjema

School of Public and Environmental Affairs
Indiana University
Bloomington, Indiana

Academic Press
San Diego New York Boston London Sydney Tokyo Toronto

This book is printed on acid-free paper. ♾

Academic Press, Inc.
A Division of Harcourt Brace & Company
525 B Street, Suite 1900, San Diego, California 92101-4495

United Kingdom Edition published by
Academic Press Limited
24-28 Oval Road, London NW1 7DX

Library of Congress Cataloging-in-Publication Data

Haitjema, H. M. (Henk M.)
Analytic element modeling of groundwater flow / by H. M. Haitjema.
p. cm.
Includes index.
ISBN 0-12-316550-4 (alk. paper)
1. Groundwater flow--mathematical models. I. Title.
GB1197.7.H335 1995
551.49'01'5118--dc20 95-16533
CIP

PRINTED IN THE UNITED STATES OF AMERICA
95 96 97 98 99 00 BC 9 8 7 6 5 4 3 2 1

To Bieneke

This Page Intentionally Left Blank

Contents

Preface

The purpose of this text is to provide both professionals and students in groundwater hydrology with a practical introduction to the analytic element method and the use of elementary analytic solutions in solving groundwater flow problems. The design of analytic element models requires substantial expertise in engineering mathematics and computer programming, and is discussed in *Groundwater Mechanics* by Strack (1989). The current text, however, focuses not on the design of analytic element models, but on their *use*! Consequently, the detailed and often involved derivations of the various analytic elements are omitted. Instead, the basic concepts behind the method are illustrated by presenting a number of elementary analytic solutions and applying them to practical groundwater flow problems. In particular, I have set out to promote a stepwise approach to groundwater flow modeling, progressively using more sophisticated or detailed solutions as insight into the problem grows. Where possible, data uncertainties are resolved through hypothesis testing—by presenting several alternative solutions. This approach is in contrast to the more rigid, but often employed, practice of constructing a "best fit model." Although the analytic element method is particularly well suited for this stepwise modeling procedure, the concept applies equally well to modeling projects carried out with other numerical models; see Ward *et al.* (1987).

An educational version of the analytic element software GFLOW is included with this text. The GFLOW package consists of a data preprocessor GAEP and the analytic element model GFLOW1. A set of GFLOW1 input-data files are provided to allow the reader to reproduce the various solutions to groundwater flow problems discussed in this text. The relevant data files are identified in the captions of the figures that display these solutions. Many of the data files contain instructions for

additional experimentation with the problem at hand. Refer to the file "readme" on the distribution diskette for installation and operating procedures for GFLOW.

The approach to groundwater flow modeling presented in this text reflects the influence of my mentors combined with my own experiences in teaching and practicing groundwater hydrology. I am particularly grateful to the inspiring lectures of Prof. A. Verruijt, Prof. L. Huisman, and Prof. G. de Josselin de Jong at the Civil Engineering Department of the Technical University Delft, The Netherlands. Dr. P. A. Vermeer at the Geotechnical Laboratory of the Civil Engineering Department was the first to introduce me to the elegance and power of analytic solutions to groundwater flow problems. Prof. Verruijt offered me a research position and started my career in academia. Prof. de Josselin de Jong further stimulated my interest in analytical solutions until his advisee Dr. O. D. L. Strack invited me to Minnesota. There, under contract with the U.S. Army Corps of Engineers, I worked on the implementation of his newly conceived analytic element method. After completing my Ph.D. studies under Prof. Strack, I started to teach and further develop the analytic element method at the School of Public and Environmental Affairs of Indiana University. The current text evolved from my course "Groundwater Flow Modeling" and my groundwater flow consulting experiences.

I am indebted to many of my students who provided feedback on the manuscript, improving its clarity and focus. Specifically, I thank my Ph.D. advisees: Dr. S. R. Kraemer, Dr. S. Mitchell-Bruker, Mr. J. Wittman, Mr. V. A. Kelson, and Mr. K. Luther, with whom I discussed much of the material and its presentation in this text. Mr. V. A. Kelson wrote part of the GFLOW software (the preprocessor GAEP) included with this text and assisted in preparing one of the case studies in Chapter 6. Dr. Lloyd Townley provided valuable feedback on Section 5.3.7.

This text has been prepared with the typesetting program TEX,[1] by Donald E. Knuth, using the macro LATEX by Leslie Lamport. The preparation of this manuscript diverted my attention from many other important activities, including spending time with my children, Coraline (14), Mart (12), and Charles (10). I could not have completed this text without the unwavering support of my wife, Bieneke, to whom I dedicate this work.

H. M. Haitjema

[1] TEX is a trademark of the American Mathematical Society.

Chapter 1

Introduction

The mention of groundwater flow modeling usually evokes images of a model grid or element network, depending on whether one is a finite difference or finite element modeler. Of course, groundwater flow modeling is nearly synonymous with *computer modeling*. Solving groundwater flow problems by drawing flownets, or applying conformal mapping techniques, seems an activity of the past (Muskat, 1937; Harr, 1962). The use of computer models does not require a background in advanced engineering mathematics, or so it is believed. The ingenuity and elegance of classical analytic solutions to groundwater flow have been largely replaced by the versatility of numerical algorithms and the computational power of the digital computer. Many see an advantage here: The hydrologist can now concentrate on *groundwater hydraulics* rather than being distracted by tiresome mathematical manipulations.

The shift from analytical to numerical modeling of groundwater flow is also reflected in the current training of groundwater hydrologists. After introducing such basics as Darcy's law and continuity of flow, the discussions quickly focus on the application of numerical models. This emphasis on numerical modeling, early on in the training, often deprives the hydrologist of the insight in basic groundwater hydraulics that comes from solving elementary flow problems *analytically*. The basic concept of superposition, for instance, is undoubtedly taught in every groundwater hydrology course, but it is not applied when creating a finite difference or finite element solution. The consequences of this single-sided training may be illustrated by the following anecdote. Once, the validity of my analytic solution to a regional groundwater flow problem, superimposing over a hundred elementary solutions to the governing differential equation, was called into question by a conference attendee who asked: "How can you trust your solution if you

have no grid in which to check the water balance?" The critique came from a very responsible finite difference modeler who indeed is conscious of the need to check the water balance in finite difference models. That analytic solutions to the governing differential equation satisfy the water balance *exactly*, however, was forgotten.

Elementary analytic solutions, such as a well in a uniform flow field or areal recharge on an aquifer between two parallel streams, provide much insight in the role that various aquifer parameters play in determining the groundwater flow patterns. For instance, in many cases of aquifer remediation or wellhead protection, the groundwater capture zones for wells can be sketched by hand using three points on the capture zone envelope that are easily determined from field data. Such a "back of the envelope" capture zone estimate is a valuable check on any computer-generated capture zone. From a simple one-dimensional solution we learn that, in general, groundwater mounding in regional aquifers is proportional to the ratio of recharge over transmissivity while it is proportional to the *square* of the average distance between surface waters. There are many more examples of how elementary analytic solutions provide important insights in the behavior of groundwater flow. Occasionally, a simple analytic solution will suffice to answer the questions for which a numerical model may otherwise be employed. In fact, the important step of *model selection* (Anderson and Woessner, 1992) cannot be taken properly without a good insight in the basic behavior of the groundwater flow system at hand. Perhaps the best way to select a (computer) model is after some simple hand calculations (analytic solutions) have been done.

As with so many things, the pendulum swings back and forth. Currently, there is a renewed interest in analytic approaches to groundwater flow modeling. Although analytic solutions usually require more severe simplifications of the flow system (horizontal aquifer base, uniform conductivity, etc.) than numerical solutions do, they also require correspondingly fewer input data. The latter feature is attractive because field data acquisition is time-consuming and expensive, while some parameters remain uncertain anyhow (e.g., spatial distributions of hydraulic conductivities and recharge rates). For the purpose of wellhead protection, for instance, EPA developed the analytical computer model WHPA, which uses conformal mapping and imaging techniques to solve basic groundwater flow problems (Blandford and Huyakorn, 1990). WHPA is widely used by the drinking-water industry to delineate capture zones for their well fields. In 1981 Strack introduced the "Analytic Element Method," by which complex regional flow problems can be solved by superposition of many (hundreds) analytic solutions or *analytic elements* (Strack and Haitjema, 1981a, 1981b). The analytic element method combines the elegance and accuracy of analytic

solutions with the power of the digital computer in an attempt to get the best of both worlds. Although analytic element models are easy to use, they are difficult to build; they employ complex analytic solutions, whose development requires advanced mathematical skills and whose implementation in a computer code requires specialized programming skills. A rigorous treatment of these analytic elements and their numerical implementation is found in a text by Strack (1989). The current text focuses on the *application* of the analytic element method, while the theoretical basis for the method is presented step by step through a series of analytic solutions to elementary flow problems. The theoretical discussions are interspersed with computer exercises which demonstrate the concepts by applying them to practical problems.

The approach to groundwater flow modeling promoted in this text is that of *stepwise modeling* and *hypothesis testing*, instead of finding "the best-fit model." More often than not, the enthusiastic groundwater modeler loses himself or herself in the overwhelming complexity of the hydrogeology and the effort to include it all in the model. The quality of a groundwater flow simulation is then measured by the degree of complexity and detail of the model and model input data. Variations in aquifer properties and recharge rates, transient effects, and transport phenomena are all incorporated in the model because they *exist*, not because they *matter*. Extensive model calibration efforts are directed at finding the conductivity or conductivities, the aquifer recharge rate or rates, etc. Such a complex model becomes a card-house of assumptions; if one assumption is shown to be in error, the whole model collapses under the pressure of suspicion. In a stepwise modeling procedure, in contrast, we will gradually build up complexity and only to the degree necessary. In this way the relative importance of the various hydrogeologic parameters is better understood and documented. Data uncertainties are dealt with by modeling bounding parameter values and assessing their impact in view of the *modeling objectives*. This hypothesis testing approach can often replace expensive and time-consuming field data acquisition, or at least demonstrate objectively which additional field data are of importance for the project. This kind of groundwater flow modeling places the responsibility for the outcome of a study entirely with the groundwater hydrologist — where it belongs! This way the quality of the work depends on the expertise of the hydrologist, not on the bells and whistles of the software or on the (mechanical) adoption of some established modeling protocol.

The text is subdivided into six chapters, including this introduction. In Chapter 2, I review some of the basics of groundwater hydrology, such as Darcy's law and conservation of mass, and show how they are combined into a governing differential equation. Chapter 3 is devoted to "Dupuit–

Forchheimer flow," in most other texts referred to as two-dimensional flow. We will discover, however, that the Dupuit–Forchheimer assumption is less restrictive than the term "two-dimensional flow" suggests. In fact, as we will discover, Dupuit–Forchheimer models can handle most of our modeling needs. In Chapter 4, we will briefly address three-dimensional flow problems. At the end of that chapter I will show how three-dimensional analytic elements (e.g., a partially penetrating well) can simply be included in a Dupuit–Forchheimer model, at least for the case of confined flow. Such a hybrid 2D-3D model is computationally very efficient: Complicated three-dimensional functions are evaluated only where needed, e.g., near a partially penetrating well. In Chapter 5, I formally introduce the analytic element method, although for all of our previous computer modeling exercises we have already been using the analytic element model GFLOW1. In that chapter I formulate a stepwise modeling approach for which the analytic element method is uniquely suited. We also systematically explore the effect of more complex conceptual models — for instance, when to use three-dimensional flow or transient flow, and what is the effect of variations in aquifer properties or aquifer recharge. Finally, in Chapter 6, I discuss three groundwater flow modeling projects (case studies) to which the analytic element method has been applied.

Chapter 2

Basic Concepts

Groundwater is present and in motion in almost all geological formations. In some materials, such as clay or rock, movement is very slow as compared to the groundwater flowing in sand and gravel formations. Highly fractured rock, however, may exhibit groundwater discharges equal to or in excess of sand and gravel *aquifers*. Any geological formation from which water can be pumped in "usable quantities" [a few gallons per minute (GPM) or more] is, at least according to regulatory agencies, an aquifer worthy of our attention. These aquifers comprise our groundwater resource and are the subject of the groundwater modeling discussions in this text.

For most practical engineering purposes, it is sufficient to consider average groundwater flow rates and directions. We rarely have to concern ourselves with the erratic movement of water on the (microscopic) scale of individual pores. With that stipulation, the movement of groundwater is quite accessible to mathematical descriptions. The governing equations for groundwater flow are based on two fundamental principles: Darcy's law and conservation of mass.

2.1 Darcy's Law

In 1856 the French engineer Darcy conducted a series of experiments on the flow of water through columns of sand (Darcy, 1856). Figure 2.1 is a copy of the original figure in his report. Water, introduced at the top of the iron pipe, is forced downward through a column of sand and exits through a faucet at the bottom. Water pressures are monitored by manometers connected to the top and the bottom of the sand column.

Darcy's experiment is schematically represented in Figure 2.2. The wa-

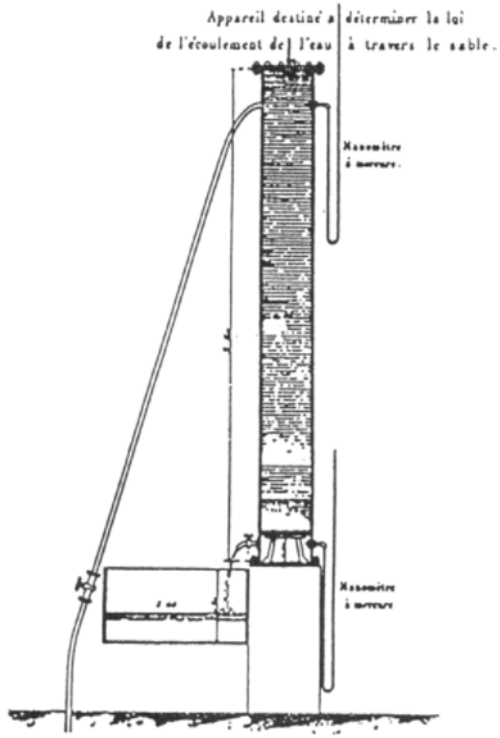

Figure 2.1: Darcy's experiment as shown in his paper from 1856.

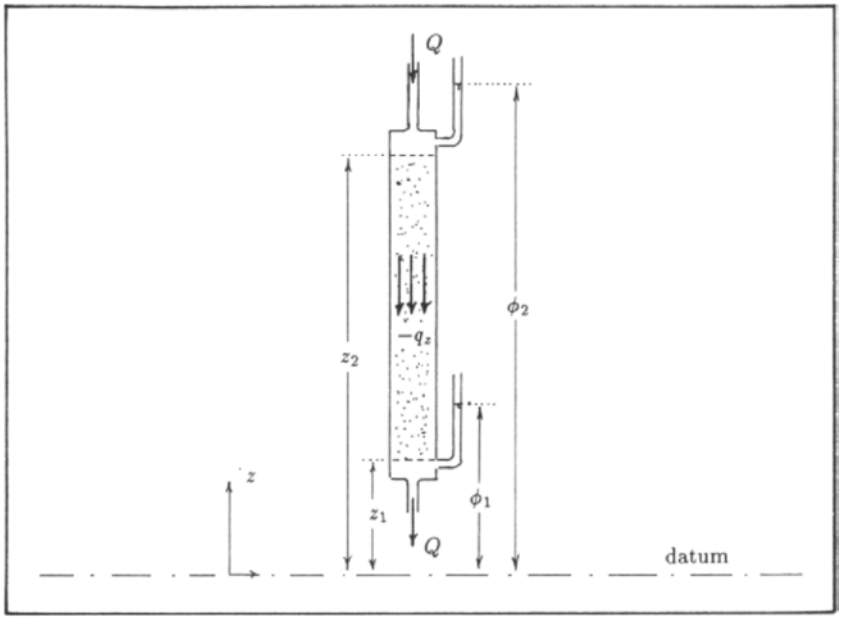

Figure 2.2: Schematic diagram of Darcy's experiment.

ter levels in the manometers[1] are ϕ_1 and ϕ_2 $[L]$ as measured with respect to some horizontal datum. Throughout this text I will report the dimensions of newly introduced properties between square brackets, in which L, T, and M stand for length, time, and mass, respectively.

These water levels ϕ_1 and ϕ_2 are referred to as *hydraulic heads*, or *heads* for short. The top of the sand column is at $z = z_2$ where the head is ϕ_2, while the bottom is at $z = z_1$ with head ϕ_1 (see Figure 2.2). The difference in head $(\phi_2 - \phi_1)$ is the driving force that moves the water through the sand.

Darcy found the following relationship between the flow rate Q $[L^3/T]$[2] and the head difference $(\phi_2 - \phi_1)$:

$$Q = kA\frac{\phi_2 - \phi_1}{z_2 - z_1} \tag{2.1}$$

where A $[L^2]$ is the cross-sectional area of the sand column and $z_2 - z_1$ $[L]$ is its length; see Figure 2.2. The parameter k $[L/T]$ is a proportionality

[1] Darcy employed mercury-filled manometers, but translated the rise of mercury into water elevations.

[2] Dimensions are given between [ ]: L is length, T is time, and M is mass.

constant found to be dependent on the type of sand in the apparatus; it is termed the *hydraulic conductivity.*

Equation (2.1) may be generalized for use in the analysis of groundwater flow. The head distribution in the sand column varies linearly from ϕ_1 to ϕ_2 for increasing values of z. This may be understood by applying (2.1) to sections of the column. For instance, a manometer connected to the sand column midway between z_1 and z_2 must exhibit a head midway between ϕ_1 and ϕ_2 in order for (2.1) to be valid. Consequently, we may write the head as a linear function of z:

$$\phi(z) = \frac{\phi_2 - \phi_1}{z_2 - z_1} z + \frac{\phi_1 z_2 - \phi_2 z_1}{z_2 - z_1} \tag{2.2}$$

The term $(\phi_2 - \phi_1)/(z_2 - z_1)$ in (2.1) appears to be the derivative of $\phi(z)$,

$$\frac{d\phi}{dz} = \frac{\phi_2 - \phi_1}{z_2 - z_1} \tag{2.3}$$

The flow rate Q in (2.1) may be normalized with respect to the cross-sectional area A of the sand column, yielding the *specific discharge* $q_z = -Q/A$ $[L/T]$. The index z indicates that the specific discharge is parallel to the z-direction, while the minus sign indicates that the flow in Figure 2.2 occurs in the negative z-direction. Darcy's relationship (2.1) may therefore be rewritten as

$$q_z = -k \frac{d\phi}{dz} \tag{2.4}$$

Equation (2.4) no longer refers to the specific dimensions or design of Darcy's apparatus. It simply states that if, in a sand body (aquifer), the derivative of the head in z-direction is known, the specific discharge in the z-direction follows from (2.4). It seems intuitive that the result (2.4) holds in any direction, including the x- and y-direction of a Cartesian coordinate system. All three components of the *specific discharge vector* in the aquifer then follow from

$$\begin{aligned} q_x &= -k \frac{\partial \phi}{\partial x} \\ q_y &= -k \frac{\partial \phi}{\partial y} \\ q_z &= -k \frac{\partial \phi}{\partial z} \end{aligned} \tag{2.5}$$

The partial derivatives of $\phi(x, y, z)$ in (2.5) represent the three components of the *hydraulic gradient.* Equation (2.5) may be written in a more compact form by use of the indicial notation or tensor notation:

$$q_i = -k \partial_i \phi \qquad (i = 1, 2, 3) \tag{2.6}$$

where q_i represents the three components of the specific discharge vector q_x, q_y, and q_z, while ∂_i represents the three partial derivatives of ϕ with respect to x, y, and z.

Hydraulic conductivity values

The hydraulic conductivity values vary widely depending on the geological formations. In Table 2.1 approximate ranges for k are given for several soil types. The k-value ranges in tables are too broad and too unreliable,

Table 2.1: Some approximate ranges for k in different soil types.

soil type	k in ft/day
gravel	> 500
sand and gravel	200 - 500
coarse sand	50 - 200
medium sand	20 - 50
fine sand	1 - 20
silty sand	0.1 - 1
silt	0.01 - 0.1
peat	0.001 - 0.01
sandy clay	0.0001 - 0.001
clay	< 0.0001

however, to be used for practical computations. Instead, these values should be obtained from so-called "pumping tests" in the field, see Section 3.6.4, or from ... groundwater flow modeling, as we will discuss later. I did not present any k-values for rock in Table 2.1, since they depend heavily on the degree of fracturing of the rock. In fact, it is often questionable whether or not flow in a fractured rock aquifer can be described by Darcy's law, which brings us to the next issue.

2.1.1 The Representative Elementary Volume

When rewriting (2.1) in the form of (2.4), it was tacitly assumed that Darcy's experiment remains valid on any scale, including on the scale of a single point. This is obviously not true. That single point, for instance, may fall inside a sand grain where neither water pressure (or head) nor groundwater velocity can be defined. Yet in our mathematical analyses we will pretend that soil and water form a continuum, so that we may write our relationships for any point in the porous (continuous) medium. This

is an acceptable practice, provided that we do not attempt to make any observations at a single point. Our observations of heads and groundwater velocities, for example, should be averages over a sufficiently large aquifer volume as to allow for proper averaging of these quantities. The smallest possible volume acceptable for our observations is called the *representative elementary volume* or *REV*. In sand and gravel aquifers the REV may be less than a few cubic inches. In fractured rock, however, far larger volumes may need to be considered. In some cases, the fractured rock system continues to behave discretely even on a regional scale. In those cases the basic equations developed in this chapter do not apply.

2.1.2 Average Groundwater Velocity

The dimensions of the specific discharge vector are those of a velocity $[L/T]$, which has led to the term "Darcy velocity" for q_i in (2.6). In fact, in his report, Darcy himself referred to it as a velocity. The term, however, is misleading and is better avoided! The specific discharge is not a velocity, but a discharge rate per unit area. The *average groundwater velocity* v in Darcy's apparatus is

$$v = \frac{Q}{nA} \tag{2.7}$$

where n is the soil porosity: the fraction of the soil volume occupied by pore space. The term nA in (2.7) is thus the cross-sectional area available for the discharge rate Q to flow through. Only when there would be no soil particles ($n = 1$) would the specific discharge represent the average groundwater flow velocity. The average groundwater velocity vector v_i in an aquifer is, with Q/A being the specific discharge,

$$v_i = \frac{q_i}{n} \tag{2.8}$$

2.1.3 Intrinsic Permeability

Hubert (1940) pointed out that the *hydraulic conductivity* k depends not only on the soil type, but also on the density and viscosity of the pore fluid which flows through the soil:

$$k = \frac{\kappa\gamma}{\mu} = \frac{\kappa\rho g}{\nu\rho} = \frac{\kappa g}{\nu} \tag{2.9}$$

where κ $[L^2]$ is called the *intrinsic permeability* or just *permeability*. The other properties in (2.9) are

γ $[M/L^2T^2]$ is the unit weight of the pore fluid,

μ $[M/LT]$ is the dynamic viscosity of the pore fluid,

ρ $[M/L^3]$ is the density (unit mass) of the pore fluid,

ν $[L^2/T]$ is the kinematic viscosity of the pore fluid, and

g $[L/T^2]$ is the acceleration of gravity.

The intrinsic permeability concept is popular in the oil industry where the simultaneous movement of gas, oil, and water needs to be considered. In the context of groundwater flow the intrinsic permeability is usually not used except, for instance, when dealing with problems of severe groundwater contamination — for example, in the case of pure TCE (trichloroethylene) sinking to the bottom of an aquifer. For some fluids the values for ρ and ν are given in Table 2.2. I added the density and viscosity for *air* to Table 2.2

Table 2.2: Density and viscosity values for some fluids and air.

fluid or gas	density ρ [g/cm^3]	kin. viscosity ν [cm^2/s]
fresh water	1.000	0.013
sea water	1.025	0.014
gasoline	0.680	0.005
crude oil	0.860	0.12
TCE (trichloroethylene)	1.464	0.0039
air	1.247×10^{-9}	0.142×10^{6}
Acceleration of gravity g is 998.1 cm/s^2.		

so that the hydraulic conductivity may be converted into an *air conductivity* by use of (2.9). This air conductivity is useful in the context of "soil venting", a technique for cleaning up the unsaturated zone of a shallow aquifer. The subject of modeling air flow through porous media, however, is beyond the scope of this text. The interested reader is referred to Johnson *et al.* (1990).

2.1.4 Laminar Flow

Darcy's experimental law represents a linear relationship between the hydraulic gradient and the specific discharge vector, indicating laminar flow conditions. However, rapid flow through large pore spaces may become turbulent, in which case it cannot be described by Darcy's laminar flow

law. Such conditions are possible in large fractures in rock or, for instance, in coarse gravel formations close to high-capacity wells.

Validity of Darcy's Law

The validity of Darcy's law may be verified by calculating the value of a dimensionless number used in fluid dynamics: the *Reynolds number*. The Reynolds number is defined differently depending on the character of the flow problem. For flow between two parallel plates, an approximation to fracture flow, the Reynolds number may be defined as

$$Re_{(rock)} = \frac{dv}{\nu} \tag{2.10}$$

where d $[L]$ is the fracture aperture, v the average groundwater velocity in the fracture, and ν the kinematic viscosity of the groundwater. Laminar flow conditions are ensured when

$$Re_{(rock)} < 800 \tag{2.11}$$

For flow through sand and gravel aquifers, the Reynolds number may be defined as

$$Re_{(soil)} = \frac{Dq}{\nu} \tag{2.12}$$

where D $[L]$ is the average grain diameter and q the specific discharge. Laminar flow conditions are ensured when

$$Re_{(soil)} < 1 \tag{2.13}$$

To illustrate the validity of Darcy's law, consider a sand and gravel aquifer with an average grain size of 10^{-3} m, a hydraulic conductivity of 10^{-2} m/s, and a hydraulic gradient of 10^{-2}. The kinematic viscosity of water is approximately 10^{-6} m^2/s. The specific discharge is the product of hydraulic conductivity and hydraulic gradient: $q = 10^{-2} \times 10^{-2} = 10^{-4}$ m/s. With these values the Reynolds number becomes [see (2.12)]:

$$Re_{(soil)} = \frac{10^{-3} \times 10^{-4}}{10^{-6}} = 10^{-1} < 1 \tag{2.14}$$

The values just used represent rather extreme conditions of rapid flow in a course sand and gravel aquifer, yet the flow is well within the laminar range. In most sand and gravel aquifers, laminar flow is ensured. However, fractured rock aquifers may frequently exhibit turbulent flow because of large fracture apertures.

Contaminant Spreading

The laminar nature of groundwater flow has an important implication regarding the movement of contaminated groundwater. On the macroscopic scale, "water particles" tend to move parallel to each other in an orderly linear motion, rather than the turbulent mixing that occurs in some rapidly flowing surface waters. Consequently, mechanical mixing of clean and contaminated groundwater does not, in general, occur in aquifers! Instead, it is molecular diffusion which drives some contaminants from contaminated water to adjacent clean water. This diffusive process is enhanced by the irregular nature of flow paths on the scale of the aquifer pores. This process is known as *microscopic hydrodynamical dispersion* (Bear, 1972). Aquifer inhomogeneities on a macroscopic scale, such as clay layers or gravel pockets, also contribute to contaminant spreading: *macroscopic dispersion.* Contaminant spreading perpendicular to the (average) direction of flow, *transverse dispersion*, is usually small and fairly predictable. Contaminant spreading into the direction of flow, *longitudinal dispersion*, is often orders of magnitude larger than transverse dispersion and more difficult to assess. Longitudinal dispersion comes about by contaminant movement speeded up along *preferential pathways* (gravel layers) and slowed down through, for example, layers of silt or clay.

Microscopic dispersion by itself is of little practical consequence, but macroscopic dispersion may be significant. Macroscopic dispersion can be described by a continuum model, the *transport equation*, provided the observations and predictions are made on a sufficiently large scale: the REV for the macroscopic dispersive process. The theory and practice of dispersive transport modeling, however, is still the subject of fundamental research (Anderson and Woessner, 1992), and is not included in this text. For examples of further reading on this matter the reader is referred to Javandel *et al.* (1984), Sudicky (1989), and Strack (1992).

2.1.5 Pore Pressure and Head

It may be noted that Darcy's law has not been formulated in terms of water pressures, but in terms of (hydraulic) heads. The concept of a head is more useful here than that of a pressure. This may be illustrated with reference to Figure 2.2. If the heads ϕ_1 and ϕ_2 in Figure 2.2 are equal, no flow would occur through the sand; $d\phi/dz = 0$ in (2.4). Yet the water pressure in the sand, called *pore pressure*, at z_1 would be larger than the pore pressure at z_2! This is because of a "hydrostatic pressure distribution" in the sand column which is caused by gravity and does not constitute a driving force for flow. However, when considering Darcy's law in a horizontal direction

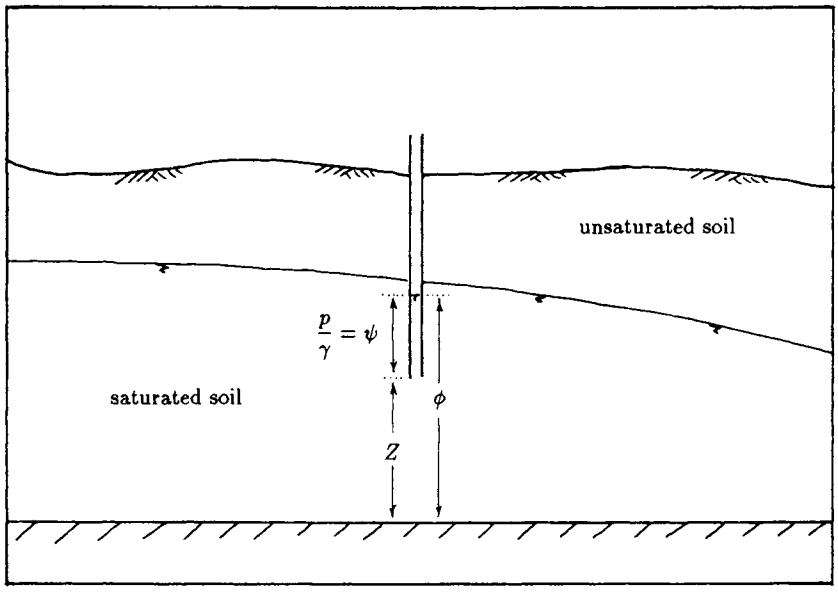

Figure 2.3: Piezometer to measure heads and pore pressure

(e.g., the x- or y-direction), a zero head gradient does indeed imply a zero pressure gradient.

The relationship between head and pore pressure is illustrated in Figure 2.3. A pipe is installed in the saturated zone of an aquifer. The open bottom of the pipe is located at an elevation Z above some horizontal datum: Z is the *elevation head.* The groundwater rises in the pipe to an elevation ϕ above the datum: the "hydraulic head," or "piezometric head," or just "head." The pipe in Figure 2.3 is also referred to as a *piezometer.* The height ψ of the water column in the piezometer is called the *pressure head.* It is a direct measure of the pore pressure immediately below the piezometer. Heads and pore pressure p are related as follows:

$$\phi = \psi + Z = \frac{p}{\gamma} + Z = \frac{p}{\rho g} + Z \tag{2.15}$$

In words: the piezometric head is the sum of the pressure head and the elevation head. Rewriting (2.15) yields for the pore pressure

$$p = \gamma\psi = \gamma(\phi - Z) = \rho g(\phi - Z) \tag{2.16}$$

Darcy's law can be formulated in terms of the pore pressure p by combining

(2.6) and (2.15):

$$q_i = -\frac{k}{\gamma}\partial_i p - k\delta_{3i} \tag{2.17}$$

where δ_{3i} is part of the Kronecker Delta δ_{ij}, which is equal to 1 if $i = j$ and equal to 0 if $i \neq j$. Consequently, q_z $(i = 3)$ contains the extra term $-k$ which accounts for the hydrostatic pressure distribution when $q_3 = q_z = 0$.

2.1.6 Anisotropic Hydraulic Conductivity

Thus far we have tacitly assumed that the hydraulic conductivity is the same in all directions: the aquifer is assumed to have an *isotropic hydraulic conductivity*. In reality, however, geological formations are often more permeable in one direction than in another. Many thin, nearly horizontal clay layers in a sand and gravel aquifer, for instance, may reduce the vertical permeability. Fractured rock may exhibit different permeabilities in different horizontal directions depending on the dominant fracture orientations. Under these anisotropic conditions, the specific discharge vector may not be co-linear with the hydraulic gradient vector, as was assumed in developing (2.5). The general linear relationship between the two vector fields q_i and $\partial_i \phi$ is

$$q_i = -k_{ij}\partial_j \phi \qquad (i = 1, 2, 3 \text{ and } j = 1, 2, 3) \tag{2.18}$$

where summation is implied over the index j. Throughout this text the Einstein summation convention is adopted, summing over those indices which occur twice in a multiplication. Equation (2.18) may be written out as

$$\begin{aligned} q_x &= -k_{xx}\frac{\partial \phi}{\partial x} - k_{xy}\frac{\partial \phi}{\partial y} - k_{xz}\frac{\partial \phi}{\partial z} \\ q_y &= -k_{yx}\frac{\partial \phi}{\partial x} - k_{yy}\frac{\partial \phi}{\partial y} - k_{yz}\frac{\partial \phi}{\partial z} \\ q_z &= -k_{zx}\frac{\partial \phi}{\partial x} - k_{zy}\frac{\partial \phi}{\partial y} - k_{zz}\frac{\partial \phi}{\partial z} \end{aligned} \tag{2.19}$$

The second-order tensor with components k_{ij} is the *hydraulic conductivity tensor*, which has four components in two dimensions and nine components in three dimensions. It is generally accepted that the hydraulic conductivity tensor is symmetric:

$$k_{ij} = k_{ji} \tag{2.20}$$

which leads to only three independent components in two dimensions and six independent components in three dimensions. Observe from (2.19) that a particular component of flow depends not only on the gradient in its own

direction, but also on the components of the hydraulic gradient in the other coordinate directions. In general, therefore, flow in anisotropic media is not co-linear with the hydraulic gradient in that medium.

Principal Directions

The components k_{ij} do depend on the choice of the coordinate system. It is possible to rotate a coordinate system in such a way that all components k_{ij} for which $i \neq j$ are zero. Denoting the coordinate directions of the rotated system by $\bar{x}$, $\bar{y}$, and $\bar{z}$ yields for the specific discharges in those directions

$$\begin{aligned} q_{\bar{x}} &= -k_{\bar{x}\bar{x}} \frac{\partial \phi}{\partial \bar{x}} = -k_1 \frac{\partial \phi}{\partial \bar{x}} \\ q_{\bar{y}} &= -k_{\bar{y}\bar{y}} \frac{\partial \phi}{\partial \bar{y}} = -k_2 \frac{\partial \phi}{\partial \bar{y}} \\ q_{\bar{z}} &= -k_{\bar{z}\bar{z}} \frac{\partial \phi}{\partial \bar{z}} = -k_3 \frac{\partial \phi}{\partial \bar{z}} \end{aligned} \tag{2.21}$$

The directions $\bar{x}$, $\bar{y}$, and $\bar{z}$ are called the *principal directions* of the hydraulic conductivity tensor, while k_1, k_2, and k_3 are referred to as the *principal hydraulic conductivities.* Observe from (2.21) that the specific discharge vector in a principal direction is again co-linear with the hydraulic gradient. In the real world this occurs when the coordinate axes are chosen parallel and perpendicular to clay layers in a sand and gravel aquifer or to major fracture planes in fractured rock aquifers. In the case of aquifers with horizontal clay layers, (2.21) reduces to

$$\begin{aligned} q_x &= -k_h \frac{\partial \phi}{\partial x} \\ q_y &= -k_h \frac{\partial \phi}{\partial y} \\ q_z &= -k_v \frac{\partial \phi}{\partial z} \end{aligned} \tag{2.22}$$

where k_h is the horizontal hydraulic conductivity, and k_v is the vertical hydraulic conductivity.

2.2 Continuity of Flow

If the head $\phi(x, y, z)$ is known throughout an aquifer, the groundwater movement can be calculated everywhere by use of (2.6). However, as a rule the head distribution is not known, and an additional equation is required. This equation is provided by the realization that no water can

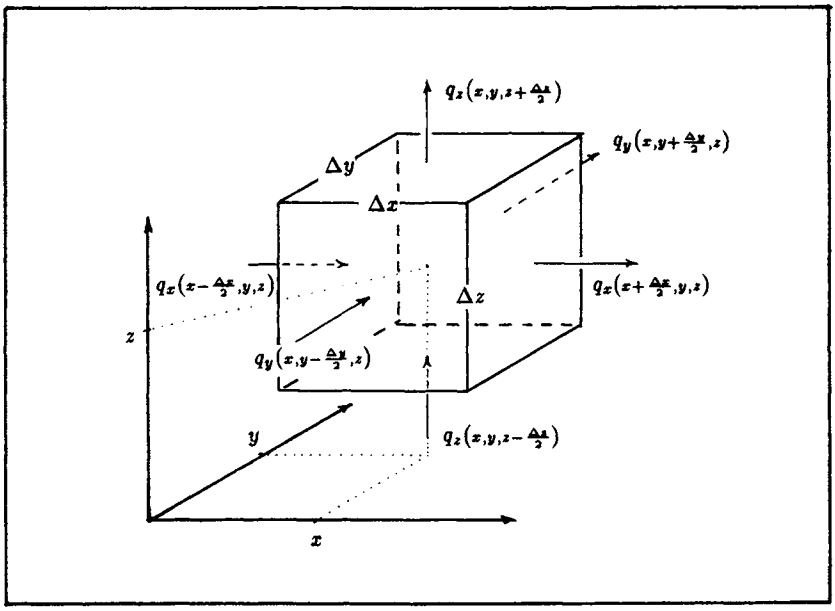

Figure 2.4: Continuity of flow.

spontaneously disappear or appear at a particular point in the aquifer: conservation of mass. If we consider water incompressible, conservation of mass implies conservation of volume, or for water in motion, continuity of flow.

We will derive a mathematical formulation for continuity of flow by writing a water balance for a small block of soil and water in an aquifer (see Figure 2.4). The sides of the block are parallel to the coordinate directions x, y, z, and measure Δx, Δy, and Δz, respectively. We consider the specific discharge vectors at the centers of all six sides of the block. On each side, only one component of the specific discharge vector is pointing into or away from the block; the other two components are parallel to the side. For instance, the inflow into the block on the side that is facing us in Figure 2.4 is only the y-component of the specific discharge vector, the x- and z-components being parallel to that side. We will assume that the specific discharge at the center of a side represents the average for that entire side, an assumption which will be more accurate the smaller the block. Water balance for the block means

$$\text{total inflow} = \text{total outflow}$$

or

$$\text{total outflow} - \text{total inflow} = 0$$

which leads to (see Figure 2.4)

$$\begin{aligned} & (q_x(x+\tfrac{\Delta x}{2},y,z) - q_x(x-\tfrac{\Delta x}{2},y,z))\Delta y \Delta z \\ + \; & (q_y(x,y+\tfrac{\Delta y}{2},z) - q_y(x,y-\tfrac{\Delta y}{2},z))\Delta x \Delta z \\ + \; & (q_z(x,y,z+\tfrac{\Delta z}{2}) - q_z(x,y,z-\tfrac{\Delta z}{2}))\Delta x \Delta y = 0 \end{aligned} \tag{2.23}$$

The specific discharge vector components are labeled to indicate their position on the sides of the block. Both sides of (2.23) are divided by the volume of the block, $\Delta x \Delta y \Delta z$, which leads to

$$\begin{aligned} & \frac{q_x(x+\frac{\Delta x}{2},y,z) - q_x(x-\frac{\Delta x}{2},y,z)}{\Delta x} \\ + \; & \frac{q_y(x,y+\frac{\Delta y}{2},z) - q_y(x,y-\frac{\Delta y}{2},z)}{\Delta y} \\ + \; & \frac{q_z(x,y,z+\frac{\Delta z}{2}) - q_z(x,y,z-\frac{\Delta z}{2})}{\Delta z} = 0 \end{aligned} \tag{2.24}$$

In the limiting case that $\Delta x \to 0$, $\Delta y \to 0$, and $\Delta z \to 0$, the quotients in (2.24) become partial derivatives:

$$\frac{\partial q_x}{\partial x} + \frac{\partial q_y}{\partial y} + \frac{\partial q_z}{\partial z} = 0 \tag{2.25}$$

The continuity equation (2.25) may also be written in tensor notation as

$$\partial_i q_i = 0 \tag{2.26}$$

2.3 Laplace's Equation

The continuity equation may be combined with Darcy's law to form the basic governing differential equation for steady-state groundwater flow. Combining (2.25) with (2.5) yields

$$\frac{\partial}{\partial x}\left[-k\frac{\partial \phi}{\partial x}\right] + \frac{\partial}{\partial y}\left[-k\frac{\partial \phi}{\partial y}\right] + \frac{\partial}{\partial z}\left[-k\frac{\partial \phi}{\partial z}\right] = 0 \tag{2.27}$$

or

$$\frac{\partial^2 \phi}{\partial x^2} + \frac{\partial^2 \phi}{\partial y^2} + \frac{\partial^2 \phi}{\partial z^2} = 0 \tag{2.28}$$

There are several ways of abbreviating (2.28). Using tensor notation:

$$\partial_{ii}\phi = 0 \tag{2.29}$$

where ∂_{ii} symbolizes the second partial derivative and, of course, where the repetition of i implies summation. A popular way of writing (2.28) is in terms of the so-called "symbolic notation":

$$\nabla^2 \phi = 0 \tag{2.30}$$

where ∇^2 (pronounced "nabla-second") is called the "operator of Laplace" and has the same meaning as ∂_{ii} in (2.29).

The second-order partial differential equation given in (2.28) through (2.30) is called the *equation of Laplace.* The equation is universally used in physics to describe phenomena such as the conduction of heat through solids, the flow of electricity through conductors, and the diffusion of gases. Equation (2.30) is therefore also known as the "diffusion equation." It may be confusing, however, to refer to groundwater flow as diffusion. Flow is not driven by groundwater "concentration gradients," as in the case of real diffusion, but by head gradients. Contaminants in groundwater, however, do in part spread under the influence of (contaminant) concentration gradients, although this influence is small.

It is not difficult to find general solutions to Laplace's equation. The difficulty in applying (2.30) to a real-world groundwater flow problem is constructing a particular solution to (2.30) that satisfies the complex set of boundary conditions formed by streams, lakes, wetlands, wells, etc. In order to accomplish this, we will have to compromise, making simplifying assumptions where possible to bring a solution within reach.

This Page Intentionally Left Blank

Chapter 3

Dupuit–Forchheimer Flow

We have, quite naturally, developed our basic equations for a three-dimensional space. Our world is three-dimensional, and so is the flow of groundwater. Groundwater flowlines may be curved in both the horizontal and vertical plane, as illustrated in Figure 3.1. Water enters the aquifer through areal infiltration, resulting from precipitation, and discharges in streams and lakes that are connected to the groundwater. The vertical scale of the cross-section over the flowline is exaggerated for clarity, a common practice in geological sciences. Observe from Figure 3.1 that the groundwater flow is predominantly horizontal. This is even more apparent when plotting the cross-section in Figure 3.1 to scale, which may look like Figure 3.2, where a part of the cross-section in Figure 3.1 is depicted. The preceding considerations suggest that when following a (fictitious) water particle from entry to exit, most of its movement will be horizontal.

A few years after Darcy's publication, Dupuit (1863) presented regional groundwater flow solutions based on the assumption that flowlines are predominantly horizontal and velocities do not vary over the aquifer depth. Later, Forchheimer (1886) independently suggested the same approximation, since then termed the *Dupuit-Forchheimer approximation.* If flow is assumed to be only horizontal, then

$$q_z = 0 \tag{3.1}$$

which leads with Darcy's law (2.5) to

$$\frac{\partial \phi}{\partial z} = 0 \tag{3.2}$$

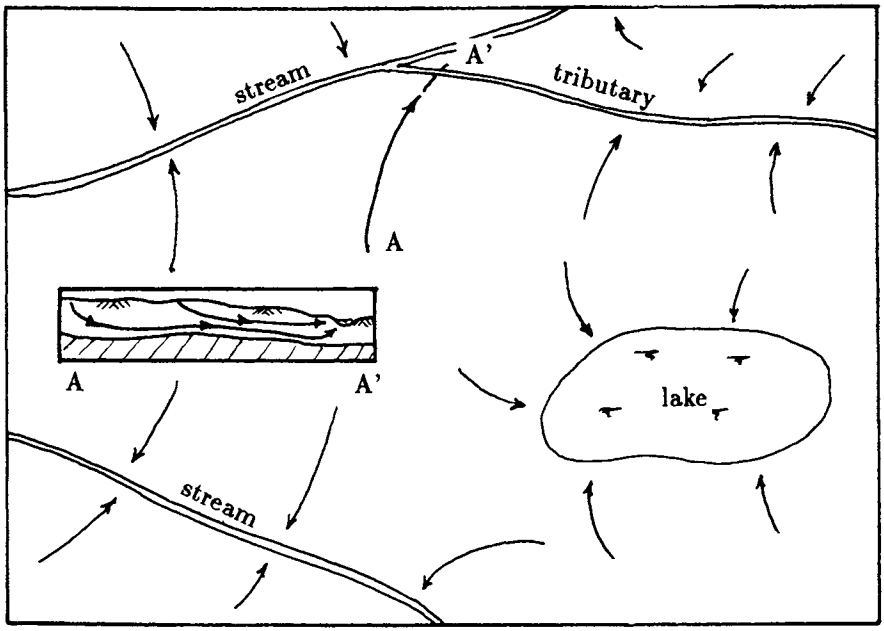

Figure 3.1: Three-dimensional flowlines in a regional aquifer. The cross-section (inset) is taken along the flowline and has an exaggerated vertical scale.

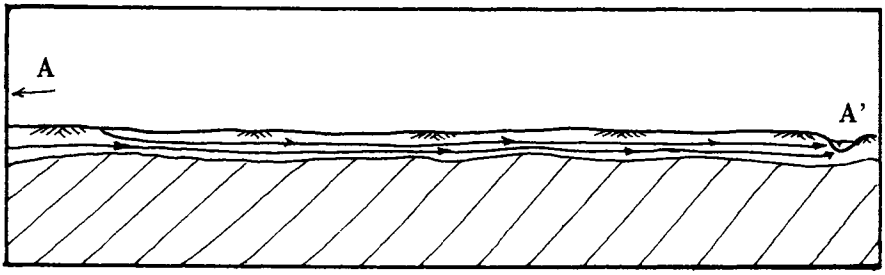

Figure 3.2: Cross-section over flowline plotted to scale.

Equations (3.1) and (3.2) represent the traditional interpretation of the Dupuit–Forchheimer approximation, reducing three-dimensional flow problems to two-dimensional ones. In applying the Dupuit–Forchheimer approximation, however, only the assumption (3.2) is needed: Heads do not vary with depth. Kirkham (1967) showed that (3.2) does not necessarily require (3.1), but may also be the result of an infinite vertical hydraulic conductivity in the (hypothetical) aquifer,

$$q_z = \lim_{\substack{k_z \to \infty \\ \partial\phi/\partial z \to 0}} \left(-k_z \frac{\partial \phi}{\partial z} \right) \neq 0 \tag{3.3}$$

In fact, in as early as 1952, Polubarinova-Kochina presented approximate values for q_z in a Dupuit–Forchheimer model (Polubarinova-Kochina, 1962). It took more than 30 years before a complete theory for tracing three-dimensional streamlines in Dupuit–Forchheimer models was published (Strack, 1984). Comparisons with two-dimensional solutions in the vertical plane (Strack, 1984) and fully three-dimensional solutions (Haitjema, 1987a) reveal a surprising accuracy for these approximate streamlines for most practical cases of regional flow.

The Dupuit–Forchheimer approximation, of course, is based on the condition that the length of a flowline is large as compared to the aquifer thickness (see Figures 3.1 and 3.2). This condition is frequently met in groundwater flow problems associated with water resources issues. Prolific aquifers are usually relatively thin, varying in thickness between a few feet and one or two hundred feet. Sand and gravel aquifers several hundred feet thick are an exception, while the distances between streams are often measured in miles. Groundwater flow in such aquifers is sometimes referred to as shallow flow, a term which may cause confusion, as it may equally well occur in deep confined aquifers. In this text we will refer to *Dupuit–Forchheimer flow* whenever we are dealing with flow in aquifers that are thin compared to their lateral extent.

The Dupuit–Forchheimer approximation leads to one of the most dramatic simplifications of real-world groundwater flow problems: reducing three-dimensional flow problems to those of two-dimensional horizontal flow. Although this is usually not stated, all two-dimensional horizontal flow models can be interpreted as Dupuit–Forchheimer models. The method, however, is not universally acclaimed. Muskat (1937) considered many of its applications "questionable" and referred to the Dupuit–Forchheimer theory as "untrustworthy." Unfortunately, the power of the Dupuit–Forchheimer approximation is often underestimated. Many applications of three-dimensional flow models are, in my estimation, overkill. In most cases, as we will see later, a Dupuit–Forchheimer model

could have done the job, saving resources and cost.

The remainder of this chapter is devoted to the development of elementary solutions to Dupuit–Forchheimer flow. We will start with one-dimensional flow and gradually build up our arsenal of practical solutions, forming a basis for modeling real-world groundwater flow problems. In the process, we will develop some special mathematical tools which will enhance our problem-solving capabilities.

3.1 Elementary Solutions

Groundwater hydrologists distinguish between two basic types of flow: confined flow and unconfined flow. Confined flow occurs in an aquifer which is sandwiched between two "impermeable" geological formations, e.g., a layer of saturated sand and gravel between two clay layers. The notion "impermeable" is relative; it means that the permeability of the confining layers is negligible compared to the aquifer permeability. Such relatively impermeable confining layers are called *aquicludes*, and confined aquifers are sometimes referred to as *artesian aquifers*. We assume that in a confined aquifer the cross-section of the flow regime, the saturated aquifer height, is known and independent of the flow. Unconfined aquifers, in contrast, have as their upper aquifer boundary the water table, whose position depends on the groundwater flow regime and is a priori not known. Most unconfined aquifers are shallow aquifers near the soil surface. A sand and gravel formation may have a confining layer, but still exhibit unconfined flow, simply because the water table does not reach the confining layer.

We will investigate some elementary cases of confined and unconfined flow, emphasizing the differences as well as the similarities in flow characteristics.

3.1.1 One-Dimensional Confined Flow

In Figure 3.3, some flowlines are shown between two rivers in contact with a confined aquifer. The same figure also provides a cross-section over one of the flowlines which forms a straight line between the two rivers; hence, there is no flow perpendicular to the plane of the cross-section. As a first approximation, in solving the regional flow problem, we will consider the flow in the cross-section representative for the entire region. In keeping with the Dupuit–Forchheimer approximation, we further replace the cross-section in Figure 3.3 by the schematic cross-section in Figure 3.4. The fully penetrating streams and perfectly horizontal upper and lower aquifer boundaries will ensure horizontal flow.

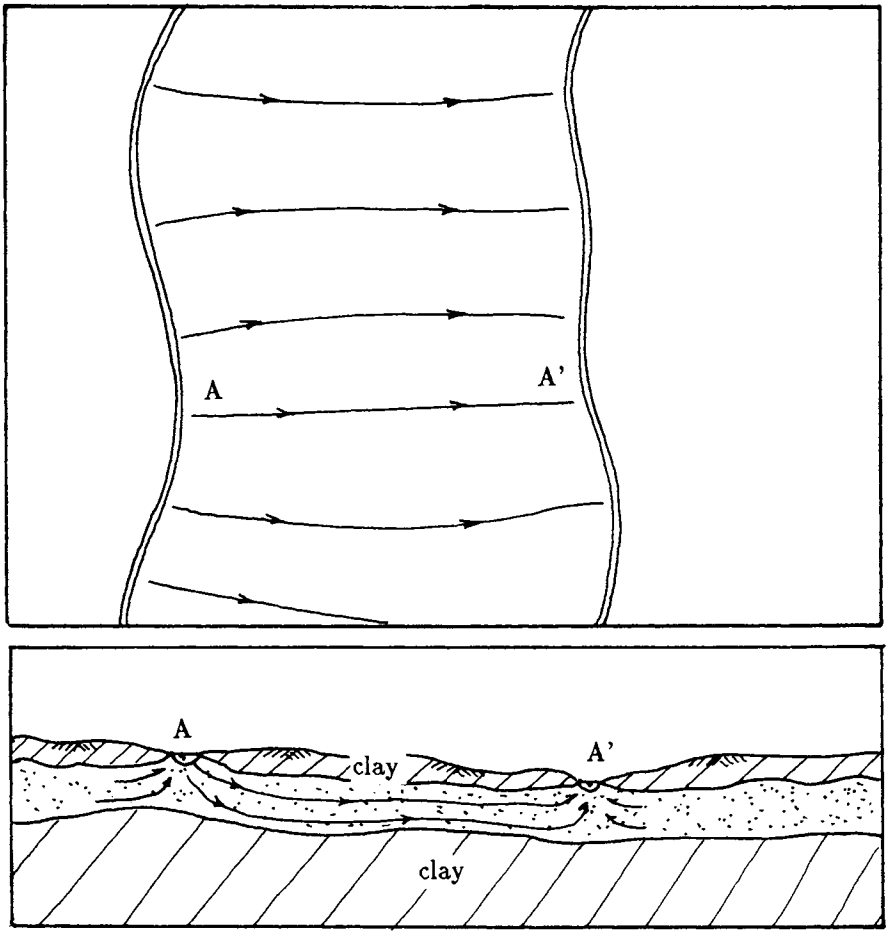

Figure 3.3: Cross-section over a straight streamline in a confined aquifer between two streams.

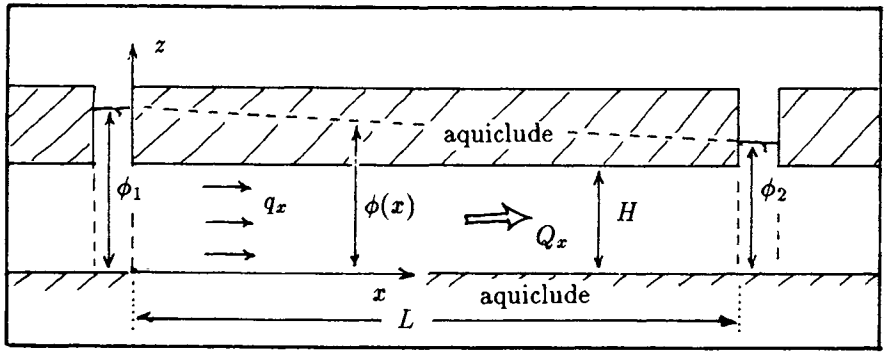

Figure 3.4: One-dimensional confined flow.

Our task is to determine the head distribution $\phi(x)$ in the aquifer, after which we can calculate the specific discharge by use of Darcy's law. The flow problem in Figure 3.4 reminds us of Darcy's experiment, with the column full of sand being horizontal rather than upright. In that case, we already know the head distribution from Darcy's experiment: It varies linearly between the heads at either end of the column. In terms of the parameters in Figure 3.4:

$$\phi(x) = \frac{\phi_2 - \phi_1}{L} x + \phi_1 \tag{3.4}$$

It should also be possible to obtain (3.4) by formally solving the governing differential equation (2.30). Since there is no flow in the y- and z-directions, the partial derivatives of ϕ with respect to y and z are zero, so that (2.30) reduces to

$$\frac{d^2\phi}{dx^2} = 0 \tag{3.5}$$

which is Laplace's equation for one-dimensional flow. The general solution to (3.5) is

$$\phi = Ax + B \tag{3.6}$$

where A and B are constants which must be selected in such a way that (3.6) meets the boundary conditions. That (3.6) is indeed a solution to (3.5) may be verified by substituting it in (3.5). Differentiating (3.6) once yields A. Differentiating it twice, as prescribed by (3.5), implies differentiating the constant A, which yields zero, so that (3.5) is indeed satisfied.

We still need to resolve the unkown constants A and B. With reference to Figure 3.4, the boundary conditions of our groundwater flow problem are

$$x = 0 \quad \phi = \phi_1 \tag{3.7}$$

$$x = L \quad \phi = \phi_2 \tag{3.8}$$

Substituting the first boundary condition (3.7) into the general solution (3.6) yields

$$B = \phi_1 \tag{3.9}$$

Solving for A by substituting (3.8) and (3.9) into (3.6) yields

$$A = \frac{\phi_2 - \phi_1}{L} \tag{3.10}$$

Substituting the expressions for the constants A and B into the *general solution* (3.6) gives us the *particular solution* to our problem:

$$\phi = \frac{\phi_2 - \phi_1}{L} x + \phi_1 \tag{3.11}$$

which is indeed the linear head distribution we anticipated in (3.4).

The procedure given by (3.5) through (3.11) is the formal way of solving a boundary value problem. In words: First find the general solution to the differential equation; next, define the boundary conditions for the problem at hand; and finally, resolve the unkown constants in the general solution by use of the boundary conditions. The boundary conditions for our one-dimensional problem, heads at the streams, were formulated entirely in terms of specified heads: a *boundary condition of the first kind* or *Dirichlet condition.* It appears from (3.11) that this leads to a solution independent of any aquifer parameters, such as hydraulic conductivity or aquifer thickness: The head distribution is simply a straight line from ϕ_1 at $x = 0$ to ϕ_2 at $x = L$.

Rule 3.1 *Solutions to Laplace's equation, subject to Dirichlet conditions, are fully determined by these boundary conditions.*

Not all groundwater flow solutions are governed by Laplace's equation, however, and not all boundary conditions are Dirichlet conditions. When a known amount of water is withdrawn from or infiltrated into the aquifer, we speak of a flux specified boundary: a *boundary condition of the second kind* or *Neumann condition.* Most real world problems have *mixed* boundary conditions: a combination of Dirichlet and Neumann conditions. We will discuss such mixed boundary-value problems elsewhere in this chapter, where we will find that Rule 3.1 may have a significant impact on our modeling results.

Rule 3.2 *In regions where head-specified boundary conditions are abundant, e.g., many streams and lakes, the modeled heads are relatively insensitive to the choice of aquifer parameters (k and H), but are mostly determined by the heads specified at the surface waters.*

The specific discharge q_x in the aquifer is obtained by applying Darcy's law to (3.11):

$$q_x = -k\frac{\partial \phi}{\partial x} = -k\frac{\phi_2 - \phi_1}{L} = k\frac{\phi_1 - \phi_2}{L} \tag{3.12}$$

In Darcy's original experiment, a total flow rate for the column Q $[L^3/T]$ was used; see (2.1). We may also introduce a total flow rate for our one-dimensional aquifer by considering the total flow over the aquifer height H and over some width of the aquifer measured perpendicular to the plane of Figure 3.4. If we select a width of 1 (foot or meter depending on our unit system), we may define the *discharge* in the x-direction Q_x $[L^2/T]$ as

$$Q_x = \int_0^H q_x dz \tag{3.13}$$

In a Dupuit–Forchheimer model, q_x does not vary over the aquifer height, so that (3.13) reduces to

$$Q_x = H q_x \tag{3.14}$$

While the head distribution (3.11) depends only on the boundary conditions, the specific discharge q_x also depends on the hydraulic conductivity k, see (3.12). Furthermore, the discharge (3.14) depends on the aquifer thickness H.

Rule 3.3 *While groundwater flow solutions may look alike in terms of piezometric head surfaces, they may exhibit significantly different discharges depending on aquifer parameters.*

Notice that the aquifer porosity does not enter any of our formulas yet. Only when calculating average groundwater velocities is the porosity n of importance:

$$v_x = \frac{q_x}{n} \tag{3.15}$$

Rule 3.4 *Steady-state solutions to groundwater flow, in terms of heads and discharges, do not depend on the aquifer porosity. Average groundwater velocities do.*

Discharge Potential for Confined Flow

In Dupuit–Forchheimer models, it turns out to be convenient to formulate our flow problems in terms of discharges integrated over the aquifer height, rather than in terms of specific discharges. Expanding our discussion, for a moment, to both x and y dimensions, we introduce the *discharge vector* with components Q_x and Q_y:

$$\begin{aligned} Q_x &= Hq_x \\ Q_y &= Hq_y \end{aligned} \tag{3.16}$$

We can express Q_x and Q_y in terms of ϕ by applying Darcy's law to (3.16):

$$\begin{aligned} Q_x &= Hq_x = H\left[-k\frac{\partial\phi}{\partial x}\right] \\ Q_y &= Hq_y = H\left[-k\frac{\partial\phi}{\partial y}\right] \end{aligned} \tag{3.17}$$

Since both k and H are independent of x and y, we can rewrite (3.17) as

$$\begin{aligned} Q_x &= -\frac{\partial[kH\phi]}{\partial x} \\ Q_y &= -\frac{\partial[kH\phi]}{\partial y} \end{aligned} \tag{3.18}$$

We replace the term $kH\phi$ in (3.18) by a new variable Φ, so that

$$\begin{aligned} Q_x &= -\frac{\partial\Phi}{\partial x} \\ Q_y &= -\frac{\partial\Phi}{\partial y} \end{aligned} \tag{3.19}$$

The auxiliary function $\Phi(x, y)$ is called the *discharge potential*:

$$\Phi = kH\phi \tag{3.20}$$

The product of hydraulic conductivity and aquifer thickness (kH) is often referred to as the aquifer *transmissivity* T:

$$T = kH \tag{3.21}$$

The use of potentials in conjunction with laminar flow is not new. In fact, the entire mathematical framework of solving laminar flow problems is often referred to as "potential theory." In general, we have "potential flow" if the flow vector field forms the gradient vector field of some scalar potential function. This is the case in (3.19), where Q_x and Q_y are the components of the discharge vector field and are equal to the (negative) components $\partial\Phi/\partial x$ and $\partial\Phi/\partial y$ of the potential gradient vector field. The negative sign in (3.19) does not detract from our concept of potential flow, as it could easily have been incorporated in the definition of Φ. Along these lines we could also have called the head ϕ a potential, as it differs by only the factor $(-k)$ from the formal definition of a potential; see (2.5). Bear (1972) called ϕ a "pseudopotential." Hubert (1940) introduced a "fluid potential," the acceleration of gravity g $[L/T^2]$ times the head: $g\phi$. Strack (1981a, 1981b) introduced discharge potentials to facilitate the description of combined confined and unconfined flow, as well as flow in aquifers with horizontal clay laminae (Strack and Haitjema, 1981a, 1981b). In this text we will adopt Strack's discharge potential concepts, introducing them step by step in the next sections, where we will refer to them as *potentials* for short.

Laplace's equation may also be written in terms of Φ. Multiplying both sides in (2.28) through by kH and taking $\partial^2\phi/\partial z^2$ equal to zero yields

$$\frac{\partial^2\Phi}{\partial x^2} + \frac{\partial^2\Phi}{\partial y^2} = 0 \tag{3.22}$$

When (3.19) is substituted into (3.22), we obtain the continuity equation in terms of discharges,

$$\frac{\partial Q_x}{\partial x} + \frac{\partial Q_y}{\partial y} = 0 \tag{3.23}$$

The continuity equation (3.23) can also be obtained by considering inflow and outflow for an elementary aquifer section, following a procedure similar to the one outlined in Section 2.2.

For our case of one-dimensional flow, Laplace's equation (3.22) reduces to

$$\frac{d^2\Phi}{dx^2} = 0 \tag{3.24}$$

There is no difference between solving the original differential equation (3.5) in terms of ϕ and solving the new differential equation (3.24) in terms of Φ. All we have to do is replace ϕ by Φ in the solution (3.11),

$$\Phi = \frac{\Phi_2 - \Phi_1}{L}x + \Phi_1 \tag{3.25}$$

The constants Φ_1 and Φ_2 are the potentials at the aquifer boundaries and can be calculated using (3.20),

$$\Phi_1 = kH\phi_1 \quad ; \quad \Phi_2 = kH\phi_2 \tag{3.26}$$

The discharge Q_x is obtained by applying Darcy's law in terms of potentials. With (3.19) and (3.25), we get

$$Q_x = -\frac{d\Phi}{dx} = -\frac{\Phi_2 - \Phi_1}{L} = \frac{\Phi_1 - \Phi_2}{L} \tag{3.27}$$

The discharge Q_x, as given by (3.27), is meaningful to us in physical terms, but the potential Φ as given by (3.25) seems a rather abstract quantity. Indeed, we cannot measure Φ in the field. We can, however, measure the head ϕ. Assuming we know the aquifer thickness H and hydraulic conductivity k, the head ϕ may be obtained from the potential Φ by inverting (3.20):

$$\phi = \frac{\Phi}{kH} \tag{3.28}$$

Equation (3.28) may be applied to Φ for any value of x, so that we can calculate ϕ from (3.25) for any value of x.

At this point there seems to be no advantage in introducing the potential Φ. In fact, in the foregoing analysis it is merely a detour: We had obtained $\phi(x)$ already in (3.11) without the use of this auxiliary function Φ. The advantages of introducing Φ, however, will become apparent in the next few sections, starting with unconfined flow.

Exercise 3.1 *The following data are given for the flow problem in Figure 3.4. The aquifer is 2,000 feet long and 40 feet thick. The hydraulic conductivity is 10 ft/day. The water levels in the stream to the left and the right of the aquifer are 60 feet and 50 feet above the aquifer base, respectively.*

(a) Calculate the head ϕ and the discharge Q_x at the center of the aquifer ($x = L/2$). Perform your analysis in terms of heads.

(b) Answer the same questions as under (a), but now perform your analysis in terms of discharge potentials.

(c) Calculate the discharge Q_x at $x = 0$ and at $x = L$. Comment on your findings.

(d) Repeat your calculations for (b), but now use $k = 20\ ft/day$.

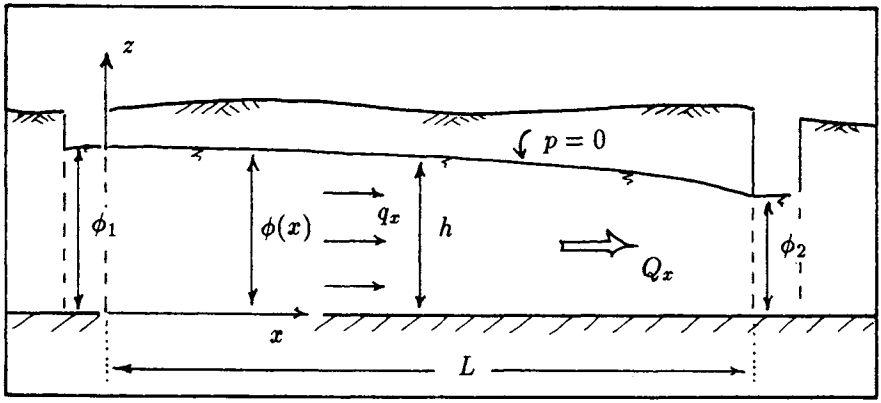

Figure 3.5: One-dimensional unconfined flow.

3.1.2 One-Dimensional Unconfined Flow

Assume that the confining layer in Figure 3.3 is absent. Figure 3.4 would then look like Figure 3.5, where the flow domain is bounded below by a confining layer and above by the *water table*. That upper boundary, the water table, is somewhat fuzzy. In reality, there is a transition from dry or slightly moist soil near the surface to fully saturated soil below the water table. There is groundwater flow in the *unsaturated zone* above the water table; this is referred to as unsaturated flow. In general, however, the unsaturated zone is thin as compared to the saturated zone, while its hydraulic conductivity is lower than that of the saturated zone. Consequently, the *horizontal unsaturated flow* is often negligible when compared to the saturated flow. In this text we will only deal with flow below the water table: saturated flow. The water table itself is defined as the surface where the pore pressure is atmospheric, and thus $p = 0$. It is therefore also called the *phreatic surface*. In the context of solving boundary value problems (our steady-state groundwater flow problems), the water table is also referred to as a *free surface*, as its position is not known in advance: It depends on the solution to the problem.

In solving for $\phi(x)$ in Figure 3.5, we cannot make a direct comparison with Darcy's experiment, as we did in the case of confined flow. Instead, we will follow the discharge vector and discharge potential approach introduced earlier.

Discharge Potential for Unconfined Flow

The total discharge Q_x in the aquifer of Figure 3.5 follows from [see also (3.14)]

$$Q_x = hq_x \tag{3.29}$$

where h is the saturated aquifer thickness. However, if we measure the head ϕ with respect to the aquifer bottom, as is done in Figure 3.5, the head and the aquifer thickness are the same:

$$\phi = h \tag{3.30}$$

Consequently, (3.29) becomes

$$Q_x = \phi q_x \tag{3.31}$$

or, with Darcy's law,

$$Q_x = \phi \left[-k \frac{d\phi}{dx} \right] \tag{3.32}$$

We want to write Q_x as the negative derivative of a discharge potential Φ, similar to (3.19); hence,

$$Q_x = -\frac{d\Phi}{dx} \tag{3.33}$$

Equations (3.32) and (3.33) are identical when Φ is chosen as

$$\Phi = \tfrac{1}{2} k \phi^2 \tag{3.34}$$

which is readily seen by substituting (3.34) into (3.33):

$$Q_x = -\frac{d\Phi}{dx} = -\frac{d}{dx}[\tfrac{1}{2} k \phi^2] = -\tfrac{1}{2} k 2\phi \frac{d\phi}{dx} = \phi \left[-k \frac{d\phi}{dx} \right] \tag{3.35}$$

which is indeed identical to (3.32).

Equation (3.33) may be generalized for two-dimensional flow to Equations (3.19), which were obtained for the case of confined flow. Hence, the discharge vector Q_i, in terms of potentials, is defined in the same way for confined and unconfined flow. The potential Φ, however, is defined differently: Compare (3.34) with (3.20).

The continuity equation for unconfined flow, in terms of discharges, may be obtained by a procedure similar to that outlined in Section 2.2, which leads to

$$\frac{\partial Q_x}{\partial x} + \frac{\partial Q_y}{\partial y} = 0 \tag{3.36}$$

which is, of course, the same as for confined flow; see (3.23). Since, for both types of flow, the continuity equations in terms of Q_i and Darcy's law in terms of Φ are the same, then so are the differential equations in terms of Φ. We reached an important conclusion: The differential equations for unconfined and confined flow are the same, but then so are their solutions. Thus, the solution to the flow problem given in Figure 3.5 is given by (3.25):

$$\Phi = \frac{\Phi_2 - \Phi_1}{L} x + \Phi_1 \tag{3.37}$$

The constants Φ_1 and Φ_2 are defined with (3.34) as

$$\Phi_1 = \tfrac{1}{2} k \phi_1^2 \quad ; \quad \Phi_2 = \tfrac{1}{2} k \phi_2^2 \tag{3.38}$$

It is, of course, possible to write the differential equation for unconfined flow in terms of the head ϕ. Substituting (3.34) into (3.22) yields

$$\frac{\partial^2 [\frac{1}{2} k \phi^2]}{\partial x^2} + \frac{\partial^2 [\frac{1}{2} k \phi^2]}{\partial y^2} = 0 \tag{3.39}$$

which reduces to

$$\frac{\partial^2 \phi^2}{\partial x^2} + \frac{\partial^2 \phi^2}{\partial y^2} = 0 \tag{3.40}$$

This equation was first presented by Forchheimer, and he applied it to a variety of problems (Forchheimer, 1930). The solution to the problem in Figure 3.5, in terms of the head ϕ, is obtained by replacing Φ by ϕ^2 in (3.37):

$$\phi^2 = \frac{\phi_2^2 - \phi_1^2}{L} x + \phi_1^2 \tag{3.41}$$

or

$$\phi = \sqrt{\frac{\phi_2^2 - \phi_1^2}{L} x + \phi_1^2} \tag{3.42}$$

Note that, as in the case of confined flow, the solution for ϕ (3.42) does not depend on k, but only on the head specified boundary conditions, consistent with Rule 3.1. The differential equations, and thus the solutions in terms of heads are different for confined and unconfined flow conditions; compare (3.42) with (3.11). Consequently, in textbooks, these types of flow are routinely treated in separate chapters with separate solutions. In order to avoid these differences and simplify the treatment of unconfined flow, the variable aquifer thickness h in Figure 3.5 is sometimes replaced by an average aquifer thickness $\bar{h}$. In so doing, the average thickness $\bar{h}$ takes the place of H in confined aquifers, thus approximating unconfined flow by confined flow solutions. When formulating the problem in terms of discharge

potentials, however, there is no need for such an approximation, as there is no distinction between confined and unconfined flow! Once boundary conditions in terms of heads are "translated" in terms of potentials, the same solution applies to flow in confined and unconfined aquifers.

Exercise 3.2 *The following data are given for the flow problem in Figure 3.5. The aquifer is 2,000 feet long. The hydraulic conductivity is 10 ft/day. The water levels in the stream to the left and the right of the aquifer are 60 feet and 50 feet above the aquifer base, respectively.*

(a) Calculate the head ϕ and the discharge Q_x at the center of the aquifer ($x = L/2$). Perform your analysis in terms of heads.

(b) Answer the same questions as under (a), but now perform your analysis in terms of discharge potentials.

(c) Calculate the discharge Q_x at $x = 0$ and at $x = L$. Comment on your findings.

(d) Repeat your calculations under (b), but now use $k = 20\ ft/day$.

3.1.3 Combined Confined and Unconfined Flow

In Figure 3.6, a one-dimensional flow problem is depicted that is partially confined and partially unconfined. The unconfined flow conditions, on the right-hand side of the aquifer, are caused by the low water level in the stream on the right, being below the upper confining layer. When we formulate our problem in terms of heads, two different solutions apply to the problem in Figure 3.6. The solution to the confined section follows from (3.11) as

$$\phi = \frac{H - \phi_1}{l} x + \phi_1 \qquad (0 \leq x \leq l) \tag{3.43}$$

where l is the length of the confined aquifer zone, and where H is the head at $x = l$. The solution for the unconfined zone follows from (3.42) as

$$\phi = \sqrt{\frac{\phi_2^2 - H^2}{L - l}(x - l) + H^2} \qquad (l \leq x \leq L) \tag{3.44}$$

Both solutions (3.43) and (3.44) contain the unknown position ($x = l$) of the interface between confined and unconfined flow. We need an additional equation to resolve l. That equation is obtained by considering continuity of flow across the interface between confined and unconfined flow. Denoting

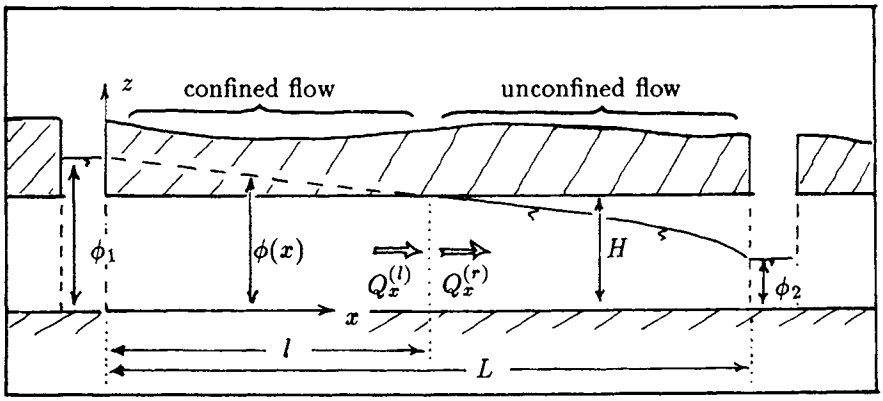

Figure 3.6: One-dimensional combined confined and unconfined flow.

$Q_x^{(l)}$ and $Q_x^{(r)}$ as the discharge to the left and to the right of the interface, respectively, continuity of flow implies

$$Q_x^{(l)} = Q_x^{(r)} \tag{3.45}$$

Using Darcy's law, this leads to

$$H\left[-k\frac{d\phi}{dx}\right]^{(l)} = H\left[-k\frac{d\phi}{dx}\right]^{(r)} \tag{3.46}$$

After dividing both sides by $-kH$ and substituting (3.43) and (3.44) in the right-hand and left-hand side of (3.47), respectively, we obtain

$$\frac{H-\phi_1}{l} = \frac{1}{2}\frac{(\phi_2^2 - H^2)/(L-l)}{\sqrt{\frac{\phi_2^2-H^2}{L-l}(x-l)+H^2}} \qquad (x=l) \tag{3.47}$$

Since we are evaluating (3.47) at the interface between confined and unconfined flow ($x = l$), it reduces to

$$\frac{H-\phi_1}{l} = \frac{\phi_2^2 - H^2}{2H(L-l)} \tag{3.48}$$

which yields for l

$$l = \frac{2HL(H-\phi_1)}{\phi_2^2 - 2H\phi_1 + H^2} \tag{3.49}$$

Substitution of (3.49) into (3.43) and (3.44) finally allows us to calculate the head for every value of x in the aquifer.

Exercise 3.3 *The following data are given for the flow problem in Figure 3.6: The aquifer is 2,000 feet long and 50 feet thick. The hydraulic conductivity is 10 feet/day. The water levels in the stream to the left and the right of the aquifer are 60 feet and 45 feet above the aquifer base, respectively.*

(a) What is the position $x = l$ of the interface between confined and unconfined flow?

(b) What is head at the center of the aquifer ($x = L/2$)?

(c) What is the discharge at $x = 0$, $x = l$, and $x = L$? Comment on your answer.

Discharge Potentials for Combined Confined and Unconfined Flow

The procedure for solving combined confined and unconfined flow, as outlined earlier, is not attractive. Although it can be done for our case of one-dimensional flow, it becomes quite impractical when we are dealing with more general two-dimensional flow problems. Imagine the complex shape of the interface between unconfined flow near a well field and the confined flow elsewhere in the aquifer. Trying to find this complex boundary by requiring continuity of flow across it is no small task.

It is possible, however, to exploit the similarity between the solutions for confined and unconfined flow in terms of discharge potentials. The idea is to write one solution of the form (3.25) and (3.37) for the flow problem in Figure 3.6:

$$\Phi = \frac{\Phi_2 - \Phi_1}{L} x + \Phi_1 \tag{3.50}$$

The potential Φ_1 may be calculated from ϕ_1 with the definition of the potential for confined flow (3.26), while Φ_2 may be calculated by use of (3.38). The difficulty with this approach is that the potential function $\Phi(x)$ would have different values just to the left and just to the right of the interface between confined and unconfined flow. Not to mention that we still do not know where that interface is. With $\Phi^{(l)}(l)$ and $\Phi^{(r)}(l)$ being the potentials just left and right of the interface, the jump is

$$\Phi^{(l)}(l) - \Phi^{(r)}(l) = kHH - \tfrac{1}{2}kH^2 = \tfrac{1}{2}kH^2 \tag{3.51}$$

where $\Phi^{(l)}(l)$ has been evaluated with the potential definition (3.20) for confined flow, and $\Phi^{(r)}(l)$ has been calculated with the potential definition (3.34) for unconfined flow. In order for (3.50) to be useful to us, the potential function should be continuous everywhere, and thus also across the

interface between confined and unconfined flow. Strack (1981a) suggested subtracting the constant $\frac{1}{2}kH^2$ from the earlier definition of the discharge potential for confined flow (3.20); see also Strack and Haitjema, (1981a):

$$\Phi = kH\phi - \tfrac{1}{2}kH^2 \tag{3.52}$$

This modification has no impact on the flow solution, since the discharge vector Q_i is the negative *gradient* of the potential. Differentiating (3.52) or (3.20) gives the same result (the same discharge); the extra constant vanishes. With (3.52) instead of (3.20), the potential at the interface between confined and unconfined flow has the same value, whether we use the definition for confined flow (3.52) or for unconfined flow (3.34): $\Phi(l) = \frac{1}{2}kH^2$. The complete solution to the combined confined and unconfined flow problem is defined by (3.50) and the following definitions for Φ_1 and Φ_2:

$$\Phi_1 = kH\phi_1 - \tfrac{1}{2}kH^2 \qquad \Phi_2 = \tfrac{1}{2}k\phi_2^2 \tag{3.53}$$

Note that the solution has been obtained without prior knowledge of the location of the interface between confined and unconfined flow! We know that the potential is larger than $\frac{1}{2}kH^2$ in zones of confined flow, while for unconfined flow conditions the potential is smaller than $\frac{1}{2}kH^2$. Hence, by comparing the value of $\Phi(x)$ with the constant $\frac{1}{2}kH^2$, we know the local type of flow. We need to know the local type of flow in order to obtain heads from (3.50). Inverting (3.52) and (3.34) yields for ϕ

$$\phi = \frac{\Phi + \frac{1}{2}kH^2}{kH} \qquad (\Phi \geq \tfrac{1}{2}kH^2) \tag{3.54}$$

$$\phi = \sqrt{\frac{2\Phi}{k}} \qquad (\Phi \leq \tfrac{1}{2}kH^2) \tag{3.55}$$

The usefulness of discharge potentials is now more evident. Dupuit–Forchheimer flow may be solved in terms of these potentials without giving consideration to whether the flow conditions in the domain are confined or unconfined. All that is needed is knowledge of the flow conditions at the aquifer boundaries, the streams in our example, so that the heads can be translated into potentials by use of the proper formula. The boundary or boundaries between confined and unconfined flow may be obtained afterward by setting Φ equal to $\frac{1}{2}kH^2$.

Exercise 3.4 *The following data are given for the flow problem in Figure 3.6. The aquifer is 2,000 feet long and 50 feet high. The hydraulic conductivity is 10 feet/day. The water levels in the stream to the left and the right of the aquifer are 60 feet and 45 feet above the aquifer base, respectively.*

(a) What is the potential Φ at the center of the aquifer ($x = L/2$)? Is the flow there confined or unconfined? Explain your answer.

(b) What is head in the center of the aquifer ($x = L/2$)?

(c) What is the location ($x = l$) of the interface between confined and unconfined flow? Show your approach.

3.1.4 Two-Dimensional Potential Flow

While discussing some elementary one-dimensional flow problems we introduced, step by step, a potential theory tailored to deal with Dupuit–Forchheimer flow in both confined and unconfined aquifers. Next, we will briefly summarize our results.

The total flow, integrated over the aquifer height, is described by the discharge vector Q_i, and defined as

$$Q_x = Hq_x \qquad Q_y = Hq_y \qquad (\phi \geq H) \tag{3.56}$$

$$Q_x = \phi q_x \qquad Q_y = \phi q_y \qquad (\phi \leq H) \tag{3.57}$$

where $\phi \geq H$ indicates confined flow conditions, while $\phi \leq H$ implies unconfined flow conditions. If there is no upper confining layer, H may be considered infinite, so that the flow conditions are always unconfined. The continuity of flow equation, in terms of Q_i, is

$$\partial_i Q_i = 0 \qquad (i = 1, 2) \tag{3.58}$$

In words: The *divergence* of the discharge vector is zero. The discharge vector Q_i is also defined as the negative gradient of a scalar potential Φ,

$$Q_i = -\partial_i \Phi \tag{3.59}$$

The discharge potential is defined differently for confined and for unconfined flow:

$$\begin{aligned} \Phi &= kH\phi - \tfrac{1}{2}kH^2 \qquad (\phi \geq H) \\ \Phi &= \tfrac{1}{2}k\phi^2 \qquad (\phi \leq H) \end{aligned} \tag{3.60}$$

The head is obtained from the potential by

$$\begin{aligned} \phi &= \frac{\Phi + \frac{1}{2}kH^2}{kH} \qquad (\Phi \geq \tfrac{1}{2}kH^2) \\ \phi &= \sqrt{\frac{2\Phi}{k}} \qquad (\Phi \leq \tfrac{1}{2}kH^2) \end{aligned} \tag{3.61}$$

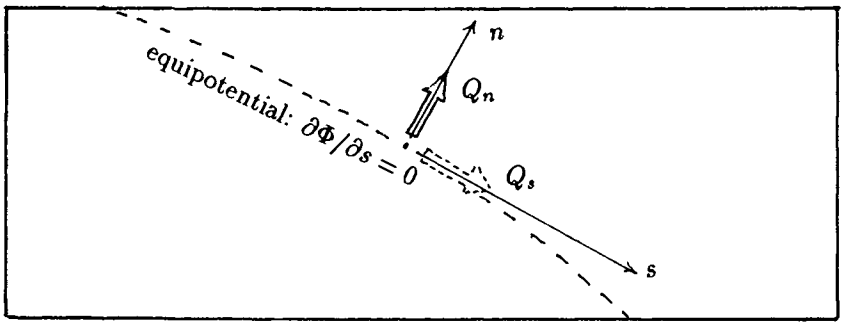

Figure 3.7: Groundwater flow is normal to equipotentials.

Combining (3.59) and (3.58) yields the differential equation of Laplace,

$$\partial_{ii}\Phi = 0 \qquad (i = 1, 2) \tag{3.62}$$

or, in symbolic notation,

$$\nabla^2\Phi = 0 \tag{3.63}$$

which governs both confined and unconfined flow.

From here on, we will treat all problems of Dupuit–Forchheimer flow by use of the discharge vector and discharge potentials defined here.

3.1.5 Equipotentials and Streamlines

The potential function $\Phi(x, y)$ may be viewed as a surface in three dimensions with the surface elevation at x and y equal to the value of $\Phi(x, y)$. We can draw contours on that surface for equal values of Φ, just as we draw contours on a topographical map to indicate terrain elevations. Each contour is a locus of points with the same value for the potential: an *equipotential.*

Groundwater flow occurs perpendicular or normal to these equipotentials. This may be understood by use of Figure 3.7, where a section of an equipotential is depicted together with the components of the discharge vector at a point on the equipotential. The components of the discharge vector are with respect to a local s,n coordinate system, with Q_s tangential to the equipotential and Q_n normal to the equipotential. The discharge vector components are, with Darcy's law,

$$\begin{aligned} Q_s &= -\frac{\partial\Phi}{\partial s} \\ Q_n &= -\frac{\partial\Phi}{\partial n} \end{aligned} \tag{3.64}$$

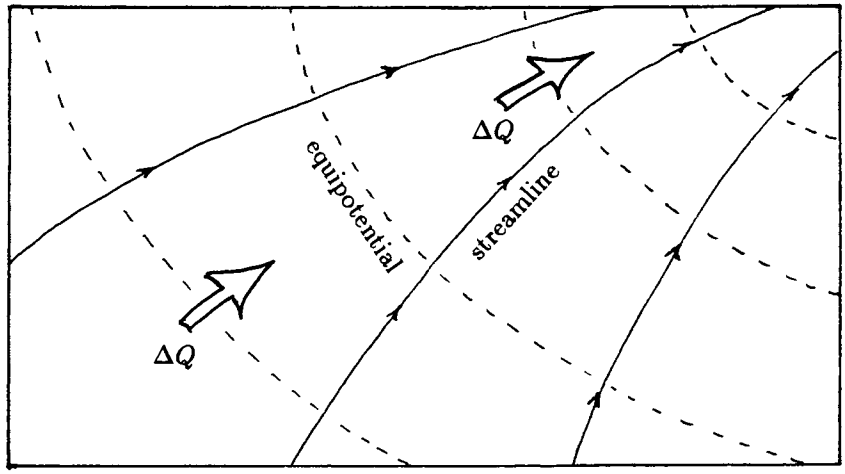

Figure 3.8: Streamlines are normal to equipotentials.

The derivative of the potential into the direction s, along the equipotential, is zero. This follows immediately from the definition of the equipotential, along which Φ is constant:

$$\frac{\partial \Phi}{\partial s} = 0 \tag{3.65}$$

With (3.65) the tangential component Q_s along the equipotential vanishes. Consequently, the only flow component at a point on an equipotential is Q_n, which is normal to the equipotential.

If we follow a (fictitious) water particle through the aquifer, its path will cross equipotentials under 90^0 angles, by virtue of our preceding analysis. Under steady-state flow conditions, the pathlines of water particles are called *streamlines*. In Figure 3.8, a few streamlines and equipotentials are sketched. Flow, of course, is in the direction of descending potential values, as follows from (3.64). Note that the total amount of water ΔQ $[L^3/T]$ that moves between two streamlines does not change, regardless of whether the streamlines converge or diverge. By definition of a streamline, there is no water that can cross a streamline, and hence no water can be added to or escape from the domain bounded by two streamlines. Of course, the discharge rate will increase when streamlines converge and decrease when streamlines diverge.

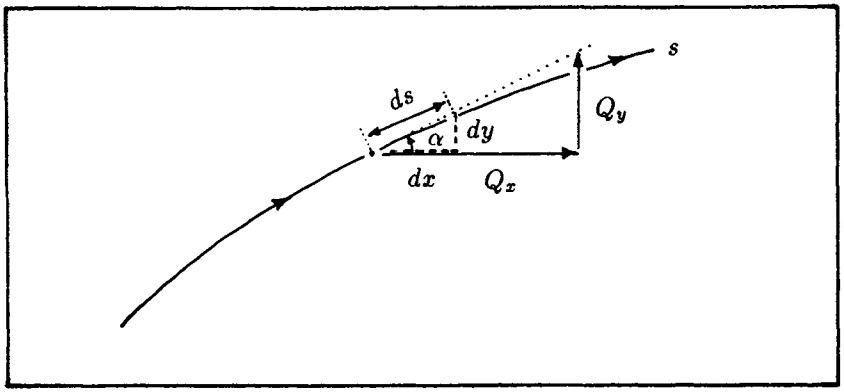

Figure 3.9: Discharge vector tangential to a streamline.

3.1.6 The Stream Function

The equipotentials in Figure 3.8 can be obtained by calculating Φ at a grid of points in the flow domain and using a contouring routine to generate the equipotentials. The accuracy of that procedure can be increased at will by increasing the density of grid points in the region. The streamlines in Figure 3.8, however, were just sketched in as lines normal to the equipotentials.

It appears that, for groundwater flow problems governed by Laplace's equation, there exists a scalar function $\Psi(x, y)$ which is constant along streamlines. This *stream function*, therefore, can be contoured in the same manner as the potential function, yielding streamlines. Just like the potential function, this stream function satisfies the equation of Laplace.

We will first demonstrate the existence of Ψ. The vector Q_i, in Figure 3.9, is tangential to a streamline, so that

$$\tan\alpha = \frac{dy}{dx} = \frac{Q_y}{Q_x} \tag{3.66}$$

The x and y values of points on the streamline are functions of position measured by the curvilinear coordinate s along the streamline. Thus, x and y are functions of s, so that (3.66) may be written as

$$\frac{dy/ds}{dx/ds} = \frac{Q_y}{Q_x} \tag{3.67}$$

or

$$Q_y\frac{dx}{ds} - Q_x\frac{dy}{ds} = -\frac{\partial\Phi}{\partial y}\frac{dx}{ds} + \frac{\partial\Phi}{\partial x}\frac{dy}{ds} = 0 \tag{3.68}$$

where use has been made of Darcy's law for Q_i. The stream function Ψ is defined as being constant along a streamline:

$$\frac{d\Psi}{ds} = 0 \tag{3.69}$$

Writing the total derivative in (3.69) in terms of partial derivatives yields

$$\frac{d\Psi}{ds} = \frac{\partial \Psi}{\partial x}\frac{dx}{ds} + \frac{\partial \Psi}{\partial y}\frac{dy}{ds} = 0 \tag{3.70}$$

Comparing (3.68) with (3.70) results in the following fundamental relations:

$$\begin{aligned} \frac{\partial \Psi}{\partial x} &= -\frac{\partial \Phi}{\partial y} \\ \\ \frac{\partial \Psi}{\partial y} &= +\frac{\partial \Phi}{\partial x} \end{aligned} \tag{3.71}$$

The equations (3.71) are called the *Cauchy-Riemann* equations. The function Ψ which satisfies (3.71) for a particular potential function Φ is the stream function that belongs to that potential function.

Next we will prove that Ψ also satisfies Laplace's equation. It follows from (3.71) and Darcy's law that

$$\begin{aligned} Q_x &= -\frac{\partial \Phi}{\partial x} = -\frac{\partial \Psi}{\partial y} \\ \\ Q_y &= -\frac{\partial \Phi}{\partial y} = +\frac{\partial \Psi}{\partial x} \end{aligned} \tag{3.72}$$

Applying continuity of flow, $\partial_i Q_i = 0$, yields

$$\frac{\partial^2 \Psi}{\partial x \partial y} = \frac{\partial^2 \Psi}{\partial y \partial x} \tag{3.73}$$

Equation (3.73) is the mathematical expression of the single-valuedness of the stream function. We know that the potential function is also single-valued! If it were not, we could have more than one value of Φ at a single point in the aquifer, implying more than one head or pressure at the same point. Clearly, this is not physically possible; thus,

$$\frac{\partial^2 \Phi}{\partial x \partial y} = \frac{\partial^2 \Phi}{\partial y \partial x} \tag{3.74}$$

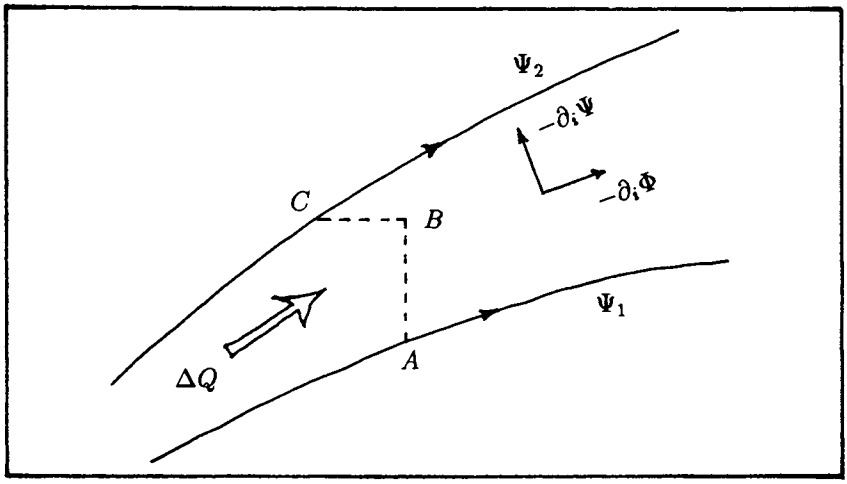

Figure 3.10: The total flow between two streamlines.

Application of (3.74) to (3.71) leads to Laplace's equation for Ψ:

$$\partial_{ii}\Psi = 0 \tag{3.75}$$

Functions which satisfy the equation of Laplace are called *harmonic functions.* The functions Φ and Ψ are related by the Cauchy-Riemann equations and are called *conjugate harmonic functions.* Hence, Ψ is a conjugate harmonic function of Φ, and vice versa.

Rule 3.5 *A stream function exists if, and only if, the potential function is harmonic — that is, it satisfies the equation of Laplace.*

It follows from (3.72) that the discharge vector can be calculated from either the derivatives of Φ or the derivatives of Ψ. We will use the expression of Q_i in terms of derivatives of Ψ to calculate the amount of flow between two streamlines. Consider the two streamlines depicted in Figure 3.10. The total flow ΔQ $[L^3/T]$ between the two streamlines must cross the lines AB and CB, parallel to the y- and x-axes, respectively. The flow across AB is obtained by integrating Q_x over AB, while the flow across CB is obtained by integrating Q_y over CB:

$$\begin{aligned} \Delta Q &= \int_A^B Q_x dy + \int_C^B Q_y dx = -\int_A^B \frac{\partial \Psi}{\partial y} dy + \int_C^B \frac{\partial \Psi}{\partial x} dx \\ &= \Psi_A - \Psi_B + \Psi_B - \Psi_C = \Psi_A - \Psi_C \end{aligned} \tag{3.76}$$

Since the Ψ values at A and C are Ψ_1 and Ψ_2, respectively, the total discharge ΔQ becomes

$$\Delta Q = \Psi_1 - \Psi_2 \tag{3.77}$$

Rule 3.6 *The total flow between two streamlines is equal to the difference between the stream function values of these streamlines.*

The orientation of the flow can also be derived from the Ψ values of the streamlines. With reference to Figure 3.10, it is defined by the following rule.

Rule 3.7 *The potential Φ decreases in the direction of flow, while the stream function Ψ decreases in a direction to the left and normal to the direction of flow.*

In other words: The *negative* gradients of Φ and Ψ form a right-hand Cartesian coordinate system, with $-\partial_i\Phi$ pointing into the direction of flow; see Figure 3.10.

3.1.7 Flow Net

Streamlines and equipotentials are often combined into a *flow net* in such a way that the total flow ΔQ between successive streamlines is always the same and equal to the difference in potential between two successive equipotentials. This is accomplished as follows.

We refer to the directions $-\partial_i\Phi$ and $-\partial_i\Psi$ in Figure 3.10 as the s- and n-directions, respectively. The two negative gradients may then be written as

$$-\partial_i\Phi = -\frac{d\Phi}{ds} \qquad\qquad -\partial_i\Psi = -\frac{d\Psi}{dn} \tag{3.78}$$

Applying the Cauchy–Riemann equations and approximating the derivatives in (3.78) by "finite differences" yields

$$Q_s \simeq -\frac{\Delta\Phi}{\Delta s} = -\frac{\Delta\Psi}{\Delta n} \tag{3.79}$$

The total flow ΔQ between two streamlines (see Figure 3.11) becomes, with (3.79),

$$\Delta Q = \Delta n|Q_s| = \Delta n\frac{|\Delta\Phi|}{\Delta s} = |\Delta\Psi| \tag{3.80}$$

If the distance Δn between streamlines is chosen equal to the distance Δs between equipotentials, (3.80) reduces to

$$\Delta Q = |\Delta\Phi| = |\Delta\Psi| \tag{3.81}$$

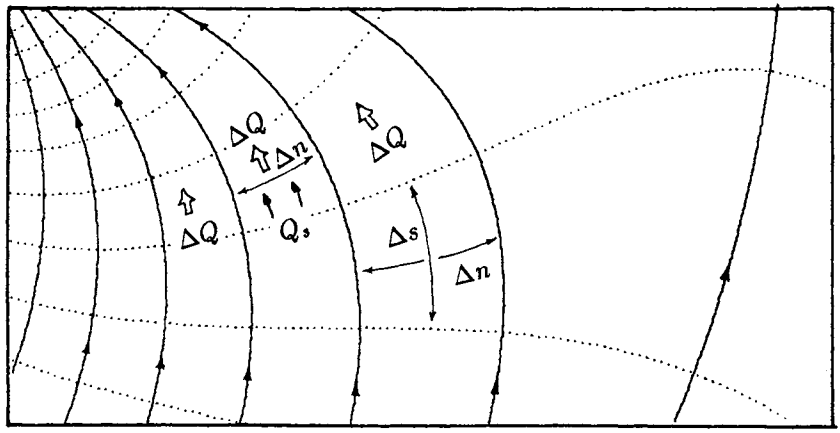

Figure 3.11: Flow net.

Therefore, if we plot equipotentials and streamlines in such a manner that they form "squares," that is (on average) the distance Δs and Δn are the same (see Figure 3.11), the flow in each "flow channel" is the same and equal to $\Delta\Phi$, the difference in the potential between two successive equipotentials.

Flow nets can be constructed graphically, a practice often used in engineering to obtain solutions to, for example, flow underneath dams. For further reading on this matter, the reader is referred to Harr (1962) and Cedergren (1967). The flow nets presented in this text have been generated by use of the computer model GFLOW1, which optionally adds streamlines with the same increment in Ψ as the increment $\Delta\Phi$ it uses to plot the equipotentials. It is important to note that flow nets involve the stream function, which exists only when Φ satisfies the equation of Laplace; see rule 3.5.

Rule 3.8 *A flow net can be constructed if, and only if, the groundwater flow problem is governed by Laplace's equation.*

Next we will present the potential and stream function for some elementary flow problems, and illustrate them by plotting some flow nets.

3.1.8 Radial Flow toward a Well

One of the best-known solutions to two-dimensional groundwater flow is that of flow towards a well. If flow in the aquifer is due to the well alone, the flow pattern is radially symmetric, as indicated in Figure 3.12. The origin of a radial (r, θ) coordinate system is chosen at the center of the well. Because of radial symmetry, there is only flow parallel to the direction r.

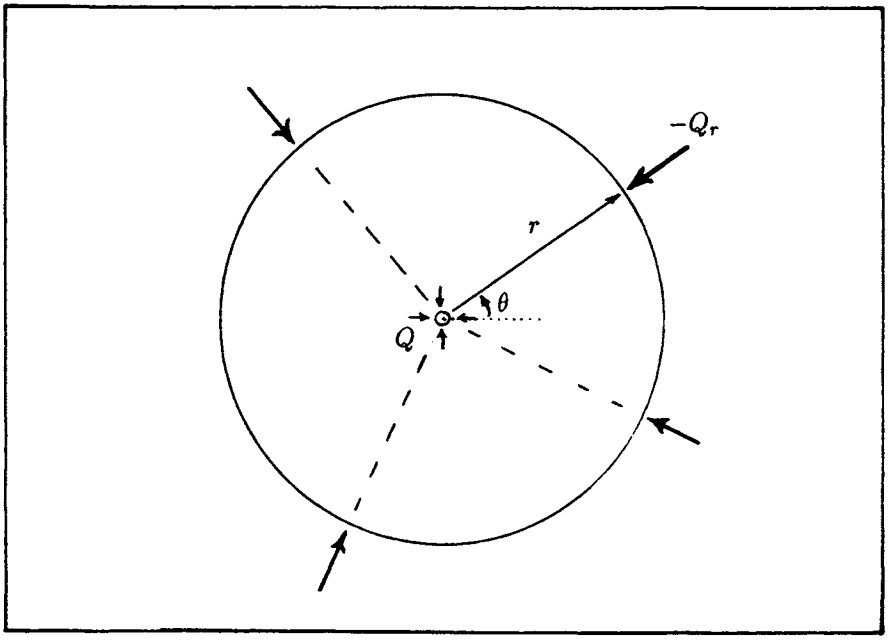

Figure 3.12: Radial flow toward a well.

Applying continuity of flow across a circle of radius r around the well gives (see Figure 3.12)

$$Q = 2\pi r(-Q_r) \tag{3.82}$$

where Q $[L^3/T]$ is the discharge (pumping rate) of the well, and where $(-Q_r)$ is the discharge vector component across the circle per unit length of the circle. The negative sign in front of Q_r indicates that the flow occurs in the negative r-direction; see Figure 3.12. The discharge vector component Q_r satisfies Darcy's law:

$$Q_r = -\frac{d\Phi}{dr} \tag{3.83}$$

Combining (3.82) and (3.83) yields

$$\frac{d\Phi}{dr} = \frac{Q}{2\pi r} \tag{3.84}$$

The potential Φ is obtained by integrating (3.84) with respect to r:

$$\Phi = \int \frac{d\Phi}{dr} dr = \int \frac{Q}{2\pi}\frac{1}{r} = \frac{Q}{2\pi}\ln r + C_w \tag{3.85}$$

where C_w is a constant of integration which may be chosen to satisfy some boundary condition. For instance, if at a distance R from the well the potential is given to be Φ_0,

$$r = R \qquad \Phi = \Phi_0 \tag{3.86}$$

we can find C_w by substituting (3.86) into (3.85),

$$\Phi_0 = \frac{Q}{2\pi} \ln R + C_w \tag{3.87}$$

which yields for C_w

$$C_w = \Phi_0 - \frac{Q}{2\pi} \ln R \tag{3.88}$$

Combining (3.88) with (3.85) gives the potential for a well with discharge Q and subject to the boundary condition (3.86);

$$\Phi = \frac{Q}{2\pi} \ln \frac{r}{R} + \Phi_0 \tag{3.89}$$

where use has been made of the fundamental relation $\ln a - \ln b = \ln a/b$.

The potential Φ depends on r only, as stated at the outset of this derivation; hence, all points on a circle with the well at its center have the same value for the potential. A well, by itself, generates circular equipotentials concentric about the well axis.

Exercise 3.5 *Prove that Equation (3.89) satisfies the equation of Laplace.*

Exercise 3.6 *Construct a flow net for a well using eight streamlines.*

Unconfined Flow near the Well

The flow conditions in the aquifer may be confined, unconfined, or both, as illustrated in Figure 3.13. The water level in the well is assumed to be equal to the head in the aquifer just outside the well bore. In reality, this is merely an approximation, since close to the well the Dupuit–Forchheimer approximation becomes inaccurate. Resistance to vertical flow, resistance across the well screen, and turbulent flow conditions just outside the well all contribute to the tendency of the water level in the well to be lower than our Dupuit–Forchheimer estimate. Thus, if the Dupuit–Forchheimer solution predicts unconfined conditions near the well, the flow in the real world is almost certainly unconfined as well.

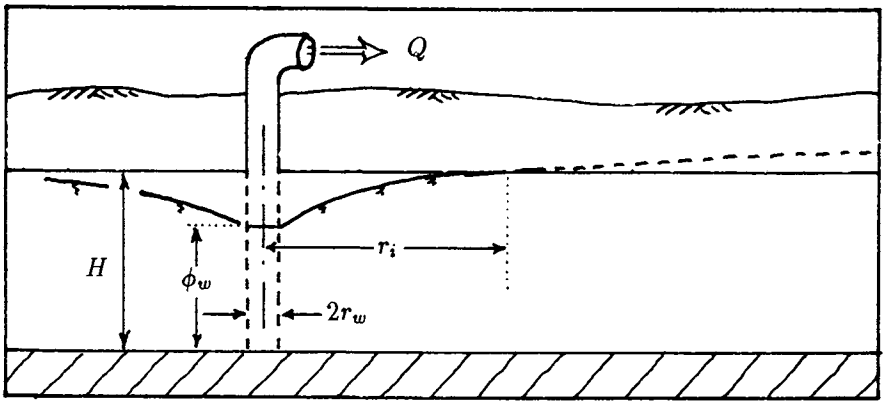

Figure 3.13: Unconfined flow near a well in a confined aquifer.

We can investigate the flow conditions near the well as follows. Assume that the radius of the well bore is r_w. The potential Φ_w in the aquifer, at the well bore, follows from

$$\Phi_w = \frac{Q}{2\pi} \ln \frac{r_w}{R} + \Phi_0 \tag{3.90}$$

The flow conditions near the well are unconfined if $\Phi_w < \frac{1}{2}kH^2$, where H is the aquifer thickness. Assuming, for a moment, that this is the case, the location r_i of the interface between unconfined and confined flow follows from

$$\tfrac{1}{2}kH^2 = \frac{Q}{2\pi} \ln \frac{r_i}{R} + \Phi_0 \tag{3.91}$$

where use has been made of the fact that at the interface the head is H, so that the potential is $\frac{1}{2}kH^2$. The radius r_i of the unconfined zone is, with (3.91),

$$r_i = R\, e^{\frac{2\pi(\frac{1}{2}kH^2 - \Phi_0)}{Q}} \tag{3.92}$$

If (3.92) yields a value for r_i larger than R, the aquifer is everywhere ($r_w \leq r \leq R$) unconfined. If r_i is smaller than r_w, the aquifer is everywhere confined.

Exercise 3.7 *The following data are given for the flow problem in Figure 3.13:* $R = 1,000\ feet$, $r_w = 0.5\ foot$, $H = 50\ feet$, $k = 20\ ft/day$, $Q = 25,000\ ft^3/day$, *and the head at a distance* R *from the well is* $\phi_0 = 60$ *feet above the aquifer base.*

(a) Calculate the (approximate) water level in the well.

(b) If the flow conditions at the well bore are unconfined, calculate the position of the interface r_i between the unconfined and the confined zone.

(c) Calculate the discharge Q_r at three different distances from the well: 1, 10, *and* 100 *feet.*

(d) Repeat the calculations under (a) for the following values of r_w: 10, 1, 0.1, *and* 0 *feet. Explain your answers.*

Stream Function for a Well

The streamlines for a well are radials emanating from the center of the well, see Figure 3.12. The stream function Ψ is given by

$$\Psi = \frac{Q}{2\pi}\theta \tag{3.93}$$

which is consistent with both Rule 3.6 and Rule 3.7. The angle θ may also be expressed in terms of the coordinates x and y:

$$\Psi = \frac{Q}{2\pi} \arctan \frac{y}{x} \tag{3.94}$$

Some caution is required in evaluating the arctangent in (3.94). Pocket calculators usually return values for the arctangent between $-\pi/2$ and $\pi/2$, assuming a positive value for x in (3.94). For negative values of x, the following corrections should be made: If $y < 0$, subtract $-\pi$; if $y > 0$, add π. When (3.94) is programmed on a computer, an arctangent function may be available with two arguments (x and y), so that no corrections should be necessary.

Branch Cut

The stream function (3.93) exhibits a jump when the principal value of the angle θ jumps from $+\pi$ to $-\pi$ across its *branch cut*; see Figure 3.14. The branch cut of the angle θ may be chosen differently than in Figure 3.14, but will always exhibit a jump of 2π. With the origin of the coordinate system at the center of the well, the stream function has the value $+Q/2$ just above the negative x-axis, and $-Q/2$ just below the negative x-axis. Previously, however, we featured the single-valuedness of the stream function. The reason for the jump in Figure 3.14 is that at the well itself the divergence of the discharge vector is not zero, but equal to the discharge of the well. Consequently, Laplace's equation does not apply at the well! The well itself, therefore, should not be considered part of the flow domain. This is

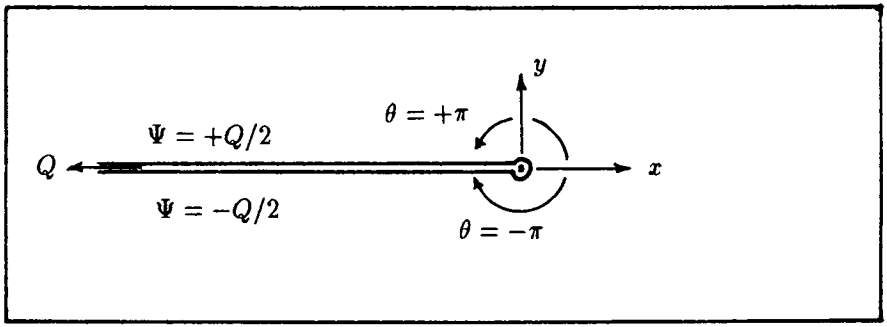

Figure 3.14: Branch cut in the stream function for a well with discharge Q.

no problem, since we do not evaluate heads and flow inside the well radius. Because the center of the well is a *singular* point, the stream function is many-valued along a line from the well to infinity: the negative x-axis in Figure 3.14. As a more physical interpretation of this, we may imagine the flow domain (a two-dimensional plane) to be cut open along the negative x-axis and around the well, eliminating the well from the flow domain. The water that flows toward the well, inside the flow domain, is removed through the slit along the negative x-axis. Therefore, there is a (fictitious) flow Q, from the well through the slit, toward infinity. In fact, this flow is consistent with the behavior of the stream function across the slit, whose jump Q suggests a flow in the slit (branch cut) of Q; see Rule 3.6. The direction of the flow in the slit is from the well toward infinity, consistent with Rule 3.7.

3.1.9 Principle of Superposition

The solution to more than one well can be obtained by simply adding the solutions for each individual well. This is a powerful feature of groundwater flow solutions and is due to the linear nature of the governing differential equation. This is how it works.

Consider the potential $\Phi_1(x, y)$ due to well #1 and the potential $\Phi_2(x, y)$ due to well #2, in Figure 3.15. The distances from well #1 and well #2 to a point P in the flow domain are r_1 and r_2, respectively. The potential at P due to well #1 with discharge Q_1 is

$$\Phi_1 = \frac{Q_1}{2\pi} \ln r_1 + C_1 \tag{3.95}$$

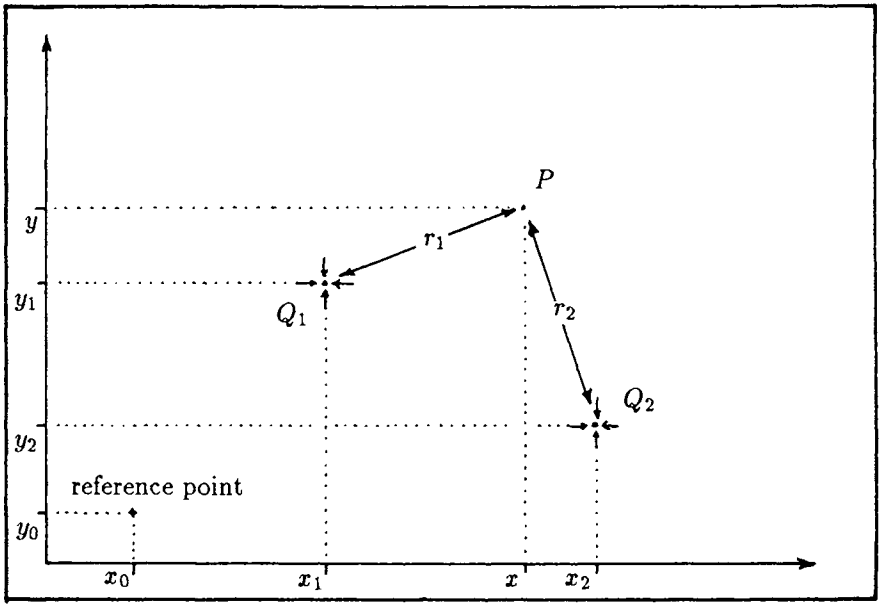

Figure 3.15: Locations of two nearby wells in an aquifer.

The potential at P due to well # 2 with discharge Q_2 is

$$\Phi_2 = \frac{Q_2}{2\pi} \ln r_2 + C_2 \tag{3.96}$$

The integration constants C_1 and C_2 are not yet defined at this point. Each of the solutions satisfies the equation of Laplace; thus, for Φ_1,

$$\partial_{ii}\Phi_1 = 0 \tag{3.97}$$

and for Φ_2,

$$\partial_{ii}\Phi_2 = 0 \tag{3.98}$$

We can sum the two equations (3.97) and (3.98):

$$\partial_{ii}\Phi_1 + \partial_{ii}\Phi_2 = 0 \tag{3.99}$$

or, because the differential equations are linear in terms of Φ_1 and Φ_2,

$$\partial_{ii}(\Phi_1 + \Phi_2) = 0 \tag{3.100}$$

Replacing the sum of the potentials Φ_1 and Φ_2 by Φ,

$$\Phi = \Phi_1 + \Phi_2 \tag{3.101}$$

yields for (3.100)

$$\partial_{ii}\Phi = 0 \tag{3.102}$$

What we showed is that if Φ_1 and Φ_2 each satisfy Laplace's equation, then so does their sum Φ. In other words: The sum of several groundwater flow solutions is also a groundwater flow solution. The last statement is not always true, as we will see later, but is for now the practical implication of *the principle of superposition* of solutions.

The solution to the flow problem in Figure 3.15, flow towards two wells, is obtained by adding (3.95) and (3.96):

$$\Phi = \frac{Q_1}{2\pi} \ln r_1 + \frac{Q_2}{2\pi} \ln r_2 + C \tag{3.103}$$

where C is the sum of C_1 and C_2 and may be chosen to satisfy some boundary condition, e.g., that the potential is equal to Φ_0 at some *reference point* (x_0, y_0):

$$x = x_0 \text{ and } y = y_0 \qquad \Phi = \Phi_0 \tag{3.104}$$

The distances r_1 and r_2 can be written in terms of the Cartesian coordinates of the wells and of point P (see Figure 3.15):

$$\begin{aligned} r_1 &= \sqrt{(x - x_1)^2 + (y - y_1)^2} \\ r_2 &= \sqrt{(x - x_2)^2 + (y - y_2)^2} \end{aligned} \tag{3.105}$$

The complete solution, which also satisfies the boundary condition (3.104), is

$$\begin{aligned} \Phi \;=\; & \frac{Q_1}{2\pi} \ln \frac{\sqrt{(x - x_1)^2 + (y - y_1)^2}}{\sqrt{(x_0 - x_1)^2 + (y_0 - y_1)^2}} \\ & + \frac{Q_2}{2\pi} \ln \frac{\sqrt{(x - x_2)^2 + (y - y_2)^2}}{\sqrt{(x_0 - x_2)^2 + (y_0 - y_2)^2}} + \Phi_0 \end{aligned} \tag{3.106}$$

Superposition also applies to the stream function, since Laplace's equation in terms of Ψ is also linear; see (3.75). The stream function for the two wells is

$$\Psi = \frac{Q_1}{2\pi} \arctan\left(\frac{y - y_1}{x - x_1}\right) + \frac{Q_2}{2\pi} \arctan\left(\frac{y - y_2}{x - x_2}\right) \tag{3.107}$$

A flow net for the two wells is plotted in Figure 3.16, where the dotted lines are equipotentials and the solid lines are streamlines. The calculations

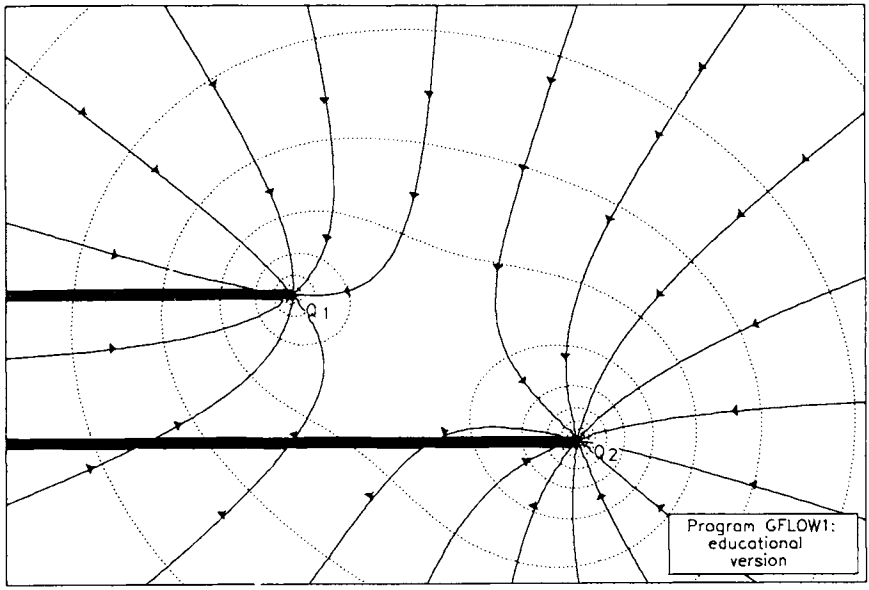

Figure 3.16: Equipotentials and streamlines due to superposition of two nearby wells. (GFLOW1 data file: problem1.dat)

necessary to produce Figure 3.16 are laborious and have been carried out with the computer model GFLOW1. The program calculates Φ and Ψ at a grid of points, evenly distributed over the domain in Figure 3.16, after which a contouring routine generates the equipotentials and streamlines for specified values of Φ and Ψ, respectively. The rather thick horizontal lines emanating from the wells are an artifact of the contouring routine, which cannot handle discontinuous functions. These thick lines, therefore, mark the positions of the branch cuts for the wells. The Ψ value along a streamline is constant, by definition, but jumps when the streamline crosses a branch cut. The jump equals the discharge rate of the well to which the branch cut belongs.

The input data for Figure 3.16 is stored in the file *problem1.dat* on the distribution diskette included with this text. You may further investigate the concept of superposition by following the instructions included in this data file.

Exercise 3.8 *Try to sketch the* **bounding streamlines** *that separate the* **capture zones** *of the two wells in Figure 3.16.*

Nonlinear Laplace Equation

The principle of superposition depends, as we have seen, on the linearity of the differential equation of Laplace. We have formulated the equation of Laplace in terms of discharge potentials, resulting in the same *linear* differential equation for confined and unconfined flow. However, when formulating Laplace's equation in terms of heads, the differential equation for unconfined flow is *not linear*; see (3.40), which contains ϕ^2. Consequently, we cannot superimpose solutions in terms of the head ϕ for the case of unconfined flow. The fact that Laplace's equation in terms of discharge potentials is always linear, regardless of the flow type, is what makes superposition of solutions (in terms of Φ) always possible. This is one of the incentives to formulate groundwater flow problems in terms of discharge potentials rather than heads.

Rule 3.9 *Unconfined flow solutions in terms of heads cannot be superimposed. Solutions in terms of discharge potentials can always be superimposed.*

3.1.10 A Well in a Uniform Flow Field

The principle of superposition is, of course, not limited to adding wells. A very practical problem, for instance, is that of a well superimposed onto a uniform flow field. The potential for a uniform flow Q_0 in the x-direction is, integrating Darcy's law,

$$\Phi = \int [-Q_x] dx = -\int Q_0 dx = -Q_o x + C_u \tag{3.108}$$

where C_u is a constant of integration. The stream function for uniform flow in the x-direction is

$$\Psi = -Q_0 y \tag{3.109}$$

Equation (3.109) satisfies Laplace's equation and generates the proper uniform flow rate in view of Rule 3.6 and Rule 3.7.

For convenience, we will select the origin of our coordinate system at the center of the well; see Figure 3.17. The combined potential for the well and the uniform flow field is obtained by adding (3.108) and (3.85):

$$\Phi = -Q_0 x + \frac{Q}{2\pi} \ln \sqrt{x^2 + y^2} + C \tag{3.110}$$

The constant C is the sum of C_u and C_w and may be chosen to satisfy some potential at some reference point; see (3.104).

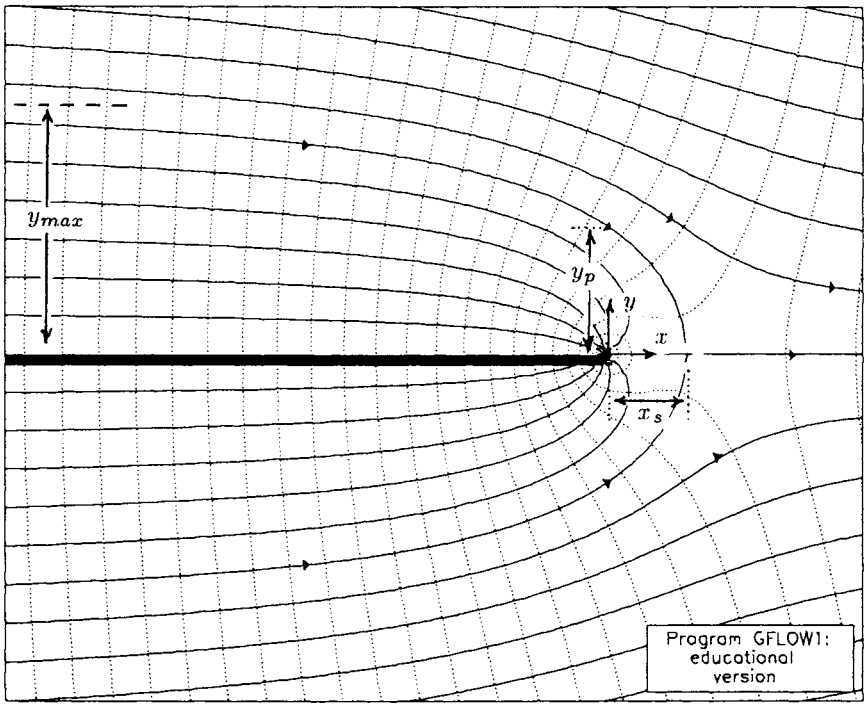

Figure 3.17: A well intercepting water from a uniform flow field. (GFLOW1 data file: problem2.dat)

The stream function is obtained by adding (3.94) and (3.109):

$$\Psi = -Q_0 y + \frac{Q}{2\pi} \arctan \frac{y}{x} \tag{3.111}$$

The flow net in Figure 3.17 has been generated with GFLOW1 and the input data file *problem2.dat*. You may further investigate this solution by following the instructions included in this data file.

Exercise 3.9 *For the case of Figure 3.17:*

(a) Determine the Ψ value(s) of the bounding streamlines, which delineate the capture zone of the well.

(b) Determine the Ψ value(s) of the streamlines along the x-axis.

Explain your answers.

3.1.11 Capturing Contaminant Plumes with a Recovery Well

The flow problem depicted in Figure 3.17 is of considerable practical importance. One of the most common techniques for aquifer restoration is the so called "pump and treat" method. Contaminated groundwater, emanating from some "point source," is intercepted by a recovery well, removed from the aquifer, treated, and discharged in a nearby surface water or (sometimes) reinjected into the aquifer. The flow problem depicted in Figure 3.17 may be seen as a first approximation to a recovery well system. In Figure 3.17 the existing regional flow field is locally approximated by uniform flow, and the recovery system is represented by a single well. The question is: What is the minimum discharge rate of the well which will still remove all contaminated groundwater? Another way of looking at the problem is to find the minimum size of the capture zone that is still sufficient to include the entire contaminant plume. By overlaying the capture zone of the well over the contaminant plume boundaries, we can determine whether or not all contaminated water will be recovered, or if some of it will escape (see Figure 3.18).

The capture zone may be generated by use of a computer model, as done in Figure 3.17. It is quite simple, however, to make a fairly accurate sketch of the capture zone based on a few simple hand calculations. To do so, we will determine three critical measurements of the capture zone: (1) the location of the tip downstream from the well, (2) the width opposite the well, and (3) the width (infinitely) far upstream from the well. With these three measurements, we can make a useful sketch of the capture zone.

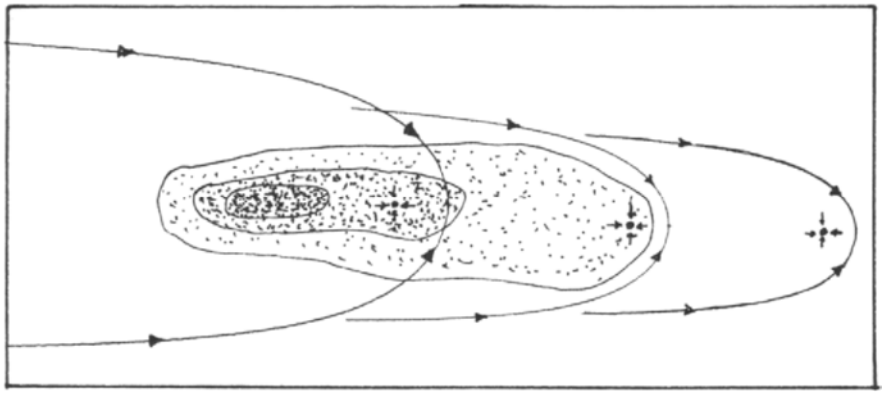

Figure 3.18: Capturing contaminant plumes with a recovery well.

Stagnation Point

The tip of the plume occurs at a point where the "pull" of the well balances the uniform flow. At this point there is no groundwater flow: It is called a *stagnation point.* In view of the symmetry in Figure 3.17, we conclude that the stagnation point must occur on the x-axis ($y = 0$), where it is indeed visible in Figure 3.17 as the point where the bounding streamlines meet. Assume that the stagnation point occurs at a distance x_s from the well. We know that Q_x is zero at the stagnation point and hence,

$$Q_x = -\frac{\partial \Phi}{\partial x} = 0 \qquad (x = x_s) \tag{3.112}$$

so that with (3.110),

$$-\frac{\partial \Phi}{\partial x} = Q_0 - \frac{Q}{2\pi\sqrt{x^2+y^2}}\frac{1}{2}\frac{2x}{\sqrt{x^2+y^2}} = 0 \quad (x = x_s \; ; \; y = 0) \tag{3.113}$$

where use has been made of the chain rule when differentiating the natural logarithm. Equation (3.113) yields for x_s

$$x_s = \frac{Q}{2\pi Q_0} \tag{3.114}$$

Width of Capture Zone

We will first determine the width of the capture zone opposite the well. The Ψ value at the stagnation point is zero, as follows from (3.111) by substituting the coordinates of the stagnation point $(x_s, 0)$. The bounding

streamlines, which define the capture zone, share the stagnation point; thus, their Ψ value is also equal to zero. We select a point P $(0, y_p)$ on the bounding streamline above the well, see Figure 3.17. Evaluating (3.111) at P yields

$$0 = -Q_0 y_p + \frac{Q}{2\pi} \arctan \frac{y_p}{0} \tag{3.115}$$

The arctangent in (3.115) is $\pi/2$, so that y_p becomes

$$y_p = \frac{Q}{4Q_0} \tag{3.116}$$

The maximum elevation y_{max} of the bounding streamline occurs (infinitely) far upstream from the well; see Figure 3.17. With (3.111) and $x \to -\infty$:

$$0 = -Q_0 y_{max} + \frac{Q}{2\pi} \arctan \frac{y_{max}}{-\infty} \tag{3.117}$$

The arctangent in (3.117) is π, so that y_{max} becomes

$$y_{max} = \frac{Q}{2Q_0} \tag{3.118}$$

The maximum width w of the capture zone, therefore, is

$$w = \frac{Q}{Q_0} \tag{3.119}$$

The result (3.119) might have been anticipated by realizing that far upstream the influence of the well is negligible; the flow is nearly uniform. Sufficiently far upstream from the well, the total flow within the capture zone approaches wQ_0. This flow must equal the total well discharge Q; hence equation (3.119).

We found that the width of the capture zone opposite the well is $Q/2Q_0$, while the maximum width upstream from the well is Q/Q_0. These measurements, together with the location of the stagnation point, are indicated on Figure 3.19, which may be used as a flash card for pump and treat systems. If the aquifer transmissivity and the local hydraulic gradient of the ambient groundwater flow are known, Q_0 can be calculated and Figure 3.19 may be used to prepare some first estimates of required pumping rates and well locations for a pump and treat system.

3.1.12 Well Doublet for Air-Conditioning

Air-conditioning systems for large public or corporate buildings often use groundwater in their heat exchangers. Groundwater has a rather constant temperature of approximately 10^0C ($\sim 50^0$F) year around. The used

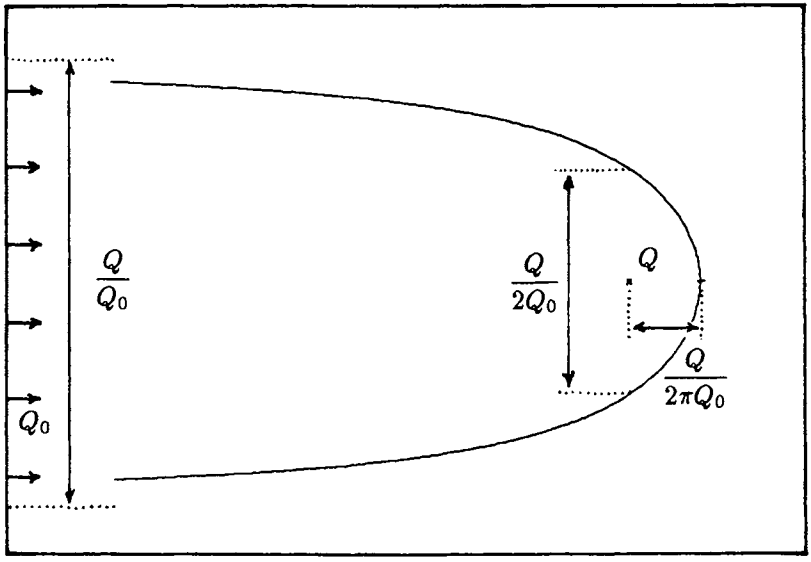

Figure 3.19: Capture zone dimensions of a recovery well in a uniform flow field.

groundwater, warmed in the heat exchanger, is either discharged in a nearby surface water or *reinjected* in the aquifer by use of a *recharge well.* In the latter case, it is important to design the *well doublet* (combination of discharge and recharge well) in such a manner that recirculation of the warmed water is avoided, or at least minimized.

In Figure 3.20, a flow net is depicted for a well doublet with the discharge well at $(-d, 0)$ and the recharge well at $(d, 0)$. The pumping and injection rates are Q and $-Q$, respectively. The potential function for Figure 3.20 is

$$\Phi = \frac{Q}{2\pi} \ln \frac{r_1}{r_2} + \Phi_0 \tag{3.120}$$

or, in terms of Cartesian coordinates,

$$\Phi = \frac{Q}{4\pi} \ln \frac{(x+d)^2 + y^2}{(x-d)^2 + y^2} + \Phi_0 \tag{3.121}$$

The factor 4π in (3.121) results from replacing $\ln(r_1/r_2)$ in (3.120) by $\frac{1}{2}\ln(r_1^2/r_2^2)$. The stream function is

$$\Psi = \frac{Q}{2\pi} \left[\arctan\left(\frac{y}{x+d}\right) - \arctan\left(\frac{y}{x-d}\right) \right] \tag{3.122}$$

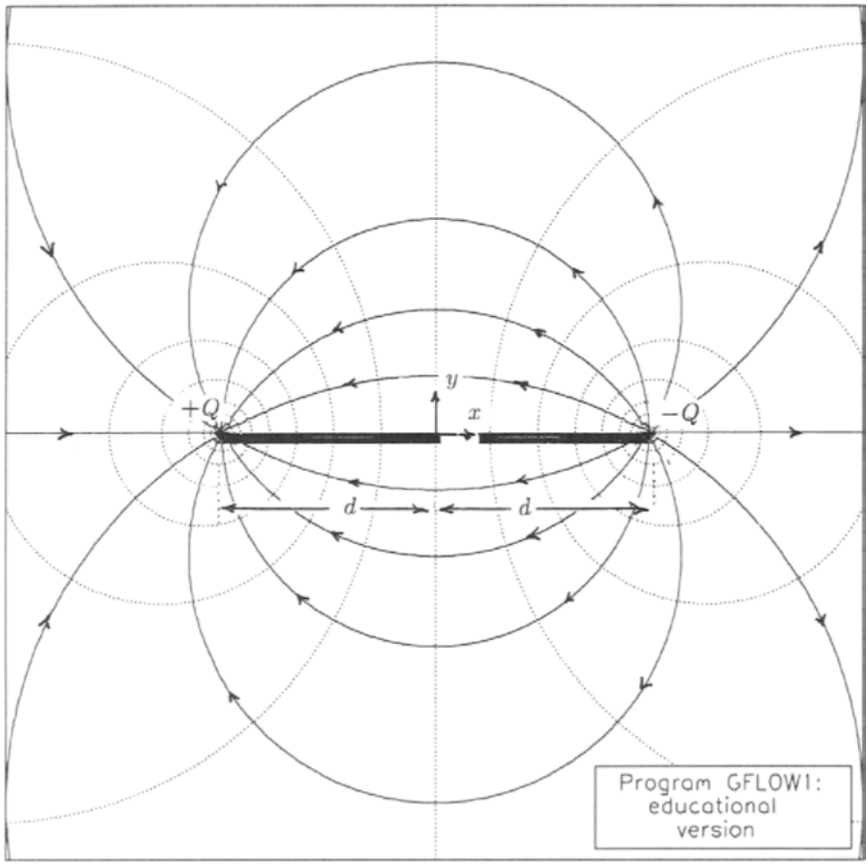

Figure 3.20: Flow due to a discharge well and recharge well of equal strength. (GFLOW1 file: problem3.dat)

The flow in Figure 3.20 is due to the wells alone and is steady-state; thus, the wells have been operating forever. Under these conditions, there is total recirculation! The only cooling of the groundwater is due to heat conduction to adjacent geological formations.

The Effects of Regional Flow

In general, however, there is already flow in the aquifer prior to the installation of the well doublet. The recharge well is placed downstream from the discharge well in order to reduce recirculation. Approximating the ambient flow near the wells by uniform flow, we obtain the following solutions for

the potential and stream function:

$$\Phi = -Q_0 x + \frac{Q}{4\pi} \ln \frac{(x+d)^2 + y^2}{(x-d)^2 + y^2} + \Phi_0 \tag{3.123}$$

$$\Psi = -Q_0 y + \frac{Q}{2\pi} \left[\arctan\left(\frac{y}{x+d}\right) - \arctan\left(\frac{y}{x-d}\right) \right] \tag{3.124}$$

Flow nets are plotted in Figure 3.21 for three cases: (a) no recirculation with two stagnation points between the wells, (b) just no recirculation with one stagnation point midway between the wells, and (c) some recirculation with two stagnation points on the y-axis midway between the wells. The origin of the coordinate system in Figure 3.21, although not indicated, is midway between the well and the recharge well, as in Figure 3.20.

Of practical importance to us are the conditions under which case (b), the critical case with just no recirculation, occurs. Specifically, we want to know, for a given uniform flow rate, what relationship between well discharge and distance between the wells will just prevent recirculation. For case (b), the stagnation point occurs at the origin of the coordinate system. There is no flow at the stagnation point, so that

$$Q_x = -\frac{\partial \Phi}{\partial x} = 0 \qquad (x = y = 0) \tag{3.125}$$

Setting the derivative of (3.123) with respect to x equal to zero yields

$$0 = -Q_0 + \frac{Q}{4\pi} \left[\frac{2(x+d)}{(x+d)^2 + y^2} - \frac{2(x-d)}{(x-d)^2 + y^2} \right] \quad (x = y = 0) \tag{3.126}$$

which yields

$$\frac{Q}{\pi d Q_0} = 1 \tag{3.127}$$

Equation (3.127) provides the critical condition for which there is just no recirculation. When the factor $Q/\pi d Q_0$ is larger than 1, there will be recirculation; see Figure 3.21.

Exercise 3.10 *For case (c) in Figure 3.21:*

(a) Calculate the positions y_1 and y_2 on the y-axis of the stagnation points. Hint: You may make use of (3.126) without setting y equal to zero.

(b) What is the value of the stream function Ψ at each of the stagnation points?

(c) What is the percentage of water that is being recirculated?

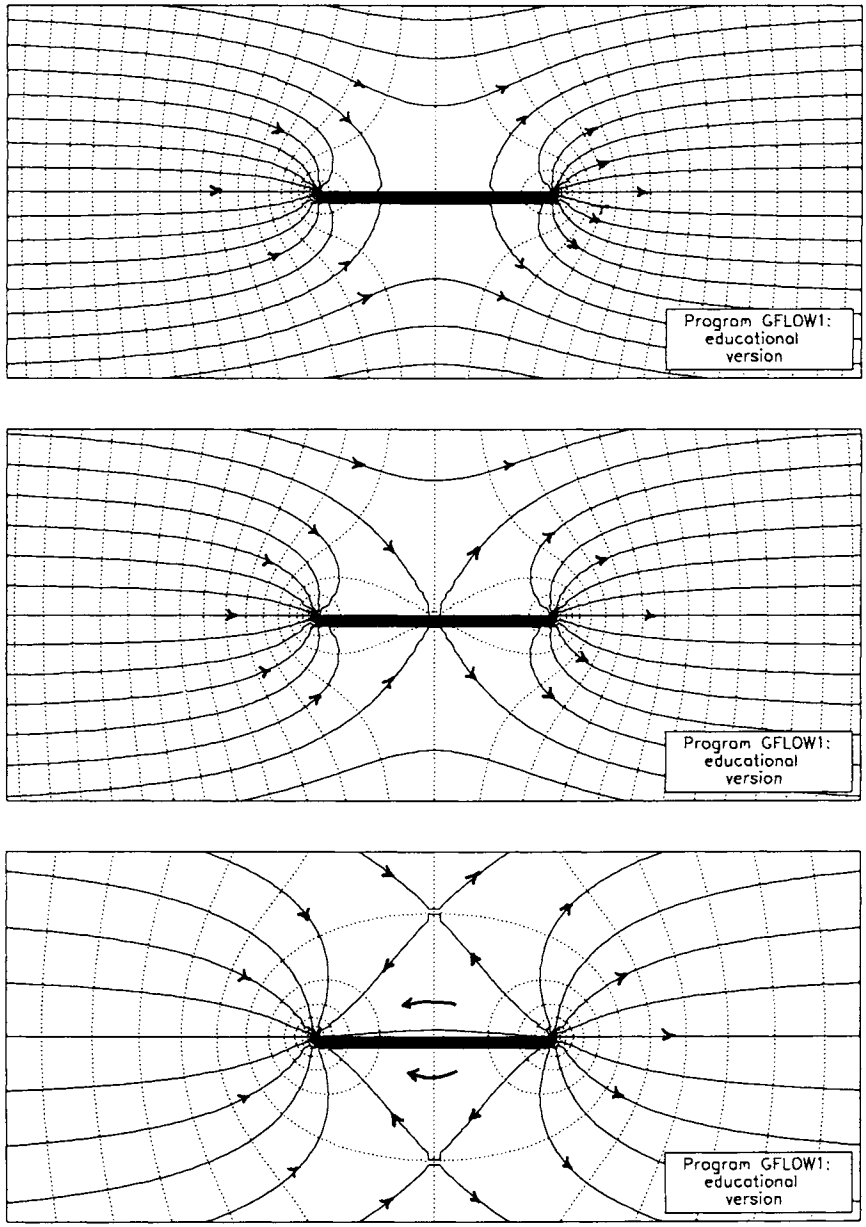

Figure 3.21: Three cases of a well and recharge well in a uniform flow field: (a) $Q/\pi dQ_0 = 0.8$, (b) $Q/\pi dQ_0 = 1$, and (c) $Q/\pi dQ_0 = 2$. (Case (b) in GFLOW1 file: problem4.dat)

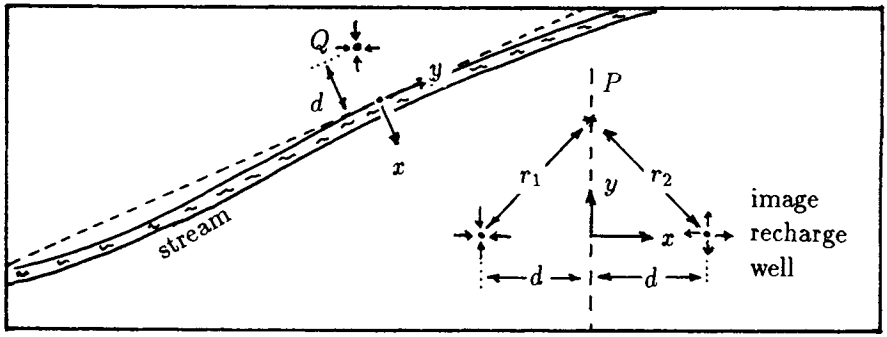

Figure 3.22: A well near a stream, approximated by a well near a straight equipotential.

3.1.13 Method of Images

Our groundwater flow solutions so far have not included any realistic boundary conditions, such as streams or lakes. In a Dupuit–Forchheimer model, the heads underneath a stream or lake are given by the water elevation in that stream or lake, respectively. When a well is pumped near a stream, for instance, the heads along that stream should not be affected. Our basic solutions for one or more wells, as formulated earlier, cannot satisfy such a constant-head (or constant-potential) condition along streams and lakes. In fact, our solutions generate *drawdowns* everywhere, except at a single reference point.

There is a simple technique (perhaps trick is a better word) to create some basic boundary conditions. Adding imaginary wells to our real wells, at strategic locations in the flow domain, allows us to generate infinitely long straight equipotentials or no-flow boundaries, and circular equipotentials.

Infinitely Long Straight Equipotential Boundary

In Figure 3.22 a well is depicted at a distance d from a stream boundary. The well should not affect the heads (potentials) along the stream boundary. In order to achieve this, in an approximate manner, the stream boundary is replaced by a straight line: the y axis in Figure 3.22. Our objective is to let the well pump while keeping the potential along the y-axis constant. The solution to this problem is already known to us! Review the equipotentials plotted in Figure 3.20. Midway between the discharge and recharge well there is a vertical straight equipotential: the y-axis. If we would only consider the equipotentials to the left of the y-axis, we have the solution to our problem of a well near a stream as illustrated in Figure 3.22. In using the solution to the well doublet in Figure 3.20, for the problem in

Figure 3.22, the recharge well is *fictitious*, added only as a trick to obtain the equipotential conditions along the y-axis. The recharge well is an *image* of the pumping well with respect to the stream boundary.

The solution to the potential and stream function are given by (3.121) and (3.122), respectively. The equipotentials are circles with their centers on the x-axis; see Figure 3.20. The equipotential midway between the well and the recharge well is a circle with its center infinitely far away on the x-axis. Consequently, the equipotential through $x = y = 0$, the y-axis, is an infinitely long straight line. The streamlines are also circles, but with their centers on the y-axis. The straight streamline along the x-axis is a circle with its center infinitely far away on the y-axis.

That all points on the y-axis indeed have the same potential is readily seen from Equation (3.120) and Figure 3.22. For all points on the y-axis, the distances r_1 and r_2 are the same. Consequently, the $\ln(r_1/r_2)$ in (3.120) becomes $\ln 1$, which is zero. Therefore, along the y-axis the potential is equal to Φ_0; the y-axis is an equipotential.

In Figure 3.23, a flow net is plotted in the flow domain to the left of the stream of Figure 3.22; it is the left half of the flow net in Figure 3.20. In Figure 3.23, we pretend that the stream is supplying the water for the well. As appears from Figure 3.20, in our mathematical model, that water is actually coming from the image recharge well. The solution is, of course, approximate; the real potential conditions along the stream differ somewhat from the ones produced in Figure 3.23.

3.1.14 A Well near a Polluted Stream

The only flow in Figure 3.23 is due to the well. In general, however, there is some ambient flow, usually toward the stream. The stream in Figure 3.24, therefore, is depicted as a receiving stream. The regional groundwater flow toward the stream, in the vicinity of the well, is approximated by uniform flow.

The problem is similar to the one depicted in Figure 3.22, except for the addition of uniform flow. The problem resembles that of the well doublet in a uniform flow field discussed before. The potential and stream function are given by (3.123) and (3.124), respectively. The flow nets in Figure 3.21 are now reinterpreted as those for a well in a uniform flow field near a stream (y-axis). Only the left halves of the flow nets in Figure 3.21 are real; the other halves occur on the other side of the stream and are fictitious. In Figure 3.25, these flow nets are superimposed onto the domain to the left of the stream in Figure 3.24. The three cases, reinterpreted for the problem in Figure 3.24, are: (a) no water is pumped from the river, (b) critical case of no water pumped being from the river, and (c) some water is pumped from

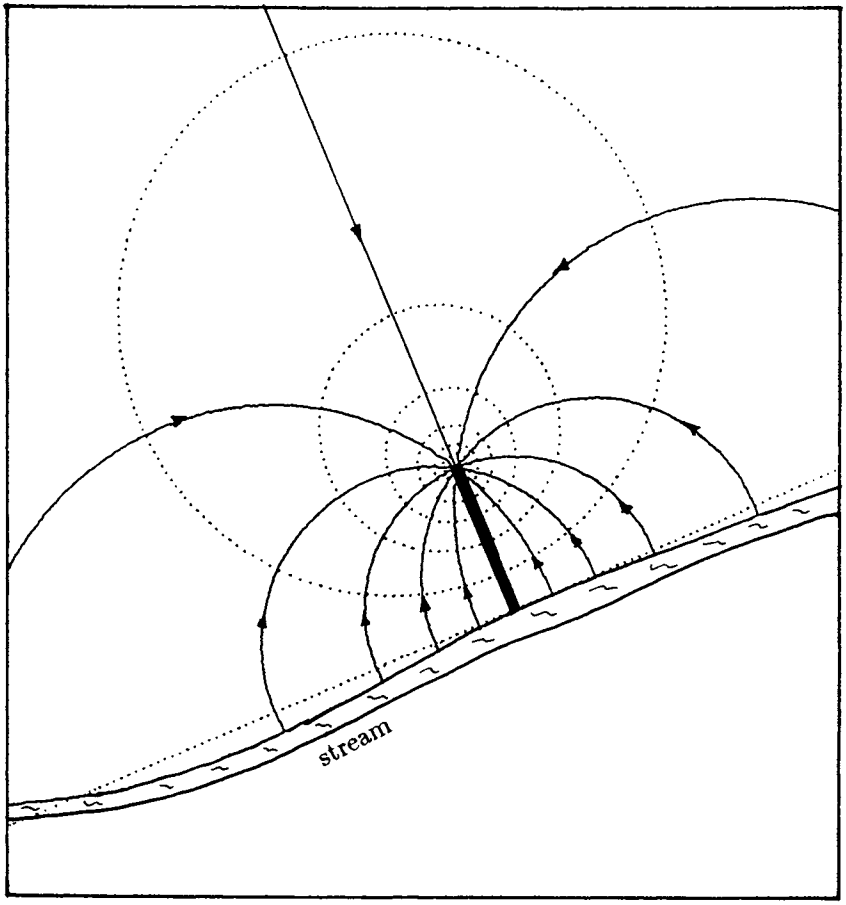

Figure 3.23: Equipotentials and streamlines for a well near a stream.

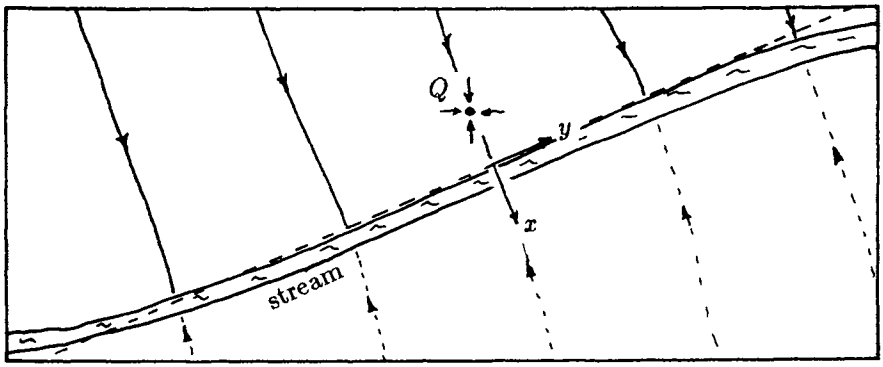

Figure 3.24: A well near a polluted stream.

the river. The solution is approximate, because the straight equipotential in combination with the uniform flow neither accurately reflects the ambient flow conditions near the stream nor accurately satisfies the actual boundary conditions along the stream.

3.1.15 A Well near a Rock Outcrop

The method of images, used above, employed an image recharge well in order to obtain a straight equipotential boundary near a discharge well. We will show that when using an image discharge well, a no-flow boundary is obtained instead of an equipotential boundary.

Consider a well near a rock outcrop, as depicted in Figure 3.26. The no-flow boundary may also be a sheet piling (with their slots sealed with bentonite) or a bentonite "slurry trench." If the boundary is approximated by an infinitely long, straight no-flow boundary (y-axis in Figure 3.26), it may be modeled by an image pumping well. The potential and stream function are

$$\Phi = \frac{Q}{4\pi} \ln \left[\frac{(x+d)^2 + y^2}{(x_0+d)^2 + y_0^2} \times \frac{(x-d)^2 + y^2}{(x_0-d)^2 + y_0^2} \right] + \Phi_0 \tag{3.128}$$

and

$$\Psi = \frac{Q}{2\pi} \left[\arctan\left(\frac{y}{x+d}\right) + \arctan\left(\frac{y}{x-d}\right) \right] \tag{3.129}$$

A flow net for this case is plotted in Figure 3.26. That the well and image well indeed create a no-flow boundary along the y-axis is seen from (3.129) by substituting $x = 0$, yielding

$$\Psi = \frac{Q}{2\pi} \left[\arctan \frac{y}{+d} + \arctan \frac{y}{-d} \right] = \frac{Q}{2\pi} [\theta_1 + (\pi - \theta_1)] = \frac{Q}{2} \tag{3.130}$$

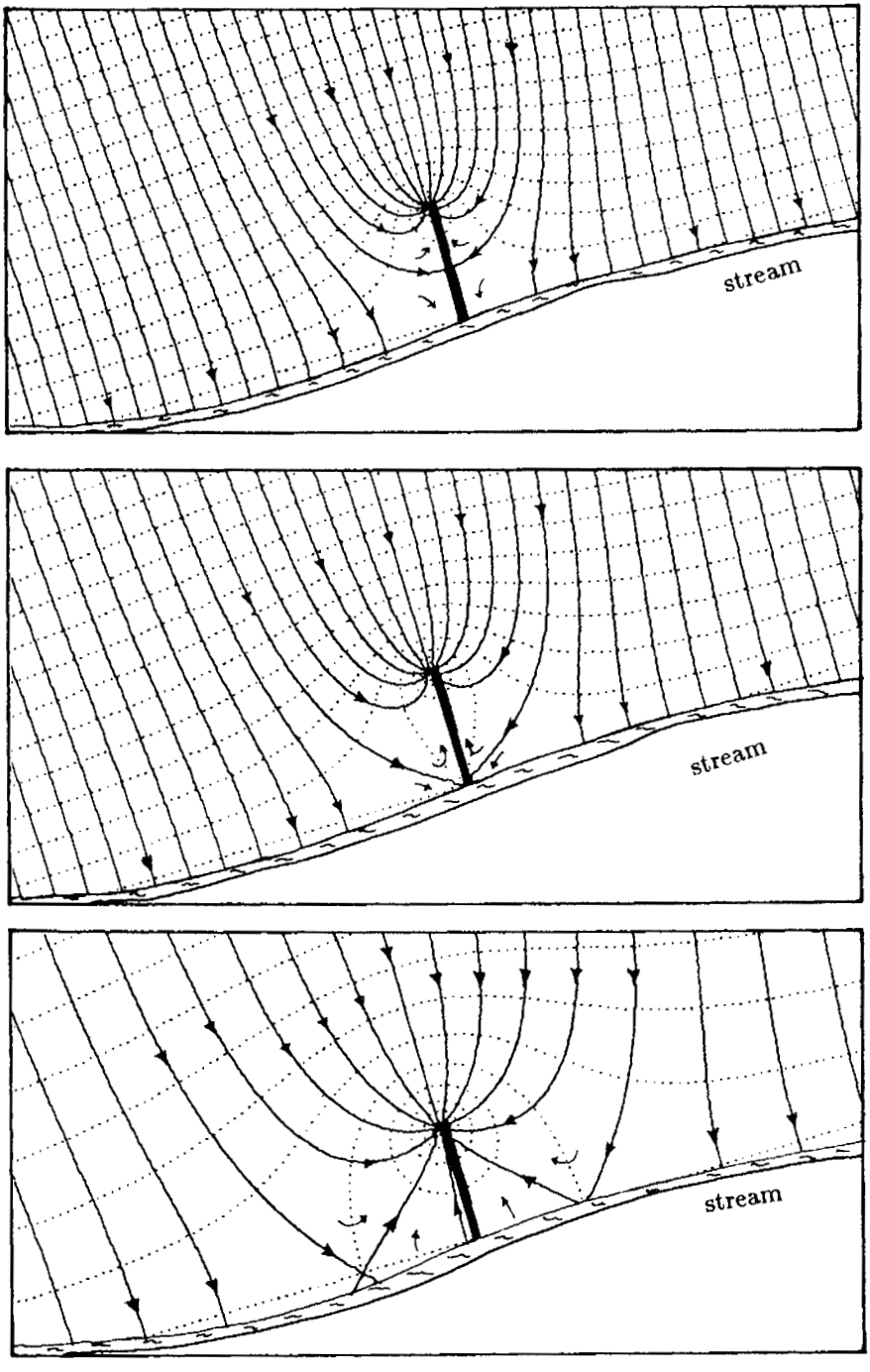

Figure 3.25: Three cases of a well near a polluted stream: (a) $Q/\pi dQ_0 = 0.8$, (b) $Q/\pi dQ_0 = 1$, and (c) $Q/\pi dQ_0 = 2$. (Case (b) in GFLOW1 file: problem4.dat)

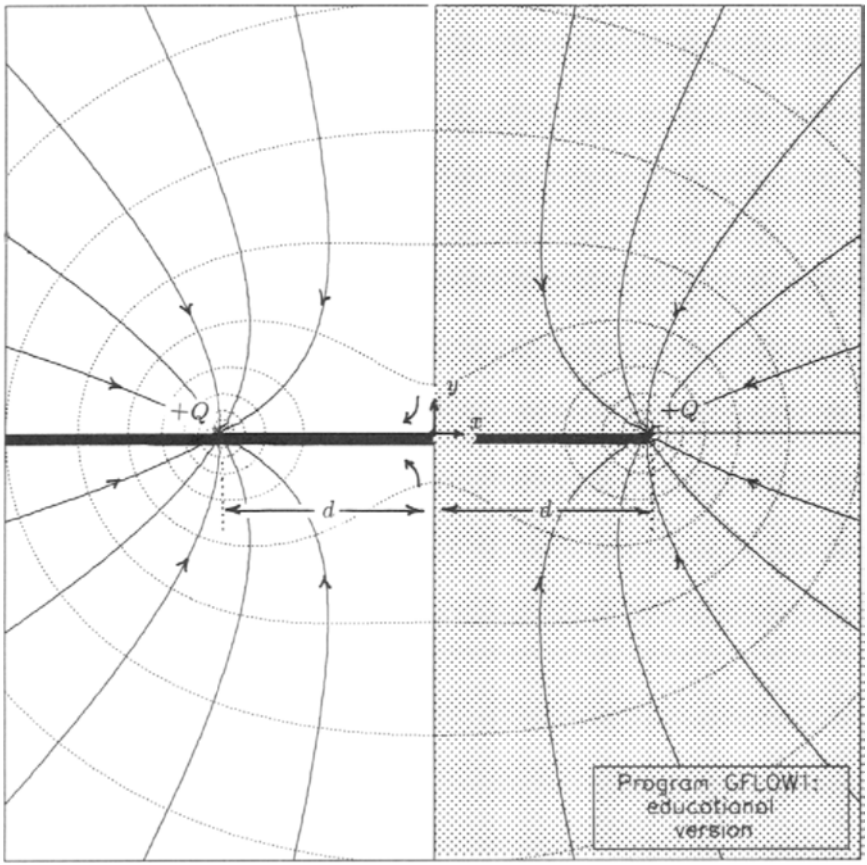

Figure 3.26: A well near a rock outcrop. (GFLOW1 data file: problem5.dat)

The Ψ value along the y-axis is constant $(Q/2)$, so that the y-axis is a streamline across which there cannot be any flow: The y-axis is a no-flow boundary.

It is possible to mix the equipotential and no-flow boundaries for some cases. For instance, a well near an equipotential boundary and a no-flow boundary, which are perpendicular, may be provided with images with respect to both boundaries. It is also necessary, however, to image the image well and image recharge well. For the case where the equipotential and no-flow boundary are perpendicular, full symmetry is obtained with a total of three images. In most general cases of intersecting equipotential and no-flow boundaries, however, the number of images is infinite! It is, of course, still possible to create approximate solutions by taking only a finite number of images into account.

Exercise 3.11 *Define the image wells and/or image recharge wells for the following cases:*

(a) A well to the left of the y-axis which is an equipotential boundary, and above the x-axis, which is a no-flow boundary.

(a) A well midway between two parallel equipotential boundaries. The distance from the well to either boundary is d.

Indicate in a sketch the position and discharge (+ for pumping and − for injection) of the well and its images. Present an approximate solution when necessary. You may test your solutions in program GFLOW1.

3.1.16 A Well near a Circular Lake or inside a Circular Island

Earlier we have seen that the combination of a well and a recharge well generates circular equipotentials with the wells off-center; see Figure 3.20. Assume, for a moment, that one of the circles around the recharge well in Figure 3.20 is a circular lake. In that case, the recharge well and the equipotentials inside that circle are fictitious; the recharge well is an image of the well with respect to the *circular equipotential boundary* formed by the lake boundary. Another way of interpreting the equipotentials in Figure 3.20 is to envision the well as being positioned off-center in a circular island, the boundary of which is one of the circular equipotentials around the well itself. Again the recharge well is now regarded as an image of the well with respect to the island boundary.

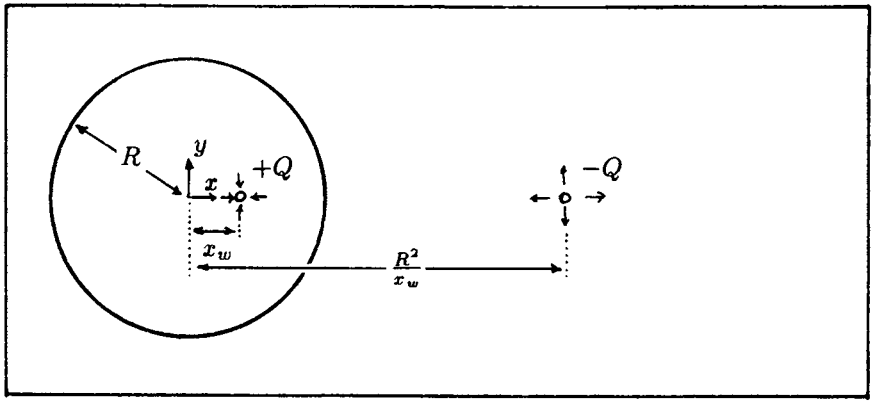

Figure 3.27: Eccentric well inside a circular island.

Eccentric Well Inside a Circular Island

The latter situation is depicted in Figure 3.27, where the coordinate system has been shifted with respect to the one in Figure 3.20: The origin is now at the center of the circular island. The radius of the island is R, while the well is located at $x = x_w$ and $y = 0$. The position of the image recharge well is at $x = R^2/x_w$ and $y = 0$. The potential is given by

$$\Phi = \frac{Q}{4\pi} \ln \left[\frac{(x - x_w)^2 + y^2}{\left(x - \frac{R^2}{x_w}\right)^2 + y^2} \frac{R^2}{x_w^2} \right] + \Phi_0 \tag{3.131}$$

where Φ_0 is the potential at the boundary of the circular island.

We will demonstrate that (3.131) satisfies the condition of a constant potential Φ_0 at the boundary of the island, where

$$x^2 + y^2 = R^2 \tag{3.132}$$

First we rewrite (3.131) as follows:

$$\Phi = \frac{Q}{4\pi} \ln \left[\frac{(x^2 + y^2 - 2xx_w + x_w^2)R^2}{(x^2 + y^2 - 2x\frac{R^2}{x_w} + \frac{R^4}{x_w^2})x_w^2} \right] + \Phi_0 \tag{3.133}$$

Substituting (3.132) in (3.133) yields

$$\frac{Q}{4\pi} \ln \left[\frac{(R^2 - 2xx_w + x_w^2)R^2}{(R^2 - 2x\frac{R^2}{x_w} + \frac{R^4}{x_w^2})x_w^2} \right] + \Phi_0 =$$

$$\frac{Q}{4\pi}\ln\left[\frac{R^2-2xx_w+x_w^2}{x_w^2-2xx_w+R^2}\right]+\Phi_0=$$

$$\frac{Q}{4\pi}\ln 1+\Phi_0=\quad\Phi_0 \tag{3.134}$$

The stream function for the well inside the island is

$$\Psi=\frac{Q}{2\pi}\left[\arctan\left(\frac{y}{x-x_w}\right)-\arctan\left(\frac{y}{x-\frac{R^2}{x_w}}\right)\right] \tag{3.135}$$

Well near a Circular Lake

As discussed, Figure 3.27 can also be interpreted as that of a well outside a circular lake, provided that the recharge well is replaced by a well and the well inside the circular equipotential (now the lake boundary) becomes a recharge well. The solution is the same as in (3.131), except with the well and recharge well interchanged:

$$\Phi=\frac{Q}{4\pi}\ln\left[\frac{\left(x-\frac{R^2}{x_w}\right)^2+y^2}{(x-x_w)^2+y^2}\,\frac{x_w^2}{R^2}\right]+\Phi_0 \tag{3.136}$$

Similarly, the stream function becomes

$$\Psi=\frac{Q}{2\pi}\left[\arctan\left(\frac{y}{x-\frac{R^2}{x_w}}\right)-\arctan\left(\frac{y}{x-x_w}\right)\right] \tag{3.137}$$

3.1.17 A Circular Lake in a Uniform Flow Field

Observe that the flow field in the vicinity of the origin in Figure 3.20, midway between the well and the recharge well, is nearly uniform. The streamlines will straighten further if we move the well and recharge well further apart. In order to maintain a certain "uniform" flow rate near the origin, we must increase the strength of the well and recharge well proportionally to their distance from the origin. In the limiting case, where the well and recharge well are moved infinitely far apart, while their strengths are increased to infinity, the flow field is exactly uniform. We will use this "trick" for creating uniform flow to construct a solution to a circular lake in a uniform flow field (see also Strack, 1989).

In Figure 3.28 a circular lake is depicted with a recharge well to the left and a discharge well to the right. Each well has an image inside the lake to maintain the (circular) equipotential boundary. If the well and

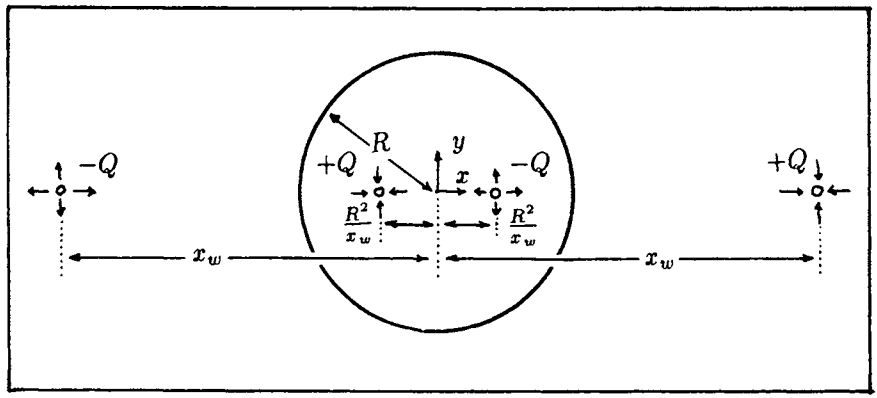

Figure 3.28: Creating uniform flow near a circular lake.

the recharge well are moved farther and farther away from the lake, the images are moving closer and closer together. In the limit, where the well and recharge well are approaching plus and minus infinity, respectively, the images coincide at the center of the lake. The well and recharge well are located at $x = x_w$ and $x = -x_w$, respectively. The potential Φ is, with reference to (3.131),

$$\Phi = \frac{Q}{4\pi}\left[\ln\frac{(x-x_w)^2+y^2}{\left(x-\frac{R^2}{x_w}\right)^2+y^2}\,\frac{R^2}{x_w^2} - \ln\frac{(x+x_w)^2+y^2}{\left(x+\frac{R^2}{x_w}\right)^2+y^2}\,\frac{R^2}{x_w^2}\right] + \Phi_0 \quad (3.138)$$

We recombine the terms related to the wells and their images:

$$\Phi = \frac{Q}{4\pi}\left[\ln\frac{\left(x+\frac{R^2}{x_w}\right)^2+y^2}{\left(x-\frac{R^2}{x_w}\right)^2+y^2} - \ln\frac{(x+x_w)^2+y^2}{(x-x_w)^2+y^2}\right] + \Phi_0 \quad (3.139)$$

Writing out the quadratic terms yields

$$\Phi = \frac{Q}{4\pi}\left[\ln\frac{x^2+y^2+2xx_w+\frac{R^4}{x_w^2}}{x^2+y^2-2xx_w+\frac{R^4}{x_w^2}} - \ln\frac{x_w^2+x^2+2xx_w+y^2}{x_w^2+x^2-2xx_w+y^2}\right] + \Phi_0 \quad (3.140)$$

which can be rearranged as

$$\Phi = \frac{Q}{2\pi}\ln\left[\ln\frac{1+\frac{R^2}{x_w^2}\left(\frac{R^2+2xx_w}{x^2+y^2}\right)}{1+\frac{R^2}{x_w^2}\left(\frac{R^2-2xx_w}{x^2+y^2}\right)} - \ln\frac{1+\frac{x^2+2xx_w+y^2}{x_w^2}}{1+\frac{x^2-2xx_w+y^2}{x_w^2}}\right] + \Phi_0 \quad (3.141)$$

We are interested in the limiting case where both x_w and Q approach infinity. We define Q_0 as

$$Q_0 = \lim_{\substack{Q\to\infty \\ x_w\to\infty}} \frac{Q}{\pi x_w} \tag{3.142}$$

The logarithms in (3.141) can be written in terms of four logarithms of the form $\ln(1+\epsilon)$, which can be replaced by ϵ, since we will let $x_w \to \infty$, and hence $\epsilon \to 0$. We write for (3.141)

$$\Phi = \lim_{\substack{Q\to\infty \\ x_w\to\infty}} \frac{Q}{4\pi}\left[\frac{R^2}{x_w^2}\frac{4xx_w}{x^2+y^2} - \frac{4xx_w}{x_w^2}\right] + \Phi_0 \tag{3.143}$$

Taking the limit gives

$$\Phi = -Q_0\left[x - \frac{xR^2}{x^2+y^2}\right] + \Phi_0 \qquad (x^2+y^2 \geq R^2) \tag{3.144}$$

which is the potential for a lake in a uniform flow field. Equation (3.144) is, of course, only meaningful outside the lake.

The conjugate stream function to (3.144) is

$$\Psi = -Q_0\left[y + \frac{yR^2}{x^2+y^2}\right] \tag{3.145}$$

The terms containing R^2 in (3.144) and (3.145) are the potential and stream function, respectively, of a *dipole*: the mathematical result of the two coinciding images at the lake or island center. In Section 3.7.5 I will revisit this function, while the interested reader may also refer to Strack (1989).

Exercise 3.12 *Show that (3.144):*

(a) yields a constant potential along the lake boundary;

(b) reduces to the potential for uniform flow when evaluated (infinitely) far from the lake;

(c) is the conjugate harmonic of (3.145).

3.1.18 Ambient Flow Field near a Well

Circular lakes are not common, but may serve as approximations to more natural lakes. The solution obtained earlier, however, can be directly applied to a non-pumping well in a regional flow field. The well bore takes

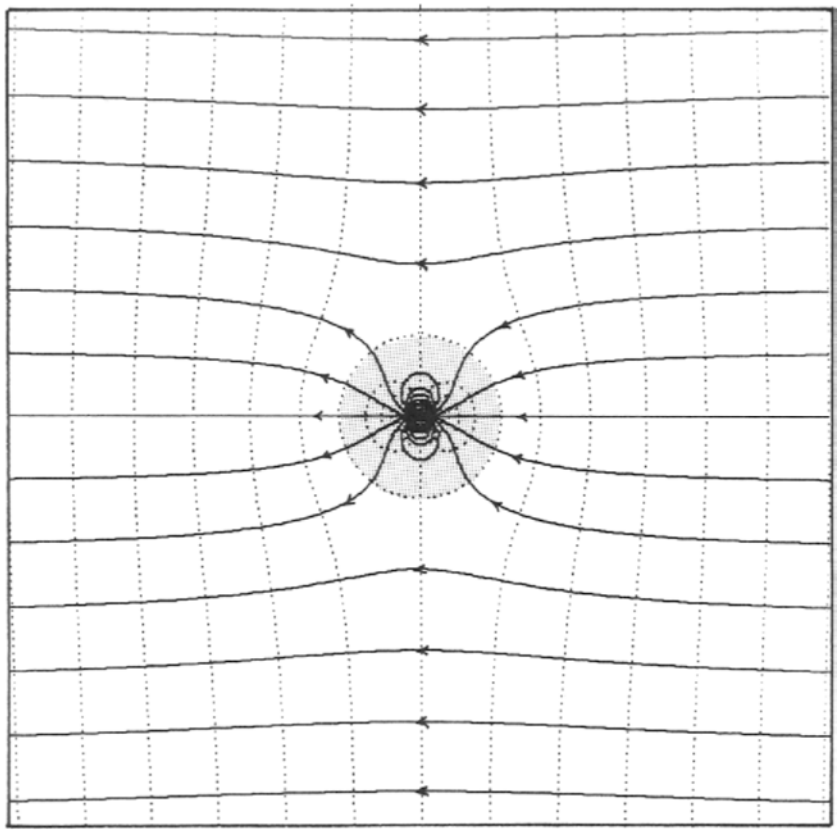

Figure 3.29: Ambient flow field near a non-pumping well.

the place of the lake, while the regional flow is approximated by uniform flow. Equations (3.144) and (3.145) describe the effect of the (dormant) well on the regional flow field, as illustrated by the flow net in Figure 3.29. The flow net inside the well is due to the dipole and has been shaded to indicate that it is not part of the flow domain. It appears from Figure 3.29 that the effect is quite local; just a few well diameters away from the well, the flow becomes nearly uniform again.

Ambient flow rates have been estimated by releasing a tracer in a well and pumping it back after a given time interval (Leap and Kaplan, 1988). In order to conduct such experiments, it is necessary to take into account the effect of the well on the nearby flow field. Observe that the uniform (regional) flow converges toward the well bore and diverges away from the

well. The groundwater discharge rate, just upstream or downstream from the well, is in the x-direction and follows from differentiating (3.144) as

$$Q_x = -\frac{\partial \Phi}{\partial x} = Q_0 \left[1 - \frac{R^2}{x^2 + y^2} + \frac{x R^2 2x}{(x^2 + y^2)^2} \right] \tag{3.146}$$

which becomes, for $x = \pm R$ and $y = 0$,

$$Q_x = 2Q_0 \qquad (x = \pm R \ ; \ y = 0) \tag{3.147}$$

The discharge rate, and thus also the velocity, near the well is twice that of the ambient (uniform) flow. Of course, when moving away from the well the flow rate will gradually reduce to Q_0.

Net Inflow Rate of the Lake

Our solution for a lake so far does not account for any net inflow into the lake or outflow from the lake. Interpreting Figure 3.29 as flow due to a circular lake in a uniform flow field, we note that all water that enters the lake to the left leaves it on the right. In reality, the lake may lose water through an outlet stream, evaporation, or both. From the perspective of the aquifer, the lake is discharging. A recharging lake may obtain its water from a stream which ends in the lake, from overland flow in the surrounding watershed, or from both.

We can account for net inflow in the lake by placing a fictitious well at the center of the lake. Since a well, by itself, has circular equipotentials, the equipotential conditions on the circular lake boundary are not disturbed. The complete solution for Φ becomes

$$\Phi = -Q_0 \left[x - \frac{x R^2}{x^2 + y^2} \right] + \frac{Q}{4\pi} \ln \frac{x^2 + y^2}{R^2} + \Phi_0 \tag{3.148}$$

The complete solution for the stream function becomes

$$\Psi = -Q_0 \left[y + \frac{y R^2}{x^2 + y^2} \right] + \frac{Q}{2\pi} \arctan \frac{y}{x} \tag{3.149}$$

where Q is the net discharge rate of the lake, positive for inflow and negative for outflow.

3.1.19 Large-Diameter Well

Strictly speaking we should always use (3.148) and (3.149) when dealing with a well in a uniform flow field, in order to maintain a constant potential (water level) along the well perimeter. However, the well radius is

usually very small compared to the scale of the flow regime in which we are interested. When R is small, the effect of the dipole term in (3.148) is insignificant (Figure 3.29) and may be omitted, as we usually do. In practical terms this means that, in our model, there is a very small gradient across the well screen, which might have been corrected by including the dipole term, hence using (3.148) instead of (3.110).

There do exist very large-diameter wells, dug by hand, in shallow aquifers. Such wells are useful when the aquifer is very shallow, restricting the drawdown and, consequently, the productivity of a conventional well. Under these conditions, the water table in a conventional well would quickly drop to the aquifer bottom, even for moderate pumping rates. The most important advantage of a large-diameter well is its large storage capacity. This allows a pump to run at full capacity for some time, after which it is shut down to allow the water level in the well to restore itself. A conventional well, with little or no storage, may have unacceptably short pumping times. A large-diameter well has also a somewhat larger average yield, but this may also be achieved by drilling more than one conventional well.

In Figure 3.30 a flow net is plotted for a large-diameter well in a uniform flow field. Because of its large diameter, the flow net has been made with (3.148) and (3.149). The flow net inside the well has been erased, because it is not part of the flow domain.

Figure 3.30 may also be interpreted as that of a circular lake in a uniform flow field, whereby the lake receives water from the aquifer. This water leaves the lake through a surface water outlet, evaporation, or both.

3.2 Areal Recharge

In the groundwater flow problems discussed so far, the water entered the aquifer at discrete locations: through a stream, a lake, or a recharge well. When introducing regional (uniform) flow, we did not elaborate on the source of the groundwater; it came from somewhere far away (mathematically speaking, from infinity). Ultimately, all groundwater comes from precipitation. Rainwater, for instance, may run off into streams or lakes, after which some of it infiltrates into the aquifer ("losing streams"). In general, however, most of the precipitation (rain, snow, etc.) infiltrates into the soil close to where it hits the surface. Some of this infiltrated water is evaporated back into the atmosphere, or taken up by plants and then transpirated off into the atmosphere. Combined, these processes are called *evapotranspiration*. Water that is not evapotranspirated flows downward through the upper unsaturated zone of the soil (*vadose zone*) until it reaches the (saturated) aquifer. This form of *areal recharge* is usually the

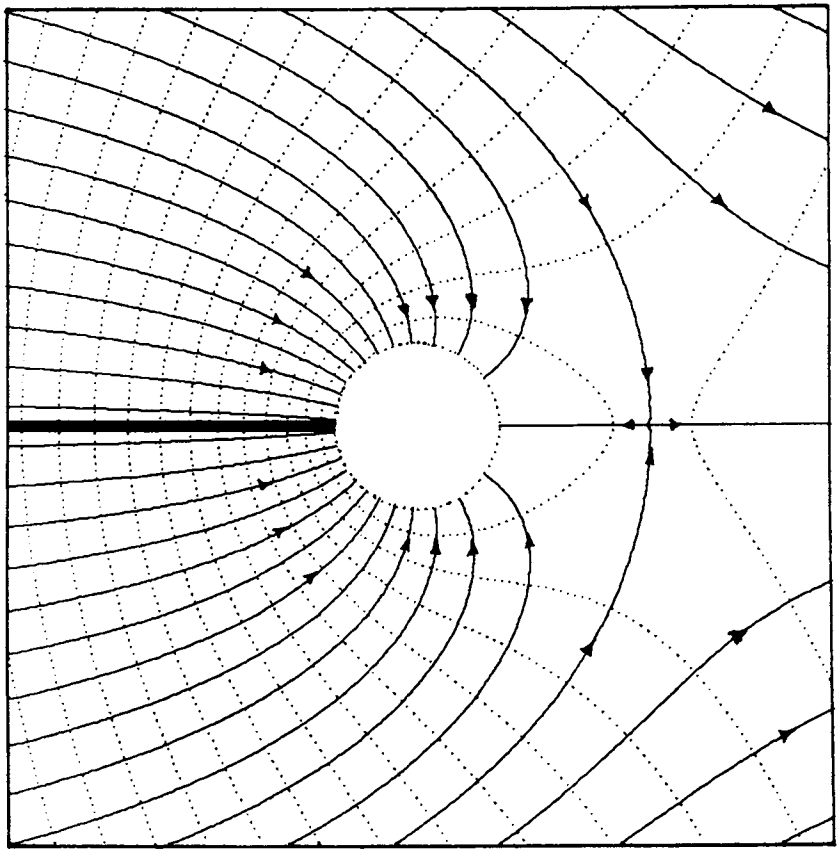

Figure 3.30: Flow net near a large-diameter well.

most important source for groundwater, at least when viewed on a regional scale.

Most climates exhibit wet and dry seasons, causing temporal variations in areal recharge. Different soils have different infiltration capacities, causing spatial variations in recharge. It is possible, and sometimes necessary, to include these variations in our mathematical models. In this section, however, we will limit ourselves to steady-state flow, assuming a recharge rate that is constant in time. This constant recharge rate may be seen as the yearly average for the region. Since the actual recharge rate varies seasonally, our groundwater flow solution will only reflect average conditions; hence, summer and winter flow patterns may differ from our steady-state solution. When necessary, we can and will consider recharge rates that differ from place to place.

3.2.1 Poisson's Equation

Areal recharge causes a vertical downward flow into the aquifer, equal to the areal recharge rate. In a Dupuit–Forchheimer model, however, we either ignore vertical flow, or we treat it in an approximate manner as we will discuss at the end of this chapter. Consequently, we cannot prescribe a vertical specific discharge along the upper aquifer boundary (the water table). Instead, we will include the areal recharge in the continuity equation, which, combined with Darcy's law, will result in a new differential equation for Dupuit–Forchheimer flow: Poisson's equation.

In Figure 3.31, the inflows and outflows are depicted for an elementary aquifer volume of a Dupuit–Forchheimer model. The elementary volume is a column of soil and water that extends over the full saturated aquifer height and has a cross-section that measures Δx by Δy. The center of the column is at the point x, y. The areal recharge rate due to precipitation is N $[L/T]$. The dimensions of N are length over time, because it is a volume of water per unit time per unit area. The dimensions of recharge, therefore, are the same as those commonly used for rainfall: inches per year. We write the continuity of flow equation in the form

$$\text{outflow} - \text{inflow} = 0$$

Combining terms of Q_x and Q_y yields (see Figure 3.31)

$$\begin{aligned} &\left[Q_x(x+\tfrac{\Delta x}{2},y) - Q_x(x-\tfrac{\Delta x}{2},y)\right]\Delta y \\ &+ \left[Q_y(x,y+\tfrac{\Delta y}{2}) - Q_y(x,y-\tfrac{\Delta y}{2})\right]\Delta x + \\ &-N\Delta x\Delta y = 0 \end{aligned} \tag{3.150}$$

We will perform a few operations on (3.150). First, we divide both sides by $\Delta x\Delta y$, then we pass through the limit for $\Delta x \to 0$ and $\Delta y \to 0$, and

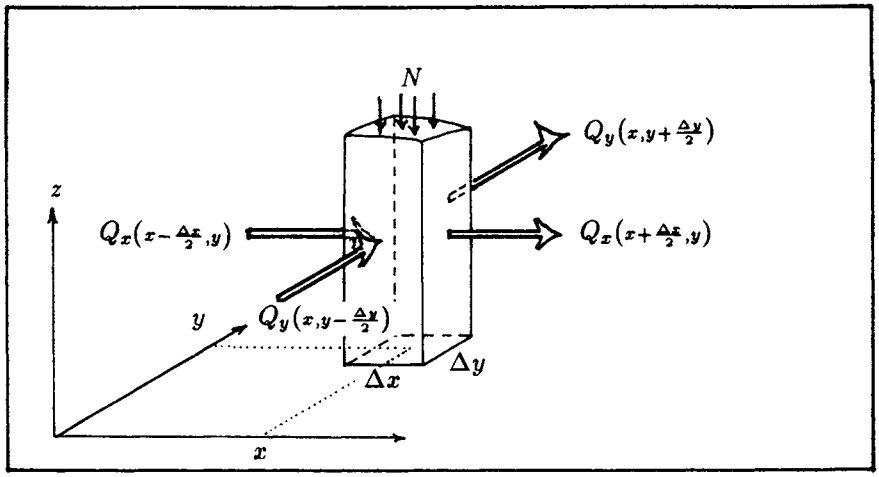

Figure 3.31: Continuity of flow in a Dupuit–Forchheimer model with areal recharge.

finally we bring the term with N to the right-hand side of the equation. The result is

$$\frac{\partial Q_x}{\partial x} + \frac{\partial Q_y}{\partial y} = N \tag{3.151}$$

Combining (3.151) with Darcy's law [see (3.19)] results in the differential equation for Dupuit–Forchheimer flow with areal recharge, which is called Poisson's equation:

$$\frac{\partial^2 \Phi}{\partial x^2} + \frac{\partial^2 \Phi}{\partial y^2} = -N \tag{3.152}$$

As we did before, we may abbreviate (3.152) by writing it in index notation as

$$\partial_{ii}\Phi = -N \tag{3.153}$$

with $(i = 1, 2)$. In symbolic notation, it becomes

$$\nabla^2 \Phi = -N \tag{3.154}$$

Observe that the only difference between Laplace's equation and Poisson's equation is the term $-N$ on the right-hand side of the equation; compare (3.63) and (3.154). The added term is the "source term" that recharges the aquifer in the Dupuit–Forchheimer model.

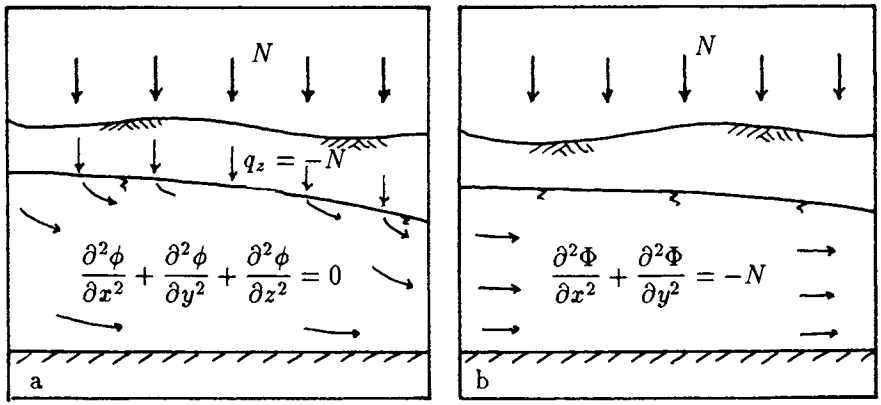

Figure 3.32: Areal recharge in a three-dimensional model (a) and in a Dupuit-Forchheimer model (b).

Areal Recharge in a Three-Dimensional Model

As mentioned before, the actual effect of areal recharge is that of vertical downward flow into the aquifer. In a truly three-dimensional model, therefore, the areal recharge is introduced as a Neumann boundary condition, prescribing a vertically downward specific discharge along the upper aquifer boundary; see Figure 3.32a. In a Dupuit-Forchheimer model, as we have seen, the areal recharge is introduced not as a boundary condition, but as a source term in the differential equation. This leads to the replacement of Laplace's equation by Poisson's equation, see Figure 3.32b.

Rule 3.10 *In a Dupuit-Forchheimer model, steady-state flow with areal recharge is governed by Poisson's equation, while in a three-dimensional model, the areal recharge is a boundary condition to Laplace's equation.*

In the next sections we will explore some elementary solutions to Poisson's equation. These solutions will provide us with some insight into the effects of areal recharge on regional groundwater flow systems.

3.2.2 One-Dimensional Flow with Recharge

We will start with a simple example, solving the same one-dimensional flow problem as in Section 3.1.2, except now there is an areal recharge rate N; see Figure 3.33. Since there is no flow in the y-direction, so that $\partial^2\Phi/\partial x^2 = 0$, Poisson's equation reduces to

$$\frac{d^2\Phi}{dx^2} = -N \tag{3.155}$$

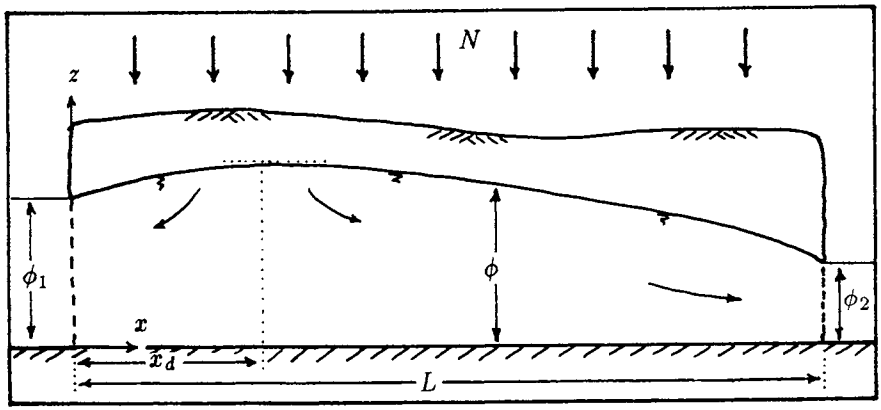

Figure 3.33: One-dimensional unconfined flow with recharge.

The general solution to (3.155) is

$$\Phi = -\frac{N}{2}x^2 + Ax + B \tag{3.156}$$

where A and B are constants to be selected in such a manner that the boundary conditions are satisfied. That (3.156) indeed satisfies Poisson's equation may be verified by substituting it into (3.155). The particular solution that satisfies the boundary conditions in Figure 3.33 ($x = 0$; $\Phi = \Phi_1$ and $x = L$; $\Phi = \Phi_2$) is given by

$$\Phi = -\frac{N}{2}x(x - L) + \frac{\Phi_2 - \Phi_1}{L}x + \Phi_1 \tag{3.157}$$

At first glance, Equation (3.157) does not resemble (3.156). They are the same, however, if A and B in (3.156) are chosen as

$$A = \frac{N}{2}L + \frac{\Phi_2 - \Phi_1}{L} \qquad B = \Phi_1 \tag{3.158}$$

The form of (3.157) makes it easy to see that the boundary conditions are satisfied. Substituting $x = 0$ in (3.157) sets the first two terms to zero, so that $\Phi = \Phi_1$. Substituting $x = L$ sets the first term in (3.157) equal to zero, while the other two terms reduce to Φ_2. Observe that (3.157) is equal to the solution without rainfall (3.37) plus a term that represents the contribution of the recharge, so that

$$\Phi_{recharge} = -\frac{N}{2}x(x - L) \tag{3.159}$$

This added term (3.159) satisfies Poisson's equation. Since Equation (3.37) did already satisfy the boundary conditions, the added term ($\Phi_{recharge}$) has been written in such a way that it does not contribute to the boundaries of the aquifer: $\Phi_{recharge}$ is zero for $x = 0$ and for $x = L$.

Superimposing Laplace and Poisson Solutions

The preceding discussion introduces an interesting concept. Apparently, we can write a solution to a groundwater flow problem with areal recharge as the sum of two solutions: A solution that satisfies Laplace's equation, plus one that satisfies Poisson's equation:

$$\Phi = \Phi_{Laplace} + \Phi_{Poisson} \tag{3.160}$$

where $\Phi_{Poisson}$ fulfills the role of $\Phi_{recharge}$ in (3.159). The combined solution Φ must satisfy Poisson's equation, as indeed it does:

$$\nabla^2\Phi = \nabla^2\Phi_{Laplace} + \nabla^2\Phi_{Poisson} = 0 + (-N) = -N \tag{3.161}$$

This leads to the following general principle.

Rule 3.11 *An existing groundwater flow solution to Laplace's equation may be expanded to include areal recharge by adding one particular solution to Poisson's equation. The combined solution will then satisfy Poisson's equation.*

Water Divide

Let us return to the problem depicted in Figure 3.33. It seems that a *water divide* exists at a distance x_d from the left-hand stream boundary. Water that is infiltrating to the left of the water divide is flowing to the left and leaves the aquifer through the left-hand stream. Water which infiltrates to the right of the water divide is moving to the right and ends up in the right-hand stream. At the water divide itself, the horizontal groundwater velocities are zero, as if a groundwater particle at that point cannot decide which way to go. This condition of zero horizontal flow allows us to determine the location x_d of the water divide as follows. We set Q_x equal to zero and use Darcy's law:

$$Q_x = -\frac{d\Phi}{dx} = 0 \tag{3.162}$$

Thus, at the water divide the derivative of the potential is zero, which means that the derivative of the head ϕ is zero as well. This is also evident

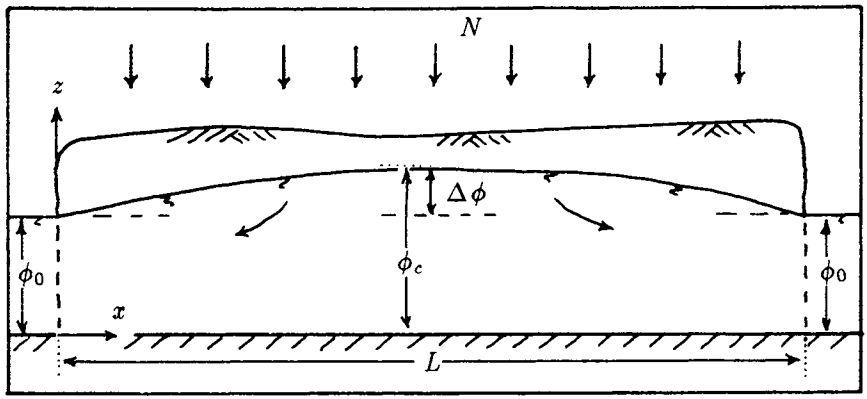

Figure 3.34: Groundwater mounding due to areal recharge.

from Figure 3.33, where the water table exhibits a horizontal tangent (zero slope) at the water divide. Differentiating (3.157) and setting it zero for $x = x_d$ yields

$$-Nx_d + \frac{NL}{2} + \frac{\Phi_2 - \Phi_1}{L} = 0 \tag{3.163}$$

which results in the following expression for x_d:

$$x_d = \frac{L}{2} + \frac{\Phi_2 - \Phi_1}{NL} \tag{3.164}$$

If the water levels in the two streams are the same, and hence if $\Phi_1 = \Phi_2$, the location of the water divide is $x_d = L/2$. The water divide for that case occurs midway between the two streams, as intuitively seems right. It is possible for x_d to assume values smaller than zero or larger than L, depending on the values of Φ_1 and Φ_2. In those cases there simply is no water divide in the aquifer; all infiltrated rainwater moves to the right if $x_d \leq 0$ or to the left if $x_d \geq L$.

Groundwater Mounding

If we compare the groundwater table in Figure 3.5 with the water table in Figure 3.33, we see that areal recharge raises the groundwater table, causing *groundwater mounding*. The degree of groundwater mounding depends on several factors, such as the recharge rate, the aquifer hydraulic conductivity, and the distance between the streams. To gain insight into the role of these parameters, we will consider the special case whereby the water levels in the two streams are the same: $\phi_1 = \phi_2 = \phi_0$ (see Figure 3.34). With Φ_1

equal to Φ_2, the second term on the right-hand side in (3.157) vanishes; hence,

$$\Phi = -\frac{N}{2}x(x - L) + \Phi_0 \tag{3.165}$$

The maximum head ϕ_c occurs midway between the two streams (see Figure 3.34) and follows from (3.165) by setting $x = L/2$:

$$\tfrac{1}{2}k\phi_c^2 - \tfrac{1}{2}k\phi_0^2 = \frac{NL^2}{8} \tag{3.166}$$

where (3.34) has been used to replace the potentials by heads (water table elevations). We may rewrite (3.166) as follows:

$$\tfrac{1}{2}k(\phi_c - \phi_0)(\phi_c + \phi_0) = \frac{NL^2}{8} \tag{3.167}$$

The mounding $\Delta\phi$ in the center of the aquifer is $\Delta\phi = \phi_c - \phi_0$, which becomes, with (3.167),

$$\Delta\phi = \frac{NL^2}{8k\bar{\phi}} \tag{3.168}$$

where $\bar{\phi}$ is the average head in the aquifer defined by

$$\bar{\phi} = \frac{\phi_c + \phi_0}{2} \tag{3.169}$$

We may introduce an average transmissivity $\bar{T} = k\bar{\phi}$, with which Equation (3.168) becomes

$$\Delta\phi = \frac{NL^2}{8\bar{T}} \tag{3.170}$$

The mounding appears to be very sensitive to the distance between the two streams: It is proportional to L squared! Furthermore, the mounding is linearly proportional to the recharge rate N, while it is inversely proportional to the (average) transmissivity $\bar{T}$. Although these results were obtained for this special case of one-dimensional flow, we may generalize our findings to real-world regional settings. The geometry of the streams and lakes then take the place of the parameter L in Figure 3.34. This geometry is always given and does not change. What is usually not given is the average areal recharge rate and the average aquifer transmissivity. During groundwater modeling exercises we often try to match modeled heads with observed heads. In the presence of areal recharge we could also say that we are trying to match modeled groundwater mounding with observed groundwater mounding. We can change the mounding in the model by changing either the recharge rate N or the hydraulic conductivity k. As appears from (3.170), increasing N has the same effect as decreasing k (thus decreasing $\bar{T}$). This leads to the following conclusion:

Rule 3.12 *Trying to match modeled groundwater mounding with observed groundwater mounding provides insight in the ratio of recharge over transmissivity (N/T). By itself, however, it cannot lead to an estimate of either one of these parameters individually.*

We will come back to this issue in Chapter 5 when discussing computer modeling of regional flow.

Exercise 3.13 *The following data are given for the case of Figure 3.33:* $N = 4$ *inches/year,* $k = 30$ *ft/day,* $L = 5,000$ *ft,* $\phi_1 = 35$ *ft, and* $\phi_2 = 30$ *ft.*

(a) Calculate the head ϕ_c *at the center of the aquifer.*

(b) Calculate the discharge Q_x *in the aquifer at: (1) the left-hand stream, (2) the center of the aquifer, and (3) the right-hand stream.*

(c) Calculate the position x_d *of the water divide.*

(d) What is the largest value $(\phi_1)_{max}$ *of the water level in the right-hand stream for which there is still a water divide in the aquifer?*

3.2.3 Radial Flow with Recharge

Another elementary solution to Poisson's equation is that of areal recharge on a circular island. The problem may seem contrived, but will prove useful as a building block for more realistic flow problems. We will derive the solution using continuity of flow considerations rather than integrating the differential equation, as we did in Section 3.1.8 for the solution for a well. Applying continuity of flow to the problem depicted in Figure 3.35 leads to the following observation. The total amount of water per unit time that crosses the circle with radius r in Figure 3.35 is equal to the recharge rate N times the surface area of the circle. The discharge vector Q_r, across the circle, is defined as the amount of water per unit time per unit length of the circle. Consequently, Q_r is equal to the total flow across the circle divided by the circumference of the circle:

$$Q_r = \frac{N\pi r^2}{2\pi r} = \frac{Nr}{2} \tag{3.171}$$

Because of radial symmetry, the potential depends only on the radial distance r, so that with Darcy's law,

$$Q_r = -\frac{d\Phi}{dr} \tag{3.172}$$

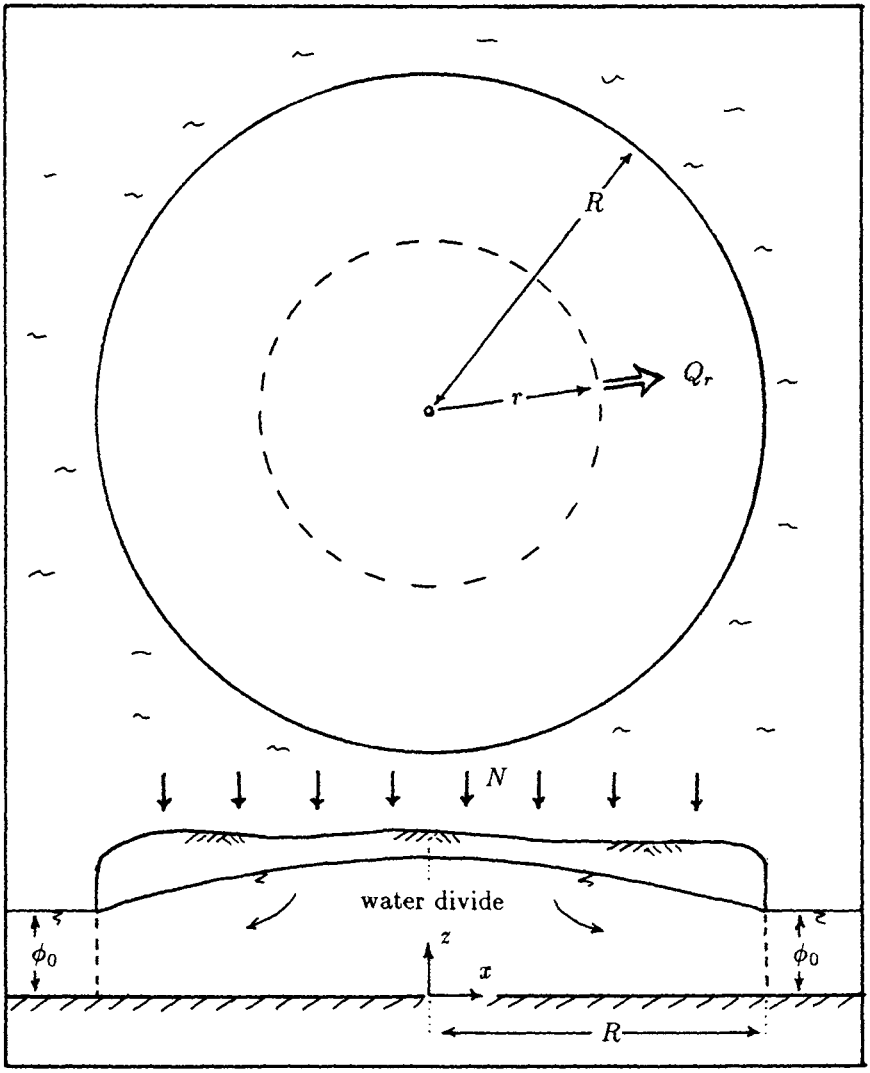

Figure 3.35: Areal recharge on a circular island.

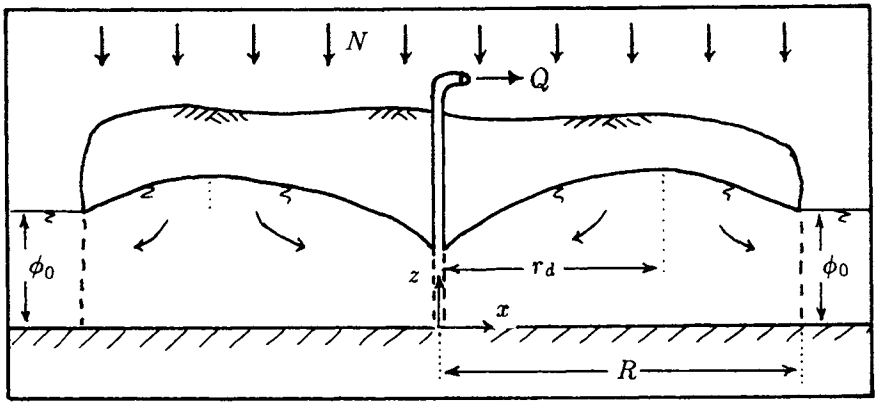

Figure 3.36: A well at the center of a circular island with areal recharge.

As follows from (3.171) and (3.172), the potential Φ can be obtained by integrating (3.171) with respect to r, yielding

$$\Phi = -\frac{N}{4}r^2 + C \tag{3.173}$$

where C is a constant of integration. At the boundary of the island, thus for $r = R$, the head is given: $\phi = \phi_0$. With this boundary condition (3.173) becomes

$$\Phi = -\frac{N}{4}(r^2 - R^2) + \Phi_0 \tag{3.174}$$

The maximum value for the potential, and thus also for the water table, occurs at the center of the island where r is equal to zero. The groundwater, therefore, mounds up like a dome with a *water divide* at the center of the island, see Figure 3.35. For this case of radial flow, the water divide is a single point. Previously, when discussing one-dimensional flow (see Figure 3.33), the water divide was a line perpendicular to the plane of the figure.

A Well at the Center of the Island

In Figure 3.36, the problem depicted in Figure 3.35 has been expanded by adding a well at the center of the island. In Section 3.2.2, we discussed the concept of superimposing a solution to Poisson's equation onto a solution to Laplace's equation. Applying this concept to the problem in Figure 3.36 leads to the superposition of (3.174) onto the solution for a well at the center of the island without recharge, as given by (3.89),

$$\Phi = -\frac{N}{4}(r^2 - R^2) + \frac{Q}{2\pi}\ln\frac{r}{R} + \Phi_0 \tag{3.175}$$

Water Divide

Figure 3.36 exhibits a water divide on either side of the well. In fact, the water divide is a concentric circle about the well with radius r_d. This radius can be determined by use of the condition that the horizontal discharge Q_r, at the water divide, is equal to zero, as was done for the one-dimensional flow problem (Section 3.2.2). This leads to the following analysis. Using Darcy's law we have

$$Q_r = -\frac{d\Phi}{dr} = 0 \qquad (r = r_d) \tag{3.176}$$

Differentiating (3.175) and substituting the result into (3.176) gives

$$\frac{Nr_d}{2} - \frac{Q}{2\pi}\frac{1}{r_d} = 0 \tag{3.177}$$

This yields for the location of the water divide

$$r_d = \sqrt{\frac{Q}{\pi N}} \tag{3.178}$$

The result (3.178) could also have been obtained in a more direct manner, by inspection of Figure 3.36. Note that all infiltrated water within the circular water divide ends up in the well. The well discharge Q, therefore, is equal to the total amount of aquifer recharge that falls inside the (circular) water divide. Mathematically, this means

$$Q = N\pi r_d^2 \tag{3.179}$$

which leads directly to the expression for r_d as given by (3.178).

Just as in the case of one-dimensional flow, there may not always be a water divide. If the well pumps more water than is recharged on the entire island, the water divide is pushed beyond the island boundary. In practical terms, this means that there is no water divide. The well pumps up all of the aquifer recharge plus some water from outside the island. The critical case, of course, is when r_d just equals R, which is the case when $Q = N\pi R^2$.

3.2.4 Circular Irrigator or Percolating Pond

The solutions to Poisson's equation presented so far are instructive for illustrating some basic concepts, such as groundwater mounding and water

divides. They are, however, of limited practical use. We will rarely encounter parallel streams, much less circular islands. Yet, as we will see, we can use the solution (3.174) to construct a useful elementary solution to Poisson's equation, which can be combined with other elementary solutions.

In the upper part of Figure 3.37, a circular recharge area is depicted in plan view: a source disc. Inside the area there is a recharge rate N, so that the flow in the aquifer underneath the source disc is governed by Poisson's equation. Outside the source disc, where there is no areal recharge, the flow is governed by Laplace's equation. The recharge area may be thought of as belonging to a circular irrigator, the upper cross-section in Figure 3.37, or a percolating pond or wetland, the bottom cross-section. In all cases we assume that the recharge rate (percolation rate) is equal to N. The solution to the problem in Figure 3.37 needs to satisfy Poisson's equation underneath the source disc ($r \leq R$) and Laplace's equation on the outside ($r > R$). The solution is given by Strack (1989) and has the following form:

$$\begin{aligned} \Phi &= -\frac{N}{4}(r^2 - R^2) + C \qquad (r \leq R) \\ \Phi &= -\frac{NR^2}{2} \ln \frac{r}{R} + C \qquad (r > R) \end{aligned} \tag{3.180}$$

Note that we are actually dealing with two solutions: one for the inside of the source disc, and one for the outside. The inside solution is that of recharge on a circular island; see (3.174). The outside solution, the second formula in (3.180), is that of a recharge well at the center of the source disc. The recharge well has an injection rate that is just equal to the total recharge of the source disc. Both solutions exhibit radial flow, and both solutions send the same total amount of water across the boundary of the source disc. Consequently, the discharge rate Q_r is continuous across the boundary: $Q_r^{(i)} = Q_r^{(o)}$ (see Figure 3.37). We may verify this continuity condition by differentiating both expressions in (3.180) and substituting $r = R$. Calculating $Q_r^{(i)}$ for the inside solution gives

$$Q_r^{(i)} = -\frac{d\Phi}{dr} = -\frac{d}{dr}\left[-\frac{N}{4}(r^2 - R^2) + C\right] = \frac{N}{2}r \quad (r \leq R) \tag{3.181}$$

Calculating $Q_r^{(o)}$ for the outside solution leads to

$$Q_r^{(o)} = -\frac{d\Phi}{dr} = -\frac{d}{dr}\left[-\frac{NR^2}{2} \ln \frac{r}{R} + C\right] = \frac{NR^2}{2r} \quad (r > R) \tag{3.182}$$

The discharge vector at the boundary of the circle is obtained by setting r

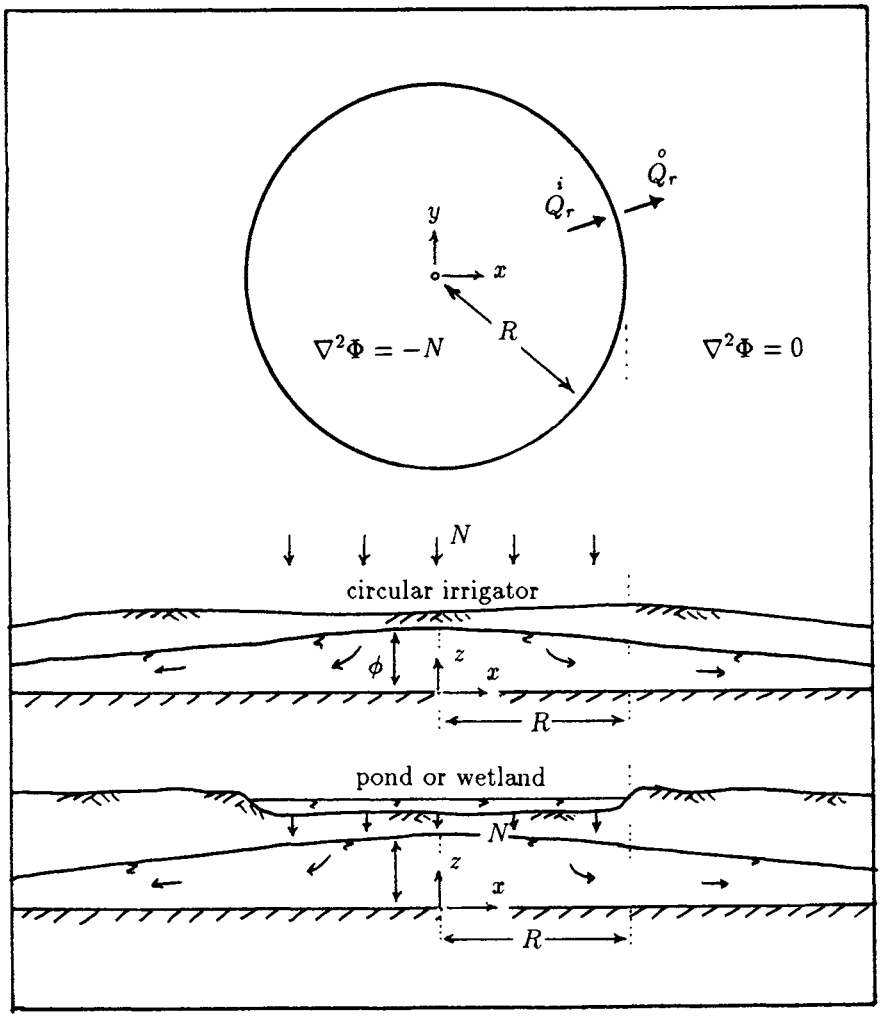

Figure 3.37: Plan view and cross-sections of a circular irrigator and pond or wetland, respectively.

equal to R, which yields

$$Q_r^{(i)} = Q_r^{(o)} = \frac{N}{2}R \qquad (r = R) \tag{3.183}$$

The inside and outside solution, therefore, fit together in that they assure continuity of flow across the boundary of the disc. The two solutions must also fit together by having the same head (or potential) at the disc boundary. This is readily verified by substituting $r = R$ in both expressions in (3.180). The potential at $r = R$ is equal to C, a constant of integration which can be calculated by requiring a particular head at some reference point in the aquifer, as we did when superimposing wells in Section 3.1.9.

It seems a little awkward to have two solutions for a single flow problem. It may be helpful, for that matter, to write these solutions symbolically as one solution, as follows:

$$\Phi = N\, G_p(x, y, x_0, y_0, R) \tag{3.184}$$

What we did in (3.184) is to write the potential as the product of the recharge rate N times a *coefficient function* G_p. With reference to (3.180), the coefficient function is defined as

$$G_p(x, y, x_0, y_0, R) = \\ -\frac{1}{4}\left[(x - x_0)^2 + (y - y_0)^2 - R^2\right] \qquad (\sqrt{(x-x_0)^2+(y-y_0)^2} \leq R) \tag{3.185}$$

$$G_p(x, y, x_0, y_0, R) = \\ -\frac{R^2}{4} \ln \frac{(x - x_0)^2 + (y - y_0)^2}{R^2} \qquad (\sqrt{(x-x_0)^2+(y-y_0)^2} \geq R)$$

where the radial distance r has been expressed in terms of the point x, y, at which the potential is calculated, and the center of the disc x_0, y_0. In the second formula of (3.185), we also used the basic relation $\ln a = \frac{1}{2} \ln a^2$. The coefficient function G_p is now "hiding" the two different solutions for inside and outside the circular area. Imagine this function programmed in Fortran: We would have one function subprogram G_p with the arguments listed in (3.184). Inside the function subprogram, a test would be conducted to determine whether the point x, y is inside or outside the disc. Based on the outcome of that test, the function subprogram would select one of the two expressions in (3.185). For us, the user, it looks as if we have just one function G_p which represents a pond, a wetland, or a circular irrigator.

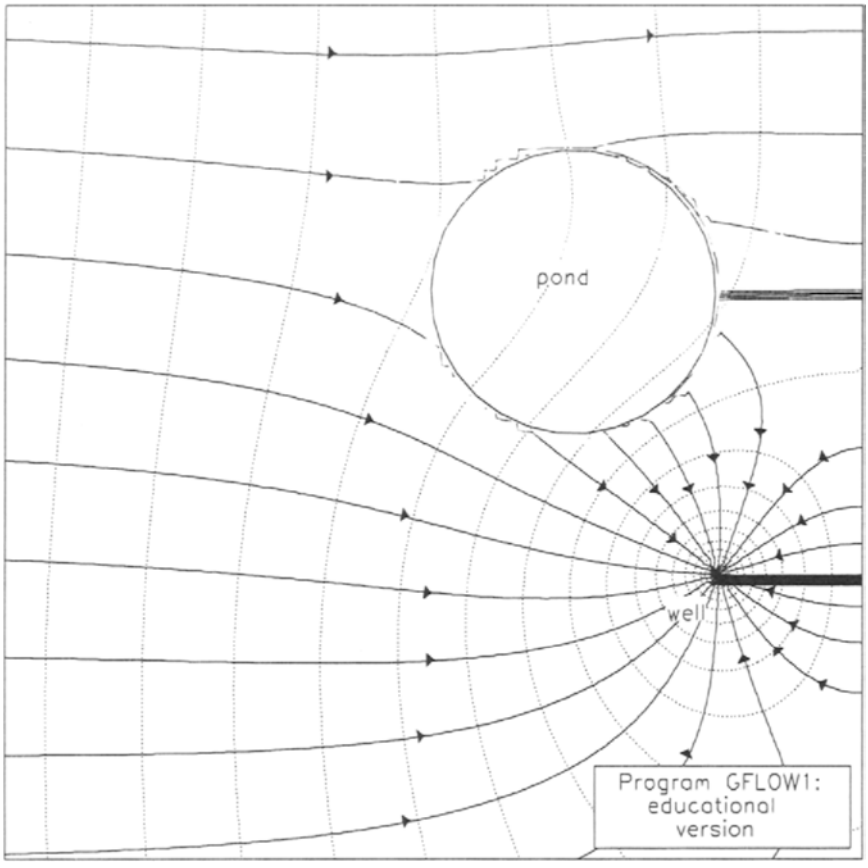

Figure 3.38: Flownet for a well near a pond and a stream. (GFLOW1 data file: problem6.dat)

3.2.5 Well near a Pond and a Stream

The preceding elementary solution can be combined with other, previously obtained, solutions. In Figure 3.38, a flow net is plotted for a well near a pond and a stream. There is also a regional uniform flow rate Q_0 toward the stream. The well and the pond both have images with respect to the stream boundary in order to obtain an equipotential condition along the stream. The solution for the flow problem depicted in Figure 3.38 is

$$\Phi = \frac{Q}{4\pi} \ln \frac{(x - x_w)^2 + (y - y_w)^2}{(x + x_w)^2 + (y - y_w)^2} - Q_0 x$$
$$+N \left[G_p(x, y, x_0, y_0, R) - G_p(x, y, -x_0, y_0, R) \right] + \Phi_0 \quad (3.186)$$

The second function G_p in (3.186) is the image of the pond with respect to the stream boundary: the y-axis in Figure 3.38. Since we only consider points x, y to the left of the stream, we will always be outside the image pond! Consequently, we will always be using the second formula in (3.185) for the image pond. Hence, we might also have written

$$\begin{aligned}\Phi = &\frac{Q}{4\pi}\ln\frac{(x-x_w)^2+(y-y_w)^2}{(x+x_w)^2+(y-y_w)^2} - Q_0 x \\ &+NG_p(x,y,x_0,y_0,R) + \frac{NR^2}{4}\ln\frac{(x+x_0)^2+(y-y_0)^2}{R^2} \\ &+\Phi_0 \end{aligned} \tag{3.187}$$

Equation (3.187) is essentially the same as (3.186), except that in (3.187) we recognized the fact that we are always using a well to represent the image pond.

You may have noticed that the flow net in Figure 3.38 is incomplete: there are no streamlines underneath the pond, just equipotentials. The reason for this is not that there are no streamlines there, but that the *stream function*, used to generate them, *does not exist underneath the pond.* This is a consequence of Rule 3.5, which says that the stream function exists only if the potential function satisfies the equation of Laplace. Underneath the pond, therefore, where the governing differential equation is Poisson's equation, the stream function does not exist. Yet when the data file "problem6.dat" is run to reproduce Figure 3.38, red (stream)lines do appear underneath the pond. The reason for this is that the flow problem in Figure 3.38 does include solutions to Laplace's equation (well, image well, and image pond) which do generate Ψ-values underneath the pond. The contouring routine, which produces the streamlines, does not distinguish between these and the legitimate Ψ-values outside the pond. In producing Figure 3.38, therefore, the "streamlines" underneath the pond have been erased.

3.2.6 Tracing Streamlines

Although the stream function may not exist underneath the pond, streamlines do exist, of course. It is just that we do not have a (valid) stream function to generate them. Next we will discuss an alternative way to determine streamlines, a procedure for which we do not need a stream function. In Figure 3.39, a streamline section is depicted with two points defined on the streamline: $\overset{1}{x}_i$ and $\overset{2}{x}_i$. The points may be defined either in two dimensions ($i = 1, 2$) or in three dimensions ($i = 1, 2, 3$). Associated with each of these points is a *residence time* t_1 and t_2, respectively. The residence

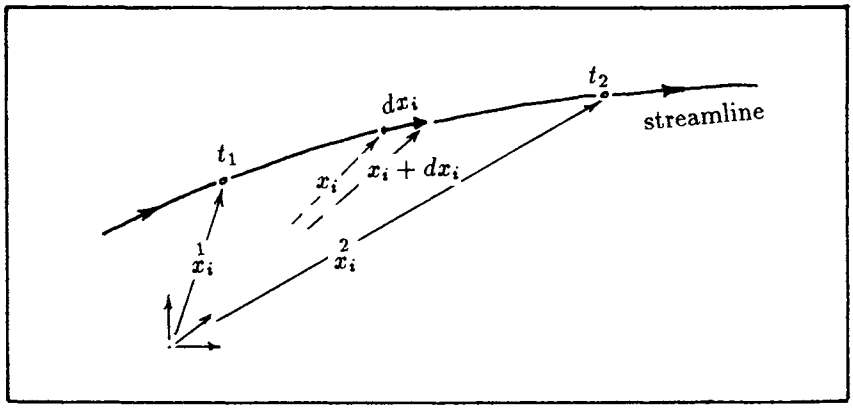

Figure 3.39: Tracing streamlines.

time is the time it takes a water particle to move from its entry point in the aquifer to the location in question: point $\overset{1}{x}_i$ or $\overset{2}{x}_i$ in Figure 3.39. Consequently, in view of the direction of flow in Figure 3.39, the residence time t_2 is larger than the residence time t_1. Our objective is to find successive points x_i along the streamline. The computational procedure for *tracing* a streamline will be explained with reference to Figure 3.39.

Assume we know the location $\overset{1}{x}_i$ on the streamline and want to determine the location $\overset{2}{x}_i$. We may calculate $\overset{2}{x}_i$ by use of the following definite integral:

$$\overset{2}{x}_i = \overset{1}{x}_i + \int_{\overset{1}{x}_i}^{\overset{2}{x}_i} dx_i \tag{3.188}$$

where dx_i is an infinitesimal vector along the streamline; see Figure 3.39. We may rewrite the integral in (3.188) in terms of residence times as

$$\overset{2}{x}_i = \overset{1}{x}_i + \int_{t_1}^{t_2} \frac{dx_i}{dt} dt \tag{3.189}$$

The term dx_i/dt is the definition of the groundwater flow velocity v_i, so that (3.189) may also be written as

$$\overset{2}{x}_i = \overset{1}{x}_i + \int_{t_1}^{t_2} v_i dt \tag{3.190}$$

As appears from (3.190), tracing streamlines is accomplished by integrating the velocity of a groundwater particle with respect to its residence time. The integration can be carried out analytically, but only for a few trivial

cases. In general, when streamlines are traced in groundwater flow models, (3.190) will have to be integrated numerically.

3.2.7 Travel Times

The concept of a *residence time* or *travel time* (which is the same) should not be confused with *real time*. In other words, the fact that there are residence times associated with our groundwater flow solutions does not mean that our solutions are time-dependent: We are still only talking about steady-state groundwater flow. The function of residence time in (3.190) is that of a parameter with which we measure distance along a streamline, in much the same way as light-years are used to measure distances between celestial bodies. On the other hand, following that analogy, if a star is 100 light-years away from us, the light from that star has traveled for a *time* period of 100 years before it arrived at our location. Similarly, if the residence time or travel time of a water particle is 100 years, then that particle has traveled for a period of 100 years through the aquifer before arriving at its current position.

Travel times are important in the context of groundwater pollution. Short travel times, on the order of a few days or months, imply that contaminants are moving quickly through the aquifer with little time to decay, volatilize, or otherwise be reduced in concentration. When travel times of contaminants are in the order of several years or decades, as is not uncommon, then there is substantial "response time" to intercept the contaminants. Furthermore, because of the long travel time, the contaminant concentrations may have been substantially reduced by adsorption to the soil, and by physical, chemical, and biological degradation processes.

Program GFLOW1 supports the computation of travel times along streamlines by plotting markers on the streamlines at specified travel time intervals. For instance, if the travel time interval is specified to be one year, the total travel time (in years) of a water particle traveling along a streamline can be found by simply counting the number of markers on that streamline.

Exercise 3.14 *Following the instructions in the file* problem6.dat, *trace some streamlines inside and outside the pond in Figure 3.38. Plot markers for residence times using several different time intervals.*

3.2.8 Wellhead Protection

Drinking-water companies, which use groundwater as a resource, employ high-capacity wells that are usually clustered in one or more *well fields*.

Groundwater flow patterns in and near these well fields are of interest from the perspective of *wellhead protection*. Under the U.S. Environmental Protection Agency's wellhead protection program, drinking-water companies must develop a plan to protect the integrity of the groundwater entering their production wells. These plans call for land use restrictions based on the *capture zones* of the wells in combination with groundwater travel times within these capture zones (USEPA, 1987). The capture zone of a well is defined as the domain under which part or all of the groundwater ends up in the well. Consequently, land use restrictions may apply to parts of these capture zones. For instance, in zones where the groundwater reaches a well within one or two years, land use control is more urgent than in other parts of a capture zone, where the travel times are one or more decades. Groundwater modeling is usually the only practical way to delineate these capture zones and estimate the groundwater travel times in them.

In Figure 3.40, the capture zones and some travel time *isochrones* are depicted for a fictitious well field intercepting water from a uniform flow field. As observed from Figure 3.40, there may be more than one capture zone belonging to a single well. For instance, the most downstream well in Figure 3.40 has a capture zone that is split up into two subzones, one above and one below the capture zone of the center well. The lower subzone, in turn, is also broken up into two zones, located above and below the most upstream well, respectively. The example well field has only three wells, real world well fields may have more wells, resulting in even more complex capture zone patterns.

Isochrones of travel times are lines from which all water particles travel to the well in an equal amount of time. The capture zones and isochrones in Figure 3.40 have been generated with EPA's well-head protection code W*h*AEM (Well-head Analytic Element Model). The code automatically generates the capture zones and isochrones based on a few simple user instructions.

In Figure 3.41, the same setting as depicted in Figure 3.40 has been modeled with GFLOW1. Unlike W*h*AEM, GFLOW1 does not support special routines to automatically generate capture zones and isochrones of travel times. Instead of the solid line isochrones in Figure 3.40, in Figure 3.41 sets of streamlines have been plotted using markers to indicate travel time intervals. These streamlines have been traced backwards in time starting at the wells. The marker patterns mark the positions of the travel time isochrones, as indicated in Figure 3.41. The markers are alternating dashes or triangles which are oriented perpendicular to a line from the well to the marker. In this manner it is easier to decide which markers belong to which well.

The capture zones in Figure 3.41 are not sharply defined, they may

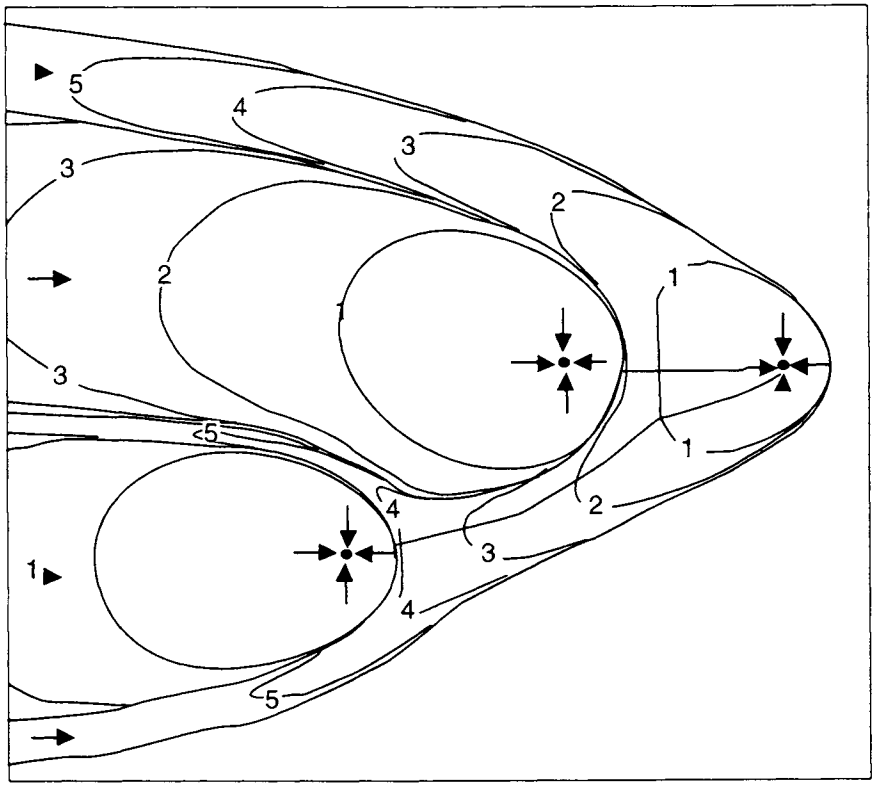

Figure 3.40: Capture zones and isochrones for a well field in a uniform regional flow field as produced by USEPA's program WHAEM. The isochrones are labeled in years.

be delineated with greater accuracy by tracing additional streamlines in between the streamlines that currently bound neighboring capture zones. Keep in mind, however, that the capture zones in both Figure 3.40 and Figure 3.41 are obtained by use of average pumping rates for the wells and under steady-state groundwater flow conditions. In reality, the various wells are rarely pumped at these average rates. Instead, a particular well may be pumped to capacity for several months, after which it is switched off for a few months. Combined with seasonal variations in recharge, this will cause the actual capture zones to vary in time, particularly near the wellfield. The precision in the delineation of the capture zones in Figure 3.40, therefore, is of only relative practical value. In Chapter 5 we will revisit this issue when comparing transient and steady-state flow solutions.

Exercise 3.15 *Following the instructions in file* problem7.dat, *recreate the travel-time capture zones in Figure 3.41 by starting streamlines from cursor-selected points. Also create new tavel-time capture zones by changing the direction of the uniform flow field.*

3.3 Multiple Aquifers

Real-world aquifers rarely resemble the nice homogeneous sand boxes we sketched in the previous sections. Aquifers are defined by geological formations, and they inherit all their complexity. Geological formations are often *stratified*, which means that they are composed of roughly horizontal layers of both low- and high-permeability soils or rocks. Even if we speak about a sand and gravel aquifer, we are probably still dealing with a stratified aquifer. When drilling a well in such an aquifer, we usually encounter different layers of sand and gravel, whose conductivities may differ by several factors. Yet, as we will see in Section 3.4, for most practical purposes we may still treat them as single homogeneous aquifers. Even drilling through some occasional clay does not automatically imply that our single-aquifer representation will be unreasonable. For instance, if an aquifer is mostly sandy with some small horizontal clay lenses, its hydraulic behavior will be quite similar to that of our homogeneous sand boxes; see Figure 3.42a. On the other hand, if the clay layer or layers show up in all borings in the area, we may really be dealing with multiple aquifers rather than one single aquifer. These clay layers may be locally permeable, leaking water from one aquifer into another. They may also be locally absent, connecting the adjacent aquifers and making them act (locally) as one single aquifer; see Figure 3.42b.

It is important to point out that the situation depicted in Figure 3.42b

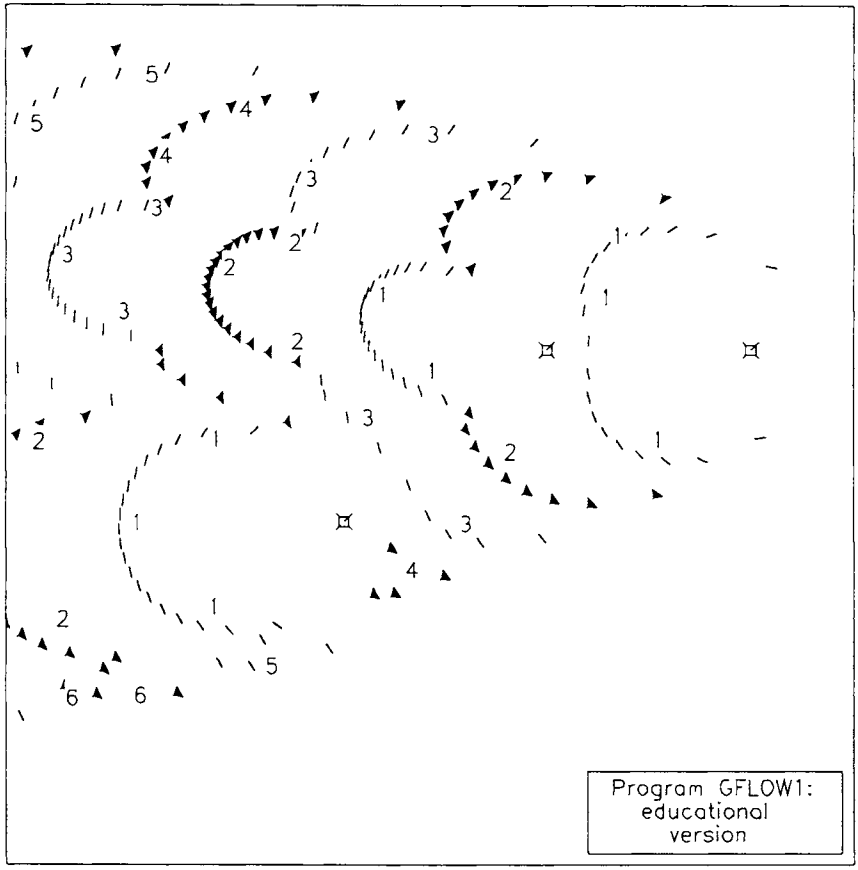

Figure 3.41: Isochrones for a well field in a uniform flow. The isochrones are labeled in years. (GFLOW1 file: problem7.dat)

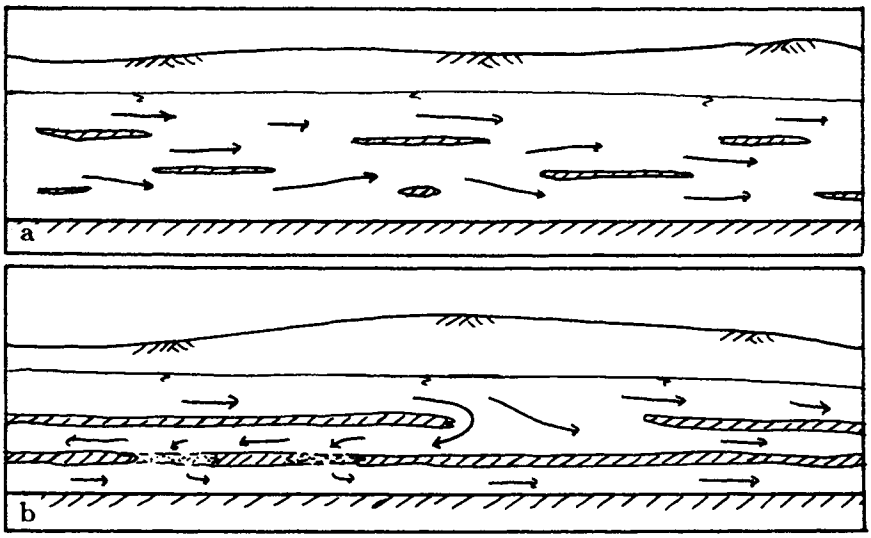

Figure 3.42: A single aquifer with small clay lenses (a), and multiple aquifers separated by discontinuous or locally leaky clay layers (b).

does not automatically require a three-dimensional groundwater flow model. If the distances between interconnections or leakage areas are large as compared to the thicknesses of the aquifers, we can still apply the Dupuit–Forchheimer approximation to each of the individual aquifers. This leads to multi-aquifer Dupuit–Forchheimer models, which are often referred to as *multi layer models* or *quasi three-dimensional models*. Many numerical models support multiple layers. At the time of this writing, there is only one operational analytic element model designed to solve multiple aquifer flow: MLAEM (Multi-Layer Analytic Element Model). The code has been written by Strack and applied to several large scale projects (e.g., de Lange, 1991).

The description of flow in such interconnected multiple-aquifer systems is exceedingly complicated. It requires detailed knowledge about the separating clay layers: Where are they absent, and if leaking, what are their spatially varying resistances to (vertical) flow? Groundwater flow modeling under these conditions is difficult. The hydrologist must deal with many uncertain parameters and try to match modeled piezometric head surfaces with observed heads in several aquifers simultaneously. In many cases piezometric head data are not even available for all aquifers (or are insufficient).

In this section, we will try to gain some insight into multiple aquifer

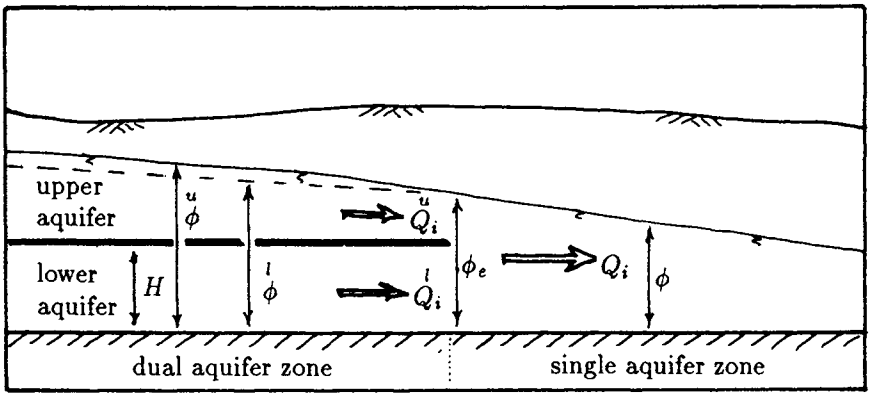

Figure 3.43: Flow in an aquifer with a discontinuous aquiclude.

flow by considering two interconnected aquifers, which locally act as one aquifer, while they are elsewhere fully separated. Hence, the clay layer is either present and impermeable, or it is absent: We do not consider leakage through the clay layer. We will introduce a new potential function, *the comprehensive potential*, in order to facilitate the description of flow in these dual aquifer systems.

3.3.1 The Comprehensive Potential

Strack (1981a, 1981b) introduced the concept of a comprehensive potential to solve flow in aquifers with clay laminae. The technique was first applied to the dual aquifer system near the Tennessee-Tombigbee Waterway (Strack and Haitjema, 1981a, 1981b).

We will explain the comprehensive potential concept with reference to Figure 3.43, which exhibits two zones: a single aquifer zone and a dual aquifer zone. In the dual aquifer zone, we distinguish between an upper and a lower aquifer, separated by an impervious clay layer. The heads in both the upper and lower aquifer are measured with respect to the base of the lower aquifer. At the edge of the clay layer, the heads in the upper, lower and single aquifer zone are the same:

$$\overset{u}{\phi}_e = \overset{l}{\phi}_e = \phi_e \tag{3.191}$$

Similarly, at the clay layer edge, the vectorial sum of the discharge vectors in the upper and lower must equal the discharge vector in the single aquifer zone:

$$\overset{u}{Q}_i + \overset{l}{Q}_i = Q_i \qquad \text{(at clay layer edge)} \tag{3.192}$$

Equation (3.192) is simply a statement of continuity of flow. The discharge potential in the single aquifer zone is given by (3.34),

$$\Phi = \tfrac{1}{2}k\phi^2 \tag{3.193}$$

The discharge potential for the lower aquifer is given by (3.60) as

$$\begin{aligned} \overset{l}{\Phi} &= kH\overset{l}{\phi} - \tfrac{1}{2}kH^2 \qquad (\overset{l}{\phi} \geq H) \\ \overset{l}{\Phi} &= \tfrac{1}{2}k\overset{l}{\phi}^2 \qquad (\overset{l}{\phi} \leq H) \end{aligned} \tag{3.194}$$

where the second equation applies to unconfined conditions in the lower aquifer (not depicted in Figure 3.43). The discharge potential for the upper aquifer is defined as

$$\overset{u}{\Phi} = \tfrac{1}{2}k(\overset{u}{\phi} - H)^2 \tag{3.195}$$

This is a new potential definition, whose validity may be verified by applying Darcy's law,

$$\overset{u}{Q}_i = -\frac{\partial \overset{u}{\Phi}}{\partial x_i} = -\tfrac{1}{2}k2(\overset{u}{\phi} - H)\frac{\partial \overset{u}{\phi}}{\partial x_i} = q_i(\overset{u}{\phi} - H) \tag{3.196}$$

where $\overset{u}{\phi} - H$ is the saturated aquifer thickness of the upper aquifer, so that indeed $\overset{u}{Q}_i = q_i(\overset{u}{\phi} - H)$. In writing (3.195), we have ignored the thickness of the clay layer. We have also tacitly assumed that the hydraulic conductivity in the upper and lower aquifer are the same. These restrictions are not necessary, but are applied here to simplify our expressions.

Comprehensive Flow

We introduce the concept of comprehensive flow in the dual aquifer zone, which states that

$$Q_i = \overset{u}{Q}_i + \overset{l}{Q}_i \tag{3.197}$$

In words, the comprehensive discharge vector is the vectorial sum of the discharge vectors in the upper and lower aquifer. We may also envision comprehensive flow as *the* discharge vector that would occur in a hypothetical single aquifer that replaces the dual aquifer system. Expression (3.197) leads, with Darcy's law, to the relation

$$\frac{\partial \Phi}{\partial x_i} = \frac{\partial \overset{u}{\Phi}}{\partial x_i} + \frac{\partial \overset{l}{\Phi}}{\partial x_i} \tag{3.198}$$

or, integrated,

$$\Phi = \overset{u}{\Phi} + \overset{l}{\Phi} \tag{3.199}$$

give or take a constant of integration. The potential Φ in (3.199) is called the *comprehensive potential*. Its (negative) derivative is the comprehensive discharge vector in the dual aquifer zone.

Observe from (3.192) that (3.197) also holds at the clay layer edge, whereby Q_i is the discharge vector in the single aquifer. Consequently, (3.198) must also hold at the clay layer edge, with $\partial\Phi/\partial x_i$ equal to the derivative of the potential (3.193) in the single aquifer zone. If (3.198) holds at the clay layer edge, so must (3.199), so that the comprehensive potential must equal the single aquifer potential at the clay layer edge, except perhaps for a constant of integration. We may verify this by setting (3.193) equal to the sum of (3.194) and (3.195), and setting all heads equal to ϕ_e (we are at the clay layer edge):

$$\begin{aligned} \tfrac{1}{2}k\phi_e^2 &= \tfrac{1}{2}k(\phi_e - H)^2 + kH\phi_e - \tfrac{1}{2}kH^2 \\ &= \tfrac{1}{2}k\phi_e^2 - kH\phi_e + \tfrac{1}{2}kH^2 + kH\phi_e - \tfrac{1}{2}kH^2 = \tfrac{1}{2}k\phi_e^2 \end{aligned} \tag{3.200}$$

Indeed, at the clay layer edge, the comprehensive potential for the dual aquifer zone equals the single aquifer potential. As it appears, no additional constant of integration is needed in (3.199).

The comprehensive potential offers an interesting perspective. If we can translate all boundary conditions for a dual aquifer flow problem in terms of this comprehensive potential, we can construct a solution in terms of this potential as if we deal with a single homogeneous aquifer, completely ignoring the clay layers. This solution will be the complete groundwater flow solution in single aquifer zones, where the clay layer is really absent! In these single aquifer zones we can calculate heads by inverting (3.193), while we can calculate the discharge vector by differentiating the comprehensive potential. In zones where the clay layer is present, however, we are not yet done! The head obtained from the comprehensive potential is neither the upper nor the lower head, although, as we will see later on, it is not without physical meaning either. The derivative of the comprehensive potential, as we have already seen, also has a physical meaning: It is the sum of the upper and lower discharge vectors in the dual aquifer zone. In order to illustrate the use of the comprehensive potential, we will apply it to some elementary groundwater flow problems.

3.3.2 One-Dimensional Dual Aquifer Flow

The setting in Figure 3.44 is similar to the one in Figure 3.33, except for the clay layer which protrudes into the aquifer over a distance x_e. The

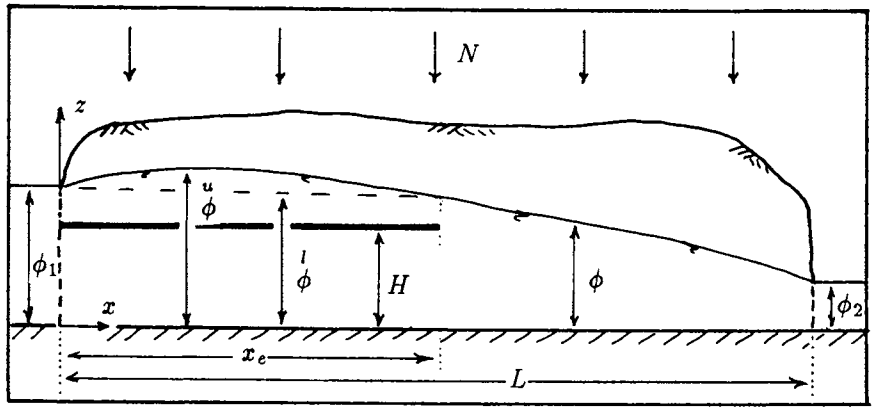

Figure 3.44: One-dimensional flow in an aquifer with a clay layer.

aquifer underneath the clay layer has a thickness H, while the thickness of the clay layer itself is ignored. We have two boundary conditions:

$$\begin{aligned} x = 0 \qquad & \phi = \phi_1 \\ x = L \qquad & \phi = \phi_2 \end{aligned} \tag{3.201}$$

The first step in our solution procedure is to determine the comprehensive potential $\Phi(x)$ in the aquifer. To that end, we need to reformulate the boundary conditions (3.201) in terms of comprehensive potentials. For the right-hand boundary ($x = L$), this is easily done; the comprehensive potential is equal to the single aquifer potential, so that

$$\Phi_2 = \tfrac{1}{2} k \phi_2^2 \tag{3.202}$$

The situation on the left-hand boundary requires some thought. Both the lower and the upper aquifer have the same head ϕ_1 at $x = 0$. We are, in fact, at the left-hand edge of the clay layer! Thus, we may consider the aquifer at $x = 0$ a single aquifer zone (of zero extent), just as we consider the point x_e (at the other edge) to be part of the single aquifer zone to its right. If we are in a single aquifer zone, at $x = 0$, then the comprehensive potential at that point is equal to the single aquifer potential; hence,

$$\Phi_1 = \tfrac{1}{2} k \phi_1^2 \tag{3.203}$$

Exercise 3.16 *Demonstrate that the same result would have been obtained by using (3.194) and (3.195) to calculate the potentials in the lower and upper aquifer, respectively, and then calculate the comprehensive potential by use of (3.199).*

Once the boundary conditions are known in terms of Φ, we can (for now) forget about the clay layer! The solution is the same as for a homogeneous unconfined aquifer with areal recharge and is given by (3.157),

$$\Phi = -\frac{N}{2}x(x-L) + \frac{\Phi_2 - \Phi_1}{L}x + \Phi_1 \tag{3.204}$$

The comprehensive potential in (3.204) is also the single aquifer potential in the single aquifer zone ($x_e \leq x \leq L$): To the right of the clay layer, we are done!

What is left is to solve the flow problem in the upper and lower aquifer, and thus find $\overset{u}{\Phi}$ and $\overset{l}{\Phi}$. First, we need the boundary conditions for both the upper and lower aquifers. We already have the boundary conditions on the left-hand side: $x = 0$; $\overset{u}{\phi}=\overset{l}{\phi}= \phi_1$. Because of (3.204), we now also have the boundary conditions on the right-hand side of the upper and lower aquifer! The head ϕ_e at the clay layer edge can be calculated from

$$\phi_e = \sqrt{\frac{2\Phi(x_e)}{k}} \tag{3.205}$$

where $\Phi(x_e)$ is calculated by substituting $x = x_e$ into (3.204). The solution for the lower aquifer is that for one-dimensional flow in a confined aquifer (no recharge) [see (3.25)],

$$\overset{l}{\Phi}= \frac{\overset{l}{\Phi}_e - \overset{l}{\Phi}_1}{x_e}x + \overset{l}{\Phi}_1 \qquad (0 \leq x \leq x_e) \tag{3.206}$$

Similarly, we may obtain the solution for the upper potential, which is that for one-dimensional flow in an unconfined aquifer with recharge [see (3.204)],

$$\overset{u}{\Phi}= -\frac{N}{2}x(x-x_e) + \frac{\overset{u}{\Phi}_e - \overset{u}{\Phi}_1}{x_e}x + \overset{u}{\Phi}_1 \qquad (0 \leq x \leq x_e) \tag{3.207}$$

In fact, it is not even necessary to solve both the upper and lower potentials from scratch. Once we obtained, for instance, the potential for the lower aquifer (3.206), we could have written for the upper aquifer

$$\overset{u}{\Phi}(x) = \Phi(x) - \overset{l}{\Phi}(x) \qquad (0 \leq x \leq x_e) \tag{3.208}$$

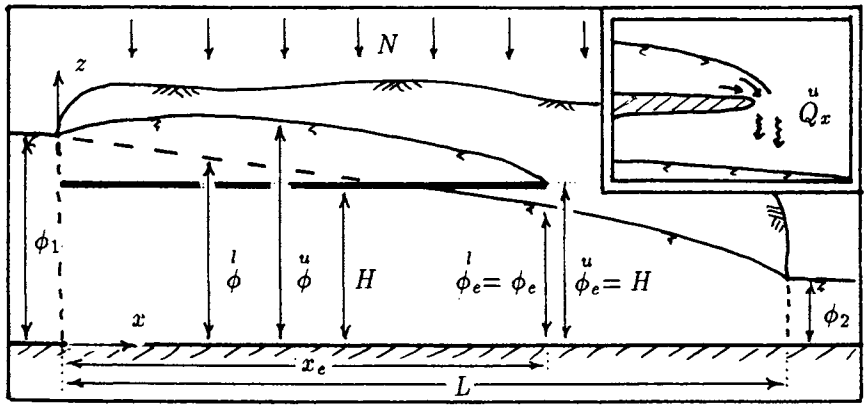

Figure 3.45: Unconfined flow conditions in the lower aquifer near the clay layer edge.

using the definition of the comprehensive potential (3.199). Both potentials on the right-hand side of (3.208) can be calculated using (3.204) and (3.206), respectively, so that $\overset{u}{\Phi}(x)$ is known for all values of x without using (3.207).

Unconfined Flow Conditions in the Lower Aquifer

In Figure 3.44 the flow conditions in the lower aquifer are depicted as everywhere confined. Depending on the parameters of the problem, however, the head at the clay layer edge may be below the clay layer, as illustrated in Figure 3.45. At the clay layer edge, in Figure 3.45, the head in the lower aquifer equals the head in the single aquifer, but these heads do not equal the head in the upper aquifer. Hence, the condition (3.191) is not valid! The head in the upper aquifer is "perched up" by the clay layer to at least the height of the clay layer. In reality, there is a strong curvature of the streamlines toward the clay layer, with water from the upper aquifer percolating downward into the lower or single aquifer; see inset in Figure 3.45. There is significant resistance to vertical flow just before the water starts percolating over the edge. Consequently, our Dupuit–Forchheimer solution in the upper aquifer is not too reliable near the edge. Neither do we know exactly what boundary condition we must select at that point. For simplicity, we will assume that the water table in the upper aquifer just touches the clay layer edge, leading to the following boundary conditions:

$$\overset{u}{\phi}_e = H \qquad \overset{l}{\phi}_e = \phi_e \tag{3.209}$$

Continuity of flow must still apply, of course, so that (3.192) still holds. We will demonstrate that at the clay layer edge the comprehensive potential as defined by (3.199) is still equal to the single aquifer potential (3.193),

$$\tfrac{1}{2}k\phi_e^2 = \tfrac{1}{2}k(\overset{u}{\phi}_e - H)^2 + \tfrac{1}{2}k\,\overset{l}{\phi}_e{}^2 = \tfrac{1}{2}k(H-H)^2 + \tfrac{1}{2}k\phi_e^2 = \tfrac{1}{2}k\phi_e^2 \qquad (3.210)$$

The upper potential in (3.210) is zero, while the lower (unconfined) potential equals the single aquifer potential: Indeed, the comprehensive potential equals the single aquifer potential at the clay layer edge. When solving for the comprehensive potential, therefore, it is not necessary to know the flow conditions at the clay layer edge in advance. However, when solving for the upper potential, we should realize that the upper head can never be lower than the clay layer elevation, so that if at the clay layer edge $\phi_e < H$, the head in the upper aquifer is $\overset{u}{\phi}_e = H$.

Exercise 3.17 *The following data are given for the case of one-dimensional flow in an aquifer with a clay layer, like the one depicted in Figure 3.44 or Figure 3.45:*
$L = 5000$ *ft*, $x_e = 3000$ *ft*, $H = 50$ *ft*, $\phi_1 = 60$ *ft*, $\phi_2 = 30$ *ft*, $N = 0.002$ *ft/day, and* $k = 10$ *ft/day.*

(a) What is the head at the edge of the clay layer ($x = x_e$)*?*

(b) What is the discharge rate Q_x *at the right-hand aquifer boundary* ($x = L$)*?*

(c) What are the discharge rates $\overset{u}{Q}_x$ *and* $\overset{l}{Q}_x$ *in the upper and lower aquifer, respectively, at the left-hand aquifer boundary* ($x = 0$)*?*

(d) Answer the questions (a), (b), and (c) for the case that $N = 0$ *ft/day.*

The advantage of the comprehensive potential formulation is significant. Without it, the dual aquifer system in Figure 3.44, for example, must be broken up into three individual aquifers: the upper, lower, and single aquifer. Next, we would have to solve the flow problem in these three aquifers separately, for which we need boundary conditions. At $x = 0$ and $x = L$, these boundary conditions are known, but at the clay layer edge ($x = x_e$), the boundary condition (head) is not known! Assuming saturated conditions in the lower aquifer, we can state that all three aquifers have the same head ϕ_e at $x = x_e$. We may solve the three flow problems in terms of this, as yet unknown, head ϕ_e, and then use continuity of flow across the clay layer edge to resolve ϕ_e. If we find that ϕ_e is smaller than the clay

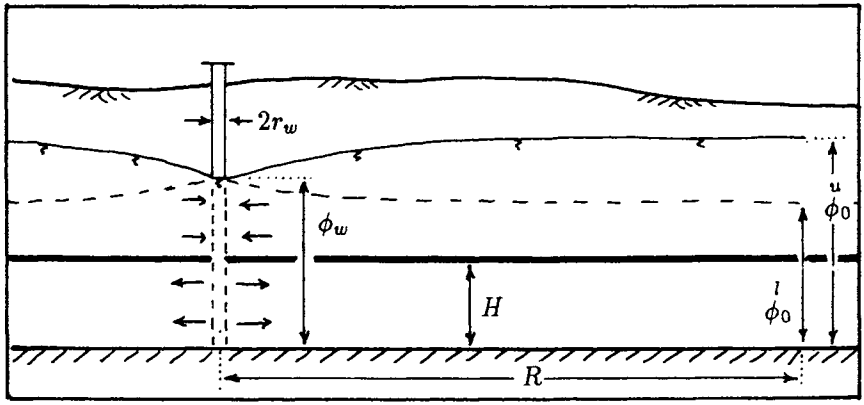

Figure 3.46: An abandoned well screened in two aquifers.

layer elevation H, the solution is in error. We have to redo our solutions by setting $\overset{u}{\phi}_e = H$, which leads directly to the solution for the upper aquifer. Then we can solve the lower and single aquifer problems with the, as yet unknown, head ϕ_e at $x = x_e$, and resolve ϕ_e by use of continuity of flow across the clay layer edge.

Such a procedure may be doable for simple cases of one-dimensional flow. It is quite hopeless for two-dimensional flow cases where the clay lenses may be arbitrarily shaped. In contrast, by solving the flow problem first in terms of the comprehensive potential, we immediately have the solution in all single aquifer zones. Consequently, we also immediately have the head along all clay layer edges, without the need to apply continuity of flow conditions across those boundaries. The solution procedures for the upper and lower aquifers then are straightforward.

3.3.3 The Abandoned Well

An important case of multiple aquifer flow is that due to a well screened in more than one aquifer. Even if the well is not in use (not pumping), it still serves as a shortcut between aquifers.

In Figure 3.46, an abandoned well is depicted with its well screen connecting two aquifers. At a distance R from the well, the heads in the upper and lower aquifer are $\overset{u}{\phi}_0$ and $\overset{l}{\phi}_0$, respectively. Let us assume, for simplicity, that there are no other flow features in the aquifer beyond the (abandoned) well. The question is, what happens at the well? What is the water level in the well, and what, if any, is the flow in the well? We do know, of course, that there is no net flow from the well — in other words, no water

is removed from the aquifer system!

We follow the same approach as we did for the one-dimensional problem: first solve for the comprehensive potential. At a distance R from the well we can calculate the comprehensive potential:

$$\Phi_0 = \overset{u}{\Phi}_0 + \overset{l}{\Phi}_0 = \tfrac{1}{2}k(\overset{u}{\phi}_0 - H)^2 + kH\ \overset{l}{\phi}_0 - \tfrac{1}{2}kH^2 \tag{3.211}$$

The well in Figure 3.46 is not pumping and, as was given, there are no other flow features in the aquifer. Thus, the comprehensive potential in the aquifer is constant and equal to (3.211): $\Phi(x,y) = \Phi_0$. The comprehensive potential at the well, therefore, is also equal to (3.211),

$$\Phi_w = \Phi_0 \tag{3.212}$$

We may argue that the well bore actually creates a (very small) single aquifer zone. Just as we imagined the left-hand stream in Figure 3.44 to create an infinitely small single aquifer zone at $x = 0$, so does the well create an infinitely small single aquifer zone at the well perimeter $r = r_w$. Consequently, the water level in the well is equal to the comprehensive head at the well perimeter, which is

$$\phi_w = \sqrt{\frac{2\Phi_0}{k}} \tag{3.213}$$

This comprehensive head has a value somewhere in between the upper and lower aquifer heads $\overset{u}{\phi}_0$ and $\overset{l}{\phi}_0$. With the upper aquifer head higher than the lower aquifer head in Figure 3.46, the well is "pumping" in the upper aquifer and "injecting" water in the lower aquifer. The potential in the upper aquifer, therefore, has the form

$$\overset{u}{\Phi} = \frac{Q}{2\pi}\ln\frac{r}{R} + \overset{u}{\Phi}_0 \tag{3.214}$$

while the potential in the lower aquifer is

$$\overset{l}{\Phi} = -\frac{Q}{2\pi}\ln\frac{r}{R} + \overset{l}{\Phi}_0 \tag{3.215}$$

The discharge rate Q in both expressions is the same; it is the extraction rate in the upper aquifer and the injection rate in the lower aquifer. Q can be calculated from either (3.214) or (3.215). Using (3.214),

$$Q = \frac{(\overset{u}{\Phi}_w - \overset{u}{\Phi}_0)2\pi}{\ln\frac{r_w}{R}} \tag{3.216}$$

where $\overset{u}{\Phi}_w$ is the potential in the upper aquifer at the well perimeter and follows from

$$\overset{u}{\Phi}_w = \tfrac{1}{2}k(\phi_w - H)^2 \tag{3.217}$$

where ϕ_w is given by (3.213).

Exercise 3.18 *The following data are given for the problem in Figure 3.46:* $\overset{u}{\phi}_0 = 90$ *ft,* $\overset{l}{\phi}_0 = 80$ *ft,* $R = 5000$ *ft,* $H = 50$ *ft,* $r_w = 0.5$ *ft, and* $k = 30$ *ft/day.*

(a) What is the head ϕ_w *at the well?*

(b) What is the discharge rate Q *in the well?*

(c) Show that (3.214) and (3.215) satisfy the comprehensive potential (3.211).

The situation depicted in Figure 3.46 is an extreme case whereby different geological formations are completely separated, except for the well bore. Since without the well the upper aquifer would have had a consistently higher water table, the "inactive" well leaks water from the upper into the lower aquifer. Most aquifers do exhibit some form of aquifer stratification, with different heads in different strata. A well which is screened across these strata will cause a "short circuit" and, when not pumping, moves water from some strata into others. In recharge areas, thus usually away from surface waters, an abandoned well will "pump" water from higher strata into deeper aquifer zones. In discharge areas, thus near receiving streams or lakes, the flow in the well is reversed; water from deeper zones is discharged into the upper portions of the aquifer. A well does not have to be abandoned for this to happen: The same exchange of water occurs in wells that are temporarily not in use, such as domestic wells between pumping periods.

This short-circuiting of multiple aquifer wells has major implications in terms of contaminant transport. Imagine that the upper aquifer in Figure 3.46 is contaminated, while the lower aquifer is still clean, as is not uncommon. Wells that are screened in both aquifers may function as contaminant sources for the lower aquifer. If the flow directions in the lower aquifer are different from those in the upper aquifer, contaminants may move in unexpected directions, suggesting major contaminant spreading. For this reason, nowadays wells are limited (by law) to be screened in only one aquifer. In addition, separating clay layers, which are penetrated during well construction, must be sealed off. These seals are often created by pumping bentonite (a swelling clay) into the annular space between the well casing and the clay formation.

We have learned something else from this problem: The head in the well depicted in Figure 3.46 is equal to the comprehensive head. This leads to the following general rule:

Rule 3.13 *The comprehensive head at a point in a multiple aquifer system is equal to the water level in a fictitious (non-pumping) well that penetrates all aquifers at that point.*

With this rule, some physical meaning is given to the comprehensive head ϕ derived from the comprehensive potential Φ outside single aquifer zones.

Aquifers with Different Hydraulic Conductivities

The upper and lower aquifer in Figure 3.46 may have different hydraulic conductivities: $\overset{u}{k}$ and $\overset{l}{k}$, respectively. The expressions for the upper aquifer and lower aquifer potentials then become (see Strack, 1981a)

$$\overset{u}{\Phi} = \tfrac{1}{2}\,\overset{u}{k}\,(\overset{u}{\phi} - H)^2 \tag{3.218}$$

$$\overset{l}{\Phi} = \overset{l}{k}\,H\,\overset{l}{\phi} - \tfrac{1}{2}\,\overset{l}{k}\,H^2 \quad (\overset{l}{\phi} \geq H) \tag{3.219}$$

$$\overset{l}{\Phi} = \tfrac{1}{2}\,\overset{l}{k}\overset{l}{\phi}^2 \quad (\overset{l}{\phi} \leq H)$$

The comprehensive potential at the well, assuming confined conditions everywhere, is

$$\Phi = \tfrac{1}{2}\,\overset{u}{k}\,(\overset{u}{\phi}_0 - H)^2 + \overset{l}{k}\,H\,\overset{l}{\phi}_0 - \tfrac{1}{2}\,\overset{l}{k}\,H^2 \tag{3.220}$$

or, in terms of the head ϕ_w at the well,

$$\Phi = \tfrac{1}{2}\,\overset{u}{k}\,(\phi_w - H)^2 + \overset{l}{k}\,H\phi_w - \tfrac{1}{2}\,\overset{l}{k}\,H^2 \tag{3.221}$$

The head ϕ_w may be calculated from (3.221) by substituting (3.220) for Φ.

Exercise 3.19 *The following data are given for the problem in Figure 3.46:* $\overset{u}{\phi}_0 = 75$ *ft,* $\overset{l}{\phi}_0 = 20$ *ft,* $R = 5000$ *ft,* $H = 50$ *ft,* $r_w = 0.5$ *ft,* $\overset{u}{k} = 20$ *ft/day and* $\overset{l}{k} = 50$ *ft/day.*

(a) What is the comprehensive potential at the well (in ft^3/day*)?*

(b) Assuming that the head ϕ_w *at the well is below the clay layer, what is the expression for the comprehensive potential in terms of* ϕ_w*?*

(c) What is the head ϕ_w *at the well?*

(d) What is the discharge rate Q *in the well?*

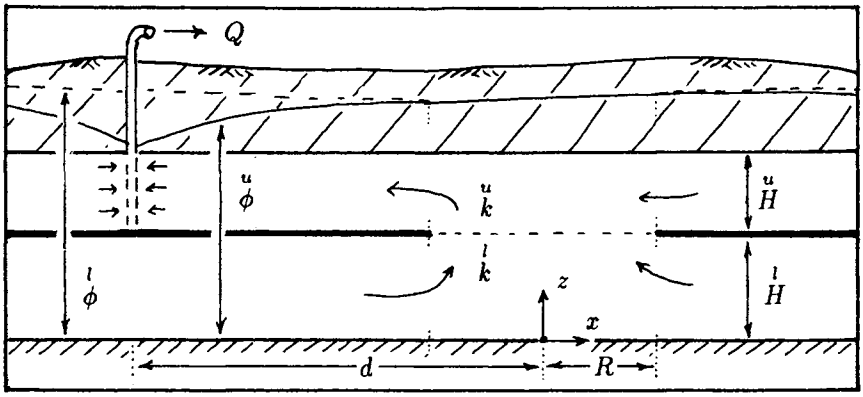

Figure 3.47: Well in the upper aquifer near a circular opening in the clay layer.

3.3.4 Well near a Circular Opening in a Clay Layer

A well which is screened in only one aquifer may still affect the flow in overlying or underlying aquifers through (nearby) connections. In such a case, the well may be expected to draw water from more than one aquifer, as we will illustrate.

In Figure 3.47, a well is depicted near a circular opening in the (impermeable) clay layer between an upper and lower aquifer. The well is screened in the upper aquifer only. The upper and lower aquifers have hydraulic conductivities $\overset{u}{k}$ and $\overset{l}{k}$, respectively, and are continuous across the opening in the clay layer. This causes the single aquifer zone to have two layers with two different hydraulic conductivities; see Figure 3.47. We will assume that the difference between $\overset{u}{k}$ and $\overset{l}{k}$ is small enough that we can treat the flow in the clay layer opening as Dupuit–Forchheimer flow. In practice, this means that $\overset{u}{k}$ and $\overset{l}{k}$ need to be within the same order of magnitude (a difference of less than a factor 10). The flow conditions in both aquifers remain confined with the solid and dashed curves in Figure 3.47, representing the piezometric head in the upper and lower aquifers, respectively. The discharge potentials in the upper and lower aquifer are defined as

$$\overset{u}{\Phi}=\overset{u}{k}\overset{u}{H}\overset{u}{\phi} \qquad \overset{l}{\Phi}=\overset{l}{k}\overset{l}{H}\overset{l}{\phi} \tag{3.222}$$

Since we do not anticipate unconfined flow conditions, the constant $-\frac{1}{2}kH^2$ [see, e.g., (3.219)] has been left off. Prior to pumping, the heads in both aquifers are the same and equal to ϕ_0. The origin of our coordinate system is

chosen as the center of the circular opening in the clay layer. At a reference point $x = L$ and $y = 0$, the heads in both aquifers remain unaffected during pumping, whereby

$$\overset{u}{\phi}=\overset{l}{\phi}= \phi_0 \qquad (x = L \ ; \ y = 0) \tag{3.223}$$

The well is located in the upper aquifer at $x = -d$, $y = 0$. The radius of the opening in the clay layer is R, whereby $R < d$.

As before, we first determine the comprehensive potential. The only flow feature in the aquifer system is the well. In terms of the comprehensive potential Φ, it does not matter that the well pumps in the upper aquifer only; hence, Φ is

$$\Phi = \frac{Q}{4\pi} \ln \frac{(x+d)^2 + y^2}{(L+d)^2} + \Phi_0 \tag{3.224}$$

which satisfies the boundary condition at the reference point, see (3.223). Expression (3.224) is the complete solution in the single aquifer zone, and thus inside the circular opening. The head inside the opening follows from (3.224) with

$$\Phi = \overset{u}{\Phi} + \overset{l}{\Phi} = (\overset{u}{k}\overset{u}{H} + \overset{l}{k}\overset{l}{H})\phi \tag{3.225}$$

With (3.224) and (3.225), we can calculate the head distribution along the perimeter of the opening in the clay layer, and thus along the boundary of the upper and lower aquifers. This head distribution, however, is not a simple one. In general, we would proceed with a numerical solution — for instance, by use of GFLOW1. For this special case of a circular opening, it is possible to arrive at a (simple) closed-form analytic solution by use of a "trick." This is how.

The same head distribution along the clay layer edge as obtained from (3.224) may be obtained from

$$\Phi = \frac{Q}{4\pi} \ln \left(\frac{(x + \frac{R^2}{d})^2 + y^2}{(L+d)^2} \frac{d^2}{R^2} \right) + \Phi_0 \tag{3.226}$$

which represents a well inside the opening. That (3.226) and (3.224) indeed generate the same potential along the circular boundary of the opening in the clay layer may be verified by substituting $x^2 + y^2 = R^2$ into both (3.224) and (3.226). The equivalence of the two potentials along the circular boundary may also be understood from an earlier analysis. Expression (3.226) represents an image of the well with respect to the circle, as was done in Section 3.1.16. In (3.136), the image *recharge well* was used to maintain equipotential conditions along the circle. Therefore, the image

recharge well counteracted the well. In other words, as much as the well lowered the potential at a particular point along the circle, the recharge well raised it by that same amount! Consequently, along the circular boundary, the effects of the well and the image recharge well are equal but opposite. If we replace the image recharge well by a well, the effects of the well and the image well will be the same: Equations (3.224) and (3.226) generate the same potential along the circle. Note, however, that (3.226) does **not** satisfy the boundary condition (3.223) at the reference point!

Exercise 3.20 *Prove mathematically that (3.224) and (3.226) yield the same potential at* $x^2 + y^2 = R^2$.

Next we will solve the potential $\overset{l}{\Phi}$ for the lower aquifer. The circular boundary of the opening in the clay layer also forms an internal boundary for the lower aquifer. The head distribution along this boundary is obtained from

$$\phi = \frac{\Phi}{\overset{u\,u}{kH} + \overset{l\,l}{kH}} \qquad (x^2 + y^2 = R^2) \tag{3.227}$$

where Φ is obtained from (3.226) and use is made of the definition of the comprehensive potential:

$$\Phi = \overset{u}{\Phi} + \overset{l}{\Phi} = \overset{u\,u}{kH}\,\phi + \overset{l\,l}{kH}\,\phi = (\overset{u\,u}{kH} + \overset{l\,l}{kH})\phi \tag{3.228}$$

The potential $\overset{l}{\Phi}$ along the boundary is, with (3.222) and (3.227),

$$\overset{l}{\Phi} = \left(\frac{\overset{l\,l}{kH}}{\overset{u\,u}{kH} + \overset{l\,l}{kH}} \right) \Phi \qquad (x^2 + y^2 = R^2) \tag{3.229}$$

Replacing Φ by (3.226) yields

$$\overset{l}{\Phi} = \frac{\overset{l\,l}{kH}}{\overset{u\,u}{kH} + \overset{l\,l}{kH}} \left[\frac{Q}{4\pi} \ln \left(\frac{(x + \frac{R^2}{d})^2 + y^2}{(L+d)^2} \frac{d^2}{R^2} \right) + \Phi_0 \right] \qquad (x^2 + y^2 = R^2) \tag{3.230}$$

The solution (3.230) has been constructed to satisfy the boundary condition along the circular opening in the clay layer. However, (3.230) does not satisfy the boundary condition at the reference point, since (3.226) did not, either. We need another "trick" to adjust the lower potential at the reference point, while at the same time the potentials along the circular

opening generated by (3.230) must not be disturbed. The solution to our problem is to add a well at the center of the circular opening, as follows:

$$\overset{l}{\Phi} = \frac{\alpha Q}{4\pi} \ln\left(\frac{(x+\frac{R^2}{d})^2+y^2}{(L+d)^2}\frac{d^2}{R^2}\right) + \frac{\beta Q}{4\pi}\ln\left(\frac{x^2+y^2}{R^2}\right) + \overset{l}{\Phi}_0 \qquad (x^2+y^2 \geq R^2) \tag{3.231}$$

where α is the factor in front of the potential in (3.230),

$$\alpha = \frac{\overset{l}{k}\overset{l}{H}}{\overset{u}{k}\overset{u}{H} + \overset{l}{k}\overset{l}{H}} \tag{3.232}$$

and where β is chosen in such a way that the potential at the reference point is $\overset{l}{\Phi}_0$, which is the case for

$$\beta = \alpha\left(\frac{\ln\frac{dL+R^2}{LR+dR}}{\ln\frac{R}{L}}\right) \tag{3.233}$$

The condition $(x^2+y^2=R^2)$ in (3.230) has been relaxed to $(x^2+y^2 \geq R^2)$ in (3.231), since the potential $\overset{l}{\Phi}$ satisfies all boundary conditions in the lower aquifer and is, therefore, valid in the entire lower aquifer.

The solution in the upper aquifer simply follows from the definition of the comprehensive potential,

$$\overset{u}{\Phi} = \Phi - \overset{l}{\Phi} \qquad (x^2+y^2 \geq R^2) \tag{3.234}$$

There is no real need to pursue the solution for the upper aquifer any further; values for $\overset{u}{\Phi}$ can be calculated at any point in the aquifer using (3.234) with (3.226) and (3.231). For illustrative purposes, however, we will write an explicit expression for $\overset{u}{\Phi}$ by substituting (3.226) and (3.231) into (3.234), so that

$$\begin{aligned}\overset{u}{\Phi} &= \frac{Q}{4\pi}\ln\left(\frac{(x+d)^2+y^2}{(L+d)^2}\right) - \frac{\alpha Q}{4\pi}\ln\left(\frac{(x+\frac{R^2}{d})^2+y^2}{(L+d)^2}\frac{d^2}{R^2}\right) \\ &\quad - \frac{\beta Q}{4\pi}\ln\left(\frac{x^2+y^2}{R^2}\right) + \overset{u}{\Phi}_0 \qquad (x^2+y^2 \geq R^2)\end{aligned} \tag{3.235}$$

Exercise 3.21 *Demonstrate that (3.235) satisfies the boundary conditions along the circular opening in the clay layer and at the reference point $x = L$ and $y = 0$.*

Flow nets for the upper and lower aquifer are depicted in Figure 3.48. The

flow net for the single aquifer zone, the circular opening, is shown as part of the flow net for both the upper and the lower aquifer, respectively. The equipotentials are continuous at the clay layer edge (circle), which is a consequence of the single-valuedness of the head. However, the streamlines do not line up at the boundary of the circular opening, because they represent flow "channels" in three different aquifer zones. Observe that the well in the upper aquifer obtains part of its water from the lower aquifer by drawing it through the opening in the clay layer.

Unconfined Flow Conditions

We limited ourselves to confined flow conditions in order to facilitate the analytical solution presented here. If flow conditions had been (partly) unconfined, all potentials would not have been linear functions of the head, preventing the operation in (3.228) and, with it, the successive steps to arrive at the potentials for the upper and the lower aquifers. Under such circumstances, however, it is still possible to arrive at an approximate solution to the problem by introducing an average value for $\overset{u}{H}$ along the clay layer boundary. This may be obtained by averaging the head along the circular boundary. With this average upper aquifer thickness, we may adopt the potential definitions (3.222) along the opening and use (3.228) through (3.235) to obtain approximate solutions for the upper and lower potentials. However, as a result of our approximation of $\overset{l}{\Phi}$ and $\overset{u}{\Phi}$ at the circular opening (when conditions are unconfined), we are not satisfying the boundary conditions along the circular opening exactly!

3.3.5 Water Quality Sampling in a Domestic Well

The concepts of comprehensive flow and a comprehensive potential need not be limited to only two aquifers, of course. Some aquifers exhibit many permeable strata separated by nearly impervious layers. A good example of such an aquifer is a *shale aquifer*, which allows horizontal water movement along so-called *bedding planes*, but has a substantial resistance to vertical groundwater movement. These aquifers are usually not very productive, making them unsuitable for high-capacity industrial or city wells. For domestic water usage, however, the shale aquifer may be adequate, provided the well is constructed to tap several bedding planes at the same time.

In a sense, the domestic well in a shale aquifer is a multiple aquifer well, causing a short circuit between aquifers as discussed in Section 3.3.3. In most situations, the heads in the upper aquifers (bedding planes) will be somewhat larger than in deeper aquifers, unless the well is near a discharge

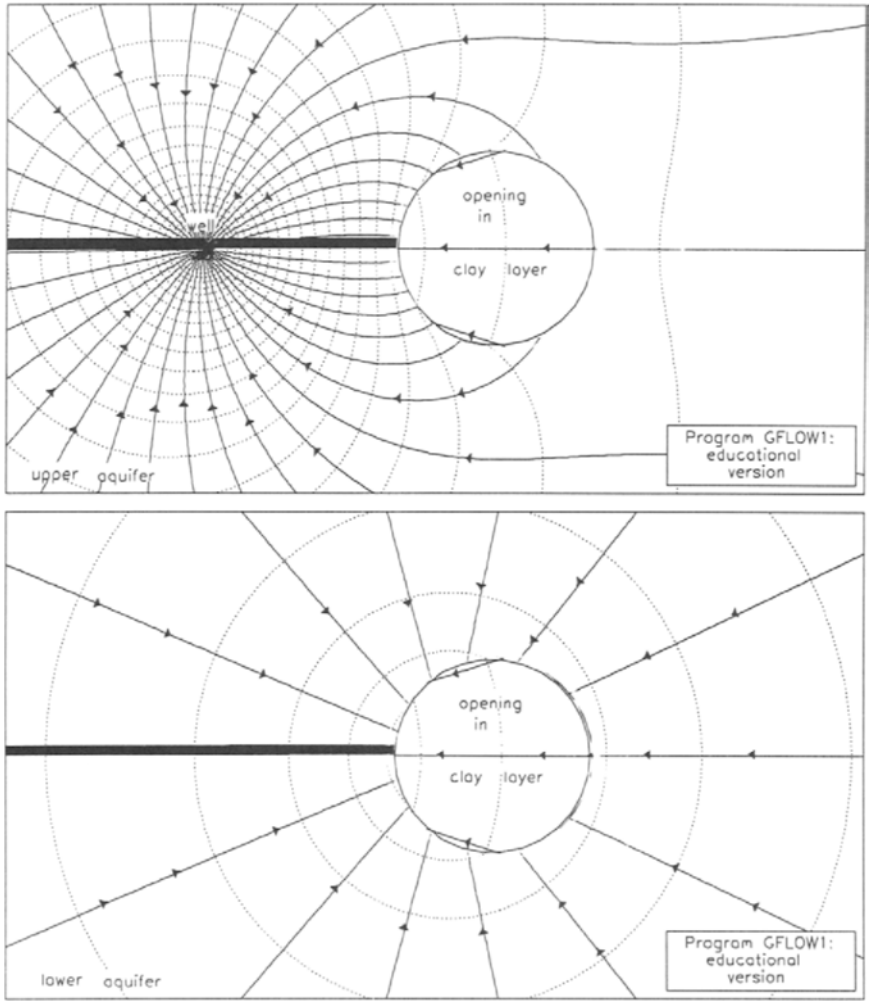

Figure 3.48: Flow in the upper and lower aquifer toward a well in the upper aquifer. (GFLOW1 file: problem8.dat)

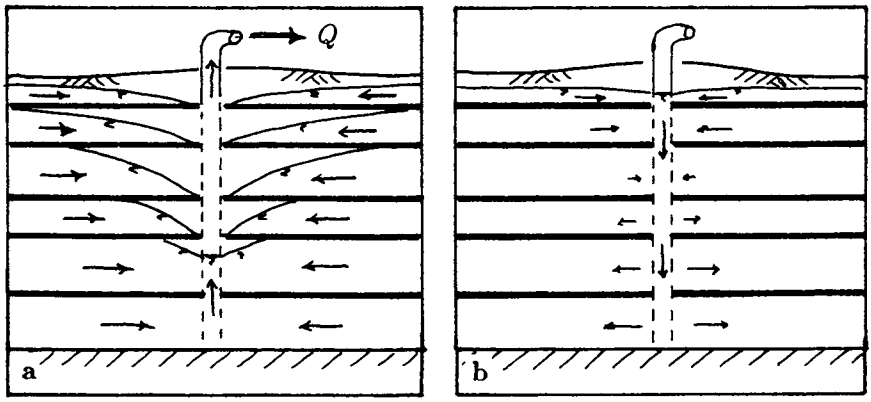

Figure 3.49: Multiple aquifer flow near a well during pumping (a) and when the pump is off (b).

area (stream or lake). Since domestic wells are pumped intermittently, there is the potential for downward flow in the well between pumping cycles (see Figure 3.49b). If the upper aquifer(s) are contaminated, contaminant movement into the lower aquifers will occur. Whether or not this leads to a further spreading of contaminants depends on the average discharge of the well in relation to the intensity of flow from higher aquifers into deeper aquifers when the pump is off. Once the pump is switched on, the flow in all aquifers will be toward the well, see Figure 3.49a. If the downward flow is moderate, the contaminants flowing into the lower aquifers may be pumped back completely by the well. This potential periodic contaminant movement from higher aquifer strata into lower ones can have a significant impact on the water quality of the well. This may be illustrated by the following hypothetical example.

For computational convenience, we will simplify the situation in Figure 3.49 by considering five aquifers which will always remain confined, unlike what is depicted in Figure 3.49. The aquifers have constant transmissivities denoted by $\overset{i}{k}\overset{i}{H}$, where $i = 1, 2, 3, 4, 5$. The well has a pumping rate Q and a radius r_w. At a distance R from the well, the heads in the five aquifers are constant and equal to $\overset{i}{\phi}_0$, where $i = 1, 2, 3, 4, 5$. It is given that the upper aquifer is contaminated with a contaminant concentration C_1. During pumping, the well water is a mixture of water coming from all five aquifers. If only the uppermost aquifer is contaminated, the concentration of contaminants in the well effluent is much smaller than C_1. In between pumping periods, there may be flow from the upper aquifers into the deeper

aquifers, depending on the values of the heads $\overset{i}{\phi}_0$. If this is the case, the contaminant concentration in the well may be significantly higher when the pump is off than when the pump is running. We will illustrate this with a numerical example.

Consider the following data: $\overset{i}{k}$= 10 ft/day and $\overset{i}{H}$= 5 ft for $i = 1, 2, 3, 4, 5$; $\overset{i}{\phi}_0$= 40, 39, 38, 37, 36 ft for $i = 1, 2, 3, 4, 5$, respectively; $R = 5000$ ft; $r_w = 0.25$ ft; $Q = 10$ GPM (1925.28 ft^3/day).

This leads to the following potentials in the aquifers at a distance R from the well:

$$\overset{i}{\Phi}_0 = \overset{i}{k}\overset{i}{H}\overset{i}{\phi}_0 = 2000,\ 1950,\ 1900,\ 1850,\ \text{and}\ 1800\,\frac{\text{ft}^3}{\text{day}} \tag{3.236}$$

for $i = 1, 2, 3, 4, 5$, respectively.

We first consider the situation with the pump off. For simplicity, we will assume that when the well is shut off or turned on, steady-state conditions will be reached instantly. Although this is not really true, the assumption is a first approximation to the problem and will still provide us with insight into the consequences of cyclic pumping on the quality of the well water.

If the pump is off, there is no net flow in the aquifer system, so that the comprehensive potential at the well is

$$\Phi_w = \sum_{i=1}^{5} \overset{i}{\Phi}_0 = 9500\,\frac{\text{ft}^3}{\text{day}} \tag{3.237}$$

The head at the well can be obtained from [see also (3.225)]

$$\phi_w = \frac{\Phi_w}{\sum_{i=1}^{5} \overset{i}{k}\overset{i}{H}} = 38\,\text{ft} \tag{3.238}$$

If we compare the head in the well with those in the aquifers at a distance R from the well, it becomes clear that the upper two aquifers are discharging water into the well, and the lower two aquifers are being recharged by the well, while the middle aquifer has no flow. Note that while the pump is off, the well is "pumping" or "injecting" in four of the five aquifers. We denote the discharge rates for the aquifers as $\overset{i}{Q}_0$ and calculate them as follows:

$$\overset{i}{Q}_0 = \frac{2\pi\,\overset{i}{k}\overset{i}{H}\,(\phi_w - \overset{i}{\phi}_0)}{\ln\frac{r_w}{R}} = 63.44,\ 31.72,\ 0,\ -31.72,\ \text{and}\ -63.44\,\frac{\text{ft}^3}{\text{day}} \tag{3.239}$$

for $i = 1, 2, 3, 4, 5$, respectively. These discharge rates add up to zero, so that there is indeed no comprehensive flow. Given some time, the concentration C_0 in the well becomes

$$C_0 = \frac{\overset{1}{Q_0}\, C_1}{\underset{1}{Q_0} + \underset{2}{Q_0}} = 0.666\, C_1 \tag{3.240}$$

Equation (3.240) provides the ultimate concentration in the well with the pump off. But what is the concentration in the well if it is pumping? With the pump on, the comprehensive potential at the well is

$$\Phi_w = \frac{Q}{2\pi} \ln \frac{r_w}{R} + \Phi_0 = 6465.39 \frac{\text{ft}^3}{\text{day}} \tag{3.241}$$

The head at the well becomes

$$\phi_w = \frac{\Phi_w}{\sum_{i=1}^{5} \overset{i}{k}\overset{i}{H}} = 25.86\,\text{ft} \tag{3.242}$$

Each aquifer is five feet thick ($\overset{i}{H} = 5$) so that the top of the upper aquifer is 25 ft above the base of the lower aquifer (the datum for the heads). Consequently, as appears from (3.242), the flow conditions in all aquifers remain confined (again contrary to what is depicted in Figure 3.49). The contributions to the well discharge of the five aquifers are denoted by $\overset{i}{Q}$ with $i = 1, 2, 3, 4, 5$ and are calculated as follows:

$$\overset{i}{Q} = \frac{2\pi\, \overset{i}{k}\overset{i}{H}\, (\overset{i}{\phi_w} - \overset{i}{\phi_0})}{\ln \frac{r_w}{R}} = 448.50,\ 416.78,\ 385.06,\ 353.33,\ \text{and}\ 321.61 \frac{\text{ft}^3}{\text{day}} \tag{3.243}$$

for $i = 1, 2, 3, 4, 5$, respectively. The concentration in the well, after some time of pumping, will approach the following value:

$$C = \frac{\overset{1}{Q}\, C_1}{\sum_{i=1}^{5} \overset{i}{Q}} = 0.233\, C_1 \tag{3.244}$$

The concentration of contaminants in the well, during pumping, drops to 35% of the concentration in the well with the pump off; compare (3.240) and (3.244). Of course, these changes do not occur abruptly. When the pump stops, it will take time for the steady-state discharges (3.239) to occur, and for the concentration (3.240) to be realized. Conversely, when the pump

is being restarted, some contaminated water that was infiltrated into the deeper aquifers will be pumped back, keeping the concentration initially above the one calculated in (3.244). The actual time-dependent behavior of the contaminant concentration in the well will depend on many factors, including aquifer properties and pumping regimes.

The preceding calculations demonstrate a mechanism for "self cleaning" of the well during pumping. This has important consequences for water sampling protocols applied to domestic wells. Currently, when sampling *monitoring wells*, it is customary to remove about four to five well volumes of water before a sample is taken. The reason for this is that stagnant water in the monitoring well may have a contaminant concentration that is not representative for the aquifer. For instance, volatile organic compounds (VOCs) may have decreased in the well water due to long exposure to the air, causing many of the VOCs to volatilize and leave the well water. The same sampling protocol is often applied to domestic wells. In stratified aquifers, however, the well water may not be truly stagnant, as we have seen, but may move contaminants from higher aquifers into lower aquifers while the pump is off. The resulting initially high contaminant concentrations may be missed if the well is pumped extensively before samples are taken.

To test this concept in the field, a domestic well in Bridgewater, New Jersey, was sampled three times: after one-half, two, and four well volumes of water were removed. The respective contaminant (chloroform) concentrations were 85, 65, and 57 ppb (Haitjema, 1987c). The contaminant concentration obtained according to protocol (obtained from the last sample) was 33% less than what was there initially! Of course, the occupants of the residence served by the well do not discard four well volumes of water every time the pump starts. Consequently, they are exposed to the full range of concentrations found during this experiment.

3.4 Heterogeneous Aquifers

In the previous section we discussed geological stratigraphies that caused hydraulic separation of different horizontal permeable strata: multiple aquifers (see Figure 3.42b). Multiple aquifers, in general, exhibit different heads in different aquifers, and thus at different depths. If the low permeable formations are isolated lenses, as in Figure 3.42a, they may cause some increased resistance to vertical flow, but may not translate into significant vertical differences in head. With or without the clay layers in Figure 3.42a, it is likely that the hydraulic conductivity in real-world aquifers varies with depth, while the head does not, at least not significantly.

The hydraulic conductivity may also vary regionally. For instance, a

stream in a regional till aquifer (mixtures of sandy clay and silt) may be surrounded by a sand and gravel zone, called a *channel deposit* or *alluvium* if deposited by the stream and *outwash* if resulting from glaciers. The sand and gravel zone may be an order of magnitude more conductive than the till. The hydraulic conductivity may also vary on a more local scale, because of clay and silt inclusions in a predominantly sand and gravel aquifer, or gravel pockets in a till aquifer.

In this section we will discuss some consequences of these different types of aquifer inhomogeneities. In all cases we will assume that the Dupuit–Forchheimer assumption remains valid: The head does not vary with depth.

3.4.1 Reduced Vertical Hydraulic Conductivity

A reduction in vertical hydraulic conductivity may be the result of many clay lenses in a sand and gravel aquifer, as illustrated in Figure 3.42a, or may occur in fractured rock aquifers where flow occurs predominantly in horizontal *bedding planes* interconnected locally by vertical fractures. When viewed on a large enough scale, the many discrete heterogeneities may be blended into a continuum: a homogeneous *anisotropic aquifer*. In the case of reduced vertical hydraulic conductivity, the principal directions of the *hydraulic conductivity tensor* are in the horizontal and vertical directions, respectively [see (2.22)],

$$\begin{aligned} q_x &= -k_h \frac{\partial \phi}{\partial x} \\ q_y &= -k_h \frac{\partial \phi}{\partial y} \\ q_z &= -k_v \frac{\partial \phi}{\partial z} \end{aligned} \tag{3.245}$$

with the vertical hydraulic conductivity k_v smaller than the horizontal hydraulic conductivity k_h:

$$k_v < k_h \tag{3.246}$$

The condition (3.246) does not encourage the adoption of the Dupuit–Forchheimer assumption, which implies that the vertical hydraulic conductivity is infinite (Kirkham,1967)! Next we will investigate the effect of a reduction of the vertical hydraulic conductivity on the validity of the Dupuit–Forchheimer assumption.

Continuing with the three-dimensional description of flow, we substitute

(3.245) in the continuity equation (2.25):

$$\frac{\partial q_x}{\partial x} + \frac{\partial q_y}{\partial y} + \frac{\partial q_z}{\partial z} = \frac{\partial(-k_h \frac{\partial \phi}{\partial x})}{\partial x} + \frac{\partial(-k_h \frac{\partial \phi}{\partial y})}{\partial y} + \frac{\partial(-k_v \frac{\partial \phi}{\partial z})}{\partial z} = 0 \quad (3.247)$$

which becomes

$$k_h \left(\frac{\partial^2 \phi}{\partial x^2} + \frac{\partial^2 \phi}{\partial y^2} \right) + k_v \frac{\partial^2 \phi}{\partial z^2} = 0 \quad (3.248)$$

the differential equation for three-dimensional anisotropic flow with k_h and k_v as the principal hydraulic conductivities.

Transformation into an Isotropic Flow Domain

To obtain a solution to (3.248), it is convenient to transform the actual flow domain (coordinates x, y, z) into a fictitious domain with coordinates $\bar{x}$, $\bar{y}$, and $\bar{z}$. We use the following transformation:

$$x = \bar{x} \qquad y = \bar{y} \qquad z = \sqrt{\frac{k_v}{k_h}}\,\bar{z} \quad (3.249)$$

with which (3.248) becomes

$$\frac{\partial^2 \phi}{\partial \bar{x}^2} + \frac{\partial^2 \phi}{\partial \bar{y}^2} + \frac{\partial^2 \phi}{\partial \bar{z}^2} = 0 \quad (3.250)$$

which is Laplace's equation for a homogeneous *isotropic* aquifer. That (3.250) and (3.248) are indeed equivalent may be verified by substituting (3.249) into (3.250). We write (3.250), by use of the chain rule, as

$$\frac{\partial^2 \phi}{\partial x^2} \left(\frac{\partial x}{\partial \bar{x}} \right)^2 + \frac{\partial^2 \phi}{\partial y^2} \left(\frac{\partial y}{\partial \bar{y}} \right)^2 + \frac{\partial^2 \phi}{\partial z^2} \left(\frac{\partial z}{\partial \bar{z}} \right)^2 = 0 \quad (3.251)$$

The derivatives of x, y, and z with respect to $\bar{x}$, $\bar{y}$, and $\bar{z}$, respectively, are obtained from (3.249):

$$\frac{\partial x}{\partial \bar{x}} = 1 \qquad \frac{\partial y}{\partial \bar{y}} = 1 \qquad \frac{\partial z}{\partial \bar{z}} = \sqrt{\frac{k_v}{k_h}} \quad (3.252)$$

so that (3.251) becomes

$$\frac{\partial^2 \phi}{\partial x^2} + \frac{\partial^2 \phi}{\partial y^2} + \frac{\partial^2 \phi}{\partial z^2} \frac{k_v}{k_h} = 0 \quad (3.253)$$

which is the same as (3.248), as asserted.

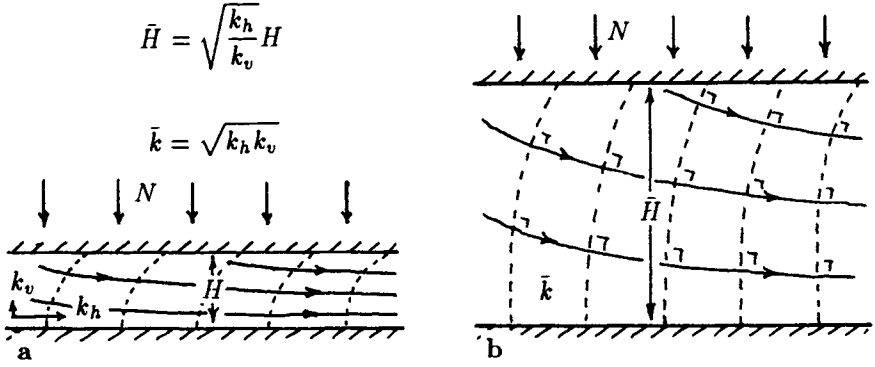

Figure 3.50: Real (a) and transformed (b) flow domain of an aquifer with a low vertical hydraulic conductivity.

The groundwater flow problem may be solved in the $\bar{x}, \bar{y}, \bar{z}$-domain, where the aquifer has a thickness $\bar{H}$:

$$\bar{H} = \sqrt{\frac{k_h}{k_v}} H \tag{3.254}$$

The isotropic hydraulic conductivity $\bar{k}$ in the transformed domain is

$$\bar{k} = \sqrt{k_h k_v} \tag{3.255}$$

The expression for $\bar{k}$ may be understood from a simple thought experiment. Assume a horizontal discharge $Q_x = Hq_x$ in the aquifer depicted in Figure 3.50a. The horizontal discharge in the transformed domain, Figure 3.50b, must be the same for reasons of continuity of flow:

$$Q_x = -k_h H \frac{\partial \phi}{\partial x} = -\bar{k} \bar{H} \frac{\partial \phi}{\partial \bar{x}} \tag{3.256}$$

which is true with (3.254) and (3.255) and in view of (3.252).

Equipotential and streamlines obtained in the transformed domain are transformed back into the actual x, y, z flow domain. It is noted that equipotentials and streamlines which are perpendicular to each other in the isotropic (transformed) domain are, in general, no longer perpendicular in the actual flow domain. In order to obtain solutions to flow in anisotropic aquifers, transformation rules are required for both Dirichlet- and Neumann-type boundary conditions, but a discussion of these rules is outside the scope of this text. For further reading refer to Harr (1962), Verrijt (1970), and Strack (1989). It suffices here to state that equipotentials

and streamlines in the actual domain remain equipotentials and streamlines in the transformed domain.

In Figure 3.50, both the actual and the transformed domain are depicted for the case that the vertical hydraulic conductivity is *10 times* the horizontal hydraulic conductivity. The aquifer height in the transformed domain is $\sqrt{k_h/k_v} = \sqrt{1/0.1} = 3.162$ times as large as in the actual domain. In the beginning of this chapter, I reasoned that if the aquifer thickness is small with respect to the lateral distance between boundary conditions (streams, lakes, wells, etc.), the Dupuit–Forchheimer assumption may be adopted. As is seen from Figure 3.50, the effect of reducing the vertical hydraulic conductivity is the same as that of increasing the aquifer height. Consequently, in order to use the Dupuit–Forchheimer assumption in aquifers with a reduced vertical hydraulic conductivity, larger distances between boundary conditions are required. In Section 5.3.4, I will show that, in order for the Dupuit–Forchheimer assumption to be valid in isotropic aquifers, the minimum distance between boundary conditions must be about two times the saturated aquifer thickness. Under conditions of decreased vertical hydraulic conductivity, this rule of thumb applies to the aquifer thickness in the transformed domain, which leads to the following rule for the actual domain.

Rule 3.14 *In order for the Dupuit–Forchheimer assumption to be valid in an aquifer with a reduced vertical hydraulic conductivity, the minimum distance between boundary conditions must be* $2\sqrt{k_h/k_v}$ *times the saturated aquifer thickness.*

Before we leave the subject of anisotropy, a word of caution. The occurrence of many clay laminae in an aquifer is often modeled by introducing anisotropy. However, not all groundwater flow characteristics are equally well represented in the anisotropic continuum model. Discontinuous clay laminae may create locally perched water table conditions and locally discrete downward pathways for groundwater, which are different from the water tables and flow paths in the continuum model where we assumed uniform vertical resistance. Consequently, whereas the anisotropic model may be a fair representation for the average flow conditions on a regional scale, it may fail to represent local groundwater pathways and associated travel times.

3.4.2 Aquifer Stratification

In Section 3.3.4, we discussed a single aquifer zone, the circular opening in the clay layer, which consisted of two different strata with two different hydraulic conductivities. Aquifers quite often consist of layers of different

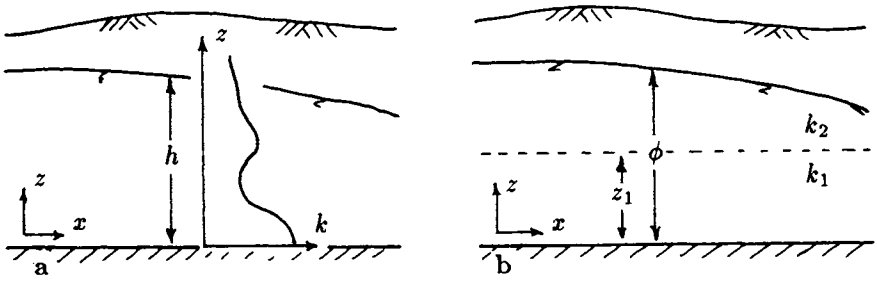

Figure 3.51: Hydraulic conductivity varies with depth (a) and a stratified aquifer (b).

geologic formations, and thus different hydraulic conductivities. Girinski (1946) introduced a potential function for Dupuit–Forchheimer flow in an aquifer with a continuously varying vertical hydraulic conductivity $k(z)$ (see Figure 3.51a):

$$\Phi = \int_0^h k(z)(\phi - z)dz \tag{3.257}$$

where h is the saturated aquifer thickness. The integral in (3.257) may be evaluated for the case of a finite number of horizontal aquifer strata. We will perform the integration for the case where the aquifer consists of only two layers, as depicted in Figure 3.51b. We will break the integral in (3.257) up into two integrals, one for each layer, and replace the saturated thickness h by the head ϕ:

$$\Phi = k_1 \int_0^{z_1} (\phi - z)dz + k_2 \int_{z_1}^{\phi} (\phi - z)dz = -\tfrac{1}{2}k_1(\phi - z)^2|_0^{z_1} - \tfrac{1}{2}k_2(\phi - z)^2|_{z_1}^{\phi} \tag{3.258}$$

which yields, after some elementary algebra,

$$\Phi = k_1\phi z_1 - \tfrac{1}{2}k_1 z_1^2 + \tfrac{1}{2}k_2(\phi - z_1)^2 \tag{3.259}$$

Equation (3.259) is the same as (3.220) if H is replaced by z_1, ϕ_0 is replaced by ϕ, and $\overset{u}{k}$ and $\overset{l}{k}$ are replaced by k_1 and k_2, respectively. The Girinski potential, therefore, is the "comprehensive potential" for a stratified aquifer. Similar expressions may be developed for aquifers with more than two strata. Following Strack (1989), the comprehensive potential for

confined flow in an aquifer with m strata is

$$\Phi = \sum_{i=1}^{m} \left[T_i(\phi - b_i) - \tfrac{1}{2} k_i (b_{i+1} - b_i)^2 \right] \qquad (\phi \geq b_{m+1}) \tag{3.260}$$

where b_i is the elevation of the base of the i^{th} stratum and b_{m+1} is the elevation of the aquifer top. The transmissivity T_i is given by

$$T_i = k_i (b_{i+1} - b_i) \tag{3.261}$$

The total transmissivity for the confined aquifer is

$$T = \sum_{i=1}^{m} T_i \tag{3.262}$$

The flow conditions are just confined when the head ϕ equals the upper aquifer boundary, which yields the potential

$$\Phi_c = \sum_{i=1}^{m} \left[T_i(b_{i+1} - b_i) - \tfrac{1}{2} k_i (b_{i+1} - b_i)^2 \right] \qquad (\phi = b_{m+1}) \tag{3.263}$$

For confined flow conditions, the head ϕ can be calculated from the potential Φ using

$$\phi = b_{m+1} + \frac{\Phi - \Phi_c}{T} \qquad (\Phi \geq \Phi_c) \tag{3.264}$$

Unconfined flow conditions occur when the head ϕ is lower than the aquifer top b_{m+1}. The head may be just below the aquifer top or below the base of one or more of the upper aquifer strata. If the head is just equal to the base of layer n, the potential Φ_n becomes

$$\Phi_n = \sum_{i=1}^{n-1} \left[T_i(b_n - b_i) - \tfrac{1}{2} k_i (b_{i+1} - b_i)^2 \right] \qquad (\phi = b_n) \tag{3.265}$$

If the head is above the base b_n but below the base b_{n+1}, the comprehensive potential for *unconfined* flow becomes

$$\Phi = \sum_{i=1}^{n-1} T_i(\phi - b_n) + \Phi_n + \tfrac{1}{2} k_n (\phi - b_n)^2 \qquad (b_n \leq \phi \leq b_{n+1}) \tag{3.266}$$

The head ϕ follows from inverting (3.266):

$$\phi = b_n - \frac{T_{n-1}}{k_n} + \sqrt{\left(\frac{T_{n-1}}{k_n} \right)^2 + \frac{2(\Phi - \Phi_n)}{k_n}} \qquad (\Phi_n \leq \Phi \leq \Phi_{n+1}) \tag{3.267}$$

For a more complete discussion of the potential functions for stratified aquifers and their relation to Girinski potentials, refer to Strack (1989). The potentials for a stratified aquifer are implemented in two commercially available analytic element models, SLAEMS[1] (arbitrary number of layers) and TWODAN[2] (two layers), and in the public domain code SLWL (Strack, 1989). These codes are useful in areas where aquifer stratification manifests itself by a number of distinct layers that occur throughout the model area. Often, however, aquifer stratification varies spatially, making it difficult to correlate the various permeable strata encountered in different borings. Under these conditions it is still possible to model groundwater flow in a single layer (single aquifer) model, provided a weighted average is used for the hydraulic conductivity. In Figure 3.52a an aquifer with five strata is depicted. The hydraulic conductivities and layer thicknesses are denoted by k_1 through k_5 and H_1 through H_5, respectively. The average hydraulic conductivity k follows from

$$k = \frac{\sum_{i=1}^{5} k_i H_i}{\sum_{i=1}^{5} H_i} \tag{3.268}$$

The homogeneous aquifer representation, Figure 3.52b, will provide piezometric head surfaces and discharge rates similar to those of the stratified aquifer in Figure 3.52a. This may be understood by interpreting the potential function for the homogeneous model aquifer as the *comprehensive potential* for the actual stratified aquifer. In fact, under confined flow conditions, the homogeneous aquifer may be given the exact same transmissivity as the stratified aquifer, and the resulting piezometric head surfaces will be identical for both aquifers. In Chapter 5, Section 5.3.5, however, we will see that under *unconfined* flow conditions, some differences do occur in the piezometric head surfaces, particularly in areas of large drawdowns.

Variations in q_i and v_i over the Aquifer Height

The specific discharge in the stratified aquifer is not constant over the aquifer height, as in the homogeneous model aquifer, but depends on the aquifer stratum in which we consider the flow. Under Dupuit–Forchheimer conditions, variations in specific discharge will be proportional to variations in the hydraulic conductivity between the different strata. For instance, in layer number 3, the specific discharge $\overset{3}{q}_i$ is

$$\overset{3}{q}_i = \frac{k_3}{k} q_i \tag{3.269}$$

[1]SLAEMS is a trademark of Strack Consulting, Inc.
[2]TWODAN is a trademark of Fitts Software, Inc.

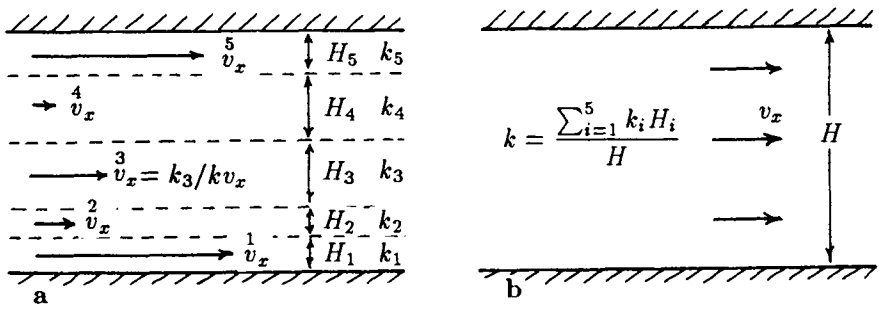

Figure 3.52: Replacing a stratified aquifer (a) by a homogeneous aquifer (b).

where q_i is the specific discharge in the homogeneous model aquifer; see Figure 3.52. This may lead to significant variations in the specific discharge, as hydraulic conductivity between strata may vary by as much as a factor of 10. It is mentioned that for variations in hydraulic conductivity in excess of a factor of 10, the Dupuit-Forchheimer assumption becomes suspect. In that case it will be necessary to treat the aquifer as a multi-aquifer system with leaky separating layers.

The groundwater flow velocities in the various layers will vary in the same manner as the specific discharge, unless there are different porosities in the layers. In that case, the velocities may vary less or more than the specific discharges, depending on the porosities involved. For instance, the velocity $\overset{3}{v}_i$ in layer 3 is $\overset{3}{q}_i / n_3$, where n_3 is the porosity in layer 3. Expressed in terms of the velocity v_i in the homogeneous model aquifer,

$$\overset{3}{v}_i = \frac{n}{n_3} v_i \tag{3.270}$$

where n is the porosity in the homogeneous aquifer.

In summary, replacing a stratified aquifer by a homogeneous aquifer will have little effect on the piezometric head surface or discharge vector field — none under confined, and some under unconfined, flow conditions. However, the specific discharges and velocities in the various aquifer strata, and thus at different depths, may differ by several factors from the "average" values obtained from the homogeneous aquifer model.

3.4.3 Regional Variations in Transmissivity

A different type of aquifer heterogeneity results from lateral variations in aquifer thickness and/or hydraulic conductivity. These conditions may occur both on the regional and the local scale. On the regional scale, changes in hydraulic conductivity are often seen near streams, where highly permeable "channel deposits" (alluvium) are embedded in more moderately permeable regional aquifer material. Moreover, these alluvial stream channels may also incise the bedrock, resulting in an increased aquifer thickness, and thus increased transmissivity. On the local scale, hydraulic conductivity variations may be due to gravel pockets in a sandy aquifer or clay inclusions in a sandy or gravely aquifer. In addition, there may also be local variations in aquifer thickness.

In this section we will look at some solutions for regions with different hydraulic conductivities. Variations in aquifer thickness will not be explicitly addressed, but their effect on the transmissivity can often be approximated by changing the hydraulic conductivity instead of the aquifer thickness, resulting in the same variation in the transmissivity. For a discussion of how to model these variations in aquifer thickness explicitly, reference is made to Strack (1989).

The Jump in the Discharge Potential

In Figure 3.53, part of an aquifer is shown in plan view with two different hydraulic conductivities separated by an abrupt interface. The hydraulic conductivities to the left and right of the interface are k_1 and k_2, respectively. The solution to the flow problem in Figure 3.53 must satisfy two conditions at the interface: (1) the head must be continuous across the interface, and (2) there must be continuity of flow across the interface. The continuity of flow requirement is self-evident, while the continuity of the piezometric head follows from the physical necessity of a single pore pressure at any one point in the aquifer, and hence also at the interface between the two hydraulic conductivities in Figure 3.53. The continuity of the head does *not* imply continuity of the potential function. Denoting the potential just to the left of the interface by Φ_1 and that just to the right by Φ_2, we observe the following jump $\Delta\Phi$ across the interface:

$$\Delta\Phi = \Phi_1 - \Phi_2 = \tfrac{1}{2}k_1\phi^2 - \tfrac{1}{2}k_2\phi^2 = (k_1 - k_2)\tfrac{1}{2}\phi^2 \tag{3.271}$$

which may be written as

$$\Delta\Phi = \frac{k_1 - k_2}{k_1}\Phi_1 \tag{3.272}$$

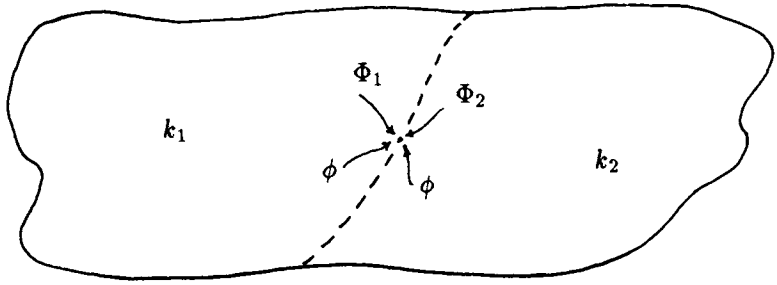

Figure 3.53: Discontinuous hydraulic conductivity.

or

$$\Delta\Phi = \frac{k_1 - k_2}{k_2}\Phi_2 \tag{3.273}$$

A similar analysis for confined flow conditions leads to the same result, (3.272) or (3.273). As it appears, the condition of a continuous head at the interface translates into the requirement of a jump in the discharge potential as defined by (3.272) or (3.273). Solutions to flow in aquifers with zones of different hydraulic conductivities, therefore, are obtained by generating a jump in the potential Φ that satisfies (3.272) or (3.273).

Exercise 3.22 *Show that the jump in the discharge potential across an interface between two different hydraulic conductivities in a* confined *aquifer is also defined by (3.272) or (3.273).*

3.4.4 A Well opposite a Straight Inhomogeneity Boundary

There exist a few exact analytic solutions to flow in an aquifer with zones of different hydraulic conductivity. A classical example is shown in Figure 3.54, where a well is located at a distance d from a straight infinitely long interface between two zones of different hydraulic conductivity. The solution consists of two parts: the potential $\Phi_1(x, y)$ in the left-hand domain where the well occurs, and the potential $\Phi_2(x, y)$ on the other side of the interface. The solutions are available in textbooks on potential flow,

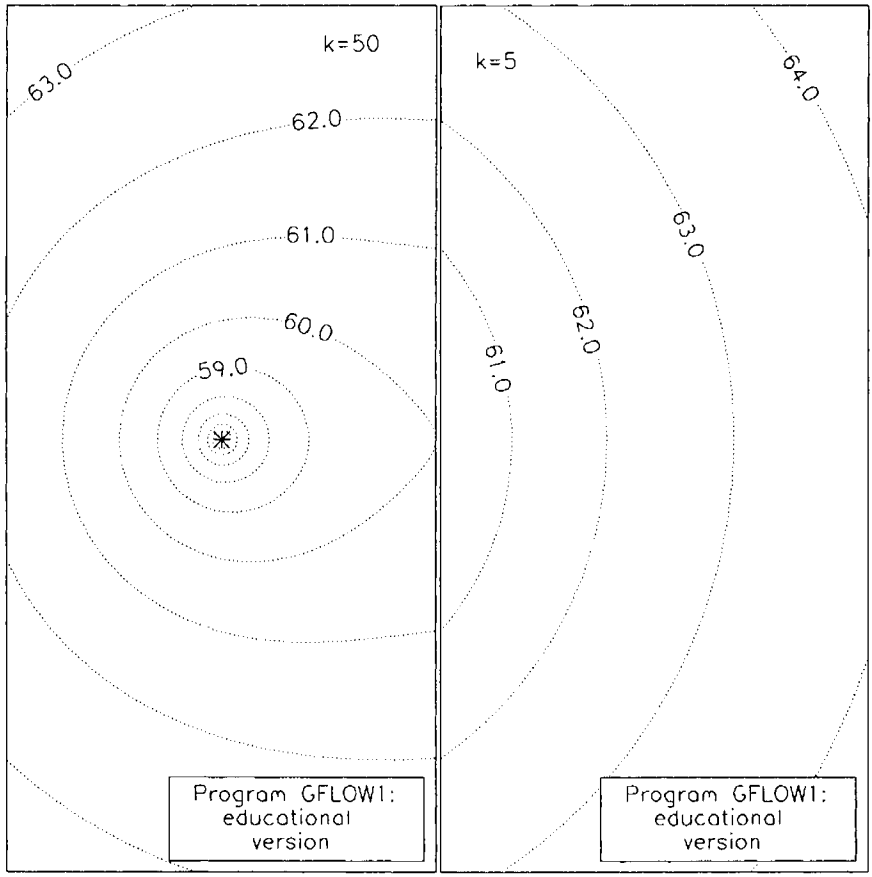

Figure 3.54: Well opposite a straight infinitely long interface between two zones of different hydraulic conductivity. (GFLOW1 file: problem9.dat)

e.g., Kellogg (1929), and are in terms of our parameters:

$$\Phi_1(x,y) = \frac{Q}{4\pi} \ln \frac{(x-x_w)^2+y^2}{R^2} + \frac{k_1-k_2}{k_1+k_2} \frac{Q}{4\pi} \ln \frac{(x+x_w)^2+y^2}{R^2} + \Phi_1(0,R) \tag{3.274}$$

and

$$\Phi_2(x,y) = \frac{2k_2}{k_1+k_2} \frac{Q}{4\pi} \ln \frac{(x-x_w)^2+y^2}{R^2} + \Phi_2(0,R) \tag{3.275}$$

The two potentials (3.274) and (3.275) must satisfy the two conditions discussed earlier: the jump in the potential, e.g., (3.273), and continuity of flow across $x = 0$. Subtracting (3.275) from (3.274), for a point at the interface ($x = 0$), yields

$$\begin{aligned} \Delta\Phi &= \Phi_1(0,y) - \Phi_2(0,y) \\ &= \left[1 - \frac{k_1-k_2}{k_1+k_2}\right] \frac{Q}{4\pi} \ln \frac{x_w^2+y^2}{R^2} + \Phi_1(0,R) \\ &\quad - \frac{2k_2}{k_1+k_2} \frac{Q}{4\pi} \ln \frac{x_w^2+y^2}{R^2} - \Phi_2(0,R) \quad (x=0) \end{aligned} \tag{3.276}$$

which reduces to

$$\Delta\Phi = \frac{2(k_1-k_2)}{k_1+k_2} \frac{Q}{4\pi} \ln \frac{x_w^2+y^2}{R^2} + \frac{k_1-k_2}{k_2} \Phi_2(0,R) \quad (x=0) \tag{3.277}$$

Equation (3.277) may be written as

$$\Delta\Phi = \frac{k_1-k_2}{k_2} \left[\frac{2k_2}{k_1+k_2} \frac{Q}{4\pi} \ln \frac{x_w^2+y^2}{R^2} + \Phi_2(0,R) \right] = \frac{k_1-k_2}{k_2} \Phi_2(0,y) \tag{3.278}$$

which is indeed equal to (3.273), as asserted.

The continuity of flow condition at $x = 0$ implies

$$\frac{\partial \Phi_1}{\partial x} = \frac{\partial \Phi_2}{\partial x} \quad (x=0) \tag{3.279}$$

Substituting (3.274) and (3.275) into (3.279) gives

$$\begin{aligned} &\frac{Q}{4\pi} \left[\frac{2(x-x_w)}{(x-x_w)^2+y^2} + \frac{k_1-k_2}{k_1+k_2} \frac{2(x+x_w)}{(x+x_w)^2+y^2} \right] \\ &= \frac{Q}{4\pi} \left[\frac{2k_2}{k_1+k_2} \frac{2(x_w-x)}{(x_w-x)^2+y^2} \right] \quad (x=0) \end{aligned} \tag{3.280}$$

which becomes, after we set $x = 0$ and divide through by $Q/4\pi$,

$$\left[\frac{k_1 - k_2}{k_1 + k_2} - 1\right] \frac{2x_w}{x_w^2 + y^2} = -\frac{2k_2}{k_1 + k_2} \frac{2x_w}{x_w^2 + y^2} \tag{3.281}$$

This is indeed true; hence, the continuity of flow requirement is also satisfied.

The piezometric contours in Figure 3.54 have been generated by running GFLOW1 twice, once for the solution to the left of the interface and once for the right-hand-side solution. In practice, as for the case of a well near a no-flow boundary, the interface does not have to be infinitely long and straight in order to make use of the foregoing solutions. They will provide a good approximation if, for instance, the well is near the boundary of an alluvial channel, which can be locally approximated by a straight line.

Exercise 3.23 *Demonstrate that (3.274) reduces to the solution for a well near a straight equipotential for the limiting case that k_2 becomes infinitely large ($k_2 \to \infty$) and to the solution for a well near a rock outcrop by setting $k_2 = 0$.*

Exercise 3.24 *Change the hydraulic conductivity contrast in the problem depicted in Figure 3.54 by following the instructions in the file* problem9.dat *provided on the distribution diskette.*

3.4.5 A Circular Inhomogeneity in a Uniform Flow Field

In Section 3.1.17, we developed a solution for a circular lake in a uniform flow field. In the context of Dupuit–Forchheimer flow, the circular lake may be viewed as a cylinder, extending over the aquifer height, with an infinite hydraulic conductivity. In fact, in Figure 3.30, we used the circular lake solution to simulate a large-diameter well, which is indeed a cylinder in the aquifer without aquifer material and thus with an infinite hydraulic conductivity.

It appears that the solution for a lake in a uniform flow field is a special case of a circular inhomogeneity with arbitrary interior hydraulic conductivity; see Carslaw and Jaeger (1959). The solution is formulated in terms of an inside and outside potential Φ_i and Φ_o, respectively:

$$\Phi_i(x, y) = -Q_0 \frac{2k_i}{k_o + k_i} x + \Phi_i(0, 0) \quad (x^2 + y^2 \leq R^2) \tag{3.282}$$

and

$$\Phi_o(x,y) = -Q_0\left[x + \frac{k_o - k_i}{k_o + k_i}\frac{xR^2}{x^2+y^2}\right] + \frac{k_o}{k_i}\Phi_i(0,0) \quad (x^2+y^2 \geq R^2) \tag{3.283}$$

where k_i and k_o are the inside and outside hydraulic conductivity, respectively, and where $\Phi_i(0,0)$ is the inside potential at the center of the circle which serves as the origin of the x, y coordinate system. The stream function for the inside and outside domain are

$$\Psi_i(x,y) = -Q_0\frac{2k_i}{k_o + k_i}y \quad (x^2+y^2 \leq R^2) \tag{3.284}$$

and

$$\Psi_o(x,y) = -Q_0\left[y - \frac{k_o - k_i}{k_o + k_i}\frac{yR^2}{x^2+y^2}\right] \quad (x^2+y^2 \geq R^2) \tag{3.285}$$

Observe that the inside potential (3.282) represents horizontal uniform flow, regardless of the difference between k_i and k_o, which may also be seen from the inside stream function (3.284). Also notice that the expressions (3.283) and (3.285) reduce to (3.144) and (3.145), respectively, for the limiting case that the inside hydraulic conductivity becomes infinitely large ($k_i \to \infty$).

Exercise 3.25 *Demonstrate that both the head and the flow across the circular inhomogeneity boundary are continuous. Note: Continuity of the head implies that $\Phi_i = k_i/k_o\Phi_o$ along the circular boundary, while continuity of flow implies that the stream function is continuous along the circular boundary. Explain why.*

In Figure 3.55, streamlines are presented for various contrasts in the inside and outside hydraulic conductivity. Notice that the effects on the flow regime are local: The flow field is nearly uniform again at a distance of about two times the inhomogeneity diameter away from the inhomogeneity. This was also observed for the extreme case of an infinite interior hydraulic conductivity, see Figure 3.30. We will revisit this issue in Chapter 5, where we will model inhomogeneities of arbitrary shape.

3.4.6 A Well at the Center of a Circular Slurry Trench

Some aquifer inhomogeneities are manmade. For instance, in attempts to contain groundwater contamination, a *slurry wall* may be installed around the contaminated aquifer zone. A *slurry wall* or *slurry trench* is a trench-like excavation backfilled with a bentonite clay (slurry) to create a low permeable wall. Often the slurry wall solution is combined with a pump

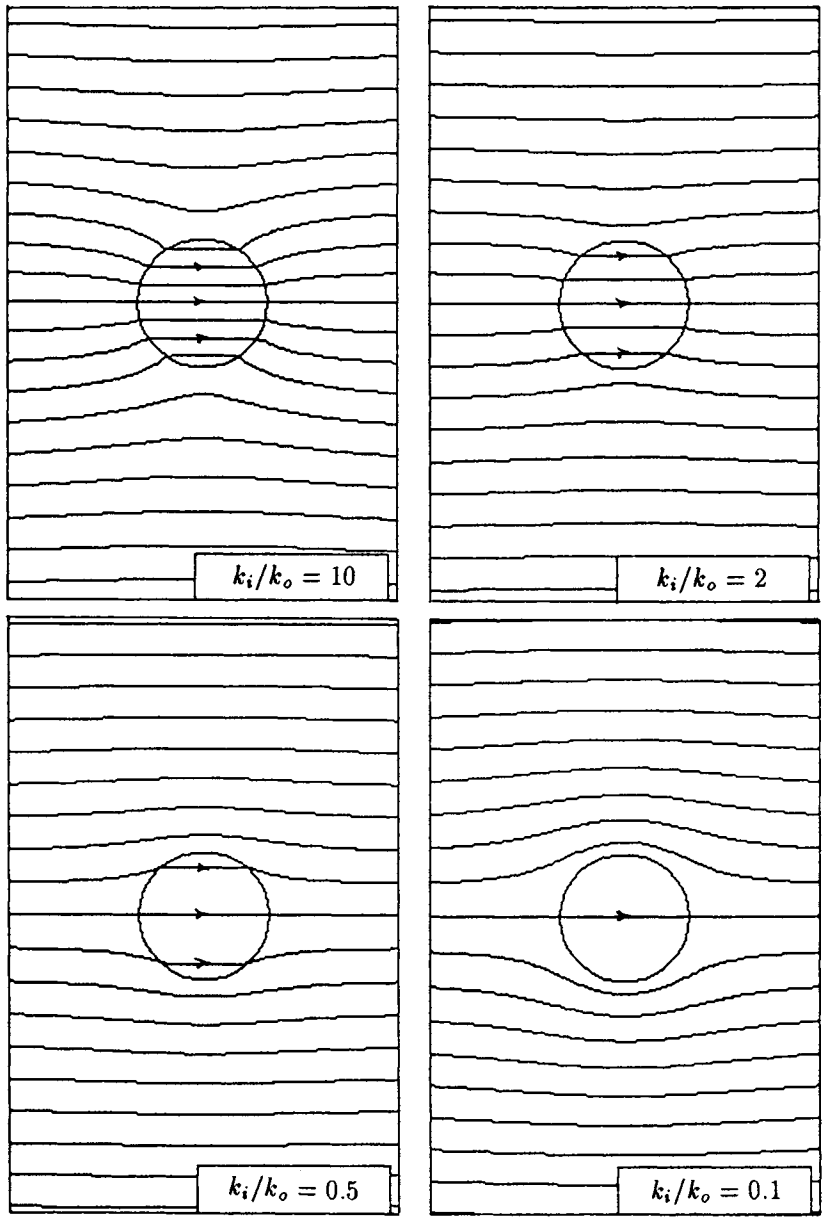

Figure 3.55: Circular inhomogeneities in a horizontal uniform flow field. The hydraulic conductivities inside and outside the circle are k_i and k_o, respectively.

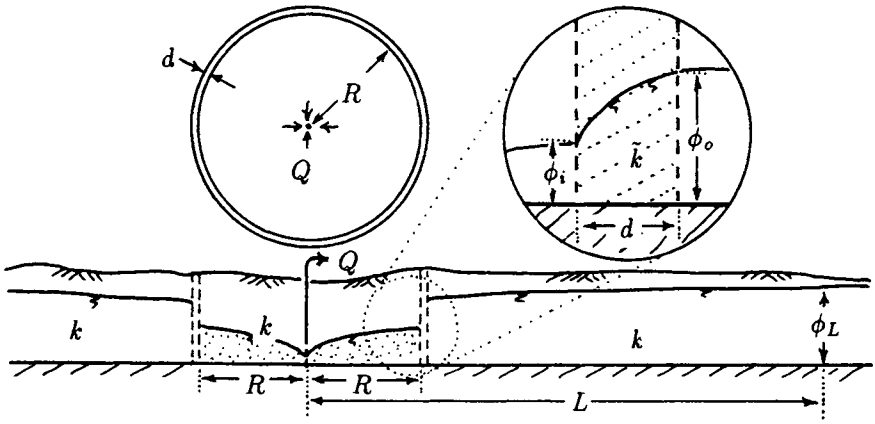

Figure 3.56: Well at the center of a circular slurry wall.

and treat system to clean up the aquifer and further ensure contaminant containment. Next we will analyze a simplified system of a slurry wall in combination with a recovery well.

In Figure 3.56, both the plan view and a cross-section of a well at the center of a circular slurry wall are depicted. The aquifer inside the slurry wall is assumed to be contaminated. The slurry wall is not impervious, but has a conductivity $\tilde{k}$ and a thickness d; see Figure 3.56. The radius of the slurry wall is R. Assuming radial flow, we provide two solutions, one for the aquifer outside the slurry wall,

$$\Phi(r) = \frac{Q}{2\pi} \ln \frac{r}{L} + \Phi_L \quad (r > R + d \; ; \; L > R) \tag{3.286}$$

and one for the aquifer inside the slurry wall,

$$\Phi(r) = \frac{Q}{2\pi} \ln \frac{r}{L} - \Delta\Phi + \Phi_L \quad (r < R \; ; \; L > R) \tag{3.287}$$

where $\Delta\Phi$ is the difference in the potential in the aquifer just outside the wall, Φ_o, and just inside the wall, Φ_i:

$$\Delta\Phi = \Phi_o - \Phi_i \tag{3.288}$$

where

$$\Phi_o = \tfrac{1}{2} k \phi_o^2 \qquad \Phi_i = \tfrac{1}{2} k \phi_i^2 \tag{3.289}$$

Neither of these potentials are a priori known. The problem can be solved, however, by writing an expression for the difference in the potentials just

inside the slurry wall as opposed to those in the aquifer on either side of the slurry wall:

$$\tilde{\Phi}_i = \frac{Q}{2\pi} \ln \frac{R}{R+d} + \tilde{\Phi}_o \tag{3.290}$$

where $\tilde{\Phi}_i$ is the potential just inside the slurry wall on the well side, and where $\tilde{\Phi}_o$ is the potential just inside the slurry wall near the outer interface between bentonite and aquifer (see the inset in Figure 3.56):

$$\tilde{\Phi}_o = \tfrac{1}{2}\tilde{k}\phi_o^2 \qquad\qquad \tilde{\Phi}_i = \tfrac{1}{2}\tilde{k}\phi_i^2 \tag{3.291}$$

Expression (3.290) may be seen as that of the potential $\tilde{\Phi}_i$ at a well of radius R and known potential $\tilde{\Phi}_o$ at radius $R+d$, whereby the "aquifer" is the slurry wall. This leads to a difference $\Delta\tilde{\Phi}$:

$$\Delta\tilde{\Phi} = \tilde{\Phi}_o - \tilde{\Phi}_i \tag{3.292}$$

or, in terms of the potentials in the aquifer on either side of the slurry wall,

$$\Delta\Phi = \frac{k}{\tilde{k}}\Delta\tilde{\Phi} \tag{3.293}$$

which becomes, with (3.290),

$$\Delta\Phi = \frac{k}{\tilde{k}}\frac{Q}{2\pi} \ln \frac{R+d}{R} = \frac{k}{\tilde{k}}\frac{Q}{2\pi} \ln\left(1 + \frac{d}{R}\right) \tag{3.294}$$

Assuming that the thickness d of the slurry wall is small compared to its radius R, hence $d/R \ll 1$, expression (3.294) reduces to

$$\Delta\Phi = \frac{Q}{2\pi}\frac{dk}{R\tilde{k}} \tag{3.295}$$

where use has been made of $\lim_{\epsilon\to 0} \ln(1+\epsilon) = \epsilon$. It is convenient to introduce a resistance c for the slurry wall defined as

$$c = \frac{d}{\tilde{k}} \tag{3.296}$$

The resistance c has the dimension of time. The solution in the aquifer enclosed by the slurry wall is finally written in the form

$$\Phi = \frac{Q}{2\pi}\left[\ln\frac{r}{L} - \frac{kc}{R}\right] + \Phi_L \quad (r < R\ ;\ L > R) \tag{3.297}$$

Observe that (3.297) reduces to that of a well in an infinite homogeneous aquifer for the case that the resistance c becomes zero, and hence when

there is no slurry wall. Both terms between the square brackets in (3.297) are negative; hence, the term kc/R contributes to the drawdowns inside the slurry wall. This is intuitively right: The more effective the slurry wall (the higher its resistance c), the lower the drawdowns, or, given the drawdowns, the lower the pumping rate Q.

Exercise 3.26 *Calculate the maximum possible well discharge Q when the following data are given: $k = 10^{-4}$ m/s, $\tilde{k} = 10^{-7}$ m/s, $L = 1{,}000$ m, $R = 100$ m, $d = 1$ m, $r_w = 0.2$ m, and $\phi_L = 6$ m. The maximum possible pumping rate is defined as the rate by which the head at the well (radius r_w) is just one meter above the aquifer bottom: $\phi_w = 1$ m. Assume unconfined flow conditions.*

Exercise 3.27 *Solve the same problem as in Exercise 3.26, but now assume an average areal recharge rate of $N = 0.002$ ft/day on the aquifer inside the slurry wall (not outside the slurry wall). What might be the purpose of artificial recharge on the area inside the slurry wall?*

3.5 Approximate Vertical Flow

As mentioned at the beginning of this chapter, the traditional interpretation of the Dupuit–Forchheimer approximation is that vertical flow is ignored, which leads to vertical equipotential surfaces:

$$\frac{\partial \phi}{\partial z} = 0 \tag{3.298}$$

Yet ignoring vertical flow is conceptually troublesome when we consider areal infiltration due to precipitation or leakage into an adjacent aquifer. In unconfined aquifers, the phreatic surface (upper aquifer boundary) is curved, also implying vertical flow in the aquifer. Clearly, water must be moving in a vertical direction, even though the condition (3.298) suggests otherwise. This apparent paradox in Dupuit–Forchheimer models was addressed by Kirkham (1967), who suggested viewing Dupuit–Forchheimer flow as occurring in aquifers with an infinite vertical hydraulic conductivity. In such a model, vertical flow can occur without a vertical gradient in the hydraulic conductivity, as expressed by (3.3):

$$q_z = \lim_{\substack{k_z \to \infty \\ \partial\phi/\partial z \to 0}} \left(-k_z \frac{\partial \phi}{\partial z} \right) \neq 0 \tag{3.299}$$

In 1952 the Russian mathematician Polubarinova-Kochina showed in her book *Theory of Ground Water Movement* how approximate vertical flow

components can be calculated in Dupuit–Forchheimer models as a result of the curving phreatic surface. Her book was translated into English by de Wiest (Polubarinova-Kochina, 1962). In 1984, Strack published a comprehensive theory of estimating three-dimensional streamlines in Dupuit–Forchheimer models (Strack, 1984). His expressions for q_z include both the effects of the curvature of the phreatic surface and the effects of areal recharge and leakage. Comparisons with exact two-dimensional solutions in the vertical plane (Strack, 1984) and complete three-dimensional solutions (Haitjema, 1987a) demonstrate a surprising accuracy of the approximate three-dimensional streamlines for many practical cases. In fact, as we will see in Section 5.3.4, the approximate three-dimensional streamlines are often more realistic than the piezometric head distributions obtained from Dupuit–Forchheimer models.

The implications are significant. One of the most persuasive arguments for the use of a three-dimensional groundwater flow model is the need for a description of flow paths in three dimensions. This is particularly important when dealing with point-source groundwater contamination. However, if three-dimensional flow patterns can be adequately approximated using a Dupuit–Forchheimer model, then there may be little advantage in implementing a full blown three-dimensional model. This is only true, of course, when the prerequisite for adopting the Dupuit–Forchheimer assumption is met: The distance between boundary conditions must be large as compared to the saturated thickness of the aquifer. See also Rule 3.14.

Next, I will present an abbreviated version of the theory of approximate three-dimensional streamlines in Dupuit–Forchheimer models. For a comprehensive treatise, refer to Strack (1984, 1989). Comparisons with complete three-dimensional flow solutions are deferred to Chapter 5.

3.5.1 Vertical Flow from Continuity Considerations

The vertical component of flow q_z cannot be obtained from Darcy's law, as is evident from (3.299). Instead, we will estimate q_z from continuity considerations. In a three-dimensional flow regime, continuity of (steady-state) flow implies that the divergence of the specific discharge vector is zero, see (2.25):

$$\frac{\partial q_x}{\partial x} + \frac{\partial q_y}{\partial y} + \frac{\partial q_z}{\partial z} = 0 \tag{3.300}$$

which gives us an expression for the derivative of q_z:

$$\frac{\partial q_z}{\partial z} = -\left[\frac{\partial q_x}{\partial x} + \frac{\partial q_y}{\partial y}\right] \tag{3.301}$$

Continuity of flow in a Dupuit–Forchheimer model is [see (3.151)],

$$\frac{\partial Q_x}{\partial x} + \frac{\partial Q_y}{\partial y} = \frac{\partial}{\partial x}(hq_x) + \frac{\partial}{\partial y}(hq_y) = N \tag{3.302}$$

where h is the saturated aquifer thickness, and N the areal recharge rate.

Confined Flow Conditions

At first we will assume that $h = H$ is constant, so that (3.302) becomes

$$\frac{\partial q_x}{\partial x} + \frac{\partial q_y}{\partial y} = \frac{N}{H} \tag{3.303}$$

which, substituted in (3.301), yields

$$\frac{\partial q_z}{\partial z} = -\frac{N}{H} \tag{3.304}$$

Integration of (3.304) results in an expression for q_z:

$$q_z = \int -\frac{N}{H} dz = -\frac{N}{H} z + C \tag{3.305}$$

There is no vertical flow at the aquifer bottom, $z = 0$, so that the constant in (3.305) is zero:

$$q_z = -\frac{N}{H} z \tag{3.306}$$

The vertical flow in a Dupuit–Forchheimer model of a confined aquifer seems to vary linearly between $q_z = -N$ at the aquifer top and $q_z = 0$ at the aquifer bottom; see Figure 3.57.

Unconfined Flow Conditions

Under unconfined flow conditions, h is not constant in (3.302). Applying the chain rule to (3.302) yields

$$\frac{\partial h}{\partial x} q_x + h\frac{\partial q_x}{\partial x} + \frac{\partial h}{\partial y} q_y + h\frac{\partial q_y}{\partial y} = N \tag{3.307}$$

which may be reorganized as

$$\frac{\partial h}{\partial x} q_x + \frac{\partial h}{\partial y} q_y + h\left[\frac{\partial q_x}{\partial x} + \frac{\partial q_y}{\partial y}\right] = N \tag{3.308}$$

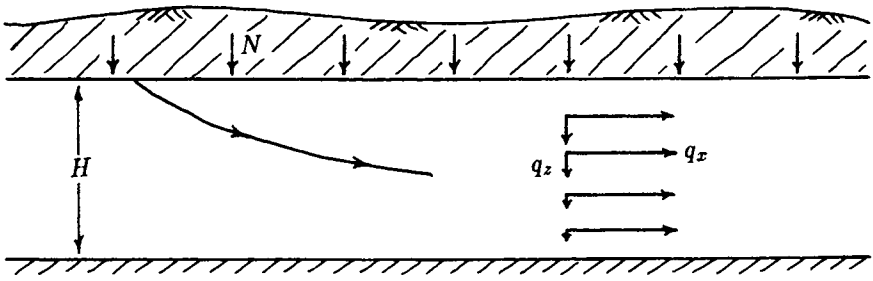

Figure 3.57: Vertical flow in a confined Dupuit–Forchheimer model due to areal recharge.

Using (3.301) and switching to index notation gives for the derivative of q_z

$$\frac{\partial q_z}{\partial z} = \frac{1}{h}\left[\partial_i h\, q_i - N\right] \qquad (i = 1, 2) \tag{3.309}$$

which, integrated over the saturated aquifer height, results in the following expression for q_z:

$$q_z = \frac{z}{h}\left[q_i \partial_i h - N\right] \qquad (i = 1, 2) \tag{3.310}$$

With h being equal to the piezometric head ϕ, when measured with respect to the aquifer bottom, and using the discharge vector Q_i, expression (3.310) may also be written as

$$q_z = \frac{z}{\phi}\left[\frac{Q_i}{\phi}\partial_i \phi - N\right] \qquad (i = 1, 2) \tag{3.311}$$

The first term between the square brackets in (3.311) is due to the curving phreatic surface and was also found by Polubarinova-Kochina (1962). The analysis may be expanded to include leakage through the aquifer bottom N_b out of a deeper aquifer. If the leakage rate N_b is known, the following general expression for q_z is obtained (see Strack, 1984, 1989):

$$q_z = \frac{z}{\phi}\left[\frac{Q_s}{\phi}\frac{\partial \phi}{\partial s} - N_t - N_b\right] + N_b \tag{3.312}$$

where s is measured along the streamline in the horizontal plane and where N_t is the infiltration at the aquifer top. The total areal infiltration in the aquifer, therefore, is $N = N_t + N_b$; see Figure 3.58.

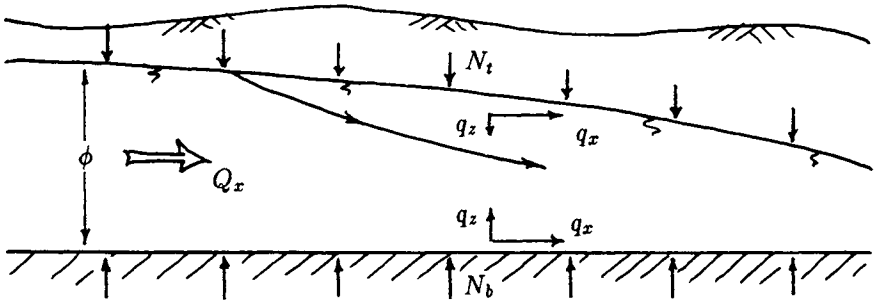

Figure 3.58: Vertical flow in an unconfined Dupuit–Forchheimer model due to areal recharge and leakage through the aquifer bottom.

In GFLOW1, streamline tracing is routinely done in three dimensions using (3.312). In Figure 3.59, the same flow problem is depicted as in Figure 3.38. Three streamlines have been traced starting from the left boundary of Figure 3.59, passing underneath the circular recharge area, and ending at the well. The tick marks on the left-hand side of the streamlines, underneath the circular recharge area, indicate the depth of the streamline. Each tick mark signals a depth increase of 5 (e.g., feet). Since the streamlines started at the aquifer top (elevation 50), the successive tick marks indicate elevations of 45, 40, 35, etc. Notice that the tick marks are most closely spaced at the upstream end of the recharge area, where the horizontal velocities are smaller than they are further downstream toward the well. Consequently, the streamlines descend more steeply into the aquifer on the upstream side than on the downstream side of the recharge area.

Exercise 3.28 *Refer to the instructions in the data file* proble10.dat, *included on the distribution diskette, for further experimentation with three-dimensional streamlines in GFLOW1.*

Next we will illustrate the concept of three-dimensional streamlines in Dupuit–Forchheimer models for a few simple flow cases.

3.5.2 A Well in a Dual Aquifer near a Polluted Stream

In Figure 3.60, a cross-section is depicted over an aquifer between two parallel streams. The stream on the left-hand side is polluted. The aquifer on the right-hand side is separated into an upper and lower aquifer by an impermeable (thin) clay layer. A domestic well is present in the upper aquifer.

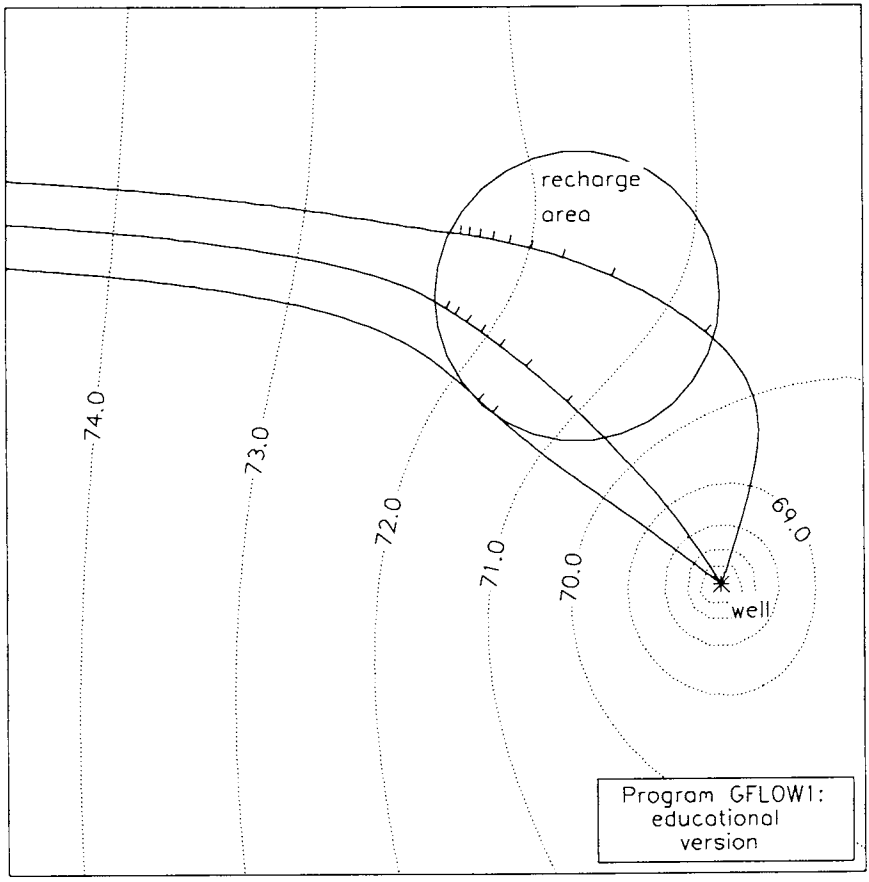

Figure 3.59: Streamlines with tick marks indicating their vertical elevation. Each tick mark indicates a depth increment of 5. (GFLOW1 data file: proble10.dat)

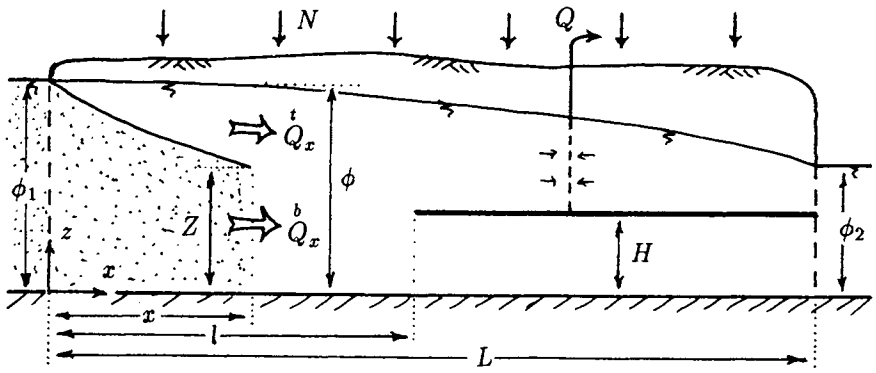

Figure 3.60: A well in a dual aquifer near a polluted stream.

Although the well is intermittently pumping small amounts of water, we will ignore its effect on the groundwater flow regime. This allows us to treat the flow in the aquifers as one-dimensional Dupuit-Forchheimer flow.

Of interest is whether or not the well in the upper aquifer receives polluted water from the stream on the left? To begin with, only in cases where the groundwater movement is everywhere to the right, and hence when there is no groundwater divide in the aquifer, will polluted stream water enter the aquifer and potentially pollute the well. In that event, the question may also be phrased as follows: Will a streamline emanating at the saturated aquifer top at the left-hand stream end up above or below the clay layer (see Figure 3.60)? If that critical streamline ends up above the clay layer, some polluted stream water will enter the upper aquifer and pollute the well.

The vertical position of the streamline at any point (for any x) in the aquifer may be obtained directly from continuity of flow considerations, thus bypassing the use of (3.312), as follows. The discharge Q_x is written as the sum of two discharges,

$$Q_x = \overset{t}{Q}_x + \overset{b}{Q}_x \tag{3.313}$$

where $\overset{t}{Q}_x$ and $\overset{b}{Q}_x$ are the discharges above and underneath the streamline, respectively. The elevation z of the streamline follows from

$$\frac{z}{\phi} = \frac{zq_x}{\phi q_x} = \frac{\overset{b}{Q}_x}{Q_x} \tag{3.314}$$

where use is made of the fact that in a Dupuit-Forchheimer model, q_x is

constant over the aquifer height (provided the aquifer is not stratified). The discharge Q_x is obtained by differentiating the comprehensive potential Φ [see (3.204)],

$$\Phi = -\frac{N}{2}x(x-L) + \frac{\Phi_2 - \Phi_1}{L}x + \Phi_1 \tag{3.315}$$

so that

$$Q_x = -\frac{\partial \Phi}{\partial x} = Nx - \frac{NL}{2} + \frac{\Phi_1 - \Phi_2}{L} \tag{3.316}$$

The discharge $\overset{b}{Q}_x$ follows from

$$\overset{b}{Q}_x = Q_x - \overset{t}{Q}_x = Q_x - Nx \tag{3.317}$$

The last term (Nx) in (3.317) equals the recharge that entered the aquifer between the left-hand stream ($x = 0$) and the point x; see Figure 3.60. Combining (3.314) through (3.317) yields for z

$$z = \phi \left[1 - \frac{Nx}{Nx - \frac{NL}{2} + \frac{\Phi_1 - \Phi_2}{L}} \right] \tag{3.318}$$

The well will become polluted if, for $x = l$ in (3.318), z becomes larger than H.

Exercise 3.29 *Answer the question whether or not the well receives any contaminants from the stream when the following data are given:* $\phi_1 = 50$ *ft,* $\phi_2 = 30$ *ft,* $H = 22$ *ft,* $L = 2000$ *ft,* $l = 1000$ *ft,* $k = 10$ *ft/day, and* $N = 2 \times 10^{-3}$ *ft/day.*

The preceding problem may be seen as a simplified version of the problem of pollutants passing underneath a partially penetrating well. The clay layer in Figure 3.60 was needed in order to maintain Dupuit–Forchheimer conditions near the well. It has been tacitly assumed, therefore, that the well is screened over the entire upper aquifer. Without the clay layer, a complete three-dimensional solution would be required in order to answer the question whether the pollutants would enter the partially penetrating well or pass underneath. We will discuss such a solution in Chapter 4.

3.5.3 Contaminant Concentration in a Well

Three-dimensional streamline tracing can be used not only to determine whether or not a well will become polluted, but also to what extent. Consider the situation depicted in Figure 3.61. Streamlines emanating from the rear and front of the contaminated area will arrive at different elevations at

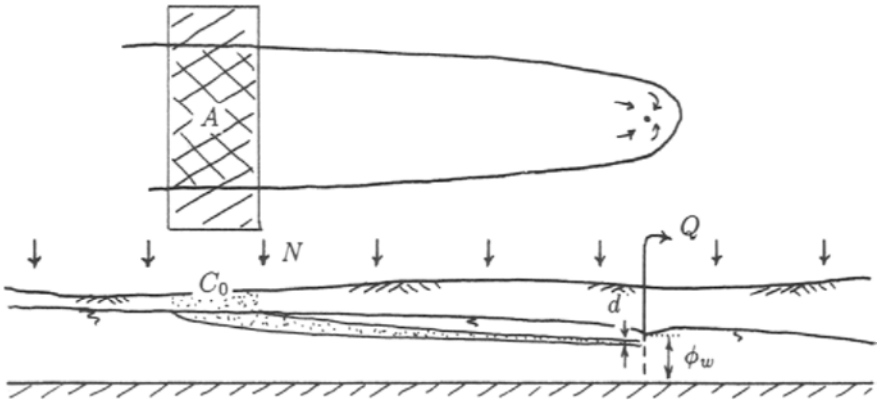

Figure 3.61: Contaminant plume intercepting a well.

the well. They form the bounding streamlines of the contaminant plume in the vertical plane, ignoring diffusion (dispersion) of the contaminants across streamlines. We can calculate these elevations by tracing three-dimensional streamlines using (3.312), e.g., using GFLOW1. Comparing the thickness d of the contaminant plume near the well with the total saturated thickness ϕ_w at the well allows us to estimate the contaminant concentration in the well. For the case of a conservative tracer, a compound which does not adsorb to the soil or (partly) disappear due to physical or (bio)chemical processes, the concentration C_w in the well is simply

$$C_w = \frac{d}{\phi_w} C_0 \tag{3.319}$$

where C_0 is the concentration of the water that leaches through the contaminated area into the aquifer.

If we are indeed dealing with a conservative tracer, there is a more direct way to estimate the concentration C_w at the well. If the areal recharge rate is N, C_w follows from a simple mass balance consideration:

$$C_w = \frac{AN}{Q} C_0 \tag{3.320}$$

where A is the contaminated area that contributes to the well, N is the areal recharge rate, and Q is the total well discharge. Simple mass balance computations such as these are often useful to estimate the impact of groundwater contamination on a receptor. Contaminant decay due to volitalization, radioactive decay, or (bio)chemical reactions will lead to lower

actual concentrations, thus making the mass balance approach a conservative one when trying to estimate maximum possible concentrations.

3.6 Transient Flow

So far we have only concerned ourselves with steady-state flow, without much justification. Groundwater flow is nearly always transient; for instance, varying recharge rates tend to make groundwater levels rise in the winter and drop in the summer. There are also manmade transient effects: Intermittent pumping of large industrial or public water supply wells, or the addition of extra wells, results in groundwater flow patterns that change over time. Consequently, our steady-state solutions must be interpreted as long-term average conditions. The piezometric head surfaces of these steady-state solutions, therefore, are unlikely to match observed piezometric heads at any one time. This has significant implications for so-called model calibration procedures, an issue we will discuss in more detail in Chapter 5.

Modeling transient groundwater flow is far more involved than steady-state flow modeling. It requires more sophisticated models and, most of all, many more field data. These additional data include the storage capacity of the aquifer (which may vary over the model area) as model input data, and time series of piezometric heads, distributed over the model area, for model calibration purposes. To avoid these complications, we will limit ourselves, when possible, to the modeling of average conditions: steady-state flow. Moreover, even when transient groundwater flow modeling is called for, it is good practice to start with steady-state modeling before attempting to include any transient effects.

In this section, and in Chapter 5, we will pay limited attention to transient flow with the objective of understanding its relative importance. Next we will derive the governing differential equation for transient groundwater flow, present the well-known solution of Theis for a well that starts pumping, and apply the results to the evaluation of pumping tests. We will also compare the effects of periodic pumping in a confined and an unconfined aquifer.

3.6.1 The Boussinesq Equation

To obtain the differential equation for transient flow, we have to revisit the concept of continuity of flow. In Figure 3.62, an elementary volume in an unconfined aquifer is depicted. The elementary volume is a rectangular column centered at the point x, y and with its sides parallel to the x-

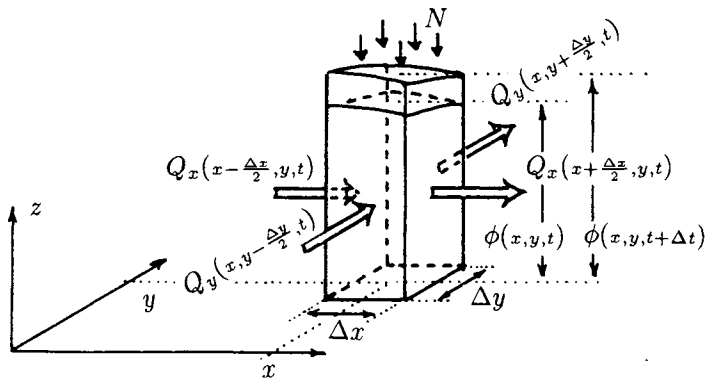

Figure 3.62: Continuity of transient flow in an unconfined aquifer.

and y-axes. The widths of the sides are Δx and Δy, respectively, while the height of the column is ϕ. Actually, the height of the column varies in time due to transient flow conditions. In Figure 3.62, the height is depicted at times t and $t + \Delta t$: $\phi(x,y,t)$ and $\phi(x,y,t+\Delta t)$, respectively. The total discharges that enter or leave the column through the four sides are indicated in Figure 3.62. Note that in addition to labeling these discharge vector components according to their position, I have also labeled them as occurring at time t. During the times t and $t+\Delta t$, the groundwater table in Figure 3.62 rises, increasing the saturated aquifer thickness and thus allowing more water to enter the column during that time period than what is leaving the column: Water is being *stored* in the aquifer. In words: Inflow equals outflow plus storage during the time interval Δt. To translate this continuity concept in mathematical terms, I am rewriting the continuity statement as

outflow - inflow = - storage + recharge

where the inflow term has been broken up into inflow through the sides of the column and areal recharge on the top of the column. Writing this out in terms of the parameters indicated in Figure 3.62, we get

$$\begin{aligned}&[Q_x(x+\tfrac{\Delta x}{2},y,t) - Q_x(x-\tfrac{\Delta x}{2},y,t)]\,\Delta y\Delta t\\ &+ [Q_y(x,y+\tfrac{\Delta y}{2},t) - Q_y(x,y-\tfrac{\Delta y}{2},t)]\,\Delta x\Delta t\\ &\quad = -n[\phi(x,y,t+\Delta t) - \phi(x,y,t)]\Delta x\Delta y \quad + \quad N\Delta x\Delta y\Delta t \quad (3.321)\end{aligned}$$

Equation (3.321) is written in terms of volumes of water $[L^3]$ that enter, leave, or are stored in the aquifer column during the time step Δt. The storage term in (3.321) (first term on the third line) is the volume of the

aquifer between the groundwater table at time t and at time $t + \Delta t$ multiplied by the porosity n. Hence, the storage term as written in (3.321) represents the total volume of groundwater stored in the upper part of the aquifer column, between the phreatic surfaces at time t and $t + \Delta t$.

Dividing both sides of (3.321) by the factor $\Delta x \Delta y \Delta t$ leads to the following finite difference expression:

$$\begin{aligned} &\frac{Q_x(x+\frac{\Delta x}{2},y,t) - Q_x(x-\frac{\Delta x}{2},y,t)}{\Delta x} \\ &+\frac{Q_y(x,y+\frac{\Delta y}{2},t) - Q_y(x,y-\frac{\Delta y}{2},t)}{\Delta y} \\ &= -n\frac{\phi(x,y,t+\Delta t) - \phi(x,y,t)}{\Delta t} \quad + \quad N \end{aligned} \tag{3.322}$$

After we take the limit for $\Delta x \to 0$, $\Delta y \to 0$ and $\Delta t \to 0$, the continuity equation becomes

$$\frac{\partial Q_x}{\partial x} + \frac{\partial Q_y}{\partial y} = -n\frac{\partial \phi}{\partial t} + N \tag{3.323}$$

Substituting Darcy's law (3.20) into (3.323) yields

$$\nabla^2 \Phi = n\frac{\partial \phi}{\partial t} - N \tag{3.324}$$

which is known as the *Boussinesq equation.* Since we are dealing with unconfined flow conditions, Φ contains ϕ^2, which makes the differential equation nonlinear in terms of ϕ. Writing (3.324) in terms of Φ does not help, since the right-hand side would then contain the square root of Φ; the equation remains nonlinear. When we solve (3.324) numerically, e.g., using the finite difference method, its nonlinear character poses no obstacle, but only a few analytic solutions to (3.324) are known (Boussinesq, 1904; Aravin and Numerov, 1965).

Equation (3.324) may be approximated by a linear equation which is easier to solve. I will write (3.324) in terms of Φ, which involves the term $\partial\Phi/\partial t$:

$$\frac{\partial \Phi}{\partial t} = \frac{\partial(\frac{1}{2}k\phi^2)}{\partial t} = \phi k\frac{\partial \phi}{\partial t} \tag{3.325}$$

Combining (3.325) and (3.324) yields

$$\nabla^2 \Phi = \frac{n}{k\phi}\frac{\partial \Phi}{\partial t} - N \tag{3.326}$$

The differential equation can now be linearized by replacing the factor $n/k\phi$ by $n/k\bar{\phi}$, where $\bar{\phi}$ is constant:

$$\nabla^2 \Phi = \frac{S}{k\bar{\phi}}\frac{\partial \Phi}{\partial t} - N \tag{3.327}$$

I have also replaced the porosity n by the *storage coefficient* S, which is dimensionless. The latter substitution is important, since the aquifer porosity tends to overestimate the actual available storage. The reason for this is that some of the pore space may already contain water prior to becoming saturated (rising groundwater table) or, when the water table drops, not all water may be drained at once from the now unsaturated zone. We may write S as

$$S = n_e \leq n \tag{3.328}$$

where n_e stands for *effective porosity*, which is usually smaller than the total aquifer porosity n. It is customary to use a *specific storage coefficient* S_s, defined as

$$S_s = \frac{S}{\bar{\phi}} \tag{3.329}$$

with which (3.327) becomes

$$\nabla^2 \Phi = \frac{S_s}{k} \frac{\partial \Phi}{\partial t} - N \tag{3.330}$$

Confined Aquifers

In confined aquifers, storage is accomplished by expanding the aquifer and compressing the groundwater. As you can imagine, these effects are small compared to the storage due to variations in the water table (thus, aquifer thickness) in unconfined aquifers. As a result, the storage coefficient S in (3.327) or the specific storage coefficient S_s in (3.330) is often several orders of magnitude smaller for confined aquifers than for unconfined aquifers. For confined flow, S_s is given by

$$S_s = \gamma_w (m_v + n/K_w) \tag{3.331}$$

where m_v is the "coefficient of volume compressibility" of the aquifer material, and where γ_w and K_w are the unit weight and "bulk modulus" for the groundwater, respectively.

The unit weight and bulk modulus of pure water at 4^oC are: $\gamma_w = 10$ [kN/m^3] and $K_w = 2.3 \times 10^9$ [kN/m^2]. The bulk modulus for groundwater may have a somewhat lower value due to dissolved gases. Some typical values for the volume compressibility m_v are given below (after Freeze, 1979).

Soil type	m_v in m^2/kN
clay	$10^{-3} - 10^{-5}$
sand	$10^{-4} - 10^{-6}$
gravel	$10^{-5} - 10^{-7}$
jointed rock	$10^{-5} - 10^{-7}$
sound rock	$10^{-6} - 10^{-8}$

The derivation of (3.331) requires knowledge of some basic concepts from soil mechanics, in particular Terzaghi's theory of one-dimensional consolidation. The following assumptions underly (3.331):

- The aquifer deforms only in the vertical direction (one-dimensional consolidation).
- The deformations are small, leaving the hydraulic conductivity and porosity unaltered.
- The aquifer behaves linearly elastic.
- The total vertical stresses in the aquifer remain the same.

These assumptions appear reasonable for most cases of transient confined flow.

The differential equation (3.330) is the same for both confined and unconfined flow. For confined flow, however, the differential equation (3.330) is *linear* by nature, since the specific storage coefficient S_s does not depend on ϕ, compare (3.329) and (3.331). The recharge term N, for confined flow, either is due to leakage through the confining layers or is equal to zero when the aquifer is bounded by aquicludes.

3.6.2 Theis' Solution for a Well

Equation (3.330) is commonly known as the *diffusion equation*, for which various solutions can be found in the literature; see, for instance, Carslaw and Jaeger (1959). In 1935, Charles V. Theis published a paper in which he applied the solution for transient heat conduction due to an instantaneous line source to the case of flow toward a well that starts pumping at some time t_0 (Theis, 1935). His classic paper opened the way to meaningful calculations of transient groundwater flow. Theis' solution, for instance, forms the basis for the evaluation of pumping tests used to determine aquifer parameters, as we will discuss elsewhere in this section.

In terms of the discharge potential Φ, Theis' solution is, assuming no recharge [$N = 0$ in (3.330)],

$$\Phi(r,t) = -\frac{Q}{4\pi} E_1(u) + \Phi_0 \qquad (t > t_0) \tag{3.332}$$

where r is the radial distance from the well, Φ_0 the initial potential at time t_0, and where u is defined as

$$u = \frac{S_s r^2}{4k(t - t_0)} \tag{3.333}$$

The function E_1 in (3.332) is a form of the so-called exponential integral function:

$$E_1(u) = \int_u^\infty \frac{e^{-\xi}}{\xi} d\xi \tag{3.334}$$

In many groundwater textbooks, the integral (3.334) is referred to as the "well function" $W(u)$. With that notation (3.332), looks like

$$\Phi(r,t) = -\frac{Q}{4\pi} W(u) + \Phi_0 \qquad (t > t_0) \tag{3.335}$$

Verification of Theis' Solution

The solution (3.332) may be obtained from the diffusion equation by use of Laplace transformations (see, e.g., Carslaw and Jaeger, 1959). We will omit this derivation, but instead demonstrate that (3.332) satisfies the differential equation (3.330), the boundary condition at the well with radius r_w,

$$Q_r = -\frac{\partial \Phi}{\partial r} = \frac{Q}{2\pi r_w} \quad (r = r_w \; ; \; t > t_0) \tag{3.336}$$

and the *initial condition* in the aquifer,

$$\Phi = \Phi_0 \quad (r > 0 \; ; \; t \leq t_0) \tag{3.337}$$

To verify that (3.332) satisfies the differential equation, we rewrite (3.330) in terms of cylindrical coordinates (see, e.g., Korn and Korn, 1968):

$$\frac{\partial^2 \Phi}{\partial r^2} + \frac{1}{r}\frac{\partial \Phi}{\partial r} = \frac{S_s}{k}\frac{\partial \Phi}{\partial t} \tag{3.338}$$

where N is assumed zero. We will demonstrate the validity of (3.332) by substituting it in (3.338). To do this we will need the first and second derivative of E_1 with respect to r. The first derivative is

$$\frac{\partial E_1(u)}{\partial r} = \frac{\partial}{\partial r}\int_u^\infty \frac{e^{-\xi}}{\xi} d\xi = -\frac{e^{-u}}{u}\frac{\partial u}{\partial r} \tag{3.339}$$

where use is made of Leibnitz's rule for the differentiation of integrals,

$$\frac{\partial}{\partial x}\int_{f_1(x)}^{f_2(x)} F(y,x)dy = \int_{f_1(x)}^{f_2(x)} \frac{\partial F}{\partial x}dy + F(f_2,x)\frac{\partial f_2}{\partial x} - F(f_1,x)\frac{\partial f_1}{\partial x} \quad (3.340)$$

With F a function of ξ only ($y = \xi$) and f_2 being a constant ($f_2 = \infty$), only the last term of (3.340) remains, which yields (3.339). By use of (3.333), expression (3.339) becomes

$$\frac{\partial E_1(u)}{\partial r} = \frac{e^{-u}}{u}\frac{2S_s r}{4k(t-t_0)} = -2\frac{e^{-u}}{r} \quad (3.341)$$

The second derivative of E_1 with respect to r becomes

$$\frac{\partial^2 E_1(u)}{\partial r^2} = 2\frac{e^{-u}}{r}\frac{\partial u}{\partial r} + 2\frac{e^{-u}}{r^2} = \frac{e^{-u}}{r^2}(4u+2) \quad (3.342)$$

The derivative of E_1 with respect to t becomes

$$\frac{\partial E_1}{\partial t} = -\frac{e^{-u}}{u}\frac{\partial u}{\partial t} = \frac{e^{-u}}{t-t_0} \quad (3.343)$$

Substituting (3.332) into the differential equation (3.338), using (3.341) through (3.343), yields

$$-\frac{Q}{4\pi}\frac{e^{-u}}{r^2}(4u+2) + \frac{Q}{4\pi}2\frac{e^{-u}}{r} \stackrel{?}{=} -\frac{S_s}{k}\frac{Q}{4\pi}\frac{e^{-u}}{t-t_0} \quad (3.344)$$

I divide both sides of the equation by $-Q/\pi r^2$ and combine the two terms on the left-hand side:

$$ue^{-u} \stackrel{?}{=} \frac{S_s r^2}{4k(t-t_0)}e^{-u} = ue^{-u} \quad (3.345)$$

so that (3.338) is indeed satisfied, as asserted.

Next we need to verify the boundary condition (3.336). The discharge Q_r at the well screen ($r = r_w$) follows from

$$Q_r(r_w,t) = -\frac{\partial \Phi}{\partial r} = -\frac{Q}{2\pi r_w}e^{-u_w} \quad (3.346)$$

where u_w is defined as

$$u_w = \frac{S_s r_w^2}{4k(t-t_0)} \quad (3.347)$$

Expression (3.346) differs from the required boundary condition (3.336) by the factor e^{-u_w}. As is seen from (3.347), the parameter u_w depends on

time, and hence the inflow into the well varies with time. However, since r_w^2 is small in (3.347), the factor e^{-u_w} in (3.346) is nearly 1, except for very small times $(t - t_0)$:

$$Q_r(r_w) \approx -\frac{Q}{2\pi r_w} \quad (u_w \ll 1) \tag{3.348}$$

Strictly speaking, therefore, the boundary condition (3.336) is only exactly met when r_w becomes vanishingly small ($r_w \to 0$). In practice, the well radius is usually sufficiently small for (3.348) to be true.

Finally, we need to verify the initial condition (3.337). When t is less than t_0, Theis' solution does not apply, which means that the potential is equal to the initial value Φ_0. When t is equal to t_0, the parameter u becomes infinitely large, so that for E_1:

$$\lim_{t \to t_0} E_1(u) = \lim_{u \to \infty} E_1(u) = \int_{\infty}^{\infty} \frac{e^{-\xi}}{\xi} d\xi = 0 \tag{3.349}$$

With E_1 becoming zero, Theis' solution reduces to the constant potential Φ_0; see (3.332). This completes the verification of Theis' solution.

Numerical Evaluation of E_1

The exponential integral function E_1 is a tabulated function, similar to the logarithmic function, for instance. Below a listing of a Basic subprogram is provided for approximating the function $E_1(u)$:

```
500 REM
510 REM   function E1(u)
520 REM
530 u2=u*u
540 u3=u2*u
550 u4=u3*u
560 if u-.5 GOTO 610
570 u5=u4*u
580 E1=-.57721566#+.99999193#*u-.24991055#*u2+5.519968e-02*u3
590 E1=E1-9.76004e-03*u4+1.07857e-03*u5-LOG(u)
600 RETURN
610 E1=u4+8.5733287401#*u3+18.059016973#*u2
615 E1=E1+8.6347608925#*u+.2677737343#
620 u1=u4+9.5733223454#*u3+25.6329561486#*u2
625 u1=u1+21.0996530827#*u+3.958496228#
```

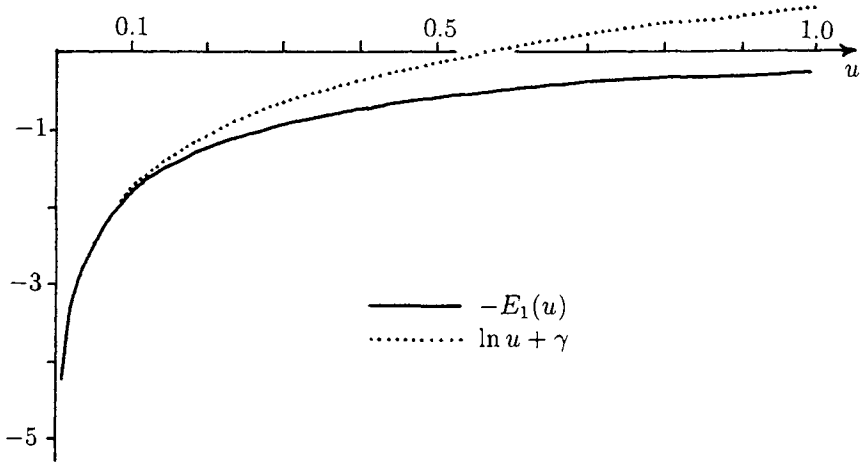

Figure 3.63: Comparison between $-E_1(u)$ and $(\ln u + \gamma)$.

```
630 u0=0
640 if u>500 GOTO 660
650 u0=EXP(-u)
660 E1=E1/(u*u1)*u0
670 RETURN
```

In Figure 3.63, I plotted the function $-E_1(u)$ together with the function $(\ln u + \gamma)$, where γ is Euler's constant:

$$\gamma = 0.57721566 \tag{3.350}$$

Note that for small values of u, less than 0.1, the two functions become nearly equal,

$$E_1(u) \approx -(\ln u + \gamma) \qquad (u \ll 1) \tag{3.351}$$

Hence, close to the well (small r) or after sufficient time has elapsed since the onset of pumping (large $t - t_0$), the exponential integral function may be approximated by a logarithm plus Euler's constant. Cooper and Jacob (1946) used this approximation to develop an approximate method for the evaluation of pumping tests.

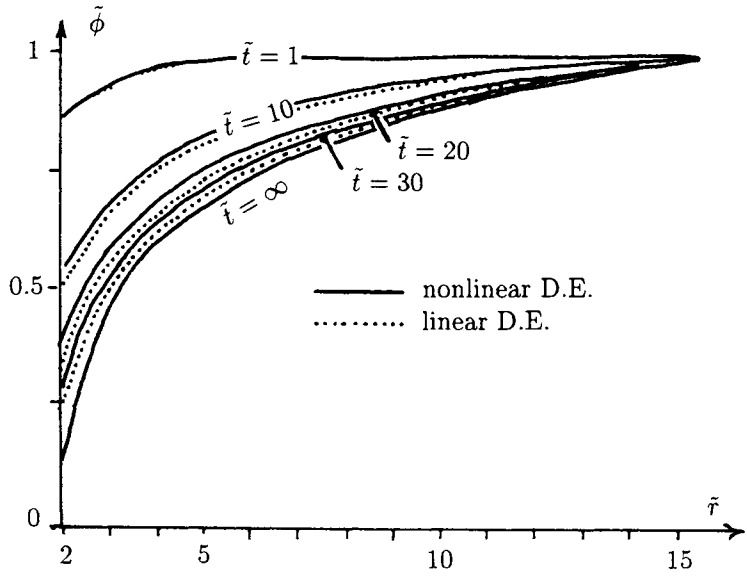

Figure 3.64: Comparison of a linear with a nonlinear finite difference solution for flow toward a well in an unconfined aquifer. (After Haitjema and Strack, 1983).

Nonlinear Effects

I mentioned that the nonlinear character of the Boussinesq equation poses little difficulty when we seek numerical solutions, but requires linearization of the differential equation to facilitate analytical solutions, such as Theis' solution. In order to gain some insight in the importance of this nonlinear effect, I have solved the problem of flow towards a well that starts pumping at time t_0, the problem for which Theis' solution was developed, by use of finite differences for both the linearized equation (3.330) and for the original Boussinesq equation (3.324). The results are plotted in Figure 3.64 in terms of the following dimensionless parameters:

$$\tilde{\phi} = \frac{\phi}{\phi_0} \qquad \tilde{r} = \frac{r}{\phi_0} \qquad \tilde{t} = \frac{kt}{\phi_o} \tag{3.352}$$

where ϕ_0 is the initial head in the aquifer and where k is the aquifer hydraulic conductivity. In generating the linear solution, I defined the specific

storage coefficient S_s as

$$S_s = \frac{S}{\phi_0} \tag{3.353}$$

The following data were used in Figure 3.64: The well discharge $Q = 1.5k\phi_0^2$, the well radius $r_w = 2\phi_0$, the grid spacing $\Delta r = 0.2\phi_0$, and the time step $\Delta t = 0.001\phi_0/k$. The well radius r_w is unusually large in order to allow for large pumping rates and thus large drawdowns in the aquifer. Since the finite difference solution for the linear case is a numerical version of Theis' solution, the well discharge is not constant, but given by (3.346). What is different from Theis' solution in Figure 3.64 is that the head was kept constant (equal to ϕ_0) at a distance $10\sqrt{2}\phi_0$ from the well axis.

It appears that the nonlinear effects are fairly small, even though the drawdowns are large; hence, the head ϕ differs significantly from the initial head ϕ_0 used in (3.353) to linearize the differential equation.

Superposition in Space and Time

Since the differential equation (3.330) is linear in terms of Φ, we can apply the principle of superposition. With reference to Figure 3.20 and Figure 3.22, we may write the potential due to a "transient" well near a stream with the use of an image "transient" recharge well:

$$\Phi = \frac{Q}{4\pi}\left[E_1(u_2) - E_1(u_1)\right] + \Phi_0 \tag{3.354}$$

where u_1 and u_2 are defined as

$$u_1 = \frac{S_s\{(x+d)^2 + y^2\}}{4k(t-t_0)} \qquad u_2 = \frac{S_s\{(x-d)^2 + y^2\}}{4k(t-t_0)} \tag{3.355}$$

For a sufficiently large time period since the onset of pumping, both u_1 and u_2 become very small, so that the approximation (3.351) may be used:

$$\Phi = \frac{Q}{4\pi}\left[\ln u_1 - \ln u_2\right] + \Phi_0 \qquad (t \to \infty) \tag{3.356}$$

The term γ in (3.351) cancels out in (3.356). Using (3.355), we may rewrite (3.356) as

$$\Phi = \frac{Q}{4\pi} \ln\left[\frac{S_s\{(x+d)^2 + y^2\}}{4k(t-t_0)} \frac{4k(t-t_0)}{S_s\{(x-d)^2 + y^2\}}\right] + \phi_0 \tag{3.357}$$

which reduces to the steady-state solution (3.121),

$$\Phi = \frac{Q}{4\pi} \ln \frac{(x+d)^2 + y^2}{(x-d)^2 + y^2} + \Phi_0 \tag{3.358}$$

The solution to transient flow for a well near a stream (straight equipotential boundary) as given by (3.354) with (3.355) converges to a steady-state solution for long pumping times of the well. Under these steady-state conditions, the well is receiving all its water from the stream (the recharge well in our imaging scenario). Without this nearby boundary condition, however, the Theis' solution will *never* converge to a steady-state solution. The well in Theis' solution (3.332) is obtaining all its water from storage in the aquifer and will never come to equilibrium with a surface water feature supplying the water to the well, as in the preceding example. Consequently, when evaluating Theis' solution for increasingly large times, the drawdowns in the aquifer will continue to increase. This will result in negative potentials in the vicinity of the well (thus negative heads), a clearly nonsensical solution. Some consultants use a "hundred day pumping scenario" for Theis' solution to predict long-term (read steady-state) drawdowns. There is no basis for such a procedure, and it should be expected to produce arbitrary results.

Rule 3.15 *Theis' solution, by itself, is fundamentally unsuitable to produce steady-state drawdowns. For very large times, the aquifer will everywhere be pumped dry.*

Exercise 3.30 *Investigate the behavior of Theis' solution by calculating the discharge potential Φ_w at the well for various times since the onset of pumping. Use the following data: $Q = 50,000\ ft^3/day$; $k = 50\ ft/day$; $\phi_0 = 50\ ft$; $r_w = 0.5\ ft$; and $S_s = 0.002$. Calculate Φ_w for the following times: 1 , 10 , 100 and 1,000 days. You may use the Basic function subprogram listed in this section or program GFLOW1 (see also file* proble11.dat *on the distribution diskette). Compare your results with a steady-state solution assuming the head remains at ϕ_0 at a distance of $5,000\ ft$ from the well.*

Theis' solution may also be superimposed in time. For instance, consider the case of a well that starts pumping at time t_0 and is switched off at a later time t_1. The solution to that problem can be written in terms of two solutions, one between time t_0 and time t_1,

$$\Phi = -\frac{Q}{4\pi} E_1(\overset{0}{u}) + \Phi_0 \qquad (t_0 \leq t < t_1) \tag{3.359}$$

and one for times larger than t_1,

$$\Phi = \frac{Q}{4\pi} \left[-E_1(\overset{0}{u}) + E_1(\overset{1}{u}) \right] + \Phi_0 \qquad (t \geq t_1) \tag{3.360}$$

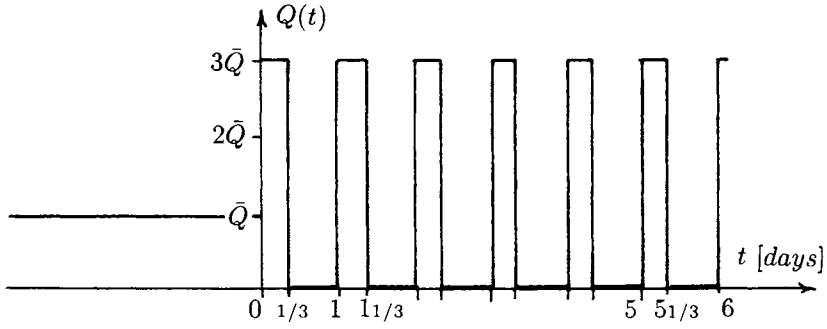

Figure 3.65: Pumping scenario for an industrial well.

where $\overset{0}{u}$ and $\overset{1}{u}$ are given by

$$\overset{0}{u} = \frac{S_s r^2}{4k(t - t_0)} \qquad \overset{1}{u} = \frac{S_s r^2}{4k(t - t_1)} \tag{3.361}$$

The second Theis' solution in (3.360) is a recharge well with the same pumping rate as the original well and in the same location. Thus, at time t_1 (and thereafter) the pumping well is "extinguished" by a recharge well of the same strength.

Exercise 3.31 *Demonstrate that after a sufficiently long time ($t \to \infty$) the potential in the aquifer is restored to its initial value Φ_0 for all values of r.*

3.6.3 Periodic Pumping

In steady-state groundwater models, wells are pumping continuously at an average rate. In reality, this is rarely the case. Some industrial wells, for instance, may only pump during working hours. In Figure 3.65, a pumping scenario is depicted for a hypothetical well. Starting at time zero, the steady-state average pumping rate is replaced by daily pumping periods of eight hours followed by 16 hours with the pump off. On average, the pumping rate is $\bar{Q}$, the same as that prior to time zero. The well is located at a distance d from a stream. The piezometric contours in Figure 3.66 are produced with GFLOW1 for the case of confined flow conditions. The confined aquifer has a thickness H and an initial head ϕ_0 measured with respect to the aquifer base. The data used in producing Figure 3.66 are $k = 100$ ft/day ; $S = 0.001$; $\phi_0 = 100$ ft ; $H = 50$ ft ; $\bar{Q} = 100,000$

ft^3/day ; $d = 500$ ft, and $r_w = 0.5$ ft.

For the case of unconfined flow, Figure 3.67, all data are the same except that the aquifer thickness equals the piezometric head and the storage coefficient is much larger: $S = 0.2$. GFLOW1 requires the storage coefficient S as input, which is given above. The specific storage coefficient is: $S_s = S/H = 2 \times 10^{-5}$ ft^{-1} for the confined case and $S_s = S/\phi_0 = 2 \times 10^{-3}$ ft^{-1} for the unconfined case.

The contour plots for time = 0 days in Figures 3.66 and 3.67 are due to the steady-state pumping $\bar{Q}$ prior to the periodic pumping. At times 5 days and 6 days the pump has just been off for a period of 16 hours, while at time 5.3 days we are close to the end of an eight-hour pumping period; see Figure 3.65. Consequently, the well has created a significant "cone of depression" in the third diagram from the top in Figure 3.66 and Figure 3.67, where the time is 5.3 days, while the drawdowns are much smaller in the diagrams for times 5 and 6 days. In fact, in Figure 3.66 the heads have been restored to within one foot of the initial head (100 ft), so that only one contour is plotted in these diagrams: the 100 ft contour along the stream on the right-hand side.

Comparing the piezometric contour plots in Figures 3.66 and 3.67, it appears that the transient effects in the confined aquifer are much more pronounced than in the unconfined aquifer. The time-dependent effects in the confined aquifer are felt farther from the well and cause larger variations in the head than for the case of unconfined flow. In fact, when compared to each other, the effects of starting or stopping pumpage are almost instantaneous in a confined aquifer. Our steady-state modeling, therefore, seems more reasonable in unconfined aquifers than in confined aquifers. We will explore this issue further in Section 5.3.7.

Exercise 3.32 *Further explore the issue of periodic pumping by following the instructions in the file* proble11.dat *provided on the distribution diskette.*

3.6.4 Pumping Test

Theis' solution is widely used in the evaluation of pumping tests. These tests are of limited duration, varying between one and three days, so that Theis' solution does not lead to unrealistic drawdowns, see Exercise 3.30. The purpose of the pumping test is to compare calculated drawdowns with observed drawdowns in an attempt to determine the transmissivity T and specific storage coefficient S_s for the aquifer.

For the case of confined flow, we can obtain the drawdown $\phi_0 - \phi$, at

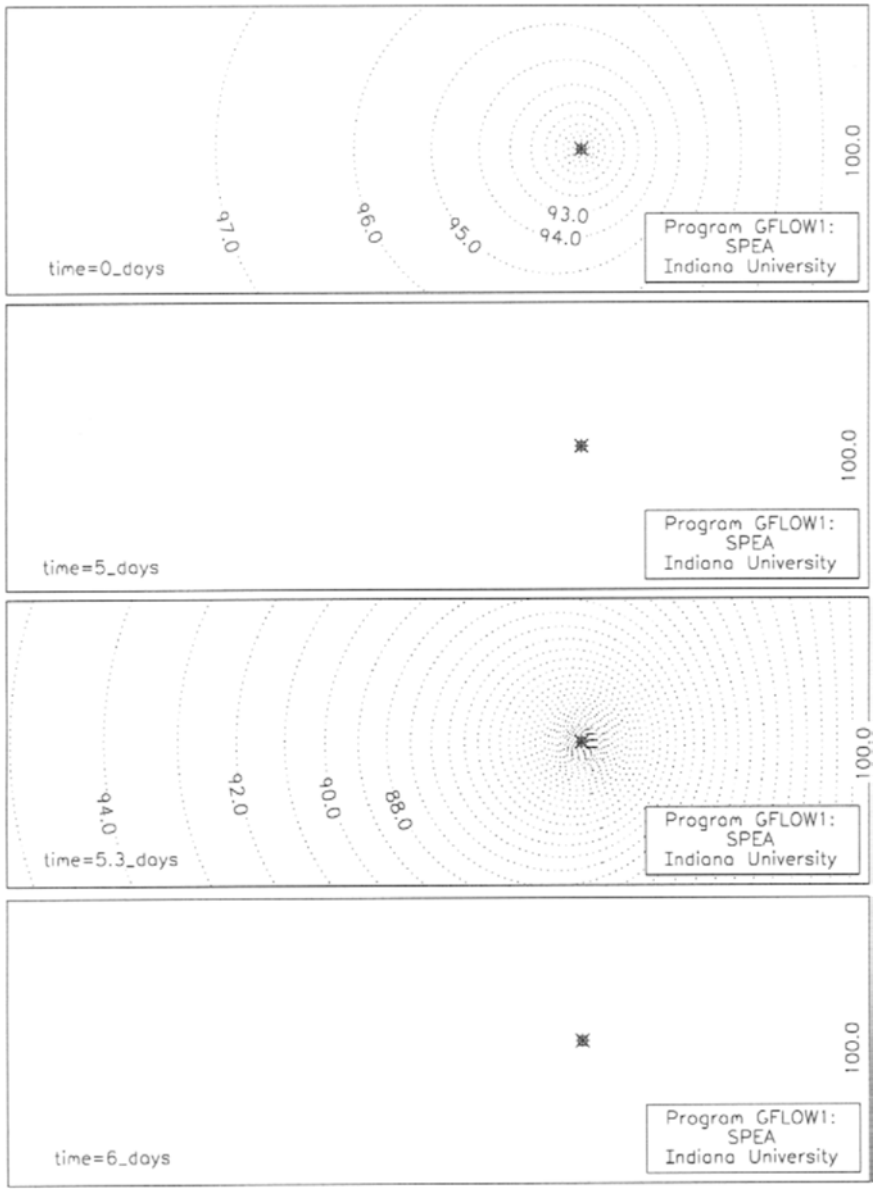

Figure 3.66: Transient piezometric head contours of a periodically pumped well near a stream. Groundwater flow conditions are confined. (GFLOW1 file: proble11.dat)

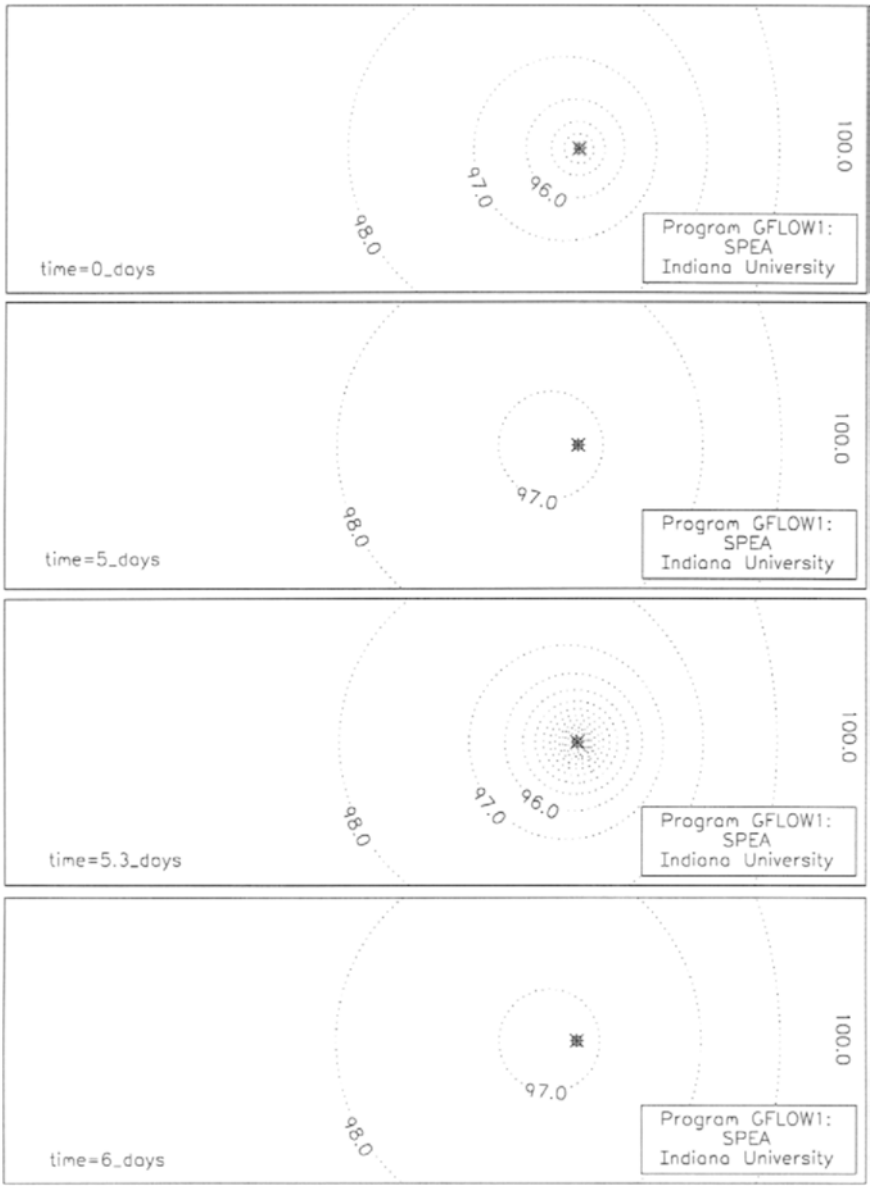

Figure 3.67: Transient piezometric head contours of a periodically pumped well near a stream. Groundwater flow conditions are unconfined. (GFLOW1 file: proble11.dat)

time t and distance r from the well, from (3.332) as

$$\phi_0 - \phi = \frac{Q}{4\pi T} E_1(u) \tag{3.362}$$

The time interval $t - t_0$ is related to u [see (3.333)],

$$t - t_0 = \frac{S_s r^2}{4k} \frac{1}{u} \tag{3.363}$$

I am rewriting the identities (3.362) and (3.363) by taking the logarithm of both sides of the equations:

$$\log(\phi_o - \phi) = \log \frac{Q}{4\pi T} + \log E_1(u) \tag{3.364}$$

and

$$\log(t - t_0) = \log \frac{S_s r^2}{4k} + \log \frac{1}{u} \tag{3.365}$$

The function $E_1(u)$ is plotted versus $1/u$ on so-called double logarithmic paper; hence, we are actually plotting the logarithms of these parameters. The resulting curve is called a *type curve* for Theis' solution. Next we plot the observed drawdown $\phi_0 - \phi$ at a certain distance r from the well (hence in a particular piezometer) versus time $t - t_0$, also on double logarithmic paper.

If the drawdowns in the aquifer behave according to our theory, they should produce curves of the same shape. However, these curves are shifted along both the horizontal and vertical axes; see Figure 3.68. The shift along the horizontal axis follows from (3.365) and is equal to $\log(S_s r^2/4k)$, while the shift along the vertical axis follows from (3.364) and is $\log(Q/4\pi T)$. Placing the two graphs on top of each other in such a manner that the measured drawdowns (data points) match the type curve, and measuring the horizontal and vertical shifts, allows us to determine the transmissivity T and specific storage coefficient S_s. The determination of these parameters may be facilitated by selecting a convenient"match point" on the plane of the type curve: the point $1/u = 1$ and $E_1(u) = 1$. Projecting this match point onto the axes of the field data graph yields directly the shift factors mentioned earlier, as the logarithms of E_1 and $1/u$ in (3.364) and (3.365) become zero. The projection of the match point on the $t - t_0$ axis yields $t_1 - t_0$, while the projection on the $\phi_0 - \phi$ axis yields $\phi_0 - \phi_1$; see Figure 3.68. The transmissivity then follows from (3.364) with $\log E_1(u) = \log 1 = 0$,

$$T = \frac{Q}{4\pi(\phi_0 - \phi_1)} \tag{3.366}$$

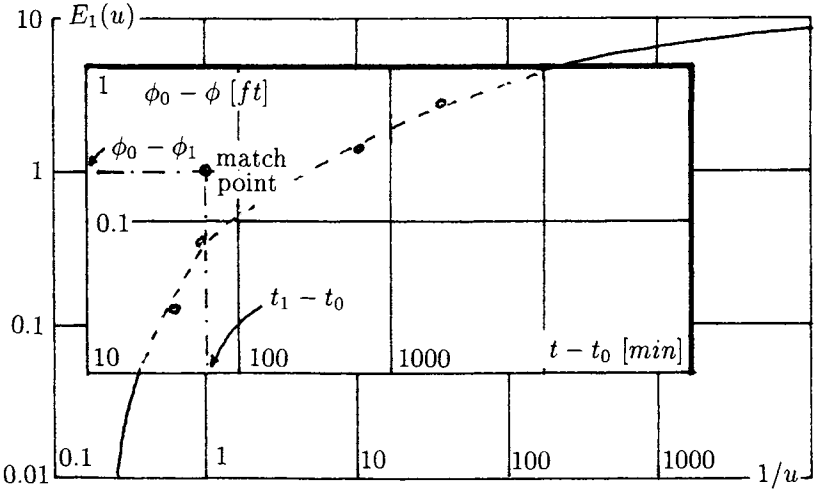

Figure 3.68: Comparing observed drawdowns with a type curve based on Theis' solution.

while the specific storage coefficient follows from (3.365) with $\log 1/u = \log 1 = 0$,

$$S_s = \frac{4k(t_1 - t_0)}{r^2} \tag{3.367}$$

The hydraulic conductivity k in (3.367) follows from (3.366) by dividing the transmissivity T by the average aquifer thickness. The aquifer thickness is usually determined separately from drilling records (well logs).

Pumping Tests under Complex Hydrogeological Conditions

Theis' solution is only accurate in confined aquifers which do not receive water from or lose water to other aquifers through leakage. Even in non-leaky unconfined aquifers, Theis' solution is an approximation, not only because of the linearization of the differential equation, but also because the storage coefficient depends on the unsaturated conditions in the aquifer zone above the groundwater table; see Neumann (1975). Different analytic solutions have been developed for aquifers under different flow conditions. These solutions are used to evaluate pumping tests by essentially the same graphical method as discussed earlier, but using different type curves. The

reader is referred to other textbooks for a thorough discussion of the various pumping test evaluation techniques, e.g., Freeze and Cherry (1979) and Davis and DeWiest (1966).

Imperfect Pumping Tests

Frequently, the conditions under which pumping tests are conducted are less than ideal. Sometimes a technical problem arises which interrupts the pumping for a few hours. In other cases, a nearby high-capacity well is pumped intermittently, potentially influencing the observed drawdowns in the piezometers. Under these conditions, it may be better not to rely on the curve matching procedure outlined earlier, but to simulate the actual pumping test scenario, complete with pumping interruptions and nearby pumping, on a computer. GFLOW1 supports Theis' solution, and the program may be used to superimpose "transient wells" in both time and space to carry out such a pumping test simulation. The aquifer parameters are then estimated by a trial-and-error procedure, attempting to match computed drawdowns in the piezometers with those observed.

3.7 Complex Potential Theory

Although we considered vertical flow in our Dupuit–Forchheimer models, the governing differential equations are two-dimensional in nature: describing horizontal flow. We developed solutions to three different differential equations: Laplace's equation (3.63), Poisson's equation (3.153), and Boussinesq's equation (3.324). In Chapter 5 we will solve regional groundwater flow problems by combining many (hundreds) of elementary solutions to these differential equations: the *analytic element method.* It appears that the vast majority of *analytic elements* that constitute our model are solutions to Laplace's equation. In Section 3.1.6, we learned that if the discharge potential Φ satisfies Laplace's equation, and hence is a harmonic function, there also exists a conjugate harmonic function: the stream function Ψ. In this section we will see that both the potential function and stream function can be combined into one *complex potential* function Ω. By solving our problems in terms of this complex potential function, we hit two birds with one stone: We are getting both Φ and Ψ for essentially the same effort as solving for Φ alone.

In the sections that follow, we will very briefly review the basics of complex numbers and complex functions. Next I will present the complex potential for some elementary solutions to Laplace's equation. The theory in this section is relevant to the mathematical description of the analytic el-

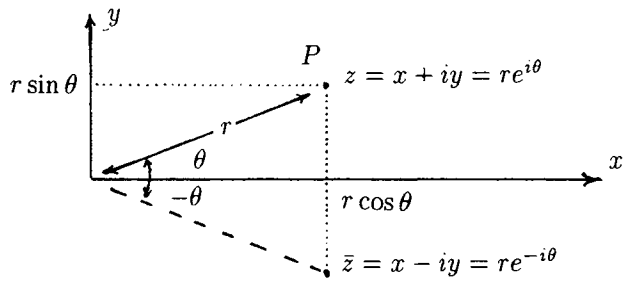

Figure 3.69: A point in a complex plane.

ements and their implementation in GFLOW1 as outlined in Sections 5.1.2 through 5.1.5. The reader who is only interested in the application of the analytic element method may safely skip this section. Conversely, for a more thorough treatment of the theory of complex variables and complex potential theory the reader is referred to, for example, Churchill (1960), Nehari (1952), and Von Koppenfels and Stallmann (1959). For an extensive treatise on the application of complex potential theory to the field of groundwater flow, reference is made to Strack (1989).

3.7.1 Complex Numbers

The point P in the two-dimensional plane of Figure 3.69 is defined by the Cartesian coordinates (x, y) or by the polar coordinates (r, θ). The point P may also be defined by the complex variable z, whereby

$$z = x + iy \tag{3.368}$$

The coordinates x and y are referred to as the *real* and *imaginary* parts of the complex number z, respectively:

$$x = \Re(z) \qquad y = \Im(z) \tag{3.369}$$

The x-axis and the y-axis of the complex plane are referred to as the *real axis* and *imaginary axis*, respectively. The symbol i is defined as

$$i = \sqrt{-1} \qquad \text{or} \qquad i^2 = -1 \tag{3.370}$$

With reference to Figure 3.69, I rewrite (3.368) in terms of the distance r and angle θ:

$$z = r(\cos\theta + i \sin\theta) \tag{3.371}$$

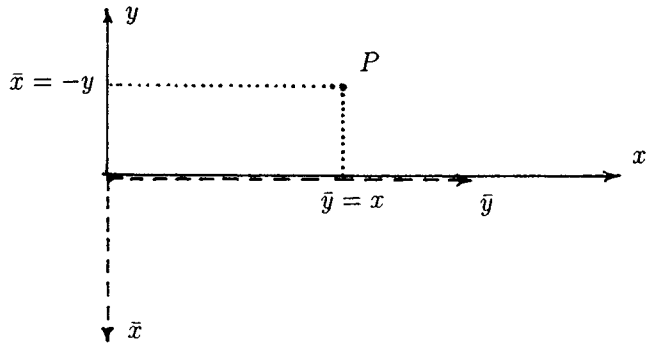

Figure 3.70: Multiplication by i represents a clockwise coordinate system rotation over an angle of $\pi/2$.

which may be rewritten, using Taylor series expansions for the sine and the cosine (e.g. Strack, 1989), as

$$z = r\, e^{i\theta} \tag{3.372}$$

The distance r between the origin and the point P is called the *modulus* of z, written as $|z|$, and the angle θ is called the *argument* of z and is written as $\arg(z)$. Associated with every complex number z is its *conjugate* $\bar{z}$:

$$\bar{z} = x - iy \tag{3.373}$$

which may be interpreted as the image of point P with respect to the real axis (x-axis); see Figure 3.69. The modulus of z is then defined by

$$|z| = \sqrt{z\bar{z}} = \sqrt{x^2 + y^2} \tag{3.374}$$

where use has been made of $i^2 = -1$.

Multiplication of z by i may be interpreted as a clockwise rotation of the coordinate system over an angle of $\pi/2$:

$$i\, z = ix + i^2 y = -y + ix \tag{3.375}$$

In terms of the new $\bar{x}, \bar{y}$-coordinates we have $\bar{x} = -y$ and $\bar{y} = x$, see Figure 3.70. Division by i is carried out as follows:

$$\frac{z}{i} = \frac{i}{i}\frac{z}{i} = \frac{iz}{i^2} = -iz \tag{3.376}$$

We have performed some algebraic operations on complex variables, such as multiplication and division by i and the multiplication of the two complex variables z and $\bar{z}$; see (3.374). In general, multiplication of complex numbers is most conveniently done by representing them in the form of polar coordinates [see (3.372)]:

$$z_1 z_2 = |z_1| e^{i\theta_1} |z_2| e^{i\theta_2} = |z_1||z_2| e^{i(\theta_1+\theta_2)} \tag{3.377}$$

Addition of complex numbers simply implies addition of their real and imaginary parts:

$$z_1 + z_2 = (x_1 + x_2) + i(y_1 + y_2) \tag{3.378}$$

3.7.2 Complex Potential and Discharge Function

At the beginning of this section I mentioned that solutions to Laplace's equation (in two dimensions) can be formulated in terms of a complex potential function:

$$\Omega(z) = \Phi(z) + i\Psi(z) \qquad\qquad z = x + iy \tag{3.379}$$

Ω is a function of the complex variable z and has a real and an imaginary part: the discharge potential Φ and the stream function Ψ, respectively. Both Φ and Ψ are real functions which each depend on z, and hence on x and y. Expression (3.379) involves *four* real variables: x, y, Φ, and Ψ. Written in the form of (3.379), however, it involves only two complex variables: Ω and z.

That there indeed exists a class of functions of the form (3.379), whose real and imaginary parts are the discharge potential and stream function for a groundwater flow problem, is not immediately obvious. In fact, not all complex functions do — only those that are *continuous* and *differentiable.* These restrictions on Ω seem reasonable, as we already know that they apply to the real functions Φ and Ψ, except perhaps in some isolated points (singularities).

Continuity of the complex function Ω is conditional on the existence of the following limit:

$$\lim_{z \to z_0} \Omega(z) = \Omega_0 \tag{3.380}$$

whereby the value of Ω_0 is independent of the path followed in the complex plane; see Figure 3.71.

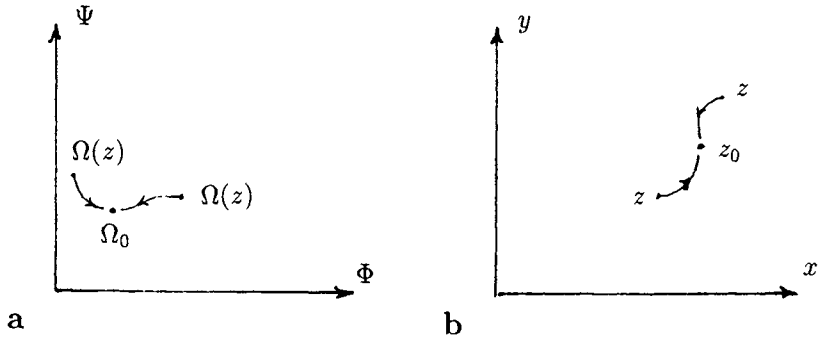

Figure 3.71: Ω is continuous near z_0.

Analytic Functions

The derivative of the complex function Ω is defined as

$$\Omega'(z_0) = \left(\frac{d\Omega}{dz}\right)_{z=z_0} = \lim_{z\to z_0} \frac{\Omega(z) - \Omega(z_0)}{z - z_0} \tag{3.381}$$

The derivative (3.381) is only meaningful if its value is independent of the path along which z approaches z_0. A differentiation path is not an issue for real functions of one variable. For complex functions, however, differentiability requires that both (3.380) and (3.381) be path-independent.

Complex functions that are differentiable are called *analytic functions*. If Ω is indeed analytic, we should be able to differentiate it in two different ways, e.g., by letting z approach z_0 along a path parallel to the x-axis or by letting z approach z_0 along a path parallel to the y-axis, and still obtain the same result. Let's see what restrictions this places on Φ and Ψ, the real and imaginary part of Ω.

Differentiating Ω along a path parallel to the x-axis yields

$$\begin{aligned}\Omega'(z_0) &= \lim_{x\to x_0}\left(\frac{\Phi(x,y_0) - \Phi(x_0,y_0)}{x - x_0} + i\frac{\Psi(x,y_0) - \Psi(x_0,y_0)}{x - x_0}\right) \\ &= \frac{\partial\Phi}{\partial x} + i\frac{\partial\Psi}{\partial x}\end{aligned} \tag{3.382}$$

Differentiating Ω along a path parallel to the y-axis yields

$$\begin{aligned}\Omega'(z_0) &= \lim_{y\to y_0}\left(\frac{\Phi(x_0,y) - \Phi(x_0,y_0)}{i(y - y_0)} + i\frac{\Psi(x_0,y) - \Psi(x_0,y_0)}{i(y - y_0)}\right) \\ &= \frac{\partial\Psi}{\partial y} - i\frac{\partial\Phi}{\partial y}\end{aligned} \tag{3.383}$$

where use has been made of (3.376). Since the derivatives (3.382) and (3.383) must yield the same value, their real and imaginary parts must be the same, which yields the Cauchy–Riemann equations (3.71):

$$\frac{\partial \Psi}{\partial x} = -\frac{\partial \Phi}{\partial y}$$
$$\frac{\partial \Psi}{\partial y} = +\frac{\partial \Phi}{\partial x} \tag{3.384}$$

This is the link between our groundwater flow solutions and (analytic) complex functions. We found in Section 3.1.6 that groundwater flow problems governed by the (two-dimensional) equation of Laplace have a discharge potential and stream function which satisfy the Cauchy–Riemann conditions: They are conjugate harmonic functions. As it appears, complex analytic functions have a real and imaginary part which also satisfy the Cauchy-Riemann conditions. Consequently, it must be possible to represent the discharge potential and stream function for a groundwater flow problem, governed by Laplace's equation, as the real and imaginary part of a complex potential function.

As an example of an analytic function, consider $\Omega = z^2$. The real and imaginary parts of Ω are

$$\Omega = \Phi + i\Psi = (x + iy)^2 = x^2 - y^2 + 2ixy \tag{3.385}$$

so that Φ and Ψ are

$$\Phi = x^2 - y^2 \qquad \Psi = 2xy \tag{3.386}$$

This leads to the following partial derivatives for Φ and Ψ:

$$\frac{\partial \Phi}{\partial x} = 2x \qquad \frac{\partial \Phi}{\partial y} = -2y \qquad \frac{\partial \Psi}{\partial x} = 2y \qquad \frac{\partial \Psi}{\partial y} = 2x \tag{3.387}$$

which indeed satisfy the Cauchy–Riemann equations (3.384).

The derivative $\Omega'(z)$ becomes, with (3.382) and (3.387),

$$\Omega'(z) = \frac{\partial \Phi}{\partial x} + i\frac{\partial \Psi}{\partial x} = 2x + 2iy = 2z \tag{3.388}$$

Observe that the result $2z$ in (3.388) is the same as if we had treated the function z^2 as a real function and applied the rules for differentiation for real functions to it. This is indeed universally true. All rules for differentiating real functions also apply to differentiating complex functions.

Exercise 3.33 *Demonstrate that the following functions are analytic:*

(a) $\ln z$

(b) e^z

(c) $\sin z$ *and* $\cos z$

(d) $\sinh z$ *and* $\cosh z$

(e) $\sqrt{z}$

Demonstrate that the following functions are **not** *analytic:*

(a) $|z|$

(b) $\bar{z}$

The Discharge Function

Analogous to the definition of the discharge vector as the negative derivative of the real potential function Φ, there exists a *discharge function* which is the negative derivative of the complex potential function Ω:

$$W = -\frac{d\Omega}{dz} \tag{3.389}$$

The discharge function W has as its real and imaginary part the components of the discharge vector,

$$W = -\frac{\partial \Phi}{\partial x} + i\frac{\partial \Phi}{\partial y} = Q_x - iQ_y \tag{3.390}$$

Note that the imaginary part of W is equal to the *negative* discharge vector component Q_y: $\Im(W) = -Q_y$. It is possible to write the discharge vector as a complex variable as follows:

$$Q_x + iQ_y = \overline{W} = -\overline{\frac{d\Omega}{dz}} \tag{3.391}$$

In GFLOW1, all analytic elements that satisfy Laplace's equation are written in terms of the complex potential Ω, and their contribution to the discharge vector is evaluated by use of the discharge function W. Some analytic elements satisfy Laplace's equation in one domain and Poisson's equation in another, — for instance, the source disc in Section 3.2.4. Such an analytic element is represented by both a complex potential function and a real potential function, depending on the location of the point in

question. For instance, ,inside the boundary of the sink disc, the solution is formulated in terms of a real discharge potential only, while outside the sink disc, a complex potential function is being used to calculate its contribution to both Φ and Ψ.

Next we will present the complex potential for a few elementary functions.

3.7.3 Complex Potential for a Well and a Vortex

The complex potential for a well is given by

$$\Omega(z) = \frac{Q}{2\pi} \ln(z - z_w) + C \tag{3.392}$$

where z_w is the location of the well in the complex plane (see Figure 3.72a), and where z is the location of the point at which Ω is being calculated. The integration constant is in principle a complex number, but we may select the imaginary part Ψ equal to zero, because it does not have to match any boundary conditions. Consequently, C in (3.392) is a real constant. In order to separate (3.392) into its real and imaginary parts, it is convenient to write it in terms of polar coordinates:

$$\Omega(z) = \frac{Q}{2\pi} \ln\left(|z - z_w| e^{i\theta}\right) + C = \frac{Q}{2\pi} \left(\ln|z - z_w| + i\theta\right) \tag{3.393}$$

The real part of Ω is the discharge potential (3.85):

$$\Phi = \Re(\Omega) = \frac{Q}{2\pi} \ln r \qquad\qquad r = |z - z_w| \tag{3.394}$$

The imaginary part of Ω is the stream function (3.93):

$$\Psi = \Im(\Omega) = \frac{Q}{2\pi}\theta \tag{3.395}$$

Vortex

In Figure 3.72a the streamlines and equipotentials are sketched for a well. In Figure 3.72b the streamlines and equipotentials in Figure 3.72a have been interchanged! The radials are now equipotentials, and the circles have become streamlines. The flow pattern in Figure 3.72b is that of a *vortex* at z_w. The solution for a vortex, it seems, may be obtained by calling the discharge potential for a well the stream function and vice versa. Exchanging Φ and Ψ may be accomplished by dividing the complex potential function for a well by i:

$$\Omega = \frac{Q}{2\pi i} \ln(z - z_0) + C \tag{3.396}$$

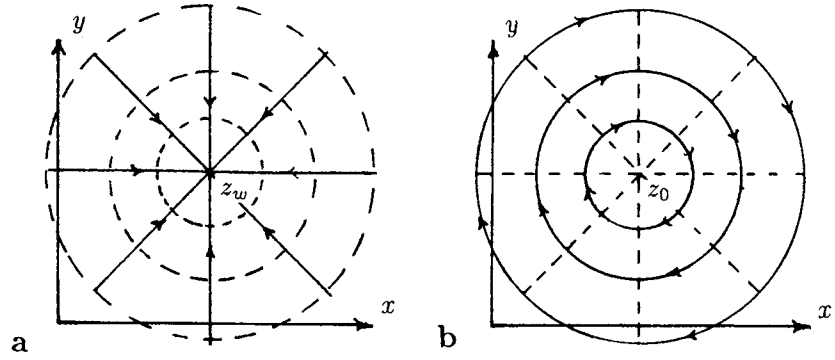

Figure 3.72: Complex potential for a vortex (b) obtained by interchanging the real and imaginary part for the complex potential for a well (a).

where z_0 is the location of the vortex. Separating the real and imaginary part of (3.396) yields the discharge potential and stream function for a vortex,

$$\Phi = \Re(\Omega) = \frac{Q}{2\pi}\theta + C \qquad \Psi = \Im(\Omega) = -\frac{Q}{2\pi}\ln|z - z_0| \tag{3.397}$$

The vortex may be used to model flow on one side of a stream near a waterfall. The vortex would be positioned at the waterfall and creates circular flow from the upstream section of the stream to the downstream section. However, since the vortex creates flow that keeps rotating around the point z_0, it cannot properly represent the flow in the aquifer on both sides of the stream. Consequently, a vortex is not a useful analytic element, since it cannot be used in the interior of a flow domain, like a well or a line sink. The vortex function, therefore, is not implemented in GFLOW1.

3.7.4 A Well in a Uniform Flow Field

The complex potential for a uniform flow field of strength Q_0 $[L^2/T]$ is given by

$$\Omega = -Q_0 z e^{-i\alpha} + C \tag{3.398}$$

where α is the orientation of the uniform flow as indicated in Figure 3.73. In order to separate (3.398) into its real and imaginary part, it is convenient to write the exponential term $\exp(-i\alpha)$ in terms of Cartesian coordinates. This yields for (3.398)

$$\Omega = -Q_0(x + iy)(\cos\alpha - i\sin\alpha) + C \tag{3.399}$$

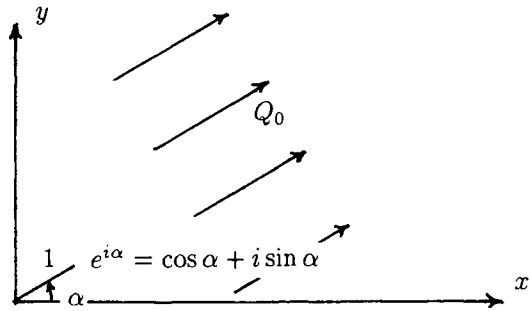

Figure 3.73: Orientation of a uniform flow field.

so that the discharge potential and stream function become

$$\Phi = -Q_0(x\cos\alpha + y\sin\alpha) \qquad \Psi = -Q_0(y\cos\alpha - x\sin\alpha) \tag{3.400}$$

For illustrative purposes I will derive the discharge vector in several different ways. Applying Darcy's law to (3.400):

$$Q_x = -\frac{\partial\Phi}{\partial x} = Q_0\cos\alpha \qquad Q_y = -\frac{\partial\Phi}{\partial y} = Q_0\sin\alpha \tag{3.401}$$

Using the Cauchy-Riemann equations (3.384):

$$Q_x = -\frac{\partial\Psi}{\partial y} = Q_0\cos\alpha \qquad Q_y = \frac{\partial\Psi}{\partial x} = Q_0\sin\alpha \tag{3.402}$$

Using the discharge function (3.390):

$$Q_x = \Re(W) \qquad Q_y = -\Im(W) \tag{3.403}$$

The discharge function W is obtained by differentiating (3.398),

$$W(z) = -\frac{d\Omega}{dz} = -\frac{d}{dz}\left(-Q_0 z e^{-i\alpha}\right) = Q_0 e^{-i\alpha} \tag{3.404}$$

Combining (3.403) and (3.404) yields

$$Q_x = Q_0\cos\alpha \qquad Q_y = Q_0\sin\alpha \tag{3.405}$$

Of course, we can superimpose complex potential functions just as we superimposed discharge potentials and stream functions. A well in a uniform flow field has the complex potential

$$\Omega = \frac{Q}{2\pi}\ln(z - z_w) - Q_0 z e^{-i\alpha} + C \tag{3.406}$$

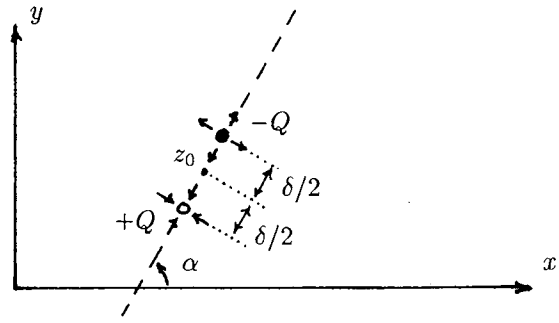

Figure 3.74: A point sink and point source pair at zero distance and with infinite discharge form a dipole.

3.7.5 A Circular Lake in a Uniform Flow Field

As a last example I will present the complex potential function for a circular lake in a uniform flow field. In Section 3.1.17, I derived the discharge potential for a circular lake in a uniform flow field by moving a point sink and a point source in opposite directions to infinity, which caused their images inside the circular lake to coincide at the center of the lake; see Figure 3.28. Since the discharges of the sink and source were chosen inversely proportional to the distance of their images, the overlapping image sink and source did not neutralize each other; instead we were left with a new kind of singularity: the *dipole*.

Complex Potential for a Dipole

A dipole with orientation α is obtained by moving a point sink and point source towards each other along a line with orientation α (see Figure 3.74), while increasing their discharge in inverse proportion to their distance. This leads to the following expression for the complex potential for the dipole:

$$\Omega = \lim_{\substack{\delta \to 0 \\ Q \to \infty}} \frac{Q\delta}{2\pi} \frac{\ln(z - (z_0 - \frac{\delta}{2}e^{i\alpha})) - \ln(z - (z_0 + \frac{\delta}{2}e^{i\alpha}))}{\delta} \tag{3.407}$$

where δ is the distance between the sink and the source. Introducing Δz_0 as

$$\Delta z_0 = \delta e^{i\alpha} \tag{3.408}$$

and defining

$$\lim_{\substack{\delta \to 0 \\ Q \to \infty}} Q\delta = s \tag{3.409}$$

I rewrite (3.407) in the form

$$\Omega = \frac{se^{i\alpha}}{2\pi} \lim_{\Delta z_0 \to 0} \frac{\ln(z - (z_0 - \frac{\Delta z_0}{2})) - \ln(z - (z_0 + \frac{\Delta z_0}{2}))}{\Delta z_0} \tag{3.410}$$

which is the definition for the negative derivative of the logarithm with respect to z_0:

$$\Omega = \frac{s\, e^{i\alpha}}{2\pi} \left(-\frac{d}{dz_0} \ln(z - z_0) \right) \tag{3.411}$$

or

$$\Omega = \frac{s}{2\pi} \frac{e^{i\alpha}}{z - z_0} \tag{3.412}$$

Complex Potential for a Circular Lake in a Uniform Flow Field

With (3.412), it is relatively easy to rewrite the expressions for Φ and Ψ [see (3.148) and (3.149)] for a circular lake in a uniform flow field in terms of a complex potential:

$$\Omega = -Q_0 \left(z - \frac{R^2}{z} \right) + \frac{Q}{2\pi} \ln \frac{z}{R} + \Phi_0 \tag{3.413}$$

where the center is at the origin of the complex plane ($z_0 = 0$) and where the lake has a radius R and net discharge (extraction rate) Q.

Exercise 3.34 *Write the real and imaginary part of (3.413) and compare them with the discharge potential and stream function given by (3.148) and (3.149), respectively.*

Chapter 4

Three-Dimensional Flow

At the beginning of Chapter 3, I argued that, in general, regional flow can be adequately described by adopting the Dupuit–Forchheimer approximation. This approximation reduces a three-dimensional groundwater flow problem to a two-dimensional one (horizontal flow), although in Section 3.5 we expanded the Dupuit–Forchheimer solution by introducing approximate vertical flow. The question, of course, is: When are we dealing with *regional* flow, and when not? Or, more to the point, when can we use the Dupuit–Forchheimer approximation, and when do we need a complete three-dimensional description of flow? Some groundwater hydrologists have expressed reservations regarding the Dupuit–Forchheimer approximation (e.g., Muskat, 1937). Faced with the reality of a complex three-dimensional geology, they intuitively reach for three-dimensional mathematical descriptions (models), considering the inadequacy of the Dupuit–Forchheimer approximation self-evident.

In some cases the need for three-dimensional solutions is obvious, — for instance, when tracing streamlines in the immediate vicinity of a partially penetrating well, or when modeling upconing of salt or brackish water underneath a partially penetrating well. The local three-dimensional geometry and importance of resistance to vertical flow, in these cases, render the Dupuit–Forchheimer approximation useless. In order to judge under which circumstances a complete three-dimensional solution to groundwater flow is called for, and when a Dupuit–Forchheimer approximation will do, we must compare solutions obtained in both manners. Such an analysis is presented in Section 5.3.4; see also Haitjema (1987a).

In this chapter I will briefly introduce three-dimensional solutions to two flow features: a partially penetrating well and a three-dimensional version of the sink disc, which are both implemented in program GFLOW1. These

three-dimensional functions are significantly more complicated than their two-dimensional counterparts (well and sink disc) discussed in Chapter 3. A particularly complicating factor is the need to satisfy the no-flow conditions at the aquifer bottom and the aquifer top. For confined flow conditions, this implies satisfying no-flow conditions along two parallel horizontal planes. For unconfined flow conditions, the upper aquifer boundary is the a priori unknown phreatic surface, adding yet another complexity.

A complete derivation of the three-dimensional potential functions for a partially penetrating well and sink disc would require a thorough treatment of three-dimensional potential theory, which is well beyond the scope of this text. Instead, I will present some basic equations followed by a mostly conceptual discussion of the three-dimensional flow features implemented in program GFLOW1. Of particular interest is the concept of combined two- and three-dimensional flow modeling, as discussed at the end of this chapter. This selective use of three-dimensional solutions, inside an otherwise two-dimensional flow model, is of significant practical value: It limits (complicated) three-dimensional flow descriptions to those areas where they are relevant: near the three-dimensional flow features themselves.

4.1 Basic Equations

The governing differential equation for steady-state three-dimensional groundwater flow, Laplace's equation, is written in symbolic and index notation as [see (2.29) and (2.30)]

$$\nabla^2\phi = \partial_{ii}\phi = 0 \qquad (i = 1, 2, 3) \tag{4.1}$$

Throughout this chapter Einstein's summation convention is implied; hence, (4.1) may be written out as [see (2.28)]

$$\frac{\partial^2\phi}{\partial x_1^2} + \frac{\partial^2\phi}{\partial x_2^2} + \frac{\partial^2\phi}{\partial x_3^2} = 0 \tag{4.2}$$

where x_1, x_2, and x_3 represent the three Cartesian coordinate directions x, y, and z. It is convenient to introduce a *specific discharge potential* Φ, defined as

$$\Phi = k\phi \tag{4.3}$$

where k is the aquifer hydraulic conductivity. The specific discharge vector q_i follows from Darcy's law,

$$q_i = -\frac{\partial\Phi}{\partial x_i} = -\partial_i\Phi \qquad (i = 1, 2, 3) \tag{4.4}$$

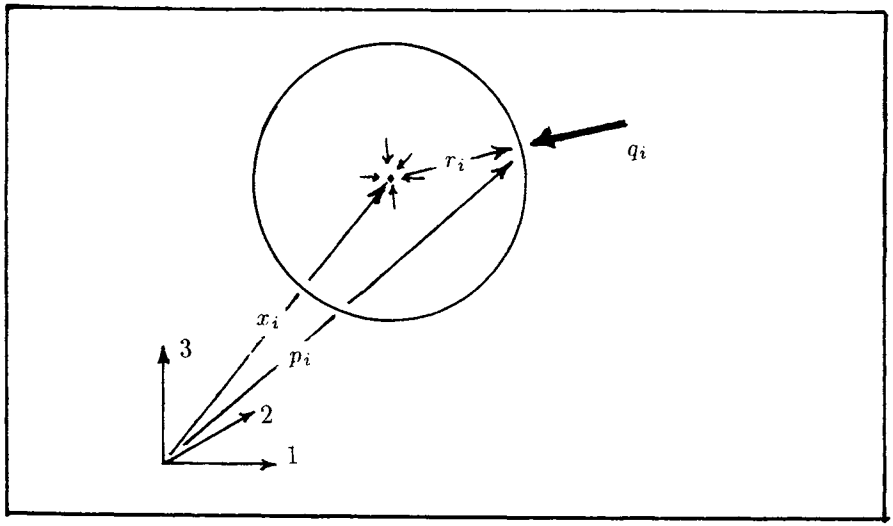

Figure 4.1: Radial flow towards a point sink.

where ∂_i is shorthand for $\partial/\partial x_i$. The units of the *specific discharge potential* are $[L^2/T]$, as opposed to the discharge potential used in Chapter 3, whose units are length *cubed* over time. Throughout this chapter we will use Φ to represent the specific discharge potential as defined by (4.3), which should not be confused with the definitions for Φ in Chapter 3.

4.1.1 The Point Sink

The simplest and best-known solution to the three-dimensional equation of Laplace is the solution for a point sink in an infinite domain. Consider the point sink with discharge Q at a point in space defined by the vector p_i; see Figure 4.1. The potential due to the point sink will be evaluated at a point defined by the vector x_i. The relative position of the point sink with respect to the point x_i is defined by the vector r_i, such that

$$r_i = x_i - p_i \tag{4.5}$$

As observed from Figure 4.1, the vector r_i points from the point sink toward x_i. The specific discharge vector q_i at x_i points toward the point sink and is therefore parallel to the vector r_i, but points in opposite direction. We will consider the flow across a sphere with radius r around p_i. Because of spherical symmetry, the specific discharge vector q_i at any point on the sphere is normal to the sphere, while its magnitude q is constant over the

sphere. Since the specific discharge is defined as the amount of flow per unit area, q is obtained by dividing the total discharge of the point sink by the area of the sphere:

$$q = \frac{Q}{4\pi r^2} \tag{4.6}$$

In this chapter I will denote the length of a vector by its symbol without the index. For example, in (4.6), q is the length of q_i and r is the length r_i. The lengths q and r are defined as

$$q = \sqrt{q_i q_i} \tag{4.7}$$

$$r = \sqrt{r_i r_i} \tag{4.8}$$

It appears from (4.6) that q is a function of r alone. Hence, with reference to (4.4) one may write

$$q = q_r = -\frac{d\Phi}{dr} \tag{4.9}$$

The potential Φ is found by integrating (4.9) with (4.6),

$$\Phi = -\frac{Q}{4\pi}\frac{1}{r} \tag{4.10}$$

whereby the constant of integration has been omitted. The potential (4.10) is known as *Newton's potential.* The location p_i of the point sink is a singular point for the potential and should be excluded from the flow domain. The specific discharge vector q_i, with components with respect to a Cartesian coordinate system, is obtained with (4.4) and (4.10) as

$$q_i = \frac{Q}{4\pi}\frac{\partial}{\partial x_i}\left(\frac{1}{r}\right) \tag{4.11}$$

The derivative of $1/r$ with respect to x_i is evaluated as follows:

$$\frac{\partial}{\partial x_i}\left(\frac{1}{r}\right) = \frac{\partial}{\partial x_i}(r_j r_j)^{-1/2} = -\tfrac{1}{2}(r_k r_k)^{-3/2} 2 r_j \frac{\partial}{\partial x_i} r_j \tag{4.12}$$

Note the use of *dummy indices*, k to define the scalar product $r_k r_k$ of the vector r_i, and j to define the derivative of this scalar product: $2r_j \partial_i r_j$. As a general rule, the same index cannot occur more than twice in a single term (multiplication of vectors and scalars). A single occurrence of an index implies a vector, while using an index twice implies a scalar. In (4.12) the indices k and j are "summed out": They define scalar products, while the single occurrence of the index i indicates that the right-hand side is a vector (as is the left-hand side). If an equation involves vectors, as in (4.12), the "free index" on either side must be the same — i for the case of (4.12).

The derivative of r_j with respect to x_i becomes, by use of (4.5),

$$\frac{\partial}{\partial x_i} r_j = \frac{\partial}{\partial x_i}(x_j - p_j) = \delta_{ij} \tag{4.13}$$

where δ_{ij} is the Kronecker Delta, defined as

$$\begin{aligned} \delta_{ij} &= 1 \qquad (i = j) \\ \delta_{ij} &= 0 \qquad (i \neq j) \end{aligned} \tag{4.14}$$

Combining (4.11) through (4.14) yields for the specific discharge vector due to a point sink

$$q_i = -\frac{Q}{4\pi} \frac{r_i}{r^3} \tag{4.15}$$

Exercise 4.1 *Demonstrate that Newton's potential $1/r$ satisfies the equation of Laplace. Hint: realize that $\delta_{ii} = 1 + 1 + 1 = 3$!*

4.1.2 Method of Images

The point sink itself is of limited practical value when modeling three-dimensional groundwater flow in aquifers. First of all, the point sink in Figure 4.1 is located in an infinite domain, while an aquifer is bounded by an *aquifer base* and *aquifer top* across which no flow occurs. Furthermore, a point sink does not resemble any real-world flow feature, but distributions of point sinks over line elements or surfaces may be used to simulate flow toward, for example, a partially penetrating well and a lake bottom, respectively. We will discuss these distributions of point sinks in the next section. Here we will first address the problem of satisfying the no-flow conditions along the aquifer base and top.

Point Sink above an Impervious Plane

In Figure 4.2 a point sink is located at a distance d above an impervious plane: the aquifer base. For now we will consider an infinite flow domain above the aquifer base, and hence no aquifer top. The no-flow condition along the aquifer base may be obtained by use of an image point sink, in the same manner in which we simulated a no-flow boundary opposite a well in two-dimensions; see Figure 3.26 in Section 3.1.15. The solution for the point sink above the aquifer base is obtained by use of (4.10):

$$\Phi = -\frac{Q}{4\pi}\left(\frac{1}{r} + \frac{1}{\bar{r}}\right) \tag{4.16}$$

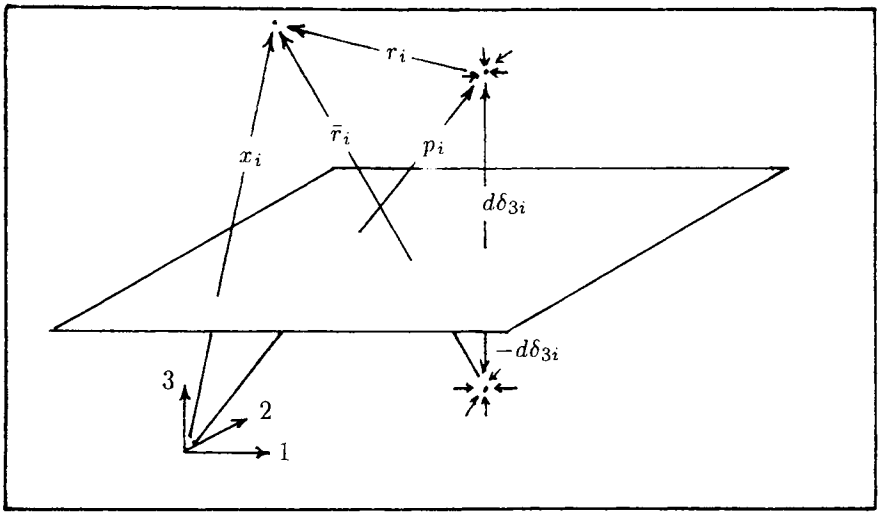

Figure 4.2: A point sink above an impervious plane.

where r is given by (4.8) with (4.5), and where $\bar{r}$ is given by (see Figure 4.2)

$$\bar{r} = \sqrt{(x_i - p_i + 2d\delta_{3i})(x_i - p_i + 2d\delta_{3i})} \tag{4.17}$$

where the components δ_{3i} of the Kronecker Delta serve as a unit vector normal to the plane in Figure 4.2. It follows from symmetry that no flow occurs across the plane $x_3 = 0$ in Figure 4.2, as for the two-dimensional case depicted in Figure 3.26.

Point Sink between Two Horizontal Impervious Planes

In Figure 4.3, the point sink is located between two horizontal impervious planes. The planes are a distance H apart, and the point sink is located at a distance d above the lower plane. The situation in Figure 4.3 may be interpreted as a point sink located inside a confined aquifer. In order to obtain no-flow conditions along both planes, images will be needed with respect to both planes. However, in order to obtain symmetry with respect to both planes (needed to create no-flow conditions along both planes), an *infinite* number of images is required.

Calculating the contribution to Φ of an infinite number of point sinks is, of course, impossible. To approximate this infinite series of point sinks, we may replace those point sinks that are sufficiently remote from the aquifer by semi-infinite line sinks (in three dimensions), see Bischoff (1981) and Haitjema (1982). In Figure 4.3, these line sinks are the vertical lines above

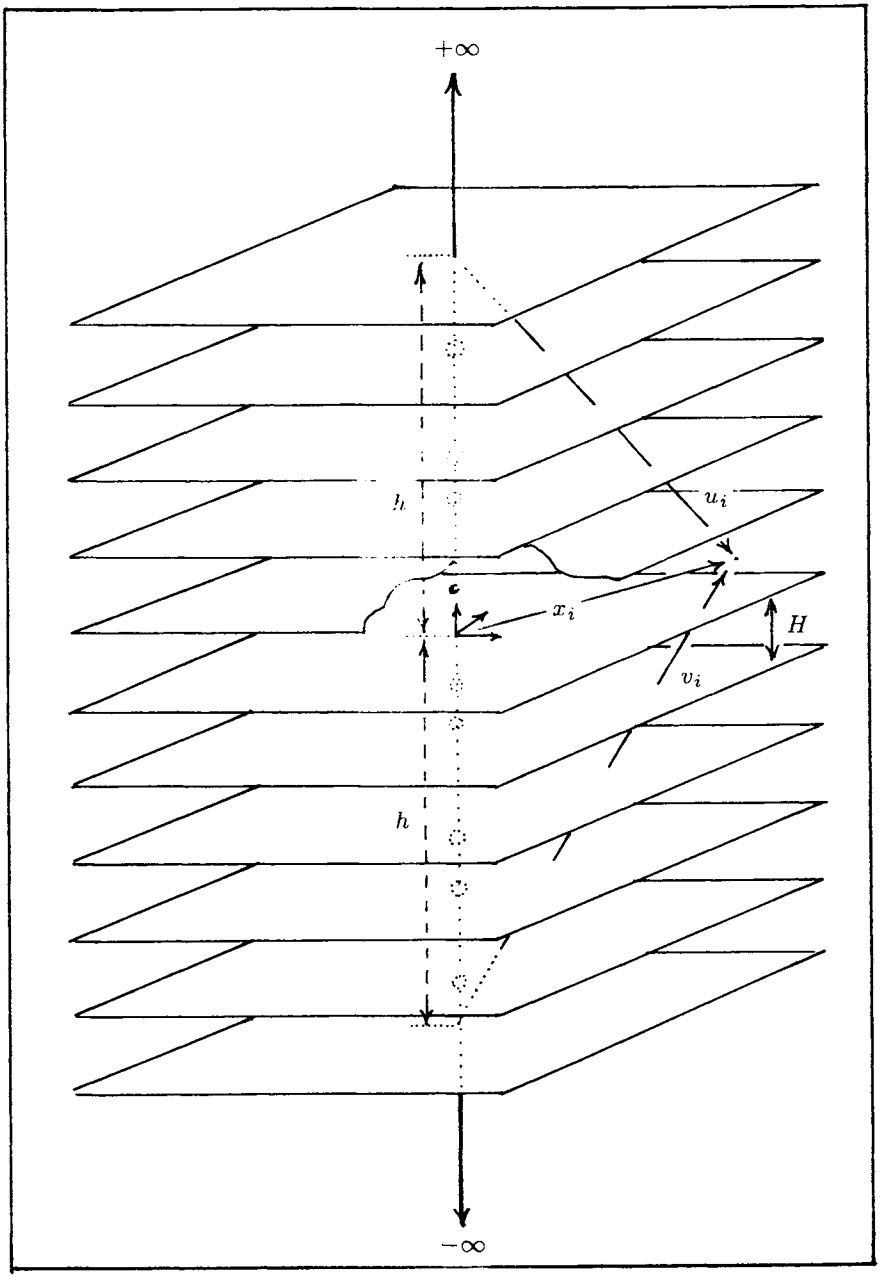

Figure 4.3: Point sink between two horizontal no-flow boundaries.

and below the last "image aquifer" with arrow heads pointing to $+\infty$ and $-\infty$, respectively. By redistributing the discharges of the point sinks over a line, we are making use of *St. Venant's principle* (see Knowles, 1965), which states that the precise geometry of a flow feature becomes less important with its distance. For the case of Figure 4.3, the flow generated by remote point sinks is nearly equal to the flow generated by a (semi-infinite) line sink with the same total discharge as the point sinks it replaces. St. Venant's principle applied to groundwater flow issues is further discussed in Section 5.3.8.

Two vertical semi-infinite line sinks are needed to replace remote image point sinks; see Figure 4.3. The semi-infinite line sink pair in Figure 4.3 may be obtained by subtracting a finite line sink from an infinite (vertical) line sink. The latter infinite vertical line sink is simply a well in a horizontal plane; the point in the horizontal plane that represents the well is a vertical infinitely long line in three-dimensional space. The specific discharge potential Φ for a semi-infinite line sink pair is written as

$$\Phi = \sigma \left[\frac{1}{2\pi} \ln \rho + \frac{1}{4\pi} \ln \frac{u+v-2h}{u+v+2h} \right] \tag{4.18}$$

where σ $[L^2/T]$ is the "sink density" along the semi-infinite line sinks, ρ is the horizontal distance from the line sinks, h is the distance from the aquifer base to the start of the semi-infinite line sinks, and u and v are the distances from the start of the semi-infinite line sink above and below the aquifer base, respectively; see Figure 4.3. The first term in (4.18) is an infinite vertical line sink which equals a well in two-dimensions, [compare (3.85)], whereby the discharge Q $[L^3/T]$ has been replaced by a discharge per unit length of the well axis (line sink) σ $[L^2/T]$. The second term in (4.18) is the potential due to a line source of length $2h$, the dotted line in Figure 4.3, which nullifies the midsection of the infinite line sink and thus creates two semi-infinite line sinks. The potential function for a three-dimensional line sink is well known in the literature, e.g., Duschek and Hochrainer (1970) and Haitjema (1982, 1985). The sink density σ in (4.18) equals the point sink discharge divided by the aquifer height:

$$\sigma = \frac{Q}{H} \tag{4.19}$$

The potential for the point sink in a confined aquifer may be written as

$$\begin{aligned} \Phi \;=\; & -\frac{Q}{4\pi} \left[\frac{1}{r} + \frac{1}{\bar{r}} + \sum_{n=1}^{M} \left\{ \frac{1}{r(n)} + \frac{1}{\bar{r}(n)} + \frac{1}{r(-n)} + \frac{1}{\bar{r}(-n)} \right\} \right. \\ & \left. - \frac{2}{H} \ln \rho - \frac{1}{H} \ln \frac{u+v-2h}{u+v+2h} \right] \end{aligned} \tag{4.20}$$

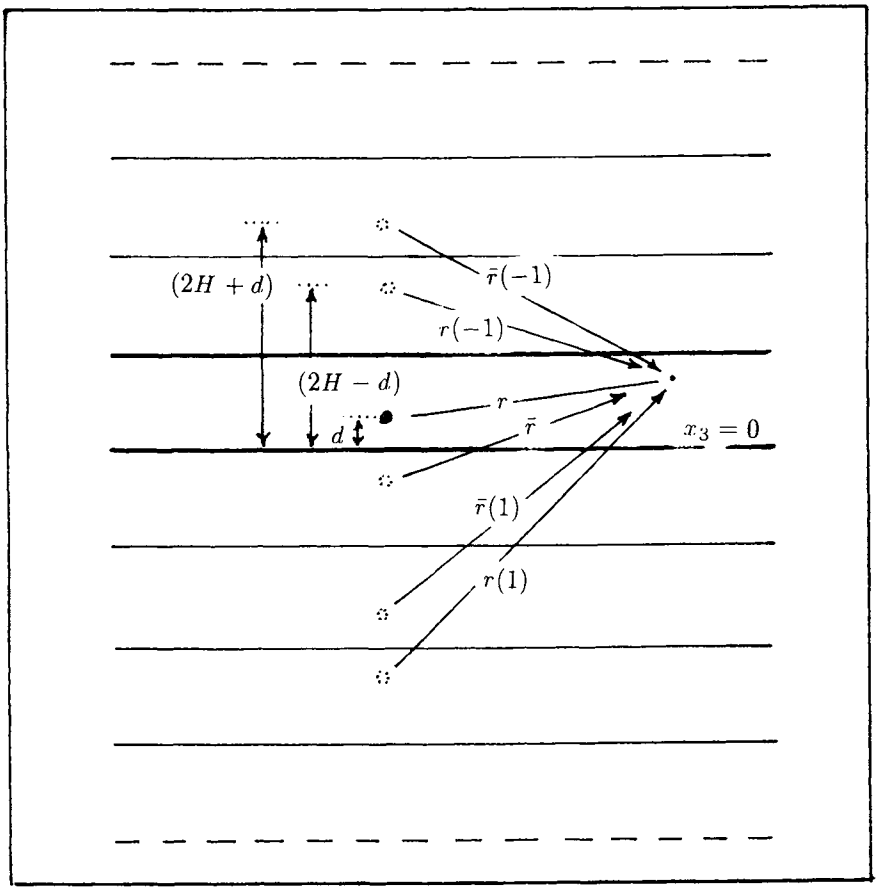

Figure 4.4: Position of image point sinks.

where $r(n)$ and $\bar{r}(n)$ are defined as [see Figure 4.4]

$$r(n) = \sqrt{(x_i + d\delta_{3i} + 2nH\delta_{3i})(x_i + d\delta_{3i} + 2nH\delta_{3i})}$$
$$\bar{r}(n) = \sqrt{(x_i - d\delta_{3i} + 2nH\delta_{3i})(x_i - d\delta_{3i} + 2nH\delta_{3i})} \tag{4.21}$$

and where h is defined as

$$h = (2M+1)H \tag{4.22}$$

The distances u and v are the lengths of the vectors u_i and v_i, which are

defined as [see Figure 4.3]

$$u_i = x_i - h\delta_{3i} \qquad v_i = x_i + h\delta_{3i} \tag{4.23}$$

In writing (4.20) through (4.23), the origin of the coordinate axis was located on the aquifer base underneath the point sink; see Figure 4.3. In (4.20) $4M + 1$ images are evaluated explicitly, while the remainder of the images are replaced by two semi-infinite line sinks. The images and semi-infinite line sinks are fully symmetric with respect to the aquifer base, while the symmetry with respect to the aquifer top can be improved arbitrarily by increasing M, and thus by evaluating more image point sinks explicitly.

4.2 Three-Dimensional Confined Flow

In the previous section we introduced the concept of three-dimensional flow in a confined aquifer for the case of flow towards a point sink. As mentioned, the point sink itself is of little practical interest, but by distributing it along line elements or over surfaces, we may model flow to, e.g., a partially penetrating well and a lake bottom, respectively. The mathematics of these *singularity distributions* along line elements or over surfaces is quite involved and outside the scope of this text. Instead, I will discuss the use of *line sinks* to model a partially penetrating well conceptually, without deriving the associated mathematical algorithms. Next I will present a three-dimensional version of the sink disc which may be used to model a shallow pond.

4.2.1 The Partially Penetrating Well

In Figure 4.5, a well is depicted which is screened over only part of the confined aquifer: a partially penetrating well. Muskat (1937) modeled the flow towards such a well by distributing point sinks along the well axis. He created a *line sink* by distributing an infinite number of point sinks along the well axis, while keeping their total discharge equal to some finite constant: the pumping rate of the well. Muskat pointed out that the sink density distribution along the line sink must increase near the ends in order to approximate a constant head along the well perimeter (well screen). Polubarinova-Kochina (1962) suggested the use of a singular sink density distribution σ along the line sink (well axis) of the form

$$\sigma(\lambda) = \frac{\sigma_0 h}{\sqrt{(1-\lambda h)(1+\lambda h)}} \quad (-1 \leq \lambda \leq +1) \tag{4.24}$$

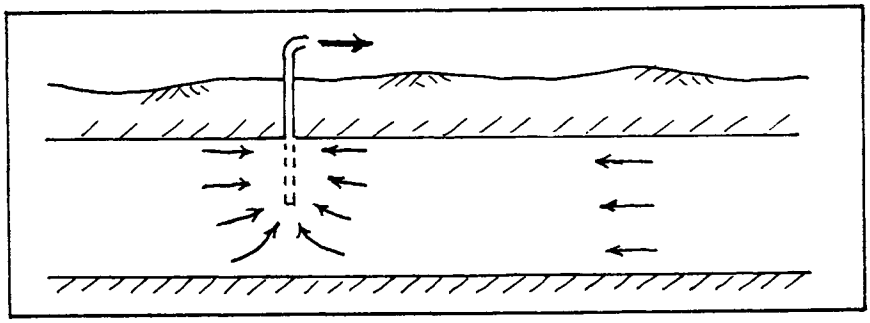

Figure 4.5: A partially penetrating well in a confined aquifer.

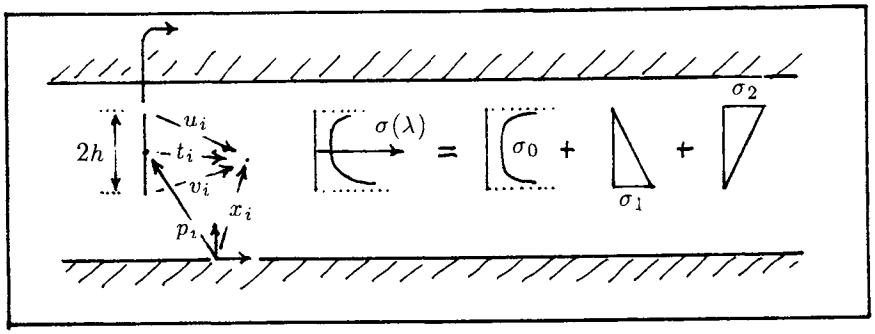

Figure 4.6: Sink density distribution along the axis of the well.

where λh is the distance from the center of the line sink to a point on the line sink: It is positive when the point is above the center, and negative when the point is below the center. The total length of the well screen is $2h$. Haitjema and Kraemer (1988) combined this strength distribution with a linear one to allow for different inflow rates near the top and bottom of the well, as may result from asymmetric positioning of the well screen in the aquifer (see Figure 4.6):

$$\sigma(\lambda) = \frac{\sigma_0}{\sqrt{(1-\lambda)(1+\lambda)}} + \frac{\sigma_1(1-\lambda)}{2} + \frac{\sigma_2(1+\lambda)}{2} \tag{4.25}$$

The specific discharge potential at a point x_i for the sink distribution (4.25) along the well axis may be writen as (see Haitjema and Kraemer, 1988)

$$\Phi(x_i) = \sigma_0 \Lambda(x_i) + \sigma_1 F(x_i) + \sigma_2 G(x_i) \tag{4.26}$$

where

$$\begin{aligned} \Lambda(x_i) &= -\frac{h}{2\pi\sqrt{uv}}K(k) \\ F(x_i) &= \frac{1}{8\pi}\left[\left(1-\frac{t_i h_i}{h^2}\right)\ln\frac{u+v-2h}{u+v+2h}+\frac{u-v}{h}\right] \\ G(x_i) &= \frac{1}{8\pi}\left[\left(1+\frac{t_i h_i}{h^2}\right)\ln\frac{u+v-2h}{u+v+2h}-\frac{u-v}{h}\right] \end{aligned} \tag{4.27}$$

The vector t_i points from the center of the well axis p_i to x_i; hence,

$$t_i = x_i - p_i \tag{4.28}$$

The parameters u and v are the lengths of the vectors u_i and v_i which point from the top and bottom of the well screen to the point x_i, respectively:

$$u_i = t_i - h_i \qquad\qquad v_i = t_i + h_i \tag{4.29}$$

The function $K(k)$ is the *complete elliptic integral of the first kind* with *modulus* k, which is defined as (Haitjema and Kraemer, 1988)

$$k^2 = \frac{h^2}{uv}\left[1-\left(\frac{u-v}{2h}\right)^2\right] \tag{4.30}$$

The specific discharge potential (4.26) does not yet include the effect of the two confining aquifer boundaries, the aquifer bottom and top. This is accomplished by imaging the line sink along the well axis with respect to both aquifer boundaries. As in the case of the point sink in the previous section, remote images are replaced by semi-infinite line sinks.

In Figure 4.7, a cross-section over the equipotential surfaces near a partially penetrating well is depicted, together with some streamlines. Observe that the streamlines become nearly horizontal at some distance from the well. The strenght parameters σ_0, σ_1, and σ_2 for this case are 53.67, 166.4647, and 164.91 ft^2/day, respectively. The difference in σ_1 and σ_2 reflects the asymmetric placement of the well in the aquifer. The strength parameters are found in the CHECK module of GFLOW1 by typing LIST PPWELL. These strength parameters have been obtained by requiring the same head at three *control points* at the well screen: one at the center of the well, and the other two at a small distance from the top and bottom of the well, respectively. For a head-specified, partially penetrating well, this leads to three equations in terms of the three strength parameters. A fourth equation is needed to define the head at a reference point at some distance from the well. If the pumping rate of the well is specified, as is the

case in Figure 4.7, the conditions required along the well screen are that the difference in the head between two successive control points is zero, which leads to only two equations. A third equation follows from requiring that the total well discharge be equal to the specified pumping rate. The total well discharge Q is found by integrating the strength (4.25) along the well axis, which yields (Haitjema and Kraemer, 1988)

$$Q = h(\pi\sigma_0 + \sigma_1 + \sigma_2) \tag{4.31}$$

In Figure 4.8, a close-up of the piezometric contours near the well screen is shown. Note that the equipotential surface near the end of the well screen is rounded, approximating the equipotential conditions along the rectangular well screen. In reality, however, the well screen is often surrounded by a gravel pack which will not exhibit the rectangular bottom depicted in Figure 4.8. In fact, the rounded shape of the equipotential near the well bottom is probably a more realistic representation of the interface between the gravel pack and the aquifer than the suggested rectangular shape of the well layout in Figure 4.8. In any case, these inaccuracies are insignificant in practice. The importance of the singular strength distribution (σ_0 in (4.25)) increases with increasing well radius. In fact, for the extreme case that the well radius becomes zero, σ_0 also becomes zero (Haitjema and Kraemer, 1988).

Exercise 4.2 *Experiment with the length of the well screen and the position of the well relative to the aquifer bottom and top by modifying the data file* proble41.dat. *For each case plot piezometric contours and trace some streamlines. Also inspect the difference in the strength parameters* σ_1 *and* σ_2.

Exercise 4.3 *Experiment with different well diameters by modifying the file* proble41.dat. *Notice how the value of* σ_0 *increases relative to* σ_1 *and* σ_2 *with increasing well diameter.*

4.2.2 The Sink Disc

In Figure 4.9, a cross-section over an aquifer underneath a lake is depicted. The lake is thought of as percolating water through a silty (low-permeable) zone above the otherwise confined aquifer. Earlier, in Section 3.2.4, we dealt with a similar situation when we discussed a circular irrigator or percolating pond. In that case, a Dupuit–Forchheimer solution was presented for a *sink disc*. Here I present the three-dimensional form of the sink disc, which is a (point) sink distribution over a horizontal disc.

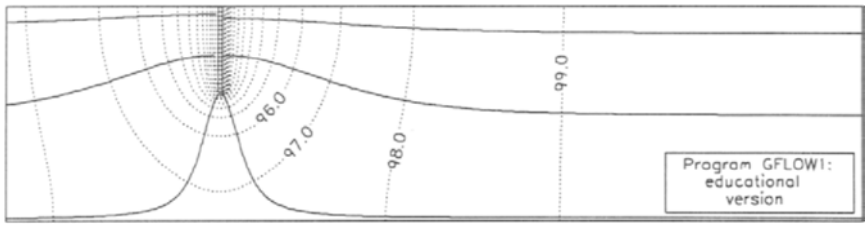

Figure 4.7: Piezometric contours and streamlines in a cross-section over a partially penetrating well in a confined aquifer. (GFLOW1 data file `proble41.dat`)

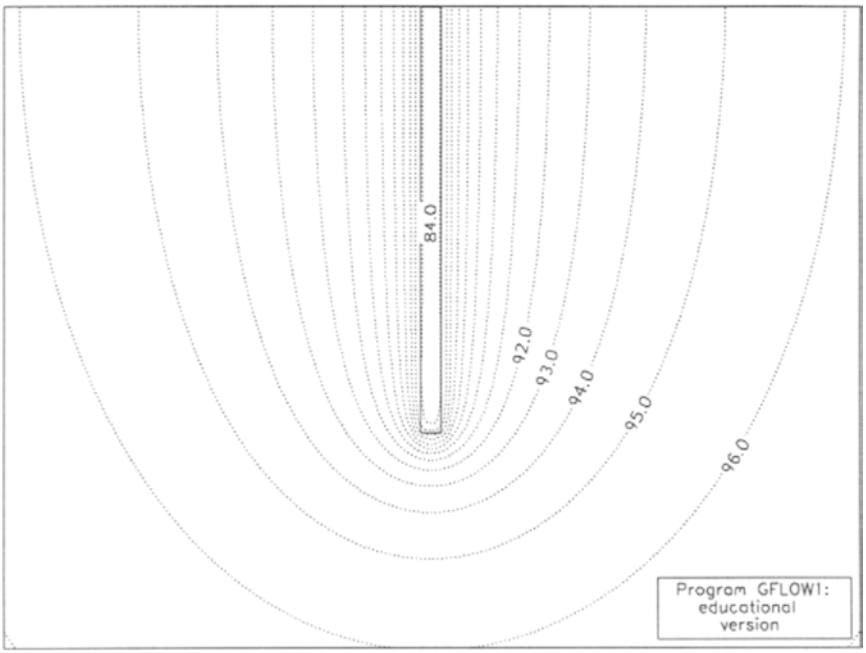

Figure 4.8: Close-up of piezometric contours near the well screen. (GFLOW1 data file `proble41.dat`)

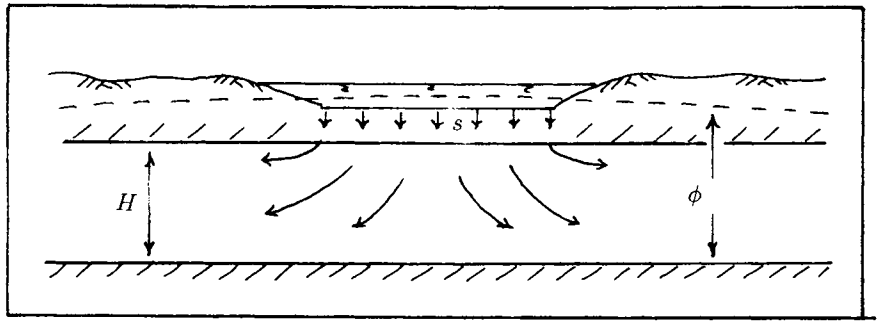

Figure 4.9: Lake infiltrating water in a confined aquifer.

The specific discharge potential Φ at the point x_i for the sink disc of radius R and sink density s is given by Haitjema (1987a):

$$\Phi(x_i) = \frac{s}{4\pi}\left[\frac{2(t^2-R^2)}{\sqrt{t^2+R^2+2\tau R}}K(k) - 2\sqrt{t^2+R^2+2\tau R}\,E(k) + \eta_i e_i \omega\right] \tag{4.32}$$

where the vector t_i points from the center of the disc toward the point x_i, and where τ_i is the projection of t_i onto the plane of the disc; see Figure 4.10. The vector η_i is perpendicular to the disc and defined by

$$t_i = \tau_i + \eta_i \tag{4.33}$$

The vector e_i is a unit vector normal to the plane of the disc which defines the orientation of the disc. The functions $K(k)$ and $E(k)$ are the complete elliptic integrals of the first and second kind, respectively; see Byrd and Friedman (1971). The modulus k is defined by (Haitjema, 1987a):

$$k^2 = \frac{4\tau R}{t^2+R^2+2\tau R} \tag{4.34}$$

The function ω is the solid angle subtended by the disc at the point x_i and is given by Haitjema (1987a):

$$\omega = \frac{2\eta_i e_i}{\sqrt{t^2+R^2+2\tau R}}\left[\frac{\tau-R}{\tau+R}\Pi(\alpha^2,k) - K(k)\right] + \overset{0}{\omega} \qquad (\tau \neq R) \tag{4.35}$$

$$\omega = -\frac{\eta_i e_i}{\eta}[2k'K(k) - \pi] \qquad (\tau = R)$$

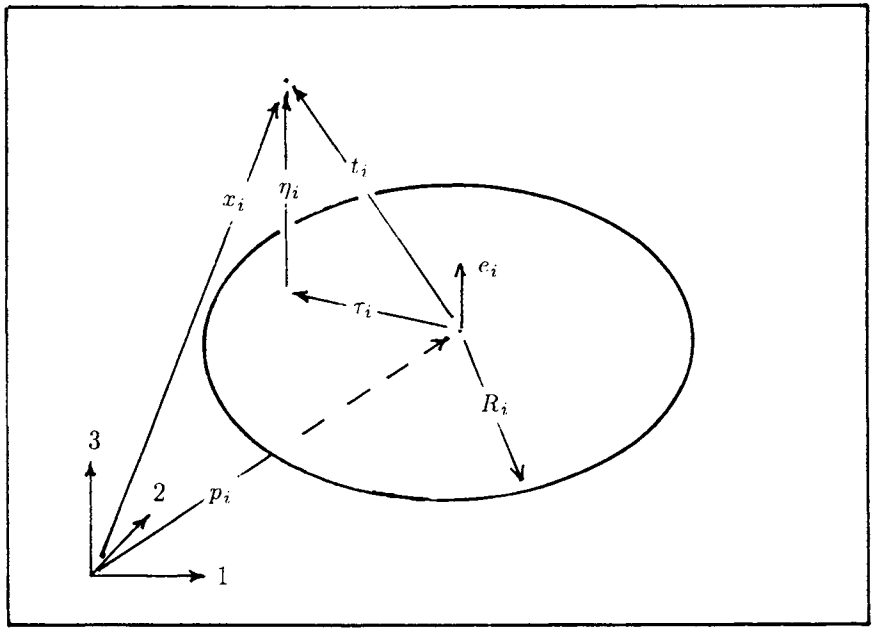

Figure 4.10: Three-dimensional sink disc.

where the constant $\overset{0}{\omega}$ is defined as

$$\begin{aligned} \overset{0}{\omega} &= 0 && (\tau > R) \\ \overset{0}{\omega} &= +2\pi && (\eta_i e_i/\eta = +1,\ \tau < R) \\ \overset{0}{\omega} &= -2\pi && (\eta_i e_i/\eta = -1,\ \tau < R) \end{aligned} \tag{4.36}$$

The term $\eta_i e_i/\eta$ switches from $+1$ to -1 when the point x_i moves from above the plane to below the plane, respectively. The *complementary modulus* k' is defined by $k'^2 = 1 - k^2$, while α^2 is defined as (Haitjema, 1987a):

$$\alpha^2 = \frac{4\tau R}{\tau^2 + R^2 + 2\tau R} \tag{4.37}$$

The specific discharge potential presented earlier does not yet include the effects of the upper and lower aquifer boundaries. As with the point sink and partially penetrating well, these no-flow boundaries are satisfied by introducing images with respect to the aquifer top and bottom. Remote image discs are replaced by semi-infinite line sinks, whereby the sink density of these image discs are redistributed over the line sink.

In Figure 4.11, piezometric contours and some streamlines are shown in a cross-section through the axis of a *source* disc at the top of a confined aquifer. A source disc is simply a sink disc with a negative sink density. Since the sink disc is the only feature in the aquifer, the flow is radially symmetric about the center of the disc.

In Figure 4.12, both a sink disc and a source disc are present. The discs have equal but opposite discharge rates and are placed inside the aquifer, away from the aquifer boundaries. The cross-section is made through the axes of both discs. As in Figure 4.11, there are no other flow features in the aquifer.

4.3 Combined Two- and Three-Dimensional Flow

Three-dimensional functions are mathematically complex and require far more computational effort than their two-dimensional counterparts: Compare, for example, the partially penetrating well functions (4.26) through (4.30) with the two-dimensional version for a fully penetrating well, which is a simple logarithm [see (3.85)]. The functions for a partially penetrating well in a confined aquifer are, in fact, even more involved than is exhibited by (4.26) through (4.30), since images and remote semi-infinite line sinks must be added, see the analysis for the point sink in a confined aquifer in

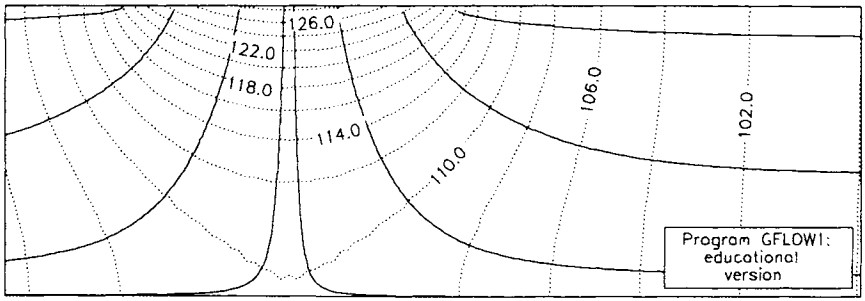

Figure 4.11: Piezometric contours and streamlines near a source disc at the aquifer top. (GFLOW1 data file proble42.dat)

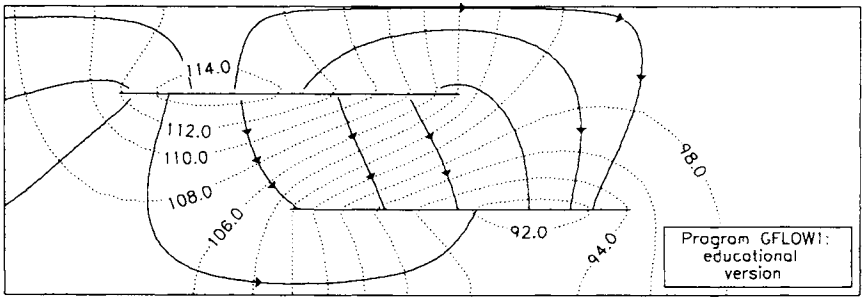

Figure 4.12: Piezometric contours and streamlines near a source disc and a sink disc in a confined aquifer. (GFLOW1 data file proble43.dat)

Section 4.1.1. Numerical techniques also experience substantial computational limitations when applied to three-dimensional flow. Consequently, three-dimensional groundwater flow modeling is often confined to relatively small areas surrounding the three-dimensional features of interest. At the same time, however, as we will see in Chapter 5, hydrological features (streams and lakes) that are rather remote from the area of interest cannot be ignored. To resolve this dilemma, Ward *et al.* (1987) suggested a "telescopic mesh refinement modeling approach" to the groundwater flow problem near the Chem-Dyne hazardous waste site in southwestern Ohio. The authors used three different groundwater models (finite difference models) for three different scales: the "regional scale," the "local scale," and the "site scale." The regional-scale two-dimensional (Dupuit–Forchheimer) model included remote hydrological features. The local-scale model obtained its conditions along the grid boundary from the regional model, while the site-scale model, in turn, received its boundary conditions from the local-scale model. Detailed three-dimensional modeling was reserved for the site scale in order to keep memory requirements and computation times manageable. It appears possible, however, to make the transition from regional Dupuit–Forchheimer flow to local three-dimensional flow within a single model, at least for the case of confined flow.

In Chapter 5 I will generalize the procedure of superposition of elementary solutions, employed in Chapter 3 (e.g., a well and a pond in a uniform flow field near a stream or lake boundary), into the *analytic element method.* Instead of using images to incorporate stream or lake boundaries, as we did in Chapter 3, within the framework of the analytic element method we are modeling these features explicitly, by use of *line sinks* in two dimensions. Haitjema (1985) showed that under confined flow conditions, two- and three-dimensional solutions (*analytic elements*) can be superimposed to form a single analytic element model. This is possible if we realize that the two-dimensional solutions to flow *in a confined aquifer* are a subset of the three-dimensional solutions in that aquifer. Consequently, as for the three-dimensional solutions, the two-dimensional (Dupuit–Forchheimer) solutions can also be written in terms of the discharge potential (4.3) which satisfies Laplace's equation in three dimensions. The two-dimensional and three-dimensional solutions in a confined aquifer, therefore, can simply be superimposed. This is quite attractive, since three-dimensional analytic elements can simply be added to a Dupuit–Forchheimer model instead of replacing the Dupuit–Forchheimer model by a three-dimensional model, as was done by Ward *et al.* (1987). In general, three-dimensional features are only needed locally, in the area of interest (in Ward's case, the Chem-Dyne hazardous waste site). The majority of flow features in the model, therefore, will be represented by the much simpler two-dimensional solutions.

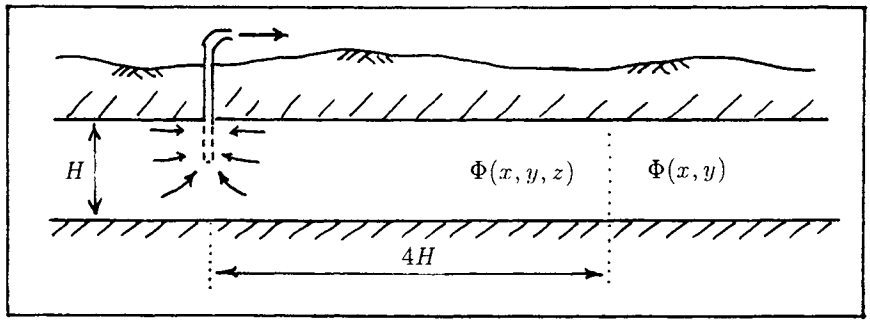

Figure 4.13: Switching from three-dimensional functions near the partially penetrating well to a Dupuit–Forchheimer solution remote from the well.

For instance, when modeling a well field in a regional setting of streams, the partially penetrating wells will generate three-dimensional flow only in the immediate vicinity of the well field, so that the streams and their tributaries away from the well field can still be modeled by two-dimensional line sinks.

This hybrid two- and three-dimensional model can be made even more efficient by exploiting the fact that three-dimensional flow features in a confined aquifer tend to generate two-dimensional horizontal flow at some distance away from the feature. For instance, in Figure 4.7, we see that at a distance of about two times the aquifer thickness, the streamlines become nearly horizontal and the equipotential surfaces become almost vertical. In other words, sufficiently far from the partially penetrating well, the flow patterns become indistinguishable from those due to a fully penetrating well. In mathematical terms, remote from the partially penetrating well the three-dimensional functions for the well and its images can be replaced by the two-dimensional solution for a fully penetrating well:

$$\Phi = \frac{Q}{2\pi H} \ln r \tag{4.38}$$

In GFLOW1, therefore, the partially penetrating well and three-dimensional sink disc are both represented by three-dimensional functions and by two-dimensional functions. Within a distance of, say, four times the aquifer thickness from the element, the three-dimensional functions are evaluated, while outside that zone the two-dimensional functions are being used; see Figure 4.13. In this manner, three-dimensional functions are evaluated very selectively, only in the immediate vicinity of a three-dimensional feature and then only the function for that feature. All other elements in the aquifer are treated as being two-dimensional, including remote three-

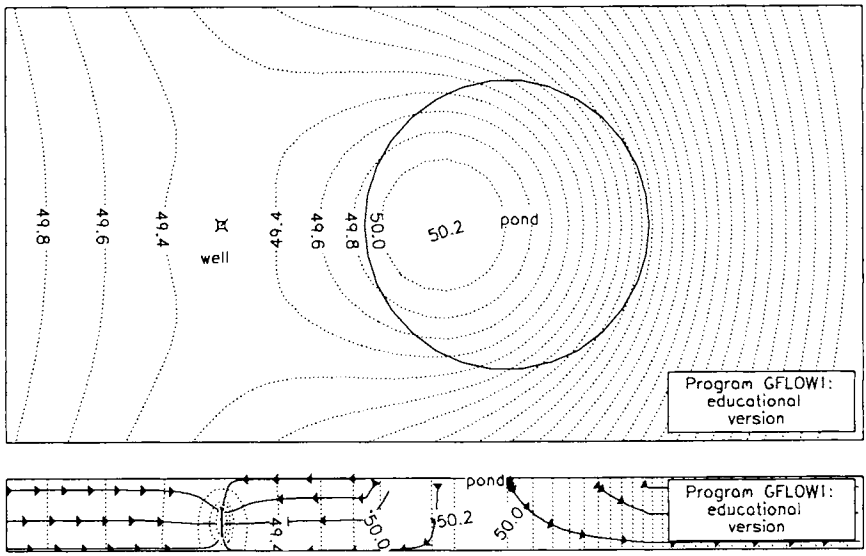

Figure 4.14: Flow near a partially penetrating well and a two-dimensional pond function. (GFLOW1 data file proble44.dat)

dimensional elements.

4.3.1 Partially Penetrating Well near a Shallow Pond

To illustrate the concept of combined two- and three-dimensional flow modeling, the problem of a partially penetrating well near a shallow pond is solved. In Figure 4.14, I combined the partially penetrating well with a two-dimensional representation of the pond as given in Section 3.2.4 by (3.184) through (3.185). In addition to the pond, there is also a uniform flow field with flow from left to right in Figure 4.14. Note that in the cross-section over the well and the pond, the streamlines underneath the pond are not perpendicular to the equipotentials. This is a consequence of modeling the pond by use of a Dupuit–Forchheimer solution by which the vertical flow is calculated in an approximate manner, as outlined in Section 3.5. In contrast, the streamlines near the well are perpendicular to the equipotentials, because the well is modeled by truly three-dimensional functions.

In Figure 4.15, the well is closer to the pond and the pond is smaller than in Figure 4.14: The radius of the pond is half the aquifer thickness. Because of this, I modeled the pond as a three-dimensional sink disc. As

in the case of Figure 4.14, there is a uniform flow from left to right in Figure 4.15. This time the streamlines are everywhere perpendicular to the equipotentials, since only fully three-dimensional functions are being used.

In Figure 4.14 I purposely chose to model the pond by use of a two-dimensional sink disc as derived in Chapter 3. I did this because the disc was large as compared to the aquifer thickness and I was content with getting truly three-dimensional flow patterns only near the well. However, the three-dimensional representation of the partially penetrating well in Figure 4.14 occurs only within a distance of four times the aquifer thickness from the well axis. For instance, underneath and to the right of the pond in Figure 4.14, the heads and flows are calculated by two-dimensional functions only. This switch from three- to two-dimensional functions (and vice versa) is made automatically in GFLOW1. In Figure 4.15 I decided to model the pond by a three-dimensional sink disc because it was small compared to the aquifer thickness and because the well was nearby; I wanted fully three-dimensional flow patterns both near the well and underneath the pond. However, here, too, GFLOW1 switches from three-dimensional functions to two-dimensional ones when we get away from the three-dimensional feature itself. For instance, at some distance to the left of the pond, outside Figure 4.15, heads and flows would be evaluated by a two-dimensional function for the well and a three-dimensional function for the pond. When we move even farther away from the pond and the well, the heads and flows are calculated by two-dimensional functions for both the well and the pond, even though both have been defined as three-dimensional features in GFLOW1. When we consider an entire regional model, it becomes clear that in most locations two-dimensional functions would be evaluated, even though several three-dimensional flow features may be included in the model. Consequently, the combined two- and three-dimensional model is nearly as efficient as a purely two-dimensional (Dupuit–Forchheimer) model.

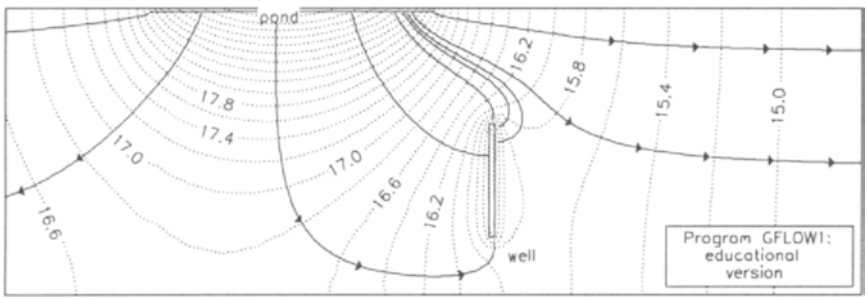

Figure 4.15: Flow near a partially penetrating well and a three-dimensional pond function. (GFLOW1 data file proble45.dat)

This Page Intentionally Left Blank

Chapter 5

Analytic Element Modeling

In the preceding chapters we have been building the theoretical framework for a mathematical description of groundwater flow. In the process we solved numerous practical problems, using what we just learned. However, most of these groundwater flow problems were severe abstractions from the real world. A recharge area or aquifer inhomogeneity, for instance, was taken to be circular, and the problem of a well near a stream was approximated by modeling a well opposite an infinitely long equipotential line. Although many of our solutions serve useful educational purposes, they are not very convincing representations of groundwater flow in regional aquifers with, among others, complex stream networks, wetlands, and varying areal recharge rates and transmissivities. It is true that there exist many more analytic solutions to groundwater flow than are presented in this text, and some of them are very ingenious. By themselves, however, they all share the limitation of a relatively simple hydrogeological setting.

In view of these limitations, and because of the widespread availability of digital computers, almost all groundwater flow problems nowadays are solved by use of *numerical methods*. The most popular approach, at least in the U.S., is the *finite difference method*. This method is conceptually very simple: The model area is overlain by a rectangular *model grid* and the differential equation is replaced by a set of *finite difference* equations in terms of the piezometric heads at the nodes of the model grid. The resulting set of linear algebraic equations is solved iteratively on a computer.

Another popular technique is the *finite element method*. The concept behind this method is to subdivide the flow domain into a network of el-

ements, in each of which a basic solution to groundwater flow is sought, e.g., uniform flow in triangular elements. Using a minimization of energy principle, all basic solutions are chosen in such a manner that together they form an approximation to the actual groundwater flow solution. Although the basic solution in each element satisfies the original differential equation, no continuity of flow is guaranteed across elements. Consequently, neither finite difference solutions (where the differential equation is approximated) nor finite element solutions satisfy regional continuity of flow automatically. In fact, a check on continuity of flow is often used to determine whether or not the numerical procedure converged to a valid solution. Another drawback of these traditional numerical methods is the fact that the groundwater flow solution is defined in terms of heads at grid nodes or element nodes alone. Anywhere else the heads must be estimated by interpolation. This is of particular concern when determining streamlines. The lack of a continuously defined piezometric head surface (or velocity vector field) may result in inaccurate streamline traces. In the context of modeling contaminant transport, these inaccuracies may contribute to *numerical dispersion.* Numerical dispersion can be minimized by refining the grid or element network, but this increases the computational effort. It is necessary, therefore, to balance the grid or element resolution against the size of the model domain in order to arrive at a computationally manageable model. These shortcomings are usually accepted in view of the versatility of the finite difference or finite element method. They can readily be applied to nonlinear differential equations and can easily accommodate aquifer inhomogeneities. The finite difference and finite element methods, and their application, are extensively discussed in textbooks, e.g., Bear and Verruijt (1987) and Anderson and Woessner (1992).

In this text we will continue to build on the analytic solutions developed in Chapters 3 and 4, rather than abandon them in the face of complex hydrogeology. We will address complex boundary conditions and inhomogeneous aquifers by combining many (several hundred) elementary analytic solutions: The *analytic elements.* This *analytic element method* provides a composite analytic solution to a regional flow problem which satisfies the differential equation everywhere: Continuity of flow is guaranteed. The heads and groundwater flow velocities are defined at any point in the flow domain; hence, there will not be numerical dispersion resulting from inaccurate groundwater flow velocities. Operationally, the analytic element method also offers advantages over the finite difference and finite element method. No design considerations for a model grid or element network are needed; instead, the hydrogeologist can input hydrological and geological features directly into the model. The absence of a model grid or element network also eliminates the compromise between model resolution and size

of the model area. The analytic element method, therefore, is relatively insensitive to scale.

In this chapter I will introduce the basics behind the analytic element method, introduce an elementary analytic element code GFLOW1, and discuss the modeling of regional groundwater flow problems by use of the analytic element method. You will discover that there is an almost seamless transition from the "hand calculations" employed in Chapter 3 to computer modeling of progressively more complex problems. In fact, I strongly recommend this procedure: First solve one or more very simple conceptualizations by hand, and then use the results to design an effective computer modeling strategy. At the very least, one should use simple hand calculations to verify whether or not the computer output is reasonable. The desirability of accompanying computer modeling by simple hand calculations, by the way, is not specific to the analytic element method; it applies to all numerical modeling techniques.

5.1 The Analytic Element Method

The analytic element method was developed at the end of the 1970s by Otto Strack at the University of Minnesota (Strack and Haitjema, 1981a, 1981b). At that time we were involved in a project for the U.S. Army Corps of Engineers to model the environmental impact of the "divide cut section" of the new Tennessee–Tombigbee Waterway (Strack *et al.*, 1980). The size of the model area and the desired resolution of the groundwater flow solution made the application of traditional numerical methods impractical. Strack developed the comprehensive potential concept (see Section 3.3.1) to deal with the dual aquifer situation in the area: the upper, unconfined Eutaw aquifer and the lower, confined Gordo aquifer. He also conceived of what is now known as the analytic element method by proposing to superimpose hundreds of line sinks to represent the surface water boundary conditions and using line doublet strings to include aquifer inhomogeneities. Especially for this project, I wrote the first analytic element program SYLENS (SteadY state flow with LENSes), which is a dual-layer Dupuit–Forchheimer model. Since that time, both the computer technology and the analytic element method have significantly advanced. SYLENS is no longer in operation, but has been superseded by several new analytic element codes.

Next I will discuss the basics of the analytic element method as implemented in the elementary program GFLOW1. These discussions are mostly conceptual in nature, with the exception of Section 5.1.2 through Section 5.1.5, where some mathematical backgrounds are provided. Yet even in those sections, I have limited the mathematics to a level that is just

enough to understand the theoretical framework of the analytic element method. The many mathematical details needed to implement the analytic elements in a computer program are outside the scope of this text, but are found in Strack (1989). In fact, the reader who is only interested in the application of the analytic element method may safely skip Sections 5.1.2 through 5.1.5.

5.1.1 Representing Hydrogeological Features by Analytic Elements

The regional groundwater flow regime interacts with available surface waters, responds to areal recharge due to precipitation, and is influenced by variations in aquifer properties. We will model these effects by use of line sinks, areal sinks, and line doublets, respectively. I will first discuss the use of these analytic elements conceptually; the associated mathematics will be discussed later on in separate sections.

In Figure 5.1, a section of a topographic map is shown. On that map we find all surface waters in the area: streams and their tributaries, ditches, lakes, and wetlands. The average surface water elevations can be estimated from the topographic map by looking for the intersections of topographic contour lines with the streams. On the original map, the topographic contour lines are thin brown lines with contour intervals of 5 or 10 feet (consult the legend on your map). In between the intersections of contour lines with streams, the surface water elevation may be estimated by interpolation. The surface water elevations obtained in this manner are, admittedly, not very precise, but for now we will accept them as adequate for our regional model.

It is noted that some surface waters are represented by solid blue lines, while others are drawn by dash-dot lines. The solid line streams are so-called *perennial* streams which flow year-round, while the dash-dot streams are *ephemeral* streams which flow intermittently. Some ephemeral streams flow during most of the winter and spring, while others flow only briefly after a rainstorm. The perennial streams, and to some extent the longer-flowing ephemeral streams, receive groundwater which sustains their flow: baseflow. Streams that flow only briefly after a rainstorm are unlikely to influence the regional groundwater flow system in any significant way. In Section 5.2 we will discuss this interaction between surface water flow and groundwater flow in more detail. For now we will assume that any surface water feature which we include in the model will be fully connected to the regional flow system. Under the Dupuit-Forchheimer assumption, the head in the aquifer underneath a stream is simply equal to the water level in that stream. This head is maintained by the stream either by allowing

groundwater to enter the stream or by infiltrating water from the stream into the aquifer. Particularly in view of the potential need to infiltrate stream water, we should be cautious not to include ephemeral streams, unless we know that they flow most of the time (are nearly perennial).

Representing Surface Waters

For the purpose of the modeling, we will break up the streams and their tributaries into many segments. Each segment, on average, may either receive groundwater (a gaining stream segment) or recharge the groundwater (a losing stream segment). In the model, we will represent each stream segment by a *line sink* which has a positive sink density when the stream is gaining, and a negative sink density when the stream is losing. A line sink may be viewed as a distribution of wells over a line element, as we will see in Section 5.1.2. In Figure 5.2, a layout of these line sinks is depicted which represents the surface waters in Figure 5.1. Note that the ephemeral streams (dash-dot lines) have not been included in the line sink network. Line sinks are also used to represent lakes, by approximating the lake boundary by a polygon of line sinks. Some of the lakes are represented by a circle: a sink disc, as discussed in Chapter 3. These sink discs will model groundwater seepage into the lake or, in case of a negative sink density, will let the lake recharge the aquifer.

Bounded versus Unbounded Model Area

Observe that the streams near the center of the map are broken up into smaller segments than those that occur near the map boundaries. We call the area of a higher data resolution, inside the dotted rectangle in Figure 5.2, the *nearfield* and the surrounding area the *farfield.* The nearfield is the area of interest for our modeling, the farfield serves as a "boundary" for that area. The analytic element method does not have a "model boundary" like the boundary of a finite difference grid or finite element network. This is actually an advantage! It is very tempting to limit the finite difference grid to the dotted area in Figure 5.2 and specify observed piezometric heads (from piezometers or domestic wells) at the boundaries of the model grid. The incentive for this is that the relatively small area can be represented by a fine grid (high resolution) without undue computational effort. However, the specified conditions on the grid boundary will significantly influence the groundwater flow solution in the model area. Where observed piezometric heads should only be used for assessing the validity of the modeling results, they are now also used to force (read bias) the model to reproduce what is observed. A better modeling approach would

Figure 5.1: Topographic map of model area.

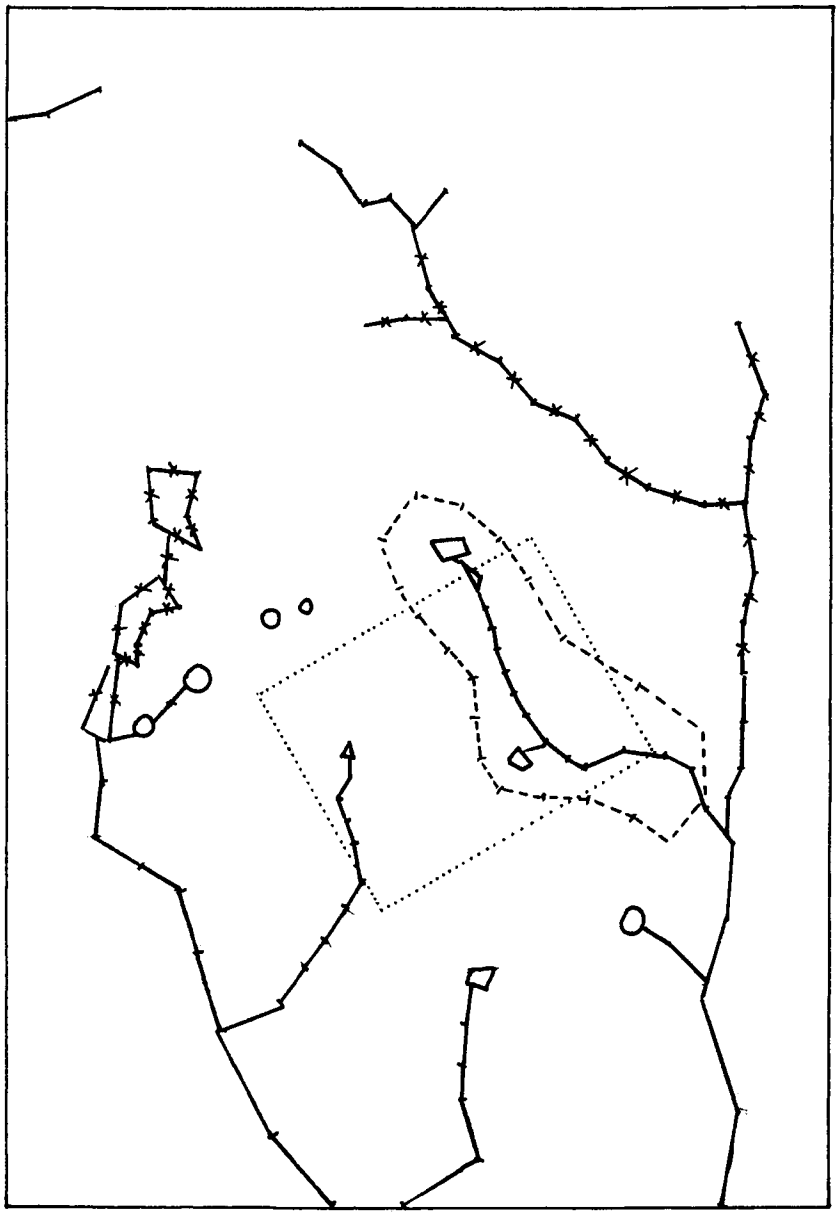

Figure 5.2: Analytic element layout for the surface water features on the topographic map. The dotted rectangle is the nearfield (area of interest).

be to overlay the entire domain in Figure 5.2, nearfield plus farfield, with a finite difference grid. The surface waters in the farfield will then ensure proper (natural) boundary conditions surrounding the nearfield. The specified conditions on the remote grid boundary are now irrelevant; they do not influence the solution in the nearfield. Since the analytic element method does not have a (grid) boundary, the inclusion of farfield features becomes an automatic necessity.

Including Aquifer Inhomogeneities

On a regional scale we may anticipate different aquifer properties in different areas. For instance, near streams one often encounters so-called *channel deposits*, zones around the stream with relatively coarse sand and gravel. Data on different aquifer thicknesses and hydraulic conductivities are, in general, not as easily obtained as the locations and water levels of surface waters. Surface geological maps and well logs, with a description of the geological formations penetrated by the well, are the primary sources for determining aquifer inhomogeneities. But determining the various hydraulic conductivities is still no simple task. When modeling groundwater flow on a regional scale, however, it is probably not necessary to deal with the many local aquifer inhomogeneities, but in the area of interest major zones of different aquifer properties should be included. A more detailed discussion on this and related issues is found in Section 5.3.3. In Figure 5.2 a dashed polygon is depicted (in the nearfield) which defines an area of a higher hydraulic conductivity than the surrounding aquifer. The polygon sides are so-called *line doublets*, which generate a jump in the discharge potential across the polygon side. The jump is chosen to satisfy the condition (3.272) discussed in Section 3.4.3, while the line doublet function itself preserves continuity of flow across the polygon side. The mathematical form of the line doublet is discussed below in Section 5.1.3.

Solving the Flow Problem

We introduced line sinks and sink discs to represent surface water features and line doublets to define a zone of different hydraulic conductivity in Figure 5.2. However, up to now, the line sinks and sink discs have unknown sink densities. It is impractical, to say the least, to attempt to determine the groundwater inflow rates or aquifer recharge rates of the surface waters in the model area. We also have not discussed how to generate the proper jump in the potential with the line doublets in Figure 5.2. As for the line sinks and sink discs, we will not attempt to specify the sink densities (infiltration or exfiltration rates), but will specify the average surface water level

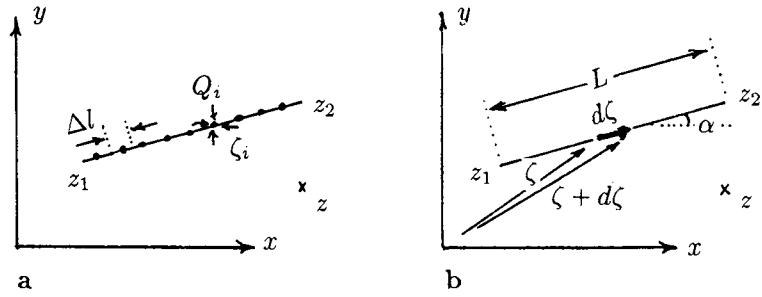

Figure 5.3: Line sink as a distribution of wells over a line element (a) for the limiting case of an infinite number of wells with a finite total discharge (b).

for each line sink or sink disc and let the program sort out the appropriate sink densities. These sink densities (line sink strengths) will be chosen in such a manner that the piezometric head in the aquifer underneath each line sink matches the specified water level for that line sink. This match will be achieved at only one particular point on each line sink: the *control point*. In Figure 5.2 some of these control points are indicated by crosses at the centers of the line sinks. By forcing the heads equal to surface water elevations, we are treating these surface water features as Dirichlet boundary conditions for the groundwater flow regime.

When dealing with inhomogeneities, we will only specify the inside and outside hydraulic conductivity of the dashed zone in Figure 5.2 and let the program adjust the line doublet strengths to create the proper jump in the discharge potential. We will discuss this in more detail in Sections 5.1.3 and 5.1.5.

5.1.2 The Line Sink

The line sink function is well known in potential theory, e.g., Kellog (1929). An extensive discussion on the topic is found in Strack (1989). Here I will provide a brief mathematical derivation of the line sink function and illustrate its effect on the groundwater flow regime.

In Figure 5.3a I present the line sink conceptually as a finite number of wells evenly distributed over a line element between the points z_1 and z_2. A real line sink is obtained if the number of wells in Figure 5.3a is infinitely large, while their total discharge remains finite: equal to the total

extraction rate of the line sink. The mathematical analysis is best carried out in terms of complex variables. The complex potential Ω_{ls} for M wells along the line element is

$$\Omega_{ls} = \sum_{i=1}^{M} \frac{Q_{(i)}}{2\pi} \ln(z - \zeta_i) \tag{5.1}$$

where $Q_{(i)}$ is the discharge rate of the ith well. On average we want the line sink to have a discharge rate of σ cubic feet per day per foot length of the line sink. If the well at ζ_i represents a section Δl of the line sink, we can write for $Q_{(i)}$

$$Q_{(i)} = \Delta l \sigma \tag{5.2}$$

with which I can rewrite (5.1) in the form

$$\Omega_{ls} = \sum_{i=1}^{M} \frac{\sigma}{2\pi} \ln(z - \zeta_i) \Delta l \tag{5.3}$$

If we represent the line sink by an infinite number of wells, hence $M \to \infty$ and $\Delta l \to 0$, the sum in (5.2) is replaced by an integral

$$\Omega_{ls} = \int_0^L \frac{\sigma}{2\pi} \ln(z - \zeta) dl \tag{5.4}$$

It would be helpful if the integral in (5.4) could be written as a complex integral in terms of the parameter ζ. To achieve this I introduce, with reference to Figure 5.3b, the infinitesimal complex variable $d\zeta$:

$$d\zeta = \Delta l e^{i\alpha} \tag{5.5}$$

where α is the angle between the line sink and the positive x-axis. With (5.5), I rewrite (5.4) as

$$\Omega_{ls} = \frac{\sigma}{2\pi} e^{-i\alpha} \int_{z_1}^{z_2} \ln(z - \zeta) d\zeta \tag{5.6}$$

The integral in (5.6) is of the form $\int \ln x \, dx = x \ln x - x$, so that the complex potential for the line sink becomes

$$\Omega_{ls} = \frac{\sigma}{2\pi} e^{-i\alpha} \left[(z - z_1) \ln(z - z_1) - (z - z_2) \ln(z - z_2) + (z_1 - z_2) \right] \tag{5.7}$$

Behavior of the Stream Function

The line sink extracts a total of σL [ft^3/day] from the aquifer, consequently it should generate a branch cut in the stream function Ψ just as a well does; see Figure 3.14 in Section 3.1.6. To illustrate the behavior of the stream function, while avoiding unnecessary algebra, I select the line sink along the x-axis: $y_1 = y_2 = 0$ and $\alpha = 0$. Furthermore, we are interested in the behavior of Ψ along the element, and thus along the x-axis: $y = 0$. With these simplifications, the stream function Ψ becomes

$$\begin{aligned}
\Psi &= \Im\{\Omega_{ls}\} \\
&= \frac{\sigma}{2\pi}\Im\{(x-x_1)(\ln|x-x_1| + i\theta_1) \\
&\quad -(x-x_2)(\ln|x-x_2| + i\theta_2) + (x_1 - x_2)\} \\
&= \frac{\sigma}{2\pi}\left[(x-x_1)\theta_1 - (x-x_2)\theta_2\right] \qquad (5.8)
\end{aligned}$$

where θ_1 and θ_2 are the arguments of the complex variables $z-z_1$ and $z-z_2$, respectively. I will distinguish between stream function values on the "plus side" of the x-axis, Ψ^+, and on the "minus side," Ψ^-. The arguments θ_1 and θ_2 have values of $+\pi$, $-\pi$, or 0, depending on the location of x relative to x_1 and x_2. This leads to the following values of Ψ^+ along the x-axis:

$$\begin{aligned}
\Psi^+ &= \frac{\sigma}{2\pi}\left[(x-x_1)(\pi) - (x-x_2)(\pi)\right] = \frac{\sigma(x_2-x_1)}{2} \qquad (x < x_1) \\
\Psi^+ &= \frac{\sigma}{2\pi}\left[(x-x_1)(0) - (x-x_2)(\pi)\right] = \frac{\sigma(x-x_2)}{2} \quad (x_1 \le x \le x_2) \\
\Psi^+ &= \frac{\sigma}{2\pi}\left[(x-x_1)(0) - (x-x_2)(0)\right] = 0 \qquad (x > x_2) \qquad (5.9)
\end{aligned}$$

On the minus side of the x-axis we have

$$\begin{aligned}
\Psi^- &= \frac{\sigma}{2\pi}\left[(x-x_1)(-\pi) - (x-x_2)(-\pi)\right] = -\frac{\sigma(x_2-x_1)}{2} \qquad (x < x_1) \\
\Psi^- &= \frac{\sigma}{2\pi}\left[(x-x_1)(0) - (x-x_2)(-\pi)\right] = -\frac{\sigma(x-x_2)}{2} \quad (x_1 \le x \le x_2) \\
\Psi^- &= \frac{\sigma}{2\pi}\left[(x-x_1)(0) - (x-x_2)(0)\right] = 0 \qquad (x > x_2) \qquad (5.10)
\end{aligned}$$

The values for Ψ^+ and Ψ^- have been plotted in Figure 5.4a. The jump $\sigma(x_2 - x_1)$, which extends from the line sink to minus infinity, represents the total discharge σL of the line sink and forms a branch cut in the flow domain, like the branch cut for the well in Figure 3.14. From x_1 to x_2 the jump in Ψ decreases linearly to zero, consistent with a constant inflow rate along the line sink.

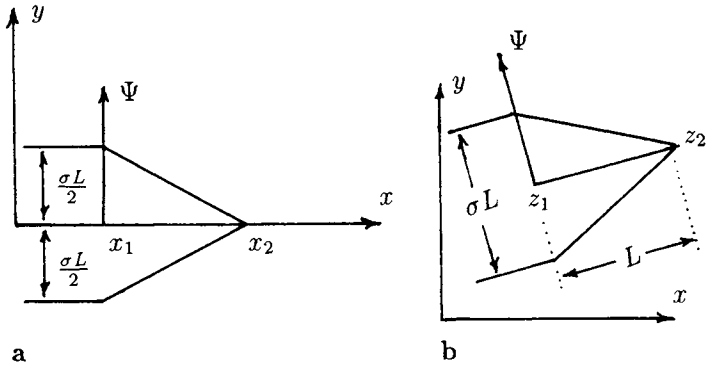

Figure 5.4: Branch cut in stream function due to a line sink along the x-axis (a) and outside the x-axis (b).

The preceding analysis can be generalized for a line sink outside the x-axis, see Figure 5.4b. The branch cut appears to extend towards infinity in the direction of the line sink. Strack (1989) maps the line sink function onto a reference plane, where the line sink falls on the real axis between -1 and 1. He also presents a "farfield expansion" for the line sink function which makes it more suitable for numerical evaluation. These analyses are outside the scope of this text, but have been implemented in program GFLOW1.

In Figure 5.5, the flow net near a line sink is shown. The branch cut in the stream function is clearly visible as a thick black line where contour lines of different Ψ values are bunched up. Observe that the potential is not constant along the line sink, but has a minimum at the line sink center. Consequently, in stringing together line sinks to model a stream (see Figure 5.2), the head underneath the stream will not exactly represent the water elevation at all points along the stream, but will oscillate somewhat between the control points where the head has been forced equal to the stream elevation.

Distributed Singularities

You may notice from Figure 5.5 that the potential is "regular" everywhere along the line sink; it does not become infinite as at the center of a well. This is not immediately obvious from (5.7), since for $z = z_1$ or $z = z_2$ one of the logarithms has an argument of zero, and thus is singular ($\ln 0 = -\infty$). However, the combination $(z - z_1)\ln(z - z_1)$ or $(z - z_2)\ln(z - z_2)$ is not singular, since $\lim_{x \to 0} x \ln x \doteq 0$. This is a peculiar result: The potential of the well function itself is singular, but if the well is distributed (integrated)

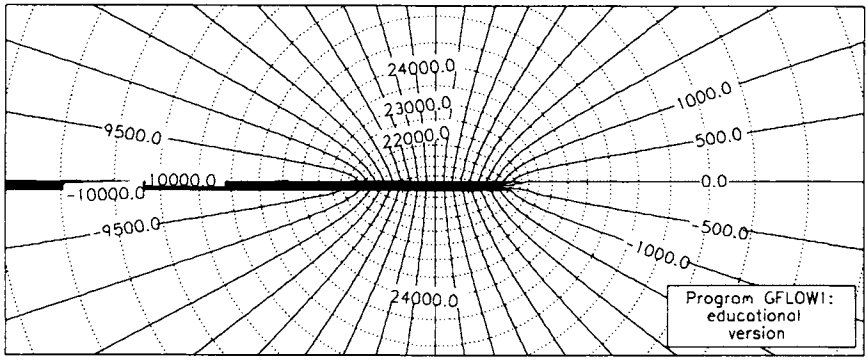

Figure 5.5: Flow net near a line sink.

over a line element, a function is obtained that is regular everywhere. Most analytic elements are "distributed singularities." In fact, the first paper about the analytic element method does not refer to analytic elements, but distributed singularities (Strack and Haitjema, 1981a, 1981b). Not all distributed singularities have potentials that are regular everywhere, and even if they do, the derivatives of the potential may still contain singularities. For instance, it may be shown that the derivative of (5.7) is singular at z_1 and z_2, resulting in infinite inflow velocities into the ends of the line sink. This implies that streamline tracing in GFLOW1 cannot be done too close to the line sink end points.

5.1.3 The Line Doublet

A line doublet is often referred to in the literature as a *double layer*, which means that it is a double singularity distribution (two layers of singularities): see, e.g., Kellogg (1929). Conceptually, the line doublet is a line sink and a line source that are moved infinitely close together, while their discharge and recharge rates are kept equal but increased to an infinitely large value; see Figure 5.6a.

I will derive a "constant strength" line doublet by carrying out this limiting procedure using the line sink function developed in Section 5.1.2. To that end I am writing (5.7) symbolically as

$$\Omega_{ls} = \sigma \Lambda_{ls}(z, z_0, L, \alpha) \tag{5.11}$$

where the *coefficient function* Λ_{ls} is defined as

$$\Lambda_{ls} = \frac{e^{-i\alpha}}{2\pi} \left[(z - z_1) \ln(z - z_1) - (z - z_2) \ln(z - z_2) + (z_1 - z_2) \right] \tag{5.12}$$

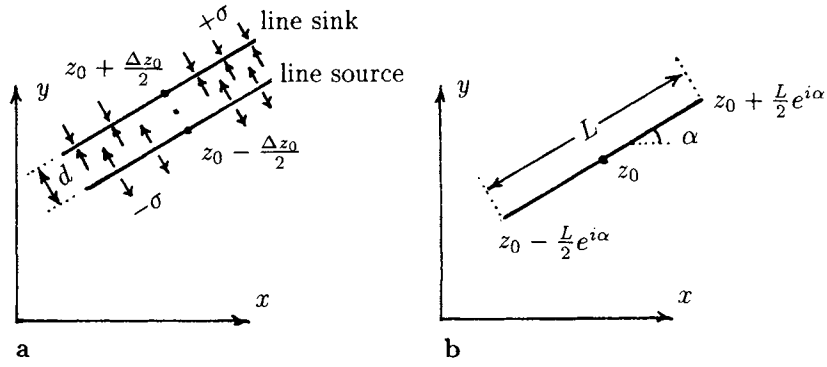

Figure 5.6: Line doublet formed by a line sink and line source pair (a) for the limiting case of zero distance d and infinite strength σ (b).

with

$$z_1 = z_0 - \frac{L}{2}e^{i\alpha} \qquad z_2 = z_0 + \frac{L}{2}e^{i\alpha} \tag{5.13}$$

and where z_0 is the center of the line sink; see Figure 5.6b. The complex potential Ω_{ld} for a line doublet is obtained for the limiting case where the distance d between the line sink and line source in Figure 5.6a goes to zero, while the discharge σ becomes infinitely large:

$$\Omega_{ld} = \lim_{\substack{d\to 0 \\ \sigma\to\infty}} \frac{\sigma d}{2\pi}\left[\frac{\Lambda_{ls}(z,z_0+\frac{\Delta z_0}{2},L,\alpha) - \Lambda_{ls}(z,z_0-\frac{\Delta z_0}{2},L,\alpha)}{d}\right] \tag{5.14}$$

where Δz_0 is defined as

$$\Delta z_0 = de^{i(\alpha+\frac{\pi}{2})} = ide^{i\alpha} \tag{5.15}$$

The line doublet strength s is defined as

$$s = \lim_{\substack{d\to 0 \\ \sigma\to\infty}} \sigma d \tag{5.16}$$

Combining (5.14) through (5.16) yields

$$\Omega_{ld} = \frac{ise^{i\alpha}}{2\pi} \lim_{\Delta z_0\to 0}\left[\frac{\Lambda_{ls}(z,z_0+\frac{\Delta z_0}{2},L,\alpha) - \Lambda_{ls}(z,z_0-\frac{\Delta z_0}{2},L,\alpha)}{\Delta z_0}\right] \tag{5.17}$$

which becomes

$$\Omega_{ld} = \frac{ise^{i\alpha}}{2\pi}\frac{d}{dz_0}\Lambda_{ls}(z,z_0,L,\alpha) \tag{5.18}$$

or with (5.12) and applying the chain rule,

$$\begin{aligned}\Omega_{ld} &= \frac{is}{2\pi}\left[\frac{d}{dz_1}\{(z-z_1)\ln(z-z_1)\}\frac{dz_1}{dz_0} - \frac{d}{dz_2}\{(z-z_2)\ln(z-z_2)\}\frac{dz_2}{dz_0}\right] \\ &= \frac{is}{2\pi}\left[-\ln(z-z_1)+\ln(z-z_2)\right] \qquad (5.19)\end{aligned}$$

where use has been made of $dz_1/dz_0 = dz_2/dz_0 = 1$; see Figure 5.6b. The complex potential for a constant strength line doublet is finally written as

$$\Omega_{ld} = \frac{is}{2\pi}\ln\left(\frac{z-z_2}{z-z_1}\right) \qquad (5.20)$$

We will investigate the behavior of both the real and imaginary part of (5.20). The real part yields the discharge potential Φ_{ld},

$$\begin{aligned}\Phi_{ld} &= \Re\{\Omega_{ld}\} = \Re\left\{\frac{is}{2\pi}\left(\ln\left|\frac{z-z_2}{z-z_1}\right| + i(\theta_2-\theta_1)\right)\right\} \\ &= \frac{s}{2\pi}(\theta_1-\theta_2) \qquad (5.21)\end{aligned}$$

The imaginary part yields the stream function Ψ_{ld},

$$\Psi_{ld} = \Im\{\Omega_{ld}\} = \frac{s}{2\pi}\ln\left|\frac{z-z_2}{z-z_1}\right| \qquad (5.22)$$

The stream function is continuous, but the potential function exhibits a jump across the line doublet, which may be seen as follows. The angle between the lines from z to z_1, and z to z_2 is equal to $(\theta_2-\theta_1)$, as can be seen from Figure 5.7 (a). If the point z approaches the line element from above, the "+ side" in Figure 5.6a, the angle $(\theta_2-\theta_1)$ becomes $+\pi$. Conversely, if the point z approaches the line element from below, the "− side" in Figure 5.6a, the angle $(\theta_2-\theta_1)$ becomes $-\pi$. Hence, in view of (5.21) the potential along the "+ side" of the line doublet is $-s/2$, while the potential on the "− side" is $+s/2$, see Figure 5.6b. The total jump in the potential across the line doublet, therefore, is equal to the line doublet strength s.

Using Line Doublets to Model an Inhomogeneity

A closed string of line doublets may be used to model a domain with a different hydraulic conductivity than the regional conductivity. I will illustrate this by use of a simple example.

Consider the triangular area depicted in Figure 5.8. The hydraulic conductivity is k on the outside and k_1 on the inside. The head in the aquifer

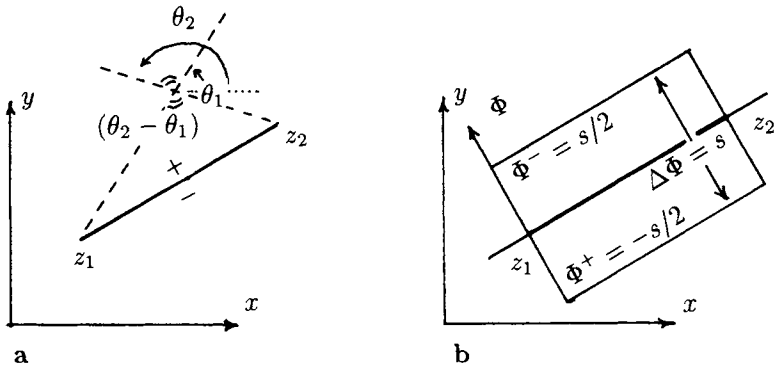

Figure 5.7: The angle $(\theta_2 - \theta_1)$ jumps across the line doublet (a), and thus the discharge potential Φ jumps across the line doublet (b).

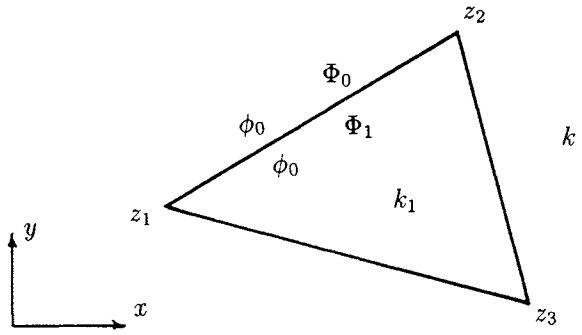

Figure 5.8: Triangular inhomogeneity in an aquifer with a constant head.

is everywhere the same: $\phi = \phi_0$. As a result, the discharge potential jumps across the sides of the triangle from Φ_0 to Φ_1, see (3.273):

$$\Delta\Phi = \Phi_1 - \Phi_0 = \frac{k_1 - k}{k}\Phi_0 \tag{5.23}$$

where Φ_0 is defined as $\Phi_0 = \frac{1}{2}k\phi_0^2$. We will generate the jump $\Delta\Phi$ by placing line doublets on the triangle sides, each with a strength equal to the jump in the potential:

$$s = \Delta\Phi \tag{5.24}$$

The discharge potential everywhere in the flow domain is equal to the potential Φ_0 plus the contribution of the three line doublets:

$$\Phi = \Re\{\frac{is}{2\pi}\left[\ln\frac{z - z_2}{z - z_1} + \ln\frac{z - z_3}{z - z_2} + \ln\frac{z - z_1}{z - z_3}\right]\} + \Phi_0 \tag{5.25}$$

which becomes

$$\Phi = \frac{s}{2\pi}\left[(\theta_1 - \theta_2) + (\theta_2 - \theta_3) + (\theta_3 - \theta_1)\right] + \Phi_0 \tag{5.26}$$

In Figure 5.9 the angles in (5.26) are indicated for both cases, z is outside the triangle and z is inside the triangle. As is seen from Figure 5.9, the three angles due to the three line doublets cancel each other out when z is outside the triangle, while they add up to 2π when z is located inside the triangle. Consequently, with reference to (5.26) the potential Φ becomes

$$\Phi = \Phi_0 \qquad (z \text{ outside the triangle}) \tag{5.27}$$

and

$$\Phi = s + \Phi_0 = \Phi_1 - \Phi_0 + \Phi_0 = \Phi_1 \qquad (z \text{ inside the triangle}) \tag{5.28}$$

where use is made of (5.24) with (5.23).

Line Doublets with Varying Strength

The preceding example nicely illustrates how line doublets are used to model domains of different hydraulic conductivity. However, the example is of little practical value. In reality there will almost always be flow in the aquifer, which leads to varying potentials along the boundary of an inhomogeneity. These varying potentials imply a variation in the jump $\Delta\Phi$, see (5.23), and thus a varying line doublet strength, see (5.24). The constant strength line doublets (5.20) are unsuitable to handle such variations in $\Delta\Phi$. Strack (1989) presents an analysis for varying strength line doublets based

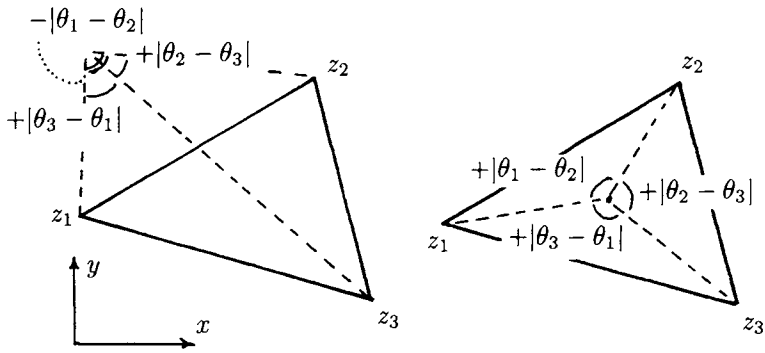

Figure 5.9: Outside the triangle the angles cancel each other out, while on the inside they add up to 2π.

on singular Cauchy integrals. His analysis leads to a generic formulation of singularity distributions which include both line sinks and line doublets of higher-order strength. The functions are mapped onto a dimensionless reference plane and accompanied by so-called farfield expansions to facilitate numerical evaluation.

In GFLOW1 line doublets are used with a parabolic strength distribution. For the triangle in Figure 5.8, this implies that a varying jump along the triangle sides can be met exactly at six different points: at the corners of the triangle and at the centers of the sides. In between these points, the jump is approximated by the parabolically varying strength s. The mathematical development of these higher-order functions is outside the scope of this text. The interested reader is referred to Haitjema and Strack (1981b) and Strack (1989). The computation of the doublet strength parameters at the nodes and centers of line doublets that define an inhomogeneity will be discussed in Section 5.1.5.

5.1.4 The Areal Sink

In Section 3.2.4 an areal source distribution with a circular boundary (sink disc) was used to model a circular irrigator or a percolating pond. We may also use this source disc to introduce areal recharge due to precipitation in a model area, simply placing a large source disc over the model domain. However, recharge rates may vary spatially, requiring the application of areal source distributions of arbitrary shape. For instance, consider an outwash plane in an otherwise till environment. The till may only allow a limited recharge rate of perhaps 2 inches per year, while the sandy and

gravely outwash may allow more than 20 inches per year of precipitation to recharge the aquifer. Next we will generalize the solution for the source disc in Section 3.2.4 to an areal sink with an arbitrary boundary and with an arbitrary sink density distribution.

I rewrite (3.180) in terms of the sink density λ rather than the source density (percolation rate) N:

$$\begin{aligned} \Phi^{(i)} &= \frac{\lambda}{4}(r^2 - R^2) + C \qquad (r \le R) \\ \Phi^{(o)} &= \frac{\lambda R^2}{2} \ln \frac{r}{R} + C \qquad (r > R) \end{aligned} \tag{5.29}$$

This gives, for (3.181) plus (3.182),

$$\begin{aligned} Q_r^{(i)} &= -\frac{d\Phi}{dr} = -\frac{d}{dr}\left[\frac{\lambda}{4}(r^2 - R^2) + C\right] = -\frac{\lambda}{2}r \quad (r \le R) \\ Q_r^{(o)} &= -\frac{d\Phi}{dr} = -\frac{d}{dr}\left[\frac{\lambda R^2}{2} \ln \frac{r}{R} + C\right] = -\frac{\lambda R^2}{2r} \quad (r > R) \end{aligned} \tag{5.30}$$

Two expressions for the discharge potential are used, $\Phi^{(i)}$ inside the sink disc ($r \le R$) and $\Phi^{(o)}$ outside ($r \ge R$). The potential $\Phi^{(i)}$ is a solution to Poisson's equation,

$$\nabla^2 \Phi^{(i)} = \lambda \tag{5.31}$$

while the outside potential $\Phi^{(o)}$ satisfies Laplace's equation:

$$\nabla^2 \Phi^{(o)} = 0 \tag{5.32}$$

This is what makes the sink disc work: Inside we have an exfiltration rate λ, while outside there is no areal exfiltration or infiltration. However, we cannot select any arbitrary solution to (5.31) and (5.32). We need to make sure that the potential function is continuous across the disc boundary and that continuity of flow is maintained across that boundary. The choices for $\Phi^{(i)}$ and $\Phi^{(o)}$ in (5.29) accomplish this, as may be seen by substituting $r = R$ in (5.29) and in (5.30).

We succeeded in finding two suitable potentials $\Phi^{(i)}$ and $\Phi^{(o)}$ because of the radial symmetry of the problem: a sink disc. In Figure 5.10, an arbitrarily shaped areal sink is depicted with a varying sink density $\lambda(x, y)$. For the case of Figure 5.10, the choices for $\Phi^{(i)}$ and $\Phi^{(o)}$ are less obvious. Strack (1989) suggested selecting any suitable function $\Phi^{(i)}$ that satisfies (5.31) and simply setting $\Phi^{(0)}$ equal to zero. These choices obviously violate

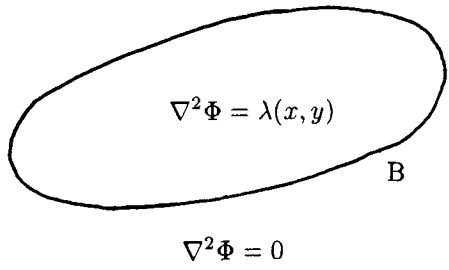

Figure 5.10: Areal sink with arbitrary boundaries and sink density $\lambda(x,y)$.

both continuity of the potential and continuity of flow across the boundary B of the areal sink. In terms of the complex potential Ω, both Φ and Ψ will jump across the boundary B, requiring additional measures. The jump in Ψ may be eliminated by use of a suitably chosen sink distribution along B, while the jump in Φ may be compensated by a suitably chosen doublet distribution along B. Observe from Figures 5.4 and 5.7 that line sinks and line doublets indeed generate jumps in Ψ and Φ, respectively. Strack (1989) shows how an arbitrarily shaped areal sink may be approximated by a polygon which sides are higher-order line sinks and line doublets to eliminate the jump in both Φ and Ψ across the polygon boundary. The analysis is quite involved, including conformal mapping and series expansions to facilitate proper numerical evaluation of the analytical functions. Although this is implemented in GFLOW1, the interested reader is referred to [Strack (1989) for further mathematical details.

Adding Recharge to Inhomogeneities

As mentioned, changes in areal recharge may occur between a relatively permeable outwash, alluvium, or channel deposits near streams and the surrounding lower permeable till. In fact, a domain with a different hydraulic conductivity usually also exhibits a different recharge rate because of precipitation, at least for the case of unconfined aquifers. The boundaries between these higher permeable zones and the lower permeable till are already included in the model by doublet strings. A line doublet with a real strength parameter creates a jump in the potential. This jump is selected in such a manner as to create a continuous head across the boundary between two different hydraulic conductivities, see Section 3.4.3. However,

we may add a second component to the strength parameter to create an additional jump to compensate for the jump caused by $\Phi^{(i)}$. Also, when the line doublet is given an imaginary strength parameter it will create a jump in Ψ! This may be seen from (5.20) through (5.22) by substituting for s the imaginary value $-is$. The expressions for Φ_{ld} and Ψ_{ld} in (5.21) and (5.22) will thus be interchanged, causing a jump in Ψ due to the branch cut of $(\theta_1 - \theta_2)$ in (5.21). Consequently, the line doublets already in place to model the jump in k can also be used to model a jump in recharge. This is accomplished with virtually no extra computational effort. The line doublet functions are evaluated anyhow to deal with the discontinuous hydraulic conductivity. All we do is modify the strength parameters to also account for the discontinuity in the recharge rate. The mathematical details of this procedure are to be found in the GFLOW User's Manual (Haitjema and Kelson, 1994).

5.1.5 Solving for Unknown Strength Parameters

At the end of Section 5.1.1, under the subheading "Solving the flow problem," I explained that the line sink strengths and line doublet strengths would be sorted out by GFLOW1. All *we* do is specify the water levels in streams and lakes and specify the hydraulic conductivity inside aquifer inhomogeneities. This *solution procedure* leads to a system of algebraic equations which is solved for the as yet unknown line sink and line doublet strengths. Here is how it works.

In Figure 5.2, crosses are placed at the center of some of the line sinks that represent the streams and lakes in the model area. These crosses indicate the location of *control points.* Each line sink has one control point at its center (although this is not indicated for all line sinks in Figure 5.2). At each of these control points, the modeler specifies the surface water elevation in the stream. For now we will assume that the surface water is in full contact with the aquifer, which implies that the head in the aquifer at a control point is the same as the surface water level at that point. Expressed in terms of discharge potentials I write for the potential at the ith control point, due to n line sinks,

$$\Phi_i = \sigma_1 Fls_{i,1} + \sigma_2 Fls_{i,2} + \sigma_3 Fls_{i,3} + ...\sigma_n Fls_{i,n} + C \qquad (5.33)$$

which is a symbolic way of writing the contributions of all the line sinks to the potential at the ith control point. The function $Fls_{i,j}$ is the coefficient function of the jth line sink evaluated at the center of the ith line sink. The function $Fls_{i,j}$ is the real part of the complex potential (5.7):

$$Fls_{i,j} = \Re\{\frac{1}{2\pi}e^{-i\alpha_j}[(z_i-(z_1)_j)\ln(z_i-(z_1)_j) - (z_i-(z_2)_j)\ln(z_i-(z_2)_j)+((z_1)_j-(z_2)_j)]\} \quad (5.34)$$

where z_i are the complex coordinates of the ith control point, $(z_1)_j$ and $(z_2)_j$ are the begin and end points of the jth line sink, and α_j is the orientation of the jth line sink. Note that the coefficient function is the potential due to the line sink with strength 1. Thus $\sigma_j Fls_{i,j}$ is the potential of the line sink with its actual strength σ_j.

Reference Point

In writing (5.33) I did not account for any feature other than line sinks. Assuming that to be the case for now, (5.33) exhibits n unknown line sink strengths σ_j $(j = 1, n)$ and the unknown constant of integration C. However, I can only write n equations of the form (5.33) for the control points at the n line sinks. This leaves us short one equation: The one for the integration constant C. We have no other option than to dream up some additional condition in order to obtain an extra equation. In most analytic element models this is done by introduction of a *reference point* at which a *reference head* is specified. It is important to realize that this is a totally arbitrary condition forced upon us by mathematical necessity: to get enough equations to solve all of our unknowns. Novice analytic element modelers are invariably confused by this mystical reference point, and often make a poor choice for this point and its associated head. Since this point is introduced for mathematical purposes, and not for hydrological reasons, we should select it in such a manner that it does not influence the modeling results in the nearfield. The reference point should be placed far away, outside the farfield features, and given a "neutral" head: approximately the average head in the model domain. In so doing, the reference point choice causes relatively flat hydraulic gradients outside our farfield, which makes it easier for the farfield features to "protect" the nearfield. If the reference head is chosen relatively high, a lot of groundwater will move toward the model area (the model area becomes a regional sink). Conversely, if the reference head is chosen relatively low, the model area acts as a regional source, providing a lot of water that flows to infinity. However, when sufficient farfield features are included in the model, these variations in the reference head will not influence the nearfield solution. This is, in fact, a good test for a proper model design: Vary the reference head and verify that the nearfield remains unaffected. On no occasion should the reference point be chosen inside the analytic elements, let alone inside the nearfield!

Matrix Equations

The resulting $n+1$ equations can be written in matrix form:

$$a_{ij}x_j = b_i \qquad (i = 1, n+1) \text{ and } (j = 1, n+1) \tag{5.35}$$

where the *coefficient matrix* a_{ij} is defined as

$$\begin{aligned} a_{ij} &= Fls_{i,j} && (i = 1, n+1) \text{ and } (j = 1, n) \\ a_{ij} &= 1.0 && (i = 1, n+1) \text{ and } (j = n+1) \end{aligned} \tag{5.36}$$

where the $(n+1)$th control point is the reference point. The *solution vector* x_j is defined as

$$\begin{aligned} x_j &= \sigma_j && (j = 1, n) \\ x_{n+1} &= C \end{aligned} \tag{5.37}$$

and the *known vector* b_i is defined as

$$\begin{aligned} b_i &= \Phi_i && (i = 1, n) \\ b_{n+1} &= \Phi_{ref} \end{aligned} \tag{5.38}$$

where Φ_{ref} is the potential at the reference point.

The matrix equations can be solved by standard solution procedures, e.g., matrix decomposition and back substitution (Forsythe *et al.*, 1977) or transpose elimination (Wassyng, 1982).

Including Inhomogeneities

Line doublets are used around domains with different hydraulic conductivity; see Section 5.1.3. The strength s of the line doublet is equal to the jump in the discharge potential across the inhomogeneity boundary, (5.24), while the jump in the potential can be expressed in terms of the potential at the boundary by (5.23). This leads to the following matrix equation at a control point on a line doublet:

$$s_i = \frac{k_1 - k}{k}\Phi_i = \frac{k_1 - k}{k}\left[s_1 Fld_{i,1} + s_2 Fld_{i,2} + \ldots + \sigma_1 Fls_{i,1} + \ldots + C\right] \tag{5.39}$$

where k_1 is the conductivity of the domain bounded by the ith line doublet and where $Fld_{i,j}$ are the line doublet coefficient functions, similar to those the line sinks. Expression (5.39) may be rewritten as

$$s_i \frac{k}{k_1 - k} = s_1 Fld_{i,1} + s_2 Fld_{i,2} + ... + \sigma_1 Fls_{i,1} + ... + C \qquad (5.40)$$

or

$$0 = s_1 Fld_{i,1} + s_2 Fld_{i,2} + ... + s_i [Fld_{i,i} - \frac{k}{k_1 - k}] + ... + \sigma_1 Fls_{i,1} + ... + C \quad (5.41)$$

The matrix equations (5.41) are added to those for the line sinks, whereby the latter equations also involve the terms with Fld due to the line doublets. The known vector elements for equations at the line doublet control points are zero, compare (5.41) with (5.33) and (5.38). In GFLOW1 line doublets are used with a parabolic strength distribution which is continuous from one line doublet to the other. For a closed string of line doublets this results in two strength parameters per line doublet, also requiring two control points per line doublet. These control points are chosen at the vertices of the polygon and at the centers of the line doublets.

Adding Other Elements

The matrix equations may be further expanded by including areal sinks with a specified head and wells with a specified head, which yields equations similar to those for the line sinks. More sophisticated analytic elements may lead to different kind of matrix equations, but are outside the scope of this text; refer to Strack (1989). In Section 5.2.3, we will discuss line sinks and areal sinks with a specified resistance between the surface water and the aquifer. As we will see, this leads to nonlinear equations with matrix coefficients which depend on the solution. Such a nonlinear set of equations is solved iteratively, adjusting matrix coefficients from one solution to another.

In addition to all analytic elements with unknown strength parameters there are also elements whose strengths are known — for instance, wells with a given pumping rate and areal recharge due to precipitation. These elements must be added to the matrix equations, but do not generate equations for themselves. Although these elements in principle occur on the right-hand side of, e.g., (5.33) and (5.41), they are moved to the left-hand side of these equations and end up in the known vector. For the equations due to the line sinks, head-specified wells, and head-specified areal sinks,

$$b_i = \Phi_i - (\Phi_{known})_i \qquad (5.42)$$

For the equations due to the line doublets,

$$b_i = -(\Phi_{known})_i \tag{5.43}$$

where $(\Phi_{known})_i$ represents the contribution to the potential of all analytic elements with known strength at the ith control point.

In GFLOW1, when solving surface water and groundwater conjunctively (see Section 5.2.4), strength parameters of line sinks that are part of a stream network may be prescribed by the surface water solution. In that case, the equation for that line sink is removed from the matrix and its contribution is incorporated in Φ_{known}. During subsequent iterations between surface water solutions and groundwater solutions, the number of equations may vary as line sinks are removed from and reintroduced into the coefficient matrix.

5.1.6 Generating Numerical and Graphical Output

Once the unknown strength parameters have been solved, the potential can be calculated at any point in the aquifer by superposition of all analytic elements:

$$\Phi(x,y) = \sum \sigma_i Fls_{(x,y),i} + \sum s_i Fld_{(x,y),i} + ... + C \tag{5.44}$$

where $Fls_{(x,y),i}$ and $Fld_{(x,y),i}$ are the coefficient functions for the ith line sink and line doublet, respectively, evaluated at the point (x,y). Expression (5.44) is not completely written out; additional analytic elements (e.g., wells and areal sinks) are implied by the dots in (5.44).

In general, the potential Φ is not referred to when modeling groundwater flow with analytic element models. The user enters heads at control points, and the program reports back heads at any point (x,y) in the aquifer. All conversions from heads to potentials and back are handled internally in the program, completely transparent to the user. The head ϕ is calculated from (5.44) by use of (3.61),

$$\begin{aligned} \phi &= \frac{\Phi + \frac{1}{2}kH^2}{kH} && (\Phi \geq \tfrac{1}{2}kH^2) \\ \phi &= \sqrt{\frac{2\Phi}{k}} && (\Phi \leq \tfrac{1}{2}kH^2) \end{aligned} \tag{5.45}$$

In analytic element models, the heads may be specified with respect to any horizontal datum, usually mean sea level (MSL). The user must also specify the elevation of the aquifer base b with respect to the same datum.

In the program these "user heads," which I will denote here by ϕ^*, are converted to "model heads," ϕ in the preceding expression, by subtracting the elevation of the aquifer base:

$$\phi = \phi^* - b \tag{5.46}$$

All heads ϕ referred to in this text are "model heads"! Input and output in GFLOW1, however, is done exclusively in "user heads" ϕ^*.

The discharge vector Q_i is obtained by differentiating Φ; see (3.59). In analytic element models this is accomplished by superposition of the *derivative functions* of all analytic elements:

$$Q_i = -\sum \sigma_j \left[Fls'_{(x,y),j} \right]_i - \sum s_j \left[Fld'_{(x,y),j} \right]_i - .... \tag{5.47}$$

with

$$Fls'_i = \frac{\partial Fls}{\partial x_i} \qquad Fld'_i = \frac{\partial Fld}{\partial x_i} \quad (i = 1, 2) \tag{5.48}$$

The specific discharge vector q_i $(i = 1, 2, 3)$ is obtained from (5.47) and (3.312):

$$\begin{aligned} q_i &= \frac{Q_i}{h} && (i = 1, 2) \\ q_3 &= \frac{z}{h}\left[\frac{Q_i}{h}\partial_i h - N_t - N_b\right] + N_b && (i = 1, 2) \end{aligned} \tag{5.49}$$

where h is the saturated aquifer thickness, N_t the recharge at the aquifer top, and N_b the leakage into the aquifer at the aquifer bottom. Only strength-specified sink discs in GFLOW1 may be given both a bottom and a top strength, which translate into $-N_b$ and $-N_t$, respectively. In zones of confined flow, the saturated aquifer thickness is constant, $h = H$, so that the first term inside the brackets for q_3 vanishes ($\partial_i H = 0$). In zones of unconfined flow the saturated aquifer thickness may be replaced by the (model) head ϕ as obtained from (5.45).

The average groundwater flow velocities v_i $(i = 1, 2, 3)$ are obtained from (5.49):

$$v_i = \frac{q_i}{n} \qquad (i = 1, 2, 3) \tag{5.50}$$

whereby n is the "effective porosity." The porosity entered in GFLOW1 is used only to calculate average groundwater flow velocities and should be interpreted as an effective porosity.

Generating Contour Plots

A customary way of presenting piezometric head distributions in aquifers is by the use of contour plots, whereby each contour represents a line of equal head, just as topographical contours represent terrain elevations. Most existing contouring software is based on interpolation of function values in a rectangular grid (or irregular grid) of points where the function values are given. This fits quite naturally with the numerical groundwater models which provide heads at the grid points of their model grid (finite differences) or at the element corners or collocation points of elements (finite elements). Analytic element models do not employ a grid or element network to generate heads or discharges. In an analytic element model, the head or discharge can be calculated at any point, not just on grid points. To facilitate contouring of, for example, heads, however, a grid of points is introduced at which the heads are calculated by (5.45) with (5.44). This grid of values is then handed to a contouring routine to generate a contour plot.

There is a fundamental difference between contour plots generated in an analytic element model and those generated in a finite difference or finite element model. After a solution is obtained in the analytic element model, a grid can be generated at any scale and with any resolution (number of grid points per unit area). Since the solution is analytic, zooming in on a smaller area and using a higher-resolution grid provides meaningful detail. In finite difference or finite element models, however, only one grid is available: the model grid. The resolution of the solution is limited by the resolution of this model grid; it is not possible (or at least not meaningful) to zoom in on a smaller area for more detail.

Tracing Streamlines

In Section 3.2.6 it was explained how streamline tracing is accomplished by integrating the velocity vector [see (3.190)]:

$$\overset{2}{x}_i = \overset{1}{x}_i + \int_{t_1}^{t_2} v_i dt \tag{5.51}$$

where $\overset{1}{x}_i$ and $\overset{2}{x}_i$ are two successive points on a streamline, and where t_1 and t_2 are the associated residence times for a water particle traveling along that streamline. In GFLOW1 this integration is carried out numerically by use of a *predictor–corrector* method. The procedure works as follows. At the point $\overset{1}{x}_i$, the velocity $\overset{1}{v}_i$ is calculated and a first estimate of $\overset{2}{x}_i$ is made

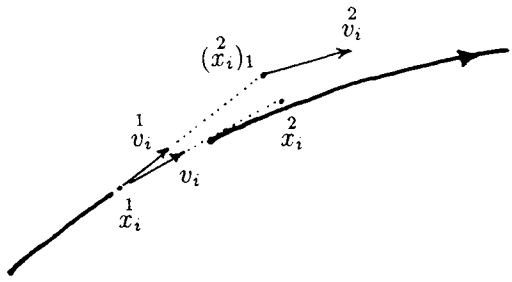

Figure 5.11: Predictor-corrector method for integrating the velocity vector along a streamline.

by stepping over a distance Δs into the direction of flow [see Figure 5.11]:

$$(\overset{2}{x}_i)_1 = \overset{1}{x}_i + \Delta s \frac{\overset{1}{v}_i}{\overset{1}{v}} \tag{5.52}$$

where $\overset{1}{v}$ is the magnitude of the velocity vector at $\overset{1}{x}_i$,

$$\overset{1}{v} = \sqrt{\overset{1}{x}_i \overset{1}{x}_i} \ (i = 1, 2, 3) \tag{5.53}$$

The value of Δs implies a particular choice for the time step Δt, but there is no need to calculate it at this point. Next the velocity $\overset{2}{v}_i$ is calculated at the point $(\overset{2}{x}_i)_1$. A new more representative velocity is obtained by taking the average of the velocities at $\overset{1}{x}_i$ and $(\overset{2}{x}_i)_1$:

$$v_i = \frac{\overset{1}{v}_i + \overset{2}{v}_i}{2} \tag{5.54}$$

The final estimate of the point $\overset{2}{x}_i$ then follows from

$$\overset{2}{x}_i = \overset{1}{x}_i + \Delta s \frac{v_i}{v} \tag{5.55}$$

where v is the magnitude of the velocity vector v_i:

$$v = \sqrt{v_i v_i} \ (i = 1, 2, 3) \tag{5.56}$$

The residence time increment Δt follows from

$$\Delta t = \frac{\Delta s}{v} \tag{5.57}$$

Note that the integration has been carried out in three dimensions. Most of our streamline traces, however, will be plotted in the horizontal plane. In GFLOW1 tick marks can be added to indicated the depth of the streamline in the aquifer, relative to the starting point.

Discontinuities in the Velocity Field

The predictor–corrector method just outlined assumes a continuous velocity field. However, the velocity field is discontinuous across line sinks and line doublets, where both the direction and magnitude of the velocity vector may jump. Consequently, the velocities $\overset{1}{v}_i$ and $\overset{2}{v}_i$, when evaluated at different sides of the line sink or line doublet, may differ significantly, which leads to a meaningless value for v_i from (5.54). During streamline tracing this may result in path lines that oscillate near line sinks or line doublets. To avoid this, GFLOW1 monitors when an intersection with a line sink or line doublet occurs and replaces the predictor–corrector procedure with Euler's method to calculate a step across that feature. In terms of the foregoing analysis this implies using $(\overset{2}{x}_i)_1$, from (5.52) as the next point on the streamline and calculating Δt from (5.57) with v replaced by $\overset{1}{v}$.

5.2 The Program GFLOW1

Most of the computer graphics in this text has been produced by the analytic element model GFLOW1, a single-layer, steady-state Dupuit–Forchheimer model which supports some transient and three-dimensional flow features. The three-dimensional features are a partially penetrating well and a three-dimensional version of the sink disc function, which are embedded in the otherwise two-dimensional Dupuit–Forchheimer model as outlined in Section 4.3. The model is particularly suitable for solving regional groundwater flow problems, including average (steady-state) stream flow. The stream and groundwater flow problems are solved conjunctively, whereby the groundwater solution dictates base flow, while the stream flow solution may limit the groundwater recharge rate of losing stream sections (Mitchell-Bruker and Haitjema,1995). Some general program features, the groundwater surface water interactions, and an example run are discussed in this section.

5.2.1 Main Program Features

GFLOW1 supports the following analytic elements:

- Steady-state wells (2D).
- Transient wells (Theis' solution).
- Partially penetrating wells (3D).
- Line sinks (drains, streams, lakes).
- Sink discs (ponds, areal recharge, wetlands).
- Three-dimensional sink discs (3D versions of two-dimensional sink discs).
- Inhomogeneities (regions with different hydraulic conductivity, porosity, and recharge).

GFLOW1 supports *interactive graphics*, which means that graphics is used within the program, and data can be obtained and changed by pointing a cursor on a feature and giving a command. On-screen editing is supported in the modules for wells, line sinks, sink discs, and inhomogeneity domains. Different colors and line types are used to distinguish between features. Graphical output includes flow nets and contour plots of heads, potentials, the stream function, and the absolute value of the discharge vector. Streamline tracing is supported with markers for travel time and streamline depth. Errors in boundary conditions and in observed heads at (observation) wells may be represented graphically, whereby line thickness and marker size are proportional to the error.

Finally, GFLOW1 supports many numerical input and output options, among which are spreadsheet files with both surface water and groundwater data along streams. The educational version of GFLOW1 (provided with this text) does not support hard-copy output of graphics, except for the option to make screen dumps using the DOS "graphics" program.

5.2.2 Program Organization

GFLOW1 is *modular* in the sense that different program functions are handled in different program modules, each with their own command menu. In Figure 5.12 a diagram is presented of the main structure of GFLOW1. The available modules in GFLOW1 are shown in Figure 5.12 in boxes connected to the MAIN PROGRAM box. When typing a module name, the user

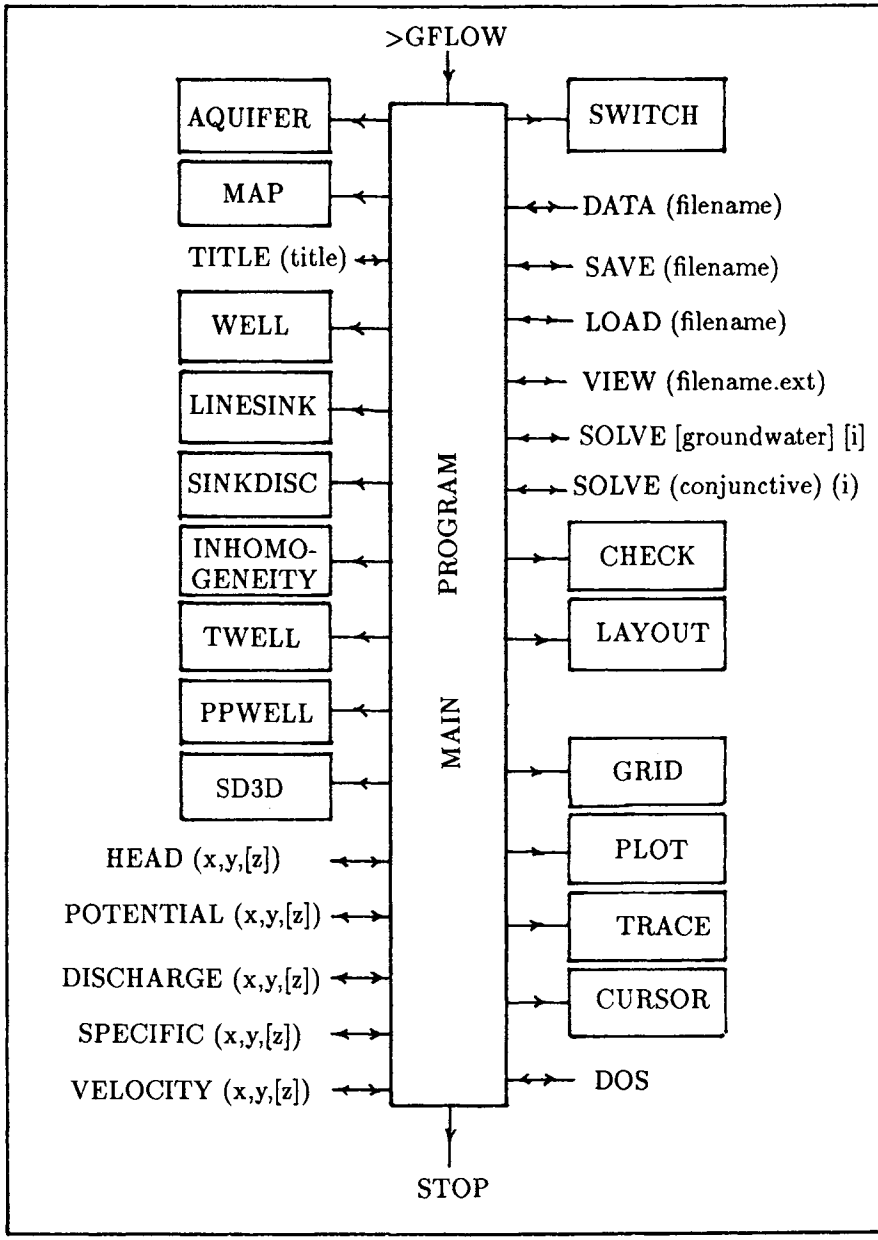

Figure 5.12: Program organization of GFLOW1.

leaves the MAIN PROGRAM, enters the module, and remains in the module until the command *return* is typed. In addition to entering modules, the user may also initiate commands which are part of the MAIN PROGRAM itself. These commands are the ones not emboxed in Figure 5.12. After such a command is executed, the user is still in the MAIN PROGRAM. A command may have one or more parameters, indicated in Figure 5.12 between parentheses. An argument between square brackets is optional; if it is omitted a default value is used.

A brief explanation of the modules and commands shown in Figure 5.12 is provided in Figure 5.13, whereby they are grouped by function. There are six main functions: input and output (IO) to disk, input of general data, input of analytic elements, generating and checking a solution, producing numerical output, and producing graphical output. These functions are not strictly separated; for instance, graphics and file IO is supported in most analytic element modules.

Command Menus

Program GFLOW1 is "command driven" in combination with command menus. A fully "menu driven" program allows the user to "point and shoot" to initiate commands and to type data in data boxes. The advantage of a menu driven program is that the user is prompted for every response, making program operation easy at first. However, when the user becomes proficient in the use of the program, the (graphical) menu interface gets in the way; you have to step through many options and menus before the desired action occurs. In addition, most data input in GFLOW1 is best done in "batch mode." rather than interactively from the keyboard or by use of a mouse. Such a batch input option requires a command structure. In an attempt to gain the best of both worlds, GFLOW1 employs commands in combination with a command menu. The command menu displays the available commands with their current parameters and options. The format of the command menu reflexes the syntax of the commands. The command menu is automatically displayed in all modules. A brief explanation of the commands in the MAIN PROGRAM is shown in Figure 5.13.

5.2.3 Resistance to Surface Water Inflow and Outflow

As explained in Section 5.1.5, the unknown strength parameters of line sinks and sink discs are solved for by requiring a specified head at a control point on that element. Under the Dupuit–Forchheimer condition, however, this implies that the head in the aquifer underneath the stream or lake is

```
------------------------- IO modules ----------------------------------------
SWITCH              Reassign logical units for input or output.
SAVE (filename)     Save solution in binary form on disc (extension: .SOL).
LOAD (filename)     Load solution from disc (extension: .SOL).
DATA (filename)     Write input data file (.dat) based on current data in program.
VIEW (fname.ext)    View ASCII file on disk (e.g. input data or error file).

------------------------- GENERAL INPUT DATA modules ------------------------
AQUIFER             Aquifer background data i.e. hydraulic conductivity, porosity,
                    aquifer thickness, uniform flow, and a reference point.
MAP                 Add background map to the layout.
TITLE (title)       16 character title included in output files.

------------------------- ANALYTIC ELEMENT modules ---------------------------
WELL                Steady state wells (2D).
PPWELL              Partially penetrating wells (3D).
TWELL               Transient wells (2D).
SINKDISC            Circular areal sink distributions (2D).
SD3D                Circular areal sink distributions (3D).
LINESINK            Line sinks to model streams (2D).
INHOMOGENEITY       Areas of different permeability, recharge, and porosity.

------------------------- SOLUTION modules -----------------------------------
SOLVE [GROUNDWATER] [i]  Solve groundwater flow problem using i iterations
                         (default: i=1).
SOLVE BASEFLOW           Solve baseflow (surface water) problem
SOLVE CONJUNCTIVE [i]    Solve groundwater and surface water conjunctively
                         using i iterations (default: i=0)
CHECK                    Check boundary conditions and piezometers.

------------------------- NUMERICAL OUTPUT modules ---------------------------
HEAD       (x) (y) [z]  Prints head at specified coordinates.
POTENTIAL  (x) (y) [z]  Prints potential at specified coordinates.
OMEGA      (x) (y)      Prints the complex potential (disch.pot. , stream function)
DISCHARGE  (x) (y)      Prints discharge vector comp. at specified coordinates
SPECIFIC   (x) (y) [z]  Prints spec. disch. vector comp. at specified coordinates.
VELOCITY   (x) (y) [z]  Prints velocity vector comp. at specified coordinates.

------------------------- GRAPHICAL OUTPUT modules ---------------------------
LAYOUT              Plot layout of hydrological features.
GRID                Set up grid for plotting (2D/3D).
PLOT                Contour plots of heads, potentials, stream function, flownet,
                    and absolute value of the discharge vector. (2D/3D).
CURSOR              Brings up layout and cursor to retrieve data (heads, etc.).
TRACE               Tracing streamlines  (2D/3D).

------------------------------------------------------------------------------

DOS                 Escape to DOS, type EXIT to return to return to GFLOW1.
STOP                Exit program to DOS, terminates program execution.
```

Figure 5.13: Printout of the command summary file: gfsum.hlp.

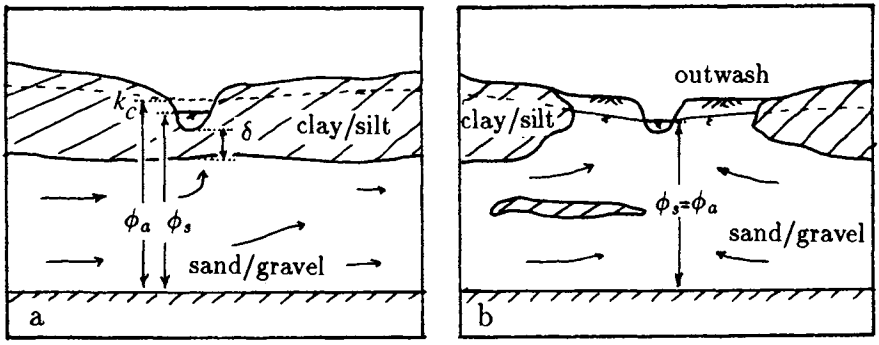

Figure 5.14: A stream with (a) and without (b) resistance to flow between aquifer and stream.

identical to the water level in the stream or lake. Restricting our discussion to streams for a moment, this is may be true in a sandy to gravelly environment, where the stream has a relatively clean sandy bottom in direct contact with the aquifer. In a till environment (mixtures of sand, silt and clay), however, there is likely to be some resistance to flow between the aquifer and the stream. This resistance may be due to a silt layer on the bottom of the stream, a silty clayey soil layer between stream bottom and aquifer, or both. The stream may, generally speaking, be in a till environment, but still in full contact with the aquifer (no resistance) if it is surrounded by a sandy or gravely outwash or "channel deposits"; see Figure 5.14. The same holds for lakes or wetlands. Depending on the geological conditions there may be substantial resistance to flow between aquifer and lake. This resistance may also be due to, or enhanced by, silt and organic deposits on the lake bottom.

In order to incorporate the situation depicted in Figure 5.14a the following boundary condition is considered at a stream or lake with resistance:

$$q_z = \frac{\phi_a - \phi_s}{c} \tag{5.58}$$

where q_z $[L/T]$ is the groundwater inflow per unit area into the surface water, and where ϕ_a and ϕ_s are the head in the aquifer and water level in the stream, respectively. The parameter c $[T]$ is the resistance to flow, defined as

$$c = \frac{\delta}{k_c} \tag{5.59}$$

where δ and k_c are the thickness and hydraulic conductivity of the clay or silt layer, respectively. When dealing with sink discs, the groundwater

inflow rate q_z is equal to the strength parameter s $[L/T]$ of the sink disc, so that with (5.58),

$$s = \frac{\phi_a - \phi_s}{c} \tag{5.60}$$

Streams are modeled by line sinks which have no width, only a length. The groundwater inflow rate into the line sink is σ $[L^2/T]$, which is the inflow rate per area $[L/T]$ multiplied by the width w $[L]$ of the stream. Consequently, Equation (5.58) becomes, in terms of σ,

$$\sigma = w\frac{\phi_a - \phi_s}{c} \tag{5.61}$$

The conditions (5.60) and (5.61) are used to replace the specified head conditions discussed in Section 5.1.5. We will illustrate this for the case of line sinks. First we express (5.61) in terms of discharge potentials. For confined flow conditions we multiply both sides in (5.61) by the aquifer transmissivity kH, which gives

$$kH\phi_a - kH\phi_s = \frac{kHc}{w}\sigma \tag{5.62}$$

or

$$kH\phi_a - \tfrac{1}{2}kH^2 - (kH\phi_s - \tfrac{1}{2}kH^2) = \frac{kHc}{w}\sigma \tag{5.63}$$

so that

$$\Phi_s = \Phi_a - \frac{kHc}{w}\sigma \qquad (\phi_a \geq H) \tag{5.64}$$

For unconfined flow conditions we multiply both sides of (5.61) by $\frac{1}{2}k(\phi_a + \phi_s)$, resulting in

$$\tfrac{1}{2}k\phi_a^2 - \tfrac{1}{2}k\phi_s^2 = \frac{k\frac{\phi_a+\phi_a}{2}c}{w}\sigma \tag{5.65}$$

which gives

$$\Phi_s = \Phi_a - \frac{k\frac{\phi_a+\phi_s}{2}c}{w}\sigma \qquad (\phi_a < H) \tag{5.66}$$

The potential in the aquifer may be expressed in terms of the strength parameters σ times coefficient functions F of all analytic elements in the flow domain, see (5.34). Writing only the contributions of the line sinks, the ith equation (at the ith line sink) becomes

$$(\Phi_s)_i = \sigma_j F_{ij} - \frac{khc}{w}\sigma_i + \ldots \tag{5.67}$$

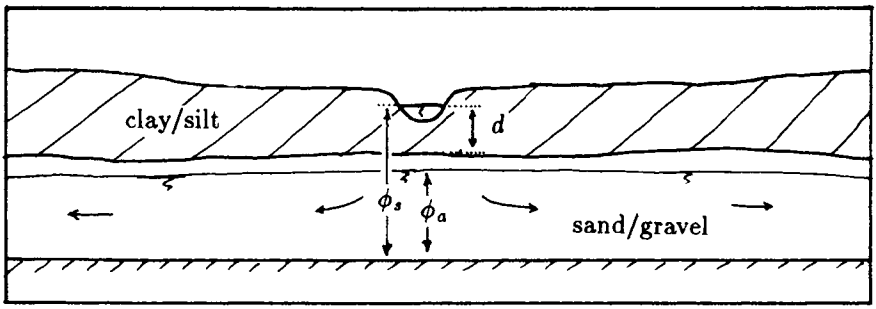

Figure 5.15: Percolating stream.

where summation is implied over j, and where h is defined with reference to (5.64) and (5.66) as

$$h = H \quad (\Phi_a \geq \tfrac{1}{2}kH^2) \qquad\qquad h = \frac{\phi_a + \phi_s}{2} \quad (\Phi_a < \tfrac{1}{2}kH^2) \tag{5.68}$$

For the case of unconfined flow, this results in a matrix coefficient for σ_i which depends on the a priori unknown head ϕ_a,

$$A_{ii} = F_{ii} - \frac{k\frac{\phi_a+\phi_s}{2}c}{w}\sigma_i \qquad (i \text{ no sum}) \tag{5.69}$$

Consequently, the set of equations becomes nonlinear and has to be solved iteratively!

The analysis for the sink disc function is similar and may be obtained from (5.62) through (5.69) by leaving off the width w and replacing σ by s. The sink disc functions, too, under unconfined flow conditions, give rise to nonlinear equations.

Percolating Surface Waters

The condition (5.58) does not apply to the extreme case in which the head ϕ_a in the aquifer drops below the resistance layer, creating unsaturated flow conditions in the aquifer underneath the stream or lake; see Figure 5.15. In order to deal with the situation in Figure 5.15 we will make two assumptions: (1) the resistance layer (silt/clay) remains saturated, and (2) the pore pressure just underneath the resistance layer is atmospheric ($p = 0$). Under these conditions the outflow rate ($-q_z$) from the stream follows from

$$-q_z = \frac{d}{c} \qquad (\phi_s - \phi_a > d) \tag{5.70}$$

where d is the depth of the bottom of the resistance layer measured from the water table in the stream; see Figure 5.15. After a solution is obtained, using equations of the form (5.67), GFLOW1 checks for the condition illustrated in Figure 5.15, eliminates the relevant equation from the matrix, and calculates σ $(= q_z w)$ from (5.70) instead.

When the resistance layer in Figure 5.15 is absent, so that the stream is in direct contact with the aquifer material, the flow rate out of a losing stream is limited by assuming that it cannot exceed the saturated hydraulic conductivity of the aquifer. In so doing, we ignore the water depth in the stream (incipient ponding) and assume atmospheric pressure between the stream bottom and the water table in the aquifer. If, after a groundwater solution is obtained, GFLOW1 detects a line sink with a negative strength in excess of the allowable percolation rate $(-\sigma/w > k)$, the relevant equation is eliminated from the matrix and the strength of the line sink is set to

$$\sigma = -wk \tag{5.71}$$

This limit on the infiltration capacity of a line sink is invoked only if the line sink has a width larger than zero. When line sinks in GFLOW1 are given a zero width, they will extract or infiltrate as much water as necessary to meet the specified head condition at their control points. Line sinks used in the farfield are best given a zero width. Line sinks used in the nearfield are best given an appropriate width, and preferably a resistance and resistance layer depth.

A similar procedure is followed for infiltrating sink discs that have a zero resistance. Percolating sink discs have a strength s which is set equal to $-k$. Sink discs, of course, have no width parameter, so that for percolating sink discs, incipient ponding is always assumed. If sink discs are used to model wetlands, this may be a reasonable assumption. Lakes or reservoirs, however, are best modeled with line sinks along their perimeter, instead of using sink discs.

5.2.4 Conjunctive Surface Water and Groundwater Flow

So far, whenever a line sink or sink disc recharges the aquifer we assumed that the necessary volume of surface water is available to realize the calculated infiltration rate. In reality, however, available stream flow is often a limiting factor on the aquifer recharge rate of a losing, and certainly of a percolating, stream. For instance, the condition illustrated in Figure 5.15 is most likely to occur in the head waters of smaller tributaries. It is questionable if sufficient stream flow is available in these stream reaches to sustain

the recharge rate calculated with (5.70). Mitchell-Bruker (1993) pioneered a strategy to include steady-state stream flow calculations in analytic element models in order to arrive at more realistic boundary conditions. A brief discussion of the implementation in GFLOW1 follows.

Stream flow, in general, is thought of as consisting of two components: *base flow* (groundwater inflow) and *overland flow*. The term *overland flow* suggests that this part of the stream flow is due to water which runs off over the terrain surface and through little gullies during a rainstorm (so called Hortonian overland flow). Hortonian overland flow, however, is very short-lived; it occurs only during and shortly after a rainstorm event: *storm flow*. Traditional techniques to distinguish between base flow and overland flow (hydrograph separation) yield overland flow rates which are much more sustained and larger than can be explained by Hortonian overland flow alone. The precise nature of overland flow is still the subject of debate and research. Depending on topographical, geological, and ecological conditions, we envision a combination of the following mechanisms for overland flow: Hortonian overland flow, unsaturated groundwater flow near streams and tributaries ("bank storage"), and saturated groundwater flow in aquifers perched above the regional aquifer.

In GFLOW1 we distinguish between three different stream flow components.

- *Base flow*: groundwater inflow from the regional aquifer
- *Overland flow*: all stream flow which is *not* base flow or storm flow
- *Head water inflow*: stream flow entering the head water of a stream in the model and coming from upstream reaches not included in the model.

The *overland flow* and the *head water inflow* are specified as input data. The *base flow* is calculated during the conjunctive groundwater and surface water solution procedure in GFLOW1. In order to perform these base flow calculations, line sinks which are used to model streams and tributaries are organized into stream networks. Starting at the head waters, the program accumulates the groundwater inflow due to each line sink, which is the line sink strength σ times the line sink length. Any specified *head water inflow* is accounted for by adding it to the base flow of the head water stream section (line sink). After the initial base flow calculations, the program scans the stream network to correct for two cases of over-infiltration. First, the base flow can become negative because of losing stream reaches. If the *stream flow*, the sum of the calculated base flow and the specified head-water and overland flow, is locally negative, the line sink strength σ

is adjusted to make the stream flow zero, rather than negative. The second case of over-infiltration may arise from the process of alternating groundwater solutions and surface water solutions. If during a surface water solution some line sinks have been given a limited negative strength (recharge rate), then they are no longer included in the matrix during the groundwater solution procedure. Yet, the new groundwater solution may have changed the conditions at some of these stream reaches so that the recharge rate, dictated by available stream flow, is now in excess of what would occur under the new groundwater flow conditions. In such a case, (5.58) is used to correct the line sink strength, and that line sink is included again in the next groundwater flow solution. Alternatively, the stream section may have been given a recharge rate (in a previous iteration) that is too small in view of the current stream flow availability. In that case the infiltration rate is corrected upward and the stream flow adjusted accordingly.

When during successive solutions no further corrections in stream flow occur, and the boundary conditions of the groundwater flow problem are sufficiently approximated, the solution procedure is completed.

5.2.5 Example Run

To illustrate the operation of program GFLOW1 a fictitious flow problem is solved. The input data file for this demonstration is demo.dat and is provided with GFLOW1. What follows is a brief discussion of some graphical output.

The layout of analytic elements and background map features for this problem is plotted in Figure 5.16. The dashed lines (long dashes) in Figure 5.16 represent some streams and their tributaries. The lines are dashed to indicate that the line sink strengths are zero, and hence no solution has been produced yet. The solid line polygon around a section of the stream in the center of the plot represents an area with a different (larger) hydraulic conductivity and areal recharge rate than the regional values. The large circle, over most of the domain, is a sink disc with a negative discharge rate used to model regional recharge due to precipitation. The remaining lines (short dashes) are background map features, representing some roads, outlining a city boundary (near center of the plot), and indicating the boundary of so-called "channel deposits" surrounding the stream that runs through the center of the plot. On a color screen, different colors are used to distinguish between the various analytic elements and map features. The streams near the center, the *nearfield*, are represented by more line sinks than those near the perimeter of the domain depicted in Figure 5.16, the *farfield*.

After the problem is solved, contours of piezometric heads may be plot-

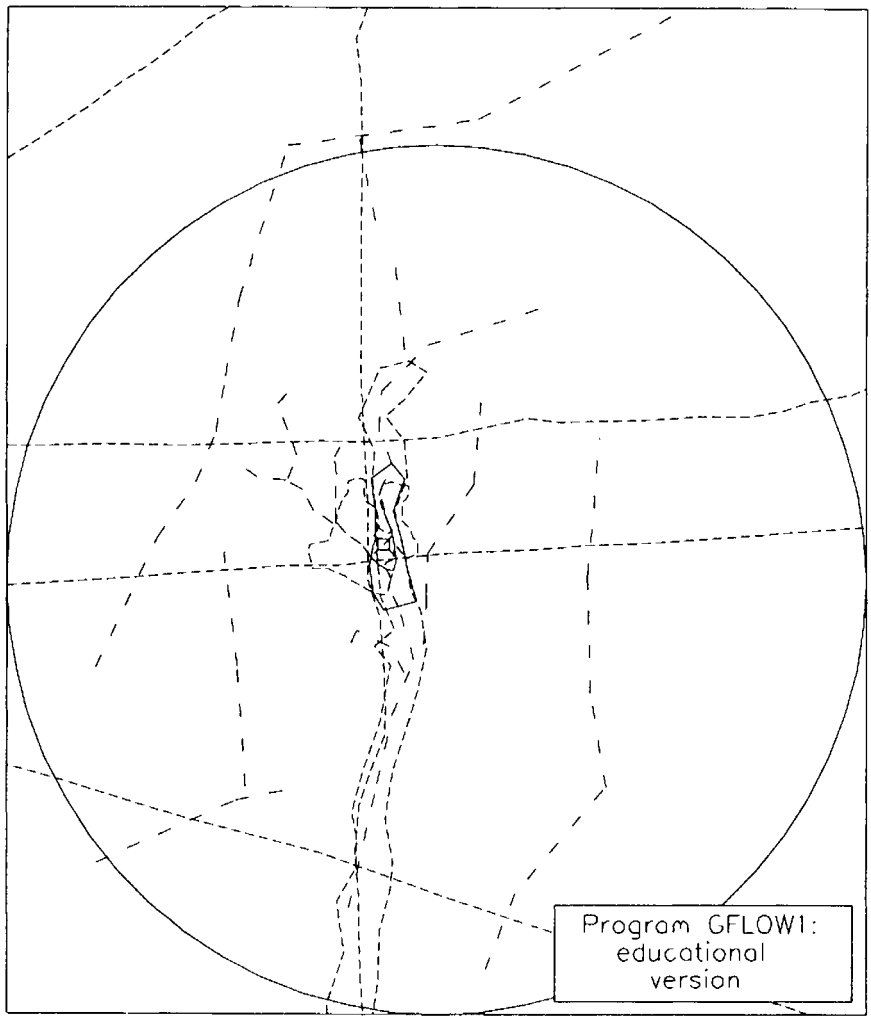

Figure 5.16: Layout of analytic elements and background map features for the demonstration problem. GFLOW1 file: demo.dat

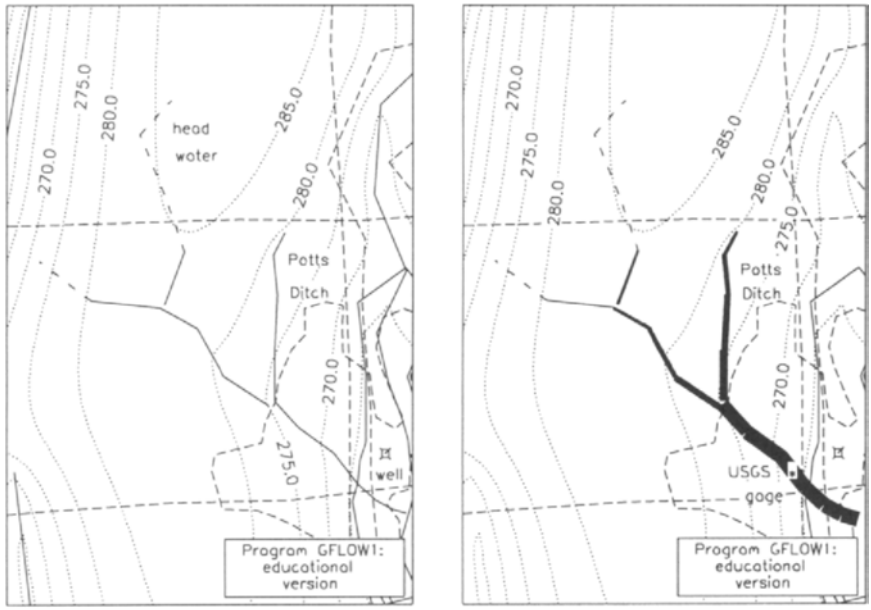

Figure 5.17: Piezometric contours for the problem in file demo.dat, regular layout (left-hand figure) and line thickness proportional to stream flow (right-hand figure).

ted, the dotted lines in Figure 5.17. The domain plotted in Figure 5.17 is considered part of the nearfield. Observe that the head waters of Potts Ditch's tributaries are dashed; they try to recharge the aquifer, but do not have the stream flow to support that recharge. Consequently, both the stream flow and the line sink strength parameters are zero. To interpret the zero stream flow in the model, remember that our solution is steady-state, and hence the dashed stream sections probably represent *ephemeral streams*, flowing only during times of high precipitation.

In the right-hand plot of Figure 5.17, a graphical representation of the stream flows is provided, whereby the line thickness of the stream is proportional to the stream flow rate. The numerical values for the heads and the stream flows in Figure 5.17 can be obtained from the graphics screen in the line sink module of GFLOW1 by use of a cursor and appropriate key strokes.

GFLOW1 together with an accompanying data preprocessor GAEP (Geographic Analytic Element Preprocessor)is called GFLOW. You may install GFLOW on a 386 or 486SX based PC with a math-coprocessor or

on a 486DX based PC. You need at least 4Mb of RAM and about 3Mb of disk space. To install the program, type A:INSTALL and follow the instructions on screen. In order to become familiar with GFLOW1, both with its capabilities and operation, you may copy the file gfintro.ps, located in the \gflow\doc subdirectory, to a PostScript[1] printer or copy the file gfintro.txt to a non-PostScript printer. You may also print the various data files (proble*.dat) in the \gflow\demo directory. Many of these files contain instructions pertinent to their use. The most elaborate instructions are found in the file problem1.dat, with additional instructions in successive files (problem2.dat, etc.) as other program features are being used. Together with gfintro.ps these files may serve as a tutorial for the use of GFLOW1.

5.3 Basic Modeling Concepts

Although gaining in popularity, groundwater flow modeling is not universally acclaimed. Many groundwater modeling projects, and their outcome, are received with a healthy amount of skepticism, and for good reason. Not seldom does the groundwater modeler appear to be a hobbyist absorbed by computer hardware and software and with an unshakable belief in the numbers or graphics produced by "the model." Similarly, some clients unwisely accept the authority of the computer and take the modeling results as absolute. Not everybody, however, is equally impressed. Many groundwater hydrologists, painfully aware of the complexity of the problem, fail to see how a computer program, provided with some crude and often unreliable data, can accurately describe the real world. Modeling "successes" are well documented, but failures are suspiciously absent from the literature. Mary Anderson (1983) critically addressed the often blind and unwarranted belief in groundwater models in an editorial in *Ground Water*: "The Emperor Has No Clothes." Konikow (1986) documented the dismal predictive performance of groundwater models dealing with contaminant transport. Some groundwater consultants are still hesitant to engage in groundwater modeling; it is known to be costly and potentially controversial.

Is groundwater flow modeling a sham? Let's hope not! The real question is, how can we use groundwater flow modeling in a productive and responsible way, improving the quality of our study and *reducing its cost*? To this end, we will redefine the role of groundwater modeling in solving groundwater flow problems. We will break with the classical project structure: (1) literature review, (2) field data collection, (3) data analysis, and (4) "construction of the model." Here, the modeling seems the *purpose* of

[1] PostScript is a trademark of Adobe Systems, Inc.

the study, while it should be one of the *means*. Instead, we will learn how to use groundwater modeling during all phases of the project, even during proposal development. We will discuss how to design simplified conceptual models of a real-world problem, and explore the validity of various simplifications.

5.3.1 Purpose of Modeling

The first and critically important step in any modeling effort is the definition of its purpose. Groundwater flow modeling can be done for a wide variety of reasons, each requiring different modeling strategies and often different models. Some possible modeling objectives follow, listed in order of increasing complexity:

1. Illustration of known groundwater flow principles
2. Determination of aquifer parameters
3. Determination of geohydrological conditions
4. Determination of groundwater flow history
5. Prediction of future groundwater flow patterns
6. Prediction of future contaminant movement
7. Basic research on flow or transport phenomena

The modeling performed in Chapter 3 can be classified under (1): illustration of known groundwater flow principles. Since we are only concerned with *principles*, relatively simple models can handle the job. In contrast, when a flow or transport phenomenon is not yet fully understood, complex models are needed, since we cannot simplify what we do not (yet) understand. With *complex* we are referring to the use of either complex algorithms or many parameters, or both. Application of groundwater models to basic research, therefore, often requires specially designed (or modified) models which may need a supercomputer to run.

Many consultants reach for the most "powerful" (read most complex) model when engaging in a modeling project. The argument goes as follows. The aquifer is stratified and laterally heterogeneous, the flow is three-dimensional and transient, there is dispersion, adsorption, volatilization, decay, bio-degradation, etc., etc.... Therefore, the more of these features are represented in the model, the more credible the modeling results are (and thus the more credible we are). The argument seems logical and self-evident, but is seriously flawed! The use of many input parameters during

research (objective 7) is only manageable, because they do not have to be related to a specific field site. Instead, these parameters are chosen arbitrarily and varied one by one to study their impact on the flow or transport problem under investigation. For a consultant, however, who is studying a particular site, multi-parameter models may pose serious data-acquisition problems, escalating project cost and delaying project completion. Worst of all, the added time, effort, and cost often fail to pay off as data uncertainty leads to questionable model input and thus questionable model output ("garbage in = garbage out").

A consultant who selects a model based on its many features, as if buying a car that is "loaded," fails to act on the first requirement of every modeling project: A well-defined purpose. This purpose may be a single item out of the list just presented, a combination of some of these items, or something else. The purpose of the modeling exercise plays an important role in model selection, as may be illustrated by an example.

In designing a "pump and treat system," the consultant may use modeling to assist in determining the average hydraulic conductivity, the possible directions and magnitudes of the ambient flow, and finally the optimum location(s) and discharge(s) of the recovery wells (objectives 2 through 6). Transport phenomena, such as dispersion and decay, are of little importance when designing a pump and treat system. Although dispersion may widen the contaminant plume somewhat beyond the average groundwater streamlines, locally that is a small effect which usually falls within the data uncertainties. It can easily be accounted for by a moderate over-design of the system. Transient and three-dimensional flow may or may not be important factors, depending on local circumstances; the same holds for aquifer heterogeneities. But even if such complexities need to be taken into account, initial basic modeling of steady-state flow in a homogeneous aquifer will still prove to be a valuable first step toward a more detailed study.

In the next sections we will concern ourselves with the important question of which phenomena to include in our modeling, and which to ignore. We will make these decisions based on field observations in combination with modeling.

5.3.2 Stepwise Modeling

The availability of field data is the main bottleneck for most groundwater studies. Uncertainties about the geology, aquifer parameters, impacts of surface waters, etc., compromise the design of a reliable conceptual model. Consequently, groundwater flow modelers have the tendency to demand ever more field data before feeling confident to engage in groundwater flow

modeling. This has traditionally led to costly data acquisition programs and long delays in producing results. In fact, every time new field data becomes available, the modeler is confronted with new complexities, which tend to lead to ... new data requests. Under this scenario, modeling is often declared unrealistic because "there is not enough data" available.

There is a different way of looking at this dilemma. If truly large amounts of field data are collected and analyzed, many of the groundwater flow questions may be answered in the process; there may not be any reason left for modeling! The answers, however, have come at great expense. A better and more cost-effective approach is to perform modeling early on in the project, prior to and concurrently with field data collection. In fact:

Rule 5.1 *Instead of collecting field data to guide modeling, modeling should be used to guide field data collection.*

Under this scenario, groundwater modeling is performed from the very beginning of the project, using what limited data is available. This initial groundwater modeling is used to increase the efficiency of field data collection, ensuring the right data are collected in the right place, and avoiding redundant or irrelevant data acquisition. The fewer data available at the outset of a project, the more potential benefit may come from (early) groundwater flow modeling. Taken to the extreme, this thinking leads to an interesting conclusion:

Rule 5.2 *The value of groundwater flow modeling is inversely proportional to the availability of data.*

The suggested interactive modeling and data acquisition process is schematically represented in Figure 5.18 and compared to the traditional approach.

The traditional approach (left-hand flow chart) is phased in four logical steps, each being completed before the next one is started. However, to minimize the risk of insufficient data during the modeling phase, data acquisition is often overdone. A frequent problem of the traditional approach is that many data are not used, while critical data are still lacking to successfully complete the modeling.

The stepwise modeling approach (right-hand flow chart) is designed to optimize the use of (expensive) data. The initial modeling is performed by use of basic data that are readily available from topographical and geological maps, and existing regional studies. Where necessary, model input parameters are estimated, while various values may be used in the model in order to assess their relative importance (sensitivity testing). Based on these initial modeling results, a data acquisition program is developed.

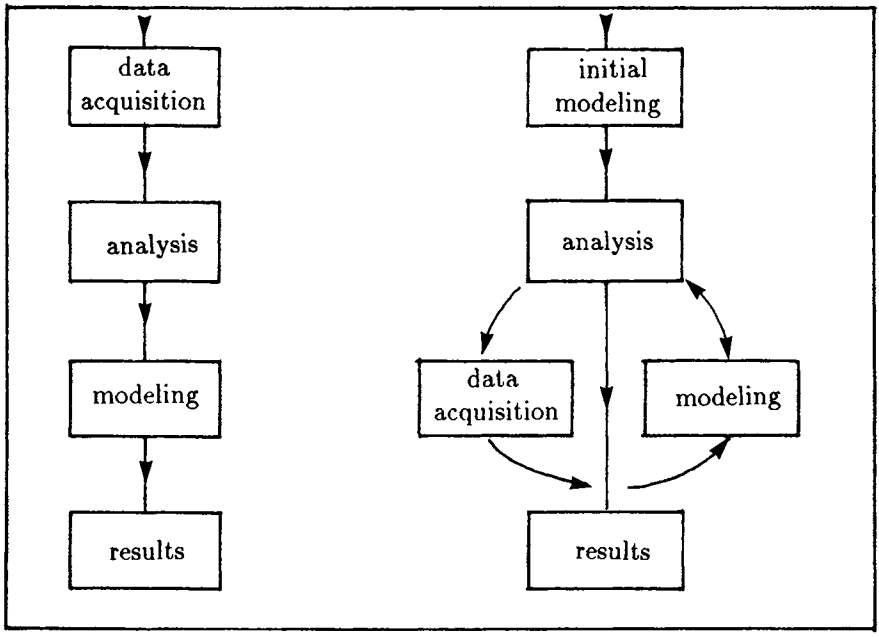

Figure 5.18: Traditional modeling and stepwise modeling.

Data acquisition may imply actual measurements in the field, extraction of data from existing maps and reports, or both. The new data are used to refine the (conceptual) model. The analysis of subsequent modeling results may lead to a reinterpretation of existing data, which in turn may lead directly to an improved (refined) model, or may require additional data collection before the model can be refined; see Figure 5.18. The process is repeated until satisfactory results are obtained.

It is important, during this process, to keep the modeling objective(s) in mind. Rather than trying to produce a perfect match between observed and modeled piezometric heads, for instance, the modeler should verify if sufficient insight into the flow problem is obtained to answer the question(s) that led to the study. For example, consider the following situation.

A study is performed to assess whether or not a particular well, near a documented contaminant spill, may become polluted. No pumping test has been conducted, leaving much uncertainty about the aquifer hydraulic conductivity. Several modeling runs are performed with different values for the regional hydraulic conductivity. Comparing modeled piezometric head distributions with observed heads does not lead to a single value for the hydraulic conductivity. If the heads compare well with observations in

one area, they appear to be in error elsewhere. Additional data collection may improve the modeling results — for instance, by spatially varying the aquifer recharge and hydraulic conductivity. However, all modeling runs suggest that the contaminant plume will comfortably miss the well. The uncertainties in the data, therefore, are irrelevant, and further data collection or modeling is not justified.

5.3.3 Designing Conceptual Models

Our computer models, whether simple or complex, are mathematical representations of *conceptual models.* A conceptual model may be defined as follows:

Rule 5.3 *A conceptual groundwater flow model is a simplification of a real-world groundwater problem such that (1) it captures the essential features of the real-world problem and (2) it can be described mathematically.*

Condition (2) needs little explanation: The sole purpose of our simplification is to make the problem fit one of our mathematical models (e.g., computer models). Condition (1) is the difficult one. When is a conceptual model an acceptable simplification of reality? The design of a conceptual model is not a simple, straightforward procedure, and it is certainly not objective! In this phase of the modeling exercise, we have to rely on the expertise and judgment of the groundwater hydrologist. Groundwater flow modeling, therefore, has often been termed an *art* instead of a science. Of course, it is both. The groundwater modeler must combine his technical knowledge with his personal creativity to come to a successful modeling project, much like an architect or engineer comes to a successful design. And just like the architect and engineer, the groundwater modeler (*not the model*) is solely responsible for the project outcome. Incidentally, some attempts are being made to exercise quality control by certifying groundwater flow models. This is, for reasons outlined earlier, just as futile as certifying the pencils, erasers, and drawing boards of architects and engineers.

There are four important ingredients that go into the design of a conceptual model:

1. Familiarity with capabilities (and limitations) of available models
2. Insight into the regional and local geology
3. Well-defined modeling objective(s)
4. Good understanding of hydraulics

First some comments on the choice of a mathematical (computer) model. It is generally accepted that the logical sequence of events is first the design of a conceptual model and then the choice of a mathematical (computer) model that fits this conceptual model. In fact, designing a conceptual model with a particular computer model in mind is seen as improper: A biased reversed procedure to favor some subjective model preference. However, there is more to a computer model than the conceptual models to which it fits. Reliability, operational efficiency, and simply the modeler's familiarity with the software are important factors in selecting a model. Therefore, as long as the conceptual model captures the essential real-world features, defined with the modeling objective(s) in mind, the use of simple and operationally convenient software is justified, even smart. Besides, if initial results indicate that the model is inadequate, they still form a nice first step toward a more comprehensive modeling effort, using a more sophisticated model.

Insight into the geology (item 2) is basic to any modeling effort. There are many questions to be asked. Which geologic formations constitute our aquifer? Do we have one or more aquifers? Are they interconnected? Which formations act as aquitards (low permeability) or aquicludes (no permeability)? How to translate the geology into a conceptual model depends, in part, on the modeling purpose (item 3). For instance, if we are interested in piezometric heads and flow patterns on a regional scale, many individual but interconnected aquifers may be combined into one homogeneous aquifer. On the other hand, if we seek to model local contaminant movement, the various aquifer strata and their interconnections may need to be represented explicitly in the conceptual model. How lumping together different geological formations affects regional or local modeling results requires a good understanding of hydraulics (item 4).

Examples

The design of conceptual models can best be illustrated with a few simple examples. In Figure 5.19 a cross-section is depicted over a hypothetical real-world aquifer system together with its conceptual model. Keep in mind that all cross-sections have an exaggerated vertical scale! The real world situation exhibits, from top to bottom, a silty, clayey till interspersed with sand lenses and locally interrupted by a silty sand. Below the till we find various sand and gravel formations with some isolated clay lenses. The rock that underlies these formations is partially fractured, mostly at the top with fewer tighter fractures deeper in the rock formation.

The conceptual model represents the sand and gravel formations, together with the upper (fractured) portions of the rock, as one homogeneous

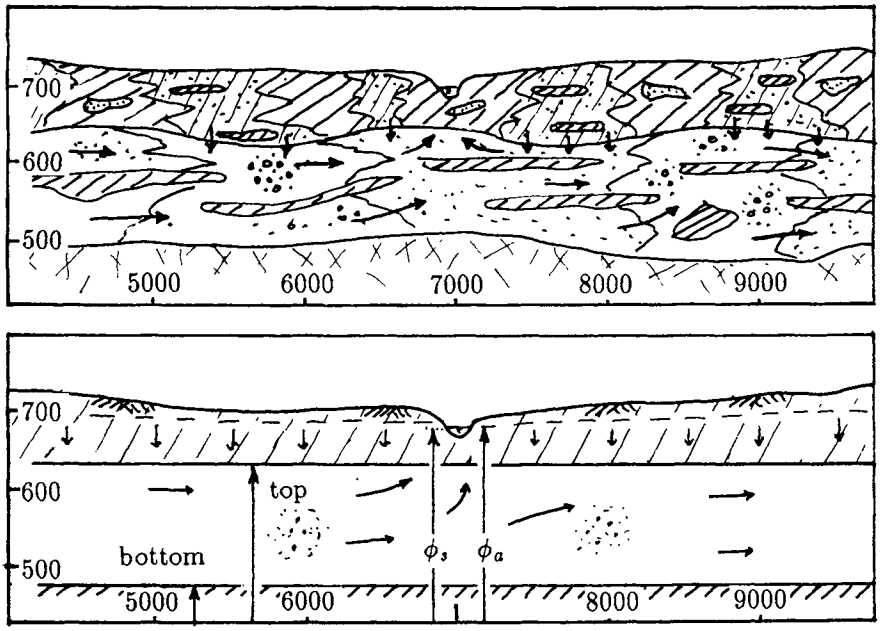

Figure 5.19: Cross-section over real-world aquifer system and its conceptual model.

confined aquifer with a horizontal impermeable bottom and a horizontal upper aquitard. The clay lenses and variations in sand or gravel contents are ignored. The aquifer recharge, which in the real-world system varies in time and in space, is replaced by an average recharge rate that is constant in both time and space.

There are three reasons for the simplification depicted in Figure 5.19:

1. The detailed geological information depicted in Figure 5.19 is simply not available, certainly not on a regional scale.

2. Even if such data were available, it is undoable to represent every clay lens, sand lens, gravel pocket, etc., in a mathematical model, particularly on a regional scale.

3. On a regional scale, the piezometric head distributions (and thus flow patterns) for the two conceptualizations in Figure 5.19 are virtually indistinguishable.

The truth of the last statement is not self-evident, but may be understood from the concept of a representative elementary volume (REV). In Section 2.1 we argued that the complex flow patterns on the scale of individual soil pores can be replaced by average flows on a scale at or beyond the REV. We may also think of an REV at or beyond which the complex flow patterns in the real world aquifer can be replaced by the average flow patterns in the conceptual model; see Figure 5.19. Strictly speaking, the scale of the REV must be determined experimentally, but in practice it is often based on intuition.

Another example is given in Figure 5.20, where part of a surface geological map is reproduced. Some of the streams are surrounded by depositions of sand and gravel referred to as channel deposits, alluvium, or outwash, depending on the geological formation process. In many cases the channel deposits extend down to the aquifer base (bedrock); see inset in Figure 5.20. The channel deposits have a significantly higher conductivity than the surrounding till aquifer. When modeling flow on a regional scale, the scale of Figure 5.20, the higher hydraulic conductivity of the channel deposits may be ignored, using a single average hydraulic conductivity for the sand and silt layers in the till. At that scale the channel deposits, however, do affect the way the streams are represented in the conceptual model. The streams without channel deposits are given a resistance to inflow or outflow, while the streams with channel deposits are represented in the model without any resistance; see Figure 5.14.

The situation is different when modeling flow on a more local scale. For instance, imagine there is a well field in the outwash aquifer (channel deposits) north of the town Greenfield, inside the circle in Figure 5.20.

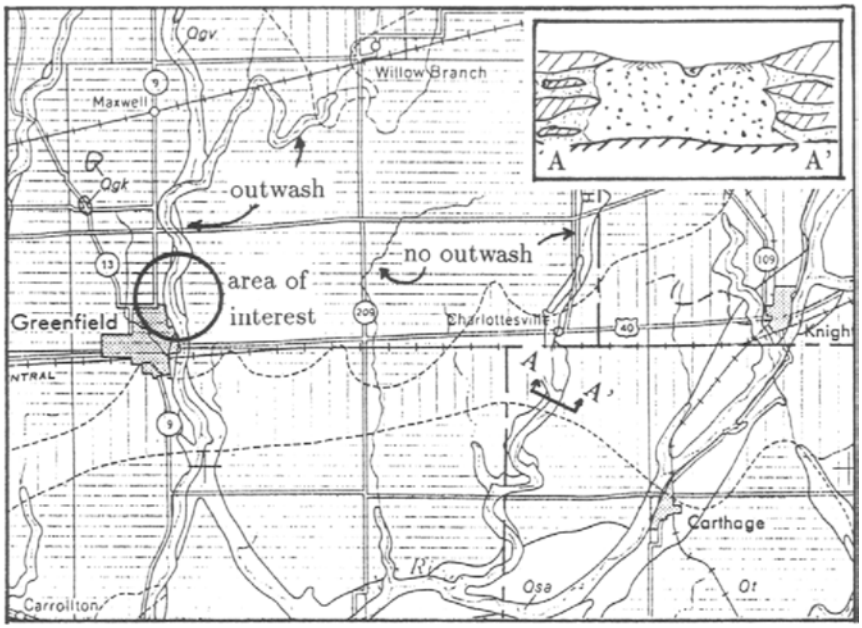

Figure 5.20: Regional flow modeling using an average hydraulic conductivity. Streams with channel deposits are given no resistance to inflow or outflow.

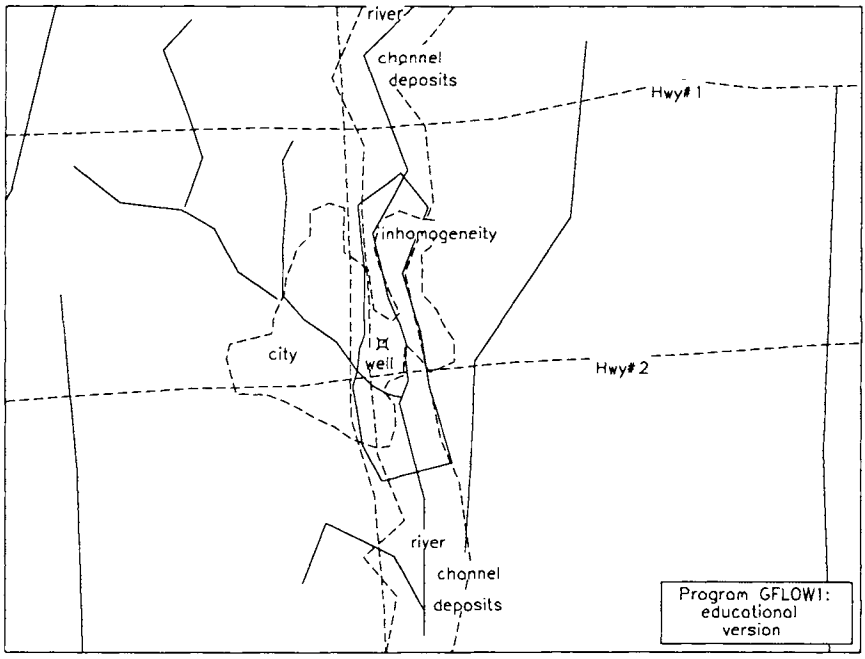

Figure 5.21: Including the channel deposits for local flow modeling. (GFLOW1 file: proble51.dat)

When modeling the flow due to the well field, the difference in conductivity between the outwash or channel deposits and the till should be included explicitly. The channel deposit boundaries on both sides of the river are modeled in GFLOW1 by an inhomogeneity area (string of line doublets) with an increased hydraulic conductivity and areal recharge rate on the inside. To illustrate this, a close-up of the analytic element layout and background map in Figure 5.16 is shown in Figure 5.21. The dashed lines represent roads, a city outline, and the outwash or channel deposit boundaries on either side of the river in the center of Figure 5.21. Only a portion of the channel deposits are modeled by the inhomogeneity area: The remaining channel deposits, away from the area of interest (city and well), are treated in the same way as in the regional model: connecting the stream to the aquifer with little or no resistance. The adequacy of this limited representation of the channel deposits is readily tested by extending the inhomogeneity in the model farther along the river and verifying that it does not indeed affect the solution in the area of interest.

Rule 5.4 *In a regional scale model, highly permeable channel deposits near*

streams are incorporated by giving little or no resistance to those streams. On a local scale, the channel deposits need to be incorporated explicitly as an area of higher conductivity.

Exactly what can and cannot be ignored in a conceptual model is not always intuitive. It requires modeling experience to design useful and responsible conceptual models, maintaining essential features while ignoring secondary effects. It may be necessary to test the adequacy of a conceptual model by comparing the modeling results of conceptual models with different complexity, which is the subject of the remainder of this section.

Exercise 5.1 *Test the adequacy of the extent of the inhomogeneity area in Figure 5.21 by following the instructions in the data file* proble51.dat *included on the distribution diskette.*

5.3.4 Dupuit–Forchheimer versus Three-Dimensional Flow

The flow patterns in, for instance, Figure 5.19 are clearly three-dimensional, which suggests the need for a three-dimensional flow model. Yet, in Chapter 3 I argued that regional groundwater flow in aquifers that are thin relative to their lateral extent may be treated as Dupuit–Forchheimer flow; see Figure 3.1 and Figure 3.2. The question then is, when do we consider the aquifer thin relative to its lateral extent? In fact, what really matters is the thickness of the aquifer compared to the distance between boundary conditions (streams, lakes, etc.). To gain insight in this issue we will compare some three-dimensional flow solutions with Dupuit–Forchheimer solutions.

Partially Penetrating Wells

In Figure 3.20 in Section 3.1.12 we investigated the flow from a recharge well toward a discharge well. Both wells were fully penetrating wells resulting in Dupuit–Forchheimer flow. In Figure 5.22, the fully penetrating wells are replaced by partially penetrating wells. The three-dimensional solution for a partially penetrating well in a confined aquifer is discussed in Section 4.2.1. The pumping and injection rate for the wells in Figure 5.22 is 50 GPM. The wells are screened from 15 feet above the aquifer bottom to 15 feet below the aquifer top, and are 200 feet apart. The aquifer is 50 feet thick and has a hydraulic conductivity of 10 ft/day. In Figure 5.22 piezometric contours are plotted along the aquifer top and in a cross-section over the wells. In the cross-section, the piezometric contours in the immediate vicinity of the well are omitted, since they are too close together for the scale

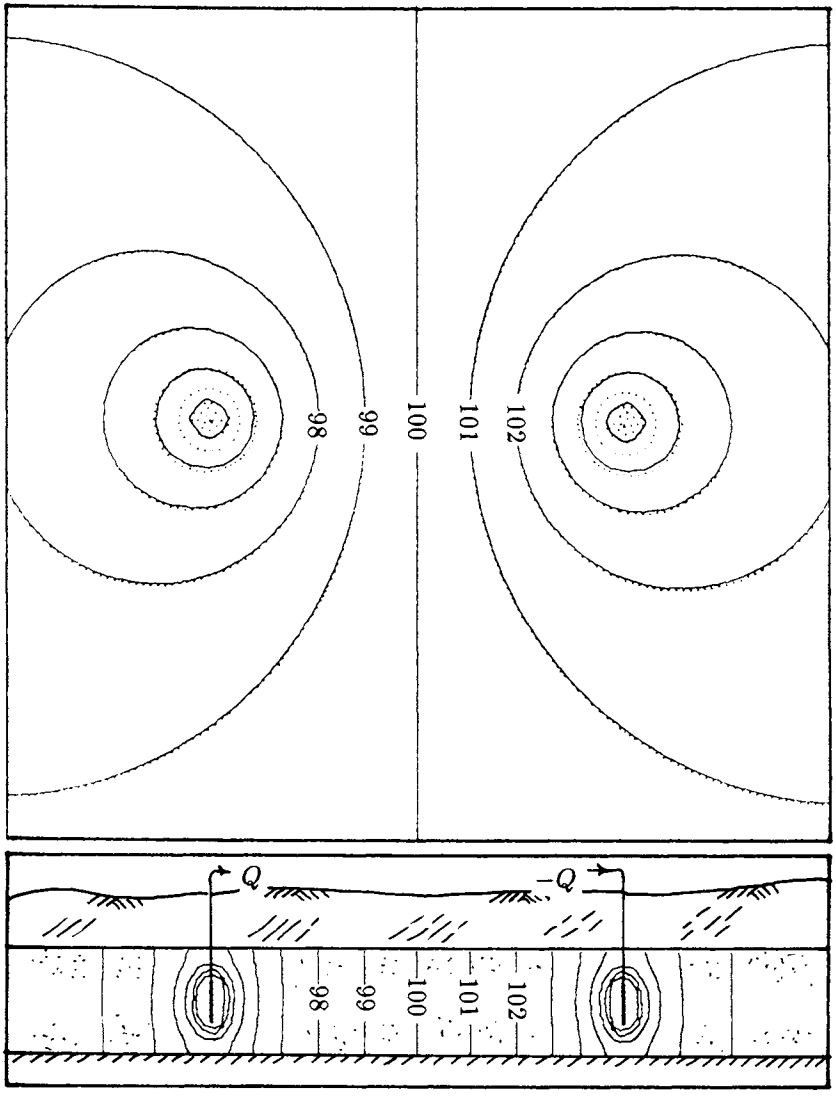

Figure 5.22: Piezometric contours in plan view and cross-section for a partially penetrating well doublet. The plan view is taken along the upper aquifer boundary. The dotted contours are from a Dupuit–Forchheimer solution. (GFLOW1 file: proble52.dat)

of Figure 5.22; they would obscure the position of the well screen. The dotted lines in the plan view contour plot represent the Dupuit–Forchheimer solution (presented earlier in Figure 3.20).

It is observed from Figure 5.22 that the three-dimensional effects are very local: They are limited to a zone that extends one to two times the aquifer thickness out from each well. Replacing a partially penetrating well by a fully penetrating well, therefore, is of little consequence for the groundwater flow solution on a regional scale. The effect is significant, however, in the immediate vicinity of the well. For instance, for the case of Figure 5.22, the head in the partially penetrating pumping well is 81.72 feet, while the head is 88.56 feet if the wells would be fully penetrating. As it seems, drawdowns in pumping wells in a Dupuit–Forchheimer model tend to be underestimated. Unfortunately, the Dupuit–Forchheimer solution is not conservative in this case: We may overestimate the pumping capacity of wells when considering allowable drawdowns in these wells. We should also become cautious when interpreting pumping test data obtained from piezometers that are relatively close to the well, where heads may vary with depth, a fact not accounted for in most pumping test evaluation methods.

Exercise 5.2 *Try several different well configurations to study the three-dimensional effects of partially penetrating wells by following the instructions in the data file* proble52.dat *included on the distribution diskette.*

Recharge Zones

Groundwater recharge areas, by their nature, must exhibit vertical components of flow. In fact, at a water divide there is only vertical flow. Consequently, some hydrologists are uncertain about using Dupuit–Forchheimer approximations in the presence of local or regional recharge. The author compared three-dimensional solutions to circular recharge areas with Dupuit–Forchheimer solutions (Haitjema, 1987a). What follows is a summary of the results presented in that paper.

The first problem is that of a circular recharge area (percolating pond) at the center of a circular island, the conceptual model of which is presented in Figure 5.23. The problem is somewhat contrived, but useful for testing the validity of the Dupuit–Forchheimer assumption under conditions of local recharge. The recharge area is modeled by a source disc of constant strength located at the aquifer top. The three-dimensional solution for a sink or a source disc is discussed in Section 4.2.2. The two no-flow boundaries (aquifer top and bottom) are included by use of images and semi-infinite line sources to approximate remote images, as was done for the partially penetrating well; see Section 4.2.1. For more details on the mathematics of this problem, refer to Haitjema (1987a).

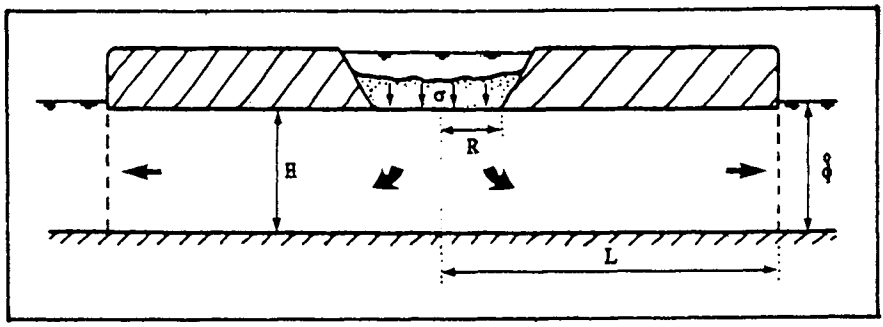

Figure 5.23: Percolating pond (circular recharge area) at the center of a circular island. (GFLOW1 file: proble53.dat) (After Haitjema, 1987a.)

In Figure 5.24, cross-sections through the equipotential surfaces near the pond are presented for three different radii of the pond: $R = 0.5H$, $R = 3H$, and $R = 6H$, where H is the aquifer thickness. The solid lines are vertical sections through the three-dimensional equipotential surfaces, while the dotted lines are sections through the corresponding Dupuit–Forchheimer surfaces. The actual equipotential surfaces are obtained by revolving the solid or dotted lines around the axis of the pond, the left-hand boundary of Figure 5.24. The equipotential surfaces are labeled in terms of the dimensionless property $k\phi/\sigma H$, where k is the aquifer hydraulic conductivity, ϕ is the piezometric head, and σ is the infiltration rate of the pond. The head at a distance L from the center of the pond is constant and equal to ϕ_0. For the case of Figure 5.24, it is given that $L/H = 100$, and $\phi_0/H = 1$.

Observe that for all three cases the three-dimensional and Dupuit–Forchheimer solutions start to coincide at approximately one aquifer thickness away from the boundary of the pond. This localized three-dimensional effect is consistent with what we saw in Figure 5.22 for the case of partially penetrating wells. Also note that when the size of the recharge area increases, the Dupuit–Forchheimer solution becomes more acceptable *underneath* the recharge area as well. However, at the center of the pond, where there is a water divide, the flow is purely vertical, and the Dupuit–Forchheimer solution fails regardless of the size of the pond.

In Figure 5.25, truly three-dimensional streamlines are compared with approximate three-dimensional streamlines in the Dupuit–Forchheimer model. The calculation of these approximate three-dimensional streamlines is discussed in Section 3.5. The length of each streamline reflects the

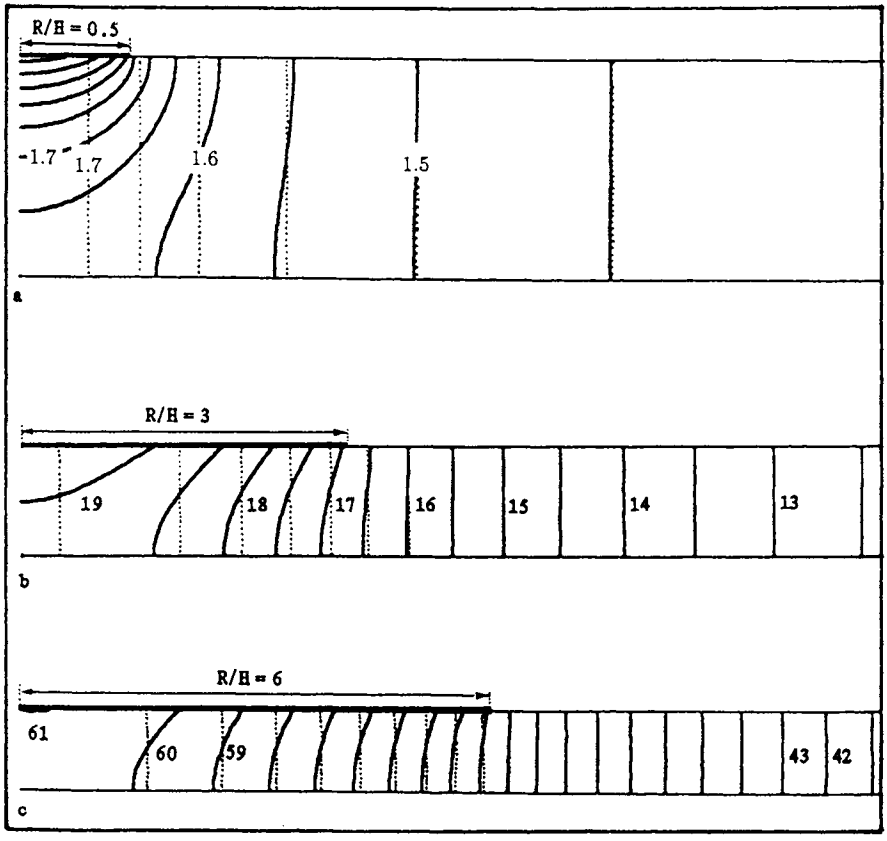

Figure 5.24: Cross-section over piezometric surfaces for ponds of three different radii. The solid lines represent the three-dimensional solution and the dotted lines represent the Dupuit–Forchheimer solution. (After Haitjema, 1987a.)

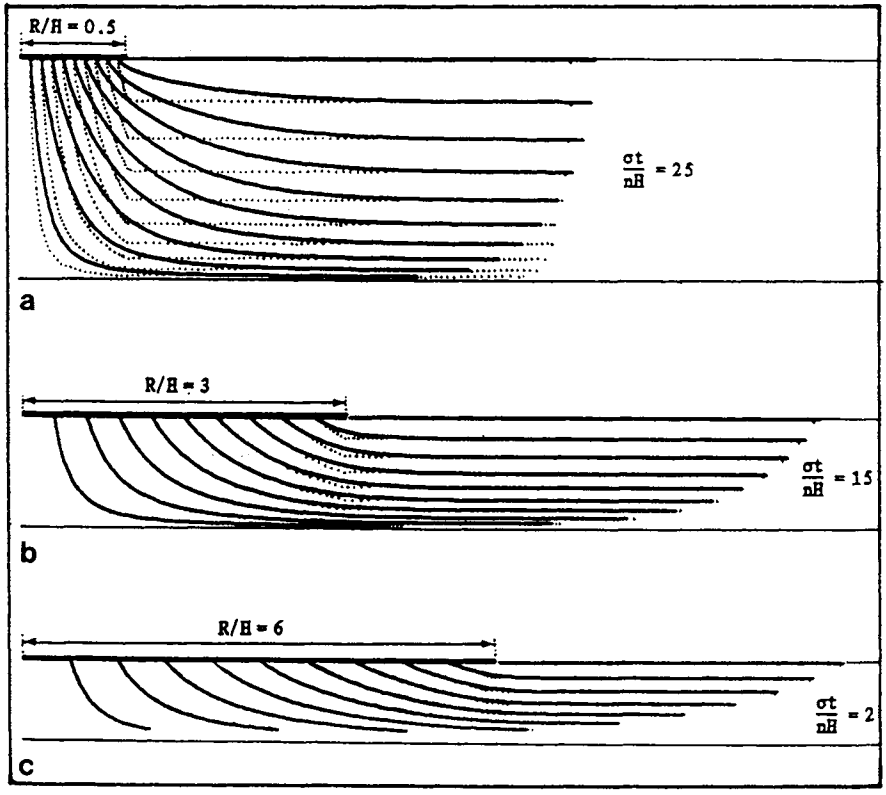

Figure 5.25: Streamlines for the three ponds. The solid lines represent truly three-dimensional streamlines, while the dotted lines are approximate streamlines in the Dupuit-Forchheimer model. (After Haitjema, 1987a.)

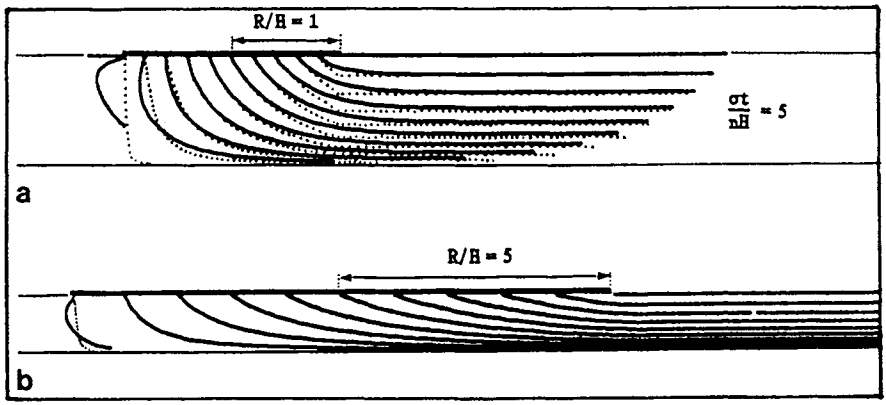

Figure 5.26: Cross-section over streamlines for a pond in a uniform flow field. The solid lines represent truly three-dimensional streamlines, while the dotted lines are approximate streamlines in the Dupuit-Forchheimer model. (After Haitjema, 1987a.)

same residence time for a water particle that travels along that streamline. This residence time is reported in Figure 5.25 by the dimensionless property $\sigma t/nH$, where t is the residence time and where n is the effective aquifer porosity. Only for the small recharge area ($R/H = 0.5$) are there significant discrepancies, and then mostly underneath or near the pond. For the case of $R/H = 6$, the differences between the approximate and exact streamlines are nearly indistinguishable on the scale of Figure 5.25.

So far we have considered radially symmetric flow, rarely encountered in reality. A non-radially symmetric solution is obtained by placing the recharge area in a regional uniform flow field. The Dupuit-Forchheimer solution to this problem is discussed in Section 3.2.4.

In Figure 5.26, a cross-section is presented over the streamlines in the plane through the center of the pond parallel to the uniform flow direction. Two cases are considered in Figure 5.26: A pond with a radius equal to the aquifer thickness, and a pond with a radius equal to five times the aquifer thickness. The uniform flow rate Q_0 in Figure 5.26 is given by the dimensionless property $2Q_0/(\sigma R) = 1$, which is the special case for which the Dupuit Forchheimer solution exhibits a stagnation point at the upstream boundary of the pond.

Plan views of streamlines, emanating at the pond outside this symmetry plane, are presented in Figure 5.27. The upper half of the figure is for the pond with radius $R = H$, while the lower half is for the case with radius $R = 5H$. Therefore, the scales for the two halves are different. The tick

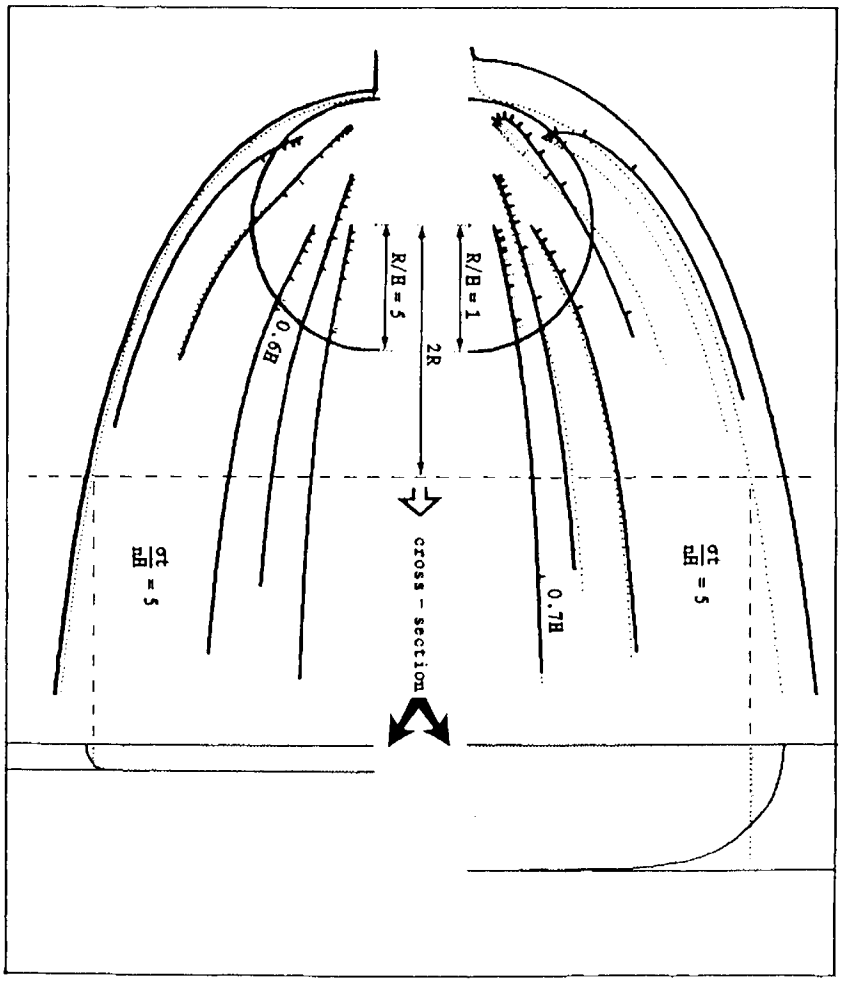

Figure 5.27: Plan view of streamlines emanating from the pond bottom. Upper half for pond with radius $R = H$, bottom half for pond with radius $R = 5H$. (After Haitjema, 1987a.)

marks on the streamlines indicate the depth of the streamline with respect to the aquifer top. Each subsequent tick mark indicates a depth increase of $0.1H$. The solid lines are the truly three-dimensional streamlines, while the dotted ones are the Dupuit–Forchheimer streamlines.

If the water in the pond were polluted, it would create a three-dimensional plume of contaminants in the aquifer. A cross-section over that plume, taken a pond diameter away from the center of the pond, is plotted in the right-hand part of Figure 5.27. The solid lines in the cross-section reflect the boundary of the plume resulting from the three-dimensional flow patterns, ignoring diffusion and dispersion. The dotted lines represent the boundary of the plume in the Dupuit–Forchheimer model.

For the large diameter pond, bottom half of Figure 5.27, the discrepancies between the truly three-dimensional flow patterns and the Dupuit–Forchheimer flow patterns are slight. The differences are more significant for the smaller pond (upper half of Figure 5.27). Particularly, the contaminant plume is wider near the top of the aquifer than predicted by the Dupuit–Forchheimer solution. Unfortunately, the Dupuit–Forchheimer solution is not conservative for this case: It underestimates the true width of the plume.

Overall, it seems that the Dupuit–Forchheimer approximation is acceptable, except if the size of the recharge area is of the same order as the aquifer thickness or smaller, or when considering the flow near stagnation points underneath the recharge area (center of the pond in Figure 5.24 and upstream boundary of the pond in Figure 5.26). When considering areal recharge due to rainfall, the "recharge area" is the entire flow domain, which is usually orders of magnitude larger than the aquifer thickness. Under these conditions both the piezometric head surfaces as well as the streamlines can be approximated quite well with a Dupuit–Forchheimer model.

Exercise 5.3 *Combine uniform flow, a three-dimensional pond, and a partially penetrating well in one problem, by following the instructions in the data file* proble53.dat *included on the distribution diskette.*

Toth's Solution to Regional Flow

The preceding conclusion, establishing the adequacy of the Dupuit–Forchheimer solution for regional flow, seems at odds with classical work by Toth (1963). Toth studied regional groundwater flow in relatively deep homogeneous aquifers. He assumed that the upper aquifer boundary, the groundwater table, would be a subdued copy of the topography, and presented an analytic solution to the boundary value problem in Figure 5.28. All sides of the domain are no-flow boundaries, except for the upper bound-

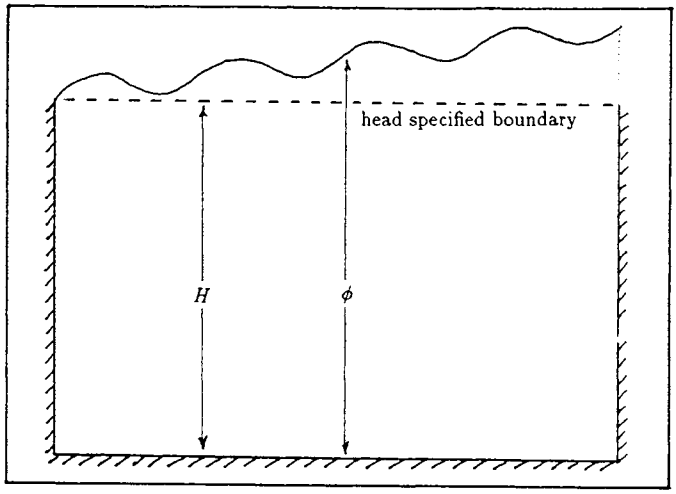

Figure 5.28: Boundary conditions for Toth's analytical solution to approximate regional flow.

ary, at which a piezometric head distribution is imposed that is derived from a hummocky topography. The vertical no-flow boundaries represent symmetry planes for a flow problem that extends well beyond the aquifer section depicted in Figure 5.28. The oscillating piezometric head is applied to the horizontal upper boundary of the rectangular flow domain. Since the aquifer thickness H is large as compared to the piezometric head (water table) fluctuations, the conceptual model in Figure 5.28 is an acceptable representation of the intended unconfined flow problem.

The analytic solution produces equipotential surfaces (lines in the two-dimensional cross-section) which are reproduced in Figure 5.29. The streamlines in Figure 5.29 are sketched in as lines perpendicular to the equipotentials. The flow patterns exhibit local shallow flow systems as well as large-scale, deeper flow systems. Toth carried out his analyses for various aquifer configurations and concluded that regional flow is, in general, characterized by three types of flow: regional, intermediate, and local flow systems (see Figure 5.30). Vertical flow is apparent in all of these systems, regardless of the scale. Others have expanded on this work (Freeze and Witherspoon, 1967), and it is generally accepted as defining the basic concepts of "regional flow" (Freeze and Cherry, 1979). The diagram in Figure 5.30, therefore, is largely responsible for the perception that vertical flow plays an important role in regional groundwater flow systems, seemingly discrediting the Dupuit-Forchheimer approximation to regional flow.

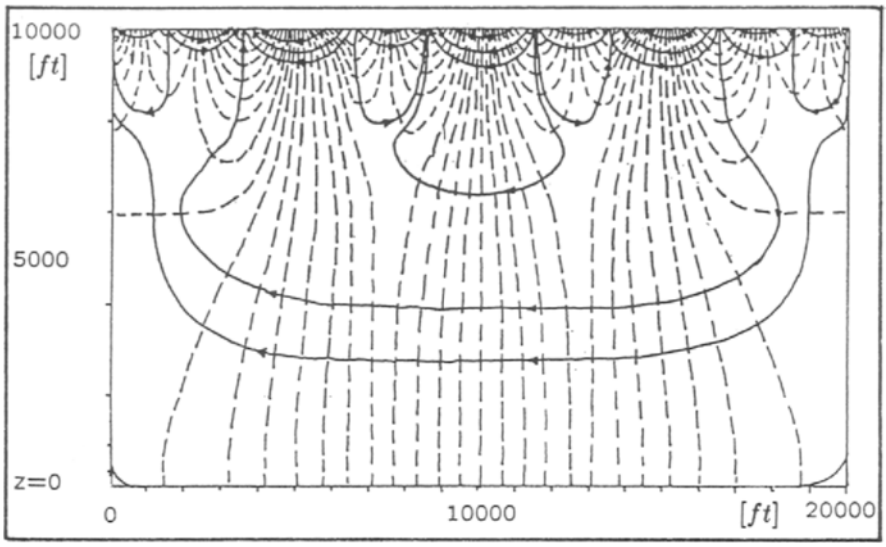

Figure 5.29: Equipotentials and streamlines in a deep regional aquifer as presented by Toth. (After Toth, 1963.)

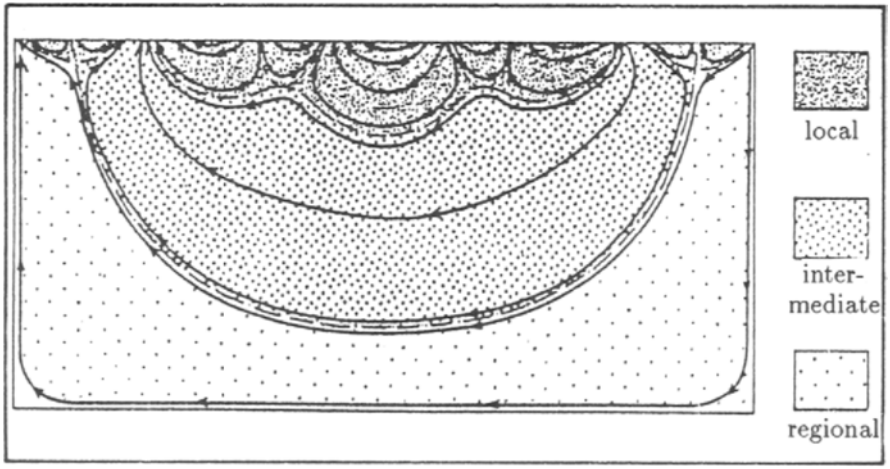

Figure 5.30: Toth's perception of regional, intermediate, and local flow. (After Toth, 1963.)

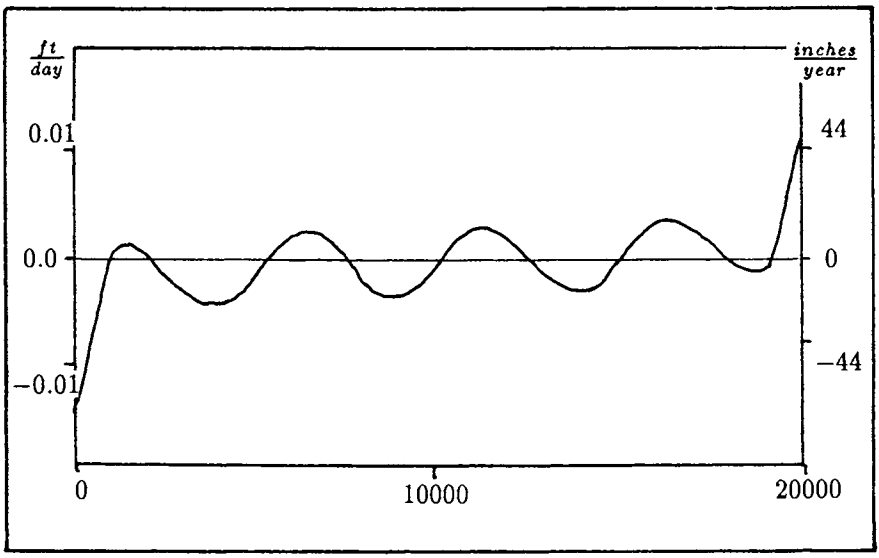

Figure 5.31: Recharge distribution for Toth's solution to regional flow for the case of $k = 0.06$ ft/day. (After Mitchell-Bruker, 1993.)

There are, however, three underlying assumptions in Toth's work which make it unsuitable for application to the type of groundwater flow systems we are concentrating on in this text: Usable aquifers from a water resources perspective. These assumptions are:

1. The depth and lateral extent of the aquifer are of the same order of magnitude.

2. The water table is controlled by the topography.

3. The aquifer hydraulic conductivity is relatively low.

The last assumption, a low hydraulic conductivity, is not explicitly stated in Toth's work, but appears necessary in order to allow for the solution presented in Figure 5.29 (see Mitchell-Bruker, 1993). Mitchell-Bruker (1993) showed that the aquifer recharge rate for Toth's solution oscillates in phase with the water table and the topography; see Figure 5.31. It is positive at topographical highs and negative at topographical lows. The extreme recharge rates can only be realized, however, for a relatively low aquifer hydraulic conductivity, less than 0.1 feet per day. For larger hydraulic conductivities, the recharge rate would exceed the available (average yearly) rainfall. An aquifer with such a low hydraulic conductivity is usually of

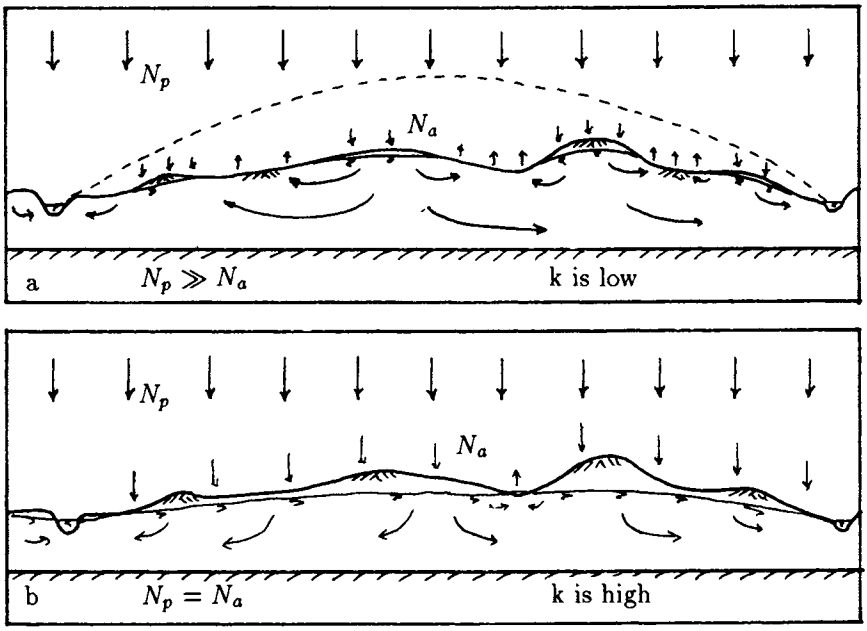

Figure 5.32: Low permeable aquifer with a topography controlled water table (a) and highly permeable aquifer with a recharge controlled water table (b).

little interest as a groundwater resource; it is not a "usable aquifer" from a regulatory perspective.

The difference between regional flow in a low permeable aquifer (say $<$ 1ft/day) versus that in a highly permeable aquifer (say $>$ 10ft/day) is illustrated in Figure 5.32. The only difference between the aquifers in Figures 5.32a and b is the hydraulic conductivity. If the potential recharge rate N_p could be infiltrated into the low permeable aquifer, the resulting water table would be the dashed line; see Figure 5.32a. The actual water table, however, is controlled by the topography, leading to a varying actual recharge rate N_a, which is positive at topographical highs and negative at topographical lows. The negative recharge rates (discharges) in the low permeable soils are in most areas small enough to be removed by evapotranspiration, rather than forming perennial surface waters.

In Figure 5.32b, where the hydraulic conductivity is high, the water table due to the potential recharge rate N_p remains below the terrain surface. In this case the actual recharge rate N_a equals the potential recharge rate N_p. Discharge of the relatively high infiltration rate N_p occurs mostly

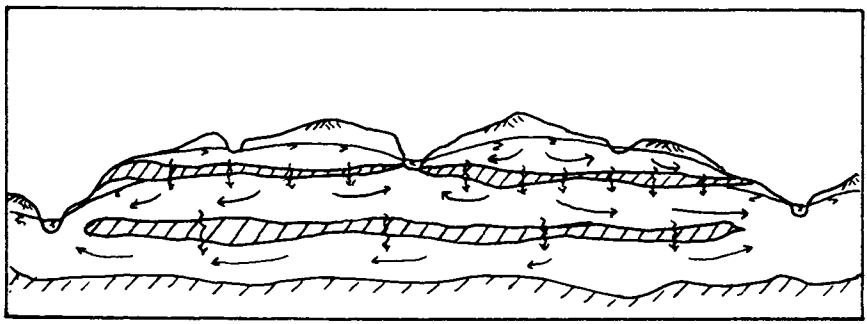

Figure 5.33: Regional, intermediate, and local flow occurring in different aquifers, each exhibiting Dupuit–Forchheimer flow.

in perennial or ephemeral surface waters, two streams and a wetland in Figure 5.32b.

Rule 5.5 *In low permeable aquifers (clayey till), the groundwater table may closely follow the topography, while in highly permeable aquifers (sand and gravel) it is controlled by areal recharge and the presence of surface waters.*

When discussing regional flow, therefore, it is important to distinguish between the "usable aquifers," which are relatively permeable and shallow, and the deep aquifer basins which on average have a relatively low permeability. In a general sense, however, Toth's concepts of regional, intermediate, and local flow remain valid for the case of stacked highly permeable aquifers. The different flow systems, however, will usually occur in different aquifers, as illustrated in Figure 5.33. The upper shallow aquifer in Figure 5.33 exhibits local flow. The aquifer below that supports mostly intermediate flow, while further down flow occurs only between major streams on a large regional scale. Each of the aquifers, however, exhibits Dupuit–Forchheimer flow. Flow systems like the one in Figure 5.33 can be modeled effectively by *multi-aquifer* models, which are also called *quasi three-dimensional* models.

A last comment on topographically controlled water tables. A highly permeable regional aquifer may be overlain by a less permeable till formation. In such formations many local *perched* groundwater flow systems may occur. This is illustrated in Figure 5.34, where the till is envisioned as a mixture of silt and fine sand with many clay lenses. Shallow piezometers will tap these perched groundwater flow systems; see Figure 5.34. These many perched water tables may be mistaken for the regional groundwater table, which has lead to the widespread belief that the concept of topogra-

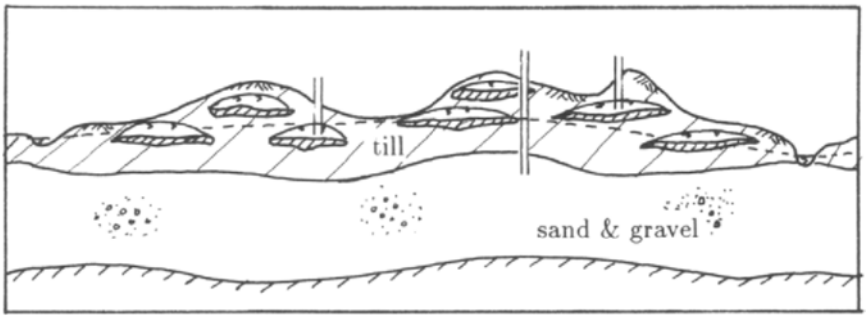

Figure 5.34: Perched water tables controlled by topography and regional piezometric surface controlled by recharge and surface waters.

phy controlled water tables is universally true. However, the actual *regional* "water table" (more accurately: piezometric surface), which is exhibited in deeper piezometers (Figure 5.34), does not follow the topography, but is controlled by the areal recharge and the presence of surface waters, as in Figure 5.32b.

Conclusion

Three-dimensional effects appear to be significant only within one or two aquifer thicknesses from a three-dimensional feature (Figure 5.22). If the three-dimensional feature is a recharge area that is many times the aquifer thickness in size, three-dimensional effects are only significant within one or two aquifer thicknesses from a stagnation point, and only when it occurs underneath that area (Figure 5.26). Consequently, in highly permeable regional aquifers, with surface waters being many aquifer thicknesses apart, groundwater flow can be adequately described with a Dupuit–Forchheimer model. When the distance between boundary conditions is close compared to the aquifer thickness, however, a three-dimensional solution may be needed (see Figure 5.29).

5.3.5 Homogeneous versus Heterogeneous Aquifers

Homogeneous aquifers do not exist, period. Even aquifers that consist of seemingly uniform sand will show both stratification and lateral variations in composition, which will cause the hydraulic conductivity to vary in all directions. The geological processes that created the subsurface formations

which make up our aquifers and separating aquitards or aquicludes are extremely varied. Some parts of an aquifer are wind-blown deposits; others are settlements of slow- or fast-flowing surface waters. Advancing and retreating glaciers, changing riverbeds, etc., all contribute to variations in aquifer materials and structure, which in turn result in significant changes in hydraulic conductivity, often of several factors.

In Section 5.3.3 I discussed the impracticality of trying to represent the actual complex geology in our mathematical models. I justified the schematization illustrated in Figure 5.19 by pointing out that we generally lack the field data to recreate reality in full detail, and even if we could, it would be impractical to implement it all in a mathematical model. Most importantly, I argued in Section 5.3.3 that there is little need to include all aquifer inhomogeneities, since their impact on the piezometric head distribution is negligible, at least on a regional scale. And herein lies the catch! Locally, aquifer heterogeneities will definitely manifest themselves, so at what scale can we ignore them?

In this section we will take a closer look at the impact of variations in conductivity on our groundwater flow solutions. I will distinguish between two kinds of aquifer heterogeneities: vertical variations in conductivity (aquifer stratification) and lateral variations in conductivity.

Stratified Aquifers

In Section 3.4.2 we learned that vertical variations in hydraulic conductivity can be incorporated in a Dupuit-Forchheimer model by use of Girinski (1946) potentials. For stratified aquifers, which contain layers with different but constant hydraulic conductivity, a set of discharge potentials can be defined, one for each layer, which, added together, form the comprehensive discharge potential for the stratified aquifer; see Section 3.4.2.

Under confined flow conditions, the piezometric head distribution will be the same, regardless of whether we represent the aquifer as stratified or homogeneous, provided that the homogeneous aquifer has an average hydraulic conductivity as defined by (3.268):

$$k = \frac{\sum_{i=1}^{5} k_i H_i}{\sum_{i=1}^{5} H_i} \tag{5.72}$$

where $k_i H_i$ is the transmissivity of the ith layer. In *unconfined* aquifers, however, the piezometric head distributions in homogeneous and stratified aquifers differ. In Figure 5.35, the flow problem of Figure 3.16 has been reproduced, except that the discharges of the two wells have been increased and the aquifer height has been raised from 50 ft to 60 ft in order to create

larger drawdowns near the wells. The aquifer in Figure 5.35 has two layers: a 40-foot thick layer with a hydraulic conductivity of 70 ft/day and above that a 20-foot thick layer with a hydraulic conductivity of 10 ft/day. If fully saturated, the transmissivity of the aquifer is $40 \times 70 + 20 \times 10 = 3000$ ft^2/day. The dotted piezometric contour lines in Figure 5.35 are produced by GFLOW1 in a homogeneous aquifer 60 feet thick and with a hydraulic conductivity of 50 ft/day, which results in the same transmissivity as for the stratified aquifer ($60 \times 50 = 3000$ ft^2/day), provided the aquifer is fully saturated. The solid contour lines in Figure 5.35 are produced by SLAEMS[2], which includes the stratification discussed earlier. The differences between the piezometric head distributions in GFLOW1 and SLAEMS are the result of different transmissivities in the two models due to unconfined flow conditions. The dropping water table near the wells reduces the saturated thickness and thus the transmissivity. In the homogeneous aquifer, the transmissivity is reduced proportionally to the reduction in saturated thickness. In the stratified aquifer, however, the upper 20 feet of the aquifer has a relatively low hydraulic conductivity, resulting in only a small reduction in transmissivity when the water table is lowered in that zone. Only when the water table is lowered into the bottom 40 feet of the aquifer, where the hydraulic conductivity is 70 ft/day, does the transmissivity reduction become more significant.

In Figure 5.36 the same situation is depicted as in Figure 5.35, except that the aquifer in Figure 5.36 has six layers each 10 feet thick, and with hydraulic conductivities of, from bottom to top, 10, 80, 10, 110, 30, and 60 ft/day, respectively. This stratification represents the maximum contrast in hydraulic conductivities (10/110) that should be attempted in a Dupuit–Forchheimer model. In fact, it is advisable to keep the contrast in conductivities below a factor of 10. When larger differences in hydraulic conductivities are encountered, the strata should be modeled as multiple aquifers. The transmissivity for the aquifer, when fully saturated, equals 3000 ft^2/day. Again, the solid lines are the piezometric contours in the stratified aquifer, while the dotted lines represent the contours in the homogeneous aquifer using the same *average* hydraulic conductivity of 50 ft/day. Notice, that the differences between the head distributions are much less for this case of six layers than for the two-layer case; compare Figure 5.35 with Figure 5.36. The largest differences occur near the wells, where the drawdowns are the largest.

It seems that aquifer stratification in unconfined aquifers does affect the piezometric head distributions, in particular where large drawdowns occur. However, when the stratification is sufficiently random, and when the av-

[2]SLAEMS is a trademark of Strack Consulting, Inc.

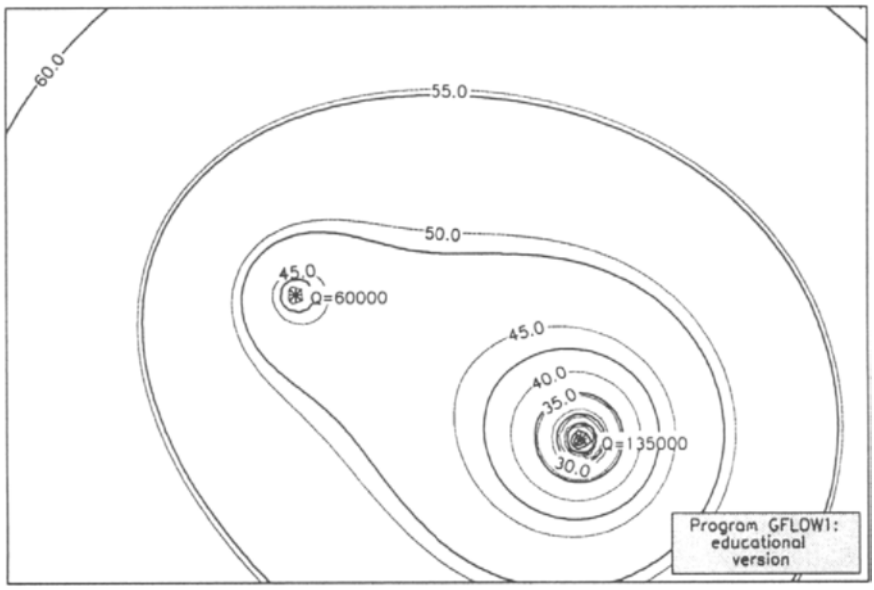

Figure 5.35: Head contours near two wells in a homogeneous aquifer (dotted lines) and in a stratified aquifer (solid lines) with *two layers*.

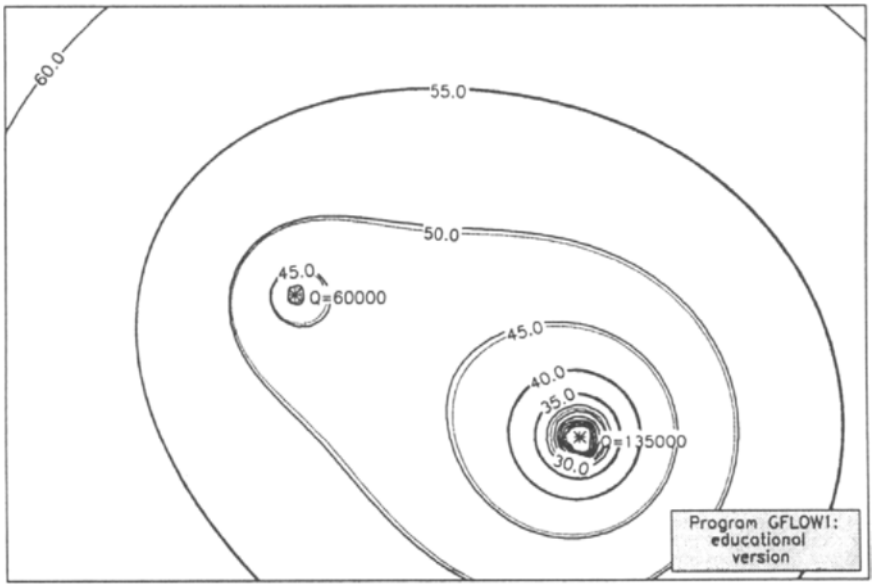

Figure 5.36: Head contours near two wells in a homogeneous aquifer (dotted lines) and in a stratified aquifer (solid lines) with *six layers*.

erage transmissivity in the homogeneous aquifer is chosen sufficiently close to the (average) transmissivity of the stratified aquifer, the homogeneous aquifer representation will yield fairly accurate solutions in terms of the piezometric head, and thus in terms of the discharges.

Rule 5.6 *When solving for piezometric heads, aquifer stratification may be ignored as long as the groundwater flow is confined. Under unconfined flow conditions, however, ignoring stratification will lead to some differences in piezometric heads, mostly in areas of large drawdowns.*

Uncertainty in Groundwater Flow Velocities

As explained in Section 3.4.2, the specific discharge at a particular location is directly proportional to the hydraulic conductivity in each stratum, and hence varies with depth (see Figure 3.52). Consequently, the groundwater velocity will also vary with depth. Furthermore, the groundwater flow velocity is also inversely proportional to the porosity, which is also likely to be different for each stratum.

Rule 5.7 *Both the specific discharges and the groundwater flow velocities are significantly different in stratified aquifers and in homogeneous aquifers. This is true even if the transmissivities of both aquifers are the same.*

A consistent uniform stratification, throughout the model domain, is unlikely to occur. Often times, the stratifications observed in different bore holes correlate poorly, so that water particles traveling at a particular elevation in the aquifer will encounter formations of different hydraulic conductivity and porosity. In view of the often nearly random distribution of the hydraulic conductivities, it is difficult, if not impossible, to determine groundwater flow velocities accurately. Our homogeneous aquifer representation provides us with an average value at any point in the aquifer, but that velocity is probably not representative of the actual velocity at that point.

Lateral Inhomogeneities

The flow patterns in Figure 3.55 in Section 3.4.5 suggest that the effect of a lateral inhomogeneity on an existing flow field is rather local. However, that conclusion is based on only a single circular inhomogeneity in an originally uniform flow field. What will be the effect of several arbitrarily shaped inhomogeneities?

In the left-hand diagram of Figure 5.37, I reproduced Figure 3.17 in Section 3.1.10, except I moved the reference point from its position at the

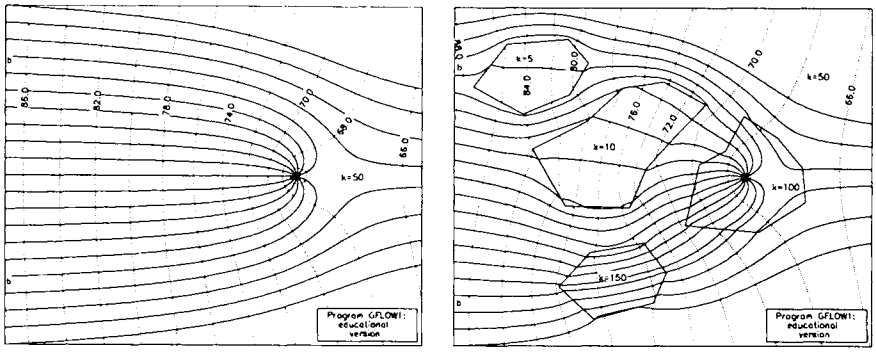

Figure 5.37: Well in a uniform flow field in a homogeneous aquifer (left) and in a heterogeneous aquifer (right).

well (see data file problem2.dat) to a distance of 1000 feet to the left of the well. In Figure 5.37, 20 streamlines were started at the left hand side of the flow domain. The streamline starting positions are spaced uniformly along the domain boundary and do not form a flow net (streamlines and equipotentials do not form squares) like that in Figure 3.17, as is apparent from Figure 5.37. In the right-hand diagram of Figure 5.37, four arbitrarily shaped domains have been added with hydraulic conductivities in the range of 5 to 150 ft/day. The background hydraulic conductivity is 50 ft/day, the same as in the left-hand diagram. One of the inhomogeneities is positioned in such a manner that it contains the well.

As may be observed from Figure 5.37, the streamlines and equipotentials in the inhomogeneous aquifer are irregular, but exhibit the same trend as those in the homogeneous aquifer. For instance, if on average the hydraulic conductivity in a heterogeneous aquifer is the same as in a homogeneous aquifer, then the average capture zone width will be the same in both aquifers, although locally they may differ. The capture zone boundaries in Figure 5.37 occur inside the streamline channels that are marked with a "b" at the left-hand boundary of the flow domain. The irregular piezometric contour lines on the right in Figure 5.37 resemble those obtained from field data, while the smooth regular contours on the left in Figure 5.37 are typical of our idealized conceptual models.

The abrupt changes in hydraulic conductivity in Figure 5.37 are an artifact of the mathematical functions used to model lateral inhomogeneities. In reality, the boundaries between the inhomogeneities may be fuzzy, exhibiting more gradual transitions in hydraulic conductivity. Although this

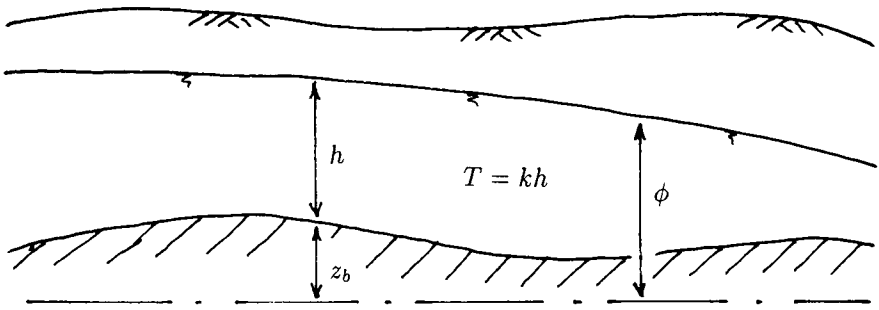

Figure 5.38: Transmissivity of unconfined aquifer depends on the elevation of the aquifer bottom.

would affect the shape of the streamlines and piezometric contours to some degree, the solution as presented in Figure 5.37 does not distract from the essential effect of lateral inhomogeneities: causing irregular contour lines and streamlines.

Variations in Aquifer Thickness and Elevation of the Aquifer Bottom

Variations in aquifer thickness have an effect similar to that of variations in hydraulic conductivity, since both affect the *transmissivity* of the aquifer. For the case of confined flow, the aquifer transmissivity T is defined as $T = kH$. Consequently, variations in aquifer thickness H have the same effect on the streamlines and equipotentials as variations in the hydraulic conductivity k. In unconfined aquifers, the transmissivity is defined as $T = kh$, where h is the saturated aquifer thickness. In Figure 5.38, h is shown to depend both on the head ϕ and aquifer bottom elevation z_b. In GFLOW1 z_b is constant, but the effect of local variations in z_b may be approximated by varying the hydraulic conductivity k instead. In general, local variations in the elevation of the aquifer bottom are much smaller than variations in hydraulic conductivity, resulting in effects on the streamlines and equipotentials less dramatic than those exhibited in Figure 5.37.

A *sloping* aquifer bottom, however, may lead to more significant variations in transmissivity that have a regional trend rather than being local and random. The impact on the streamlines and equipotentials is, therefore, more regional in nature, contrary to the local effects exhibited in Figure 5.37. In GFLOW1 the effect of a sloping aquifer bottom may be ap-

proximated by a stepwise adjustment of the hydraulic conductivity, using nested inhomogeneity domains.

The effects of lateral inhomogeneities may be summarized as follows:

Rule 5.8 *Lateral variations in transmissivity cause irregular streamlines and piezometric contours. The general trend of the flow patterns, however, is the same as for a homogeneous aquifer, provided the inhomogeneities are small compared to the size of the model domain.*

Inverse Problem

The inhomogeneities in Figure 5.37 are fictitious. Rarely are field data available to characterize the aquifer in such detail. Some computer programs will solve for hydraulic conductivities based on specified (observed) piezometric contours; these codes solve the so-called *inverse problem*. Mathematically, the problem is ill-posed (Freeze and Cherry, 1979) and can easily lead to non-unique solutions. Furthermore, we are not always certain about our "observations," either. Irregular contour lines based on observed piezometric heads should not be taken as absolute, whether they were hand-sketched by a hydrologist or produced "objectively" by statistical procedures, e.g., kriging (De Marsily, 1986). Different well screen elevations, transient effects, measurement error — all can influence the observed heads and thus the "observed piezometric contours." In any case, solving the inverse problem is difficult, requires many field data, and is still the subject of basic research.

Most consultants will not have the resources to responsibly address the inverse problem. It may be safer, therefore, to include only those inhomogeneities which are well documented, e.g., channel deposits near streams, rock outcrops, and simply *be aware* that, for instance, the solution depicted on the left in Figure 5.37 may in actuality be more like the one shown to its right. It is a good practice to experiment with a few strategically positioned inhomogeneities, in order to assess their potential impact on the groundwater flow regime. Any uncertainties arising from such experiments should be included in the conclusions of the study. Not only is such a procedure good engineering practice, it is also very educational.

5.3.6 Uniform versus Varying Aquifer Recharge

Just as there are no homogeneous aquifers, there are also no aquifers with a spatially and temporally constant recharge due to precipitation. In Section 3.2 we accounted for areal recharge (infiltration due to precipitation) by introducing a source term (N) to the governing differential equation; see (3.154). For convenience, N was assumed constant in space and

time, but in reality it depends on both. The effects of temporal variations in aquifer recharge will be discussed separately in the next section. For now, we will only consider spatial variations:

$$N = N(x, y) \tag{5.73}$$

There are a variety of factors that cause local differences in aquifer recharge, among which are the following:

- Soil conditions: Sandy soils have a larger infiltration capacity than clayey soils.
- Topographic relief: Steep slopes exhibit more surface runoff and less infiltration than moderately sloping terrain.
- Vegetation: A dense foliage intercepts and evapotranspirates much of the precipitation, leaving less for aquifer recharge.
- Density of stream network: Many streams and tributaries may increase overland runoff.

Although we may understand the effect of each of these factors individually, at least in a qualitative sense, it is less clear how they work in combination. At a few research sites, scientists have determined local infiltration rates experimentally by use of *lysimeters*. A lysimeter is a rectangular container (often made of concrete) without a lid that is dug into the ground with its rim flush with the soil surface. The container is filled with the same soil as in the surrounding area, and the vegetation inside and outside the container (lysimeter) is the same. At all times the groundwater level inside the lysimeter is kept the same as on the outside. By keeping track of the volume of water that needs to be added or removed from the lysimeter and the amount of precipitation in the area, a detailed water balance is obtained which gives accurate information on evapotranspiration and groundwater recharge rates; see Pelton (1961) and Dunne and Leopold (1978). Of course, for most groundwater flow modeling studies these data are not available, certainly not throughout the entire model domain. At best we have some estimate of the *average* recharge rate for the area, which we may then use as the basis for estimating local recharge values by considering the factors just listed.

Estimating a Regional Average Recharge Rate

The water balance concept just discussed may be applied to an entire watershed, using average precipitation and average stream flow data for the

area. In this manner, average areal recharge rates for the entire watershed can be estimated from average base flow rates in the stream network. Stream flow data are obtained from a USGS gauging station downstream from the watershed, assuming one is available, while hydrograph separation techniques can be used to obtain average base flow, e.g., Kim and Hawkins (1989).

In Section 3.2 I demonstrated that groundwater mounding in an aquifer, given a particular set of head-specified boundary conditions, is dependent on the ratio N/T, where N is the recharge rate and T the (average) aquifer transmissivity. Hence, comparisons of modeled with observed piezometric head distributions may yield an estimate for N/T. If N has been determined separately, e.g., from a base flow analysis, the average transmissivity in the (ground)watershed is found. Alternatively, if the average transmissivity in the watershed is known, e.g., from pumping tests, the modeled N/T ratio provides us with an estimate of the areal recharge rate N.

Effects of Spatially Varying Recharge

It is good practice to start a modeling project with a uniform recharge rate over the entire model area. A simple way of introducing this uniform recharge rate in GFLOW1 is to position a sink disc with a negative strength (making it a source disc) over the model area, see Figure 5.16 and the file demo.dat. Occasionally, a contrast in areal recharge is obvious and may be introduced at the outset of the modeling. For instance, consider the channel deposits surrounding the river in the center of Figure 5.16. These sandy to gravelly soils form relatively flat flood planes near the river and infiltrate significantly more water than the more clayey soils in the rest of the watershed. In the data file demo.dat, the inhomogeneity area that models the nearfield portion of the channel deposits has been given an "added exfiltration rate" of -0.001 ft/day, equal to the regional value defined by the big sink disc (see Figure 5.16 and the file demo.dat). Consequently, the channel deposits in the near field have been given twice the surrounding regional recharge rate.

During later stages of the modeling, when more insight in the geohydrology is obtained, it may be desirable to further refine the recharge distribution. In GFLOW1 this may be done by introducing inhomogeneity domains with the same hydraulic conductivity as the surrounding domain (and hence no jump in the conductivity), but with an "added exfiltration rate." However, before engaging in extensive efforts to vary the areal recharge in the model, it is advisable to first assess the importance of these refinements in view of the modeling objectives. Variations in recharge rates will certainly influence the groundwater flow patterns locally, on the scale at which these

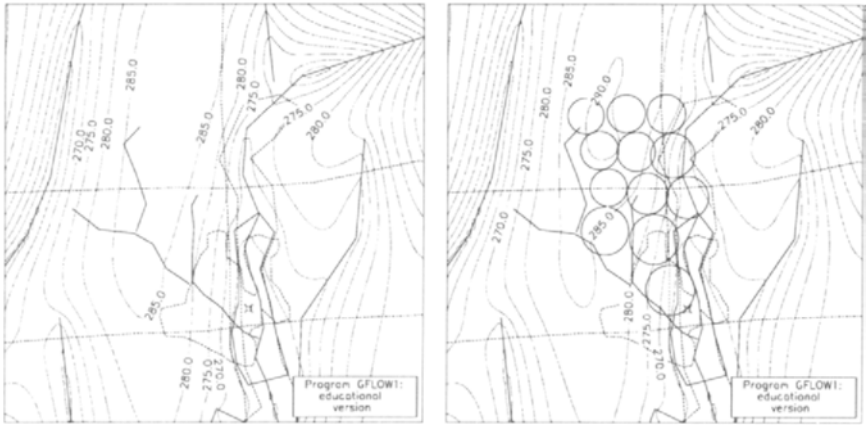

Figure 5.39: Regional piezometric contours for uniform recharge (left) and for varying recharge (right). (GFLOW1 data file proble54.dat)

variations are applied. On a larger scale, however, these recharge variations may become less important. Even when the actual recharge variations are unknown (which is the rule rather than the exception), some conceptual modeling of hypothetical recharge variations may help in deciding whether further refinements are necessary or not.

To illustrate this, I distributed 12 sink discs in the nearfield of the groundwater flow problem defined by the data file demo.dat; see the right-hand diagram in Figure 5.39. Half of the sink discs have been given a negative recharge rate, equal to the regional rate defined by the big sink disc depicted in Figure 5.16, and the other half was given the same recharge rate as the regional average. Consequently, underneath half of the discs the recharge is zero, while underneath the other half the recharge is double the regional value. In this way the total recharge has not been altered by the sink discs, but the distribution of recharge has been changed drastically and abruptly. As may be seen from Figure 5.39, on a regional scale, the general trend of the piezometric contours remains the same, although there are some differences. In Figure 5.40, a close-up is shown of the area in which the recharge is varied. On this local scale, the piezometric contours are more clearly affected by the recharge variations!

The recharge variations generated by the 12 sink discs do not, of course, represent some real-world situation. They are just an example of *conceptual* modeling to determine the possible effects of spatial variations in recharge. Depending on the purpose and scale of the modeling, different conceptual-

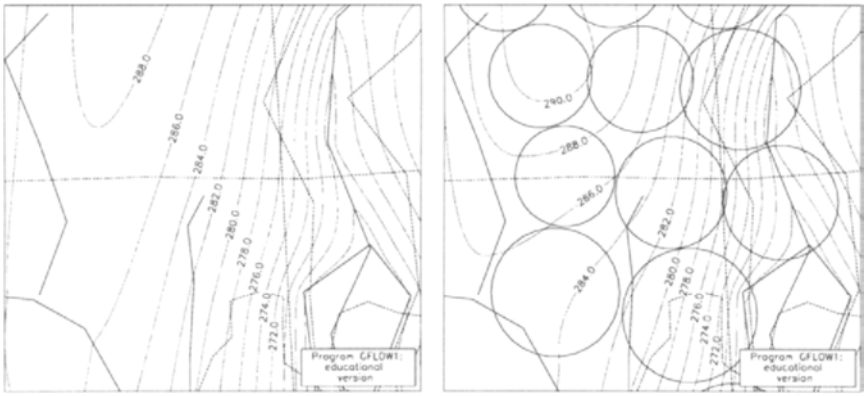

Figure 5.40: Local piezometric contours for uniform recharge (left) and for varying recharge (right). (GFLOW1 data file proble54.dat)

izations of recharge variations may have to be tested. Based on the results, additional refinements in recharge distribution may be called for, or the current (uniform) distribution may suffice. As for the example depicted in Figure 5.40, it seems that near the river, on the right-hand side of the contour plots, not much has changed as a result of the recharge variations. However, more to the left, near the water divide, both the heads and the directions of flow are noticeably affected.

5.3.7 Transient versus Steady-State Flow

With the exception of Section 3.6, all our groundwater flow modeling discussions have focused on steady-state flow, which rarely, if ever, occurs in nature. Precipitation, for instance, is far from constant over the year. In temperate climate regions in the U.S., most of the precipitation takes place during the winter, while the summers are relatively dry. The resulting aquifer recharge often peaks in the early spring and reaches a seasonal low in the late summer or early fall. These variations in precipitation and aquifer recharge cause variations in stream flow (and surface water elevations) and generate seasonal variations in piezometric heads.

So what is the rationale for *steady-state* groundwater flow modeling? It is usually argued that steady-state solutions represent *average* conditions for the year, or for several years. However, there are (at least) two concerns with our steady-state modeling of transient flow systems. In the first place, observed piezometric heads are not equal to steady-state heads, but,

depending on the time of measurement, may be larger or smaller. This, of course, greatly complicates our calibration efforts. In comparing model heads with observed heads, we have to allow for these transient variations in field data, about which we may or may not have any information. A second problem is how to interpret our model predictions. Flow patterns and piezometric heads reflect average conditions, but how meaningful are they in view of the actual transient flow patterns and heads?

In order to gain some insight into these issues, we will investigate which factors (parameters) are determining transient effects and in what way. In doing so we may distinguish between two types of transient problems:

1. Initial boundary-value problems.
2. Periodic responses to periodic forcing functions, e.g., seasonal recharge variations.

Initial Boundary Value Problems

An example of a solution to an initial boundary-value problem is Theis' solution (3.332) discussed in Section 3.6.2:

$$\Phi(r,t) = -\frac{Q}{4\pi} E_1(u) + \Phi_0 \qquad (t > t_0) \tag{5.74}$$

Theis' solution provides the response to a well which starts pumping at a time t_0. Theis' solution depends on the dimensionless parameter u, defined by (3.333), and rewritten here in the form

$$4u = \frac{Sr^2}{T(t - t_0)} \tag{5.75}$$

where S_s has been replaced by $S/\bar{\phi}$ [see (3.329)], and where $T = k\bar{\phi}$ is the (average) aquifer transmissivity. The dimensionless parameter S is the aquifer storage coefficient, and the parameter $\bar{\phi}$ represents the average saturated aquifer thickness. For the case of confined flow, $\bar{\phi}$ is equal to the aquifer height H. In addition to the factor (5.75), Theis' solution, like any other solution to an initial boundary-value problem, depends on the initial conditions -- for the case of our transient well, the constant potential Φ_0 in (5.74). In fact, for small times since the onset of pumping, the heads and flow patterns in the aquifer are dominated by the initial conditions, except in the immediate vicinity of the well [small r in (5.75))]. What constitutes a small time is defined by the dimensionless factor $4u$. When t is small, u is large and the exponential integral E_1 vanishes (see Figure 3.63), so that the initial condition Φ_0 is all that remains.

This dependency on initial conditions requires much additional data: initial heads throughout the aquifer. Be aware that it is not acceptable to use observed piezometric heads as initial conditions for the model! Such a procedure would not lead to a meaningful model calibration, because the solution would mostly depend on these observed heads rather than on the boundary conditions and aquifer parameters. Instead, one should use the heads obtained from a steady-state model, which has been properly calibrated, as the initial conditions for a transient initial boundary-value problem; see Anderson and Woessner (1992) and Franke *et al.* (1987).

Rule 5.9 *Initial conditions should be derived from modeled steady state-heads, not from observed heads.*

Periodic Solutions

Townley (1995) published a set of closed-form analytic solutions to flow in one-dimensional and radial aquifers subjected to periodic forcing functions. Instead of solving an initial value problem, he assumed that the solution is already periodic, thus bypassing the problem of selecting initial conditions. Moreover, these periodic solutions are just as sensitive to the boundary conditions as steady-state solutions (see Townley, 1995), which makes them suitable for model calibration. The periodic forcing functions considered by Townley include Dirichlet and Cauchy boundary conditions (see Section 5.3.8) with sinusoidal head variations in time, and aquifer recharge which varies sinusoidally in time. Although seasonal water table variations in streams and lakes or seasonal recharge variations are not exactly sinusoidal, and although our aquifers are usually not one-dimensional or radial in shape, these solutions may still provide us with valuable insight in the transient response of aquifers to such seasonal forcing functions.

Bounding Steady-State Solutions

A common procedure to assess the possible (extreme) effects of seasonal recharge variations on the groundwater flow patterns is to compare two different steady-state solutions: one with the maximum (monthly) recharge rate and one with the minimum (monthly) recharge rate. If these solutions are not too different from each other, our steady-state solution with a yearly average recharge rate is assumed adequate. However, if significantly different solutions are obtained, it becomes less clear how to interpret the average steady-state solution. The same strategy may be applied to seasonal variations in surface water elevations. In evaluating these "bounding" steady-state solutions, the question arises: How close will the actual

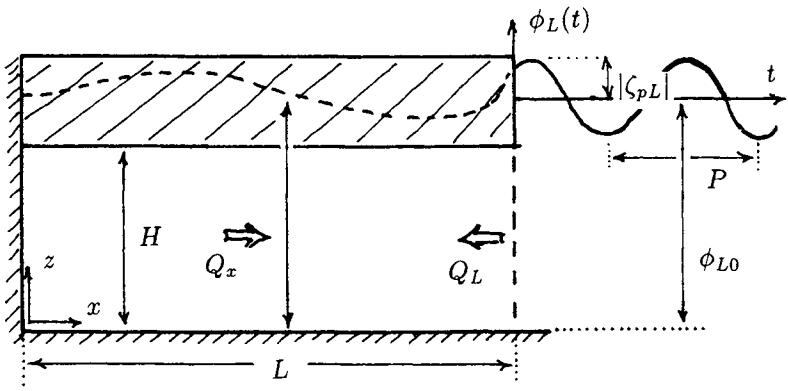

Figure 5.41: Periodic response of a one-dimensional aquifer subjected to periodic head variations at $x = L$.

transient heads and discharges in the aquifer come to these steady-state extremes?

Next I summarize the results of two of the example problems solved by Townley: flow in a one-dimensional aquifer (1) due to periodic variations in the head at the aquifer boundary, and (2) due to periodic recharge variations. These periodic solutions are compared to steady-state solutions for extreme heads at the boundary or extreme recharge rates. The objective of this comparison is to gain insight into the parameters that control these transient effects, and to assess when our bounding steady-state solutions are useful and when not.

Periodic Variations in Head at the Aquifer Boundary

In Figure 5.41, a cross-section is depicted over a one-dimensional aquifer of length L and hydraulic conductivity k. The left-hand boundary is a no-flow boundary, while the right-hand boundary is head-specified with $\phi_L(t)$:

$$\phi_L(t) = \phi_{L0} + \Delta\phi_L \cos(\omega t + \theta_p) \tag{5.76}$$

where ϕ_{L0} and $\Delta\phi_L$ are the average head and head amplitude at the boundary $x = L$, respectively. The argument of the cosine defines the period and phase of the head fluctuations:

$$\omega = \frac{2\pi}{P} \tag{5.77}$$

where P [days] is the period. For seasonal fluctuations, $P = 365$ [days]. The phase angle θ_p defines when the maximum head occurs — e.g., for $\theta_p = 0$,

the maximum head occurs at $t = 0$, 365, 730, etc., while for $\theta_p = -\pi/2$ the maximum head occurs at $t = 91.25$, 456.25, 821.25, etc. Townley simplified the mathematics by combining information on both the magnitude and phase of the periodic head variations in a single complex variable. The head $\phi(x,t)$ in the aquifer is then written as

$$\phi(x,t) = \phi_0(x) + \Re\{\zeta_p(x)e^{i\omega t}\} \tag{5.78}$$

where $\phi_0(x)$ is the average head in the aquifer at point x, and where the real part of the complex quantity in (5.78) represents the local periodic variation of the head with respect to ϕ_0. The complex variable ζ_p is defined as

$$\zeta_p(x) = \xi(x) + i\eta(x) \tag{5.79}$$

where the amplitude $\Delta\phi$ of the head variations is given by

$$\Delta\phi(x) = |\zeta_p(x)| = \sqrt{\xi^2 + \eta^2} \tag{5.80}$$

and where the phase angle $\theta_p(x)$ is given by

$$\theta_p(x) = \arg\{\zeta_p(x)\} = \arctan\left\{\frac{\eta(x)}{\xi(x)}\right\} \tag{5.81}$$

At the boundary $x = L$, the complex head variation is prescribed: $\zeta_p(L) = \zeta_{pL}$; see Figure 5.41.

Townley (1995) developed two governing differential equations. One, for the average head $\phi_0(x)$, is simply the Laplace or Poisson equation in terms of the head ϕ, rather than in terms of the discharge potential as developed in Chapter 3. The second differential equation is for the complex variable $\zeta_p(x)$, which is given below without derivation:

$$T\frac{d^2\zeta_p}{dx^2} = i\omega S\zeta_p \tag{5.82}$$

where S is the storage coefficient for the aquifer. The solution to (5.82), subject to the boundary conditions

$$\frac{d\zeta_p(0)}{dx} = 0 \quad \text{and} \quad \zeta_p(L) = \zeta_{pL} \tag{5.83}$$

is given by (Townley, 1995)

$$\zeta_p = \zeta_{pL}\left(\frac{\cosh(bx/L)}{\cosh(b)}\right) \tag{5.84}$$

where the complex constant b is given by

$$b^2 = 2\pi i \frac{SL^2}{TP} \tag{5.85}$$

The complete solution is defined by (5.78) with (5.84):

$$\phi(x,t) = \phi_{L0} + \Re\left\{\zeta_{pL}\left(\frac{\cosh(bx/L)}{\cosh(b)}\right)e^{i\omega t}\right\} \tag{5.86}$$

Observe from (5.86) and (5.85) that the transient periodic solution depends on the factor SL^2/TP, which is quite similar to the factor $4u$ for Theis' solution; as defined in (5.75). The aquifer length L takes the place of the distance r from the well, and the period P replaces the time $(t - t_0)$ since the onset of pumping.

For this simple case, the steady-state solution is a constant head in the aquifer equal to the head at the boundary $x = L$. In order to compare the transient solution (5.86) to the bounding steady-state solutions (corresponding to the maximum and minimum head at $x = L$), the amplitude $|\zeta_p(x)|$ of the head in the aquifer is compared to the amplitude $|\zeta_{pL}|$ of the head at $x = L$. This comparison is represented graphically in Figure 5.42, where $|\zeta_p|/|\zeta_{pL}|$ is plotted versus x/L for various values of SL^2/TP. The ratio $|\zeta_p|/|\zeta_{pL}|$ follows from (5.86) as

$$\frac{|\zeta_p(x)|}{|\zeta_{pL}|} = \left|\frac{\cosh(bx/L)}{\cosh(b)}\right| \tag{5.87}$$

At any point in the aquifer, we can calculate the phase angle θ_p of the periodic head variations from (5.81) with (5.84),

$$\theta_p(x) = \arg\{\zeta_p(x)\} \tag{5.88}$$

Townley (1995) presents the *phase lag* $\Delta\theta_p$, the difference between the phase angle $\theta_p(x)$ and the phase angle of the prescribed head fluctuations at $x = L$:

$$\Delta\theta_p = \arg\{\zeta_p\} - \arg\{\zeta_{pL}\} = \arg\{\frac{\zeta_p}{\zeta_{pL}}\} = \arg\left\{\frac{\cosh(bx/L)}{\cosh(b)}\right\} \tag{5.89}$$

Following Townley (1995) the phase lag $\Delta\theta_p$ may be expressed in terms of a fraction λ of the period P, whereby λ is defined as

$$\begin{aligned} \lambda &= 1 - \frac{\Delta\theta_p}{2\pi} \quad (0 \le \Delta\theta_p \le \pi) \\ \lambda &= -\frac{\Delta\theta_p}{2\pi} \quad (-\pi \le \Delta\theta_p \le 0) \end{aligned} \tag{5.90}$$

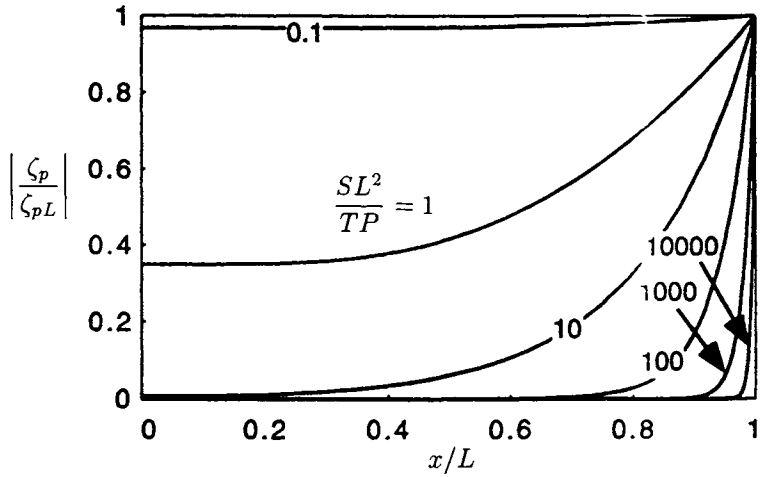

Figure 5.42: Transient head extremes as a fraction of steady-state head extremes in a one-dimensional aquifer subjected to periodic head variations at $x = L$. (After Townley, 1995.)[1]

The *phase lag time* is then defined as λP. In Figure 5.43, the phase lag parameter λ has been plotted versus x/L for various values of the factor SL^2/TP.

The aquifer inflow Q_L is defined as

$$Q_L = \Re\left\{\gamma_p e^{i\omega t}\right\} \tag{5.91}$$

where the complex parameter γ_p represents both the magnitude and the phase of the aquifer inflow variations at $x = L$. γ_p is given as (Townley, 1995)

$$\gamma_p = T\frac{\zeta_{pL}}{L} b \tanh(b) \tag{5.92}$$

or, in dimensionless form,

$$\frac{\gamma_p L}{\zeta_p T} = b \tanh(b) \tag{5.93}$$

In Figure 5.44, the dimensionless inflow $\tilde{Q}_L$, defined as

$$\tilde{Q}_L = \Re\left\{\frac{\gamma_p L}{\zeta_p T} e^{i\omega t}\right\} \tag{5.94}$$

is plotted versus x/L for various values of SL^2/TP.

[1]Figures 5.42 through 5.44 and Figures 5.47 and 5.48 are reprinted from *Advances in Water Resources*, 18(3), Lloyd Townley, "The Response of Aquifers to Periodic Forcing", pp 125 - 146, Copyright 1995, with kind permission from Elsevier Science Ltd, The Boulevard, Langford Lane, Kidlington OX5 1GB, UK.

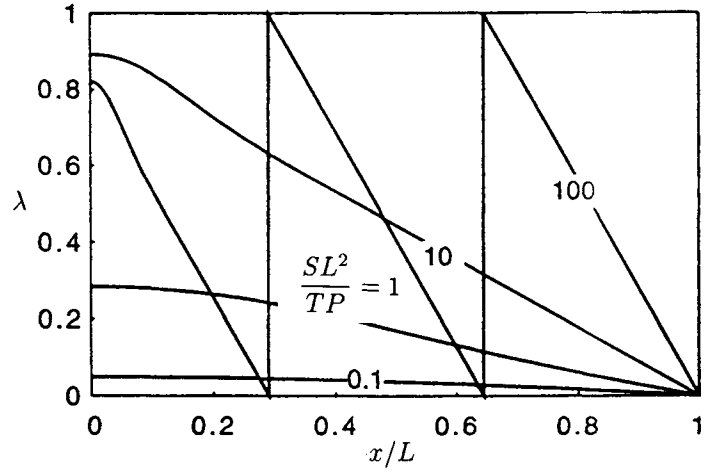

Figure 5.43: Phase lag λ, between the head in the aquifer and the head at the boundary, in a one-dimensional aquifer subjected to periodic head variations at $x = L$. (After Townley, 1995.)

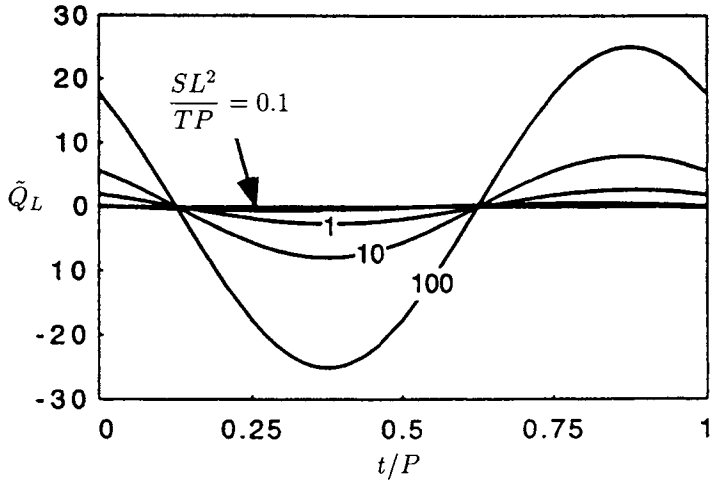

Figure 5.44: Dimensionless aquifer inflow $\tilde{Q}_L$ at $x = L$ as a function of time for the case of a periodic head at $x = L$. (After Townley, 1995.)

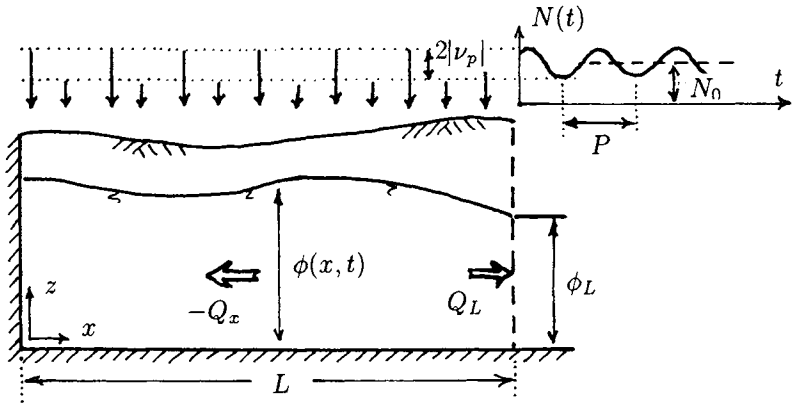

Figure 5.45: Periodic response of a one-dimensional aquifer subjected to periodic recharge variations.

Periodic Recharge Variations

In Figure 5.45, an unconfined aquifer is depicted, with a no-flow boundary at $x = 0$ and a constant head ϕ_L at $x = L$. The recharge N on the aquifer varies periodically as

$$N(t) = N_0 + \Re\left\{\nu_p e^{i\omega t}\right\} \tag{5.95}$$

where N_0 is the yearly average recharge, and where the complex parameter ν_p represents both the amplitude and phase of the recharge variations. The differential equation in terms of the complex head variation ζ_p and the complex recharge variation ν_p is (Townley, 1995)

$$T\frac{d^2\zeta_p}{dx^2} = i\omega S\zeta_p - \nu_p \tag{5.96}$$

The solution for ζ_p is (Townley, 1995)

$$\zeta_p = \frac{\nu_p}{i\omega S}\left[1 - \frac{\cosh(bx/L)}{\cosh(b)}\right] \tag{5.97}$$

The head $\phi_0(x)$ for the steady-state solution is a quadratic function in x [see (3.165)], which satisfies the no-flow condition ($d\phi_0/dx = 0$) at $x = 0$ and the prescribed head ϕ_L at $x = L$:

$$\phi_0(x) = \frac{N_0}{2T}(L^2 - x^2) \tag{5.98}$$

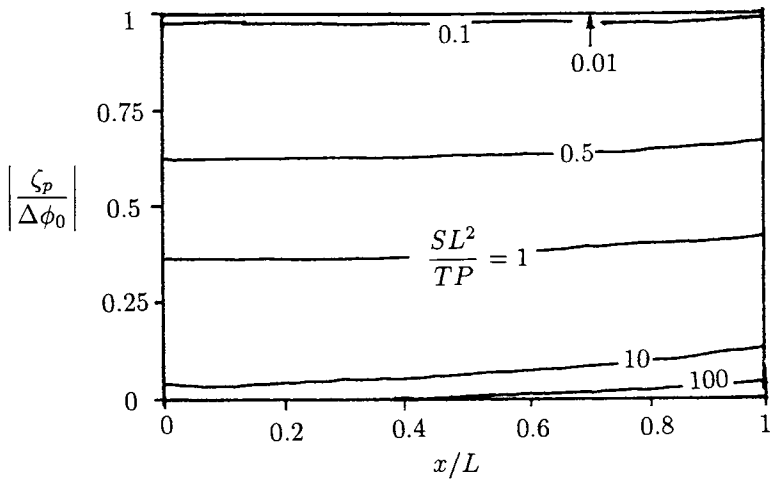

Figure 5.46: Transient head extremes as a fraction of steady-state head extremes in a one-dimensional aquifer subjected to periodic recharge variations.

I define $\Delta\phi_0(x)$ as half the difference in head between the steady-state solution with a maximum recharge rate $(N_0 + |\nu_p|)$ and with a minimum recharge rate $(N_0 - |\nu_p|)$. This yields, by use of (5.98),

$$\Delta\phi_0(x) = \frac{|\nu_p|L^2}{2T}[1 - (x/L)^2] \tag{5.99}$$

In Figure 5.46, the ratio $|\zeta_p|/|\Delta\phi_0|$ has been plotted versus x/L for various values of SL^2/TP.

In Figure 5.47, the dimensionless phase lag parameter λ for this case has been plotted versus x/L for various values of SL^2/TP.

The transient discharge (outflow) at the aquifer boundary $x = L$ is compared to the bounding steady-state outflows as follows. If the transient recharge variations would lead to instantaneous steady flow (storage coefficient equal to zero), the outflow Q_{L0} at $x = L$ would be

$$Q_{L0}(t) = N_0 L + \Re\left\{\nu_p L\, e^{i\omega t}\right\} \tag{5.100}$$

which is simply the total recharge that falls on the aquifer. The actual transient outflow Q_L is given by (see Townley, 1995)

$$Q_L(t) = N_0 L + \Re\left\{\nu_p L \left[\frac{\tanh(b)}{b}\right] e^{i\omega t}\right\} \tag{5.101}$$

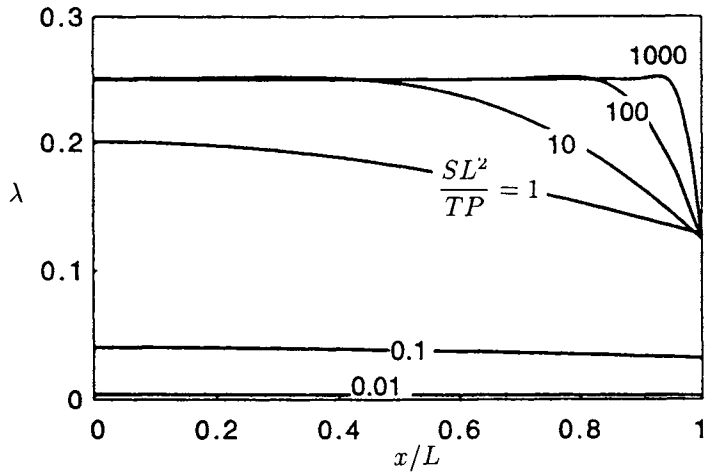

Figure 5.47: Phase lag λ, between the head in the aquifer and the recharge, in a one-dimensional aquifer subjected to periodic recharge variations. (After Townley, 1995.)

In Figure 5.48, the actual transient outflow Q_L is compared to the instantaneous outflow Q_{L0} by plotting the dimensionless parameter $\tilde{Q}_L$,

$$\tilde{Q}_L = \Re\left\{\frac{\nu_p L\left[\frac{\tanh(b)}{b}\right]}{\nu_p L} e^{i\omega t}\right\} = \Re\left\{\frac{\tanh(b)}{b} e^{i\omega t}\right\} \tag{5.102}$$

versus x/L for various values of SL^2/TP.

Interpretation of Results

The diagrams in Figures 5.42 through 5.44 and 5.46 through 5.48 exhibit a consistent pattern when distinguishing between small and large values of SL^2/TP. "Small values" are defined as $SL^2/TP \ll 1$ and "large values" as $SL^2/TP \gg 1$.

Let's first review the results for *small values* of the factor SL^2/TP. It appears from Figure 5.42 and Figure 5.46 that the extreme heads under transient conditions approach those obtained from the bounding steady-state solutions. Also, for small values of SL^2/TP, the head variations in the aquifer are more or less in phase with the head variations at the boundary; see Figures 5.43 and 5.47. Finally, for the case of Figure 5.41,

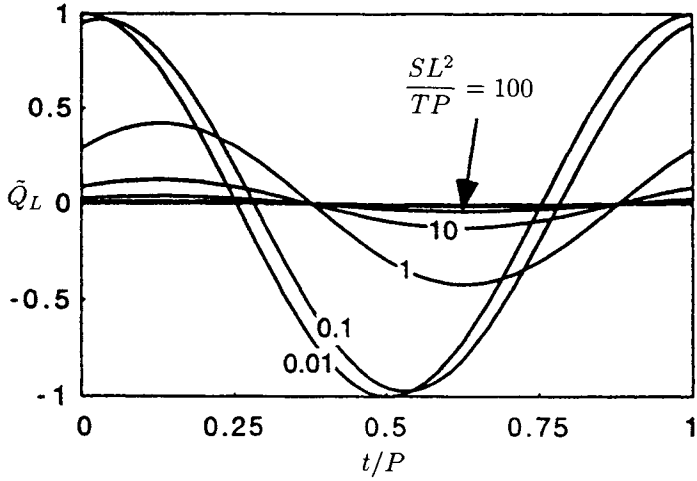

Figure 5.48: Dimensionless aquifer outflow $\tilde{Q}_L$ at $x = L$ as a function of time for the case of periodic recharge (After Townley, 1995).

the inflow at the aquifer boundary ($x = L$) is small (see Figure 5.44), which compares well with the steady-state solution for that case: no flow in the aquifer. For the case of Figure 5.45, the outflow from the aquifer, for small values of SL^2/TP, seems to be nearly equal to and in phase with the bounding steady-state solutions (assuming instantaneous steady flow for different recharge values); see Figure 5.48. In other words, for small values of SL^2/TP, the bounding steady-state solutions are a reasonable approximation of the extremes of the transient conditions in this aquifer.

This is not true for *large values* of the factor SL^2/TP! As may be seen from Figure 5.42, the head variations imposed at the aquifer boundary die out further into the aquifer. From Figure 5.43, we learn that there is also considerable phase lag between the head variations at the boundary and those at a particular point in the aquifer. And finally, for the case of Figure 5.41, we find that for large values of SL^2/TP there is, at times, some inflow and outflow at the aquifer boundary, while the steady-state solution predicts none; see Figure 5.44. Similar observations are made for the case of varying recharge. It appears from Figure 5.46 that for large values of SL^2/TP, the head variations inside the aquifer are small when compared to those due to the bounding steady-state solutions. There is again considerable phase lag (see Figure 5.47), while the aquifer outflow

is small when compared to the bounding steady-state flows and lags the recharge variations (see Figure 5.48).

In summary, when the factor SL^2/TP is large, the bounding steady-state solutions do not provide much information about the actual (transient) extreme heads and discharges in the aquifer! The only thing that may be said is that the heads in the aquifer will always remain below the extreme steady-state heads; in fact, they may not change at all in significant parts of the aquifer. On the other hand, for small values of SL^2/TP, the bounding steady-state solutions appear to be reasonable approximations of the extreme transient heads and discharges.

Practical Values for SL^2/TP

The diagrams presented earlier do not directly apply to the general case of two-dimensional flow. However, if the aquifer length L is interpreted as half the average distance between surface water features in the model domain, the trends exhibited in these diagrams may be assumed representative for our (2D) models. This possibility of generalization is also suggested by the observation that radially symmetric versions of the foregoing problems show trends very similar to those discussed earlier; see Townley (1995).

In view of this it is interesting to look at the ranges of values which the factor SL^2/TP may assume in practice. Limiting ourselves to seasonal variations, the period is 1 year: $P = 365$ [days]. The storage coefficient S may vary considerably depending on flow conditions: In unconfined aquifers, S is on the order of $S = 0.1$, while in confined aquifers, S may well be as low as $S = 0.001$. Aquifer transmissivities may also vary considerably. Deep permeable aquifers, e.g., channel deposits near a river, may have a transmissivity in the order of $T = 500,000$ [ft^2/day], while shallow till aquifers may have a transmissivity as low as $T = 100$ [ft^2/day]. For the purpose of estimating extreme values for SL^2/TP, I will assume that the half-distance L between boundary conditions varies between 500 and 5,000 [ft]. The numbers cited here do not, of course, span all possible values for these parameters, but are introduced here merely to gain some insight in the range of values we may encounter for the factor SL^2/TP. Combining these parameter values in such a manner that the smallest possible value for SL^2/TP is obtained, we get $SL^2/TP = 0.001 \times 500^2/(500,000 \times 365) = 0.00000137$. Similarly, a maximum for SL^2/TP is obtained by the following parameter combination: $SL^2/TP = 0.1 \times 5,000^2/(100 \times 365) = 68.5$. The largest values are going to be found in unconfined aquifers with a low transmissivity and distant boundary conditions. For the case of unconfined flow, I calculated three more values for SL^2/TP, using $L = 3,650$ [ft] and three

different values for the transmissivity:

$$\frac{SL^2}{TP} = \frac{0.1 \times 3,650^2}{36,500 \times 365} = 0.1$$

$$\frac{SL^2}{TP} = \frac{0.1 \times 3,650^2}{3650 \times 365} = 1.0$$

$$\frac{SL^2}{TP} = \frac{0.1 \times 3,650^2}{365 \times 365} = 10.0$$

When the same parameter values are applied to a confined aquifer, thus reducing S to 0.001, all values for SL^2/TP become equal or less than 0.1. In general terms, therefore, we may conclude that medium or low permeable unconfined aquifers exhibit local transient effects that cannot readily be approximated by bounding steady-state solutions. On the other hand, we find that:

Rule 5.10 *Highly permeable unconfined aquifers and most confined aquifers will exhibit "summer conditions" and "winter conditions" that may be approximated by steady-state solutions using recharge rates and surface water levels observed in the summer and the winter, respectively.*

5.3.8 Accuracy in Representing Boundary Conditions

Boundary conditions are a mathematical necessity for our groundwater flow problems. A "well defined" (in the mathematical sense) steady-state groundwater flow problem is defined by its governing differential equation and a *complete* set of boundary conditions. In potential theory, one distinguishes between three fundamental boundary value problems (see Bear, 1972):

1. *Dirichlet boundary value problem* or *boundary value problem of the first kind*: The head is specified along the boundary of the flow domain.

2. *Neumann boundary value problem* or *boundary value problem of the second kind*: The flux is specified along the boundary of the flow domain.

3. *Cauchy boundary value problem* or *boundary value problem of the third kind*: Both the head and the flux are specified along the domain boundary in some linear combination.

We speak of a *mixed boundary value problem* if Dirichlet conditions apply over part of the boundary and Neumann conditions apply over the remaining part. Examples of Dirichlet boundaries are streams and lakes that are fully connected to the aquifer. An example of a Neumann boundary is a discharge-specified well. In three-dimensional flow models, areal recharge due to precipitation is also a Neumann boundary condition, while in a Dupuit-Forchheimer model, the recharge is introduced as a source term in the differential equation (see Figure 3.32) and is not considered a boundary condition in the mathematical sense. An example of a Cauchy boundary is a surface water feature with resistance to flow between the surface water body and the aquifer; see Section 5.2.3.

Hydrological Versus Model Boundaries

The mathematical boundary conditions may or may not always coincide with hydrological boundaries. For instance, finite difference grids must end somewhere, forming a finite model domain. The same is true for the finite element and the classical boundary element method. When the grid boundary is chosen to coincide with a hydrological boundary (river, lake, rock outcrop, etc.), the mathematical and hydrological boundaries coincide. However, it is not always practical to extend the grid to a hydrological boundary, in which case the specified heads or specified fluxes along the grid boundary form a mathematical boundary condition, but do not represent a hydrological boundary. This may result in an incorrect representation of the flow system, even though the problem is mathematically well-defined. On the other hand, if such an "artificial boundary" is remote from the area of interest, it may have little impact on the outcome of our modeling. I discussed this matter before under the subheading "Bounded versus Unbounded Model Area" in Section 5.1.1; see also Figure 5.2. In this context it is important to note that a *groundwater divide*, as observed from piezometric contours, is *not* a hydrological boundary. Changes in model parameters, e.g., areal recharge, and pumping rates of wells, etc., may shift the water divide, but will not change, for instance, the no-flow boundary conditions along a rock outcrop. Hence, the rock outcrop is a true hydrological (no-flow) boundary, while the water divide is not. In other words, the water divide as determined from observed piezometric heads should not be used as a Neumann boundary condition, just as the observed piezometric heads themselves should not be used as Dirichlet boundary conditions. Instead, these observations should be reserved for model calibration purposes.

Rule 5.11 *Observed groundwater divides may be used for model calibration, but should* not *be used as a model boundary (no-flow boundary).*

Errors in Boundary Conditions

Rule 3.1 in Section 3.1.1 states that "Solutions to Laplace's equation, subject to Dirichlet boundary conditions, are fully determined by these boundary conditions." This rule emphasizes the dominant role of head-specified boundary conditions on our groundwater flow solutions, even though in practice we are often dealing with Poisson's equation (areal recharge) and have a mixed boundary-value problem (e.g., including discharge-specified wells). For Dirichlet boundary-value problems, governed by Laplace's equation, there is another useful theorem: the *maximum modulus theorem.* In terms of our groundwater flow problems, this theorem leads to the following rule:

Rule 5.12 *If there is no areal recharge (or leakage), both the minimum and maximum head in a domain occur at its boundaries, provided there are only head-specified boundaries.*

For a more detailed discussion and proof of the maximum modulus theorem, refer to Strack (1989). Rule 5.12 also implies that errors made in specifying the heads at the boundaries are not amplified in the interior of the flow domain. In other words, the maximum errors in the modeled heads are to be found at the boundaries. However, most of our problems are mixed boundary-value problems and are governed by Poisson's equation. Consequently, we cannot absolutely rely on the fact that the maximum errors occur at the model boundaries, although errors in boundary conditions will still dominate our model accuracy.

In representing hydrological boundaries, such as streams or lakes, in a groundwater flow model, we tend to make various kinds of errors:

1. Inaccurate representation of the surface water elevations.
2. Inaccurate representation of the stream or lake geometries.
3. Inaccurate representation of the surface water and groundwater interaction along the streams or at the lakes.

Starting with *surface water elevations*, how do we determine them? In most cases we are relying on topographic maps, usually by marking the intersections of topographic contour lines with a stream. Water levels in between those markers are estimated by interpolation. These water levels are approximate because of the limited contour resolution of the topographic map and because the actual water levels fluctuate in time based on stream flow conditions. Occasionally, in the area of interest, the modeler may possess more accurate data from direct field measurements. No matter how accurate our measurements, however, we remain confronted with the difficulty of

translating transient surface water elevations into boundary conditions for our steady-state model. It is important, therefore, to make an assessment of the possible error in the specified water levels and to keep these errors in mind when interpreting the modeling results. If these potential errors are of concern, the modeler may generate model solutions for both a low and a high estimate of the surface water elevations. In this manner a good insight is obtained into the importance of these potential errors; see Section 5.3.7. If it is not possible to improve on the surface water elevations, a choice of elevations may be used which appears conservative in view of the modeling objectives.

The second source of errors is an inaccurate representation of surface water geometries, for example, not including all stream meanders in the model. In GFLOW1 we are approximating streams by strings of straight-line elements: Line sinks. Lakes may be modeled by use of sink discs or by distributing line sinks around its perimeter. The more line sinks we use, the more accurately we are representing the stream or lake *geometry*. Modeling a stream or lake in high resolution has two advantages:

1. The geometry of the surface water is more accurately represented.
2. The variations of groundwater extraction or surface water infiltration are modeled more accurately.

We will discuss both these issues separately.

St. Venant's Principle

Errors in representing the geometry of a feature have only local implications. This may be illustrated by comparing the piezometric contours for a well and a line sink which have the same total discharge rate; see Figure 5.49. As expected, the piezometric contours near the well differ significantly from those near the line sink. However, farther away from these features the piezometric contours start to look alike. For instance, the contour lines marked 58.0 in Figure 5.49 are nearly equal for both the well and the line sink. The fact that the geometry of a feature has only a local effect is known as *St. Venant's principle* and originates from the theory of elasticity (Knowles, 1965). Of course, the total discharges must be equal (20,000 in Figure 5.49) in order for the well and line sink to behave the same at a distance.

Groundwater Inflow or Outflow along Streams

As a rule, the groundwater inflow or outflow will vary along a stream. To account for this in our analytic element model, we have to vary the strength

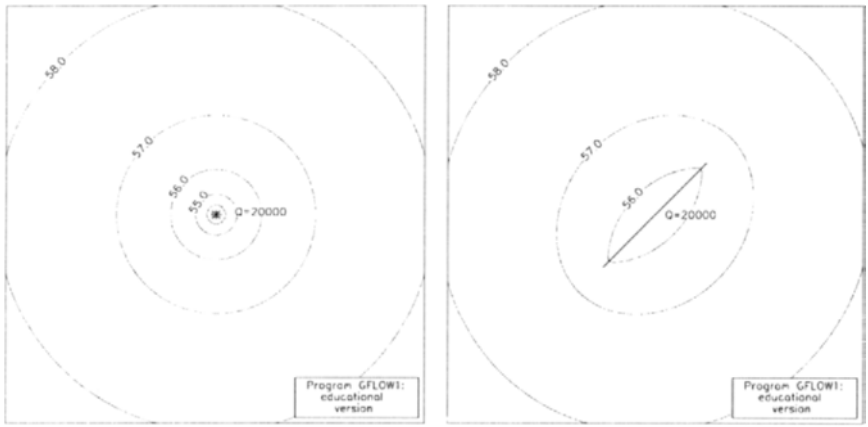

Figure 5.49: Comparing piezometric contours for a well and a line sink of equal total discharge.

distribution of the line sinks that represent the stream. In GFLOW1 each line sink has its own strength which is *constant* over the line sink. Consequently, the strength distribution along a stream is modeled as a step function that approximates the actual (gradual) changes in infiltration or exfiltration along that stream. Of course, the more line sinks are used to represent a section of a stream, the better the approximation. In the area of interest, the nearfield, a proper representation of both the stream geometry and groundwater inflow or outflow distribution is more important than in the farfield. In Figure 5.50, the analytic element layout of the nearfield for the problem in file demo.dat and some of the surrounding farfield are depicted. The figure represents a hard copy from the graphics screen produced by the cursor option in the inhomogeneity module of GFLOW1. The closed contour (solid line) near the center of the figure represents the doublet string with which the channel deposits surrounding the river are modeled. The star-shaped markers indicate the vertices of the polygon, except for the marker near the center of the polygon, which is a high-capacity well. The tick marks on the line sink strings, which are used to model the various streams and their tributaries, indicate the line sink end points.

The remote streams, near the left and right edges of Figure 5.50, are represented by fairly large line sinks: the farfield features. The streams and tributaries near the area of interest are represented by more and thus shorter line sinks: the nearfield features. Note that close to the well and

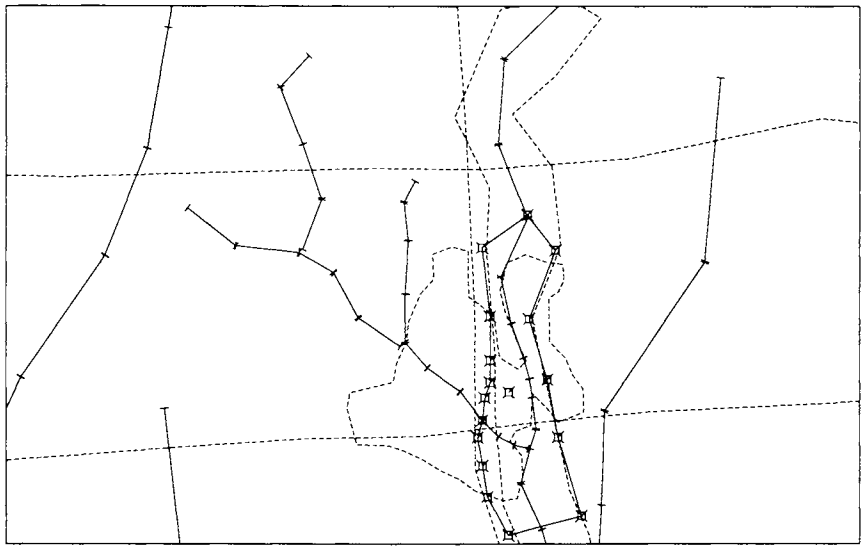

Figure 5.50: More and smaller line sinks and line doublets in area of complex flow; near well and intersection of stream with channel deposits.

the nearby intersection of a stream (Potts Ditch) with the inhomogeneity domain, both the inhomogeneity boundary and the streams are modeled in higher resolution. This is done in anticipation of the significant variations in groundwater inflow in the streams due to the (high-capacity) well. Also, the relatively large variations in the head (and thus potential) in this area require a highly variable doublet density, and thus more and shorter line doublets. The increased number of line sinks and line doublets near the well in Figure 5.50 is not so much aimed at improving the representation of the geometry (the streams and inhomogeneity boundary are nearly straight), but serves mostly to allow the strength distributions of the line sinks and line doublets to adjust more accurately to the complex flow conditions in the area. In the farfield, on the other hand, it is often acceptable to use long line sinks to roughly represent the farfield streams, ignoring meanders; see also Figure 5.16.

Resistance Elements

In a strict implementation of streams and lakes in a Dupuit–Forchheimer model, the water level in the stream or lake should be set equal to the head in the aquifer underneath it; they form Dirichlet boundary conditions. This

follows from the basic premise of the Dupuit-Forchheimer assumption that resistance to vertical flow is zero: The head is constant from the stream bottom (aquifer top) down to the aquifer bottom. In reality, however, there is often significant resistance to flow between the stream bed and the aquifer. This resistance may be due to silty or clayey sediments on the stream or lake bottom, or it may be the result of the fact that the stream or lake does not fully penetrate a till layer (mixture of sand and clay) that may overlie the regional aquifer. In Section 5.2.3, I discussed in some detail how the resistance to surface water inflow and outflow is implemented in GFLOW1. Line sinks are given three parameters to define the surface water and groundwater interactions:

1. Resistance c [days] of the soil between the river bottom and the aquifer.
2. Width w [ft] of the stream bottom.
3. Depth d [ft] of the bottom of the resistance layer below the surface water level ϕ_s in the stream.

With reference to Figure 5.14, the resistance c is defined by (5.59) as the thickness δ of the resistance layer divided by the hydraulic conductivity k_c of the resistance layer: $c = \delta/k_c$. These *resistance elements* are an example of *Cauchy boundary conditions* whereby the specified flux and head are related by (5.60) or (5.61). In some texts they are referred to as "*head-dependent flow boundaries*" (e.g., Anderson and Woessner, 1992). When the head in the aquifer ϕ_a drops below the bottom of the resistance layer, which occurs when

$$\phi_a < \phi_s - d \tag{5.103}$$

the stream or lake becomes a percolating feature; see Figure 5.14. The depth parameter d is illustrated in Figure 5.15. When the condition in (5.103) occurs, the stream section forms a Neumann boundary condition.

These resistance elements allow for a much more realistic representation of surface water boundary conditions than the Dirichlet conditions that are consistent with the Dupuit–Forchheimer model. Variations in stream resistance influence the distribution of groundwater inflow over the streams in the model area. For instance, in Figure 5.51, piezometric contours are shown in part of the nearfield of the problem in the file demo.dat. In the left-hand figure, the tributaries to Potts Ditch have the same width ($w = 10$ ft) and resistance ($c = 10$ days) as Potts Ditch itself. In the right-hand diagram the width of the tributaries has been reduced to $w = 2$ ft, while the resistance has been increased to $c = 100$ days. The latter situation may be considered more consistent with the lower stream order of the tributaries

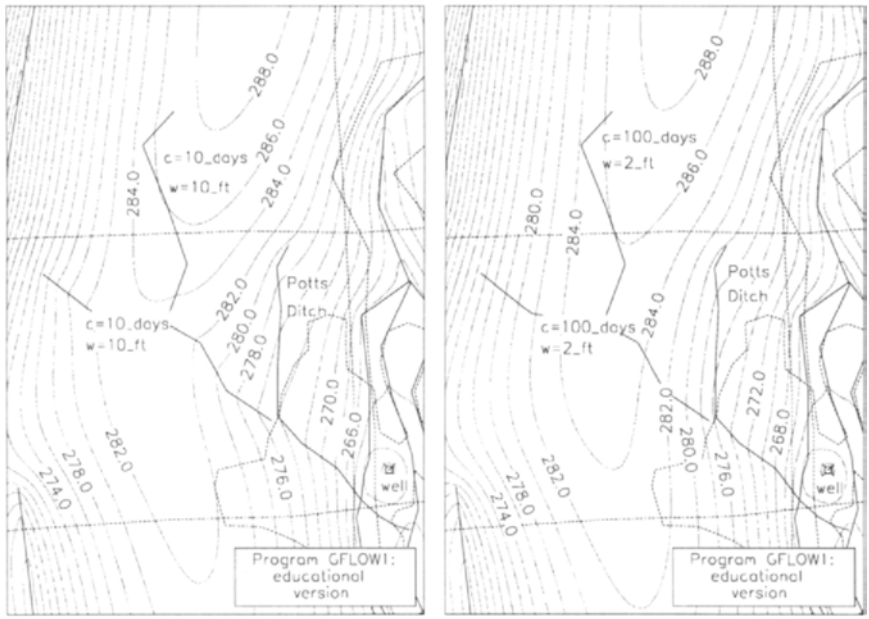

Figure 5.51: Tributaries to Potts Ditch modeled as wide, well-connected streams (left) and modeled as narrow, poorly connected streams (right).

as compared to Potts Ditch itself. As a result of the increased resistance and decreased stream width, the heads near the headwaters of the tributaries have become *lower* (see contours with elevation 286.0 and 274.0). Farther downstream along the tributaries, however, the head has become *higher* (see contours with elevations 284.0 through 276.0). Apparently, these downstream sections are groundwater discharge zones with reduced inflow into the stream due to increased resistance and decreased width. Alternatively, the headwaters are infiltrating and the increased resistance and decreased stream width have reduced the infiltration rate. This brings up another issue: Do these headwaters have enough stream flow to support the computed infiltration rates?

Including Surface Water Availability

The groundwater flow solutions depicted in Figure 5.51 have been generated by use of the "solve" command in GFLOW1, rather than the "solve conjunctive" command. Consequently, the availability of stream flow, nec-

essary to sustain the infiltration rates in the tributaries to Potts Ditch, was not considered in Figure 5.51. When stream flow and groundwater flow are solved conjunctively, the head waters of the tributaries fall dry and do not infiltrate any water into the aquifer; see Figure 5.17. As a result, the piezometric heads drop even more.

Dirichlet conditions in the farfield

As appears from this example, resistances, stream width, and surface water availability may significantly influence the groundwater flow solution. In order for these sophisticated boundary conditions to function properly, the adjacent streams and lakes must be adequately represented in the model. In other words, resistance elements and stream networks should only be used in the nearfield, *never in the farfield!* The main function of the farfield elements is to control the heads remote from the area of interest in order to avoid unrealistic groundwater movement to or from the nearfield. Farfield elements, therefore, may not behave in a hydrologically meaningful way; they may infiltrate or extract unrealistic amounts of water in order to control the (farfield) heads. Using resistance elements or stream networks in the farfield will give unpredictable and meaningless results, and they will fail to control the heads. I recommended applying only Dirichlet boundary conditions in the farfield: using line sinks that are not part of a stream network and that have a width and resistance equal to zero. In this manner we are certain that the heads in the farfield will match those defined, regardless of the required line sink strengths.

5.3.9 Field Data Requirements

In the previous section I discussed the use of resistance elements and conjunctive surface water and groundwater flow solutions in an effort to improve on the realism of our modeling. However, these resistance elements require three extra data items in addition to a surface water level: a resistance parameter, a stream width, and a resistance layer depth. To obtain reliable values (field data) for these parameters is no simple task. In fact, to obtain reliable values for any model parameter is a challenge. Field data acquisition is the number one problem of any modeling project; it frustrates every modeler. Even basic data, such as a regional average for the hydraulic conductivity and areal recharge rate due to precipitation, are often difficult to come by. And we are only talking about steady-state groundwater flow modeling. What if transient effects are to be included, or transport? Before even starting a groundwater modeling project, we should be prepared to deal with one sure thing: a chronic shortage of field data.

Groundwater flow modelers usually develop a shopping list of data needs. Anderson and Woessner (1992) presented such a list, which they adapted from Moore (1979). Their data "requirements" are subdivided into two groups: data defining the *physical* framework (first five items in the list below) and data defining the *hydrogeologic* framework of the modeling (last six items).

1. Geologic maps and cross-sections showing the areal and vertical extent and boundaries of the system.
2. Topographic maps showing the surface water bodies and divides.
3. Contour maps showing the elevation of the base of the aquifer and confining beds.
4. Isopach maps showing the thickness of aquifers and confining beds.
5. Maps showing the extent and thickness of stream and lake sediments.
6. Water table and potentiometric maps for all aquifers.
7. Hydrographs of groundwater head and surface water levels and discharge rates.
8. Maps and cross-sections showing the hydraulic conductivity and/or transmissivity distribution.
9. Maps and cross-sections showing the storage properties of the aquifers and confining beds.
10. Hydraulic conductivity and their distribution for stream and lake sediments.
11. Spatial and temporal distribution of rates of evapotranspiration, groundwater recharge, surface water–groundwater interaction, groundwater pumping, and natural groundwater discharge.

The preceding list is a literal transcription of Anderson and Woessner's (1992) Table 3.1, except I changed *map* to *maps* for the first two items. It is truly a *wish list.* Save for items (1) and (2), the geologic and topographic maps, the listed data are unlikely to be readily available. Even the available geological cross-sections are often on a scale that is insufficient for a full definition of the local stratigraphy in the model area. Acquiring all of the listed data requires extensive efforts, including drilling, hydrogeologic testing, data interpretation, and map preparation. Such activities are occasionally undertaken as part of a multiyear (and multidollar) water resource

planning project (e.g., Patrick *et al.*, 1989 and de Lange, 1991). Most consultants, however, do not have the resources to assemble all of these data prior to starting a groundwater modeling project. So now what?

In Section 5.3.2 I suggested a "stepwise" modeling procedure aimed at overcoming these almost inherent data shortages. Instead of abandoning groundwater flow modeling attempts because of a lack of data, I turned the problem around by offering *conceptual* groundwater flow modeling as an alternative to field data. For instance, consider the following approach. Assume that we are not certain whether or not a particular stream is in contact with the regional aquifer, so we model it both ways. If either way the solution in the area of interest is not significantly affected, why worry? If it does affect our solution, then we ask ourselves if a comparison of modeled heads with observed heads suggests which solution is more realistic, stream included or excluded? If the role of the stream appears important and modeling does not resolve the issue, we demonstrated the importance of this data and, perhaps, justified the expense of additional data acquisition. This approach of *hypothesis testing* may resolve many data uncertainties, and identify which data are indispensable in view of our modeling objectives.

First assembling all or most of the data in the above list and then implementing it all at once in a computer model represents the traditional left-hand flow chart in Figure 5.18. Even if all these detailed data are available, there is an argument against using them all at once. Starting with a simple groundwater model, using regional averages of the data, and making stepwise increases in the model complexity make the hydrologist experience the relative importance of the data in view of the modeling objectives. Stepwise modeling implies that initial modeling runs employ a uniform hydraulic conductivity, even though some insight may exist into conductivity variations. Similarly, model runs with a uniform areal recharge rate should precede runs with any spatial variations in recharge. Even though cyclic pumping may be locally important, initial runs should use steady-state wells with the average pumping rate. And so on. This stepwise approach also applies to issues of multiple aquifers.

Dealing with Multiple Aquifers

When interpreting geological data, it is important to realize that different geologic units may be hydraulically connected to form a single *hydrostratigraphic* unit: a single aquifer. Even when *locally* some separating strata are present, the unit may regionally still behave as one aquifer. Under these circumstances, the model solution yields *comprehensive* heads and discharges, see Section 3.3.1. The meaning of these heads or discharges depends on the local hydrogeologic conditions. In areas where the separating strata are

absent or form little resistance to flow, the modeled heads can be compared directly with those observed. In areas where the separating strata are consistently present, the different aquifer strata will exhibit different heads. The modeled (comprehensive) head will then form a weighted average of the individual heads in the various aquifer strata:

$$\phi = \frac{\sum T_i \phi_i}{\sum T_i} \tag{5.104}$$

where T_i and ϕ_i are the transmissivity and head of the ith aquifer, respectively (see also Section 3.3.5). If the area of interest is near a major stream, the channel deposits may well form a single aquifer zone embedded in the otherwise multiple aquifer environment. The single aquifer (comprehensive) model may be adequate for this case, provided we are careful in defining streams and lakes in the regional multiple aquifer domain. In multiple aquifer zones, smaller streams or lakes may only be connected to the uppermost aquifer. This may be accounted for by giving some resistance to the line sink strings or sink discs that represent these surface waters. In other cases, however, our area of interest is really a dual or multiple aquifer zone, in which case a multi-aquifer (quasi three-dimensional) model should be used. In the case of only two aquifers, GFLOW1 may be used to solve the upper and lower aquifer problem separately in the area of interest. In doing so, the comprehensive solution may be used to define Dirichlet boundary conditions along the perimeter of the dual aquifer zone (clay layer edge). However, if changes in boundary conditions are made which influence the comprehensive solution near these boundaries, the comprehensive, upper, and lower aquifer solutions need to be adjusted. Using a single aquifer model, like GFLOW1, for dual aquifer modeling leads to an iterative process: solving the comprehensive problem, solving the flow in the individual aquifers, resolving the comprehensive problem, etc.

Keep it Simple

Our models are foremost educational in nature. They educate the hydrologist regarding the behavior of a groundwater flow system, or they educate the client, the judge, or the jury regarding the consequences of some past or future action. In verbal or written presentations, we all accept the basic rule that if you can say it with few and simple words, do so! More people will listen, and they will more readily understand. The same is true for groundwater flow models (or transport models).

Rule 5.13 *The simpler the model, the easier it is to interpret its results.*

This is no invitation to oversimplify! For instance, giving detailed predictions regarding future or past contaminant concentrations, based on nothing more than groundwater travel time predictions in a homogeneous aquifer, is unwarranted. However, using a relatively simple flow model to demonstrate the possibility or impossibility that a contaminant reached a certain receptor may be quite appropriate. It is the task of the hydrologist to develop a model that has just enough realism to address the model objective(s), no more and no less. A stepwise modeling approach can accomplish this. It also avoids unnecessary field data acquisition, thus reducing field data needs.

This Page Intentionally Left Blank

Chapter 6

Field Applications

In the previous chapter, basic modeling concepts were discussed, organized by topic. Often the issues raised can only be fully appreciated in the context of a particular project where they manifest themselves. In this chapter, a number of field applications are discussed that integrate many of the concepts discussed in Chapter 5. In presenting these applications I am focusing on *modeling approaches and concepts* rather than the specific merits of the project or outcome of the study. As mentioned in Section 5.3.3 on the design of conceptual models, each groundwater hydrologist will take his or her own approach to a study. Each designs somewhat different conceptual models and uses different software, if any at all. Therefore, my approach to each of the case studies in this Chapter should be seen as an example of the application of the analytic element method; it is not the only way to solve the problem.

The modeling discussed here was carried out with several different computer programs. The first case study has been conducted by use of both the educational and professional version of GFLOW and with the finite difference model MODFLOW.[1] The data files for the educational version are supplied on the distribution diskette for further experimentation by the reader. The second case study has been conducted with the proprietary code SLAEM,[2] which is a single-layer analytic element model like GFLOW1. The last case study has been conducted with the professional version of GFLOW,[3] which is also a proprietary code.

[1] Developed by the USGS (McDonald and Harbaugh, 1988).
[2] Trademark of Strack Consulting, Inc.
[3] Trademark of Haitjema Software, LLC

6.1 Wellhead Protection

Established by the 1986 Amendments to the Federal Safe Drinking Water Act, EPA's "Wellhead Protection Program" requires the states to implement regulations aimed at protecting the groundwater resource used for the production of drinking water. Specifically, for each public supply well or well field the following measures must be taken:

- Delineate a wellhead protection area (WHPA).
- Identify potential sources of contamination in the WHPA.
- Establish management approaches to protect the groundwater in the WHPA.
- Develop a contingency plan for contamination events.
- Develop programs for public education and participation.

A WHPA is usually defined as the capture zone of the well or well field bounded by isochrones of groundwater travel time. Typically several "time of travel capture zones" are delineated: one for short travel times (between one to three years) and one or two for larger travel times, e.g., 5 or 10 years. A *five-year time of travel capture zone*, for instance, is a surface area around the well or well field underneath which groundwater will reach the wells within five years. The delineation of these capture zones is not easily done by direct field measurements. Instead, groundwater flow modeling is currently considered the best method for delineating these capture zones.

Next I will discuss the delineation of a WHPA for the well field of the city of Vincennes, Indiana. The other aspects of the wellhead protection program (source identification, management approaches, etc.) are outside the scope of this text. Part of the following discussions were adapted from a class project report submitted to me by Mr. Carl Schoedel, while the extended GFLOW and MODFLOW modeling were carried out by Mr. Victor Kelson.

6.1.1 Hydrogeology near Vincennes

The city of Vincennes is located in the Wabash river lowlands in Knox County, Indiana; see Figure 6.1. These lowlands are characterized by filled-in valleys forming a glacial outwash aquifer consisting of coarse sand and fine gravel directly resting on the underlying bedrock. The saturated aquifer thickness generally ranges between 60 to 80 feet. The U.S. Geological Survey (USGS) estimates an average hydraulic conductivity of 355 ft/day for

most of the aquifer (Shedlock, 1980). Along the eastern and western borders of the outwash, near the bedrock hills, the aquifer interlaces with zones of lower hydraulic conductivity; see Figure 6.2. The elevation of the bedrock underneath the outwash varies between 320 and 340 [ft MSL], and is approximately 340 [ft MSL] near the well field, which is located near the river just south of Vincennes; see Figure 6.1.

6.1.2 Regional Model

The regional groundwater flow model has been set up by use of a digital hydrography map (vincenne.dm) loaded into the Geographical Analytic Element Preprocessor (GAEP). A hard copy of the GAEP screen, showing part of the hydrography map near Vincennnes, is presented in Figure 6.3. The map is used as the basis for creating line sink strings to model the Wabash River and other streams and tributaries in the area. In addition to representing these hydrological boundaries, GAEP introduces regional aquifer parameters. These parameters (aquifer base, hydraulic conductivity, porosity, areal recharge rate, etc.) have been estimated from the available field data using an earlier USGS study by Shedlock (1980), and by consulting the USDA Soil Survey of Knox County, Indiana (SCS, 1981). This resulted in the use of the following parameter ranges for the regional modeling:

- Hydraulic conductivity in the outwash aquifer ranges between 250 and 450 ft/day, while in the sandstone outcrops it ranges between 10 and 115 ft/day.

- Recharge rates in the outwash range between 10 and 25 inches/year, while in the sandstone outcrops it ranges between 1 and 3 inches/year.

- Porosity ranges between 0.1 and 0.3.

- The aquifer base (bedrock surface) is modeled as being at 340 ft above mean sea level.

- Pumping rates between 2 and 5 MGD were used to simulate current pumping conditions.

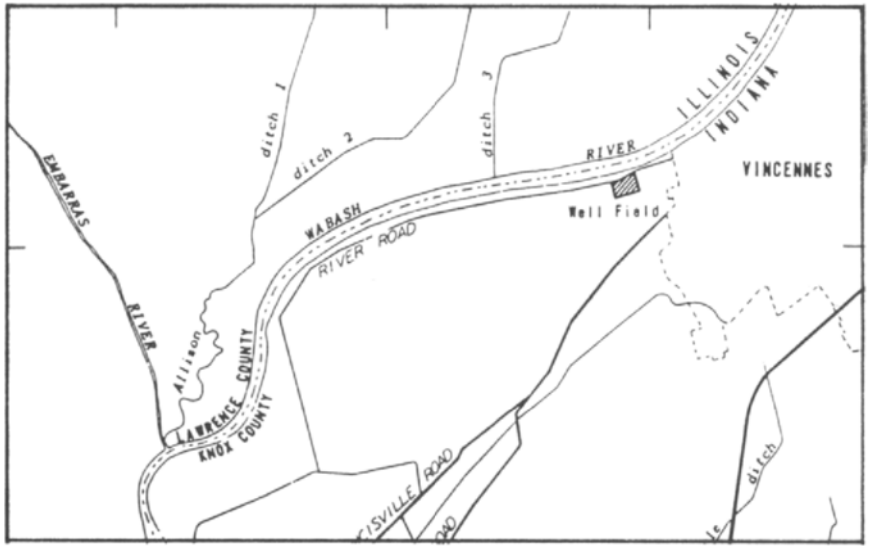

Figure 6.1: Vincennes located near the Wabash River in Knox County, Indiana. (After Shedlock, 1980.)

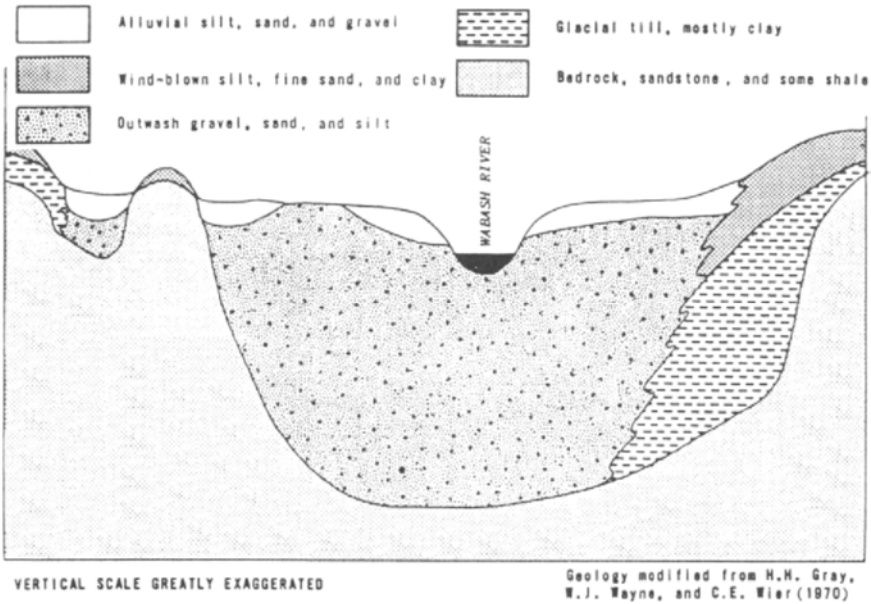

Figure 6.2: Cross-section over the outwash and sandstone aquifer near Vincennes. (After Shedlock, 1980.)

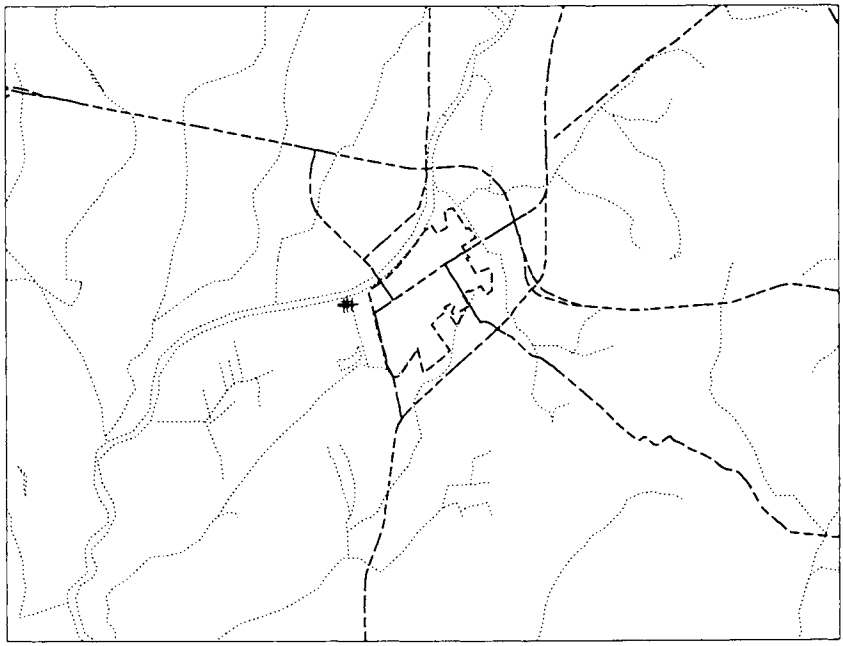

Figure 6.3: Hydrography map vincenne.dm in GAEP used to create the GFLOW1 input data file vinc01.dat.

Modeling Approach

The modeling activities consist of the following steps:

1. Set up a simple local model to get a first rough estimate of the capture zone.
2. Formulate hydrological issues to be resolved based on the preliminary model.
3. Set up a more detailed regional model to address these hydrological issues.
4. Locally refine the modeling to assess the interaction between the Wabash River and the well field.
5. Generate capture zones and isochrones for a range of model parameters.
6. Construct composite time of travel capture zones to serve as WHPAs.

Steps 1 through 4 are designed to obtain as good an insight in the hydrology near the well field as available data permits. Following the stepwise modeling approach outlined in Section 5.3.2, the modeling itself is used to formulate the most important hydrological issues and determine to which parameters the capture zones are most sensitive. The remaining uncertainties in hydrological parameters are dealt with by generating capture zones for extreme values (step 5) and incorporating them in the final WHPA (step 6).

Preliminary Capture Zone Estimate

Before setting up a complete regional groundwater flow model, a simple local flow model was created based on the concept of a well in a uniform flow field; see Section 3.1.10. For this purpose, the well field with seven wells has been represented by a single well (pumping center). The effect of the nearby Wabash river is approximated by use of an image well. The intensity $Q_0 = 23$ ft^2/day of the uniform flow was estimated from field data; using piezometric heads from USGS observations on January 23 through 25, 1978 (Shedlock, 1980), an estimated hydraulic conductivity of 355 ft/day, and an average aquifer thickness of 80 ft. The aquifer porosity was set at 20%. The resulting capture zone and time markers for one year travel times are shown in Figure 6.4. The capture zone in this and all subsequent figures has been created by back-tracing 10 streamlines along the aquifer bottom, starting from the well. The capture zone envelope may be slightly

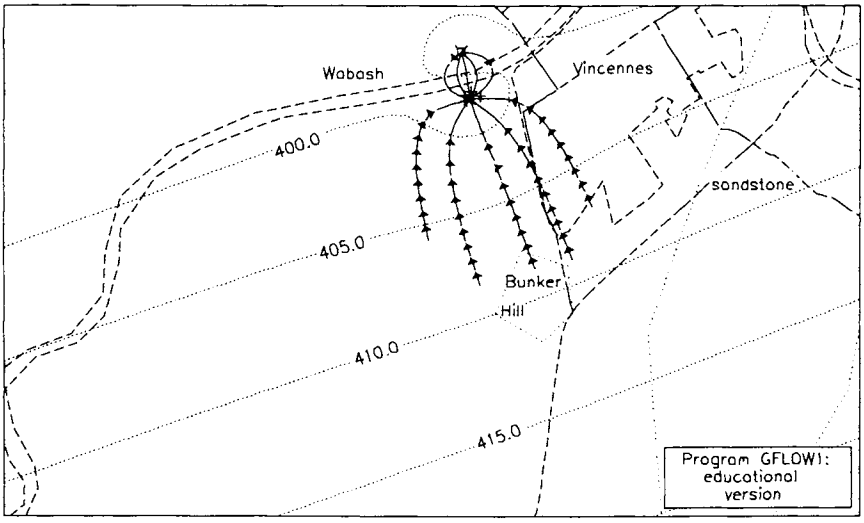

Figure 6.4: Preliminary capture zone using a "well in uniform flow" model. Arrowheads mark one-year groundwater travel time intervals. (GFLOW1 data file vincprem.dat)

wider than suggested by the streamlines in Figure 6.4, as may be seen by releasing more streamlines (e.g., 20). The arrowheads on the streamlines point into the direction of flow and are spaced at a one-year groundwater travel time interval. The image well is visible across from the Wabash River boundary, and two bedrock outcrops are displayed but not included in the modeling: "Bunker Hill," a dome-shaped sandstone outcrop inside the outwash aquifer, and the sandstone outcrop that forms the eastern outwash border.

This preliminary model raises various hydrogeological questions:

1. Will the capture zone stop at the Wabash River?
2. Will the capture zone be deflected by Bunker Hill?
3. What will be the effect of the (lower permeable) sandstone aquifer to the west of the outwash?
4. Will nearby ditches affect the capture zones?
5. What will be the effect of different assumptions on conductivity, aquifer thickness, recharge, and porosity?

Different choices for the aquifer transmissivity will change the uniform

flow rate Q_0 and make the capture zone proportionally wider or smaller; see Figure 3.19. You may visualize this by increasing or decreasing the uniform flow rate in vincprem.dat before switching it into GFLOW1 and tracing streamlines. Note that vincprem.dat already contains the commands to solve, to grid, and to set the contour levels and trace parameters. However, before back-tracing streamlines, do not forget to set the starting elevations near the aquifer bottom (e.g., H = 340 in graphics mode in the trace module). Changes in porosity will not affect the capture zone shape, but will move the isochrones closer to or further away from the well (try this in GFLOW1). Although our preliminary model may give some insight into the effects of different aquifer parameters (issue 5), the issues raised here can only be properly addressed by a more complete modeling effort, including the surface waters in the area, recharge due to precipitation, and areas of different hydraulic conductivity.

Regional Model

Using GAEP, farfield and nearfield surface water features have been introduced together with a sink disk (with negative strength) to model areal recharge due to precipitation; see the solid lines in Figure 6.5. The dotted polygons in Figure 6.5 are inhomogeneities created in GFLOW1 (using the cursor option in the inhomogeneity module). The sandstone outcrop to the east of the well field is a surrogate for the transition from outwash to sandstone which occurs all along the Wabash River, both to the east and to the west. To the west, across the river from the well field, that transition in hydraulic conductivity has been omitted altogether, while to the east a low permeable zone has been introduced to model part of the transition closest to the well field. This limited implementation of the transition from outwash to sandstone was necessitated by the limit on the number of analytic elements supported by the *educational version* of GFLOW1. Later, we will revisit this issue and model the outwash more realistically in the *professional version* of GFLOW1.

The data file vinc01.dat for Figure 6.5 has been read into GFLOW1 and a "solve" command without parameters is issued; no iterations are necessary since no resistances have (yet) been given to any of the surface water features. In Figure 6.6, piezometric contours and streamline traces are shown in a subdomain of Figure 6.5 near the well field. There are several obvious problems with this model run:

1. The well field gets all its water from a small (unnamed) ditch that is a branch of "City Ditch"; no water is obtained from the Wabash River. This is a highly unlikely situation, particularly in view of the

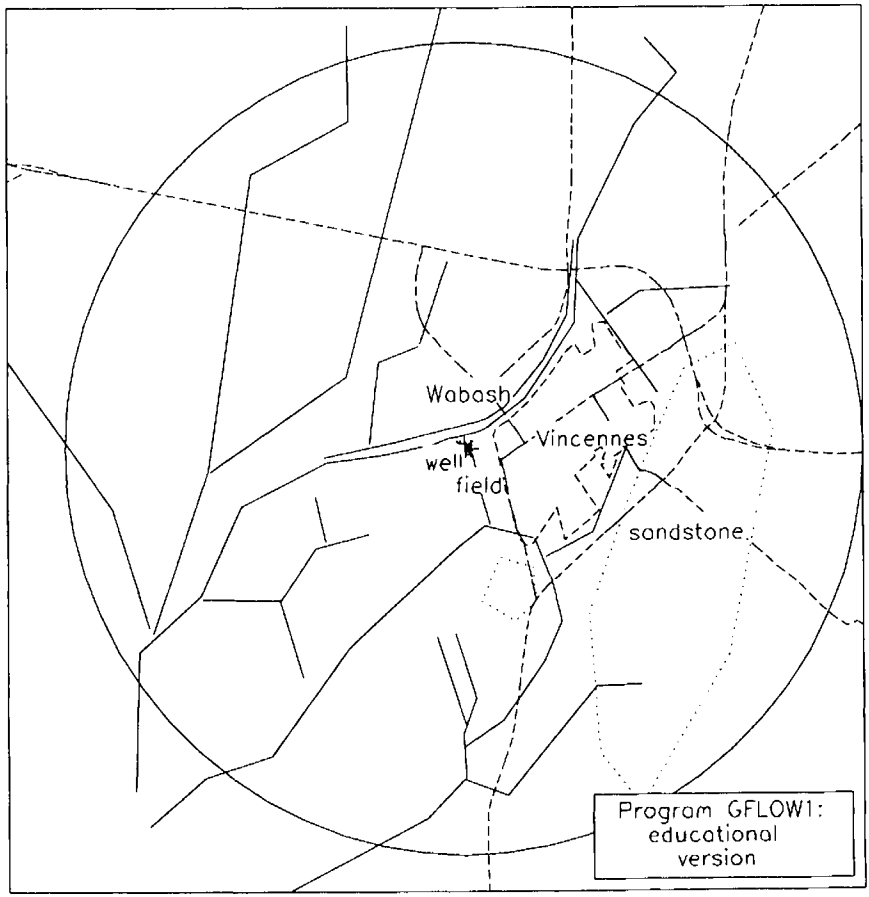

Figure 6.5: Layout of analytic elements near Vincennes, Indiana. (GFLOW1 data file vinc01.dat)

fact that the Wabash River is known to lose water near the well field (Shedlock, 1980).

2. The unnamed ditch near the well field is infiltrating over 6 cfs (cubic feet per second) to accommodate the demand of the well field, while there is no known source of water for the ditch to keep up this flow rate year-around.

3. The head waters of a stream to the south of Vincennes infiltrates large amounts of water in the sandstone aquifer (see circular contours at the line sink just above the logo). The nearby line doublet that models the jump in hydraulic conductivity from the sandstone to the outwash also shows irregular contours, suggesting that the line doublet does not maintain continuity of the head in that area. These problem areas are marked with ??? in Figure 6.6.

These unrealistic modeling results are due in part to the fact that no resistance between these small ditches or head waters of streams and the aquifer has been introduced.

In Figure 6.7, piezometric head contours and streamlines are depicted for the same area as in Figure 6.6. This time the ditches and head waters of streams in the nearfield have been given a resistance of 10 days (City Ditch has a resistance of 20 days). These values have been estimated from local soil conditions; see also Section 5.2.3. Details on the width, depth, and resistance parameters of the various surface waters may be found in the input data file vinc02.dat; you may also load the file in GFLOW1 and use the cursor option in the line sink module to point at line sinks and get their properties by pressing $< Enter >$. Instead of the ditch supplying all water for the well field, some water is now coming from the Wabash River, while the rest is captured from the regional flow toward the Wabash River. Also note that the line doublets that model the transition between the sandstone and the outwash are now performing well; there are no irregular contours like those in Figure 6.6. Still, both the ditch near the well field and Oliphant Ditch, as well as the head waters near the logo, are infiltrating water at the maximum rate allowed by the underlying soil; they are "percolating" (see also Section 5.2.3). These percolating conditions are not apparent from Figure 6.7, but may be seen on screen in GFLOW1 by selecting the "highlight percolating" option in the line sink module.

A third data file, vinc03.dat, has been created by reading vinc02.dat into GAEP and changing the line sink strings that represent the ditches and streams in the nearfield into "stream" features (properties option in the element module of GAEP). The file vinc03.dat has been "switched" into GFLOW1 and a "solve conjunctive 5" command has been given to create

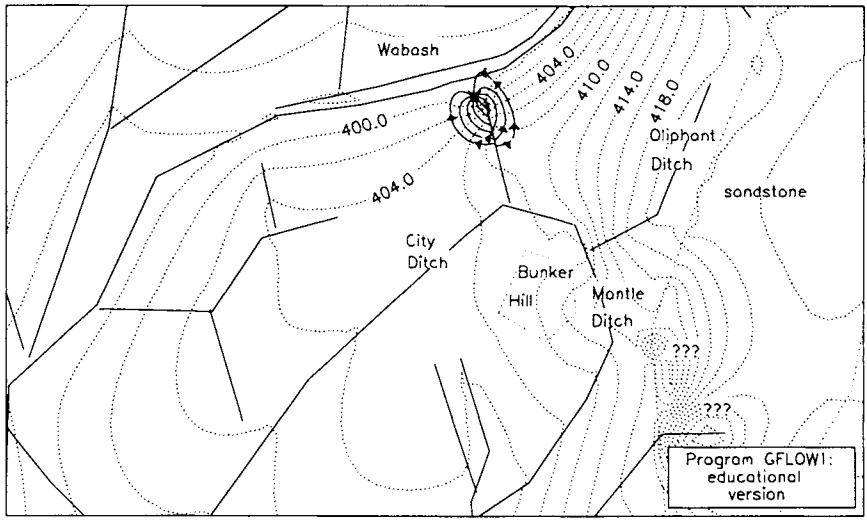

Figure 6.6: Initial model run with no resistances on surface waters. Ditches and head waters of streams are infiltrating unreasonable amounts of water. (GFLOW1 data file vinc01.dat)

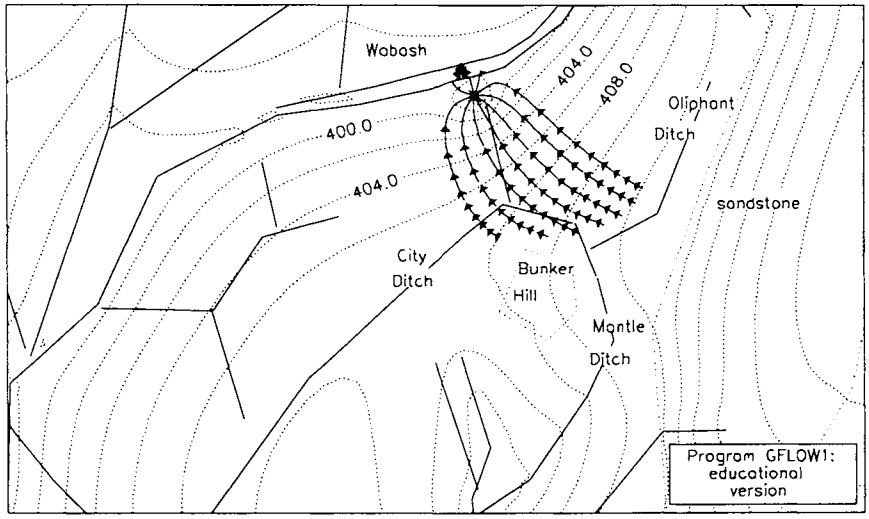

Figure 6.7: Model run with resistances added to ditches and streams. The Wabash River supplies some water to the well field. (GFLOW1 data file vinc02.dat)

a conjunctive surface water and groundwater flow solution. The resulting piezometric contours and streamlines are depicted in Figure 6.8. Note that both the ditch near the well field and Oliphant Ditch, as well as the head waters near the logo, are now dashed! Dashed line sinks have no water to infiltrate and are removed from the groundwater flow solution. This latter refinement has changed the solution only marginally; compare Figure 6.8 and Figure 6.7. In Figure 6.9, modeled heads and observed heads have been compared by using the "plot piezometer" option in the check module of GFLOW1. The piezometer file used for this comparison is usgspz.dat, which contains a selection of the water level observations made on January 23 through 25, 1978 by the USGS (Shedlock, 1980). The differences in the modeled heads and observed heads may be partly due to differences in stream levels, pumping rates, and recharge rates at the time of the observations and those used in the model. Consequently, we cannot expect a perfect match. Instead these comparisons are used to establish reasonable parameter ranges for the model, while the effect of different parameter choices on the capture zone is the subject of our modeling exercise.

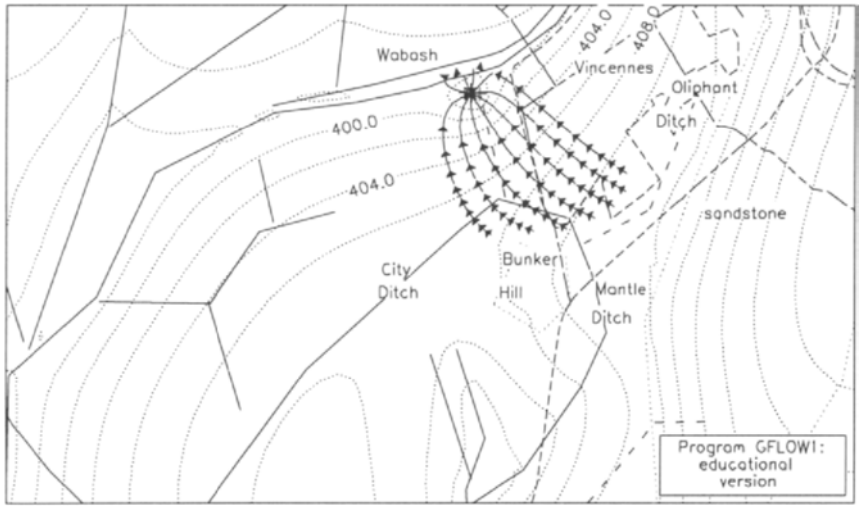

Figure 6.8: Model run with ditches and nearfield streams represented as "stream" features. Dashed lines represent line sinks that have no water to infiltrate. (GFLOW1 data file vinc03.dat)

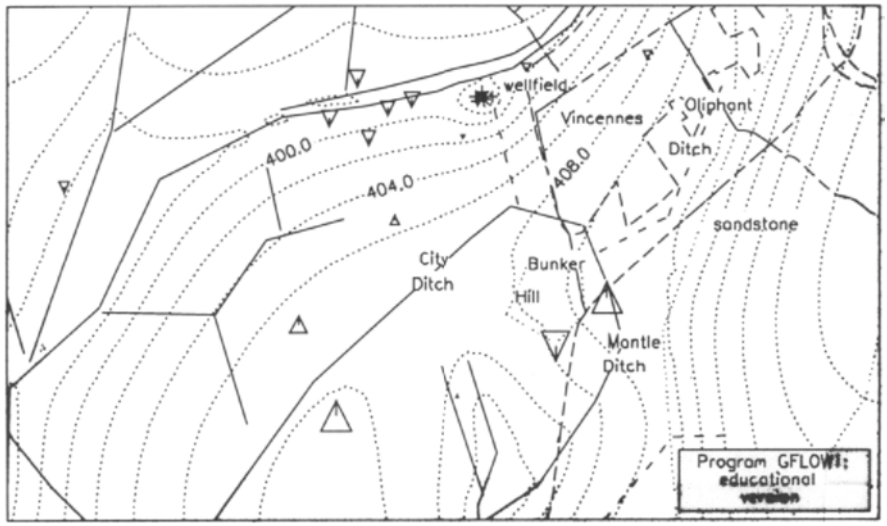

Figure 6.9: Comparison in GFLOW1 of model heads and heads measured by the USGS (Shedlock, 1980).

6.1.3 Using Partially Penetrating Wells in GFLOW1

Our modeling effort to this point has been restricted by the 100-equation limit imposed by the educational version of GFLOW1. This resulted in a limited farfield representation and a contrived representation of the transition in hydraulic conductivity between the outwash and the surrounding sandstone aquifer, the sandstone outcrop to the east of the river in Figure 6.5.

Another limitation of our modeling is the use of a Dupuit–Forchheimer model, while the well field is rather close to the river, suggesting the need for three-dimensional flow modeling. Although we can introduce a resistance between the river and the aquifer, which represents the resistance due to a sediment layer on the river bottom, we do not know what additional resistance may be introduced by vertical components of flow near the river and the wells. This vertical resistance to flow is not accounted for in the Dupuit–Forchheimer solution.

In Figure 6.10, an analytic element layout and piezometric contours are shown (in a subdomain near Vincennes) of a more complete GFLOW1 model for the Vincennes area, which is solved by the professional version of GFLOW1. The analytic element representations and aquifer parameter choices for this model differ somewhat from those in the earlier runs with the educational version, since the two models were constructed by two different modelers. Note that the outwash in Figure 6.10 is represented by a higher permeable domain on both sides of the Wabash River, rather than by the (artificial) sandstone outcrop depicted in Figure 6.5. The piezometric contours in the sandstone are omitted in Figure 6.10 to avoid clutter. The well field in Figure 6.10 is modeled by seven partially penetrating wells with their screens extending from the aquifer bottom to 10 ft above the aquifer bottom. A total discharge of 3.5 MGD has been distributed over these wells based on historic records. In Figures 6.11 and 6.12, piezometric head contours are depicted near the aquifer top and bottom, respectively, in a close-up near the well field and the river. The piezometric contours near the aquifer top (Figure 6.11) and aquifer bottom (Figure 6.12) differ only in the immediate vicinity of the wells (hardly noticeable on the scale of the figures).

The well field modeled with these seven partially penetrating wells obtains 36.1% of its water from the river, as opposed to 36.3% for the case of seven fully penetrating wells. The latter modeling, with the seven fully penetrating wells, is not presented here. In the earlier model with the educational version of GFLOW1 (data file vinc03.dat), the well field was represented by a single well which obtained 34.9% of its water from the Wabash River. In general, therefore, the extended GFLOW1 solution yields results

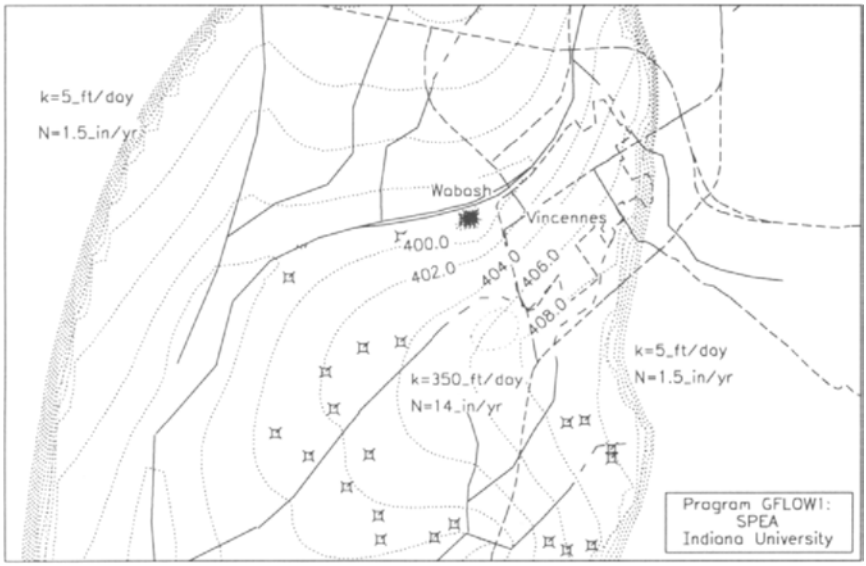

Figure 6.10: Extended analytic element layout and piezometric contours for the professional version of GFLOW1 with seven partially penetrating wells representing the well field.

that are not substantially different from those obtained from the simpler model with the educational version of GFLOW1; also compare Figure 6.10 with Figure 6.8.

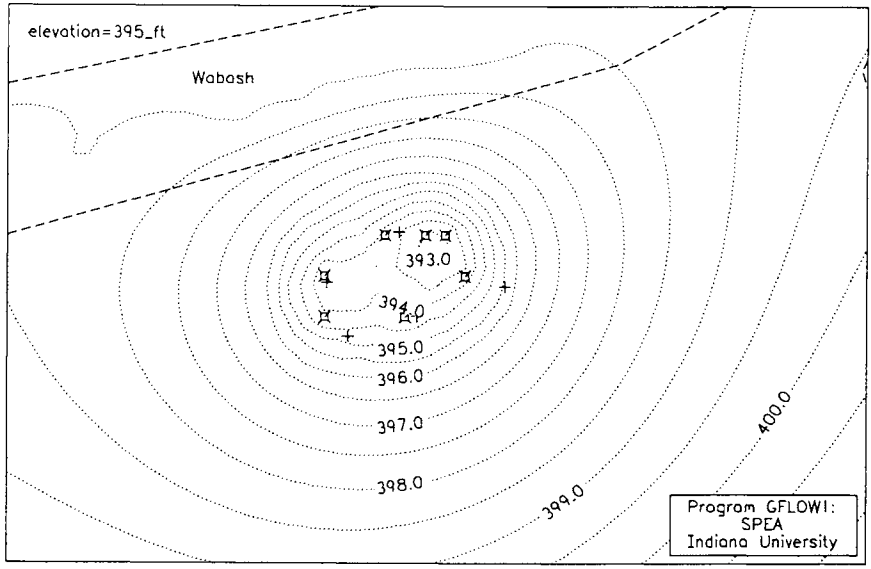

Figure 6.11: Piezometric contours near the *aquifer top* in a close-up of the seven partially penetrating wells near the Wabash River.

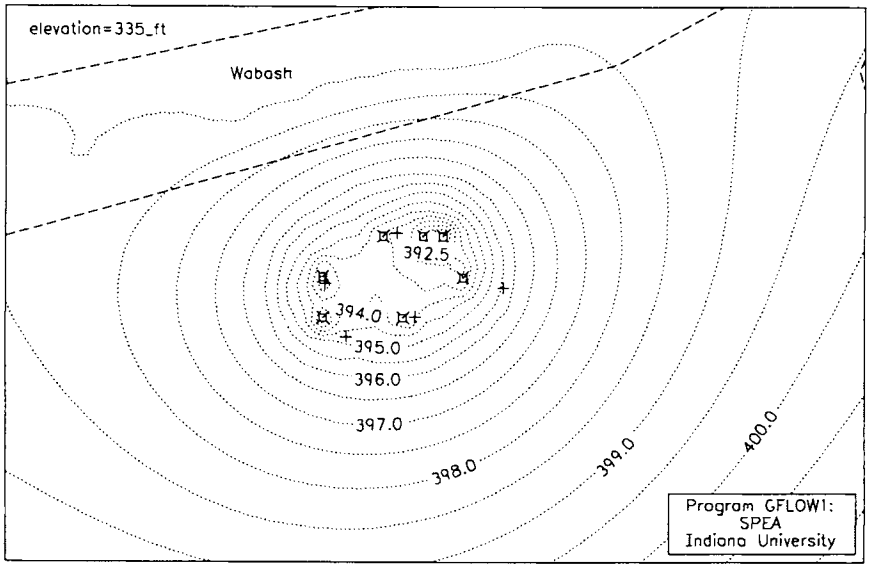

Figure 6.12: Piezometric contours near the *aquifer bottom* in a close-up of the seven partially penetrating wells near the Wabash River.

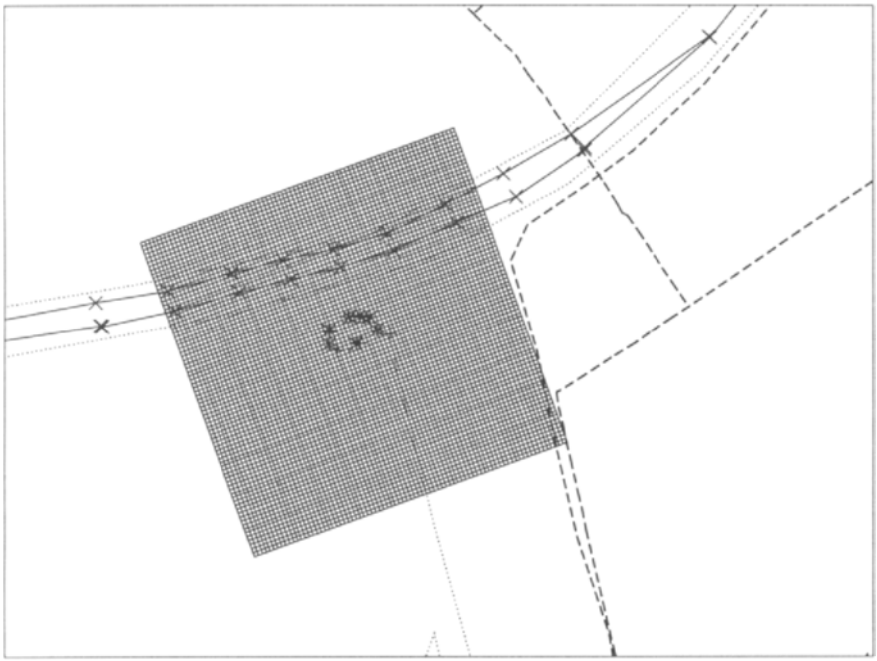

Figure 6.13: Finite difference grid in subdomain of the model area. Reproduced from GAEP's graphics screen.

6.1.4 Three-Dimensional Flow with MODFLOW

The preceding application of partially penetrating wells is not exact, since it should only be used in a confined aquifer (see Section 4.2.1), while the flow in the outwash is unconfined. Moreover, in GFLOW1, only these partially penetrating wells were treated as three-dimensional features; all other features (including the Wabash River) were represented by two-dimensional functions. To further investigate the issue of three-dimensional flow between the well field and The Wabash River, a fully three-dimensional MODFLOW solution is constructed for an area in the immediate vicinity of the well field and the Wabash River. This MODFLOW model is extracted from the GFLOW1 solution as follows.

In Figure 6.13, a reproduction of the graphics screen in GAEP is shown with a finite difference grid superimposed on an area near the well field and the Wabash River. GAEP writes a GFLOW1 script file which uses the "extract" command in GFLOW1 to extract all relevant model data for the grid, such as stream locations, resistances, conductivities, and porosities. The boundaries of the grid in Figure 6.13 are defined as Dirichlet

boundaries with specified heads obtained from the GFLOW1 solution. A special converter program combines a GAEP and GFLOW1 grid output file in a MODFLOW-compatible input data file. The latter file has been imported into MODELCAD[4] to change the two-dimensional grid into a three-dimensional grid with eight grid layers equally spaced over the aquifer height. Piezometric contours near the aquifer top and aquifer bottom are shown in Figure 6.14. These MODFLOW solutions appear nearly identical to those from GFLOW1; compare with Figures 6.11 and 6.12. Note that the domain for the MODLOW solution is somewhat different in size and rotated slightly as compared to that for the GFLOW1 solution. The amount of water that the wells obtain from the river in the MODFLOW model is 34.6%, which is for all practical purposes the same as was predicted by GFLOW1 (36.1%)

Both GFLOW1 and MODFLOW solutions, so far, assume an isotropic hydraulic conductivity, which may result in an underestimation of the resistance to vertical flow. In Figure 6.15, piezometric contours are presented near the top and bottom of the aquifer for the case of a vertical hydraulic conductivity that is 10 times less than the horizontal permeability.

In Figure 6.16, contours of equal leakage rates underneath the Wabash River are presented for the isotropic and anisotropic case. The values on the contours have units of ft/day. All water that is leaked from the Wabash River in these diagrams ends up in the well field. The amount of water that the wells obtain from the river for this anisotropic case is somewhat less than for the isotropic case: 33.1% of the total well field discharge, as opposed to 34.6%.

Resistance Layer

The three-dimensional modeling, whether with GFLOW1 or with MODFLOW, does not yield substantially different results than does the Dupuit-Forchheimer (two-dimensional) modeling. In all cases, the well field receives a little over one-third of its discharge from the Wabash River. Even the anisotropic case, with a vertical conductivity 10 times lower, made little difference. The question arises: When would we see major differences between a Dupuit-Forchheimer solution and a three-dimensional solution? To force that issue, imagine a silty clay layer 10 feet thick with a hydraulic conductivity of 0.1 ft/day that occurs at an elevation midway between the top of the well screen and the bottom of the Wabash River. A MODFLOW solution for that case is presented in Figure 6.17, where piezometric contours are depicted near the top and bottom of the aquifer. This time there

[4]Trademark of Geraghty and Miller.

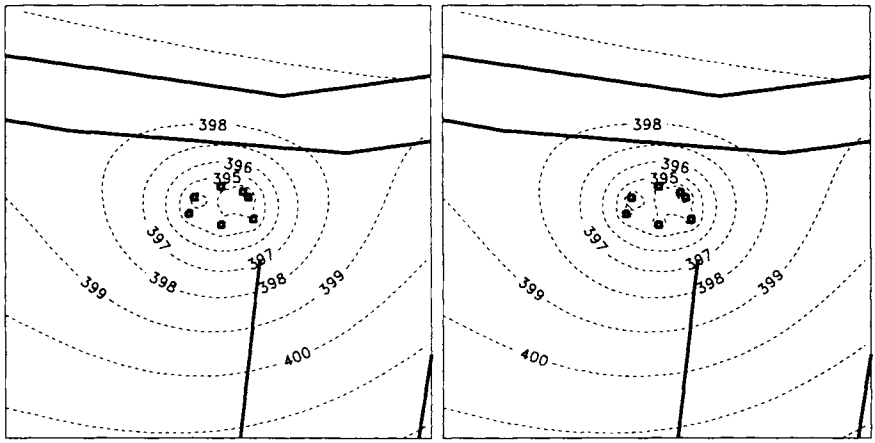

Figure 6.14: Piezometric contours near the aquifer top (left) and near the aquifer bottom (right) due to MODFLOW with seven partially penetrating wells in an *isotropic* aquifer.

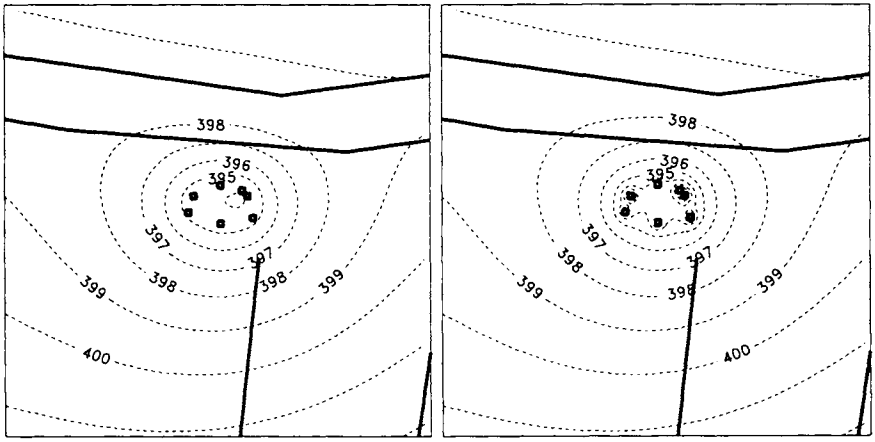

Figure 6.15: Piezometric contours near the aquifer top (left) and near the aquifer bottom (right) due to MODFLOW with seven partially penetrating wells in an *anisotropic* aquifer. The vertical hydraulic conductivity is 10 times less than the horizontal conductivity.

are clearly differences between the shallow and deep heads. For the case of Figure 6.17, the well field receives only 0.9% of its water from the Wabash River. Keep in mind, however, that this is a hypothetical case; there is no evidence of such a resistance layer in the Vincennes area.

It seems that the Dupuit–Forchheimer solution performs adequately, even though at first glance the wells are quite close to the river, suggesting the need for three-dimensional flow modeling. The extended GFLOW model did also not lead to substantially different results than were obtained earlier with the educational version. In view of this, we will continue our modeling with the educational version.

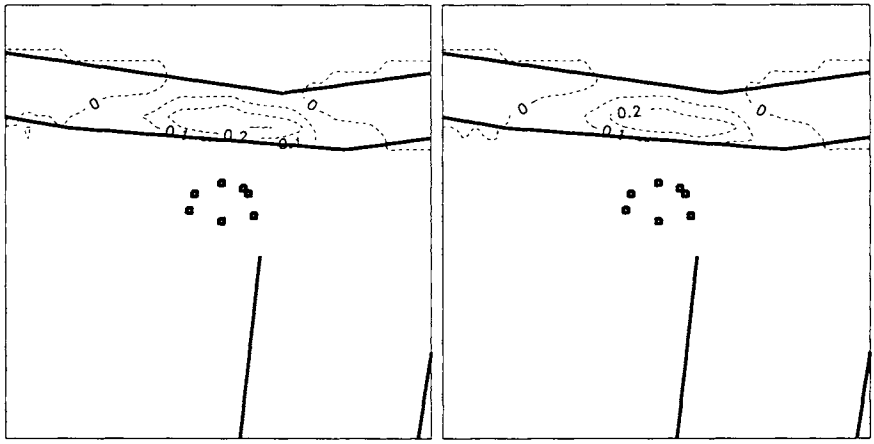

Figure 6.16: Contours of equal leakage from the Wabash River into the aquifer for the case of an *isotropic* hydraulic conductivity (left) and for the case of an *anisotropic* hydraulic conductivity (right). (MODFLOW model)

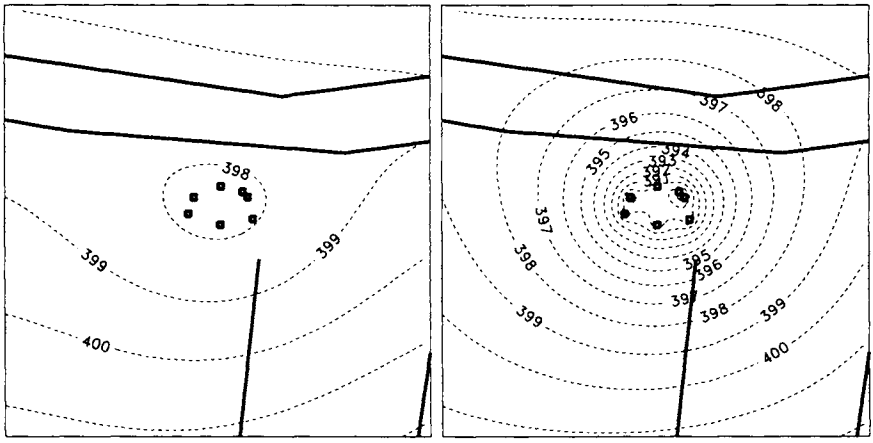

Figure 6.17: Piezometric contours near the aquifer top (left) and near the aquifer bottom (right) due to MODFLOW with a resistance layer midway in the aquifer.

Table 6.1: Effects of model parameters on the capture zone.

Parameter	Data file	Effect on capture zone
$k = 250$	vinc04.dat	slightly shorter and wider
$k = 450$	vinc05.dat	slightly longer and shorter
$n = 0.1$	vinc06.dat	much longer
$n = 0.3$	vinc07.dat	much shorter
$N = 10$	vinc08.dat	much wider, slightly shorter
$N = 25$	vinc09.dat	slightly narrower and longer
$Q = 2$	vinc10.dat	much narrower, slightly shorter
$Q = 5$	vinc11.dat	much wider, slightly longer

6.1.5 Capture Zones for Bounding Parameter Values

There is uncertainty about the value of many hydrogeological parameters, such as hydraulic conductivity, porosity, areal recharge rates, resistances between surface waters and the aquifer, etc. The model run in Figure 6.8 has been conducted with the following parameters (see data file vinc03.dat):

- Aquifer base: $base = 340$ ft MSL.
- Hydraulic conductivity of the outwash: $k = 355$ ft/day.
- Hydraulic conductivity of the sandstone outcrops: 25 ft/day.
- Recharge rate on outwash: $N = 20$ inches/year (0.004566 ft/day).
- Recharge rate on sandstone outcrops: 2 inches/year (0.0004566 ft/day).
- Porosity: $n = 0.2$.
- Pumping rate of well field: $Q = 3.5$ MGD ($467,852$ ft^3/day).
- No resistance between The Wabash River and the aquifer ($c = 0$ days).

For each of these parameters, a lower and upper bound were chosen to assess the impact on the capture zone and isochrones. These parameter choices have been based on field data and model calibration results. The runs and their results are summarized in Table 6.1, in which the effects on the capture zone are compared to the one depicted in Figure 6.8

The capture zones for the parameter choices in the table are presented in Figures 6.18 through 6.25. We learned from the MODFLOW analysis with a resistance layer between the well screens and the river that such resistance may significantly affect the contribution of the river to the well field. In Figure 6.26, a capture zone is shown for the case that the resistance between the Wabash River and the aquifer is 1 day . This results in a widening of the capture zone, while inspection of the line sinks that represent the Wabash River reveals that only 0.7% of the well field discharge comes from the river, which is about the same as for the case of the resistance layer in MODFLOW (which had also a 1 day resistance). The interaction between the river and the aquifer (and well field) appears quite important and may warrant additional field data collection.

Another uncertainty arises from the presence of the low permeable zones: Bunker Hill and the sandstone outcrop to the east. Instead of experimenting with the conductivities and recharge rates for these sandstone outcrops, a model run was conducted by which these inhomogeneities were removed altogether. The resulting capture zone is depicted in Figure 6.27 and is narrower and substantially longer than the one in Figure 6.8.

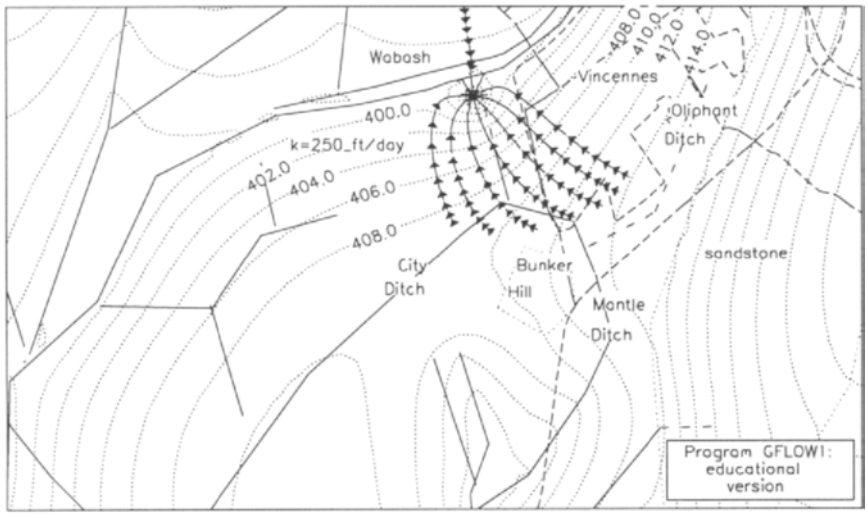

Figure 6.18: Capture zone for hydraulic conductivity in the outwash of $k = 250$ ft/day. (GFLOW1 file vinc04.dat)

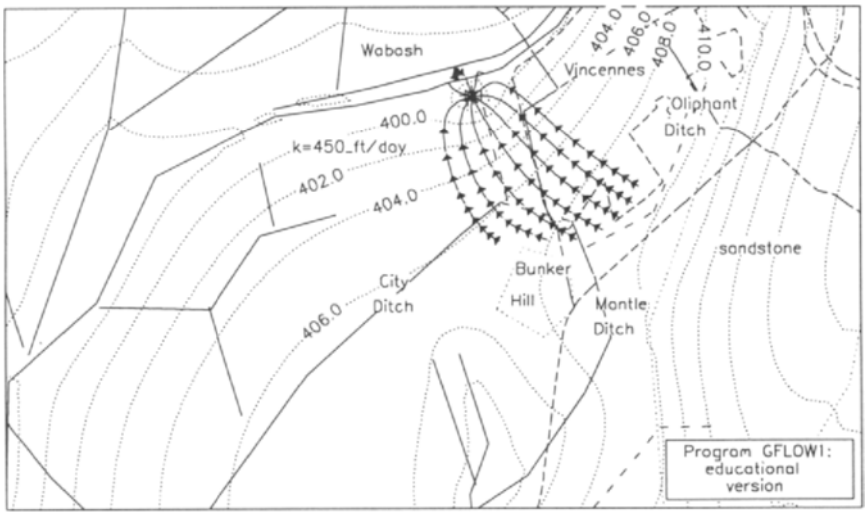

Figure 6.19: Capture zone for hydraulic conductivity in the outwash of $k = 450$ ft/day. (GFLOW1 file vinc05.dat)

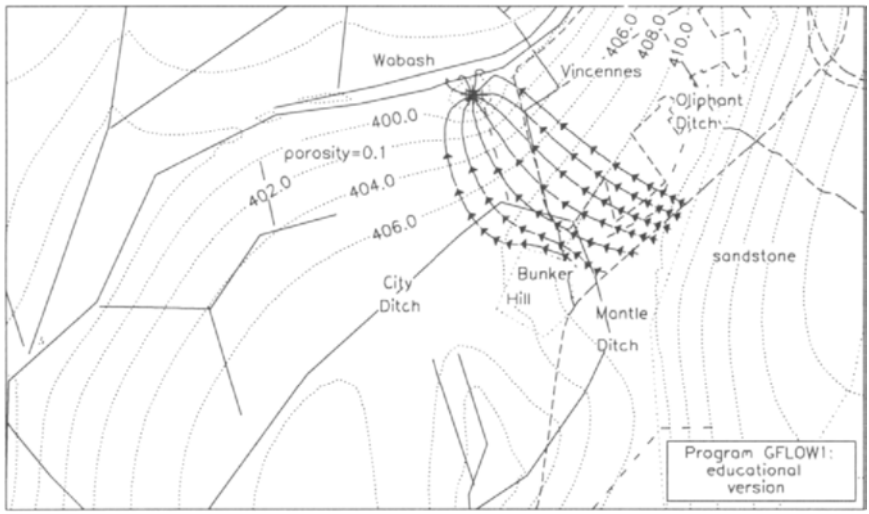

Figure 6.20: Capture zone for porosity in the outwash of $n = 0.1$. (GFLOW1 file vinc06.dat)

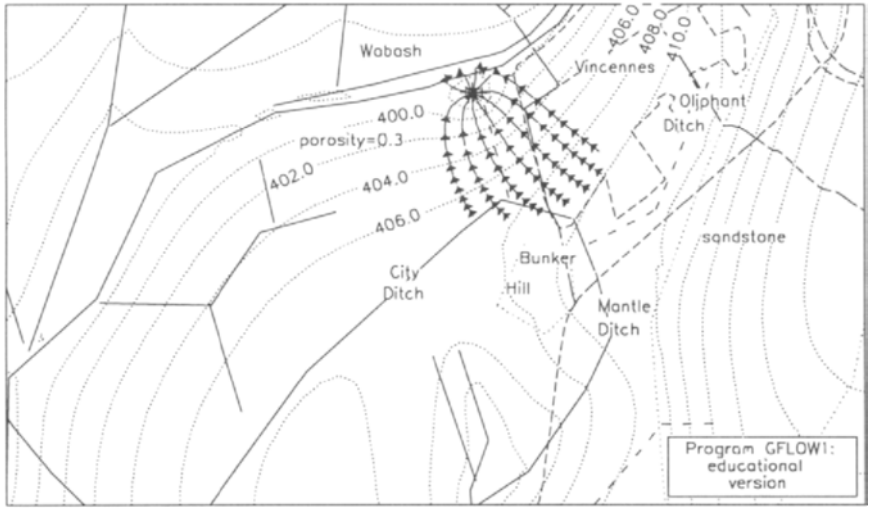

Figure 6.21: Capture zone for porosity in the outwash of $n = 0.3$. (GFLOW1 file vinc07.dat)

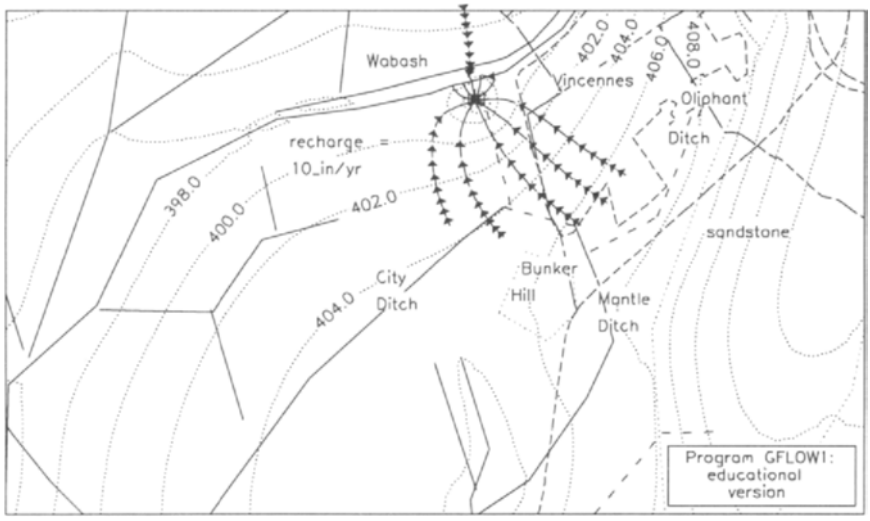

Figure 6.22: Capture zone for aquifer recharge in the outwash of $N = 10$ inches/year. (GFLOW1 file vinc08.dat)

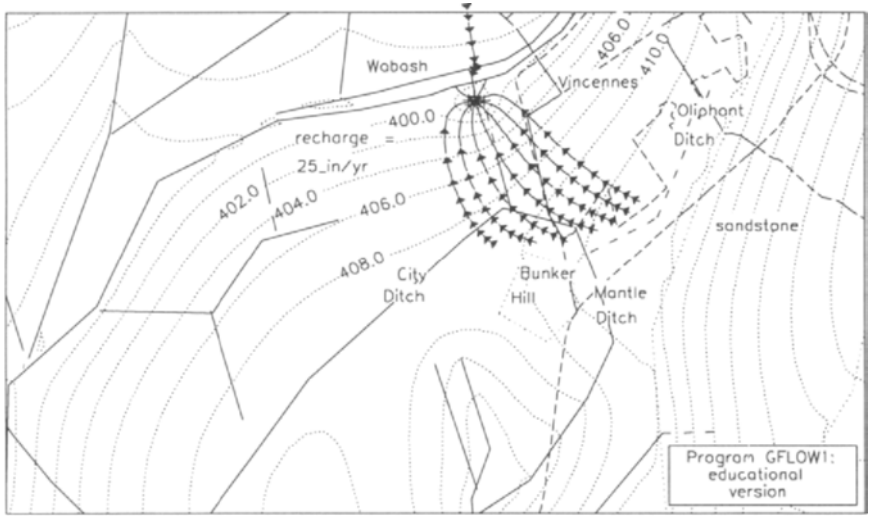

Figure 6.23: Capture zone for aquifer recharge in the outwash of $N = 25$ inches/year. (GFLOW1 file vinc09.dat)

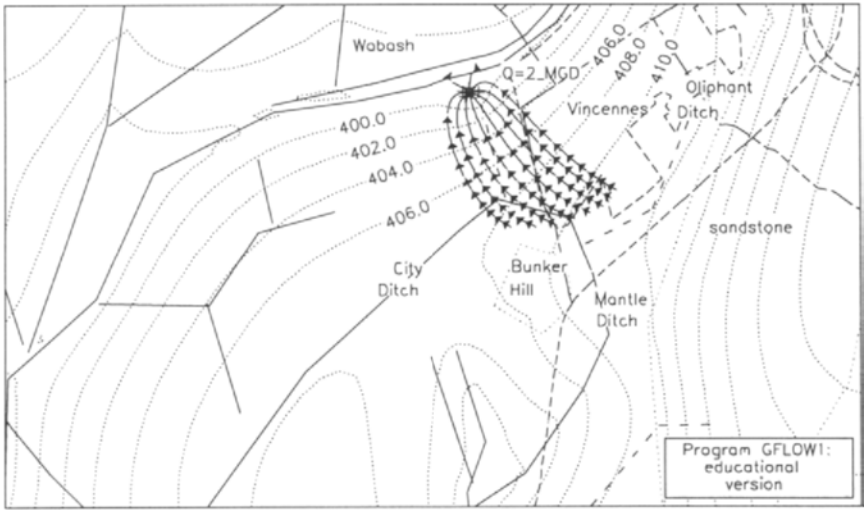

Figure 6.24: Capture zone for pumping rate of $Q = 2$ MGD. (GFLOW1 file vinc10.dat)

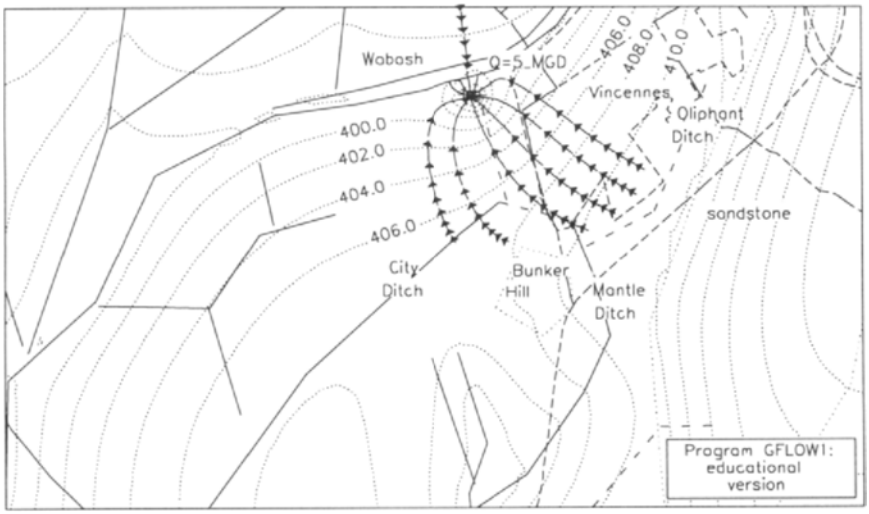

Figure 6.25: Capture zone for pumping rate of $Q = 5$ MGD. (GFLOW1 file vinc11.dat)

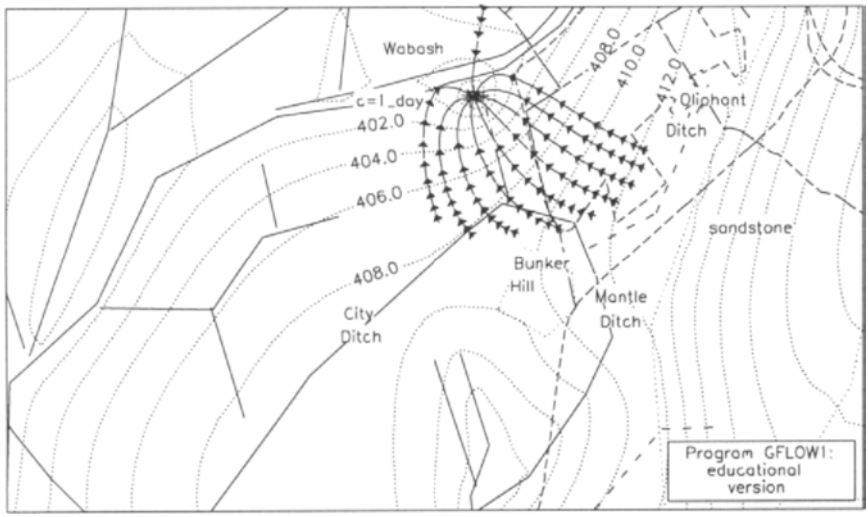

Figure 6.26: Capture zone for resistance of Wabash river of $c = 1$ days. (GFLOW1 file vinc12.dat)

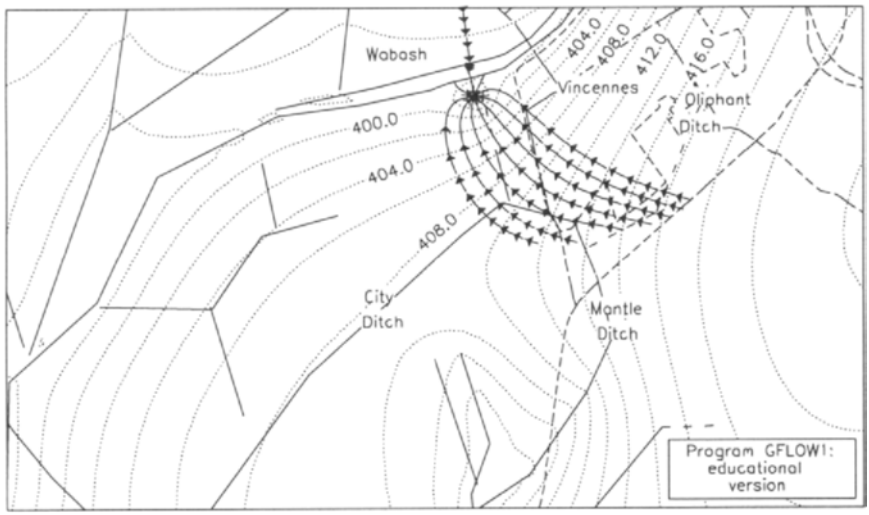

Figure 6.27: Capture zone for the case of no inhomogeneities, hence no sandstone outcrops. (GFLOW1 file vinc13.dat)

6.1.6 Establishing Wellhead Protection Areas

As pointed out before, we cannot accurately match the observed heads and modeled heads, so that we cannot decide on a single set of hydrogeological parameters. Instead, the modeling results presented in Figure 6.18 through Figure 6.27, representing a range of parameter values, are used to create a composite capture zone (see Figure 6.28), which may serve as the basis for defining well head protection areas (WHPA). This composite capture zone is quite conservative, and may be "narrowed down" by making more particular choices for the various parameter values presented in Table 6.1.

Actual Contaminant Travel Times

All isochrones for travel times reflect *average groundwater travel times* in a homogeneous aquifer under steady-state conditions. The actual travel time may be quite different. First of all, aquifers tend to exhibit stratification with layers that are more and less permeable than average. Groundwater moving in higher-permeability strata will arrive at the well earlier than predicted by our modeling. Variations in porosity will have similar effects on the actual groundwater travel times, with a lower porosity resulting in reduced travel times. The steady-state nature of our modeling is another concern. There are in general significant seasonal variations in aquifer recharge and pumping regimes. These transient effects may average out when moving farther from the well, where groundwater travel times are in the range of 5 to 10 years. Near the well, however, within a one-year isochrone, conditions may be significantly different during the summer than during the winter. In other words, the one-year time of travel capture zone is a questionable concept and may not be suitable for defining well head protection areas (WHPAs). Finally, contaminants may be retarded by adsorption to the aquifer material. This *retardation effect* depends on the contaminant in question and on the nature of the aquifer material. Fortunately, retardation *increases* the contaminant travel time, so that from this perspective the use of groundwater travel times is conservative for well head protection purposes.

6.2 Fate of Contaminants

The objective of the previous groundwater flow modeling study was to assess the consequences of groundwater contamination before it happens. Unfortunately, this proactive approach is not always possible. Numerous cases of documented groundwater pollution are currently under investigation and/or remediation. In some cases, contaminants have traveled off site

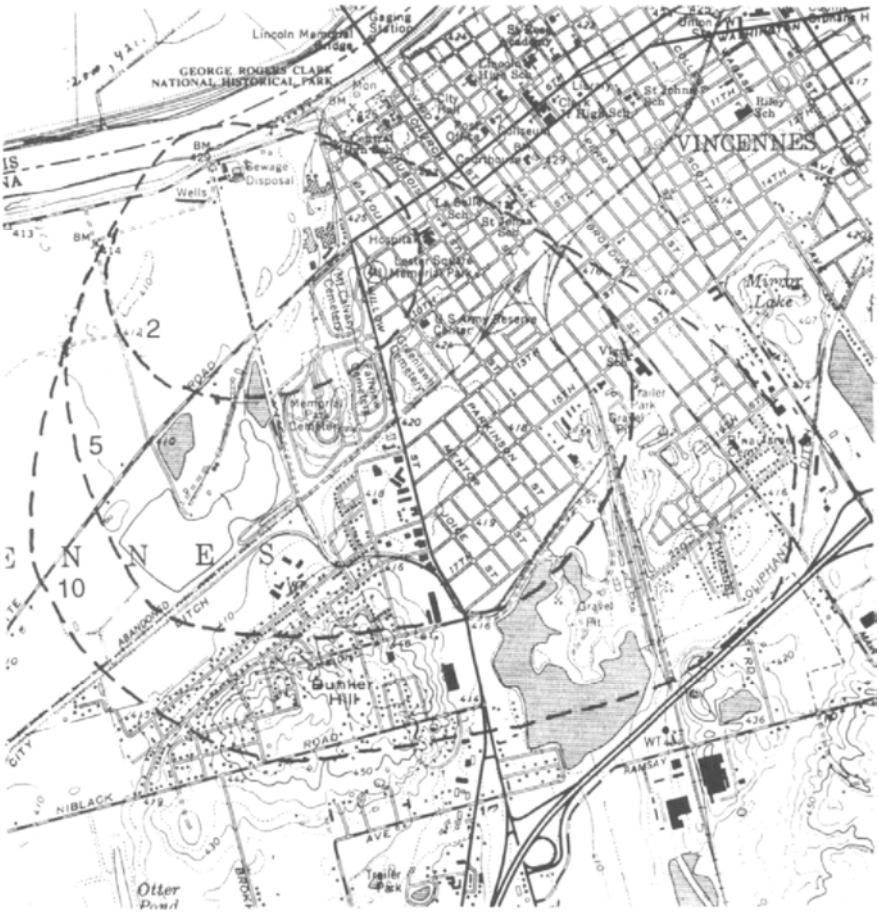

Figure 6.28: Composite time of travel capture zone with 2-, 5-, and 10-year isochrones for the Vincennes well field.

and have been detected in receptors, e.g., domestic wells. In other cases, the contaminants are known to have entered the aquifer, but it is not clear in which direction they are moving and how fast.

Next I will discuss a regional groundwater flow modeling study aimed at assessing the potential fate of contaminants released from the Four County Landfill in Fulton County, Indiana. The following summary of that study has been adapted from the journal article "Modeling Regional Ground-Water Flow in Fulton County, Indiana: Using the Analytic Element Method" (Haitjema, 1992b).

6.2.1 Environmental Impact of the Four County Landfill

In 1972, the Four County Landfill in Fulton County, Indiana (Figure 6.29) started to accept solid and liquid waste. Its controversial life as a hazardous waste landfill, in almost perpetual conflict with local citizens and both state and federal agencies, ended in early 1989 when a federal judge closed the landfill and fined its owner and operator. Closure was brought about both by a lack of compliance with regulations and by environmental concerns regarding the location and engineering design of the landfill. An important aspect of the environmental concerns is the threat that the landfill poses to the underlying regional aquifer, even though at the time no major off-site contamination of that aquifer had been demonstrated.

The author was retained by attorneys representing local citizens, who were concerned with the environmental consequences of the landfill, were plaintiffs in a civil suit against the owner and operator of the landfill, or both. The groundwater flow study was to be of limited scope, in order to control costs, while still of sufficient technical merit to answer some questions left unanswered by previous hydrogeological studies. These questions included: conflicting piezometric contour maps, different estimates of the aquifer transmissivity, and uncertainties about potential off-site movement of contaminants. To control costs, it was decided to avoid additional field data collection, but instead maximize the use of existing data through groundwater flow modeling. Data limitations were often dealt with using a hypothesis testing approach in combination with conservative assumptions regarding unknown data.

Previous Studies

In 1985 ATEC Associates, Inc., retained by the owner and operator of the landfill, Environmental Waste Control, Inc. (EWC), performed water

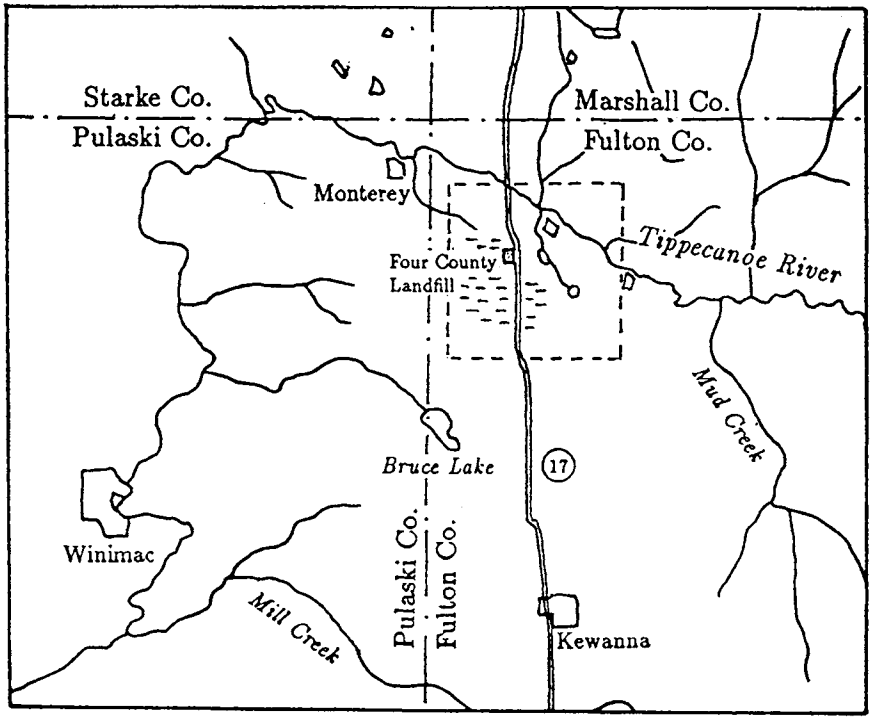

Figure 6.29: Four County Landfill (FCL) in Fulton County, Indiana. The area shown is approximately 20 by 25 miles and is included in the groundwater modeling. The dashed rectangle indicates the largest study area of previous studies. (After Haitjema, 1992b.)

quality tests on water samples from on-site monitoring wells. No evidence was found for a contaminant plume moving off-site (Weaver, 1985).

Dames & Moore, also retained by EWC, used slug tests to estimate the hydraulic conductivity of the sediments underneath the landfill and obtained values ranging from 0.017 ft/day to 12.2 ft/day (Hosfeld, 1987). In addition, detailed piezometric contour plots were presented for the landfill property, showing a mysterious "trough"-like feature. The Indiana Department of Environmental Management (IDEM), reevaluating the same data, did not report this "trough" (Autio, 1988). These conflicting conclusions about the local groundwater movements left the important question of potential off-site contaminant movement unanswered.

A local newspaper, *The Sentinel*, featured a scientific study, paid for by the paper, of the geohydrology near the FCL (Melbardis and Hall, 1987). Melbardis and Hall used both surface water elevations from topographic maps and static water level data of domestic wells, as reported by well drillers, to construct a regional piezometric contour map; see Figure 6.30a. Their contour map shows a steep groundwater gradient across the landfill at variance with observations on-site, where levels differ less than 1 foot (Hosfeld, 1987). Based on the map of Melbardis and Hall, groundwater underneath the landfill flows in a northeasterly direction. Melbardis and Hall also estimate, from literature, the hydraulic conductivity of the sand and gravel formations that make up the regional aquifer to be 250 ft/day, an order of magnitude higher than the highest conductivity reported by Dames & Moore. Assuming contaminants would be released to the regional aquifer, they estimate a total travel time from the landfill to the Tippecanoe River of 15 years.

In 1988 the USGS published its own hydrogeological study by Greeman (1988). His piezometric contour map, Figure 6.30b is based exclusively on well data and differs significantly from the one published by Melbardis and Hall, Figure 6.30a. Greeman's map exhibits a water divide south of the FCL.

Only two of the five studies include hydrogeologic information outside the landfill property itself, and none of the studies attempts to explain the observed piezometric contour patterns, leaving many questions unanswered. The two regional studies (Melbardis and Hall, 1987, and Greeman, 1988) yield different and contradictory piezometric surfaces. The steep gradients across the landfill observed by Melbardis and Hall are not found by Greeman and cannot be explained by the available geological and hydrological data. The low hydraulic conductivities and confusing groundwater gradients on-site ("trough") reported by Dames & Moore are not confirmed by other studies.

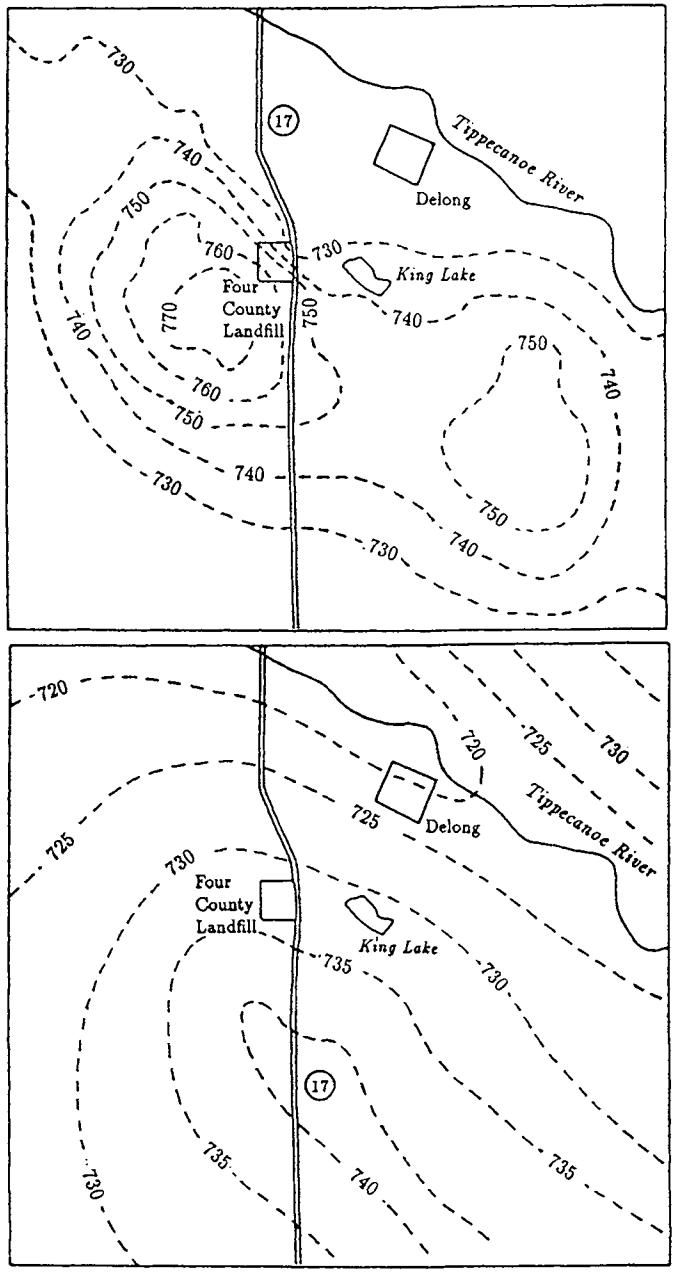

Figure 6.30: Piezometric contours [ft MSL] presented by Melbardis and Hall (1987) (a) and presented by Greeman (1988) (b). The domain of the plots is the dashed rectangle in the previous figure. (After Haitjema, 1992b.)

Geological Conditions

There is little controversy about the complex geological conditions in the area. Following the suggestions of Greeman (1988), the sediments may be grouped into two different units: (1) an upper till unit containing sand and gravel deposits and (2) a lower sand and gravel outwash with some discontinuous clay layers. The lower sand and gravel unit is the primary source of groundwater for domestic, public, and industrial use. Wells are generally less than 150 feet deep and yield from 5 to 1,000 GPM (Hosfeld, 1987). The sand and gravel deposits in the till may or may not be interconnected, depending on local presence or absence of separating clay layers, but insufficient data are available to draw a detailed stratigraphic map (Greeman, 1988). Consequently, the lower aquifer may locally exhibit different piezometric heads at different depths. Similarly, some perched aquifers are found in the upper till unit, isolating some wetlands and creeks from the lower regional aquifer.

6.2.2 Modeling Approach

One of the major concerns for modeling the groundwater flow regime near the landfill is the complexity of the geology, which often exhibits more than one aquifer unit with depth. The extent of these aquifers, their hydraulic conductivity, thickness, and connectivity to other aquifer units vary spatially and are mostly unknown. In view of these data limitations, any attempt to use a multi-aquifer groundwater flow model seems futile. In order to keep the modeling manageable, a single layer Dupuit–Forchheimer model was used: SLAEM (Single Layer Analytic Element Model), which is similar in design to GFLOW1. By using a single layer model, a comprehensive flow solution was obtained; hence, all heads are to be interpreted as "comprehensive heads." In single aquifer zones these comprehensive model heads should compare directly with those measured in the field. However, in multi-aquifer zones the observed heads may be higher or lower than the model heads, depending on the stratum in which the head has been measured. For the present study, domestic wells have been grouped into three categories related to their screen location: shallow, medium, and deep. In recharge areas, remote from streams or lakes, the heads in the shallow wells are expected to exceed the comprehensive head, while the heads in the deeper wells are expected to be lower than the comprehensive head. In discharge areas, near streams or lakes, this trend is expected to be reversed. The model head (comprehensive head) would equal an observed head if the well would penetrate (and be connected to) all strata; see Rule 3.13. In principle, when the locations of well screens and the locations of all aquifer

strata as well as their transmissivities are accurately known, the heads in the various strata can be derived from the comprehensive head (potential); see Section 3.4.2. However, these detailed data are seldom known, and certainly not in the region depicted in Figure 6.31, so that no quantitative comparisons are possible between modeled heads and observed heads, except in single aquifer domains where they should match.

Data Preparation

Nine USGS 7.5-minute topographic maps, covering an area of approximately five hundred (500) square miles surrounding the FCL, were taped together. The main streams and lakes were approximated by strings of straight line elements or quadrilaterals, respectively, which were traced on acetate overlays. SLAEM, unlike GFLOW1, uses quadrilateral surface sinks to model lakes. In GFLOW1 we would either use a sink disc or place line sinks around the lake boundary. The latter option is better, since it more accurately models the constant water table in the lake and the tendency of the lake to take most of the water out of the aquifer near its boundaries. At the center of each element, the surface water elevation was estimated from the topographic map and written near the element on the acetate. In addition, major landmarks (roads, towns, etc.) in the area near the FCL were traced on the acetate for spatial orientation of the results. All data collected on the acetates were digitized by placing each overlay on a data tablet with a 20×17 inch working area, which produced two ASCII data files (.DAT files). The first file, fcl.dat, contains all hydrologic data, including an estimate of the regional hydraulic conductivity and the areal groundwater recharge rate. The second file, fclmap.dat, contains the landmark data serving as a background for plots of piezometric contours or streamlines. A map of the hydrologic features (solid lines) and the digitized landmarks (dash-dot lines) is presented in Figure 6.31, which covers the same area as depicted in Figure 6.29. The solid line elements in Figure 6.31 are line sinks which represent Mill Creek, the Tippecanoe River, and its major tributaries. Some of the lines are interrupted because of digitizing errors. These gaps are of no consequence for the regional groundwater flow solution, and are too remote from the FCL site to be of any concern there. At the center of each line sink, the approximate water level in the creek or river, as obtained from the topographic map, is assigned to the line sink.

In the present modeling, the rivers and creeks have been assumed to be in complete contact with the aquifer. If the streams are only in partial contact with the aquifer, they should have been represented by line sinks with a bottom resistance; see Section 5.2.3. Whether or not a tributary is connected to the regional aquifer system determines whether or

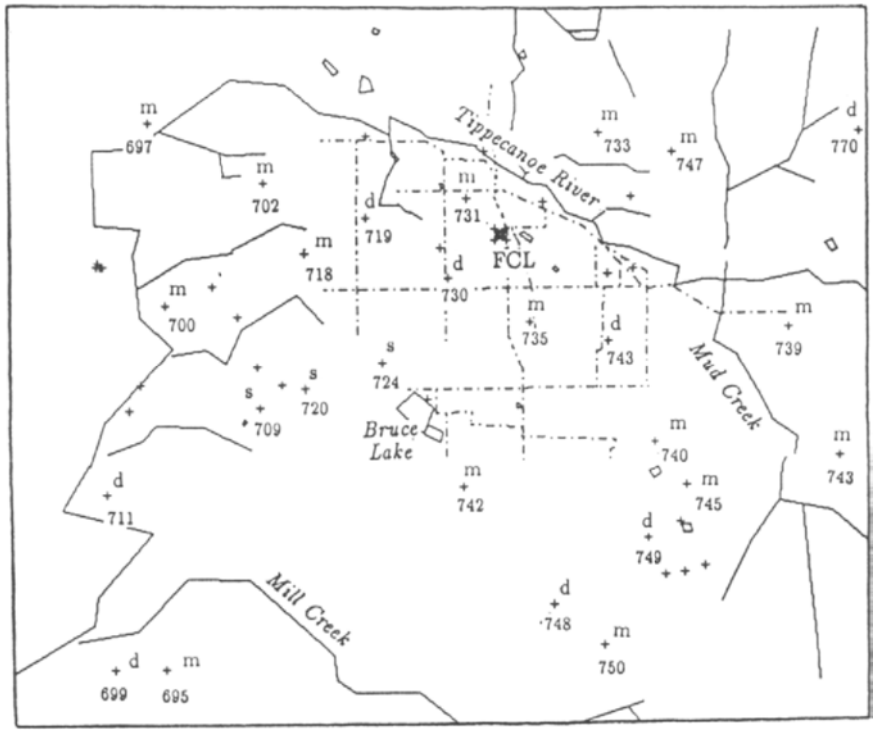

Figure 6.31: Layout of hydrological features (solid lines) and landmarks (dash-dot lines) in the area depicted in Figure 6.29. The + signs refer to domestic wells with static water levels [ft MSL] as indicated. (After Haitjema, 1992b.)

not it is included in the modeling. That decision is based in part on the sparse geological data from nearby well logs and in part on trial runs, by which modeled piezometric heads were compared to the heads in the wells (Figure 6.31), both for the case with and for the case without the tributary. In addition, the inflow or outflow rates of the tributaries, as predicted by the model, were reviewed. When they seemed unrealistically high, it was seen as another indication of poor connection to the regional aquifer. The domestic well locations (+ signs in Figure 6.31) are labeled with "s," "m," or "d," for shallow, medium, or deep wells, respectively. The static water levels indicated in Figure 6.31 are measured with respect to mean sea level (msl).

Regional Hydraulic Conductivity

The first modeling objective was to gain insight into the regional transmissivity of the aquifer. The conceptual model of the area was that of an aquifer with its base (no-flow boundary) at elevation 560 feet above MSL and an upper aquifer boundary at elevation 720 feet above MSL. This conceptualization is realistic near the FCL, but becomes a lesser approximation away from the landfill site. Depending on the modeled piezometric surface, the aquifer will be locally confined or unconfined. Groundwater mounding between streams is proportional to the ratio of N/T; see Rule 3.12. If the recharge rate N is known, the transmissivity may be found by varying the conductivity in the model and comparing the groundwater mounding with observations. Based on information from a water resources study by the "Governor's Water Resources Commission" (Clark, 1980), groundwater recharge rates in Fulton County may be in the range of 6 to 7 inches/year. I chose a conservative recharge rate of 4 inches/year (average in the State of Indiana) to avoid overestimating the hydraulic conductivity and thus overestimating the risk for groundwater contamination due to the FCL.

In Figures 6.32 through 6.34, three contour plots are depicted for three different values of the regional hydraulic conductivity: 20 ft/day, 40 ft/day, and 60 ft/day, respectively.

Superimposed on the contour plots are some water level observations from domestic wells, see also Figure 6.31. When comparing the observed water levels with the calculated levels (contours), it is important to realize that the observed levels are from different depths. In general, the shallower heads should be above the model heads, while the deeper heads should be lower than the modeled heads.

Where there are few surface water features to control the groundwater levels, the piezometric heads are most sensitive to changes in hydraulic conductivity. The calculated heads in the lower right-hand corner of Figure 6.32, for instance, are consistently higher than those observed in domestic wells, regardless of well depth. The piezometric contour that runs across the landfill (Figure 6.32) represents a head of 735 feet, at least 5 feet higher than those observed in monitoring wells on site, around 729 feet (Hosfeld, 1987). More realistic heads result from the assumed hydraulic conductivities of 40 ft/day and 60 ft/day (Figures 6.33 and 6.34, respectively). For this study I adopted the lower, more conservative hydraulic conductivity of 40 ft/day, which also produced the most realistic piezometric heads at the landfill site. This hydraulic conductivity, however, is merely a regional average and may (will) vary with location and depth.

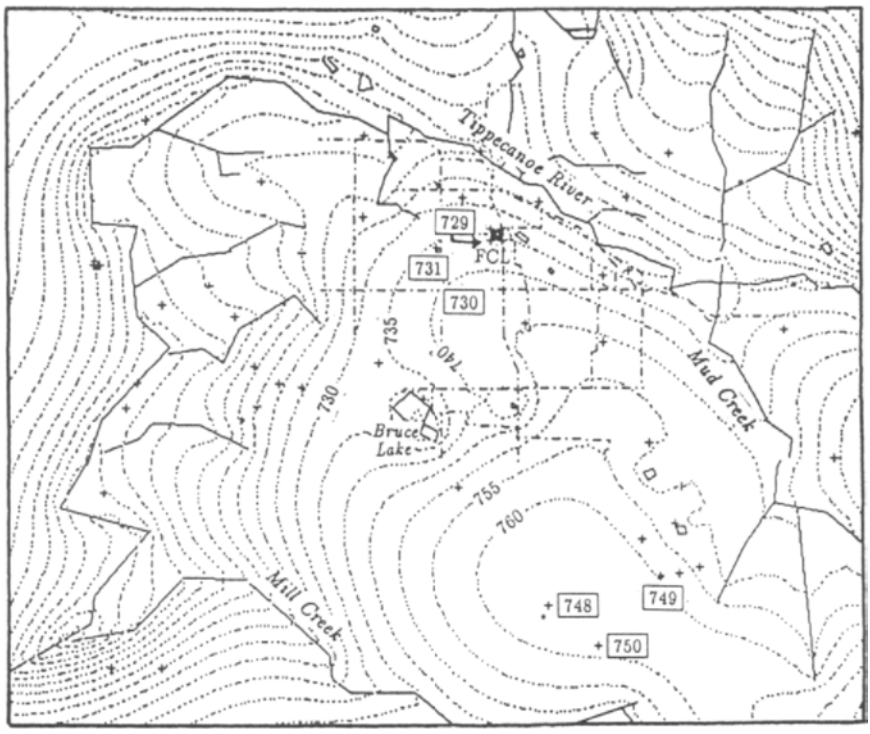

Figure 6.32: Regional piezometric contours [ft MSL] for 4 inches/year recharge and a hydraulic conductivity of 20 ft/day. (After Haitjema, 1992b.)

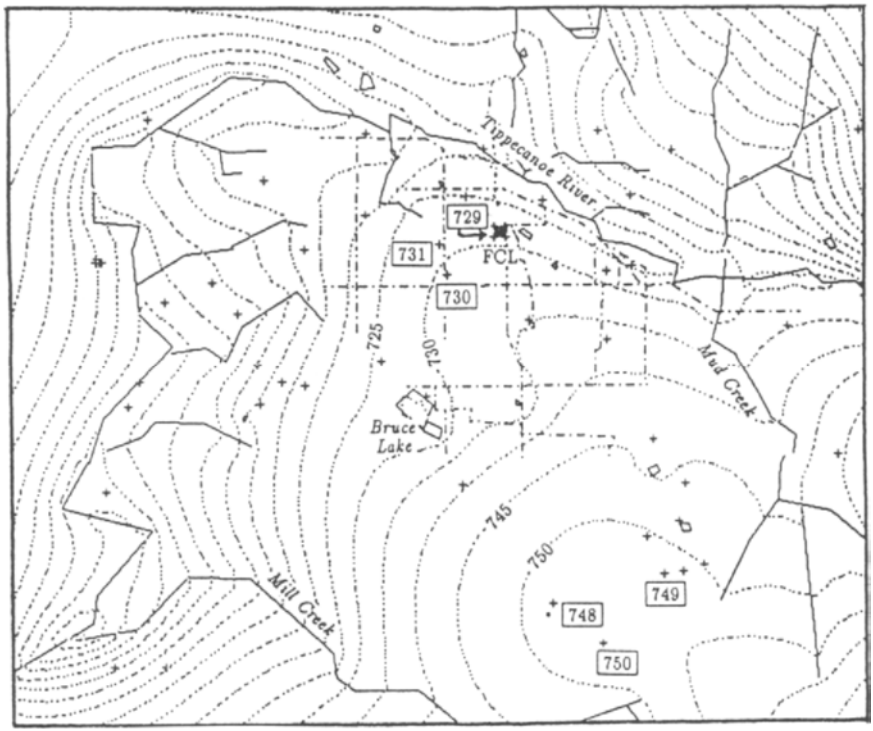

Figure 6.33: Regional piezometric contours [ft MSL] for 4 inches/year recharge and a hydraulic conductivity of 40 ft/day. (After Haitjema, 1992b.)

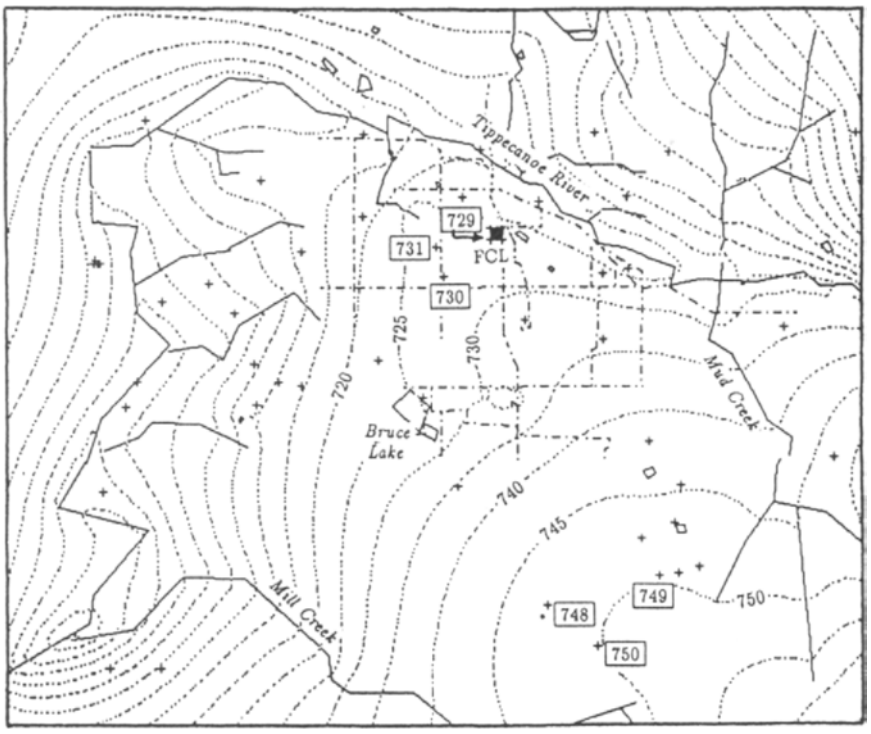

Figure 6.34: Regional piezometric contours [ft MSL] for 4 inches/year recharge and a hydraulic conductivity of 60 ft/day. (After Haitjema, 1992b.)

Area of Interest

The scale of Figures 6.32 through 6.34 is inappropriate for studying the fate of possible contaminant releases at the landfill. A close-up of the area surrounding the landfill is plotted in Figure 6.35. The area depicted in Figure 6.35 is the same as the area shown in Figure 6.30.

When comparing Figure 6.35 with Figure 6.30a it becomes evident that the contours in the latter figure represent, at least in part, perched water table conditions, rather than the regional groundwater regime. The steep gradient across the landfill, therefore, is an artifact of combining water levels from perched groundwater systems (swamps to the south and west of the landfill) with water levels from the regional system (wells on and surrounding the site).

The contours observed by Greeman (1988), which are based exclusively on well data, are in far better agreement with the calculated levels; compare Figure 6.35 with Figure 6.30b. Although the contours differ in shape and location, both the observed and calculated contours exhibit a water divide south of the landfill. For both observed and calculated data, the regional groundwater flow direction at the landfill is toward the north-northeast. This is true regardless of the assumed hydraulic conductivity in the region, (Figures 6.32 through 6.34).

6.2.3 Surface Water and Groundwater Interaction

The modeling results in Figures 6.32 through 6.35 have been obtained after several input data refinements based on comparisons of modeling results with field data and in part based on inspection of the modeling results themselves. For instance, several of the surface water features in the area are not in direct contact with the regional flow system, which became evident after the water levels in the wetlands south and west of the landfill were compared with those found in wells. It also appears that King Lake and its outlet east of the landfill do not control the heads in the regional aquifer. This is demonstrated by a model run in which little resistance to flow is assumed between King Lake and the regional flow system. In Figure 6.36, the vertical resistance to flow between the lake and the aquifer is set to 1 day, as opposed to 500 days in Figure 6.35. Using this lower resistance causes King Lake to have a greater impact on the regional flow system, raising the calculated heads at the landfill above those observed and rotating the flow to the northwest, while field observation show it to be to the northeast. Moreover, for this assumption, the surface sink that represents King Lake has an infiltration rate of 0.114757 ft/day, which translates into an annual infiltration rate of more than 500 inches/year. This seems unrealistically

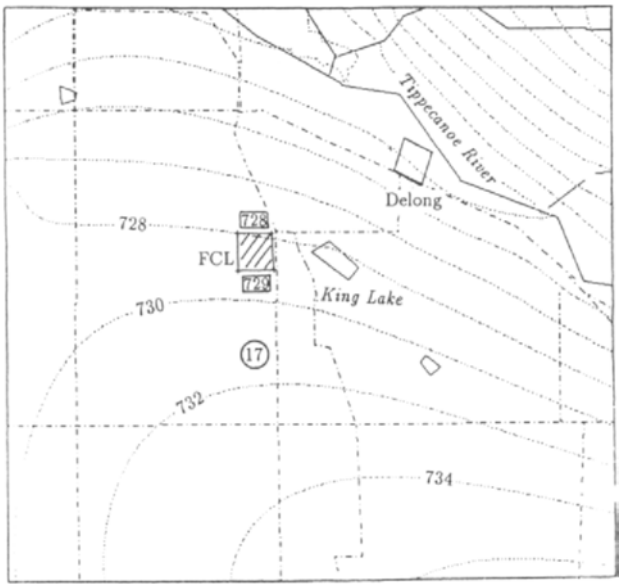

Figure 6.35: Close-up of piezometric contours near the landfill. Area shown is the same as depicted in Figure 6.30. (After Haitjema, 1992b.)

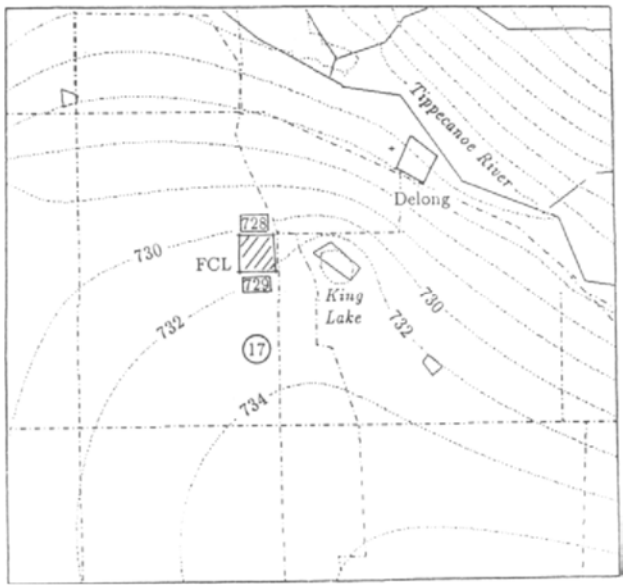

Figure 6.36: Assuming King Lake is in direct contact with the regional aquifer changes heads and flow directions underneath the FCL. (After Haitjema, 1992b.)

high, in view of both the lake's limited watershed size and the fact that it has an outlet to the Tippecanoe River. Because of the latter, some of the water from the watershed is flowing directly into the Tippecanoe River rather than infiltrating into the regional aquifer. The infiltration rate of King Lake, for the case of Figure 6.35, where the lake is given 500 days resistance, is 56 inches/year. The latter infiltration rate may still be too high, but seems possible both from a water balance perspective and in view of its effect on the regional groundwater flow regime. Similar analyses have been conducted for other surface water features in the landfill area, often resulting in adjustments of their resistance to infiltration, or sometimes their removal from the data set.

6.2.4 Potential Off-Site Contaminant Movement

The degree of connection between the various aquifer strata varies in the region. For instance, a domestic well just north of the Tippecanoe River and just west of State Road 17 exhibits artesian conditions with a head in the deeper formations standing more than 5 feet above the water level in the Tippecanoe River. At the landfill site, however, static water levels at different depths are usually within a few tenths of a foot of each other (Hosfeld, 1987), and in close agreement with the comprehensive head in the model. This is characteristic of a single aquifer zone, indicating a good connection between the various strata on site. The landfill is located on a topographic high, while surrounding water levels in the upper till are well above the levels in the regional aquifer; see Melbardis and Hall's contour map in Figure 6.30a. Consequently, there is a potential for downward movement of contaminated groundwater from the upper till into the regional aquifer. Similarly, landfill leachate may move into the regional aquifer.

If contaminants would reach the rather permeable sand and gravel formations underneath the landfill a relatively rapid northeasterly movement may follow. The aquifer thickness at the FCL is approximately 160 feet, with an average hydraulic conductivity of 40 ft/day, which results in a transmissivity of 6,400 ft^2/day. The geologic formations underneath the landfill consist of various formations with various hydraulic conductivities. Using literature values for the low permeable silt and sandy silt formations, it is estimated that the available sand and gravel zones, on average, have a conductivity of approximately 160 ft/day. This estimate is based on the following assumptions: 60 feet of silt with a conductivity of 0.1 ft/day, 60 feet of fine sand with a conductivity of 1 ft/day, and 40 feet of sand and gravel with a conductivity of 158.35 ft/day, yielding a total transmissivity of 6,400 ft^2/day.

The regional pathlines for groundwater that passes underneath the FCL

are depicted in Figure 6.37. The tick marks indicate travel times based on the average sand and gravel conductivity of 160 ft/day, and a porosity of 20%. No dispersion or retardation effects have been included in Figure 6.37. Assuming advective transport, nonreactive contaminants may reach the Tippecanoe River in about 15 years. Incidentally, this result is consistent with that reported by Melbardis and Hall, who used observed groundwater gradients northeast of the FCL and conductivities obtained from the literature (Melbardis and Hall, 1987). Of course, some fraction of the contaminants will move in lower permeable strata, and some types of contaminants will be retarded by adsorption to the aquifer material, resulting in much longer residence times. On the other hand, the transport through sand and gravel zones may still be subject to so-called "hydrodynamical dispersion," whose longitudinal component (dispersion into the direction of average groundwater flow) may further speed up the arival of the contaminants front at a down flow receptor, ultimately the Tippecanoe River. A more accurate assessment of the actual travel times of contaminants released from the landfill requires the acquisition of many more data and much more sophisticated transport modeling, both of which were outside the scope of this study.

The pathlines in Figure 6.37 represent average groundwater movement. Groundwater flow directions may vary somewhat with depth, causing contaminants to move beyond the pathlines that are depicted in Figure 6.37.

6.2.5 Conclusions

A number of questions regarding the environmental impact of the FCL have been answered by the described modeling. Aquifer hydraulic conductivities were demonstrated to be an order of magnitude higher than predicted by FCL consultants. Regional flow directions are north-northeast regardless of any uncertainties in hydrogeological parameters. The aquifers underneath the FCL appeared to be well connected, and groundwater travel times from the landfill to the Tippecanoe River may be as short as 15 years.

6.3 Drawdown Predictions

Groundwater contamination is not the only motivation for groundwater modeling, although currently it is probably the most prominent one. Groundwater availability has traditionally been the objective of many groundwater modeling studies, although more so in arid climates than in the temparate Midwest. Yet even in areas of abundant groundwater resources, the installation of new high-capacity wells may locally cause some

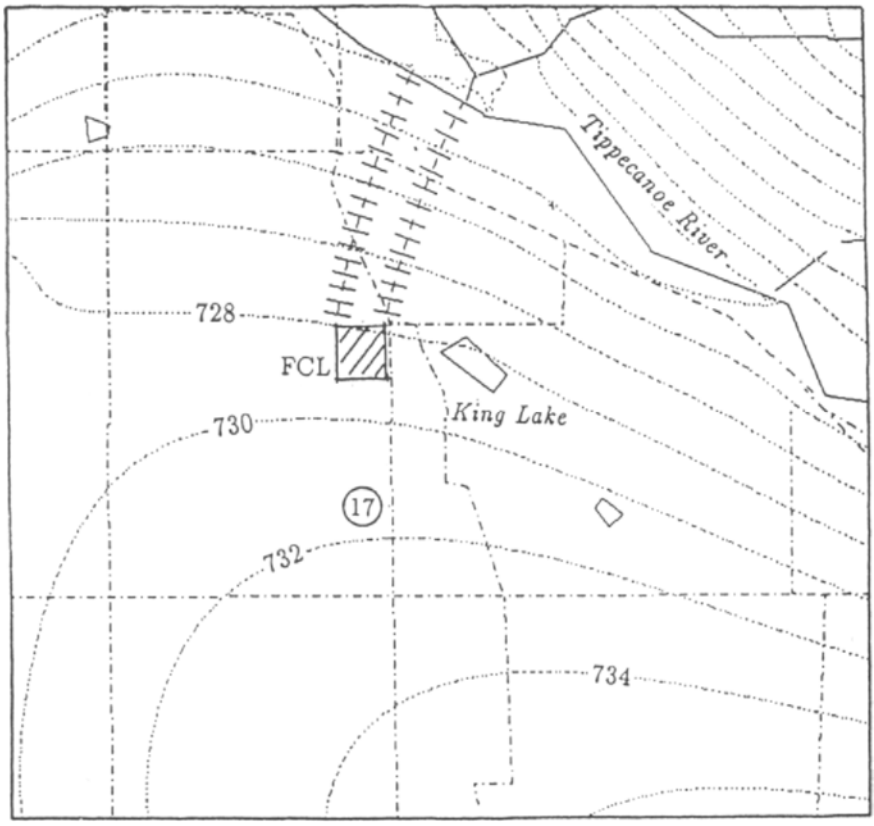

Figure 6.37: Groundwater pathlines from landfill to river through gravel zones with $k = 160$ ft/day. Tick marks indicate intervals of travel times of 1 year. (After Haitjema, 1992b.)

concern.

6.3.1 Mishawaka Well Field

In 1992 the Indiana Department of Environmental Management (IDEM) requested the author to conduct an "Environmental Impact Study of the Gumwood Road well field near Mishawaka, Indiana" (Haitjema, 1992a). The reason for this study was citizens' complaints about alleged adverse impacts of a new well field for the city of Mishawaka. Specifically, the citizens complained about (1) drawdowns that affected the operation of their own drinking water wells, (2) increased staining due to iron and manganese oxides, and (3) the fear of diversion of known or suspected groundwater contamination that would affect their wells. None of these issues are explicitly addressed under the current permitting regulations, and hence neither the city nor the regulatory agencies had investigated these issues prior to the complaints.

Next I will summarize the modeling approach used in that study and documented in a report to IDEM (Haitjema, 1992a). In doing so I will only address issue (1), the drawdowns in the domestic wells.

Previous Studies

The first study of the Gumwood Road well field was conducted before installation of any production wells. Its focus, among others, was on establishing the transmissivity of the aquifer(s) underneath the well field site and predicting long-term drawdowns near the proposed well field (Annable, 1988). The average hydraulic conductivity at the well field site was estimated at about 300 ft/day, assuming a saturated aquifer height of 124 feet. Drawdown predictions were presented for full-capacity pumping as well as for expected average pumping. These drawdowns, based on 5500 GPM pumping capacity, vary from a maximum of 10 feet near the well field to about 2 to 3 feet further away in the residential areas surrounding the well field.

My own earlier study (Haitjema, 1989) focused on potential drawdowns and the risks of diverting contaminants from known or suspected sources toward nearby domestic wells. I concluded that hydraulic conductivities in the upper aquifer, at the proposed well field site, may be substantially lower than predicted by the first study: A value of 100 ft/day was suggested. But even assuming that the hydraulic conductivity is 300 ft/day, I predicted drawdowns which are substantially higher than those reported by Annable (1988): 18 to 20 feet, as opposed to 7 to 10 feet. I did stress the fact that a significant uncertainty remains about the actual hydraulic conductivities in the area (even after both studies) and recommended a long-term pumping

test. Fears of the citizens that the AMOCO site at Granger or the nearby Douglas Road dump site could cause pollution of domestic wells near the well field were disproven. I also pointed out that water quality analyses of the production wells are not representative of the water quality in nearby domestic wells. Contaminants will reach domestic wells earlier than the production wells, and they will be less diluted in the well. Hence, public supply wells are no early warning system for domestic wells.

Under the supervision of the Indiana Department of Natural Resources (IDNR), the recommended long-duration pumping test was conducted (Barnhart and Annable, 1990). The analyses of transient responses in the various piezometers showed significant scatter: T values ranging between 146,115 GPD/ft ($\approx 20,000$ ft^2/day) and 730,575 GPD/ft ($\approx 100,000$ ft^2/day), which illustrates the heterogeneous nature of the aquifer (Haitjema, 1989). The so-called distance drawdown analyses show more consistent results and form the basis for the reported 200,000 GPD/ft average regional transmissivity. This translates into a hydraulic conductivity of 216 ft/day (using an aquifer thickness of 124 feet).

A technical report regarding the impact on nearby Juday Creek of proposed detention basins (Limno-Tech, 1991) offered two valuable analyses regarding Juday Creek: (1) stream flow measurements at different locations along the creek and (2) temperature measurements in the stream and in the sediments indicating where the creek is discharging or recharging groundwater. Since Juday Creek is the nearest surface water feature to the well field, these data are useful in assessing the regional (groundwater) hydrology. These analyses were later published in the peer-reviewed literature (Silliman and Booth, 1993).

Finally, at the time of this study, the USGS had just started a geohydrological study of the St. Joseph River basin, which includes the Gumwood Road well field. Some preliminary data from this study have been incorporated in the present analysis.

Hydrogeological Conditions

The Gumwood Road well field is located in the glacial outwash north and east of the St. Joseph River near South Bend and Mishawaka, Indiana; see Figure 6.38. These thick sand and gravel formations are a highly productive groundwater resource. Locally, the sand and gravel formations are interspersed with clay layers, locally forming dual or multi-aquifer systems, while regionally they act as one aquifer. Underneath the Gumwood Road well field there exists both a single and a dual aquifer zone (Annable, 1988), with a single aquifer domain underneath the northern part of the site and a dual aquifer system underneath the southern part. As a result of these local

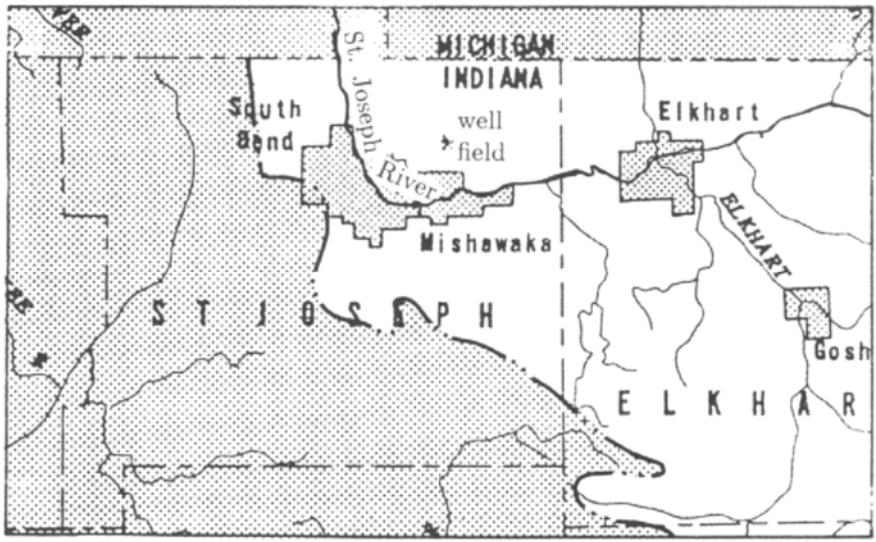

Figure 6.38: Gumwood Road well field in the glacial outwash north and east of the St. Joseph River. (Adapted from Peters, 1987.)

complexities, the pumping test results on site showed substantial scatter in predicted transmissivities and storage coefficients (Annable, 1988; Barnhart and Annable, 1990). The transmissivity for the single aquifer domain was estimated at 300,000 GPD/ft (40,110 ft^2/day). The combined transmissivities for the dual aquifer zone were close to this, 260,000 GPD/ft (34,762 ft^2/day). Based on a saturated thickness of 124 feet on site, these transmissivities translate into hydraulic conductivities of 323 and 280 ft/day, respectively. These results were obtained from a 48-hour pumping test, which suffered from two shortcomings. To begin with, the heterogeneous aquifer conditions complicate the data analysis by use of Jacob's method, which is based on homogeneous aquifer conditions. Secondly, the water pumped from the aquifer was not piped out of the area, but was discharged on site, thus potentially causing aquifer recharge not accounted for in the pumping test analysis.

The best estimate for the hydraulic conductivity in the immediate area of the well field, so far, comes from the distance drawdown analysis based on the most recent pumping test (Barnhart and Annable, 1990) and is about 216 ft/day. This value comes from the suggested transmissivity of 200,000 GPD/ft and the reported aquifer thickness (on site) of 124 feet. The evaluations of transient aquifer responses remains very inconclusive in view of the large variations in piezometer responses.

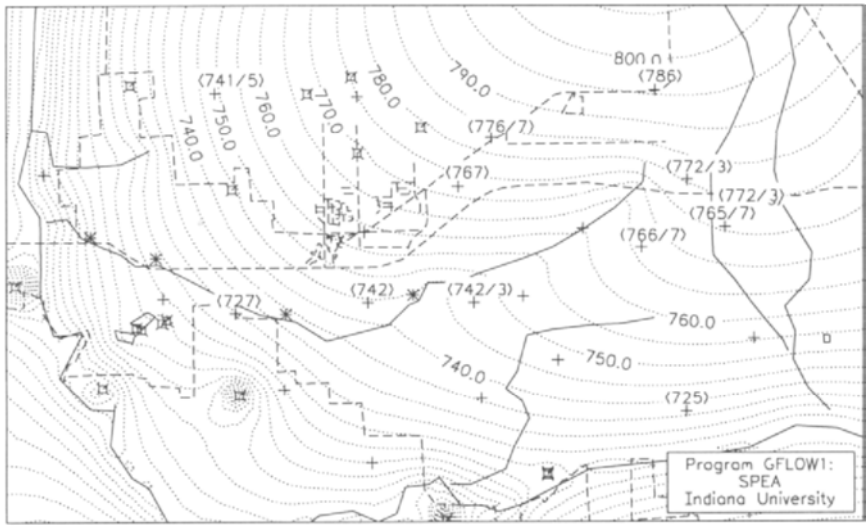

Figure 6.39: Modeled and observed piezometric heads for 15 inches/year recharge and a hydraulic conductivity of 100 ft/day.

6.3.2 Regional Hydraulic Conductivity

Regional groundwater flow modeling may be used to obtain an estimate of a regionally average transmissivity or, with known aquifer thickness, hydraulic conductivity. Here, three steady-state computer simulations are presented using GFLOW1. Each simulation uses the same recharge rate, $N = 15$ inches/year, while the hydraulic conductivity k is varied: in Figure 6.39, $k = 100$ ft/day; in Figure 6.40, $k = 150$ ft/day; and in Figure 6.41, $k = 200$ ft/day. The dotted lines represent contours of equal groundwater elevations or equal piezometric heads. The solid lines represent hydrological features, such as the St. Joseph River, and Juday Creek, while dashed lines represent landmarks, such as roads and city outlines. The small square star-like symbols represent high-capacity wells in the area which are included in the modeling with their average pumping capacity as reported to the IDNR. The plus signs indicate the locations of USGS monitoring wells with groundwater levels written above them in feet above mean sea level (msl). The groundwater levels in the wells were measured on different dates between January 25, 1991, and February 16, 1992. These observed levels are printed between angular brackets in Figure 6.39 through Figure 6.41, where the slash indicates a range of values, which were observed at different dates or at different depth.

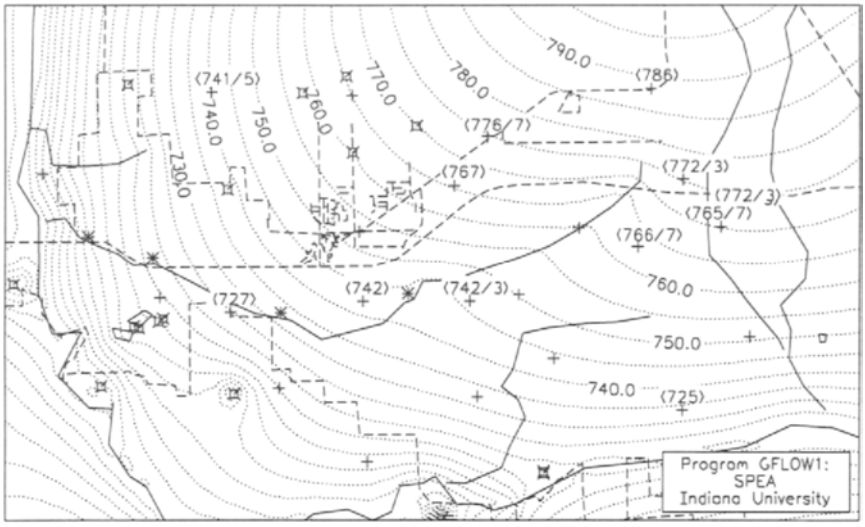

Figure 6.40: Modeled and observed piezometric heads for 15 inches/year recharge and a hydraulic conductivity of 150 ft/day.

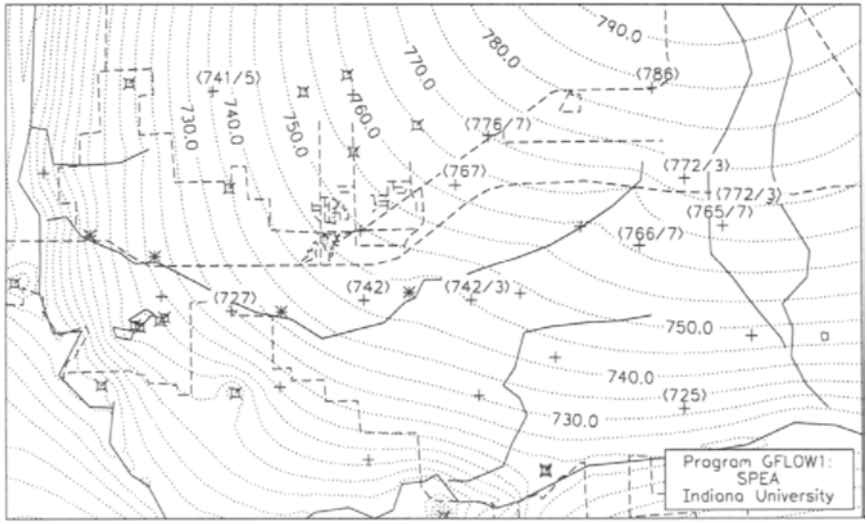

Figure 6.41: Modeled and observed piezometric heads for 15 inches/year recharge and a hydraulic conductivity of 200 ft/day.

In none of the three figures is an exact match seen between modeled and observed heads. Nor should this be expected: The model is a severe simplification of reality, which does not recognize different heads at different depths or at different times of the year. In comparing observed heads with modeled heads, therefore, one should look for general trends rather than local matches. It appears that the contours in Figure 6.40 are generally in better agreement with observed heads than in the other two figures. The contours in Figure 6.39 are generally higher than the observed heads, while the contours in Figure 6.41 are generally lower than observed. Consequently, the ratio of $N/k = \frac{15\,\text{inches/year}}{100\,\text{ft/day}}$ seems most realistic.

In Figures 6.42 through 6.44, contour plots are presented for different values of the hydraulic conductivity k, but the same ratio of N/k. The conductivities vary from 100 ft/day to 300 ft/day, while there is little difference in the piezometric contour levels. This illustrates the dependence of groundwater mounding on the factor N/k; see Rule 3.12 in Section 3.2.2. Only in areas where there is substantial pumpage do lower conductivities lead to larger drawdowns, and thus lower heads. This may be seen, for instance, by comparing the steep cone of depression near the high-capacity well in the lower left part of Figure 6.42 (upper figure) with the much weaker cone of depression for that well in Figure 6.44. A consequence of the similarity (in general) between the piezometric contours in Figures 6.42 through 6.44 is that steady-state groundwater modeling alone will not provide the average aquifer conductivity, unless a good estimate of the average recharge rate due to precipitation is available.

6.3.3 Modeling Baseflow in Juday Creek

The recharge uncertainty may be resolved by applying GFLOW1's conjunctive streamflow and groundwater flow option to Juday Creek, which is the surface water feature nearest to the well field. This option is invoked by use of the "properties" command in GAEP, changing the representation of Juday Creek from a string of line sinks into a stream. By comparing predicted base flow with observed stream flows, an additional calibration tool is obtained to select the proper N/k ratio from the cases presented in Figures 6.42 through 6.44. The Limno-Tech report (Limno-Tech, 1991) contains both stream flow measurements at various locations along Juday Creek and an analysis of temperatures of stream water and water in the stream sediments. The latter temperature measurements indicate where the stream is discharging or recharging the groundwater; see Figure 6.45. Where the temperatures in the sediments and the stream are close to each other in Figure 6.45, aquifer recharge is implied. Elsewhere the stream is receiving water from the regional aquifer. These data may be compared

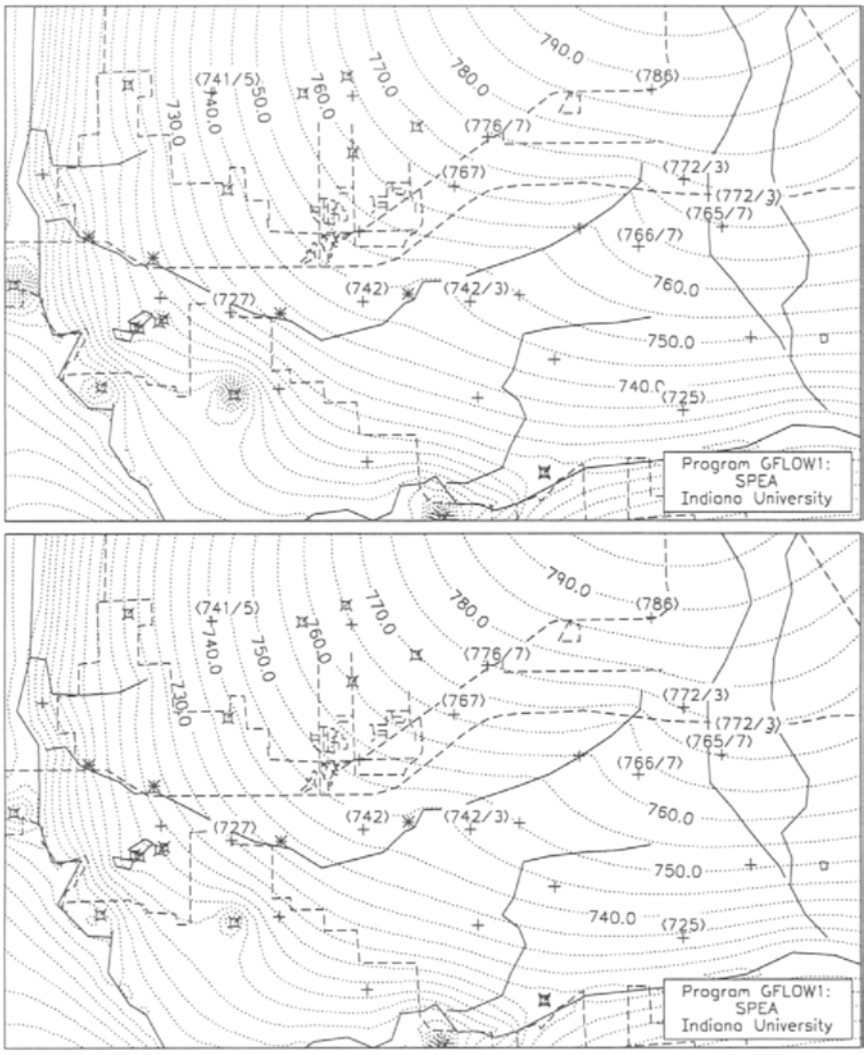

Figure 6.42: Modeled and observed piezometric heads for 10 inches/year recharge and a hydraulic conductivity of 100 ft/day (upper figure) and for 15 inches/year recharge and a hydraulic conductivity of 150 ft/day (lower figure).

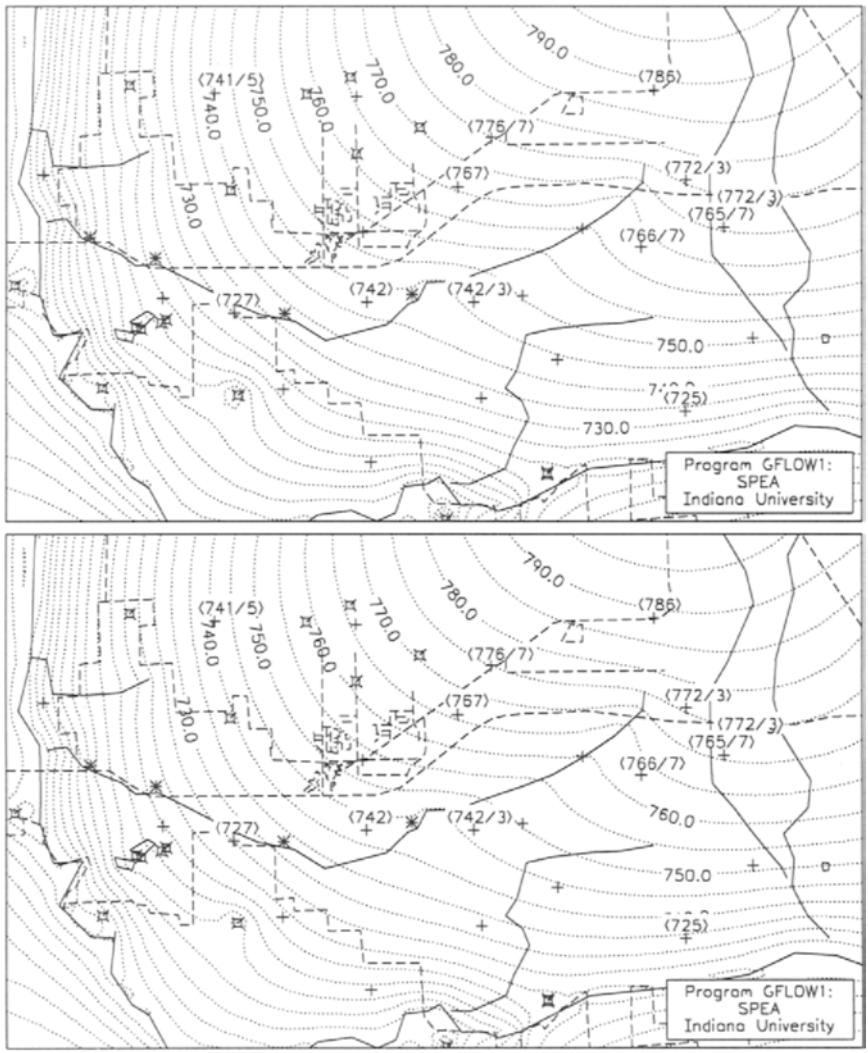

Figure 6.43: Modeled and observed piezometric heads for 20 inches/year recharge and a hydraulic conductivity of 200 ft/day (upper figure) and for 24 inches/year recharge and a hydraulic conductivity of 240 ft/day (lower figure).

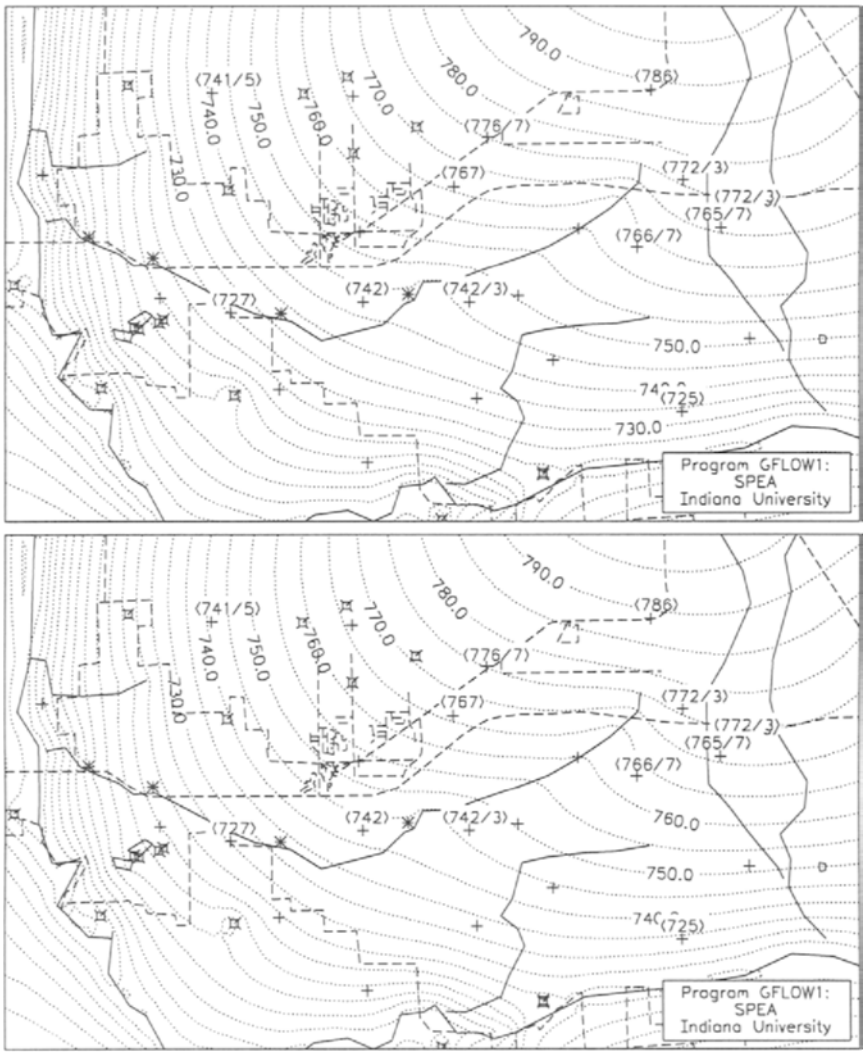

Figure 6.44: Modeled and observed piezometric heads for 26 inches/year recharge and a hydraulic conductivity of 260 ft/day (upper figure) and for 30 inches/year recharge and a hydraulic conductivity of 300 ft/day (lower figure).

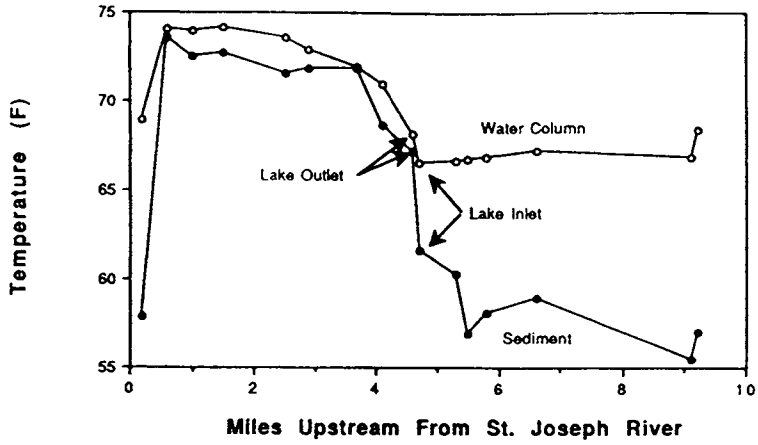

Figure 6.45: Temperature distribution in Juday Creek water and sediments. (After Silliman and Booth, 1993.)

to the modeling results where line sinks with negative sink densities are recharging the aquifer, while positive sink densities indicate groundwater inflow.

In Figures 6.46 and 6.47, modeled base flow distributions along Juday Creek are presented together with observed spring and summer flows. The modeled flow rate is printed next to the gauging station (marked by an asterisk) above the creek. Below the creek, near the gauging station, the observed low flow and high flow values are given. The cases presented in the two figures correspond to those presented in Figures 6.42 through 6.44. It appears from Figures 6.46 and 6.47 that the most likely regional conductivity is somewhere between $k = 200$ and 240 ft/day. This result is in good agreement with the distance-drawdown analyses of the latest pumping test (Barnhart and Annable, 1990). The conductivities of 200 and 240 ft/day imply areal recharge rates of 20 and 24 inches/year, respectively; see Figure 6.43. In addition, I compared recharging stream sections in the model (using the "highlight recharge" feature in the line sink module of GFLOW1) with the temperature distribution in Figure 6.45. Although not shown here, there was general agreement for the modeling runs with hydraulic conductivities between 200 and 240 ft/day.

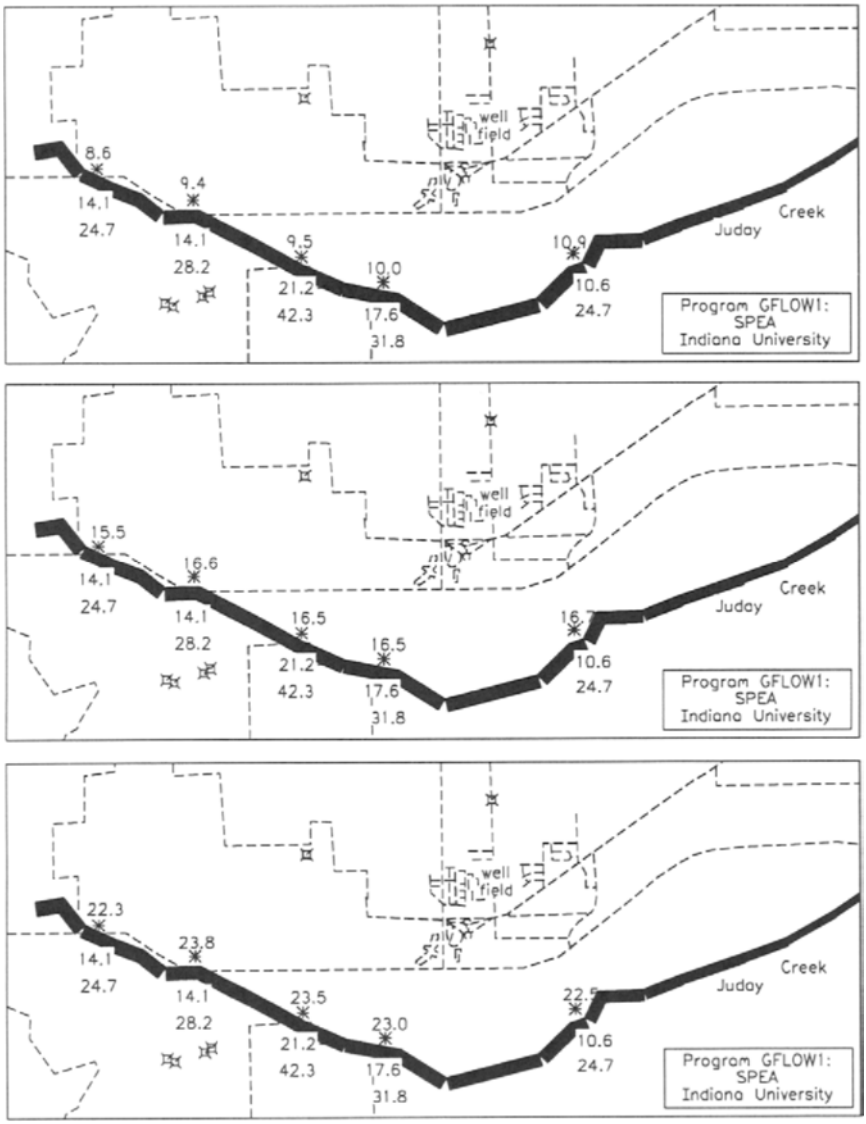

Figure 6.46: Modeled (above creek) and observed (below creek) stream flows (cfs) along Juday Creek for the case of k= 100, 150 and 200 ft/day (from top to bottom).

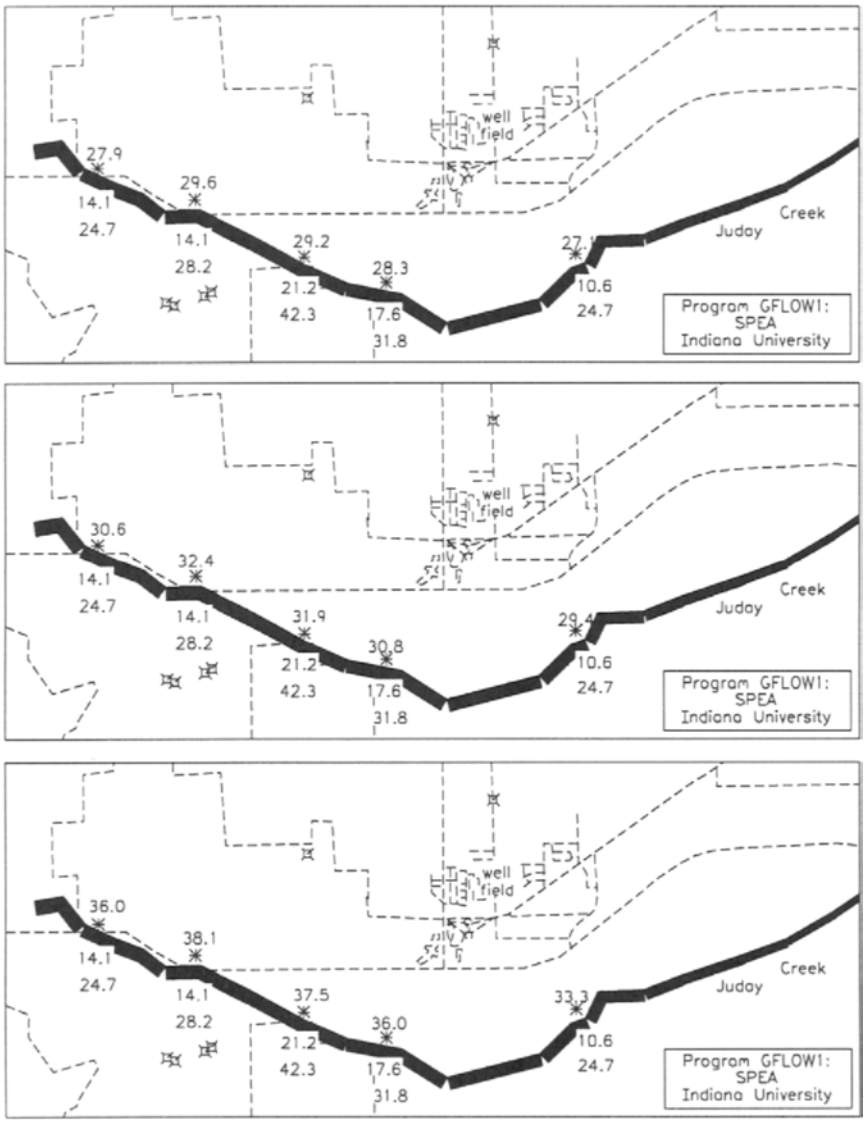

Figure 6.47: Modeled (above creek) and observed (below creek) stream flows (cfs) along Juday Creek for the case of k= 240, 260 and 300 ft/day (from top to bottom).

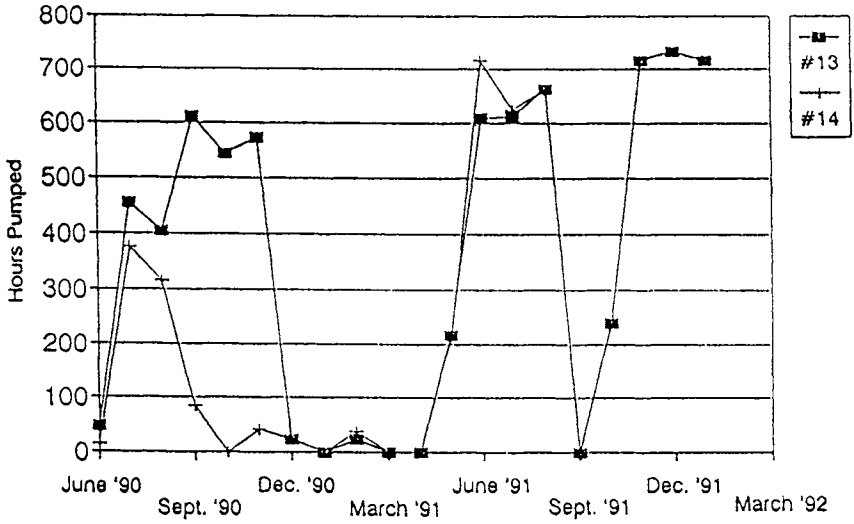

Figure 6.48: Pumping schedule of well #13 and well #14.

6.3.4 Modeling One-Year Drawdowns in Domestic Wells

At the time of this study, two production wells had been pumping for about one year. A simulation of the drawdowns caused by these wells offers yet another opportunity to assess the hydraulic conductivity near the Gumwood Road well field. The IDNR has regularly performed water level measurements in a network of domestic wells near the Gumwood Road well field. Drawdowns observed in domestic wells will be compared to simulated drawdowns using different aquifer parameters.

To isolate the effects from the well field from seasonal variations, I chose two sets of observations at approximately the same time of the year, but a year apart. These measurements were made on February 5, 1991, and on January 23, 1992. Assuming that, on these dates, the water levels would have been the same without the presence of the well field, the observed differences may be considered drawdowns due to the well field.

In Figures 6.49 through 6.52, drawdown predictions are presented for the period from February 5, 1991, to January 23, 1992, using a simulation of the pumping schedule of wells #13 and #14 presented in Figure 6.48, and using four different hydraulic conductivities (k = 150, 200, 240, and

260 ft/day) in combination with two different (phreatic) storage coefficients (S_p = 0.1 and 0.2). The dotted lines in the figure are lines of (predicted) equal drawdown, while the numbers between angular brackets above the plus signs represent the observed drawdowns in the domestic wells. The storage coefficient of S_p = 0.1 resulted from the pumping test (Barnhart and Annable, 1990), while I added the storage coefficient of S_p = 0.2 as an estimated upper bound (equal to the expected porosity). It appears that the hydraulic conductivity of 150 feet per day systematically over predicts drawdowns; see Figure 6.49. On the other hand, the hydraulic conductivity of 260 feet per day tends to underpredict the observed drawdowns, at least close to the well field; see Figure 6.52.

The transient modeling just presented does not recognize the presence of Juday Creek. Some additional modeling was performed to estimate the effect of Juday Creek by introducing image transient wells, imaged with respect to Juday Creek. The latter modeling suggested that the drawdowns in Figures 6.49 through 6.52 may be overestimated by 0.1 to 0.15 feet, a rather insignificant amount. The most likely hydraulic conductivity, therefore, is somewhere in between 200 and 240 feet per day; see Figures 6.50 and 6.51.

The drawdown simulations just discussed, may be interpreted as a pumping test with a duration of one year. This pumping test, however, cannot be interpreted in the classical way (e.g. by Theis' method) because of the irregular pumping scenario; see Figure 6.48. The simulations that have been presented here, however, circumvent the use of Theis' method for this case.

All methods used to estimate aquifer characteristics are approximate and suffer from simplifying assumptions and uncertainties in observations. However, the latest pumping test results (Barnhart and Annable, 1990), the steady-state regional computer modeling, baseflow modeling in Juday Creek, and the transient drawdown simulations, all suggest a hydraulic conductivity value somewhere between 200 and 240 feet per day. It is important to realize that this result is a regional average, which seems applicable to the Gumwood Road well field area. Elsewhere, away from the well field, however, aquifer characteristics may differ.

6.3.5 Predicting Long-Term Drawdowns

The most direct impact of the well field on the nearby domestic wells is the potential for reducing the water levels in these wells, and consequently reducing the productivity of these wells or even drying them up. Occasionally, long-term drawdown predictions are attempted by substituting a long pumping period (e.g., 100 days) in Theis' formula (e.g., Annable, 1988,

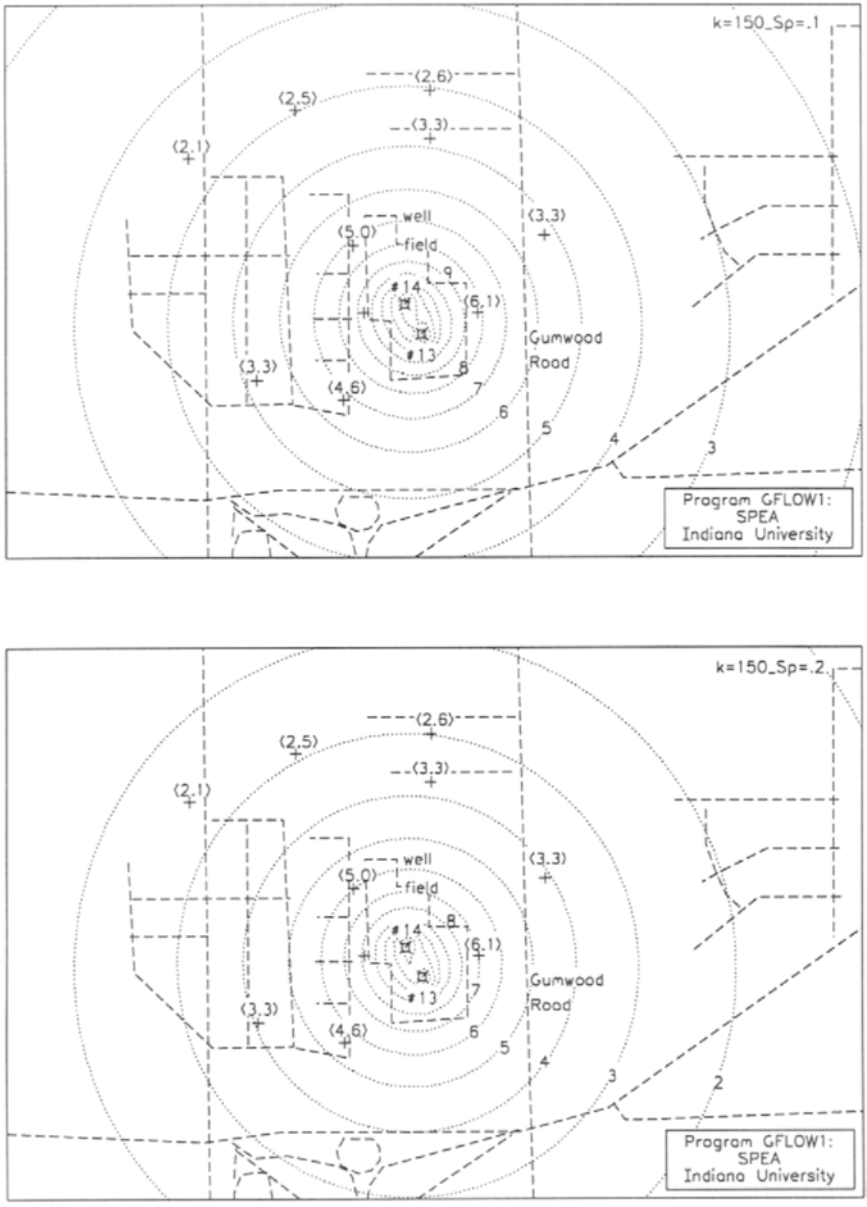

Figure 6.49: Simulated drawdown contours between 2/5/91 and 1/23/92 and observed drawdowns at domestic wells. Hydraulic conductivity is assumed to be 150 ft/day with a storage coefficient of 0.1 (upper figure) and 0.2 (lower figure).

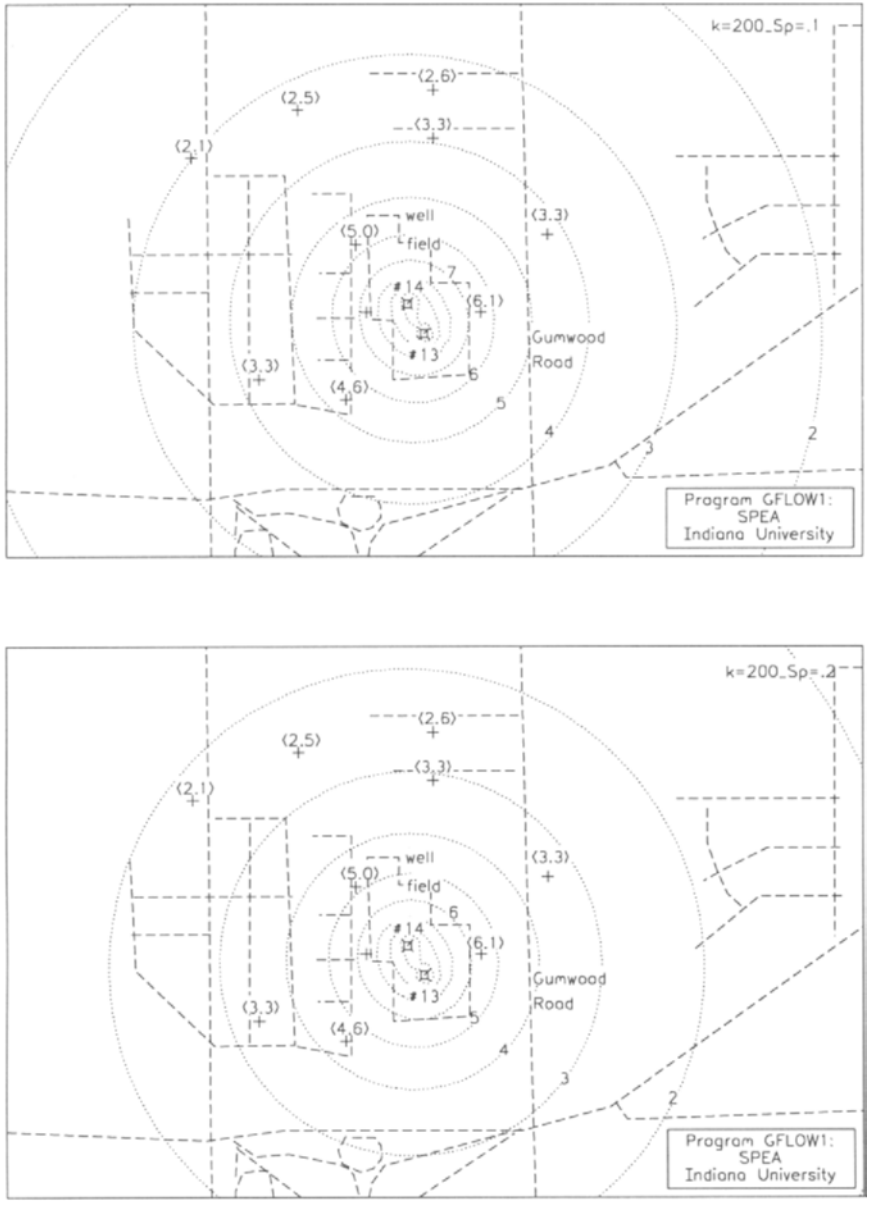

Figure 6.50: Simulated drawdown contours between 2/5/91 and 1/23/92 and observed drawdowns at domestic wells. Hydraulic conductivity is assumed to be 200 ft/day with a storage coefficient of 0.1 (upper figure) and 0.2 (lower figure).

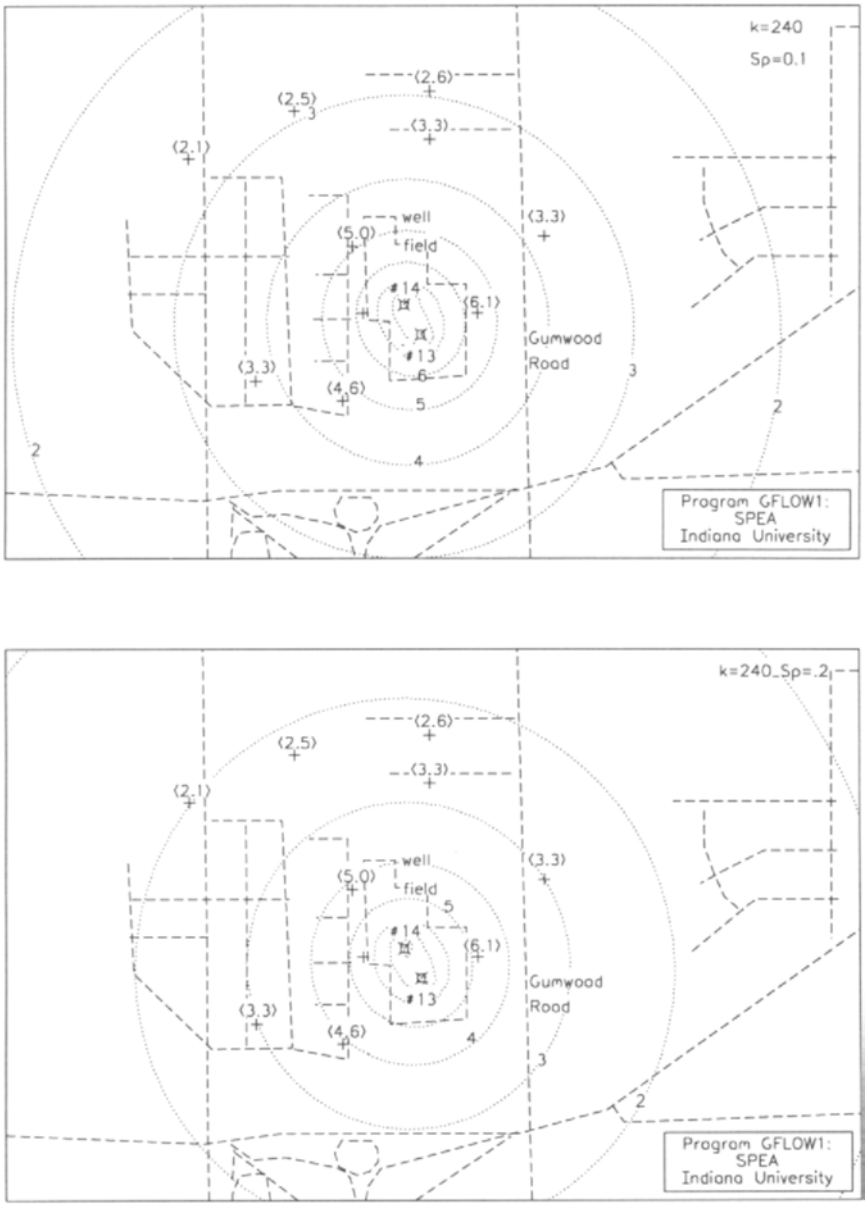

Figure 6.51: Simulated drawdown contours between 2/5/91 and 1/23/92 and observed drawdowns at domestic wells. Hydraulic conductivity is assumed to be 240 ft/day with a storage coefficient of 0.1 (upper figure) and 0.2 (lower figure).

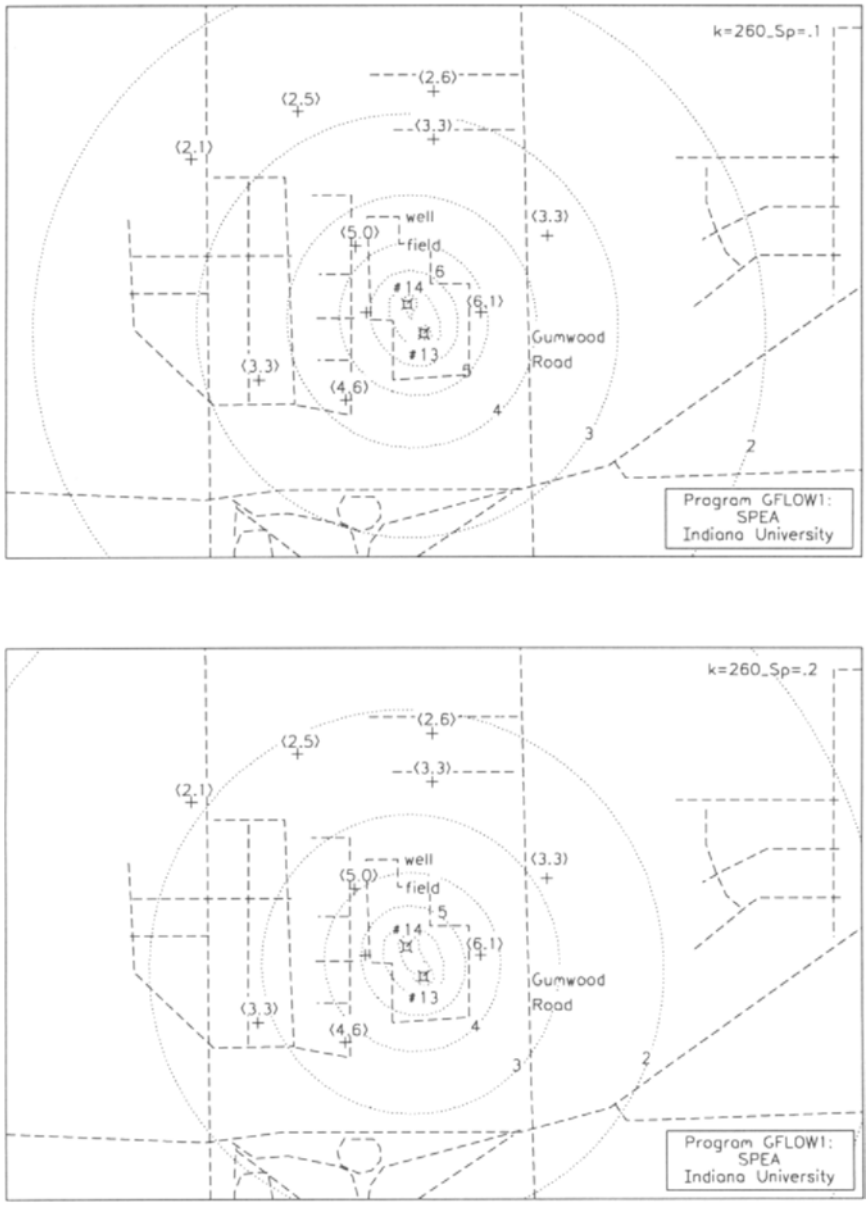

Figure 6.52: Simulated drawdown contours between 2/5/91 and 1/23/92 and observed drawdowns at domestic wells. Hydraulic conductivity is assumed to be 260 ft/day with a storage coefficient of 0.1 (upper figure) and 0.2 (lower figure).

and Barnhart and Annable, 1990). However, Theis' solution is based on the assumption that all water that flows toward the well is released from storage — freed up by lowering the water table in the aquifer. Consequently, when Theis' solution is used for very large times, very large drawdowns are obtained. In the extreme, when the pumping time is infinity, Theis' solution would predict infinitely large drawdowns. In physical terms, one could say that the Theis' solution will completely drain the aquifer if given enough pumping time; see Rule 3.15 in Section 3.6.2. This is not an error in the formula, but a fundamental limitation of the mathematical model represented by that formula. In reality, drawdowns are limited by nearby (and later on more remote) hydrological features responding to the pumping. For instance, a nearby stream or lake will receive less groundwater during pumping of the well than it did before the well was pumped. Only a regional groundwater model which includes these features can account for these changes in "boundary conditions" (responses of streams, lakes, etc.). Thus, only a steady-state regional groundwater flow model can (theoretically) predict long-term drawdowns; Theis' formula cannot!

In Figure 6.53, long-term drawdown predictions are presented for maximum pumpage of all four wells (total of 4,750 GPM), and for hydraulic conductivities of both 200 and 240 feet per day. The contours represent lines of equal drawdown. The predicted contours have been obtained by steady-state regional groundwater flow modeling, comparing piezometric heads in modeling runs with and without the production wells. The drawdown contours have been produced by use of the MINUSGRID option in the grid module of GFLOW1, subtracting two grids with heads calculated with and without pumping, repectively.

The drawdowns in Figure 6.53 are based on pumping all four wells continuously at full capacity. However, common practice is to pump a well field below its installed capacity; see Figure 6.48. The anticipated pumping scenario is an average pumping at about 40% of capacity and winter and summer pumpage that is approximately 10% lower and higher, respectively. In Figure 6.54, predicted drawdowns are presented at the end of the summer (upper figure) and at the end of the winter (lower figure). The implementation in GFLOW1 is as follows. The average pumpage of 40% is modeled by steady-state wells, while the summer and winter pumpages are modeled by adding and subtracting 10% pumpages using Theis' solution. Thus, total pumpage is 30% during six winter months and 50% during six summer months. The drawdowns presented in Figure 6.54 are after 4.5 and 5 years of transient pumping, respectively. Drawdowns in previous summers and winters (in the model) differ little, so the results in Figure 6.54 may be seen as representative for long-term pumpage.

A brief comment on the technique by which Figure 6.54 has been ob-

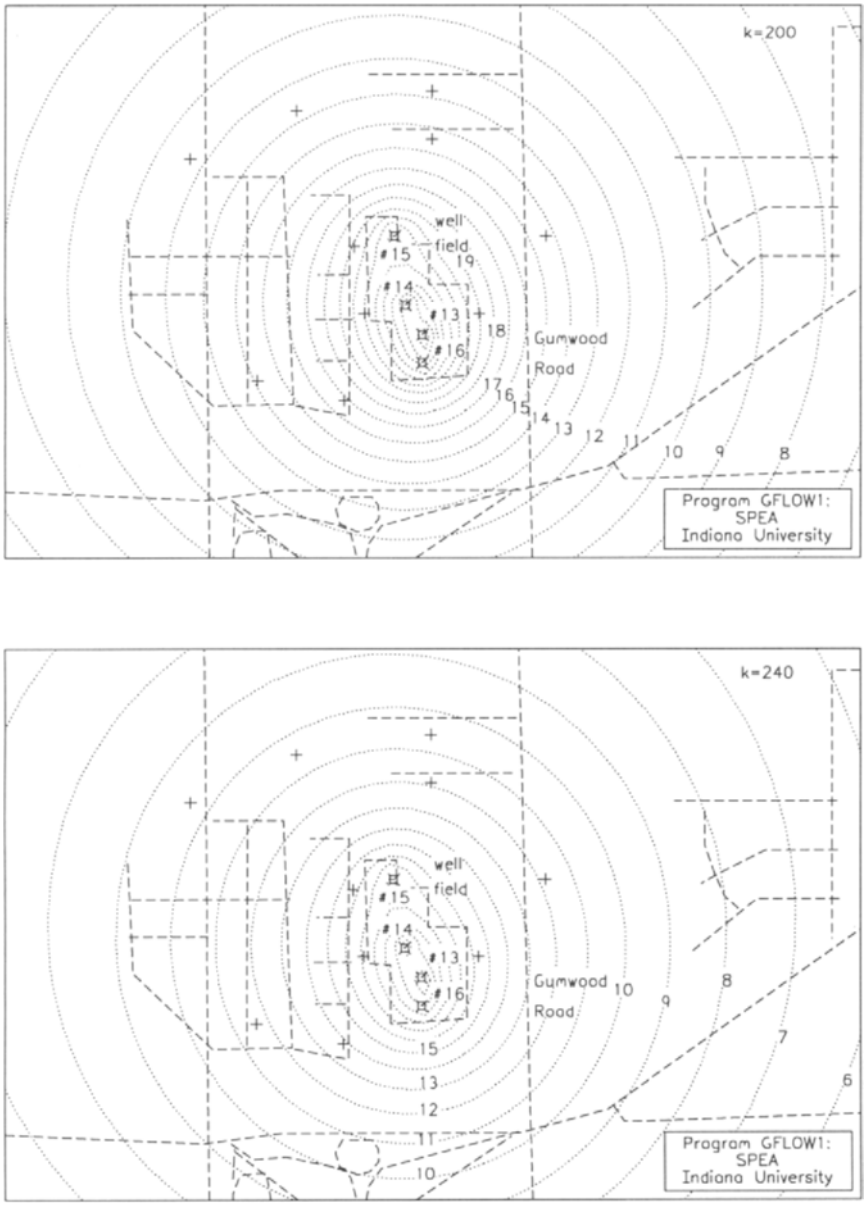

Figure 6.53: Predicted long-term drawdowns near the Gumwood Road well field. Continuous pumping at 4,750 GPM. Hydraulic conductivity of 200 ft/day (upper figure) and 240 ft/day (lower figure).

tained. Previously, I argued that the Theis' solution is unsuitable for long-term drawdown predictions, and yet I did use the Theis' solution in producing Figure 6.54. Consequently, one might expect a violation of the specified conditions along the surface waters in the area. Two factors reduce these errors, however. First of all the *average* pumping is modeled by use of a steady-state well, to which the conditions along the surface waters are correctly adjusted by the program; see also Figure 3.65 in Section 3.6.3. Secondly, the cyclic transient influences on the nearest surface waters, part of Juday Creek south of the well field, are limited by image transient wells — images with respect to Juday Creek. A check on the errors induced near Juday Creek show that they are generally smaller than 1 foot. The resulting errors at the domestic wells are still smaller: Perhaps a few tenths of a foot.

It is possible to operate the well field at only 50% of its total capacity, while still operating all wells at full capacity for the six summer months. To assess the impact of such a (theoretical) scenario, I modeled several years of six months of no pumping (winter) followed by six months of full pumping (summer). In Figure 6.55, drawdowns are presented after 4.5 years (end of winter) and 5 years (end of summer) since the onset of this cyclic pumping scenario. Prior to this cyclic pumping scenario, all wells were assumed to pump continuously at 50% capacity.

Summary

A range of possible regional (average) hydraulic conductivities has been established, between 200 and 240 ft/day, and their influence on the long-term drawdowns has been assessed. Drawdown predictions have been presented for selected wells near the well field which are being monitored by the IDNR. The predictions are based on several different pumping scenarios, with increased pumping during the summer and decreased pumping during the winter. The 50%–30% pumping scenario shows drawdowns in the domestic wells which range from 5 to 8 feet at the end of the summer. The 100%–0% pumping scenario shows drawdowns in the domestic wells which range from 8 to 16 feet at the end of the summer.

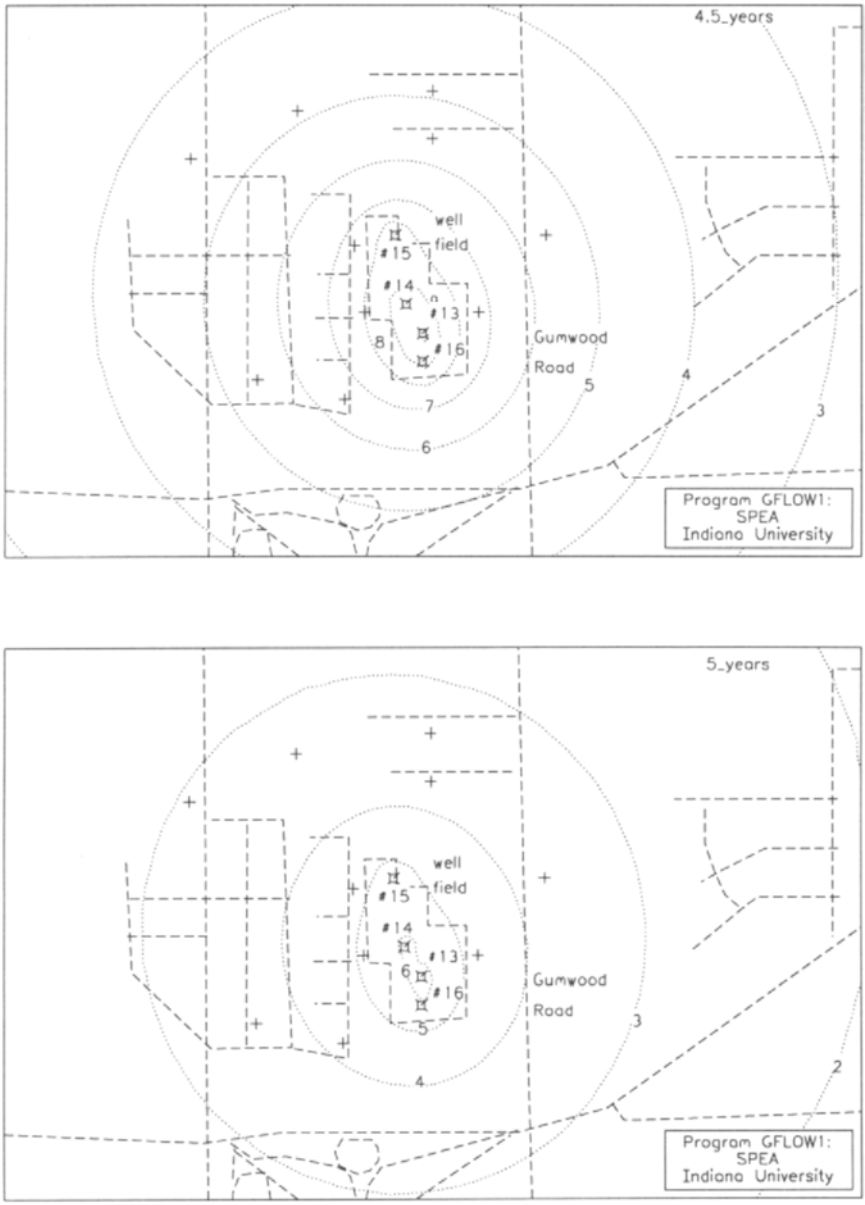

Figure 6.54: End-of-summer drawdowns (upper figure) and end-of-winter drawdowns (lower figure) resulting from 30% winter pumpage and 50% summer pumpage. The hydraulic conductivity is 240 ft/day and the storage coefficient $S_p = 0.1$.

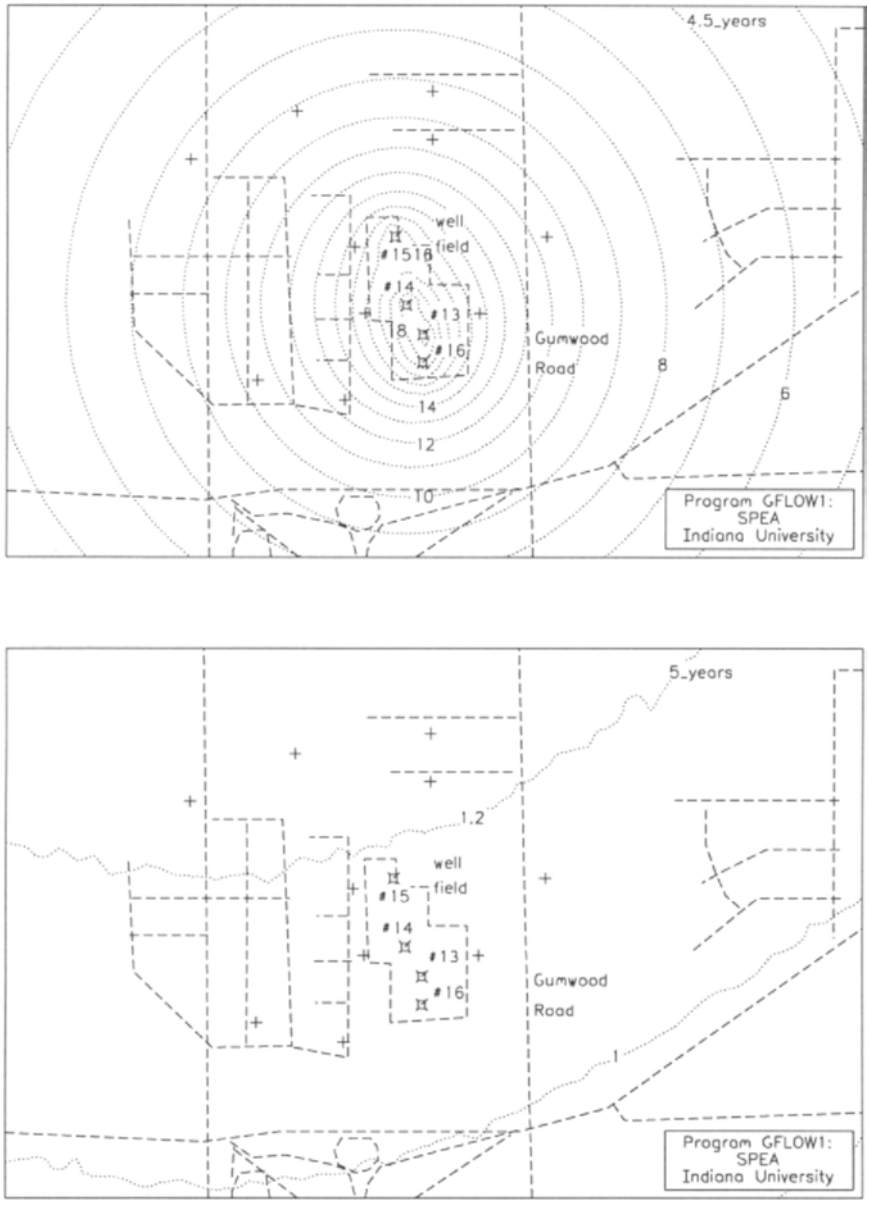

Figure 6.55: End-of-summer drawdowns (upper figure) and end-of-winter drawdowns (lower figure) resulting from 0% winter pumpage and 100% summer pumpage. The hydraulic conductivity is 240 ft/day and the storage coefficient is S_p= 0.1.

Bibliography

ANDERSON, M. P. 1983. Ground-water modeling - The emperor has no clothes. *Ground Water* 21:666–669.

ANDERSON, M. P. AND WOESSNER, W. W. 1992. Applied Groundwater Modeling. Academic Press, Inc., San Diego.

ANNABLE, J. A. 1988. Hydrogeologic study Gumwood Road Well Field, Mishawaka Municipal Utilities, Mishawaka, Indiana. Technical report, Peerless-Midwest, Inc.

ARAVIN, V. I. AND NUMEROV, S. N. 1965. Theory of Fluid Flow in Undeformable Porous Media. Daniel Davey, New York.

AUTIO, R. J. 1988. Comprehensive groundwater monitoring evaluation of Four County Landfill. Technical report, Indiana Department of Environmental Management.

BARNHART, J. R. AND ANNABLE, J. A. 1990. Mishawaka Gumwood Well Field aquifer analysis Mishawaka, Indiana. Technical report, Peerless-Midwest, Inc.

BEAR, J. 1972. Dynamics of Fluids in Porous Media. Environmental Science Series. American Elsevier Publishing Company, Inc., New York.

BEAR, J. AND VERRUIJT, A. 1987. Modeling Groundwater Flow and Pollution. Theory and Applications of Transport in Porous Media. D. Reidel Publishing Company, Dordrecht, The Netherlands.

BISCHOFF, H. 1981. An integral equation method to solve three dimensional confined flow to drainage systems. *Applied Mathematical Modeling* 5:399–404.

BLANDFORD, T. N. AND HUYAKORN, P. S. 1990. WHPA: A modular semi-analytical model for the delineation of wellhead protection areas. Technical report, U.S. EPA, Office of Ground-Water Protection.

BOUSSINESQ, J. 1904. Recherches theoriques sur l'écoulement des nappes d'eau infiltreés dans le sol. *Journal de Math. Pures et Appl.* 10:363–394.

BYRD, P. F. AND FRIEDMAN, M. D. 1971. Handbook of Elliptic Integrals for Engineers and Scientists, volume 67 of *Die Grundlehren der mathematischen Wissenschaften in Einzeldarstellungen.* Springer-Verlag, New

York.

CARSLAW, H. S. AND JAEGER, J. C. 1959. Conduction of Heat in Solids. Oxford University Press, New York, second edition.

CEDERGREN, H. R. 1967. Seepage, Drainage and Flow Nets. John Wiley & Sons, New York.

CHURCHILL, R. V. 1960. Complex Variables and Applications. McGraw-Hill, New York, 2nd edition.

CLARK, G. D. 1980. The Indiana Water Resource, Availability, Uses and Needs. Governor's Water Resources Study Commission, State of Indiana. Indiana Department of Natural Resources.

COOPER, H. H. AND JACOB, C. E. 1946. A generalized graphical method for evaluating formation constants and summarizing well history. *Trans. Am. Geophys. Un.* 27:526–534.

DARCY, H. 1856. Les Fountaines Publiques de la Ville de Dijon. Victor Dalmont, Paris.

DAVIS, S. N. AND DEWIEST, R. J. 1966. Hydrogeology. John Wiley & Sons, Inc, New York.

DE LANGE, W. J. 1991. A groundwater model of the Netherlands. Technical Report Note #90.066, The National Institute for Inland Water Management and Waste Water Treatment, Lelystad, The Netherlands.

DE MARSILY, G. 1986. Quantitative Hydrogeology. Academic Press.

DUNNE, T. AND LEOPOLD, L. B. 1978. Water in Environmental Planning. W.H. Freeman and Company, New York.

DUPUIT, J. 1863. Études Théoriques et Practiques sur le Mouvement des Eaux dans les Canaux Decouverts et à Travers les Terrains Perméables. Dunod, Paris, 2nd edition.

DUSCHEK, A. AND HOCHRAINER, A. 1970. Tensorrechnung in Analytischer Darstellung, II. Tensoranalysis. Springer-Verlag, New York, 3rd edition.

FORCHHEIMER, P. 1886. Ueber die Ergiebigkeit von Brunnen-Anlagen und Sickerschlitzen. *Architekt. Ing. Ver. Hannover* 32:539–563.

FORCHHEIMER, P. 1930. Hydraulik. Teubner, Leibzig, Berlin, 3rd edition.

FORSYTHE, G. E., MALCOLM, M. A., AND MOLER, C. B. 1977. Computer Methods for Mathematical Computations. Prentice Hall, Inc., Englewood Cliffs, NJ.

FRANKE, O. L., REILLY, T. E., AND BENNET, G. D. 1987. Definition of boundary and initial conditions in the analysis of saturated groundwater-flow systems; an introduction. Technical Report 03-B5, USGS.

FREEZE, R. A. AND CHERRY, J. A. 1979. Groundwater. Prentice-Hall, Inc.

FREEZE, R. A. AND WITHERSPOON, P. A. 1967. Theoretical analyses of regional groundwater flow: 2 Effect of water-table configuration and

subsurface permeability variation. *Water Resources Res.* 3:623–634.

GIRINSKI, N. K. 1946. Complex potential of flow with free surface in stratum of relatively small thickness and $k = f(z)$ (in Russian). *Dokl. Akad. Nauk SSSR* 51:337 – 338.

GREEMAN, T. K. 1988. Assessment of the geology, groundwater flow, and groundwater quality at Four County Landfill, Fulton County, Indiana. Technical report, U.S. Geological Survey.

HAITJEMA, H. M. 1982. Modeling Three-Dimensional Flow in Confined Aquifers using Distributed Singularities. PhD thesis, University of Minnesota. doctoral thesis.

HAITJEMA, H. M. 1985. Modeling three-dimensional flow in confined aquifers by superposition of both two- and three-dimensional analytic functions. *Water Resour. Res.* 21:1557–1566.

HAITJEMA, H. M. 1987a. Comparing a three-dimensional and a Dupuit–Forchheimer solution for a circular recharge area in a confined aquifer. *J. Hydrology* 91:83–101.

HAITJEMA, H. M. 1987b. Modeling three-dimensional flow near a partially penetrating well in a stratified aquifer. *In* Proceedings of the NWWA Conference on Solving Groundwater Problems with Models, p. 9.

HAITJEMA, H. M. 1987c. Preliminary assessment of the subsurface spreading of volatile organic compounds released at the Bridgewater Packaging Facility of Fisher Scientific Company. Technical report, Haitjema Consulting, Inc.

HAITJEMA, H. M. 1989. Preliminary study of the effects of the proposed Gumwood Road Well Field in Mishawaka on nearby domestic wells. Technical report, Haitjema Consulting, Inc.

HAITJEMA, H. M. 1992a. Environmental impact of the Gumwood Road well field near Mishawaka, Indiana. Technical report, prepared for: Indiana Department of Environmental Management.

HAITJEMA, H. M. 1992b. Modeling regional groundwater flow in Fulton County, Indiana. *Ground Water* 30:660 – 666.

HAITJEMA, H. M. AND KELSON, V. A. 1994. GFLOW User's Manual. Technical report, Haitjema Software, LCC, Indianapolis.

HAITJEMA, H. M. AND KRAEMER, S. R. 1988. A new analytic function for modeling partially penetrating wells. *Water Resour. Res.* 24:683–690.

HAITJEMA, H. M. AND STRACK, O. D. L. 1983. An initial study of thermal energy storage in unconfined aquifers. Technical report, Pacific Northwest Laboratories operated by Battelle Memorial Institute for the Department of Energy.

HARR, M. E. 1962. Groundwater and Seepage. McGraw-Hill, New York.

HOSFELD, R. K. 1987. Final hydrogeologic assessment report for the four county landfill. Technical Report Project No. 15315-003-29, Dames &

Moore, Madison, Wisconsin 53704. prepared for Environmental Waste Control, Inc.

HUBERT, M. K. 1940. The theory of groundwater motion. *J. Geol.* 48:785–944.

JAVANDEL, I., DOUGHTY, C., AND TSANG, C.-F. 1984. Groundwater Transport: Handbook of Mathematical Models. Water Resources Monograph Series 10. American Geophysical Union, Washington, D.C.

JOHNSON, P. C., KEMBLOWSKI, M. W., AND COLTHART, J. D. 1990. Quantitative analysis for cleanup of hydrocarbon-contaminated soils by in-situ soil venting. *Ground Water* 28:413 - 429.

KELLOGG, O. D. 1929. Foundations of Potential Theory, volume 31 of *Die Grundlehren der Mathematischen Wissenschaften*. Springer-Verlag, Berlin.

KIM, K. H. AND HAWKINS, R. 1989. SAM User Guide. Technical report, University of Arizona. SAM is a computer model for statistical baseflow separation.

KIRKHAM, D. 1967. Explanation of paradoxes in Dupuit–Forchheimer seepage theory. *Water Resour. Res.* 3:609–622.

KNOWLES, J. K. 1965. On Saint-Venant's principle in the two-dimensional linear theory of elasticity. *Arch. for Rational Mech. and Anal.* 21:1–22.

KONIKOW, L. F. 1986. Predictive accuracy of a ground-water model - lessons from a post audit. *Ground Water* 10:173–184.

KORN, G. A. AND KORN, T. M. 1968. Mathematical Handbook for Scientists and Engineers. McGraw-Hill Book Company, 2nd edition.

LEAP, D. AND KAPLAN, P. G. 1988. A single well tracing method for estimating regional advective velocity in a confined aquifer. *Water Resourc. Res.* 24:993 - 998.

LIMNO-TECH, I. 1991. Evaluation of potential impacts on Juday Creek from proposed detention basins. Technical report, prepared for St. Joseph County Drainage Board South Bend, Indiana.

MCDONALD, M. G. AND HARBAUGH, A. W. 1988. A modular three-dimensional finite-difference ground-water flow model. Technical report, U.S.Geological Survey.

MELBARDIS, V. V. AND HALL, R. 1987. A preliminary investigation of four county landfill, fullton county, indiana. *The Sentinel* .

MITCHELL-BRUKER, S. 1993. Modeling Steady State Groundwater and Surface Water Interactions. PhD thesis, School of Public and Environmental Affairs, Indiana University, Bloomington, IN 47405.

MITCHELL-BRUKER, S. AND HAITJEMA, H. M. 1995. On the effect of topography and recharge on regional groundwater flow: Implications for hydrological modeling. *Water Resour. Res.* . submitted for publication.

MOORE, J. E. 1979. Contributions of ground-water modeling to planning.

Journal of Hydrology 43:121–128.

MUSKAT, M. 1937. The Flow of Homogeneous Fluids through Porous Media. McGraw-Hill, Ann Arbor, Michigan.

NEHARI, Z. 1952. Conformal Mapping. McGraw-Hill, New York.

NEUMANN, S. P. 1975. Analysis of pumping test data from anisotropic unconfined aquifers considering delayed gravity response. *Water Resources Research* 11:329–342.

PATRICK, L. D., BRABETS, T. P., AND GLASS, R. L. 1989. Simulation of ground-water flow at Anchorage, Alaska, 1955-83. Technical Report 88-4139, USGS.

PELTON, W. L. 1961. The use of lysimetric methods to measure evapotranspiration. *In* Proceedings of Symposium No. 2, pp. 106–134. National Council of Canada.

POLUBARINOVA-KOCHINA, P. Y. 1962. Theory of Ground Water Movement. Princeton University Press, Princeton, New Jersey. translated from the Russian by J.M. Roger de Wiest.

SCS 1981. Soil survey of Knox County. Technical report, USDA SCS, Indianapolis.

SHEDLOCK, R. J. 1980. Saline water at the base of the glacial-outwash aquifer near Vincennes, Knox County, Indiana. Technical Report 80-65, U.S. Geological Survey, Indianapolis.

SILLIMAN, S. E. AND BOOTH, D. F. 1993. Analysis of time-series measurements of sediment teperature for identification of gaining vs. losing portions of Juday Creek, Indiana. *Journal of Hydrology* 146:131 – 148.

STRACK, O. D. L. 1981a. Flow in aquifers with clay lamina. I. The comprehensive potential. *Water Resourc. Res.* 17:985–992.

STRACK, O. D. L. 1981b. Flow in aquifers with clay lamina. II. Exact solution. *Water Resourc. Res.* 17:993–1004.

STRACK, O. D. L. 1984. Three-dimensional streamlines in Dupuit–Forchheimer models. *Water Resour. Res.* 20:812–822.

STRACK, O. D. L. 1989. Groundwater Mechanics. Prentice Hall, Englewood Cliffs, New Jersey 07632.

STRACK, O. D. L. 1992. A mathematical model for dispersion with a moving front in groundwater. *Water Resourc. Res.* 28:2973–2980.

STRACK, O. D. L. AND HAITJEMA, H. M. 1981a. Modeling double aquifer flow using a comprehensive potential and distributed singularities 1. Solution for homogeneous permeabilities. *Water Resour. Res.* 17:1535–1549.

STRACK, O. D. L. AND HAITJEMA, H. M. 1981b. Modeling double aquifer flow using a comprehensive potential and distributed singularities 2. Solution for inhomogeneous permeabilities. *Water Resour. Res.* 17:1551–1560.

STRACK, O. D. L., HAITJEMA, H. M., AND MELNYK, J. 1980. Interactive modeling of the aquifers near the, Tennessee-Tombigbee Waterway. *In* Symposium on Water and Related Land Resource Systems, Cleveland, Ohio. Int. Fed. Automat. Contr.

SUDICKY, E. A. 1989. The Laplace transform technique: A time-continuous finite element theory and application to mass transport in groundwater. *Water Resourc. Res.* 25:1833–1846.

THEIS, C. V. 1935. The relation between the lowering of the piezometric surface and the rate and duration of discharge of a well using groundwater storage. *Trans. Am. Geophys. Un.* 16th Annual Meeting, Pt. 2:519–524.

TOTH, J. 1963. A theoretical analyses of groundwater flow in small drainage basins. *J. Geophys. Res.* 68:4795–4812.

TOWNLEY, L. R. 1995. The response of aquifers to periodic forcing. *Advances in Water Recources* 18:125 – 146.

USEPA 1987. Guidelines for delineation of wellhead protection areas. Technical report, U.S.EPA-Office of Ground-Water Protection.

VERRUIJT, A. 1970. Theory of Groundwater Flow. MacMillan, London.

VON KOPPENFELS, W. AND STALLMANN, F. 1959. Praxis der Konformen Abbildungen. Springer-Verlag, Berlin.

WARD, D. S., BUSS, D. R., MERCER, J. W., AND HUGHES, S. S. 1987. Evaluation of a groundwater corrective action at the Chem-Dyne hazardous waste site using a telescopic mesh refinement modeling approach. *Water Resourc. Res.* 23:603–617.

WASSYNG, A. 1982. Solving $ax = b$: A method with reduced storage requirements. *SIAM J. Numer. Anal.* 19:197–204.

WEAVER II, J. W. 1985. Groundwater assessment plan, Four County Landfill, Fulton County, Indiana. Technical report, ATEC Associates, Ltd. revised submittal, File 5-3055.

Index

A

B

C

D

E

F

G

H

I

J

K

L

M

N

O

P

Q

R

S

T

U

V

W